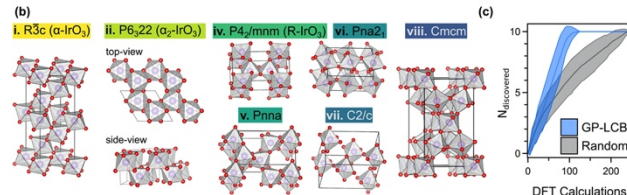
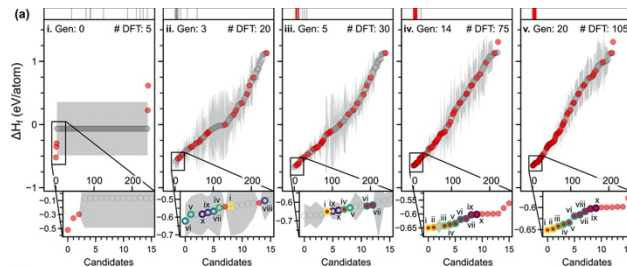
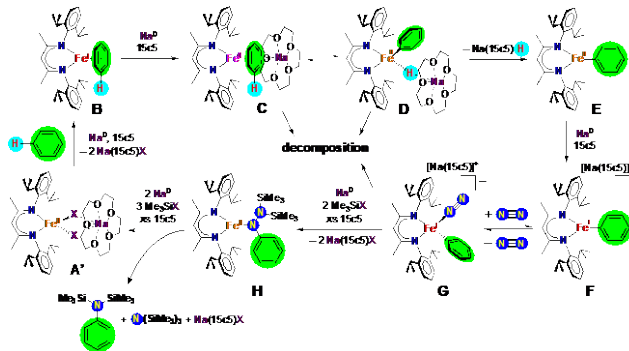
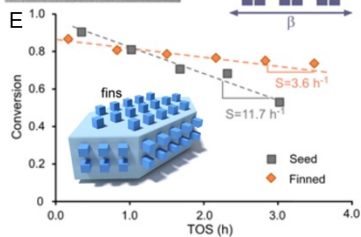
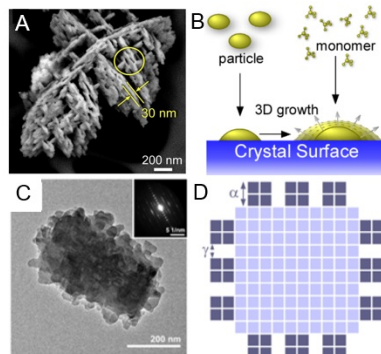
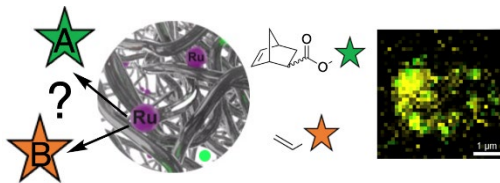


U.S. DEPARTMENT OF  
**ENERGY**

Office of  
Science

2021 Catalysis Science PI Meeting  
**Catalysis for a Circular Economy**  
Virtual Meeting  
September 20-22, 2021



Program and Abstracts for the  
2021 BES Catalysis Science Research PI  
Meeting:  
“Catalysis for a Circular Economy”



U.S. DEPARTMENT OF  
**ENERGY**

Office of  
Science

Virtual Meeting  
September 20-22, 2021

The research grants and contracts described in this document are supported by the U.S. Department of Energy, Office of Science/Basic Energy Sciences, as part of the Catalysis Science Program within the Chemical Sciences, Geosciences and Biosciences Division

## FOREWORD

The 2021 Catalysis Science Research PI Meeting is sponsored by the Division of Chemical Sciences, Geosciences and Biosciences, Office of Basic Energy Sciences (BES), U.S. Department of Energy. It is held as a virtual meeting on September 20-22, 2021. The purposes of this meeting are to discuss the recent advances in the chemical, physical, and biological bases of catalysis science, to foster exchange of ideas and cooperation among BES/Catalysis Science Program PIs, and to discuss the new science challenges and opportunities recently emerging in catalytic technologies for energy production and use.

Catalysis research activities within BES emphasize fundamental research aimed at understanding reaction mechanisms and, ultimately, controlling the chemical conversion of natural and artificial feedstocks to useful energy carriers. The long-term goals of this research are to discover fundamental scientific principles, and to produce insightful approaches for the prediction of catalyst structure-reactivity behavior. Such knowledge, integrated with advances in chemical and materials synthesis, *in-situ* and *operando* analytical instrumentation, chemical kinetics and dynamics measurements, and computational chemistry methods, will allow the control of chemical reactions along desired pathways. This new knowledge will impact the efficiency of conversion of natural resources into fuels, chemicals, materials, or other forms of energy, while minimizing the impact to the environment.

The goal of this meeting is to highlight the fundamental advances in catalysis science of relevance to the energy, economic and environmental future of the U.S. This year's meeting theme "*Catalysis for a Circular Economy*" is a reminder that catalytic processes enable the clean and continuous transformation and recovery of resources. The presentations in this meeting showcase this idea demonstrating how advancements in catalysis science lead to selective and low energy conversions of products as complex as plastics or biomass and as simple -although not less challenging- as nitrogen or CO<sub>2</sub>. This year's program includes plenary talks by international and industry speakers that provide a context on catalysis research outside of this program, as well as 4 Early Career Awardees who bring fresh and novel approaches to long standing challenges in catalytic conversions, in addition to 14 oral and 32 poster presentations by BES/Catalysis Science PIs.

Special thanks to the program investigators and their students, postdocs, and collaborators for their dedication to the continuous success and visibility of the BES/Catalysis Science Program. We also thank the Oak Ridge Institute for Science and Education staff (Linda Sievers, Connie Lansdon and Michael Sharpe) for the logistical and web support of the meeting. Finally, very special thanks go to Raul Miranda<sup>3</sup> for his longstanding and continuing contributions to the BES/Catalysis Science Program, now from his role as Team Lead for Chemical Transformations in the BES/Chemical Sciences, Geosciences and Biosciences Division.

Zdenek Dohnalek<sup>1</sup>, Brent Gunnoe<sup>2</sup>, Viviane Schwartz<sup>3</sup>, Chris Bradley<sup>3</sup> and Igor Slowing<sup>3</sup>

<sup>1</sup>Pacific Northwest National Laboratory

<sup>2</sup>University of Virginia

<sup>3</sup>Catalysis Science Program, Office of Basic Energy Sciences, US Department of Energy

# 2021 BES Catalysis Science PI Meeting

## Catalysis for a Circular Economy

September 20-22, 2021  
Virtual Meeting (All times EST)

**Program chairs:** T. Brent Gunnoe and Zdenek Dohnálek  
*University of Virginia and Pacific Northwest National Laboratory*

### Monday September 20

#### OPENING SESSION

Session Chair: **Zdenek Dohnálek**, *Pacific Northwest National Laboratory*

12:10-12:40 pm Welcoming Remarks and Program Updates

**Viviane Schwartz** and **Chris Bradley**, *DOE/BES/Catalysis Science Program*

12:40-1:00 pm BES Update

**Raul Miranda**, *Team Lead, DOE/BES/Chemical Transformations Team*

1:00-1:10 pm PI Meeting Theme – “Catalysis for a Circular Economy”

**T. Brent Gunnoe**, *University of Virginia* and **Zdenek Dohnálek**, *Pacific Northwest National Laboratory*

#### SESSION I

Session Chair: **Zdenek Dohnálek**, *Pacific Northwest National Laboratory*

##### *Plenary Presentation*

1:15-2:00 pm “Operando Insights into Electrocatalytic and Thermal Conversion of CO<sub>2</sub>”

**Beatriz Roldán-Cuenya**, *Fritz Haber Institute*

2:00-2:15 pm **Break**

## SESSION II

Session Chair: **Elizabeth Biddinger**, *The City College of New York*

### *Program PI Presentations*

2:15-2:45 pm “Imaging Single Molecule Polymerization Catalysis”

**Suzanne Blum**, *University of California Irvine*

2:45-3:15 pm “Simultaneous Upgrading CO<sub>2</sub> and Alkanes”

**Jingguang Chen**, *Columbia University*

3:15-3:30 pm **Break**

## SESSION III

Session Chair: **Steven Tait**, *Indiana University*

### *Program PI Presentations*

3:30-4:00 pm “Multifunctional Zeolites for Methane Dehydroaromatization”

**Sheima Khatib**, *Texas Tech University*

4:00-4:30 pm “Polyketoesters via Dual Alkene Hydroesterification and Carbonylation”

**Ian Tonks**, *University of Minnesota*

### *Early Career Awardees Presentations*

4:30-4:45 pm “Designing Non-covalent Interactions at the Electrode-electrolyte Interface for Nitrogen Activation”

**Sara Thoi**, *Johns Hopkins University*

4:45-5:00 pm “Building from Discrete Molecular Catalysts to Multidimensional Architectures: the Effects of Charge Delocalization and Electronic Coupling on Electrocatalysis”

**Charles McCrory**, *University of Michigan*

## POSTER SESSION I

5:00-6:00 pm

**Tuesday, September 21**

**SESSION IV**

Session Chair: **T. Brent Gunnoe**, *University of Virginia*

*Plenary Presentation*

1:00-1:45 pm “Decarbonizing Low-Cost Fossil Resources by Reactive Separation on High Temperature Liquids”

**Eric McFarland**, *University of California Santa Barbara*

*Program PI Presentation*

1:45-2:15 pm “Amines from Hydrocarbons and N<sub>2</sub>”: Combining C-H Activation and N-N Activation”

**Patrick Holland**, *Yale University*

2:15-2:30 pm **Break**

**SESSION V**

Session Chair: **Ba Tran**, *Pacific Northwest National Laboratory*

*Program PI Presentations*

2:30-3:00 pm “Solvent-mediated Cooperativity in Zeolite Pores”

**David Flaherty**, *University of Illinois Urbana-Champaign*

3:00-3:30 pm “Contributions of Cerium Catalysis to the Circular Carbon Economy”

**Polly Arnold**, *University of California Berkeley*, and *Lawrence Berkeley National Laboratory*

3:30-3:45 pm **Break**

**SESSION VI**

Session Chair: **Johannes Voss**, *SUNCAT*

*Program PI Presentations*

3:45-4:15 pm “Computational Study of Supported Organo-Vanadium Catalyst using XANES Simulations”

**Cong Liu**, *Argonne National Laboratory*

4:15-4:45 pm “Interplay of Electroadsorption and Electrocatalysis on Thin-film Oxide Surfaces”

**Jin Suntivich**, *Cornell University*

*Early Career Awardee Presentation*

4:45-5:00 pm “Electrocatalytic Grafting of PVC”

**Christo Sevov**, *Ohio State University*

## **POSTER SESSION II**

5:00-6:00 pm

### **Wednesday, September 22**

#### **SESSION VII**

Session Chair: **Frédéric Perras**, *Ames Laboratory*

*Plenary Presentation*

1:00-1:45 pm “Closing the Loop on Plastics Recycling”

**Jeff Bricker** and **Andrea Bozzano**, *UOP*

*Program PI Presentation*

1:45-2:15 pm “Selectivity Control with Organic Monolayers on Metal Oxides”

**Will Medlin**, *University of Colorado Boulder*

2:15-2:30 pm **Break**

#### **SESSION VIII**

Session Chair: **Corey Stephenson**, *University of Michigan*

*Program PI Presentations*

2:30-3:00 pm “Catalytic Rates with Active Site Specificity”

**Frank Abild-Pedersen**, *SLAC National Accelerator Laboratory*

3:00-3:30 pm “Modifying the Outer Coordination Sphere of an Artificial Enzyme for CO<sub>2</sub> Reduction”

**Wendy Shaw**, *Pacific Northwest National Laboratory*

3:30-3:45 pm **Break**

### **SESSION IX**

Session Chair: **Felipe Polo-Garzon**, *Oak Ridge National Laboratory*

#### *Program PI Presentations*

3:45-4:15 pm “Designing Zeolites with Improved Diffusion”

**Jeffrey Rimer**, *University of Houston*

4:15-4:45 pm “Cu-zeolites for Partial Methane Oxidation”

**Rajamani Gounder**, *Purdue University*

#### *Early Career Awardee Presentation*

4:45-5:00 pm “Towards a Multiscale Modeling Approach to the Electrochemical Interface with DFT Accuracy”

**Craig Plaisance**, *Louisiana State University*

### **CLOSING SESSION**

5:00-5:10 pm Final Remarks

**T. Brent Gunnoe, Zdenek Dohnálek, Viviane Schwartz, and Chris Bradley**

## POSTER SESSIONS

### Monday 20<sup>th</sup>

- 1. The Consortium for Operando and Advanced Catalyst Characterization via Electron Spectroscopy and Structure (Co-ACCESS) at SSRL**  
Simon R. Bare, Jiyun Hong, Adam S. Hoffman  
*SLAC National Accelerator Laboratory, Menlo Park, CA*
- 2. Catalytic Chloride Oxidation to Mediate Ethanol Oxidation**  
Bart M. Bartlett\*, Andrew G. Breuhaus-Alvarez, SiqiLi  
*Department of Chemistry, University of Michigan –Ann Arbor, MI*
- 3. Mechanistic studies on insertion reactions of Cu-H: Identifying kinetic regimes and substituent effects**  
Ba L. Tran, Amy L. Speelman, Jeremy D. Erickson, Monica Vasiliu, David A. Dixon, R. Morris Bullock  
*Pacific Northwest National Laboratory*
- 4. Atomic-scale interfacial structural studies of oxide-supported catalysts using XSW-XPS**  
Anusheela Das,<sup>1</sup> Yanna Chen,<sup>1</sup> Leighton Jones,<sup>1</sup> Devika Choudhury,<sup>2</sup> Denis Keane,<sup>1</sup> Tien-Lin Lee,<sup>3</sup> Jeff Elam,<sup>2</sup> George Schatz,<sup>1</sup> Michael Bedzyk<sup>1</sup>  
<sup>1</sup>*Northwestern University, Evanston, IL, USA*  
<sup>2</sup>*Argonne National Laboratory, Lemont, IL, USA*  
<sup>3</sup>*Diamond Light Source, Didcot, UK*
- 5. Electrochemical Hydrogenation and Hydrogenolysis of Furfural over Copper Acidic Media**  
Andrew S. May,<sup>1</sup> Steven M. Watt,<sup>1,2</sup> Elizabeth J. Biddinger<sup>1,2</sup>  
<sup>1</sup>*Chemical Engineering, The City College of New York, CUNY, New York, NY, (USA)*  
<sup>2</sup>*Ph.D. Program in Chemistry, The Graduate Center of the City University of New York, New York, NY*
- 6. Templated Encapsulation Promotes High-Temperature Stability in Supported Catalysts up to 1,100 °C**  
Matteo Cargnello  
*Department of Chemical Engineering, SUNCAT Center for Interface Science and Catalysis, Stanford University, Stanford, CA*

- 7. Sub Nanometer Sized Clusters for Heterogeneous Catalysis**  
Abhaya Datye, *University of New Mexico*  
Yong Wang, *Washington State University and Pacific Northwest National Laboratory*
- 8. Theory, Simulation, and Design of High-Oxidation State Main-Group Metal Catalysts for Hydrocarbon C-H Functionalization**  
Daniel H. Ess,<sup>1</sup> Shusen Chen,<sup>1</sup> Roy Periana,<sup>2</sup> Michael Konnick,<sup>3</sup> Anjaneyulu Koppaka,<sup>2</sup> Taylor Nielson,<sup>1</sup> William Hirschi,<sup>1</sup> Braden Borough,<sup>1</sup> ElaynaZalit<sup>1</sup>  
<sup>1</sup>*Department of Chemistry and Biochemistry, Brigham Young University, Provo, UT*  
<sup>2</sup>*The Scripps Research Institute, Scripps-Florida, Jupiter, FL*  
<sup>3</sup>*Hyconix Inc., Warrenville, IL*
- 9. Supramolecular Porous Assemblies of Atomically Precise Catalytically Active Cerium-Based Clusters**  
Megan C. Wasson,<sup>1</sup> Xuan Zhang,<sup>1</sup> Ken-ichiOtake,<sup>1</sup> Andrew Rosen,<sup>2</sup> Selim Alayoglu,<sup>3</sup> Matthew D. Krzyaniak,<sup>1</sup> Zhijie Chen,<sup>1</sup> Louis R. Redfern,<sup>1</sup> Lee Robison,<sup>1</sup> Florencia A. Son,<sup>1</sup> YongweiChen,<sup>1</sup> Timur Islamoglu,<sup>1</sup> Justin M. Notestein,<sup>2</sup> Randall Q. Snurr,<sup>2</sup> Michael R. Wasielewski,<sup>1</sup> Omar K. Farha.<sup>1</sup>  
<sup>1</sup>*Department of Chemistry, Northwestern University, Evanston, IL*  
<sup>2</sup>*Department of Chemical & Biological Engineering, Northwestern University, Evanston, IL*  
<sup>3</sup>*Reactor Engineering and Catalyst Testing Core, Northwestern University, Evanston, IL*
- 10. In Pursuit of Unambiguous Determination of Fe(III) versus Fe(IV) in Transition Metal Oxide Electrocatalysts**  
Lauren F. Greenlee,<sup>1,2</sup> Clemens Heske,<sup>3,4</sup> Jingyi Chen,<sup>5</sup> Tadashi Ogitsu,<sup>6</sup> Lothar Weinhardt,<sup>3,4</sup> Monika Blum,<sup>7</sup> GeletuQing,<sup>1</sup> Nan Jiang,<sup>3</sup> Sergio I. Perez Bakovic,<sup>1</sup> Stephen Faussett,<sup>3</sup> Jennifer Napoles<sup>3</sup>  
<sup>1</sup>*Ralph E. Martin Department of Chemical Engineering, University of Arkansas.*  
<sup>2</sup>*Department of Chemical Engineering, Pennsylvania State University.*  
<sup>3</sup>*Department of Chemistry and Biochemistry, University of Nevada, Las Vegas.*  
<sup>4</sup>*Institute for Photon Science and Synchrotron Radiation, Karlsruhe Institute of Technology.*  
<sup>5</sup>*Department of Chemistry and Biochemistry, University of Arkansas.*  
<sup>6</sup>*Quantum Simulations Group, Lawrence Livermore National Laboratory.*  
<sup>7</sup>*Advanced Light Source, Lawrence Berkeley National Laboratory.*
- 11. Impact of Ionic Environment on Catalytic Activity: Adsorption and Dehydration of Cyclohexanol on Zeolites in Water**  
Sungmin Kim, Niklas Pfriem, Giovanni Piccini, Mal-Soon Lee, Jian Zhi Hu, Oliver Gutiérrez-Tinoco, Roger Rousseau, Yue Liu, Johannes A. Lercher  
*Pacific Northwest National Laboratory, Richland, WA*

**12. Spectroscopic Signatures and Shape-Selective Synthesis of Cyclopentenyl Cations**

Friederike C. Jentoft,<sup>1</sup> Eric. D. Hernandez,<sup>1</sup> Babgen Manookian,<sup>2</sup> Scott M. Auerbach<sup>2</sup>

<sup>1</sup>*Department of Chemical Engineering*

<sup>2</sup>*Department of Chemistry*

*University of Massachusetts Amherst, MA*

**13. Non-Orthogonal Tandem Catalysis in Compartmentalized Nanoreactors**

Eman Ahmed,<sup>1</sup> Jinwon Cho,<sup>2</sup> Ji-il Choi,<sup>2</sup> Jaco,<sup>2</sup> Cleveland,<sup>2</sup> Sage Dubrawski,<sup>1</sup> Fangbei Liu,<sup>1</sup> Christopher W. Jones,<sup>2</sup> Marcus Weck,<sup>1</sup> Seung Soon Jang<sup>2</sup>

<sup>1</sup>*New York University, New York, NY*

<sup>2</sup>*Georgia Institute of Technology, Atlanta, GA*

**14. Catalytic Activation of C-H and O-H Bonds for the Upgrading of Alcohols**

Olaf Nachtigal, Andrew I. VanderWeide, William D. Jones

*Department of Chemistry, University of Rochester, Rochester, NY*

**15. Electronic Cooperativity in Supported Single-and Multinuclear-Sites for Catalytic C-C and C-H Bond Functionalization**

David Kaphan, Jeremy Kropf, Cong Liu, Massimiliano Delferro

*Chemical Sciences and Engineering Division, Argonne National Laboratory, Lemont, IL*

**16. Uniform Catalytic Environments at the Interface: Characterization of Sites and Distributions, Catalytic Activity and Reaction Mechanisms**

Takeshi Kobayashi, Frederic Perras, Marek Pruski, Long Qi, Aaron D. Sadow, Igor I. Slowing

*Division of Chemical and Biological Sciences, Ames Laboratory, Ames, IA*

**Tuesday 21<sup>st</sup>**

**1. Recent Advances in Carbon-Supported Single-Site Molybdenum-Dioxo Catalysis**

Yosi Kratish, Yiqi Liu, Jiaqi Li, Anusheela Das, Leighton O. Jones, Hacksung Kim, Qing Ma, Peter C. Stair, George C. Schatz, Michael J. Bedzyk, Tobin J. Marks

*Departments of Chemistry, Material Science & Engineering, and Center for Catalysis and Surface Science, Northwestern University, Evanston, IL*

- 2. Capturing the Coverage Dependence of Aromatics via Mean Field Models**  
Naseeha Cardwell,<sup>1</sup> Alyssa Hensley,<sup>1,2</sup> Jean-Sabin McEwen<sup>1</sup>  
<sup>1</sup>*The Gene and Linda Voiland School of Chemical Engineering and Bionginering, Washington State University*  
<sup>2</sup>*Department of Chemical Engineering & Materials Science, Stevens Institute of Technology, Hoboken, NJ*
  
- 3. Modulating Catalytic Properties of Targeted Metal Cationic Centers in Nonstoichiometric Mixed Metal Oxides for Electrochemical Oxygen Reduction**  
Samji Samira, John Carl A. Camayang, Xiang-Kui Gu, Eranda Nikolla  
*Department of Chemical Engineering and Materials Science, Wayne State University, Detroit, MI*
  
- 4. Sub-Monolayer is Enough: Modifying Catalyst Surfaces with Oxide Overcoats**  
Justin Notestein,<sup>1,2</sup> Alexander Ardagh,<sup>1,2</sup> Cassandra George,<sup>1,3</sup> Xin Tang,<sup>1,3</sup> Peter Stair<sup>1,3</sup>  
<sup>1</sup>*Center for Catalysis and Surface Science*  
<sup>2</sup>*Department of Chemical & Biological Engineering*  
<sup>3</sup>*Department of Chemistry*  
*Northwestern University, Evanston, IL*
  
- 5. Catalytic Conversions Involving the Addition of H–X Bonds (X = Si, B) to Carbon Dioxide**  
Daniel G. Shlian, Erika Amemiya, Serge Ruccolo, Gerard Parkin  
*Department of Chemistry, Columbia University, New York, NY*
  
- 6. Alkali-promoted Selective CO<sub>2</sub> Reduction to Alcohols from First Principles**  
Wenjie Liao,<sup>1</sup> Xuelong Wang,<sup>2</sup> Sanjaya Senanayake,<sup>2</sup> Jose A. Rodriguez,<sup>2</sup> Ping Liu<sup>2</sup>  
<sup>1</sup>*Chemistry Department, Stony Brook University, Stony Brook, NY*  
<sup>2</sup>*Chemistry Division, Brookhaven National Laboratory, Upton, NY*
  
- 7. Identifying Support Effects In CO Oxidation**  
Zachary R. Mansley,<sup>1</sup> Ryan J. Paull,<sup>1</sup> Louisa Savereide,<sup>2</sup> Emily P Greenstein,<sup>1</sup> Scott Tatro,<sup>2</sup> Abha A Gosavi,<sup>2</sup> Emily Cheng,<sup>2</sup> JianguoWen,<sup>3</sup> Kenneth R. Poepelmeier,<sup>4</sup> Justin M Notestein,<sup>2</sup> Laurence D. Marks<sup>1</sup>  
<sup>1</sup>*Department of Materials Science and Engineering, Northwestern University, Evanston, IL*  
<sup>2</sup>*Department of Chemical Engineering, Northwestern University, Evanston, IL*  
<sup>3</sup>*Center for Nanoscale Materials, Argonne National Laboratory, Lemont, IL*  
<sup>4</sup>*Department of Chemistry, Northwestern University, Evanston, IL*

- 8. Characterization of, and Hydrocarbon Functionalization with Lattice-Confined Reactive Intermediates**  
Anuvab Das, Aishanne Sur, Gerard P. Van Trieste III, Chen-Hao Wang, David C. Powers  
*Texas A&M University, College Station, TX*
- 9. Optimizing the Surface Distribution of Acid Sites for Cooperative Catalysis in Condensation Reactions Promoted by Water**  
Gengnan Li,<sup>1</sup> Bin Wang,<sup>1</sup> Takeshi Kobayashi,<sup>2</sup> Marek Pruski,<sup>2</sup> Daniel E. Resasco<sup>1</sup>  
<sup>1</sup>*Center for Interfacial Reaction Engineering (CIRE), School of Chemical, Biological and Materials Engineering, University of Oklahoma, Norman, OK*  
<sup>2</sup>*Ames Laboratory, U.S. Department of Energy, Ames, IA*
- 10. In-situ Studies for the Conversion of C-O Bonds on Complex Metal-Oxide Interfaces**  
Jose A. Rodriguez, Ping Liu, Sanjaya Senanayake, Michael G. White  
*Chemistry Department, Brookhaven National Laboratory, Upton, NY*
- 11. Catalytic Upgrading of Ethanol as a Renewable Feedstock**  
Nathaniel K. Szymczak, Corey R. J. Stephenson, Zhongyuan Li, Alex M. Davies, Emily L. Nolan  
*Department of Chemistry, University of Michigan, Ann Arbor, MI*
- 12. Size-Selected Metal Oxide Clusters as Model Inverse Catalysts**  
Y. Ma,<sup>1</sup> J. Wang,<sup>1</sup> Michael G. White<sup>1,2</sup>  
<sup>1</sup>*Department of Chemistry, Stony Brook University, Stony Brook, NY*  
<sup>2</sup>*Chemistry Division, Brookhaven National Laboratory, Upton, NY*
- 13. Molecular Transformations and Catalytic Reactions on Structurally Well-defined Catalysts**  
Zili Wu, Miaofang Chi, Sheng Dai, De-en Jiang, Stephane Irle, Felipe Polo Garzon, Aditya Savara, Zhenzhen Yang  
*Chemical Sciences Division, Oak Ridge National Laboratory, Oak Ridge, TN*
- 14. Tuning Catalytic Active Sites by Surface Modification of Supported  $\text{ReO}_4/(\text{SiO}_2\text{-Al}_2\text{O}_3)$  Catalysts for Olefin Metathesis**  
Bin Zhang,<sup>1</sup> Soe Lwin,<sup>1</sup> Shuting Xiang,<sup>2</sup> Anatoly Frenkel,<sup>2</sup> Israel E. Wachs<sup>1</sup>  
<sup>1</sup>*Operando Molecular Spectroscopy and Catalysis Laboratory, Department of Chemical & Biomolecular Engineering, Lehigh University, Bethlehem, PA*  
<sup>2</sup>*Department of Materials Science and Chemical Engineering, Stony Brook University, Stony Brook, NY*

**15. Studies of Heterogeneous Catalysis for Strategic Formation of C-C, C-O and C-N Bonds**

Liang Qi, Branden Leonhardt, Alexis T. Bell

*Chemical Sciences Division, Lawrence Berkeley National Laboratory, Berkeley, CA*

**16. “Intelligent” Ni Catalysts Based on LaMnO<sub>3</sub> Films Prepared by Atomic Layer Deposition**

Ohhun Kwon, John M. Vohs, Raymond J. Gorte

*Department of Chemical & Biomolecular Engineering, University of Pennsylvania, Philadelphia, PA*

## TABLE OF CONTENTS

<b>TITLE PAGE</b> .....	i
<b>FOREWORD</b> .....	ii
<b>AGENDA</b> .....	iii
<b>POSTER SESSIONS</b> .....	viii
<b>TABLE OF CONTENTS</b> .....	xiv
<b>ABSTRACTS</b> .....	1
<b><u>Plenary Presentations Abstracts</u></b> .....	2
<b>Operando Insight into Electrocatalytic and Thermal Conversion of CO<sub>2</sub></b> Beatriz Roldan Cuenya, <i>Fritz-Haber-Institute of the Max Planck Society, Berlin</i> .....	3
<b>Decarbonizing Low-Cost Fossil Resources by Reactive Separation on High Temperature Liquids</b> Eric McFarland, <i>University of California, Santa Barbara</i> .....	4
<b>Closing the Loop on Plastics Recycling</b> Jeffery C. Bricker and Andrea Bozzano, <i>Honeywell- UOP R&amp;D</i> .....	5
<b><u>PI Oral Presentation Abstracts</u></b> .....	6
<b>Earth-Abundant Rare Earth Catalysts with Reactive co-ligands for Sustainable Bifunctional Catalysis</b> Polly L. Arnold, <i>Lawrence Berkeley National Laboratory</i> .....	7
<b>Does Selectivity of Molecular Catalysts Change with Time? Polymerization Imaged via Single-Molecule Spectroscopy</b> Suzanne A. Blum, <i>University of California, Irvine</i> .....	8
<b>Activating CO<sub>2</sub> by H<sub>2</sub> and Light Alkanes</b> Jingguang Chen, <i>Columbia University and Brookhaven National laboratory</i> .....	11
<b>Solvent-Mediated Interactions and Catalysis within Confined Liquids</b> David W. Flaherty, <i>University of Illinois, Urbana-Champaign</i> .....	18

<b>Multinuclear Copper Active Site Requirements in Cu-Zeolites for Partial Methane Oxidation</b>	
Rajamani Gounder, <i>Purdue University</i> .....	24
<b>Amines from Hydrocarbons and N<sub>2</sub>: Combining C-H Activation and N–N Activation</b>	
Patrick L. Holland, <i>Yale University</i> .....	30
<b>Catalyst Design Strategies for Multifunctional Metal-Promoted Zeolites in Methane Dehydroaromatization</b>	
Sheima J. Khatib, <i>Texas Tech University</i> .....	35
<b>Characterizing Supported Organovanadium Catalysts with Computational K-Edge XANES</b>	
Cong Liu, <i>Argonne National Laboratory</i> .....	42
<b>Controlling Catalyst Selectivity with Organic Monolayers on Metal Oxides</b>	
J. Will Medlin, <i>University of Colorado Boulder</i> .....	43
<b>Recent Advancements in the Design of Zeolite Catalysts with Reduced Diffusion Limitations</b>	
Jeffrey D. Rimer, <i>University of Houston</i> .....	47
<b>Understanding The Contribution of The Protein Scaffold to Catalysis by Creating Artificial Enzymes</b>	
Wendy J. Shaw, <i>Pacific Northwest National Laboratory</i> .....	52
<b>Catalytic rates with active site specificity</b>	
Frank Abild-Pedersen, <i>SLAC National Accelerator Laboratory, SUNCAT Center for Interface Science and Catalysis</i> .....	53
<b>Interplay between Electroadsorption and Electrocatalysis on Thin-Film Oxide Surfaces</b>	
Jin Suntivich, <i>Cornell University</i> .....	68
<b>Polyketoester Synthesis via Dual Alkene Hydroesterification and Carbonylation Catalysis</b>	
Ian A. Tonks, <i>University of Minnesota – Twin Cities</i> .....	75
<b><u>Early Career Awardees Presentation Abstracts</u></b> .....	79
<b>Building from Discrete Molecular Catalysts to Multidimensional Architectures: The Effects of Charge Delocalization and Electronic Coupling on Electrocatalysis</b>	
Charles C. L. McCrory, <i>University of Michigan</i> .....	80

<b>Towards a Multiscale Modeling Approach to the Electrochemical Interface with DFT Accuracy</b>	
Craig Plaisance, <i>Louisiana State University</i> .....	81
<b>Electrocatalytic Grafting of Polyvinylchloride</b>	
Christo S. Sevov, <i>Ohio State University</i> .....	82
<b>Designing Non-Covalent Interactions at the Electrode-Electrolyte Interface for Nitrogen Activation</b>	
V. Sara Thoi, <i>Johns Hopkins University</i> .....	83
<b><u>PI Abstracts</u></b> .....	84
<b>The Consortium for Operando and Advanced Catalyst Characterization via Electronic Spectroscopy and Structure (Co-ACCESS) at SSRL</b>	
Simon R. Bare, <i>SLAC National Accelerator Laboratory</i> .....	85
<b>The Rational Design of Improved Iron Catalysts for CO<sub>2</sub> Hydrogenation and Related Processes</b>	
Nilay Hazari, <i>Yale University</i> and Wesley H. Bernskoetter, <i>University of Missouri</i> .....	96
<b>Carbenes as Powerful Transition-Metal Surrogates</b>	
Guy Bertrand, <i>University of California, San Diego</i> .....	102
<b>Electrochemical Hydrogenation and Hydrogenolysis of Furfural over Copper Catalyst in Acid Media</b>	
Elizabeth J. Biddinger, <i>The City College of New York, CUNY</i> .....	108
<b>Engineering Host-Guest Catalysts for the Tandem Catalytic Hydrogenation of CO<sub>2</sub> to Methanol</b>	
Jeffery A Byers, <i>University of South Carolina</i> .....	113
<b>Supported Metal Nanoparticle Catalysts and Electrocatalysts: Correlating Structure with Function through Energetics</b>	
Charles T. Campbell, <i>University of Washington</i> .....	118
<b>Chemical Imaging of Single-Particle Photoelectrocatalysis: Inter-facet junction effects on particulate photoelectrodes</b>	
Peng Chen, <i>Cornell University</i> .....	124

<b>Exploring and Exploiting the Oxidation State Void between Single Atom Catalysts and Single Atom Alloys - a Combined Model and Real Catalyst Approach</b> Phillip Christopher, <i>University of California, Santa Barbara</i> and Charles H. Sykes, <i>Tufts University</i> .....	130
<b>Electrocatalytic Oxidation of Carbon Monoxide on Metal Nanoparticles in the Presence and Absence of Interactions with Metal-Oxide Supports</b> Richard M. Crooks, <i>The University of Texas at Austin</i> .....	135
<b>Sub Nanometer Sized Clusters for Heterogeneous Catalysis</b> Abhaya Datye, <i>University of New Mexico</i> and Yong Wang, <i>Washington State University</i> .....	141
<b>Role of the Reaction Environment on the Catalytic Activation of Cellulose</b> Paul Dauenhauer, <i>University of Minnesota</i> .....	150
<b>Electronic Cooperativity in Supported Single- and Multinuclear-Sites for Catalytic C-C and C-H Bonds Functionalization</b> Massimiliano Delferro, <i>Argonne National Laboratory</i> .....	157
<b>Modeling and Design of Main-Group Metal Catalyzed Alkane C-H Functionalization Reactions</b> Daniel H. Ess, <i>Brigham Young University</i> .....	169
<b>Selenium Oxyanion Reduction</b> Alison R. Fout, <i>University of Illinois at Urbana-Champaign</i> .....	174
<b>Site Selective Deoxygenation of Cellulosic Biorenewables with Boron Catalysts</b> Michel R. Gagné, <i>University of North Carolina at Chapel Hill</i> .....	176
<b>Supported Molecular Metal Catalysts: Single-Sites to Pair-Sites to Metal Clusters</b> Bruce C. Gates, <i>University of California, Davis</i> .....	180
<b>Activation of Alkyl C-H Bonds and Dehydrogenation of Alkanes Achieved through Proton-Coupled Electron Transfer. High- and Low-Oxidation State Iridium</b> Alan S. Goldman, <i>Rutgers – The State University of New Jersey</i> .....	186
<b>Support Effect Studied on Thin-Film Perovskites.</b> Raymond J. Gorte, <i>University of Pennsylvania</i> .....	192
<b>Electrocatalytic activity of Fe(IV) model compounds <math>\text{La}_{1-x}\text{Sr}_x\text{FeO}_{3-\delta}</math> for oxygen evolution reaction in alkaline solution</b> Lauren F. Greenlee, <i>University of Arkansas</i> .....	195

<b>Development of Transition Metal Catalysts for the Functionalization of Carbon-Hydrogen Bonds: Fundamental Studies of Catalytic Hydroarylation of Olefins</b> T. Brent Gunnoe, <i>University of Virginia</i> .....	201
<b>Catalysis Program at Lawrence Berkeley National Laboratory: Harnessing Complexity for Catalytic Efficiency</b> John F. Hartwig, <i>Lawrence Berkeley National Laboratory</i> .....	207
<b>Surface and Gas Phase Chemistry of Boron-Catalyzed Oxidative Dehydrogenations</b> Ive Hermans, <i>University of Wisconsin-Madison</i> .....	235
<b>Theoretical Investigation of Heterogeneous Catalysis at the Solid-Liquid Interface for the Conversion of Lignocellulosic Biomass Model Molecules</b> Andreas Heyden, <i>University of South Carolina</i> .....	240
<b>Insights into the Behavior of Classical Catalysts in Non-Classical Environments: Rh(I) and Pt(II) Single-Site Catalysts in Phosphine MOFs as Solid-State Ligands</b> Simon M. Humphrey, <i>University of Texas at Austin</i> .....	244
<b>Data-driven discovery of intermetallic catalysts with controlled active site nuclearity</b> Michael J. Janik, <i>Pennsylvania State University</i> .....	247
<b>Spectroscopic Signatures and Shape-Selective Synthesis of Cyclopentenyl Cations</b> Friederike C. Jentoft, <i>University of Massachusetts Amherst</i> .....	251
<b>Cascade Catalysis in Tunable Multicompartment Nanoreactors</b> Christopher W. Jones, Seung Soon Jang, <i>Georgia Institute of Technology</i> and Marcus Weck, <i>New York University</i> .....	257
<b>Catalytic Activation of C-H and O-H Bonds for the Upgrading of Alcohols</b> William D. Jones, <i>University of Rochester</i> .....	264
<b>Investigating Novel Approaches for Synthesizing Supported Molecular Catalysts</b> Alexander Katz, <i>University of California, Berkeley</i> .....	269
<b>Transdisciplinary Approaches to Realize Novel Catalytic Pathways to Energy Carriers</b> Johannes Lercher, <i>Pacific Northwest National Laboratory</i> .....	276
<b>Atomic-scale Design of Metal and Alloy Catalysts: A Combined Theoretical and Experimental Approach</b> Manos Mavrikakis, <i>University of Wisconsin-Madison</i> .....	305

<b>Modulating Catalytic Properties of Metal Cationic Centers in Non-Stoichiometric Mixed Metal Oxides for Electrochemical Oxygen Reduction</b>	
Eranda Nikolla, <i>Wayne State University</i> .....	315
<b>Institute for Catalysis in Energy Processes (ICEP)</b>	
Justin M. Notestein, <i>Northwestern University</i> .....	321
<b>Fundamental studies of the multifunctional electrocatalysis on heteroatom-doped carbon (CN<sub>x</sub>) catalysts</b>	
Umit S. Ozkan, <i>The Ohio State University</i> .....	337
<b>Crystalline Matrix Isolation of Catalysts and Catalyst Intermediates</b>	
David C. Powers, <i>Texas A&amp;M University</i> .....	344
<b>Catalysis for Advanced Fuel Synthesis: Conversion of C-O and C-H bonds</b>	
José A. Rodriguez, <i>Brookhaven National Laboratory</i> .....	350
<b>Catalysis Beyond the Active Site: Identification and quantification of distinct active sites in Hf-Beta zeolites for transfer hydrogenation catalysis</b>	
Yuriy Román-Leshkov, <i>Massachusetts Institute of Technology</i> .....	366
<b>Uniform catalytic environments at the interface: characterization of sites and distributions, catalytic activity, and reaction mechanisms</b>	
Aaron D. Sadow, <i>Ames Laboratory</i> .....	373
<b>Plasma-Catalyst Modeling for Materials Selection</b>	
William F. Schneider, <i>University of Notre Dame</i> .....	385
<b>Oxidation of O-H and N-H Bonds with Non-Precious-Metal-Catalysts</b>	
Shannon S. Stahl, <i>University of Wisconsin-Madison</i> .....	388
<b>Catalytic Selective Oxidations with Porous Transition Metal Oxides</b>	
Steven L. Suib, <i>University of Connecticut</i> .....	394
<b>Tandem Upgrading and Alkylations Using Ethanol as a Building Block</b>	
Nathaniel K. Szymczak and Corey R. J. Stephenson, <i>University of Michigan</i> .....	410
<b>Ligand and Surface Cooperativity in the Stabilization of Metal-Ligand Single-site Catalysts at Surfaces</b>	
Steven L. Tait, <i>Indiana University</i> .....	413
<b>M-edge XANES Spectroscopy of Transition Metal Catalysts</b>	
Josh Vura-Weis, <i>University of Illinois at Urbana-Champaign</i> .....	419

<b>Uncovering Redox Non-Innocent Hydrogen-Bonding in Cu(I)-Diazene Complexes</b> Timothy H. Warren, <i>Georgetown University</i> .....	424
<b>Steady state oxidation of CH<sub>4</sub> on an IrO<sub>2</sub>(110) film investigated using near-ambient pressure x-ray photoelectron spectroscopy</b> Jason F. Weaver, <i>University of Florida</i> and Aravind Asthagiri, <i>Ohio State University</i> ...	429
<b>Atomically Precise Metal and Metal Oxide Clusters as Model Catalysts</b> Michael G. White, <i>Stony Brook University</i> and <i>Brookhaven National Laboratory</i> .....	434
<b>Fundamentals of Catalysis and Chemical Transformations</b> Zili Wu, <i>Oak Ridge National Laboratory</i> .....	435
<b>LIST OF PARTICIPANTS</b> .....	455

# **Abstracts**

# **Plenary Presentations**

**Operando Insight into Electrocatalytic and Thermal Conversion of CO<sub>2</sub>**

Beatriz Roldan Cuenya

Department of Interface Science, Fritz-Haber-Institute of the Max Planck Society, Berlin

**Presentation Abstract**

Tailoring the chemical reactivity of nanomaterials at the atomic level is one of the most important challenges in catalysis research. In order to achieve this elusive goal, we must first obtain a fundamental understanding of the structural and chemical properties of these complex systems. In addition, the dynamic nature of the nanoparticle (NP) catalysts and their response to the environment must be taken into consideration. To address the complexity of real-world catalysts, a synergistic approach taking advantage of a variety of cutting-edge experimental methods (EC-AFM, EC-TEM, TPD, NAP-XPS, XAS, Raman Spectr., MS/GC) has been undertaken.

This talk will provide new insights into the thermal hydrogenation and electrocatalytic reduction of CO<sub>2</sub>. Important aspects that will be discussed are: (i) the design of size- and shape-controlled catalytically active NPs (Cu, Cu-Zn, Cu-Ag) (ii) the role of the support (C, SiO<sub>2</sub>, ZnO, Al<sub>2</sub>O<sub>3</sub>, ZnOAl) on the catalytic performance and (iii) the correlation between the dynamic structure/chemical state of nanocatalysts and their reactivity and selectivity under realistic *operando* reaction conditions, i.e., at high pressure or under potential control. The results are expected to open up new routes for the reutilization of CO<sub>2</sub> through its direct conversion into valuable chemicals and fuels such as ethylene, methanol and ethanol.

**Decarbonizing Low-Cost Fossil Resources by Reactive Separation  
on High Temperature Liquids**

Eric McFarland

Department of Chemical Engineering, University of California, Santa Barbara

**Presentation Abstract**

The relatively short-term challenge of reducing atmospheric carbon dioxide emissions is among the most important problems in applied science and engineering. A rapid transition from a world powered primarily by low-cost fossil fuel combustion to more sustainable low emissions alternatives will only occur if those alternatives are widely available at comparable costs. In addition to electricity, hydrogen and other hydrogen containing fuels (e.g.  $\text{NH}_3$ ) will likely be important in future sustainable energy economies. Hydrogen is produced today, for profit, and sold under contracts for approximately  $\$1/\text{kg} = \$8.3/\text{GJ} = \$0.03/\text{kWh}$  from abundant methane by reforming and complete oxidation of the carbon from C(-4) to C(+4) producing  $\sim 7$  tons  $\text{CO}_2/\text{ton H}_2$ .

We are interested in partial oxidation of methane and other fossil resources in the absence of oxygen to produce solid carbon C(0) and valuable hydrogen containing molecules. These  $\text{CO}_2$ -free processes leave behind approximately half of the chemical oxidation potential stored by photosynthesis in the reduced carbon, however, the solid product can be stored indefinitely at low-cost. If society is willing to pay for  $\text{CO}_2$  emissions reductions, methane partial oxidation is the lowest cost source of hydrogen fuel we have.

A chemical process will be described whereby methane is decomposed to hydrogen and solid carbon using high temperature molten salts and molten metals. Solid carbon can be readily separated from several liquids resulting in process intensification and cost reduction through reactive separation in the melt-based reactor. Methane pyrolysis is equilibrium limited and thermodynamics restrict high pressure processes to very high temperatures for acceptable conversion. Heterogeneous liquid-phase catalysts increase the rate of approaching equilibrium and we have observed turnover frequencies of methane on liquid surfaces to strongly depend on the melt compositions. The relative reactivities of different melts have been investigated both experimentally and by density functional theory and *ab initio* molecular dynamics simulations. The liquid surfaces are found to facilitate both complete dehydrogenation, and the production of methyl radicals to increase the gas phase methane decomposition. There are many potential pathways for partial oxidation without oxygen for fossil resource conversion. Practical deployment requires solution of several difficult problems which will be highlighted.

**Jeffery C. Bricker and Andrea Bozzano**

**Closing the Loop on Plastics Recycling**

Jeffery C. Bricker and Andrea Bozzano  
Honeywell- UOP R&D

**Presentation Abstract**

While plastics have significant societal benefits – including lower GHG’s; the call for sustainability of plastics is accelerating. There is a significant opportunity to improve circularity through depolymerization, pyrolysis, catalytic or thermal, but viable solutions will have to meet Life Cycle Analysis, GHG and other sustainability measures and have a reliable feedstock supply at scale to achieve the desired impact. We will review the challenges facing plastic circularity, solutions, and criteria for selecting technology options. We will present Honeywell-UOP’s fully developed technology offering which meets all the sustainability criteria and has favorable economics.

# **PI Oral Presentations**

**Polly L. Arnold**

**Earth-Abundant Rare Earth Catalysts with Reactive co-ligands for Sustainable Bifunctional Catalysis**

Amy Kynman, Paul Ewing, Addison Desnoyer, Miquel Salmeron, Christopher J. Chang,  
F. Dean Toste, Laurent Maron, and Polly L. Arnold

Department of Chemistry, University of California, Berkeley, and Chemical Sciences  
Division, Lawrence Berkeley National Laboratory, Berkeley CA 94720, US

**Presentation Abstract**

Many of the rare earths (RE, group 3 and the lanthanides) are more abundant than nickel, and their halides are less toxic than those of iron. Their complexes can also exhibit strong and tunable Lewis acidity, highly ligand-dependent redox potentials, and the capacity for rapid ligand exchange reactions. Because the subtleties of structure and bonding in compounds of the rare earths are still poorly understood, their development in controlled homogeneous catalysis has trailed behind their d-block neighbors, but what we learn from studying their reactivity feeds back into a better fundamental understanding of these technology-critical elements.

We will show how organometallic chemistry can add additional functionality to the natural Lewis acidity and halophilicity of rare earth catalysts. The incorporation of hemilabile carbene donors affords catalytic CO<sub>2</sub> and related heteroallene conversions, exceptionally rapid catalytic syntheses of unusual, cyclic polylactides, and light-driven selective catalytic conversions of unactivated carbon-halogen bonds.

**Does Selectivity of Molecular Catalysts Change with Time?  
Polymerization Imaged via Single-Molecule Spectroscopy**

University of California, Irvine

**Presentation Abstract**

The chemoselectivity of molecular catalysts underpins much of modern synthetic organic chemistry. Yet little is known about the selectivity of individual catalysts because this single-catalyst-level behavior is hidden by the bulk catalytic behavior. Here, for the first time, the selectivity of individual molecular catalysts for two different reactions is imaged in real time at the single-catalyst level. This imaging is achieved through fluorescence microscopy paired with spectral probes that produce a “snapshot” of the instantaneous chemoselectivity of a single catalyst for either a single-chain-elongation or a single-chain-termination event during ruthenium-catalyzed polymerization. Superresolution imaging of multiple selectivity events, each at a different single-molecular ruthenium catalyst, indicates that catalyst selectivity may be unexpectedly spatial- and time-variable.

**DE-SC0016467: Revealing Hidden Kinetics of Molecular Polymerization Catalysts via Single-Turnover/-Particle Fluorescence Microscopy**

**Postdoc(s):** Dr. David J. Dibble, Dr. Nozomi Saito

**Student(s):** Antonio Garcia IV, Shannon J. Saluga, Pía A. López

**RECENT PROGRESS**

Statistically significant variations in chemoselectivity with time were observed (Figure 1a) in 30% of polymer aggregate particles as determined using two statistical tests (Figure 1b): 1) For statistical evaluation of changing selectivity vs. time, data was normalized and evaluated through a nonparametric, Kolmogorov-Smirnov test. This test established that the green and orange rates changed relative to each other ( $p < 0.05$ ) in a subset of particles. 2) A chi-square goodness-of-fit test was used to compare the experimental frequency of single-turnover events to a theoretical Poisson distribution. In a subset of particles, however, behavior of at least one of the reaction types (elongation or termination) did not fit a Poisson distribution ( $p < 0.05$ ). For example, the chain-elongation probability does not fit a Poisson distribution and instead is changing with time ( $p < 0.001$ ); this changing probability underpins the change in chemoselectivity with time. This behavior characterizes the range of time-variable reactivity/selectivity behaviors across the samples, which is typically obscured by ensemble measurements and is uniquely visible to subensemble experiments.

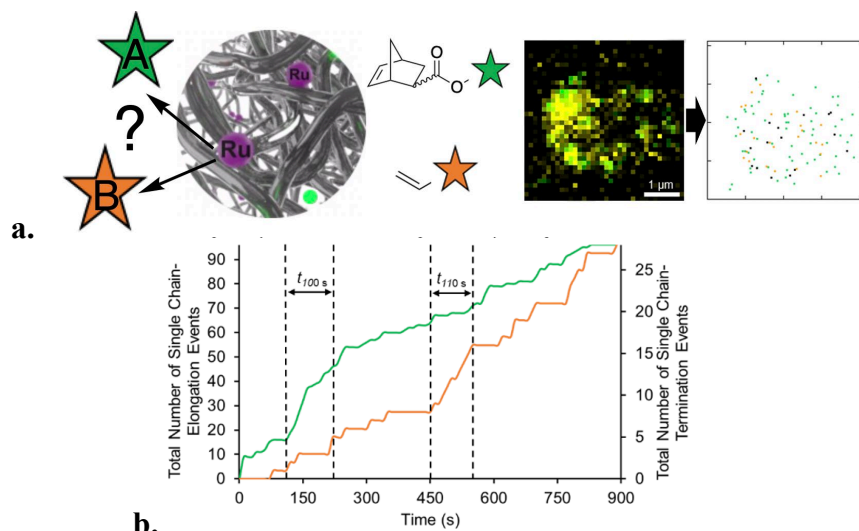


**Figure 1. a.** Overall schematic: ruthenium ring-opening metathesis polymerization catalysts chose between two monomers. Different color imaging agents enable determination of which monomer was selected. Composit images are deconvoluted using superresolution imaging to pinpoint individual molecular catalytic turnovers in space and time. **b.** Example particle exhibiting a statistically significant time variability.

**Impact:** These experiments provide spatiotemporally resolved snapshots of individual molecular catalyst selectivity at the single-turnover level, revealing catalytic behavior that is obscured by traditional ensemble measurements. These observations are consistent with dynamic catalyst microenvironments that affect chain-elongation and chain-termination reactions unequally. These unequal effects may underpin macroscopic properties of bulk polymers, for example, by broadening molecular weight distributions. The bulk characteristics of essentially all molecular catalytic reactions arise from the sum of individual choices at the single-catalyst level. The presence of space- and time-variable selectivity by individual molecular catalysts in other systems is intriguingly unknown, and the plausibility of its wider presence is bolstered by such behavior in the current system.

### Publications Acknowledging this Grant in 2018-2021

*Please classify your publications into two categories according to the source of support for the work published:*

- (I) Garcia IV, A.; Saluga, S. J.; Dibble, D. J.; López, P. A.; Saito, N.; Blum, S. A. *Angew. Chem. Int. Ed.* **2021**, *60*, 1550–1555. doi.org/10.1002/anie.202010101

### Leadership Activities

- 1) Organized the conference Probing Chemical Reactions by Single-Molecule Spectroscopy 2021, in the direct area of this DOE grant. I organized the second biannual conference in this area on June 8, 2021, held remotely due to Covid travel restrictions. My coorganizer was Prof. Randall Goldsmith at UW-Madison. The conference included 19 talks from invited principal investigators in 7 countries. Attendance was 188 participants, including other faculty, graduate students, and postdoctoral scholars.

- 2) Peer reviewer for diverse journals including *Journal of the American Chemical Society*, *Angewandte Chemie*, *Organometallics*, *Organic Letters*, *Science Advances*.
- 3) Director, UCI Field Studies in Chemistry, undergraduate student industrial internship program.
- 4) Curriculum design and teaching of graduate and undergraduate classes including Graduate Mechanisms and Undergraduate Organic Chemistry.
- 5) Teacher training program for UCI graduate students.

**Activating CO<sub>2</sub> by H<sub>2</sub> and Light Alkanes**

Jingguang Chen  
Department of Chemical Engineering, Columbia University  
Joint Appointment: Chemistry Division, Brookhaven National laboratory

**Presentation Abstract**

Converting CO<sub>2</sub> to value-added chemicals and fuels is one of the most practical routes for reducing CO<sub>2</sub> emissions while fossil fuels continue to dominate the energy sector. In this talk we will present several routes in catalytic CO<sub>2</sub> conversion: (1) CO<sub>2</sub> hydrogenation by thermocatalysis, (2) CO<sub>2</sub> reduction by electrocatalysis, and (3) simultaneous upgrading of CO<sub>2</sub> and shale gas. We will use these examples to highlight the importance of combining kinetic studies, *in situ* characterization and density functional theory calculations for the mechanistic understanding of CO<sub>2</sub> conversion. We will use the hydrogenation of CO<sub>2</sub> to methanol as an example to illustrate the challenges in achieving a net-reduction of CO<sub>2</sub> by performing mass and energy balance analysis. We will also demonstrate proof-of-principle results of several promising catalytic reactions in simultaneously converting CO<sub>2</sub> and light alkanes to syngas, olefins, aromatics and oxygenates.

**Grant number: DE-FG02-13ER16381**

**Grant Title: Metal Carbides and Bimetallic Alloys as Low-cost Electrocatalysts**

**PI:** Jingguang Chen  
**Postdoc(s):** Ji Hoon Lee (2 months)  
**Student(s):** A. Neal Biswas (12 months);  
Lea R. Winter (2 months);  
**Self-funded Visiting Students:** Qiaowan Chang (UC San Diego)  
Yumeng Liu (Peking Univ., China)  
Yao Nian (Tianjin Univ., China)  
Yan Wang (Tianjin Univ., China)

**Affiliations(s):** Department of Chemical Engineering, Columbia University  
Joint Appointment: Chemistry Division, Brookhaven National laboratory

**RECENT PROGRESS**

**1. Motivation for CO<sub>2</sub> reduction to synthesis gas**

In the past year we have performed extensive studies in developing syngas-producing electrocatalysts. We identify palladium (Pd) as a unique platform for this

application, due to its ability to transform to palladium hydride (PdH). Then we tune selectivity and optimize activity by exploring the PdH structure-function relationship, the interaction of PdH alloyed with a non-precious metal, and the reduction of Pd loading by supporting PdH on transition metal carbides. In each case we utilize in-situ synchrotron techniques to understand the Pd phase and oxidation state under reaction conditions. We also describe the observed activity and selectivity trends with density functional theory (DFT) calculations to establish descriptors for syngas production activity and selectivity on these electrocatalysts.

## **2. Tuning syngas production with palladium hydride electrocatalysts**

### **2.1 Pd/C electrocatalysts**

Palladium is a unique electroreduction catalyst, because it readily absorbs hydrogen to form palladium hydride (PdH) in aqueous electrolyte at potentials commonly used for CO<sub>2</sub> reduction. Thus, unlike most metals, Pd changes phase during the CO<sub>2</sub> reduction reaction, which results in activity trends not typical of other metallic catalysts. For example, Pd and Pt are both known to be poisoned by adsorbed CO. If the active sites during electrochemical CO<sub>2</sub> reduction consist of metallic Pd, it would be expected that CO binds too strongly to desorb, like on the Pt surface. But Pd produces a mixture of H<sub>2</sub> and CO under CO<sub>2</sub> reduction conditions, while Pt produces only hydrogen. This indicates that PdH electrocatalytic performance may depart from the expected metallic Pd performance.

We have observed the phase change from Pd to PdH using in-situ synchrotron techniques – specifically, X-ray absorption spectroscopy (XAS) and X-ray diffraction (XRD) under reaction conditions. The XRD pattern also provided direct evidence that the PdH phase under reaction conditions was  $\beta$ -PdH. The XAS and XRD indicated complete phase transformation to PdH occurred at a potential -0.5 V vs reversible hydrogen electrode (RHE), and the EXAFS showed that the phase change was reversible upon anodic potential sweeps. We also observed an increase in the peak A intensity, relative to peak B in the XANES spectra, which resulted from a decrease in the density of states above the Fermi level ( $E_F$ ) upon hydride formation. These in-situ results were characteristic of a phase transition of Pd to PdH and were used in our follow-up studies to identify the PdH phase in other Pd-based electrocatalysts.

### **2.2 Pd-based bimetallic catalysts**

Bimetallic electrocatalysts have been widely studied for CO<sub>2</sub> reduction because of their ability to modify performance beyond what would be expected from a simple physical mixture of the corresponding monometallic catalysts. Notably, the electronic interactions of two metals and the possibility of multiple functionalities at interfacial sites (e.g. preferentially adsorbing different species on different adjacent metals) can potentially result in a breaking of the linear scaling relationship that hinders utility of monometallics for CO<sub>2</sub> reduction reactions. Combining secondary metals with the versatile PdH electrocatalyst could, therefore, increase activity at lower potentials or tailor the product selection to specific applications. We explored the electrochemical syngas production performance of several different metals combined with Pd.

Pd was co-precipitated with Ag, Cu, Ni, or Co to create a PdM bimetallic with a Pd:M ratio of 8:2. XRD showed only a single phase, suggesting solid solution formation, where the secondary metal was incorporated into the Pd lattice. Each catalyst was subject

to electrochemical reduction to form a (PdM)H bimetallic phase. In-situ XAS and XRD analysis revealed a change in the oxidation state and a Pd lattice expansion, characteristic of PdH phase formation, without phase separation into PdH and M.

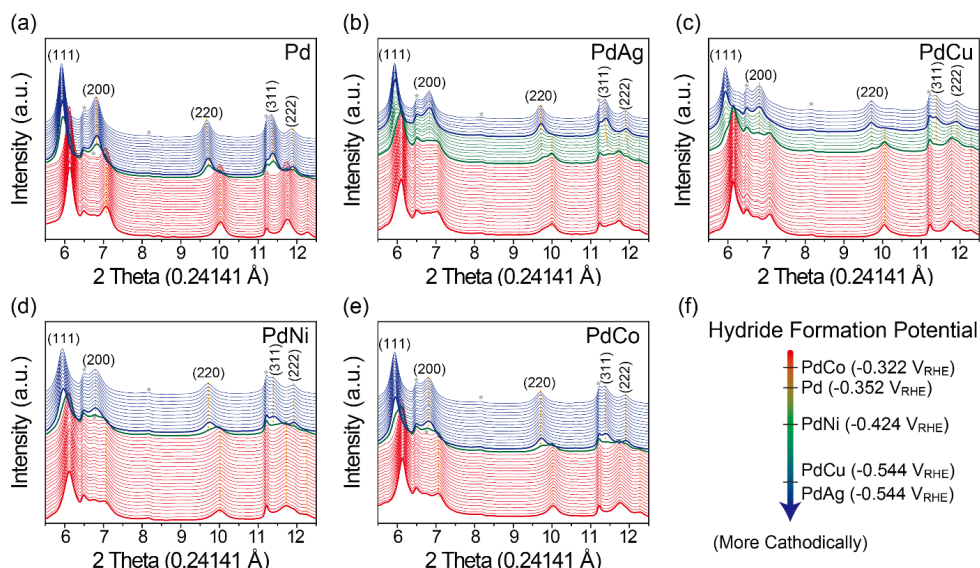


**Figure 1.** In-situ XRD characterization of Pd bimetallics in 0.5M NaHCO<sub>3</sub>. XRD patterns for (a) Pd, (b) PdAg, (c) PdCu, (d) PdNi, and (e) PdCo at potentials from 0.2 (bottom) to -0.7 (top) V vs RHE at 0.024 V intervals. Red patterns indicate Pd phase. Blue patterns indicate PdH phase. Green patterns indicate a phase transition region. (f) The schematic of hydride formation potential of the Pd-based electrocatalysts.

The electrochemical CO<sub>2</sub> reduction results indicated that the CO FE for each (PdM)H electrocatalyst at -0.9 V vs RHE followed a similar trend as the hydride formation potentials, PdCo < Pd < PdNi < PdCu < PdAg. The same trend was observed for CO:H<sub>2</sub> ratios and CO partial current density (with the exception of PdCo, which had a higher  $j_{CO}$  than PdNi). The CO partial current densities on PdNi and PdCu were especially promising, because they exceeded the activity of Pd by incorporating less expensive metals.

DFT calculations confirmed that hydride formation energy for the bimetallics followed the same trend observed in the in-situ experiments, i.e. bimetallics that required more cathodic potentials to achieve hydride phase change had higher hydride formation energies. DFT also revealed an important trend in intermediate adsorption energies that explained the different experimentally observed CO:H<sub>2</sub> ratios for each bimetallic. The binding energy for \*H and for \*HOCO (an intermediate in the CO reaction pathway) scaled linearly among the samples, which did not explain why some catalysts produced more CO than others. However, the difference between free energy change of adsorption for H and HOCO, ( $\Delta G(*H) - \Delta G(*HOCO)$ ), on different surfaces correlated well with experimentally observed CO partial current density, as seen in Figure 3d. These trends revealed that the difference in free energy is an important descriptor for PdH bimetallic electrocatalysts. Future exploration of bimetallics with different metals or metal ratios could use this descriptor as an effective screening tool for identifying active and low-cost syngas-producing electrocatalysts.

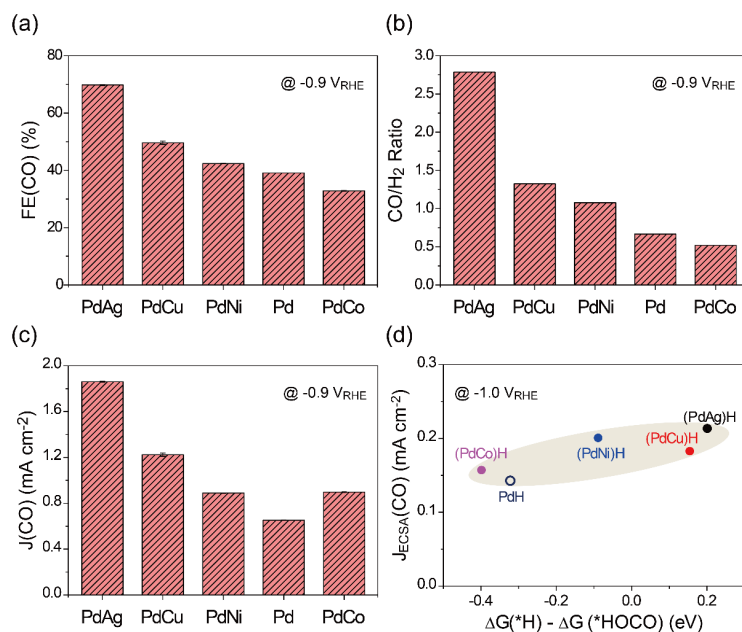


**Figure 2.** Electrochemical results for Pd bimetallic electrocatalysts. (a) CO Faradaic efficiencies, (b) CO:H<sub>2</sub> ratios, and (c) CO partial current densities for PdH and PdH bimetallics in 0.5M NaHCO<sub>3</sub> at -0.9 V vs RHE. (d) The trend between DFT calculation and CO partial current density on (PdM)H electrocatalysts.

### 2.3 Supporting low loading Pd on transition metal carbide substrates

The preceding examples showed the unique properties of PdH electrocatalysts to tune syngas production to potentially supply reactants for the Fischer-Tropsch or methanol synthesis process. In order for the syngas made from CO<sub>2</sub> to compete with traditionally manufactured products, the cost of syngas production needs to be minimized. To achieve this, the loading of the expensive Pd should be minimized while maintaining or even enhancing the current density. It is well known that carbides and nitrides of early transition metals often show similar electronic and catalytic properties as those of precious metals. Therefore, supporting low loadings of precious metals on transition metal carbides (TMC) has been previously used in our group for other electrochemical reactions to reduce precious metal loading and also to tune the catalytic activity and selectivity. Inspired by this approach, we supported Pd on several TMC substrates to reduce Pd loading and optimize syngas production.

Two layers of Pd were deposited on thin films of Mo<sub>2</sub>C, WC, NbC, and TaC to understand the product distribution trends of low-Pd loadings supported on different carbides. Pd/Mo<sub>2</sub>C and Pd/WC produced mostly H<sub>2</sub>, while Pd/NbC and Pd/TaC produced less H<sub>2</sub> and more CO, compared to the other two. Powder electrocatalysts were synthesized with 10 wt% Pd supported on high surface area NbC and TaC. The carbides were synthesized via hard templating with MCM-41 silica to avoid particle agglomeration typical with high temperature carbide synthesis. The resulting particles had BET surface areas greater than 50 m<sup>2</sup> g<sup>-1</sup>.

Once the Pd was loaded on the carbide support, electrochemical reduction was performed to form the Pd-hydride phase. As in the previous reports, in-situ XAS and XRD revealed the characteristic shifts around -0.5 V vs RHE associated with the transformation of Pd to PdH. Unlike the bimetallic XRD patterns that indicated a single phase, solid

solution, these materials showed two distinct XRD patterns for the Pd and the carbide support. During electrochemical reduction, only the Pd pattern shifted, while the carbide pattern did not. This confirms a particle-support interaction between the Pd and carbide, as opposed to the bimetallic case where metals were incorporated into the Pd lattice.

Electrochemical results revealed that 10% Pd/TaC achieved higher CO-partial current density compared to commercial 40 % Pd/C on both a geometric area basis, and on an electrochemical active surface area (ECSA) basis. This means the TaC support enables overall higher reaction rates with lower Pd loading and enhances the intrinsic activity of the PdH electrocatalyst (CO production from unmodified TaC powder is negligible). Furthermore, Pd/TaC, Pd/NbC, and Pd/C each exhibited different H<sub>2</sub>/CO ratios at given potentials, meaning that the carbide supports also impact the product selectivity of the PdH electrocatalyst.

DFT calculations were performed by optimizing the PdH layers on top of TaC(111) or NbC(111) surfaces in order to understand the observed activity and selectivity trends. It was found that surfaces with more thermodynamically favorable \*HOCO formation were more active for CO production. In this case, PdH/TaC(111) had the most favorable \*HOCO formation, followed by PdH/NbC(111), followed by PdH(111). Thus, the increase in site-normalized activity is due to the electronic modification imparted by the carbide support. Further improvement in intrinsic activity can be pursued by identifying supports that reduce the \*HOCO binding energy on PdH.

In summary, our results demonstrate high activity of Pd-based catalysts for CO<sub>2</sub>RR to produce syngas with controlled CO/H<sub>2</sub> ratios. Alloying Pd with another metal and supporting Pd over TMC substrates offer the possibility of reducing Pd loading while enhancing CO<sub>2</sub>RR activity. The combined approaches of electrochemical measurements, in-situ characterization and DFT calculations allow the identification of reaction pathways.

## **Publications Acknowledging this Grant in 2019-2021**

### *(II) Intellectually led by this grant*

1. B.M. Tackett, E. Gomez, J.G. Chen\*, “Net reduction of CO<sub>2</sub> via its thermocatalytic and electrocatalytic transformation reactions in standard and hybrid processes”, *Nature Catalysis*, 2 (2019) 381-386
2. W. Zhu, S. Kattel, F. Jiao\*, J.G. Chen\*, “Shape-Controlled CO<sub>2</sub> Electrochemical Reduction on Nano-sized Pd Hydride Cubes and Octahedra”, *Advanced Energy Materials*, 9 (2019) 1802840W.
3. Q. Zhang, Z. Jiang, B.M. Tackett, S.R. Denny, B. Tian, X. Chen, B. Wang, J.G. Chen\*, “Trends and descriptors of metal-modified transition metal carbides for hydrogen evolution in alkaline electrolyte”, *ACS Catalysis*, 9 (2019) 2415-2422.
4. J. Wang, S. Kattel, C.J. Hawxhurst, J.H. Lee, B.M. Tackett, K. Chang, N. Rui, C.-J. Liu\*, J.G. Chen\*, “Enhancing Activity and Reducing Cost for Electrochemical Reduction of CO<sub>2</sub> by Supporting Palladium on Metal Carbides”, *Angewandte Chemie International Edition*, 58 (2019) 6271-6275.
5. J.H. Lee, S. Kattel, Z. Jiang, Z. Xie, S. Yao, B.M. Tackett, W. Xu, N.S. Marinkovic, J.G. Chen\*, “Tuning the Activity and Selectivity of Electroreduction of CO<sub>2</sub> to Synthesis Gas using Bimetallic Catalysts”, *Nature Communications*, 10 (2019) 3724.

6. Q. He, J.H. Lee, D. Liu, Y. Liu, Z. Lin, Z. Xie, S. Hwang, S. Kattel\*, L. Song\*, J.G. Chen\*, “Accelerating CO<sub>2</sub> Electroreduction to CO over Pd Single-Atom Catalyst”, *Advanced Functional Materials*, 30 (2020) 2000407.
7. Q. He, D. Liu, J.H. Lee, Y. Liu, Z. Xie, S. Hwang, S. Kattel\*, L. Song\*, J.G. Chen\*, “Electrochemical Conversion of CO<sub>2</sub> to Syngas with Controllable CO/H<sub>2</sub> Ratios over Co and Ni Single-Atom Catalysts”, *Angewandte Chemie International Edition*, 59 (2020) 3033-3037.
8. B.M. Tackett, J.H. Lee and J.G. Chen\*, “Electrochemical Conversion of CO<sub>2</sub> to Syngas with Palladium-Based Electrocatalysts”, *Accounts of Chemical Research*, 53 (2020) 1535-1544.
9. Y. Liu, D. Tian, A.N. Biswas, Z. Xie, S. Hwang, J.H. Lee\*, H. Meng\* and J.G. Chen\*, “Transition Metal Nitrides as Promising Catalyst Supports for Tuning CO/H<sub>2</sub> Syngas Production from Electrochemical CO<sub>2</sub> Reduction”, *Angewandte Chemie International Edition*, 59 (2020) 11345-11348.
10. Y. Wang, Y. Nian, A.N. Biswas, W. Li, Y. Han\* and J.G. Chen\*, “Challenges and Opportunities in Utilizing MXenes of Carbides and Nitrides as Electrocatalysts”, *Advanced Energy Materials*, 11 (2021) 2002967.
11. L.R. Winter and J.G. Chen\*, “N<sub>2</sub> Fixation by Plasma-Activated Processes”, *Joule*, 5 (2021) 300-315.

(III) *Jointly funded by this grant and other grants with intellectual leadership by other funding sources*

12. W. Luc, B.H. Ko, S. Kattel, S. Li, D. Su, J.G. Chen\*, F. Jiao\*, “SO<sub>2</sub>-induced Selectivity Change in CO<sub>2</sub> Electroreduction”, *Journal of the American Chemical Society*, 141 (2019) 9902-9909.
13. H.B. Tao, J. Zhang, J. Chen, L. Zhang, Y. Xu, J.G. Chen\*, B. Liu\*, “Revealing Energetics of Surface Oxygen Redox from Kinetic Fingerprint in Oxygen Electrocatalysis”, *Journal of the American Chemical Society*, 141 (2019) 13803-1381.
14. X. Yang, S. Kattel, J. Nash, X. Chang, J.H. Lee, Y. Yan, J.G. Chen\*, B. Xu\*, “Quantification of Active Sites and Elucidation of Reaction Mechanism of Electrochemical Nitrogen Reduction Reaction on Vanadium Nitride”, *Angewandte Chemie International Edition*, 58 (2019) 13768-13772.
15. Q. Chang, P. Zhang, A.H.B. Mostaghimi, X. Zhao, S.R. Denny, J.H. Lee, H. Gao, Y. Zhang, H. Xin, S. Siahrostami\*, J.G. Chen\* and Z. Chen\*, “Promoting H<sub>2</sub>O<sub>2</sub> Production via 2-Electron Oxygen Reduction by Coordinating Partially Oxidized Pd with Defect Carbon”, *Nature Communications*, 11 (2020) 2178.
16. R. Xia, D. Tian, S. Kattel, B. Hasaa, H. Shina, X. Ma\*, J.G. Chen\* and F. Jiao\*, “Electrochemical Reduction of Acetonitrile to Ethylamine”, *Nature Communications*, 12 (2021) 1949.

#### **Awards or leadership activities during 2018-2020 calendar years**

Robert H. Wilhelm Award, American Institute of Chemical Engineers (2020)  
 R.B. Anderson Award, Canadian Catalysis Division (2020)

Web of Science Highly Cited Researcher (2019)  
President, North American Catalysis Society  
Associate Editor, ACS Catalysis

## Solvent-Mediated Interactions and Catalysis within Confined Liquids

David W. Flaherty, Daniel T. Bregante, Matthew Chan, Diwakar Shukla, David S. Potts, Chris Torres, Ohsung Kwon, E. Zeynep Ayla  
University of Illinois, Urbana-Champaign, Department of Chemical and Biomolecular Engineering

### Presentation Abstract

Solvating molecules and the environment that surround catalytic sites provide interactions that change rates and selectivities of catalytic events by orders of magnitude. Although heuristics exist for many homogeneous reactions, the interactions among solvent molecules and reactive surface intermediates remain challenging to describe. These challenges are compounded when solvents not only restructure about intermediates at active sites but also sense the presence and functionality of solid-liquid interfaces that extend beyond active sites. Understanding and exploiting these phenomena requires a conceptual framework, rooted in familiar principles, and informed by experimental methods that probe the reactivity of intermediates, the structure of the catalyst, and changes in the solvent at the reactive interface during catalysis.

Catalytic epoxidations of alkenes proceed at early transition metal active sites stabilized within the framework of zeolites. These epoxidation reactions depend on multiple factors including the dimensions and polarity of surrounding voids. The topology of the support changes the structure of the solvation shells that form about reactive species and evolve along with the reactants. Comparisons of results from kinetic, thermodynamic, spectroscopic, and synthetic experimentation provide insight to the coupled molecular interactions between catalyst surfaces, solvating molecules, and reactive species from which we can extract principles to design solid-liquid interfaces for catalysis. These findings show that individually weak but collectively significant interactions among critical transition states, solvent molecules, and the extended surface of solid catalysts present opportunities for catalyst design and reaction engineering particularly in microporous materials.

### **DE-SC0020224: The Role of Cooperative Interactions Among Surfaces, Solvents, and Reactive Intermediates in Catalysis at Solid-Liquid Interfaces**

**Student(s):** Daniel T. Bregante, Chris Torres, David Potts, Ohsung Kwon

### RECENT PROGRESS

#### **Mechanisms for Alkene Epoxidations by Organic Hydroperoxides**

Ti atoms incorporated into the framework of zeolite \*BEA (Ti-BEA) or grafted onto SBA-15 (Ti-SBA-15) catalyze alkene epoxidation with hydrogen peroxide (H<sub>2</sub>O<sub>2</sub>), t-butyl hydrogen peroxide (TBHP), or cumene hydroperoxide (CHP). The rates of epoxidation, however, differ by orders of magnitude depending on the combination of

oxidant, alkene, and support used. Within Ti-BEA, rates of 1-octene epoxidation with  $\text{H}_2\text{O}_2$  are 30- and 1700-times greater than reactions with TBHP or CHP, respectively. In contrast, 1-octene epoxidation rates in Ti-SBA-15 with  $\text{H}_2\text{O}_2$  are 7- and 40-fold higher than in reactions with TBHP or CHP, respectively. Moreover, comparisons of 1-alkene ( $\text{C}_6 - \text{C}_{10}$ ) epoxidations within Ti-BEA and Ti-SBA-15 show that turnover rates depend exponentially on chain length and sense the size of the surrounding pore for reaction with  $\text{H}_2\text{O}_2$ , TBHP, or CHP. In situ UV-Vis confirms that catalyst surface are predominantly covered by alkylperoxide intermediates at reactant ratios that contain comparable or excess amounts of oxidant to alkene. A thermodynamic model quantitatively describes how inner-sphere interactions among epoxidation transition states depend on the steric bulk of the reacting species and how these interactions are conferred by the topology of the surrounding pore. The mesopores of Ti-SBA-15 allow transition states to access conformations that lower the free energy of the complex relative to analogous transition states in Ti-BEA, which explains why epoxidation rates in mesoporous solids are less sensitive to the identity of the oxidant than within microporous silicates.

### Effects of Zeolite Topology on Catalytic Epoxidations with $\text{H}_2\text{O}_2$ at Ti-Centers

We compared activation enthalpies and entropies for 1-alkene epoxidation with  $\text{H}_2\text{O}_2$  over Ti-containing zeolites (MFI, BEA, and FAU) of varying pore size and  $(\text{SiOH})_4$  density in different solvents (i.e.,  $\text{CH}_3\text{CN}$ ,  $\text{CH}_3\text{OH}$ ,  $\text{C}_2\text{H}_5\text{OH}$ ) to develop a molecular model for how solvent molecules stabilize surface intermediates during oxidation catalysis. Turnover rates for 1-alkene (i.e., 1-hexene, 1-octene, and 1-decene) epoxidation are greater in Ti-zeolite catalysts that contain significant densities of hydrogen-bonded  $\text{SiOH}$  ( $(\text{SiOH})_x$ ; e.g., silanol nests) than within their hydrophobic analogues, regardless of the solvent choice (i.e., for  $\text{CH}_3\text{CN}$ ,  $\text{CH}_3\text{OH}$ ,  $\text{C}_2\text{H}_5\text{OH}$ ). The dependence of turnover rates on solvent identity, pore size, and  $(\text{SiOH})_x$  density reflects differences in the structure of the surrounding solvent molecules. For example, epoxidation catalysis depends on  $\text{H}_2\text{O}$  structure within  $\text{CH}_3\text{CN}$  and is reflected in differences in activation enthalpies ( $\Delta H_{\text{E,App}}^\ddagger$ ) and entropies ( $\Delta S_{\text{E,App}}^\ddagger$ ) between any given Ti-zeolite and the most-hydrophobic variant, which are defined as excess enthalpies and entropies ( $H^{\ddagger,\epsilon}$ ,  $S^{\ddagger,\epsilon}$ ), respectively (Fig. 1).

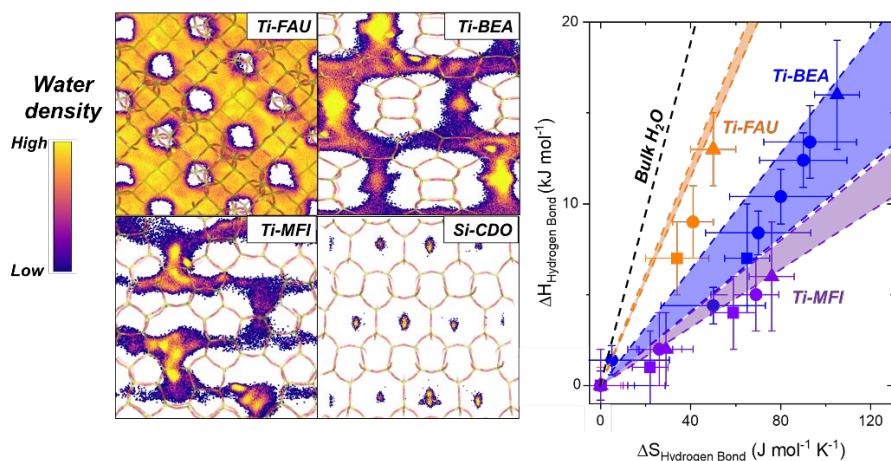


**Figure 1.** Time-averaged spatial distribution of water in Ti-zeolites and enthalpy-entropy compensation between activation parameters for epoxidation reactions.

Changes in  $H^{\ddagger,\varepsilon}$  and  $S^{\ddagger,\varepsilon}$  primarily reflect changes in the enthalpy and entropy of the epoxidation transition states, which depend sensitively on their solvating environment.  $H_2O$  molecules that congregate at  $(SiOH)_x$  within hydrophilic Ti-zeolites form distinct structures (e.g., trimers, two-dimensional chains) that must reorganize to accommodate the formation of transient surface intermediates (e.g., transition states) during catalysis. Solvent restructuring disrupts hydrogen-bonding interactions among water, other hydrogen bonding species, and surfaces. Figure 1 shows how values of  $H^{\ddagger,\varepsilon}$  change with  $S^{\ddagger,\varepsilon}$  for Ti-FAU, -BEA, and -MFI with varying densities of  $(SiOH)_x$  and shows change in enthalpy and entropy for breaking a hydrogen bond in pure  $H_2O$ .

### Mechanistic and Kinetic Influences of Solvent Identity on Epoxidations with $H_2O_2$

Ti-silicates activate  $H_2O_2$  to form Ti-hydroperoxo and Ti-peroxo intermediates that can react with alkenes to form epoxide products. 1-Octene epoxidation with  $H_2O_2$  on Ti-BEA and Ti-MFI of different hydrophilicities are conducted in methanol ( $CH_3OH$ ) and acetonitrile ( $CH_3CN$ ) solvents to elucidate the role of solvents in stabilizing kinetically relevant reactive species. Epoxidation turnover rates are higher in  $CH_3CN$  than  $CH_3OH$  for Ti-BEA, but the reverse is observed for Ti-MFI. Ti-silicates that are more hydrophilic results in higher epoxidation turnover rates than their hydrophobic counterparts, regardless of solvent identity. *In situ* UV-Vis measurements show that activation of  $H_2O_2$  is reversible in  $CH_3OH$ , but not in  $CH_3CN$ . Kinetic, spectroscopic, and thermodynamic analyses show that differences in turnover rates are mainly due to differing extent to which reactive surface species are stabilized within zeolite micropores. The mechanism and catalytic cycle of epoxidation in these Ti-zeolites and solvents are shown in **Figure 3**.

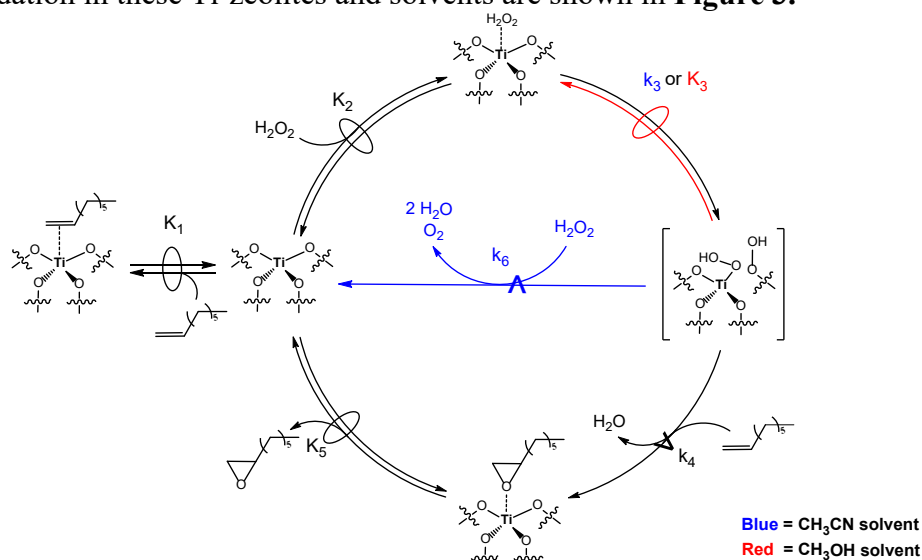


**Figure 3.** Proposed elementary steps describing 1-octene epoxidation in methanol or acetonitrile solvents over Ti-MFI and Ti-BEA catalysts.

Apparent activation free energy values obtained with transition-state theory vary with solvent identity and hydrophilicity of Ti-silicates. For instance, activation free energy values are slightly lower ( $\sim 10 \text{ kJ mol}^{-1}$ ) in  $CH_3OH$  than activation free energy values of  $CH_3CN$  within Ti-silicates of the same framework. Despite the higher activation free energy values in  $CH_3CN$ , the turnover rates of epoxidation for Ti-BEA in  $CH_3CN$  is still

higher than those for Ti-BEA in CH<sub>3</sub>OH. Conversely, turnover rates of epoxidation for Ti-MFI in CH<sub>3</sub>OH are higher than those in CH<sub>3</sub>CN. These results imply that solvent effects including hydrogen bonding numbers (or something like this) affect apparent activation free energy of zeolites of different pore sizes to different extents, which lead to differing trends in turnover rates in different between solvents.

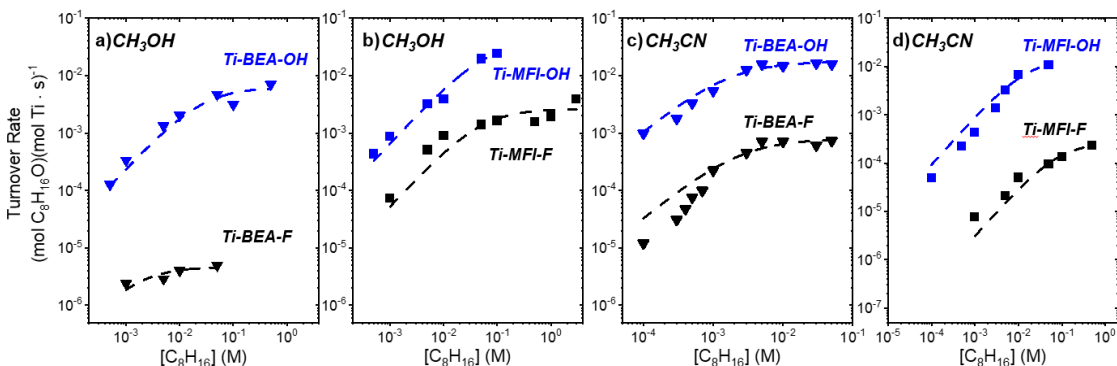


**Figure 4.** Turnover rates for the formation of C<sub>8</sub>H<sub>16</sub>O as a function of [C<sub>8</sub>H<sub>16</sub>] (0.01 M H<sub>2</sub>O<sub>2</sub>, 0.039 M H<sub>2</sub>O, 313 K) in Ti-zeolites.

Finally, hydrophilic Ti-BEA-OH and Ti-MFI-OH have activation free energy values that are 11 kJ mol<sup>-1</sup> and 15 kJ mol<sup>-1</sup> lower than their hydrophobic counterparts, respectively. The lower free energies in hydrophilic Ti-silicates can be associated to larger entropy gain from solvent reorganization within pores proximate to Ti active sites that contributes to higher epoxidation turnover rates within these zeolites. These comparisons show that stabilization of epoxidation transition states can vary between Ti-silicates of different frameworks and silanol densities, and that the hydrophilicity of Ti-silicates can be manipulated to maximize increase epoxidation turnover rates.

### Influence of Alkene Structure on Lewis-Acid Catalyzed Epoxidations

Over hydrophobic Ti-BEA-F materials that do not stabilize water networks, epoxidation turnover rates decrease monotonically as chain length increases from 1-hexene (C<sub>6</sub>H<sub>12</sub>) to 1-decene (C<sub>10</sub>H<sub>20</sub>). In contrast, rates over hydrophilic Ti-BEA-OH reach a maximum for C<sub>10</sub>H<sub>20</sub>, then decrease by 10 times to a minimum value for 1-octadecene (C<sub>18</sub>H<sub>36</sub>). The rate differences likely do not result from changes in reaction mechanism or mass transfer constraints, but rather changes in transition state stability as quantified by activation enthalpies ( $\Delta H^\ddagger$ ) and entropies ( $\Delta S^\ddagger$ ).  $\Delta H^\ddagger$  and  $\Delta S^\ddagger$  vary negligibly from C<sub>6</sub>H<sub>12</sub> to C<sub>10</sub>H<sub>20</sub> over Ti-BEA-F. However,  $\Delta H^\ddagger$  and  $\Delta S^\ddagger$  increase systematically with alkene chain length over Ti-BEA-OH, with respective differences of 68 kJ mol<sup>-1</sup> and 209 J mol<sup>-1</sup> K<sup>-1</sup> between C<sub>6</sub>H<sub>12</sub> and C<sub>18</sub>H<sub>36</sub>. The excess enthalpy and entropy of the transition state likely increase because longer alkyl chains must disrupt a greater number of H<sub>2</sub>O molecules within Ti-BEA-OH. Corresponding epoxide adsorption enthalpies, measured with isothermal titration calorimetry, increase as chain length increases and correlate to  $\Delta H^\ddagger$  measurements over Ti-BEA-OH, providing further evidence that longer alkyl chains disrupt more hydrogen bonds to alter transition state stability.

## Publications Acknowledging this Grant in 2018-2021

### (I) Intellectually led by this grant

- 1) Bregante, D. T.; Potts, D. S.; Kwon, O.; Ayla, E. Z.; Tan, J. Z.; Flaherty, D. W., “Effects of Hydrofluoric Acid Concentration on the Density of Silanol Groups and Water Adsorption in Hydrothermally Synthesized Transition Metal Substituted Silicalite-1” *Chem. Mater.* **2020**, 32, 7425-7437.
- 2) Bregante, D. T.; Tan, J. Z.; Schultz, R. L.; Ayla, E. Z.; Potts, D. S.; Torres, C.; Flaherty, D. W., “Catalytic Consequences of Oxidant, Alkene, and Pore Structure on Alkene Epoxidations within Titanium Silicates” *ACS Catal.* **2020**, 10, 10169–10184.
- 3) Bregante, D. T.; Chan, M.; Tan, J. Z.; Ayla, E. Z.; Nicholas, C. P.; Shukla, D.; Flaherty, D. W., “The Shape of Water in Zeolites and its Impact on Epoxidation Catalysis”, *accepted, Nature Catal.*
- 4) Bregante, D. T.; Wilcox, L.; Liu, C.; Paolucci, C.; Gounder, R.; Flaherty, D. W., “Dioxygen Activation Kinetics over Distinct Cu Site Types in Cu-CHA Zeolites”, *in review, ACS Catalysis*
- 5) Potts, D. S.; Bregante, D. T.; Adams, J. S.; Torres, C.; Flaherty, D. W., “Influence of Solvent Structure and Hydrogen Bonding on Catalysis at Solid-Liquid Interfaces”, *in review, Chem. Soc. Rev.*
- 6) Tan, J. Z.; Bregante, D. T.; Torres, C.; Flaherty, D. W., “Transition State Stabilization Depends on Solvent Identity, Pore Size, and Hydrophilicity for Epoxidation in Zeolites”, *in review, J. Catal.*

### (II) Jointly funded by this grant and other grants with intellectual leadership by other funding sources

- 7) Bregante, D. T.; Tan, J. Z.; Sutrisno, A.; Flaherty, D. W., “Heteroatom Substituted Zeolite FAU with Ultralow Al Contents for Liquid-Phase Oxidation Catalysis” *Catal. Sci. Tech.* **2020**, 10, 635 – 647.
- 8) Ayla, E. Z.; Potts, D. S.; Bregante, D. T.; Flaherty, D. W., “Alkene Epoxidation with H<sub>2</sub>O<sub>2</sub> over Group 4-6-Metal Substituted BEA Zeolites: Reactive Intermediates, Reaction Pathways, and Linear Free Energy Relationships” *ACS Catal.* **2021**, 11, 139-154.

### Awards or leadership activities during 2018-2020 calendar years:

2021	Eastman Foundation Distinguished Lecturer in Catalysis, Dept. of Chemical and Biomolecular Engineering, University of California, Berkeley
2019	Inaugural Student Seminar & Patten Lecture Series, Dept. of Chemical and Biological Engineering, University of Colorado, Boulder
2019	Department of Energy, Early Career Award, Catalysis Science
2019 - 2020	Early Career Advisory Board, ACS Catalysis
2019 – date	Named to Advisory Board, Cell Reports Physical Sciences
2018	Dean’s Award for Research Excellence, College of Engineering, University of Illinois
2018	Early Career Research Award, American Vacuum Society, Prairie Chapter

2020 Organizing Committee (Publications with J. Notestein, W. Medlin), 17th  
International Congress on Catalysis, San Diego, CA  
2019-2021 Spring Program Chair, ACS Division of CATL  
2017-2019 Organizing Committee (Program Chair with R. Gounder), 26th North  
American Catalysis Society Meeting, Chicago, IL

## Multinuclear Copper Active Site Requirements in Cu-Zeolites for Partial Methane Oxidation

Laura N. Wilcox<sup>1</sup>, Andrew D. Mikes<sup>1</sup>, Siddarth H. Krishna<sup>1</sup>, Rajamani Gounder<sup>1\*</sup>

<sup>1</sup>Davidson School of Chemical Engineering, Purdue University, West Lafayette, IN

### Presentation Abstract

Methane is an abundant and inexpensive alkane that can be sourced from natural and shale gas and upgraded to chemicals of higher value. Aluminosilicate zeolites exchanged with copper complexes (Cu-zeolites) facilitate partial methane oxidation (PMO) to methanol, with various proposals for mononuclear and multinuclear active site structures that form upon dioxygen activation in amounts that depend on bulk and atomic-scale zeolite properties in an imprecisely understood manner. Here, we use a high-symmetry zeolite framework (chabazite, CHA) as a model support to assist in identification of the Cu structural and site proximity requirements for activating dioxygen and methane. CHA zeolites were synthesized via routes to vary the framework Al density and arrangement, which influence the distribution of mononuclear ( $\text{Cu}^{2+}$  ( $\text{Z}_2\text{Cu}$ ),  $[\text{CuOH}]^+$  ( $\text{ZCuOH}$ )) and binuclear Cu site motifs formed after  $\text{O}_2$  treatment. Cu-CHA samples containing solely  $\text{Z}_2\text{Cu}$  sites do not undergo auto-reduction (He, 723 K) or form multinuclear  $\text{O}_x$ -bridged structures upon  $\text{O}_2$  treatment (723 K) at high temperature, and also do not form methanol from stoichiometric PMO cycles. Cu-CHA samples containing  $\text{ZCuOH}$  sites show methanol yields from stoichiometric PMO cycles and fractions of Cu that undergo auto-reduction that increase with decreasing mean distance between Cu sites. *In situ* X-ray absorption spectra (XAS) show that inert (He, 723 K) and reducing ( $\text{CH}_4$ , 473 K) treatments reduce an equivalent fraction of Cu(II) sites, implicating a common  $\text{O}_x$ -bridged binuclear Cu intermediate in  $\text{CH}_4$ - and auto-reduction pathways.  $\text{ZCuOH}$  sites are precursors to binuclear  $\text{O}_x$ -bridged structures that form upon  $\text{O}_2$  activation (723 K), identified as trans- $\mu$ -1,2-peroxo dicopper(II) and mono- $\mu$ -oxo dicopper(II) by *in situ* UV-Visible and Raman spectroscopies. These data provide new insights into how material synthesis routes and various oxidation and reduction treatments influence the number of binuclear  $\text{O}_x$ -bridged Cu sites in zeolites that facilitate partial oxidation reactions.

### DE-SC0019026: Dynamic Multinuclear Active Sites Formed from Mobilized Single Atoms on Heterogeneous Supports for Selective Oxidation Catalysis

**PI:** Rajamani Gounder

**Student(s):** Laura N. Wilcox, Andrew D. Mikes

## RECENT PROGRESS

### UV-Vis and XAS to monitor Cu sites during auto-reduction, and CH<sub>4</sub>- and CO-reduction

The distribution of framework Al atoms in CHA (Al-O(-Si-O)<sub>x</sub>-Al) between isolated ( $x \geq 3$ ) and paired ( $x = 1,2$ ) sites influences the speciation of extra-framework Cu ions, as Cu<sup>2+</sup> sites exchange at proximal Al sites (Z<sub>2</sub>Cu) and [CuOH]<sup>+</sup> complexes exchange at isolated Al sites (ZCuOH). We studied a model Cu-CHA zeolite (Si/Al = 25, Cu/Al = 0.37), prepared to contain a mixture of [CuOH]<sup>+</sup> and Cu<sup>2+</sup> (80% ZCuOH, 20% Z<sub>2</sub>Cu) sites. *In situ* UV-Vis (Fig. 1) was used to monitor the evolution of mononuclear and binuclear Cu sites after high-temperature O<sub>2</sub> activation treatments (21 kPa O<sub>2</sub>, 723 K, 2 h) and subsequent reduction either in inert auto-reduction (101 kPa He, 723 K, 2 h), CH<sub>4</sub>-reduction (4.9 kPa, 473 K, 0.5 h), and CO-reduction (5 kPa, 523 K, 1 h).

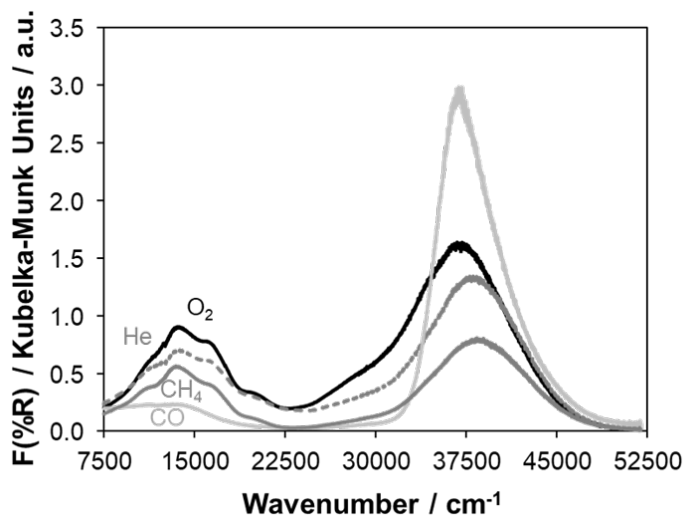


**Figure 1.** UV-Visible spectra of Cu-CHA (Si/Al = 25, Cu/Al = 0.37) after O<sub>2</sub> activation in 21 kPa O<sub>2</sub> at 723 K (black, solid) followed by the introduction of 101 kPa He at 723 K (grey, dashed). Spectrum after reduction in 4.9 kPa CH<sub>4</sub> at 473 K (grey, solid). Spectrum after reduction in 5 kPa CO at 523 K (light grey, solid).

After treatments in flowing O<sub>2</sub> at 723 K, d-d transition features (~11,059, ~13,593, ~16,379, ~20,077 cm<sup>-1</sup>) and a shoulder representative of multinuclear Cu species (24,000–30,000 cm<sup>-1</sup>) are observed, along with a ligand-to-metal charge transfer band (~30,000–50,000 cm<sup>-1</sup>) (Fig. 1). These data reproduce literature reports of UV-Vis spectra with bands (~16,500, ~19,700, ~30,000 cm<sup>-1</sup>) for multinuclear Cu-oxo species, identified with Raman spectroscopy to comprise binuclear O- and O<sub>2</sub>-bridged Cu sites. Auto-reduction, CH<sub>4</sub>-reduction, and CO-reduction led to the partial disappearance of bands for binuclear O/O<sub>2</sub>-bridged Cu species, but to a larger extent after CO reduction, suggesting that only a subset of O/O<sub>x</sub>-bridged Cu species that are CO-reducible can undergo auto-reduction or CH<sub>4</sub>-reduction. We conclude that CO reduces both mono- $\mu$ -oxo (Cu-O-Cu) and trans-peroxo (Cu-O<sub>2</sub>-Cu) species (according to Raman spectra), while auto-reduction is likely to occur on Cu-O<sub>2</sub>-Cu sites, given the elementary nature of eliminating molecular O<sub>2</sub> from each Cu-O<sub>2</sub>-Cu site to result in Cu reduction, in contrast to needing two Cu-O-Cu complexes to complete auto-reduction steps that eliminate O<sub>2</sub>.

After high-temperature O<sub>2</sub> treatment and subsequent CH<sub>4</sub> exposure, the UV-Vis spectrum (Fig. 1, grey) shows bands that remain in the d-d transition and low-energy LMCT region,

indicating that there is a fraction of binuclear Cu sites, as well as isolated ZCuOH species, that do not reduce to  $\text{Cu}^+$  in  $\text{CH}_4$  and thus would not participate in PMO cycles. Therefore,  $\text{CH}_4$  appears to reduce only a fraction of the O/O<sub>2</sub>-bridged binuclear Cu species that are present to form methoxy-bridged structures invoked previously in PMO reaction schemes. The UV-Visible spectrum collected following a subsequent CO reduction treatment (Fig. 1, lightest grey) resulted in complete disappearance of features for O/O<sub>2</sub>-bridged binuclear Cu species, again indicating that CO reduces a larger fraction of the Cu sites present than does  $\text{CH}_4$ . Comparing the UV-Vis spectra indicate that both high-temperature auto-reduction treatments in inert and moderate-temperature reduction treatments in  $\text{CH}_4$  reduce a similar subset of Cu site types, likely Cu-O<sub>2</sub>-Cu structures.

*In situ* Cu K-edge XANES spectra measured at Argonne National Laboratory at sector 10 MR-CAT (Materials Research Collaborative Access Team) with the insertion device beamline (10-ID) allowed for the determination of the fraction of  $\text{Cu}^+$  and  $\text{Cu}^{2+}$  present on each Cu-CHA sample with linear combination fitting (LCF) of XANES spectra following auto-reduction and  $\text{CH}_4$ -reduction (Fig. 2) to determine whether these treatments quantitatively result in the same fraction of  $\text{Cu}^{2+}$  to  $\text{Cu}^+$  reduction to corroborate the results from *in situ* UV-Vis spectroscopy (Fig. 1). The Cu-CHA sample containing the highest ZCuOH density showed a larger fraction of Cu sites that reduced to the  $\text{Cu}^+$  state after  $\text{CH}_4$  exposure (0.47  $\text{Cu}^+/\text{Cu}_{\text{total}}$ ) than the sample of intermediate ZCuOH density (0.35  $\text{Cu}^+/\text{Cu}_{\text{total}}$ ), consistent with the fraction of  $\text{Cu}^+$  quantified after auto-reduction experiments on these samples (0.53 and 0.34  $\text{Cu}^+/\text{Cu}_{\text{total}}$ , respectively). Negligible reduction in  $\text{CH}_4$  was observed on the Z<sub>2</sub>Cu-containing Cu-CHA control sample (0.04  $\text{Cu}^+/\text{Cu}_{\text{total}}$ ).

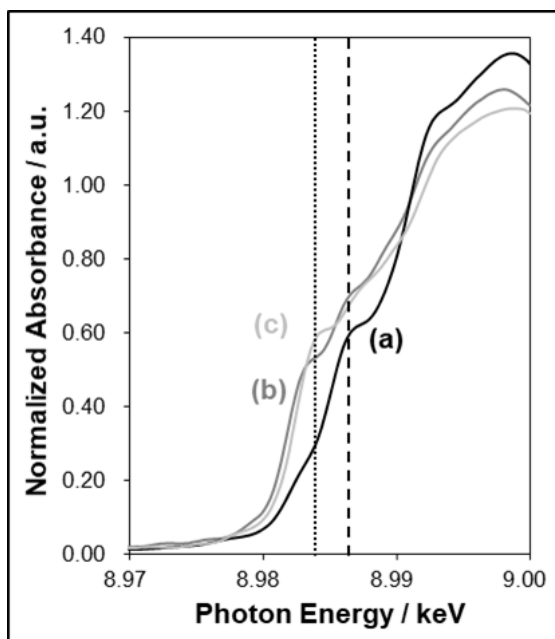


**Figure 2.** *In situ* Cu K-edge XANES spectra collected after exposure to 4.1 kPa  $\text{CH}_4$  (balance He) at 473 K on (a) Z<sub>2</sub>Cu-containing Cu-CHA (b) ZCuOH-containing Cu-CHA, and (c) mixed Z<sub>2</sub>Cu and ZCuOH-containing Cu-CHA. The line (····) at 8.983 keV denotes Cu(I) and the line (---) at 8.897 keV denotes Cu(II).

Thus, combining *in situ* XANES and UV-Vis evidence, we propose that Cu-O<sub>2</sub>-Cu site motifs undergo auto-reduction and  $\text{CH}_4$ -reduction and are relevant for PMO reaction cycles, while CO can also reduce Cu-O-Cu site motifs, some fraction of which may be irrelevant for PMO reactions. These data are being incorporated into a self-consistent mechanism for PMO comprised of elementary steps, in which O<sub>2</sub> activation can form a distribution of Cu site motifs (including Cu-O-Cu, Cu-O<sub>2</sub>-Cu,  $\text{Cu}^{2+}$ ,  $\text{CuOH}^+$ ), in which Cu-O<sub>2</sub>-Cu and two proximal Cu-O-Cu structures comprise the active pool of Cu sites that can facilitate PMO cycles.

## NH<sub>3</sub>-based reduction treatments to mobilize and activate PMO-inactive Cu sites, as monitored with UV-Vis spectroscopy and titration methods

Stoichiometric PMO data indicate that Z<sub>2</sub>Cu-only containing Cu-CHA samples are inactive for this reaction. However, NO and NH<sub>3</sub> are known to reduce Cu<sup>2+</sup> and Cu<sup>+</sup> and subsequently mobilize Cu<sup>+</sup> ions, specifically in the NO<sub>x</sub> SCR literature. Using this knowledge, we have explored the ability of NH<sub>3</sub>-only reduction followed by the introduction of NO to reduce and mobilize previously inactive Cu sites (i.e., Z<sub>2</sub>Cu) into Cu<sup>+</sup> sites that can be incorporated into the pool of PMO-active Cu sites.

We synthesized model Cu-CHA samples, including a Z<sub>2</sub>Cu-only and a mixed Z<sub>2</sub>Cu/ZCuOH-containing Cu-CHA. The change in oxidation state from Cu<sup>2+</sup> to Cu<sup>+</sup> was monitored by *in situ* UV-Visible spectroscopy during O<sub>2</sub> activation (21 kPa O<sub>2</sub>, 723 K), and then either NH<sub>3</sub>-only reduction (412 ppm) or NO+NH<sub>3</sub> co-reduction (412 ppm each) at 473 K. After O<sub>2</sub> activation, 4 distinct features in the d-d transition region for multinuclear Cu<sup>2+</sup> species are observed, and these features subsequently disappear following reduction treatments as Cu<sup>+</sup> species are formed. The d-d transition bands were integrated to estimate the fraction of Cu<sup>+</sup> remaining as a function of time (Fig. 3).

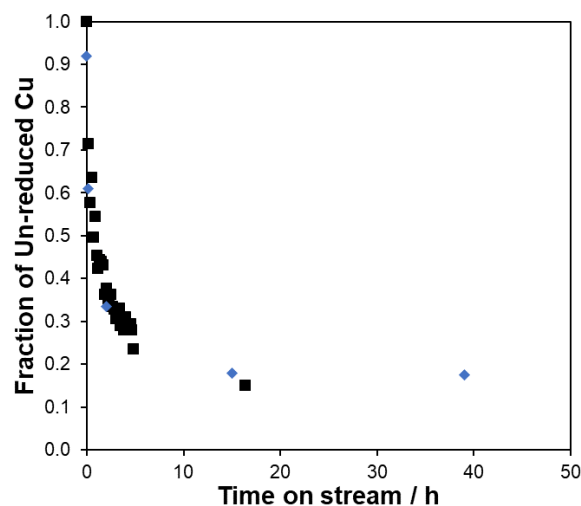


**Figure 3.** Un-reduced Cu(II) as a function of time in NH<sub>3</sub>-only flow at 473 K on a Cu-CHA with Si/Al=15, Cu/Al=0.17 (50% Z<sub>2</sub>Cu, 50% ZCuOH). The (♦) quantified the un-reduced Cu with titration methods while (■) quantified un-reduced Cu with integration of the d-d transition region (7,500-20,000 cm<sup>-1</sup>) of the UV-Visible spectra.

These data were corroborated by first developing an independent titration method in our laboratory at Purdue to quantify the remaining Cu<sup>+</sup> content on any Cu-zeolite sample of arbitrary origin or treatment history, using the well-known ability of NO+NH<sub>3</sub> co-reduction of Cu<sup>+</sup> sites with 1:1 NO:Cu stoichiometry, and then performing this titration method on Cu-CHA samples after exposure to NH<sub>3</sub>-only reduction for various lengths of time (Fig. 3). Quantitative agreement is observed between the un-reduced Cu<sup>2+</sup> fraction determined by *in situ* UV-Vis and NO+NH<sub>3</sub> titration methods, thus providing two complimentary techniques to quantify and probe the ability of NH<sub>3</sub> to reduce Cu<sup>2+</sup> ions (which are otherwise spectator species during PMO-conditions) into Cu<sup>+</sup> species that can be incorporated into the active pool of Cu sites during PMO. Ongoing work will continue to probe the NH<sub>3</sub>-reducibility of Cu on Cu-zeolites, specifically focusing on recovering Cu sites from PMO-inactive or spectator states. Developing an understanding of how Cu sites reduce and can be recovered into PMO reaction cycles will allow developing treatments to regenerate inactive Cu structures during continuous PMO reaction schemes.

## Publications Acknowledging this Grant in 2018-2021

### (IV) Intellectually led by this grant

1. Wilcox, L. N.; Krishna, S. H.; Jones, C. B.; Gounder, R.\*. Mechanistic Studies of NH<sub>3</sub>-Assisted Cu(II) Reduction of Mononuclear Cu(II) Cation Sites in Cu-CHA Zeolites. *Catalysis Science & Technology* **2021**, under review.
2. Krishna, S. H.; Jones, C. B.; Gounder, R.\*. Dynamic Interconversion of Metal Active Site Ensembles in Zeolite Catalysis. *Annual Review of Chemical & Biomolecular Engineering* **2021**, 12, 115-136.

### (V) Jointly funded by this grant and other grants with intellectual leadership by other funding sources

3. Bregante, D. T.; Wilcox, L. N.; Liu, C.; Paolucci, C.; Gounder, R.; Flaherty, D. W.\*. Dioxygen Activation Kinetics over Distinct Cu Site Types in Cu-CHA Zeolites. *ACS Catalysis* **2021**, in revision.
4. Li, H.; Paolucci, C.; Khurana, I.; Wilcox, L. N.; Göttl, F.; Albarracin-Caballero, J. D.; Shih, A. J.; Ribeiro, F. H.; Gounder, R.\*; Schneider, W. F.\*. Consequences of Exchange-Site Heterogeneity and Dynamics on the UV-Visible Spectrum of Cu-Exchanged SSZ-13. *Chemical Science* **2019**, 10, 2373-2384.

## Awards and Leadership Activities (2018-2020)

### Honors and Awards

- **2019:** Faculty Excellence Award for Early Career Research (Purdue College of Engineering)
- **2019:** R. Norris Shreve Award for Outstanding Teaching in Chemical Engineering (Purdue ChE)
- **2018:** DOE Early Career Award (Department of Energy)
- **2018:** Alfred P. Sloan Research Fellow in Chemistry (Sloan Foundation)
- **2018:** Named to “2018 Class of Influential Researchers” by *Industrial & Engineering Chemistry Research*

### Leadership Activities

- **2020-2021:** Technical Program Chair, Catalysis Club of Chicago
- **2019-2021:** Programming Chair, Area 20A: Catalysis (CRE), AIChE
- **2019-2020:** Posters, Workshops and Satellite Conferences Committee Co-Chair, 17<sup>th</sup> International Congress on Catalysis, San Diego, CA

- **2017-2019:** Technical Program Co-Chair, 26<sup>th</sup> North American Catalysis Society Meeting, Chicago, IL
- **2016-2019:** Director, Area 20A: Catalysis (CRE), AIChE
- **2016-present:** Editorial Advisory Board, *Reaction Chemistry & Engineering*
- **2017-2019:** Early Career Advisory Board, *ACS Catalysis*
- **2017-present:** Thrust/Testbed Leader, NSF ERC on Innovative and Strategic Transformation of Alkane Resources (CISTAR)

## Amines from Hydrocarbons and N<sub>2</sub>: Combining C-H Activation and N-N Activation

Patrick L. Holland  
Yale University, Department of Chemistry

### Presentation Abstract

The activation of abundant molecules (e.g. hydrocarbons, atmospheric N<sub>2</sub>) is challenging because these molecules are typically inert. We have discovered a low-coordinate iron system that mediates the one-pot conversion of petroleum-derived arenes and N<sub>2</sub> into aniline derivatives, a net formation of C–N bonds from hydrocarbons and N<sub>2</sub>. The reaction uses a mixture of sodium powder, crown ether, and trimethylsilyl bromide, and silylated anilines are isolated. Numerous iron complexes along the cyclic reaction pathway have been isolated and crystallographically characterized, and their stoichiometric reactivity outlines a mechanism for sequential C–H activation and N<sub>2</sub> functionalization. One key to this coupling reaction is the partial silylation of a reduced iron–dinitrogen complex to give a formally iron(IV) disilylhydrazido complex, which undergoes migration of a benzene-derived aryl group to the proximal N atom to form the new C–N bond. Further reduction releases the N<sub>2</sub>-derived aniline, and the resulting iron species can re-enter the cyclic pathway. This new strategy demonstrates the potential for development of catalytic reactions that incorporate abundant atmospheric N<sub>2</sub> into organic molecules.

### DE-SC0020315: Tandem Catalytic C-H Activation and N<sub>2</sub> Activation Using Iron Complexes

**Postdocs:** Daniel L. J. Broere, Erik J. T. Phipps

**Students:** Sean F. McWilliams, Samuel M. Bhutto, Junwen Xiao

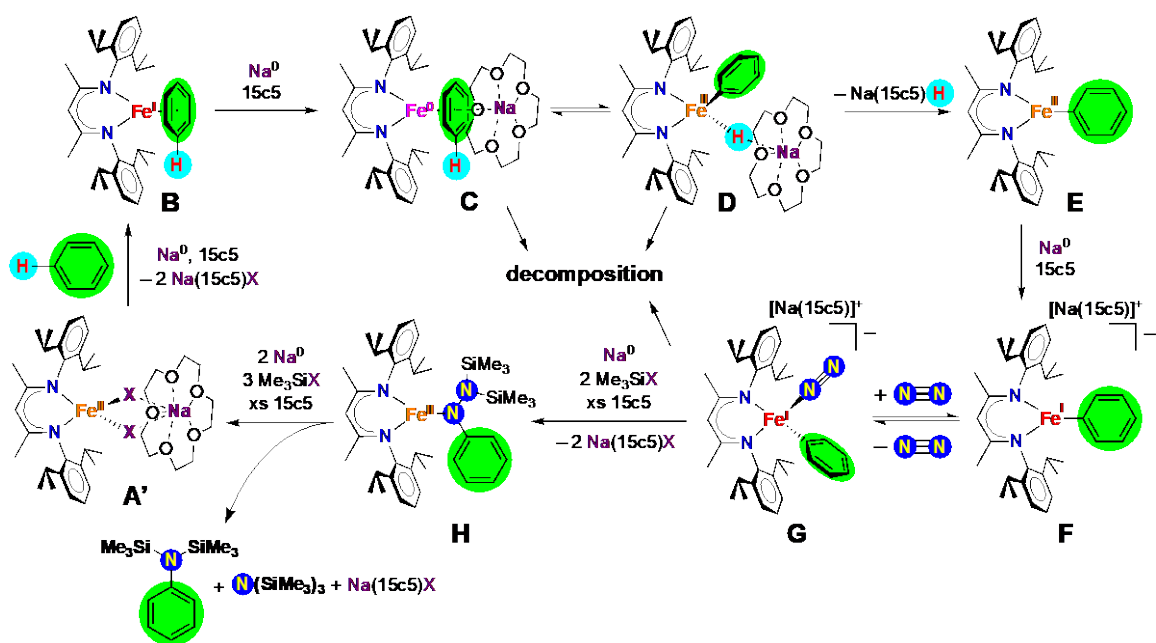
### RECENT PROGRESS

#### *Introduction*

This project aims at mechanistic understanding of the following transformation, which converts benzene and N<sub>2</sub> into substituted anilines.



We have proposed the cyclic mechanism shown in the illustration below, which is based on isolable iron compounds **A** through **H**. Starting from the left, it begins with binding of benzene (green) and C–H bond activation to form a phenyl fragment along the top. After reduction, the phenyl group migrates to N<sub>2</sub> upon silylation to form a C–N bond in silylated aniline products along the bottom. Our mechanistic efforts have focused on the distinctive steps of the reaction, namely (1) C–H activation by a high-spin metal center (**C** to **D**), (2) deposition of H (**D** to **E**), and (3) migration of a hydrocarbyl group from Fe to N<sub>2</sub> (**G** to **H**).

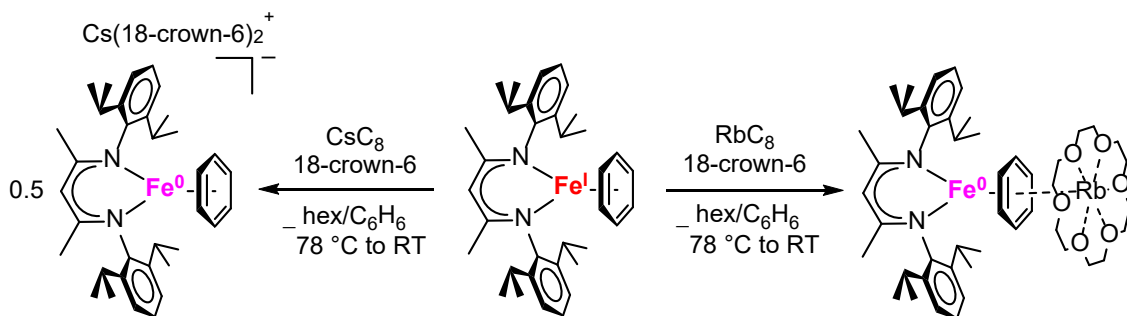


### Computational Studies on C–H Activation

We have used DFT to probe the details of the reversible C–H activation, which involves a change in spin state from **C** ( $S = 1$ ) to **D** ( $S = 2$ ). We located low-energy transition state structures (TS) on different potential energy surfaces, and the geometries of the TS indicate a concerted oxidative addition. The computations suggest that the unobserved *ortho* activation of toluene is thermodynamically feasible, even though experiments show amination in only *meta* and *para* positions. We conclude that the lack of *ortho*-aminated products is due to a kinetic barrier.

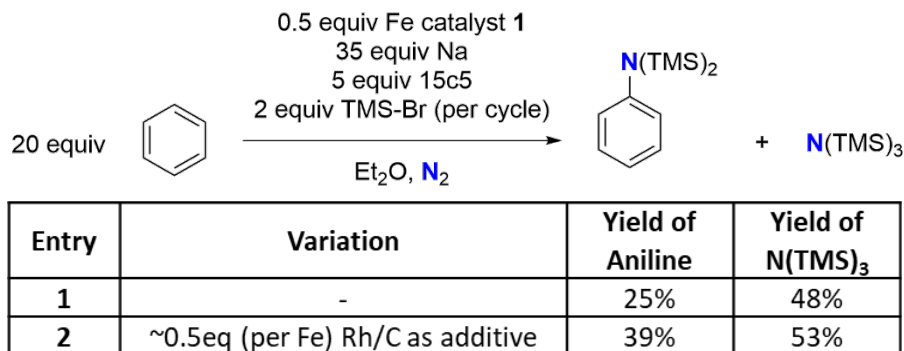
### Exploring Alkali Metal Effects on C–H Activation

The position of the equilibrium between **C** and **D** is dependent on whether the alkali metal is Na or K, and it is important to understand the energetics of these species as well as the rates of interconversion. In order to gain more data, we isolated and crystallographically characterized iron(0) benzene complexes with Rb and Cs to compare these with the reported Na and K analogues. The Rb complex has alkali metal coordinated to the arene (right), but the reduction with  $\text{CsC}_8$  instead results in an outer-sphere cation bound by two 18-crown-6 ether molecules (left).



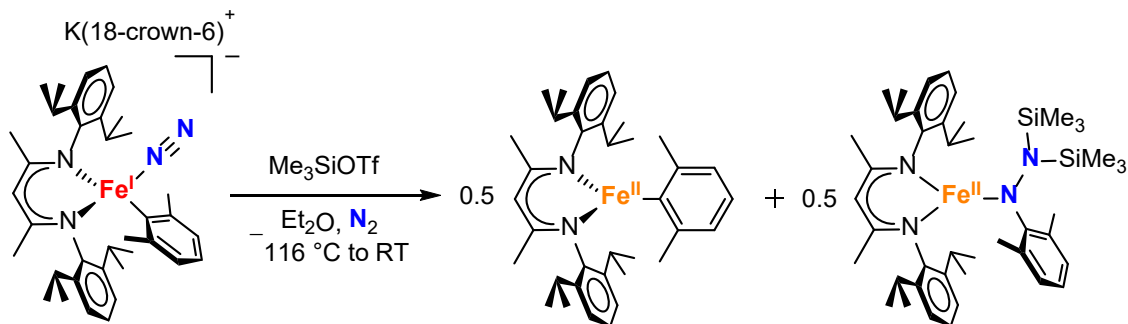
### Understanding H deposition

We hypothesized that known arene hydrogenation catalysts could deposit the H atom from **D** onto arene substrates. Indeed, the yield of silylated aniline increased when substoichiometric amounts (per iron) of Rh/C was added to the catalytic reaction mixture (see table below). In addition to being a practical solution, this lays the groundwork for mechanistic studies on H deposition.

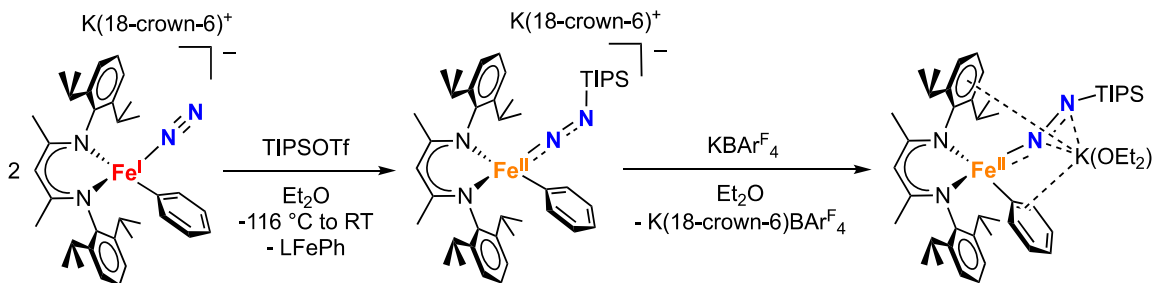


### Mechanistic Studies on Aryl Migration to an N<sub>2</sub>-derived Disilylhydrazido Ligand

In order to test the influence of sterics on the rate of migration (**G** to **H**), we prepared an iron(I) xylyl complex. Binding of N<sub>2</sub> at low temperature and subsequent silylation lead to formation of the xylylhydrazido complex, indicating that these kinetic studies will be feasible.

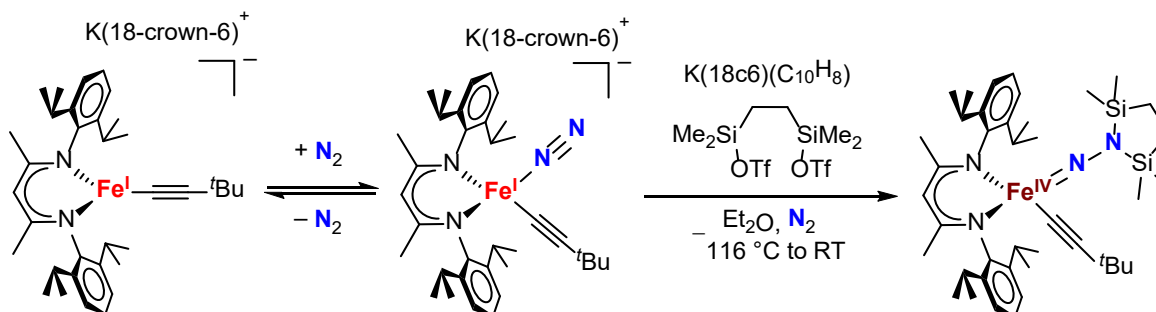


We have also varied the size of the silane. The bulky triisopropylsilyl triflate leads to isolable diazenido species, which are intermediates on the way to the disilylhydrazido species. The N–N bond in this new diazenido complex is weakened by a Lewis acidic K<sup>+</sup> cation.



### Isolation of Iron(IV) Hydrazido Complexes

In order to isolate potential intermediates in the new hydrocarbyl migration (G to H in the cycle above), we synthesized an iron(I) alkynyl complex illustrated below. It is observed to bind N<sub>2</sub> at low temperatures. Silylation of the N<sub>2</sub>-bound species resulted in the formation of an iron(IV) hydrazido complex, which was isolated and crystallographically characterized. We hypothesize that the alkynyl group does not migrate because the iron(IV) intermediate is stabilized by the greater  $\sigma$ -donating properties of the alkynyl ligand.



### Expanding the Substrate Scope

Previously, we demonstrated the ability to aminate toluene, *ortho*-xylene, and *meta*-xylene. We have now tested a number of heterocyclic substrates, and preliminary characterization of products with GC/MS indicates amination of the substrates in the table below. Other potential substrates such as naphthalene, anthracene, furan, thiophene, trifluorotoluene, and aryl halides do not give discernable amination products under the conditions employed.

Substrate	Product

### Publications Acknowledging this Grant in 2019-2021

#### (I) Intellectually led by this grant

1. McWilliams, S. M.; Broere, D. L. J.; Halliday, C. J. V.; Bhutto, S. M.; Mercado, B. Q.; Holland, P. L. Coupling Dinitrogen and Hydrocarbons through Aryl Migration. *Nature* **2020**, *584*, 221-226.
2. Weber, J. E.; Bhutto, S. M.; Genoux, A. T.-Y.; Holland, P. L. Dinitrogen Binding and Functionalization. In *Comprehensive Organometallic Chemistry IV* (O'Hare, Parkin, Meyer, Eds.), Elsevier, 2021, in press.

### **Awards and leadership activities 2018-2020**

- Watkins Lectureship, Wichita State University (2019)
- Editorial Board of *Chemical Society Reviews* (2019- )
- Editorial Board of *Chemical Science* (2019- )
- Guest Editor of *Chemical Reviews* Issue: "Reactivity of Nitrogen from the Ground to the Atmosphere" ([appeared 2020](#)) - 15 articles on various aspects of N<sub>2</sub> and nitrogen, including catalysis and nitrogenases
- [Yale Bouchet Honor Society](#) (2021)
- Volume Editor for Volume I of *Comprehensive Organometallic Chemistry IV* (to be published 2022) - 22 chapters ranging from bonding and computations, to spectroscopy, weak ligands like alkanes/N<sub>2</sub>/CO<sub>2</sub>, electrochemistry and redox-active ligands, spin states and paramagnetic organometallics, surface attachment, and modern trends in ligand and complex design. Each chapter was a collaborative endeavor between the author and myself.

## Catalyst Design Strategies for Multifunctional Metal-Promoted Zeolites in Methane Dehydroaromatization

Mustafizur Rahman<sup>1</sup>, Apoorva Sridhar<sup>1</sup>, Antonia Infantes-Molina<sup>2</sup>, Adam S. Hoffman<sup>3</sup>,  
Simon R. Bare<sup>3</sup>, Sheima J. Khatib<sup>1</sup>

<sup>1</sup> Department of Chemical Engineering, Texas Tech University, Lubbock, Texas 79409, USA

<sup>2</sup> Department of Inorganic Chemistry, Crystallography and Mineralogy. Faculty of Science. Campus de Teatinos, 29071 Malaga, Spain.

<sup>3</sup> Stanford Synchrotron Radiation Lightsource, SLAC National Accelerator Laboratory, Menlo Park, CA 94025, USA

### Presentation Abstract

Methane could be used as a building block in the chemicals manufacturing industry, but instead, large quantities of stranded shale-derived methane are being flared due to lack of existing infrastructures for their transportation to centralized processing facilities. The catalytic valorization of methane to aromatics and hydrogen, by the one-step non-oxidative methane dehydroaromatization reaction ( $6 \text{CH}_4 \rightarrow \text{C}_6\text{H}_6 + 9\text{H}_2$ ), MDA, is an attractive route for natural gas upgrade and can be implemented at the gas source, minimizing transportation costs. Our group is carrying out a systematic study of this catalytic process with the aim to answer some long-standing fundamental questions and develop strategies to mitigate technological challenges associated to MDA.

Zeolite-supported molybdenum catalysts are the most effective MDA catalysts studied so far, but they do not possess conversion and stability requirements for commercialization. Molybdenum carbide species are thought to constitute the active sites for MDA and are formed when the zeolite-supported Mo oxide species in the as-prepared catalysts are exposed to methane in the first minutes of reaction. Our group has discovered that the activation protocols employed to form the molybdenum carbides play a role on catalyst stability. We have tested different activation conditions and contrasted the structure of the fresh and spent catalysts to explain the difference in catalytic behavior. Our work has resulted in obtaining activated Mo/ZSM-5 catalysts that maintain remarkably stable benzene yields. Here we present our most recent work on the role that the acidity of the zeolite support plays on the Mo structure and performance, as well as the effect that addition of small amounts of Co and Ni promoters have on the catalytic performance.

**Grant or FWP Number:** DE-SC0019074

**PI:** Sheima J. Khatib

**Student(s):** Apoorva Sridhar, Kayla Lou Emerson

**Postdoc(s):** Mustafizur Rahman, Unmesh Menon

## RECENT PROGRESS

### *Effect of the Si/Al ratio of the ZSM-5 support on the structure and activity of Mo species*

While most work in the literature has found that catalyst deactivation by Mo aggregation can be prevented but working with catalysts with low Mo loadings, our work has demonstrated that it is possible to move to higher Mo loadings and maintain catalyst stability, despite the presence of Mo aggregates on the external surface of the zeolite, by activating Mo/ZSM-5 catalysts under reducing conditions with a slow temperature ramp. Such an activation protocol results in conversion of the Mo oxide species to their less mobile reduced form before subjecting them to reaction conditions. Based on these results we hypothesized that with higher Mo loadings and activation by temperature programmed reduction and carburization (TPR&C), we were not only preventing the external Mo aggregates from blocking the zeolite channel openings but at the same time the presence of larger amount of Mo was resulting in a larger migration of Mo species into the zeolite channels, consequently the presence of Mo sites anchored inside the channels was higher. This would also explain the higher benzene selectivity that these catalysts present compared to the He treated ones (80% versus 60%) given that the zeolite Brønsted acid sites (BAS) serve as anchoring points for the Mo oxide species inside the zeolite channels, which allows for the formation of confined Mo sites that enable shape selectivity to benzene. We further explored the effect that the number of BAS, or the Si/Al ratio would have on the dispersion and distribution of Mo species, their local structure around Mo centers (Mo coordination and cluster size), the nature of active sites, and the MDA performance in the catalysts that overwent our TPR&C activation protocol<sup>1</sup>. Previously other groups had speculated that the availability of the Al sites on the ZSM-5 support, could also impact the structures of the anchored Mo oxides, with a bigger presence of monomeric Mo oxide ( $\text{MoO}_2^{2+}$ ) species at lower Si/Al ratio, and dimeric oxides ( $(\text{Mo}_2\text{O}_5)^{2+}$ ) at higher Si/Al ratios and thus the observed differences in catalyst activity could be due to a different nature of the active sites. No direct proof for this speculation was provided spectroscopically.

In our study we prepared two groups of catalysts with low (3 wt%) and high (10 wt%) Mo loading using a HZSM-5 support with different Si/Al atomic ratios ranging from 15 to 40. In **Figure 1** we observe that as the Si/Al ratio increases, the benzene yield decreases for both low and high Mo loadings. The stability of the catalysts was also influenced by the Si/Al ration, as observed by the 1<sup>st</sup> order deactivation rate constants which drop as Si/Al increases regardless of the Mo loading (**Table 1**).

To confirm whether the local structure of the Mo sites was differing with the Si/Al ratio and could explain the differences in activity, we measured the Mo K-edge X-ray absorption

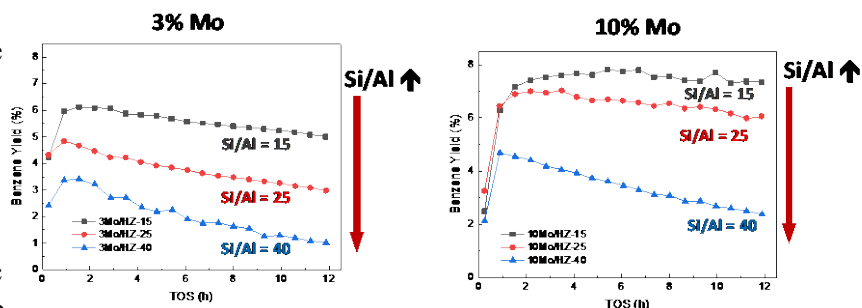


**Figure 1.** Benzene yield against TOS for 3Mo and 10 Mo catalysts using ZSM-5 with different Si/Al ratios. (Reactions performed with space velocity of 1550 ml/h-gcat in 9%  $\text{N}_2/\text{CH}_4$  at 700 °C.). After ref. [1].

**Table 1. First order deactivation rate constants ( $k_D$ ) for Mo/ZSM-5 catalysts with different Si/Al ratios. After ref. [1].**

Mo content (wt%)	Sample	$k_D$ ( $h^{-1}$ )
3% Mo	3Mo/HZ-15	0.02
	3Mo/HZ-25	0.04
	3Mo/HZ-40	0.11
10% Mo	10Mo/HZ-15	0.01
	10Mo/HZ-25	0.02
	10Mo/HZ-40	0.06

electronic transition providing information regarding the average local structure and geometry of the Mo species that are present. The intensity and peak position align better with that of  $MoO_3$  than  $MgMoO_4$ , indicating that the local structure of the Mo is not tetrahedral but octahedral in all of the catalysts. The presence of the peak in the Fourier transform of the EXAFS in the 3-4 Å range corresponds to the Mo-O-Mo scattering, indicating that there is longer range scattering present in the 10% sample compared to the 3%, suggesting the presence of small agglomerates of  $MoO_3$  species, which was in agreement with the XRD results (not shown here) where a small peak corresponding to  $MoO_3$  crystallites was detected only on the 10 wt% Mo as-prepared catalyst. The Mo K-edge XANES and Mo EXAFS data of the quenched 3 and 10 wt% Mo catalysts resembled that of  $Mo_2C$  indicating that the Mo oxide precursors were fully carburized after reduction in  $H_2$  and exposure to  $CH_4$  for two hours at high temperature (Figure 3). No features differentiate the magnitude of the Fourier transform of the EXAFS for the samples with different Si/Al ratios, suggesting that the Si/Al ratio is not a major factor in determining the local structure of the reduced Mo species.

Discarding differences in local structure of active sites being the cause for different catalytic properties at different Si/Al, an alternative explanation for the different catalytic behavior was found in the difference in the dispersion of the Mo species as a function of the Si/Al ratio. Analysis of TEM-EDS images, XPS derived surface

near edge spectra (XANES) and magnitude of the Fourier Transform extended X-ray absorption fine structure (EXAFS) spectra of Mo/HZSM-5 catalysts with Si/Al = 15 and 40 for the fresh as-prepared catalysts in ambient conditions, and the activated catalysts quenched after undergoing TPR in  $H_2$  followed by exposure to methane flow for two hours at 700°C. No differences were observed in the XANES spectra as a function of the Si/Al ratio for the as-prepared catalysts (Figure 2). All the catalysts displayed a pre-edge peak at around 20006.6 eV visible on the rising edge of the main  $1s \rightarrow 5p$  transition. This peak is assigned to the dipole-forbidden  $1s \rightarrow 4d$

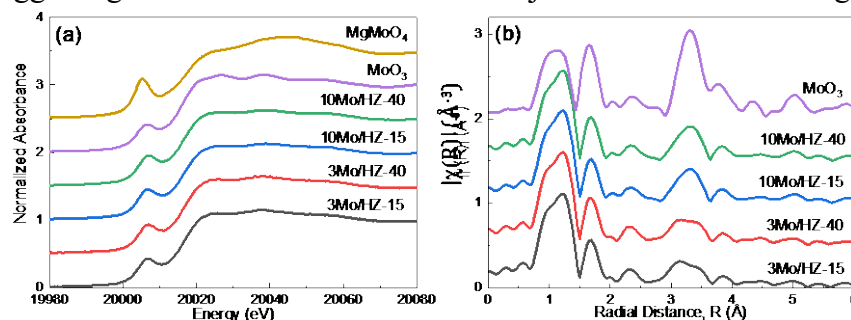


**Figure 2. (a) Mo K-edge XANES and the (b)  $k^2$ -weighted magnitude of the Fourier Transform EXAFS spectra of as-prepared catalysts. After ref. [1].**

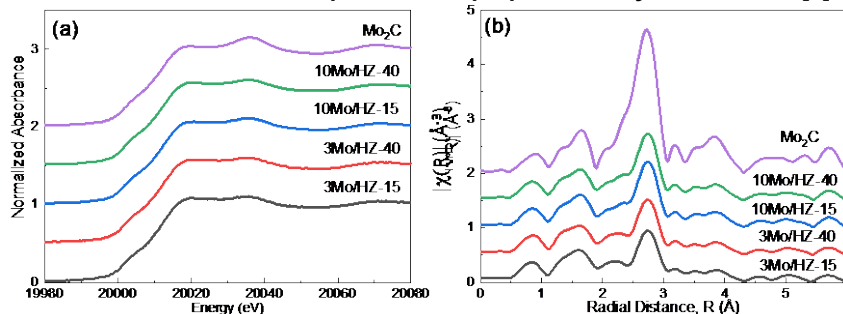


**Figure 3. (a) Mo K-edge XANES and (b)  $k^2$ -weighted magnitude of the Fourier Transform EXAFS spectra of carburized catalysts. After ref. [1].**

atomic compositions, measurement of the residual BAS by isopropylamine (IPA)-TPD, and textural properties obtained from N<sub>2</sub> adsorption/desorption isotherms (**Table 2**), suggested that the lower Si/Al ratio and higher Mo loading resulted in higher Mo occupation within the zeolite channels, which directly correlates with higher benzene selectivity. Importantly, we found that while temperature controlled H<sub>2</sub> pretreatment can improve the dispersion of the Mo species in the catalysts, even after 12 h of reaction, the Si/Al ratio has a stronger effect on catalyst stability. Low Si/Al ratios are required to maintain benzene yield over longer periods of time because they provide the necessary anchoring points required to accommodate active Mo sites in the zeolite channels.

**Table 2. Surface atomic ratios (XPS) and change in micropore volume from bare to metal impregnated zeolite (N<sub>2</sub> adsorption/desorption isotherms). After ref. [1].**

Sample	Mo/(Al+Si)	Drop in micropore volume
3Mo/HZ-15	0.018	10
3Mo/HZ-40	0.034	14
10Mo/HZ-15	0.089	26
10Mo/HZ-40	0.222	18

### ***Ex-situ formation of metal carbide species in Mo-X/ZSM-5 (X=Fe,Co, Ni) catalysts***

A catalyst design strategy employed to improve catalyst performance in MDA is the addition of metal promoters (X) to Mo/ZSM-5 catalysts. Based on our literature review, we have identified Fe, Co, and Ni as promising additives given their capacity to enhance both benzene yield and catalyst stability, and their relatively cheap price compared to other noble metal promoters. Most work in the literature shows that despite the improvement achieved in catalyst stability and benzene yield in presence of these promoters, the enhancement is short-lived. Given our discovery that Mo carbides formed by TPR&C were leading to much higher stability in production of benzene, we investigated how this activation method would affect Fe-promoted Mo/ZSM-5 catalysts<sup>2</sup>. We found that for a certain loading of Mo (6wt% Mo), there is an optimum loading of Fe (0.2 wt% Fe) that results in enhanced production of benzene and better catalyst stability. Furthermore, if the as-prepared catalyst is treated by the TPR&C activation protocol, the enhancement measured in presence of Fe additive is larger. Analysis of the conversion-selectivity plots suggest that the nature of the active sites is different in Mo versus Mo-Fe samples, but no bimetallic species were directly detected with the characterization techniques we employed. This was not surprising given the extremely low Fe loadings employed. TPR and XRD data did suggest that there was some interaction between Mo and Fe, given that the presence of Fe seems to affect the reducibility of Mo and the crystallinity of the MoO<sub>3</sub> clusters on the external surface of the zeolite. More recently, we extended our studies to employing Co and Ni additives with Mo/ZSM-5 catalysts<sup>3</sup>. We synthesized Mo-X (X = Co, Ni) catalysts using ZSM-5 as support and tested various loadings of X: 0.2, 0.6 and 1 wt% for a constant 6wt% loading of Mo. We found that the effect of adding Co and Ni to Mo/ZSM-5 catalysts varies depending on the type of pretreatment received. When Mo carbides were formed *in situ*, during the reaction induction period (after He pretreatment) the presence of additives was detrimental to their catalytic activity and benzene yield (see blue points in **Figure 4**). However, when the catalysts were treated in H<sub>2</sub>+CH<sub>4</sub>, a synergy between Mo and X was established for optimum loadings of both Co (0.6 wt%) and Ni (0.2 wt%) (red points in **Figure 4**), rendering catalysts that produced higher and more stable benzene yields. To confirm that indeed we had a synergy and not a sum of the performance of Mo and X sites in the Mo-X catalysts, we measured the catalytic activity of the single metal Co/ZSM-5 and Ni/ZSM-5 catalysts in MDA with the same loadings used in the Mo-

X catalysts; the results showed that in absence of Mo, these catalysts were just active to methane cracking, and no, or close to no products resulting from C-C coupling were detected (open symbols in **Figure 4**).

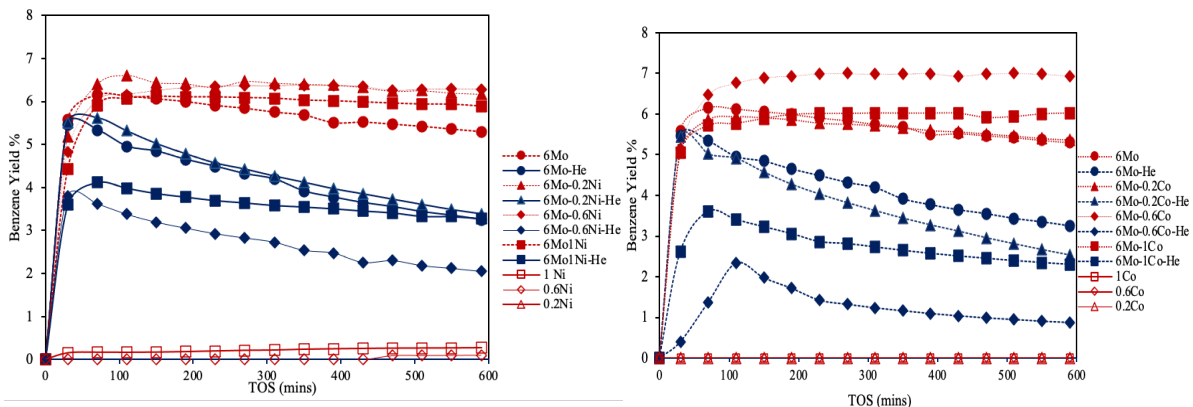


**Figure 4.** Benzene yield versus time on stream (TOS) for (a) Co-modified and (b) Ni-modified 6Mo/ZSM-5 catalysts. The blue symbols correspond to He-pretreated catalysts and red symbols correspond to precarburized catalysts. (The data points for unmodified 6Mo/ZSM-5, and single Co/ZSM-5 and Ni/ZSM-5 are included in both graphs as reference.). After ref. [3].

Structural characterization of the as-prepared catalysts by XRD<sup>3</sup> showed that when Mo and the additive species coexist, no crystalline mixed phases were observed. Similarly, the XRD patterns of the precarburized catalysts showed broad peaks corresponding to the Mo<sub>2</sub>C phase detected on the external surface in presence of both Ni and Co additives. TPR profiles of the catalysts<sup>3</sup> suggested that the presence of Co promotes the location of Mo oxides inside the zeolite channels since the intensity of the peak assigned to these species (at 580 °C) increased with Co loading, while Ni increases the reducibility of the Mo oxide species on the external surface of the zeolite and promotes the location of Mo oxides inside the channels. TPR profiles of the single metal Co and Ni/ZSM-5 samples showed no H<sub>2</sub> consumption in the case of Co, due to its high dispersion and low loading, and in the case of Ni, only a reduction peak attributed to reduction of unbound NiO was detected at the highest Ni loading employed. Further proof of the effect of X on Mo was observed by TGA of the as-prepared Mo-X catalysts (**Table 3**): with additive loading, the temperature at which the Mo species evaporate increases, thus the presence of additives further decreases the volatility and mobility of the Mo species, possibly enhancing the retention of the Mo species inside the zeolite channels and reducing catalyst deactivation.

**Table 3.** Evaporation temperature of metals in as-prepared catalysts. determined by TGA. After ref. [3].

Catalyst	Weight drop temperature (°C)
6Mo	750
6Mo-0.2Co	800
6Mo-0.6Co	815
6Mo-1Co	820
6Mo-0.2Ni	830
6Mo-0.6Ni	810
6Mo-1Ni	855

## References

- [1] Rahman, M., Infantes-Molina, A., Hoffman, A.S., Bare, S. R., Emerson, K.L., Khatib, S.J., *Fuel* **2020**, 278, 118290.
- [2] Sridhar, A., Rahman, M., Khatib, S.J., *ChemCatChem*, **2018**,10, 2571–2583
- [3] Sridhar, A., Rahman, M., Infantes-Molina, A., Wylie, B. J., Borcik, C.G., Khatib, S.J., *Appl. Catal. A: Gen.* **2020**, 589, 117247.

## Publications Acknowledging this Grant in 2018-2021

### (II) *Intellectually led by this grant*

- (1) Menon, U., Rahman, M., Khatib, J.S., A Critical Literature Review of the Advances in Methane Dehydroaromatization over Multifunctional Metal-Promoted Zeolite Catalysts, *Applied Catalysis A: General*, 2020, 608, 117870.
- (2) Rahman, M., Infantes-Molina, A., Hoffman, A., Bare, S., Emerson, K.L., Khatib\*, S.J., Effect of Si/Al ratio of ZSM-5 support on structure and activity of Mo species in methane dehydroaromatization, *Fuel*, 2020, 278, 118290.
- (3) Sridhar, A., Rahman, M., Infantes-Molina, A., Wylie, B. J., Borcik, C.G., Khatib\*, S.J., Bimetallic Mo-Co/ZSM-5 and Mo-Ni/ZSM-5 Catalysts for Methane Dehydroaromatization: A Study of the Effect of Pretreatment and Metal Loadings on the Catalytic Behavior, *Applied Catalysis A: General*, 2020, 589, 117247.
- (4) Rahman, M., Infantes-Molina, A., Boubnov, A., Bare, S.R., Stavitski, E., Sridhar, A., Khatib\*, S. J., Increasing the catalytic stability by optimizing the formation of zeolite-supported Mo carbide species ex situ for methane dehydroaromatization, *Journal of Catalysis*, **375**, 314-328 (2019).

## Awards or leadership activities during 2018-2020 calendar years

### Awards

- Whitacre Engineering Research Award (2020)
- NSF-CAREER Award (2019)
- Texas Tech Alumni Association Award (2019)
- TLPDC Spotlight Award for creatively enhancing student learning and engagement in the classroom (2019)
- Outstanding Poster Presentation Award at the Catalysis Gordon Conference (2018)
- AIChE Student Chapter Best Professor Award (2018)
- Mortar Board and Omicron Delta Kappa's Faculty Recognition Award (2018)

### Leadership Activities

- AIChE, Director (Board), Division of Catalysis & Reaction Engineering (2019-present)
- AIChE, Director (Board), Division of Fuels and Petrochemicals (2017-2020)
- AIChE, Vice Chair of the Diversity and Inclusion Task Force for Division of Catalysis & Reaction Engineering
- Southwest Catalysis Society, Director (Board) (2017-present)

- AIChE, Session Chair at Annual Meetings, Division of Catalysis & Reaction Engineering (2019-present)
- AIChE, Session Chair at Annual Meetings, Division of Fuels & Petrochemicals (2016-present)
- AIChE, NGCS (Natural Gas Conversion Symposium) Session Chair (2019)
- NAM (North American Catalysis Society Meeting) Session Chair (2019)
- Undergraduate Committee member at Department of Chemical Engineering at Texas Tech University (2017-present)
- STEP (STEM Teaching, Engagement and Pedagogy) Program Specialist at Texas Tech University (2017-present)
- Reviewer for peer-reviewed scientific journals including ACS Catalysis; Journal of Catalysis; Applied Catalysis B: General; Applied Catalysis A: General; Angewandte Chemie; Nature Communications; ChemCatChem; Chemical Engineering Science; Journal of Industrial and Engineering Chemistry; Journal of Membrane Science; Chemical Engineering Science; Materials Chemistry and Physics.
- Peer reviewer for DOE-BES (2017-present), NSF (2020-present), USDA (2018-present), ACS-PRF (2017-present), SSRL-SLAC (2020-present).

## Characterizing Supported Organovanadium Catalysts with Computational K-Edge XANES

Prajay Patel,<sup>1</sup> Jeremy Kropf,<sup>1</sup> David M. Kaphan,<sup>1</sup> Massimiliano Delferro,<sup>1</sup> and Cong Liu<sup>1\*</sup>

1. Chemical Sciences and Engineering Division, Argonne National Laboratory, Lemont, IL

A crucial consideration for supported heterogeneous catalysts is the non-uniformity of the active sites, particularly for Supported Organometallic Catalysts (SOMCs). Standard spectroscopic techniques, such as X-ray absorption spectroscopy (XAS), reflect the nature of the most populated sites, which are often intrinsically structurally distinct from the most active catalytic sites. With computational models, often only a few representative structures are used to depict catalytic active sites on a surface, even though there are numerous observable factors of surface heterogeneity that contribute to the kinetically favorable active species. A previously reported study on the mechanism of a surface organovanadium(III) catalyst [(SiO)V<sup>III</sup>(Mes)(THF)] for styrene hydrogenation yielded two possible mechanisms: heterolytic cleavage and redox cycling. These two mechanistic scenarios are challenging to differentiate experimentally since the kinetic readouts of the catalyst are identical. To showcase the importance of modeling surface heterogeneity and its effect on catalytic activity, density functional theory (DFT) computational models of a series of potential active sites of [(SiO)V<sup>III</sup>(Mes)(THF)] for the reaction pathways are applied in combination with kinetic Monte Carlo (kMC) simulations. Furthermore, the predicted V-H active species were confirmed by integrated XANES experiments and simulations. The most promising active site structure along with the optimal reaction pathway was identified and the effect of site heterogeneity was demonstrated. This work underscores the importance of modeling surface heterogeneity in computational catalysis.

### References:

- (1) Kaphan, D. M.; Ferrandon, M. S.; Langeslay, R. R.; Celik, G.; Wegener, E. C.; Liu, C.; Niklas, J.; Poluektov, O. G.; Delferro, M. Mechanistic Aspects of a Surface Organovanadium(III) Catalyst for Hydrocarbon Hydrogenation and Dehydrogenation. *ACS Catal.* **2019**, *9*(12), 11055-11066.
- (2) Patel, P.; Wells, R.; Kaphan, D.; Delferro, M.; Skodje, R. T.; Liu, C. Computational Investigation of the Role of Active Site Heterogeneity for a Supported Organovanadium (III) Hydrogenation Catalyst. *ACS Catal.* **2021**, *11*(12), 7257–7269.

## Controlling Catalyst Selectivity with Organic Monolayers on Metal Oxides

J. Will Medlin, Daniel K. Schwartz  
University of Colorado Boulder

### Presentation Abstract

Organic ligands are widely employed as surfactants for the synthesis of metal nanoparticles used in catalytic reactions. Recent studies have shown that leaving these ligands in place can have beneficial effects for catalyst performance, especially related to selectivity toward desired products. This observation suggests that it might be useful to add organic ligands even to uncoated metal nanoparticles on supported catalysts, and it has indeed been found that this strategy can lead to the ability to enhance selectivity in many reactions.

Rather than depositing ligands on the metal nanoparticles, a related strategy is to deposit them on the support, or on a catalytically active metal oxide surface. Support modification potentially avoids excessive blocking of precious metal sites but can hypothetically still provide the ability to control catalyst selectivity, especially for reactions in which rates are dominated by interfacial sites. By varying the structure and chemical functionality of the organic ligands, there are possibilities to improve catalyst activity, selectivity, and stability in reactions such as CO<sub>2</sub> hydrogenation and hydrodeoxygenation of biomass-derived oxygenates. Deposition of specific ligands on oxides can also profoundly influence catalytic activity in biphasic reaction mixtures through hydrophilic/hydrophobic effects.

### DE-SC0005239: Control of Complex Interfaces in Heterogeneous Catalysis Using Organic Monolayers

**Postdoc(s):** Jing Zhang

**Student(s):** Pengxiao Hao, Lucas Ellis, Ezra Baghdady, Zack Blanchette, Ben Greydanus, Alex Jenkins, Jordi Ballesteros-Soberanas

### RECENT PROGRESS

#### *Manipulating metal – metal oxide interfaces with organic monolayers*

The development of separate levers for controlling the bonding strength of different reactive species on catalyst surfaces is challenging but essential for the design of highly active and selective catalysts. For example, during CO<sub>2</sub> reduction, production of CO often requires balancing a trade-off between the adsorption strength of the reactant and product states: weak binding of CO is desirable from a selectivity perspective, but weak binding of CO<sub>2</sub> leads to low activity. Here, we demonstrated a new method of controlling both CO<sub>2</sub> adsorption and CO desorption over supported metal catalysts by employing a single self-assembly step where organic monolayer films were deposited on the catalyst support.

Binding of phosphonic acid monolayers on supported Pt and Pd catalysts weakened CO

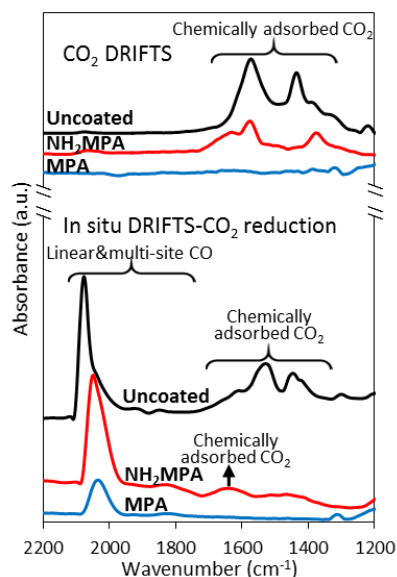


Figure 1: CO<sub>2</sub> infrared spectroscopy (top) and in situ DRIFTS during CO<sub>2</sub> hydrogenation (bottom) on Pt/TiO<sub>2</sub>. Functionalization with methyl phosphonic acid (MPA) weakened CO adsorption and nearly eliminated CO<sub>2</sub> adsorption sites, but use of an amine functional groups restored CO<sub>2</sub> adsorption and catalytic activity.

hydrogenation (RH) activity, with the degree of inhibition trending with the thiol surface coverage. This suggests that thiols do not strongly interact with the reactants and simply serve to block active sites on the Pd surface. PAs, on the other hand, were found to enhance RH when furfuryl alcohol (FA) was used as the reactant. Density functional theory calculations suggested that this enhancement was due to hydrogen-bonding interactions between FA-derived surface intermediates and PA modifiers. Here, installation of hydrogen-bonding groups on the Pd surface served to preferentially stabilize RH product states. Furthermore, the promotional effect on the RH of FA was observed to be greater when a higher-coverage PA was used, providing a rate more than twice that of the unmodified Pd/Al<sub>2</sub>O<sub>3</sub>.

Atomically dispersed precious metal catalysts maximize atom efficiency and exhibit unique reactivity. However, they are susceptible to sintering. Catalytic reactions occurring in reducing environments tend to result in atomically dispersed metals sintering at lower temperatures than in oxidative or inert atmospheres due to the formation of mobile metal-H or metal-CO complexes. We reported on a new approach to mitigate sintering of oxide supported atomically dispersed metals in a reducing atmosphere using organophosphonate self-assembled monolayers (SAMs). We demonstrated this for the case of atomically dispersed Rh on Al<sub>2</sub>O<sub>3</sub> and TiO<sub>2</sub> using a combination of CO probe molecule FTIR, temperature programmed desorption, and alkene hydrogenation rate measurements.

binding via a through-support effect. The weakened CO adsorption was generally accompanied by decreased adsorption and reactivity of CO<sub>2</sub>. However, by the incorporation of amine functions at controlled positions in the modifying film, CO<sub>2</sub> adsorption and hydrogenation reactivity could be restored (Fig. 1). Thus, both through-surface and through-space interactions could be manipulated by design of the organic modifiers. After surface modification, the catalysts exhibited significantly improved selectivity (up to ~99% at conversions near 50%) and activity toward CO production. Moreover, the rate of deactivation was notably reduced due to prevention of CO poisoning.

Interactions between surface adsorbed species can affect catalyst reactivity, and thus, the ability to tune these interactions is of considerable importance. Deposition of organic modifiers provides one method of intentionally introducing controllable surface interactions onto catalyst surfaces. In a study reported in *ACS Catalysis*, Pd/Al<sub>2</sub>O<sub>3</sub> catalysts were modified with either thiol or phosphonic acid (PA) ligands and tested in the hydrogenation of furanic species. The thiol modifiers were found to inhibit ring

Evidence suggests that SAM functionalization of the oxide provides physical diffusion barriers for the metal and weakens the interactions between the reducing gas and metal, thereby discouraging the adsorbate-promoted diffusion of metal atoms on oxide supports.

### ***Control of catalysis in biphasic mixtures***

Amphiphilic Janus particles with a catalyst selectively loaded on either the hydrophobic or hydrophilic region are promising candidates for efficient and phase-selective interfacial catalysis. In another paper published in ACS Applied Materials and Interfaces, we report the synthesis and characterization of Janus silica particles with a hydrophilic silica domain and a silane-modified hydrophobic domain produced via a wax masking technique. Palladium nanoparticles were regioselectively deposited on the hydrophobic side, and the phase selectivity of the catalytic Janus particles was established through the kinetic studies of benzyl alcohol hydrodeoxygenation (HDO). These studies indicated that the hydrophobic moiety provided nearly 100× the catalytic activity as the hydrophilic side for benzyl alcohol HDO. The reactivity was linked to the anisotropic catalyst design through microscopy of the particles. The catalysts were also used to achieve phase-specific compartmentalized hydrogenation and selective in situ catalytic degradation of a model oily pollutant in a complex oil/water mixture. We are currently applying a related strategy to prepare dynamic nanoparticle catalysts whose motion is controlled by reactions in solution.

Our work over the past year emphasized the effects of organic monolayers on both catalyst activity and stability, where SAMs were applied to both metal and metal oxide catalysts. We summarize the findings in our published work below. In addition to that work, we have continued to understand how organic coatings can be employed to create particles (such as Janus particles) that segregate to oil-water interfaces and catalyze reactions on one side of the interface; we have also used such Janus particles as active particles in single-particle tracking experiments. We are preparing to submit a manuscript in this area in August 2021.

### **Publications Acknowledging this Grant in 2018-2021**

#### *(III) Intellectually led by this grant*

1. Zhang, J.; Ellis, L. D.; Wang, B.; Dzara, M. J.; Sievers, C.; Pylypenko, S.; Nikolla, E.; Medlin, J. W., Control of interfacial acid–metal catalysis with organic monolayers. *Nature Catalysis* **2018**, *1* (2), 148-155.
2. Hao, P.; Schwartz, D. K.; Medlin, J. W., Phosphonic acid promotion of supported Pd catalysts for low temperature vanillin hydrodeoxygenation in ethanol. *Applied Catalysis A: General* **2018**, *561*, 1-6.
3. Hao, P.; Schwartz, D. K.; Medlin, J. W., Effect of surface hydrophobicity of Pd/Al<sub>2</sub>O<sub>3</sub> on vanillin hydrodeoxygenation in a water/oil system. *ACS Catalysis* **2018**, *8* (12), 11165-11173.

4. Ellis, L. D.; Ballesteros-Soberanas, J.; Schwartz, D. K.; Medlin, J. W., Effects of metal oxide surface doping with phosphonic acid monolayers on alcohol dehydration activity and selectivity. *Applied Catalysis A: General* **2019**, *571*, 102-106.
5. Ballesteros-Soberanas, J.; Ellis, L. D.; Medlin, J. W., Effects of Phosphonic Acid Monolayers on the Dehydration Mechanism of Aliphatic Alcohols on TiO<sub>2</sub>. *ACS Catalysis* **2019**, *9* (9), 7808-7816.
6. Greydanus, B.; Schwartz, D. K.; Medlin, J. W., Controlling catalyst-phase selectivity in complex mixtures with amphiphilic janus particles. *ACS applied materials & interfaces* **2019**, *12* (2), 2338-2345.
7. Jenkins, A. H.; Musgrave, C. B.; Medlin, J. W., Enhancing Au/TiO<sub>2</sub> catalyst thermostability and coking resistance with alkyl phosphonic-acid self-assembled monolayers. *ACS applied materials & interfaces* **2019**, *11* (44), 41289-41296.
8. Zhang, J.; Asokan, C.; Zakem, G.; Christopher, P.; Medlin, J. W., Enhancing Sintering Resistance of Atomically Dispersed Catalysts in Reducing Environments with Organic Monolayers. *Green Energy & Environment* **2021**.
9. Zhang, J.; Deo, S.; Janik, M. J.; Medlin, J. W., Control of Molecular Bonding Strength on Metal Catalysts with Organic Monolayers for CO<sub>2</sub> Reduction. *Journal of the American Chemical Society* **2020**, *142* (11), 5184-5193.
10. Sá, J.; Medlin, J. W., On-the-fly catalyst modification: strategy to improve catalytic processes selectivity and understanding. *ChemCatChem* **2019**, *11*, 3355-3365.
11. Coan, P. D.; Farberow, C. A.; Griffin, M. B.; Medlin, J. W., Organic Modifiers Promote Furfuryl Alcohol Ring Hydrogenation via Surface Hydrogen-Bonding Interactions. *ACS Catalysis* **2021**, *11*, 3730-3739.
12. Coan, P. D.; Griffin, M. B.; Ciesielski, P. N.; Medlin, J. W., Phosphonic acid modifiers for enhancing selective hydrodeoxygenation over Pt catalysts: The role of the catalyst support. *J. of Catal.* **2019**, *372*, 311-320.

(IV) *Jointly funded by this grant and other grants with intellectual leadership by other funding sources*

13. Coan, P. D.; Ellis, L. D.; Griffin, M. B.; Schwartz, D. K.; Medlin, J. W., Enhancing Cooperativity in Bifunctional Acid-Pd Catalysts with Carboxylic Acid-Functionalized Organic Monolayers. *J. Phys. Chem. C* **2018**, *122* (12), 6637-6647.

#### **Awards or leadership activities during 2018-2020 calendar years**

Journal associate editorship: *Catalysis Science and Technology* (since 2016)

Conference leadership: Technical program co-chair for 2020 International Congress on Catalysis (ICC) Meeting. Meeting was canceled due to the pandemic after technical program had been fully developed.

Department leadership: Dept. chair of Chemical and Biological Engineering, 2020-present.

Jeffrey D. Rimer

## Recent Advancements in the Design of Zeolite Catalysts with Reduced Diffusion Limitations

Jeffrey D. Rimer

University of Houston, William A. Brookshite Department of Chemical and Biomolecular Engineering, 4726 Calhoun Road, Houston, TX 77204-4004, USA

### Presentation Abstract

This talk will summarize our work on the rational design of zeolite catalysts, guided by the development of improved structure-performance relationships, aiming to identify next-generation heterogeneous catalysts. Realization of these goal requires concerted efforts in catalyst synthesis, testing, and modeling where the impact relies not only in the novelty and versatility of our approach, but also in the selection of economically-viable routes to generate improved catalysts for commercialization. This project has focused on three objectives: (1) Design of silicon-zoned zeolites for improved catalytic performance where or studies have shown that these materials enhance catalyst lifetime and alter selectivity; (2) Preparation of various nanosized and hierarchical zeolites with reduced mass transport limitations to minimize coking and alter catalyst activity; and (3) A new approach to reduce diffusion limitations in zeolite with varying pore dimensions involving the introduction of surface protrusions (referred to as “fins”) that dramatically improve catalyst performance.

### DE-SC0014468: Optimizing Zeolite Catalysts for the Conversion of Methanol to Hydrocarbons

**Postdoc(s):** Seungwan Seo

**Student(s):** Thuy T. Le, Heng Dai, Kumari Shilpa, Rishabh Jain, Chenfeng Huang

### RECENT PROGRESS

#### *Spontaneous assembly of self-pillared zeolite catalysts*

Conventional methods to prepare hierarchical zeolites depend upon the use of organic structure-directing agents and often require multiple synthesis steps with limited product yield and Brønsted acid concentration. Here we will discuss how the use of MEL- or MFI-type zeolites as crystalline seeds induces the spontaneous formation of self-pillared pentasil zeolites, thus avoiding, for the first time, the use of any organic or branching template for the crystallization of these hierarchical structures (Fig. 1A). The mechanism of formation was evaluated by time-resolved electron microscopy to provide evidence for the heterogeneous nucleation and growth of sequentially-branched nanosheets from amorphous precursors (Fig. 1B). The resulting hierarchical zeolites have large external surface area and high percentages of external acid sites, which markedly improves their catalytic performance in the Friedel craft alkylation and methanol to hydrocarbons reactions. These findings highlight a facile, commercially-viable synthesis method to reduce mass transport limitations and improve the performance of zeolite catalysts.

### ***Synthesis and testing of finned zeolite catalysts***

There is growing evidence for the advantages of synthesizing nano-sized zeolites with markedly reduced internal diffusion limitations for enhanced performance in catalysis and adsorption. Producing zeolite crystals with sizes less than 100 nm, however, is nontrivial, often requires the use of complex organics, and typically results in small product yield. Here, we will present an alternative approach to enhance mass transport properties of zeolites by the epitaxial growth of fin-like protrusions on seed crystals (Fig. 1C,D). We validated this generalizable methodology on two common zeolites with 3-dimensional pores (ZSM-5 and ZSM-11) and confirmed that fins are in crystallographic registry with the underlying seeds, and that secondary growth does not impede access to micropores. Molecular modelling and time-resolved titration experiments of finned zeolites probed internal diffusion and revealed substantial improvements in mass transport, consistent with catalytic tests with the methanol-to-hydrocarbon (MTH) reaction showing that these structures behave as pseudo nanocrystals with sizes commensurate to that of the fin (Fig. 1E).

We will also present recent findings showing that this approach can be applied to catalysts with restrictive pore networks. Notably, we have shown that finned ferrierite (FER), a commercial zeolite with 2-dimensional pores, behaves as a pseudo nanoparticle with dimensions smaller than any reported ferrierite catalyst in literature. Catalytic tests of both in-house and commercial ferrierite using 1-butene isomerization as a benchmark reaction reveal as much as a 3-fold enhancement of catalyst lifetime and an increase of 8 to 12% selectivity to isobutene for finned samples compared to their corresponding seeds. Collectively, these findings highlight the general applicability and advantages of introducing fins through facile and tunable post-synthesis modification to impart material properties resembling zeolite nanoparticles that are otherwise unattainable by conventional synthesis methods.

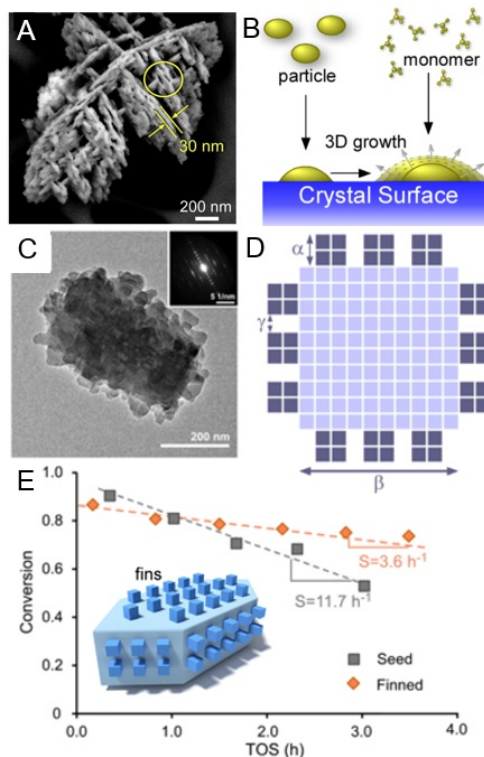


**Fig. 1.** (A) Self-pillared zeolite (MFI type) with multiple nanosheets (ca. 30 nm); (B) Diverse nonclassical pathways of zeolite growth; (C,D) Finned zeolite (commercial ZSM-5) with fins of size  $\alpha$  epitaxially grown on a seed of size  $\beta$ ; (E) MTH reaction data of finned zeolite ZSM-11.

### ***Elemental zoning enhances mass transport of zeolite catalysts***

Most approaches used to reduce mass transport restrictions focus on the synthesis of either hierarchical or nano-sized zeolites. Here, we will also demonstrate that the existence of a siliceous, catalytically-inactive exterior rim on ZSM-5 particles (i.e. Si-zoned zeolites) dramatically reduces diffusion limitations (Fig. 2A), leading to enhanced catalyst lifetime for the methanol-to-hydrocarbons reaction. Our findings revealed that binary inorganic and organic structure-directing agents enable a one-pot synthesis of silicon-zoned ZSM-5

catalysts (Fig. 2B,C) with diffusion properties that are characteristic of particles with much smaller size. Modeling cracking reactions have confirmed the passivation of external Brønsted acid sites (Fig. 2D). Operando UV-Vis diffuse reflectance spectroscopy revealed a marked reduction in external coking among Si-zoned samples. Core-shell analogues prepared by secondary growth confirmed that the introduction of a siliceous silicalite-1 exterior or pseudo ZSM-5 nanosheets grown over siliceous particles substantially reduces transport limitations and improves catalyst activity relative to ZSM-5 with a homogeneous acid site distribution (Fig. 2E).

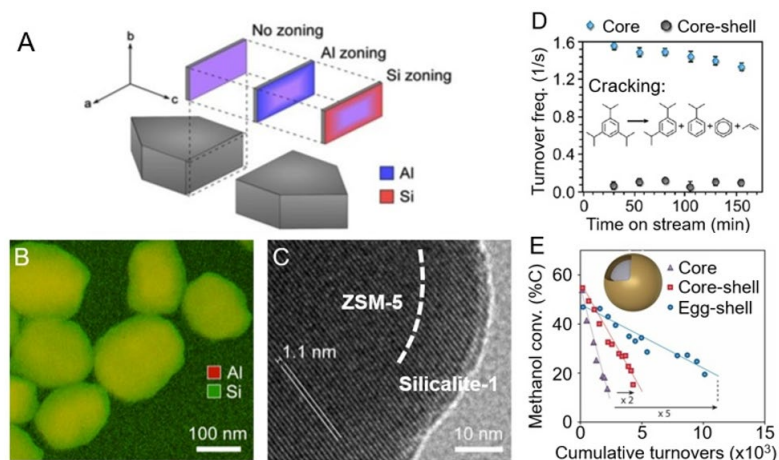


**Fig. 2.** (A) Zoning leads to spatial variations in acid sites. (B) Elemental mapping and (C) HRTEM image of core-shell ZSM-5@silicalite-1 particles. (D) Cracking (773 K) of the core-shell MFI catalyst. (E) MTH reaction (723 K) using core (ZSM-5), core-shell (ZSM-5@silicalite-1) and egg-shell (silicalite-1@ZSM-5) catalysts.

## Publications Acknowledging this Grant in 2018-2021

### (I) Intellectually led by this grant

- (1) Jain, R.; Chawla, A.; Linares, N.; Garcia Martinez, J.; Rimer, J.D. Spontaneous Pillaring of Pentasil Zeolites. *Adv. Mater.* **2021**, 33, 2100897.
- (2) Le, T.T.; Chawla, A.; Rimer, J.D. Impact of Acid Site Speciation and Spatial Gradients on Zeolite Catalysis. *J. Catal.* **2020**, 391, 56-68.
- (3) Dai, H.; Shen, Y.; Yang, T.; Lee, C.; Fu, D.; Agarwal, A.; Le, T.T.; Tsapatsis, M.; Palmer, J.C.; Weckhuysen, B.M.; Dauenhauer, P.J.; Zou, X.; Rimer, J.D. Finned Zeolite Catalysts. *Nat. Mater.* **2020**, 19, 1074-1080.
- (4) Bozhilov, K.N.; Le, T.T.; Qin, Z.; Terlier, T.; Palcic, A.; Rimer, J.D.; Valtchev, V. Time-resolved Dissolution Elucidates the Mechanism of Zeolite MFI Crystallization. *Sci. Adv.* **2021**, 7, eabg0454.
- (5) Ghosh, R.S.; Le, T.T.; Terlier, T.; Rimer, J.D.; Harold, M.P.; Wang, D. Enhanced Selective Oxidation of Ammonia in a Pt/Al<sub>2</sub>O<sub>3</sub>@Cu/ZSM-5 Core Shell Catalyst. *ACS Catal.* **2020**, 10, 3604-3617.
- (6) Kumar, M.; Berkson, Z.J.; Clark, R.J.; Shen, Y.; Prisco, N.A.; Zeng, Z.; Zheng, H.; McCusker, L.B.; Palmer, J.C.; Chmelka, B.F.; Rimer, J.D. Crystallization of Mordenite Platelets using Cooperative Organic Structure-directing Agents. *J. Am. Chem. Soc.* **2019**, 141, 20155-20165.

- (7) Qin, W.; Zhou, Y.; Rimer, J.D. Deleterious Effects of Non-framework Al Species on the Catalytic Performance of ZSM-5 Crystals Synthesized at Low Temperature. *React. Chem. Eng.* **2019**, *4*, 1957-1968.
- (8) Qin, W.; Jain, R.; Robles Hernandez, F.C.; Rimer, J.D. Organic-free Interzeolite Transformation in the Absence of Common Building Units. *Chem. Eur. J.* **2019**, *25*, 5893-5898.
- (9) Shen, Y.; Le, T.T.; Du, F.; Schmidt, J.E.; Filez, M.; Weckhuysen, B.M.; Rimer, J.D. Deconvoluting the Competing Effects of Framework Topology and Diffusion Path Length on Methanol-to-Hydrocarbons Reactions. *ACS Catal.* **2018**, *8*, 11042-11053.
- (10) Rimer, J.D.; Chawla, A.; Le, T.T. Crystal Engineering for Catalysis. *Annu. Rev. Chem. Biomol. Eng.* **2018**, *9*, 283-309.
- (11) Shen, Y.; Le, T.T.; Li, R.; Rimer, J.D. Optimized Synthesis of ZSM-11 Catalysts using 1,8-Diaminooctane as a Structure-Directing Agent. *ChemPhysChem* **2018**, *19*, 529-537.
- (12) Li, R.; Linares, N.; Sutjianto, J.G.; Chawla, A.; Garcia-Martinez, J.; Rimer, J.D. Ultrasmall Zeolite L Crystals Prepared from Highly-Interdispersed Alkali-Silicate Precursors. *Angew. Chem. Int. Ed.* **2018**, *57*, 11283-11288.
- (13) Kumar, M.; Choudhary, M.; Rimer, J.D. Transient Modes of Zeolite Surface Growth from 3D Gel-like Islands to 2D Single Layers. *Nat. Commun.* **2018**, *9*, 2129 (1-9).

***(II) Jointly funded by this grant and other grants with intellectual leadership by other funding sources***

- (14) Lu, P.; Ghosh, S.; Dorneles de Mello, M.; Kamaluddin, H.S.; Li, X.; Kumar, G.; Duan, X.; Abeykoon, M.; Boscoboinik, J.A.; Qi, L.; Dai, H.; Al-Thabaiti, S.; Narasimharao, K.; Khan, Z.; Rimer, J.D.; Bell, A.T.; Bhan, A.; Dauenhauer, P.J.; Mkhoyan, K.A.; Tsapatsis, M. Few-unit-cell MFI zeolite synthesized using a simple di-quaternary ammonium structure directing agent. *Angew. Chem. Int. Ed.* **2021**, DOI: 10.1002/anie.202104574 (In Press)
- (15) Hwang, A.; Le, T.T.; Shi, Z.; Dai, H.; Rimer, J.D.; Bhan, A. Effects of Diffusional Constraints on Lifetime and Selectivity in Methanol-to-Olefins Catalysis on HSAPO-34. *J. Catal.* **2019**, *369*, 122-132.
- (16) Li, R.; Chawla, A.; Linares, N.; Sutjianto, J.G.; Chapman, K.W.; Garcia-Martinez, J.; Rimer, J.D. Diverse Physical States of Amorphous Precursors in Zeolite Synthesis. *Ind. Eng. Chem. Res.* **2018**, *57*, 8460-8471.

**Awards or leadership activities during 2018-2021 calendar years**

2021 **National Academy of Inventors**, Senior Member

- 2021 **Associate Editor**, ACS Crystal Growth & Design
- 2020 **Edith and Peter O'Donnell Award in Engineering**, The Academy of Medicine, Engineering & Science of Texas (TAMEST)
- 2019 **Abraham E. Dukler Endowed Chair**, University of Houston
- 2018 **Norman Hackerman Award in Chemical Research**, The Welch Foundation
- 2018 **Class of Influential Researchers**, Industrial & Engineering Chemistry Research (ACS Publishing)
- 2018 **Emerging Investigators**, Molecular Systems Design & Engineering (RSC Publishing)

Wendy Shaw

## Understanding The Contribution of The Protein Scaffold to Catalysis by Creating Artificial Enzymes

Wendy J. Shaw, Joe Laureanti, Bojana Ginovska, Greg Schenter, Garry Buchko, John C. Linehan, Molly O'Hagan  
Pacific Northwest National Laboratory, Physical and Computational Sciences Directorate  
and Institute for Integrated Catalysis, Richland, WA 99354, USA

### Presentation Abstract

Enzymes are capable of shuttling gases, protons and electrons with great speed and precision. Enzymes are also capable of very specifically controlling the local environment around the catalytic active site. The superior rates and specificity of enzymes as compared to homogeneous catalysts demonstrate that the outer coordination sphere is as essential as the active site for efficient function. Our program focuses on trying to capture these desirable enzymatic traits in homogeneous catalysts. In order to achieve enzymatic rates and efficiencies for multi-proton and multi-electron reactions, as well as to understand how enzymes achieve such high performance, we are adding enzyme-inspired outer coordination spheres to molecular complexes. By covalently attaching Ni- or Rh-bis(diphosphine) complexes within a structured protein scaffold, we demonstrate that the complexes are activated for H<sub>2</sub> production or CO<sub>2</sub> hydrogenation, respectively. To develop a mechanistic understanding of the scaffold, we tested the hypothesis that a positively charged group near the active site of the CO<sub>2</sub> hydrogenation catalyst would enhance the catalytic rate by stabilizing the transition state. By modifying single amino acids to positive charges, including arginine, lysine, or histidine, we have demonstrated that a positive charge can enhance the catalytic rate, while negative charges placed near the active site inhibit activity. Using spectroscopy and molecular dynamics, we explore the effects of the influence of the outer coordination sphere on this model system. More broadly, this system provides a platform to understand the role of the scaffold for both enzymatic and synthetic systems. Combining these approaches allows us to explore and develop a mechanistic understanding of the role of the scaffold in both enzymes and molecular catalysts, allowing us to capture the essential features into homogeneous catalysts, with the potential of enhancing the rates, selectivity and specificity of the catalyst.

### FWP 47319: Low Temperature Catalytic Routes for Energy Carriers via Spatial and Chemical Organization

**PI:** Johannes Lercher

**Co-PI's:** Aaron Appel, Tom Autrey, Morris Bullock, David Dixon (U Alabama), Zdenek Dohnálek, John Fulton, Feng Gao, Bojana Ginovska, Vassiliki-Alexandra Glezakou, Jian Zhi Hu, Oliver Gutierrez Tinoco, Enrique Iglesia (UC Berkeley), Andreas Jentys, Abhi Karkamkar, Bruce Kay, Gregory Kimmel, Libor Kovarik, Joe Laureanti, Mal-Soon Lee, John Linehan, Roger Rousseau, Greg Schenter, Wendy Shaw, Janos Szanyi, Ba Tran, Huamin Wang, Yong Wang (Washington State U), Nancy Washton, Eric Wiedner.

**Catalytic rates with active site specificity**

Frank Abild-Pedersen<sup>a</sup>, Joakim Halldin-Stenlid<sup>a</sup>, Verena Streibel<sup>b</sup>, Tej S. Choksi<sup>c</sup>

<sup>a</sup>SLAC National Accelerator Laboratory, SUNCAT Center for Interface Science and Catalysis, 2575 Sand Hill Road, Menlo Park, California 94025, USA

<sup>b</sup>Technische Universität München, Walter Schottky Institut  
Am Coulombwall 4, 85748 Garching, Germany

<sup>c</sup>School of Chemical and Biomedical Engineering, Nanyang Technological University,  
62 Nanyang Drive, Singapore, 637459 Singapore

**Presentation Abstract**

The ability to predict catalytic activity from only simple structural as well as energetic features of nanoalloys is instrumental when designing heterogeneous catalysts. In this presentation I will describe a method for probing site-specific catalytic activity in which the stability of the site is applied as the only descriptor and with the ability to identify the optimal structural and chemical environments for the active site. By determining the site stability through an efficient coordination-based method we can obtain the energetics for complex nanostructures of ~10 nm size on-the-fly and with near DFT accuracy. In this presentation we examine our approach using the NO decomposition as the benchmark reaction and optimizing the catalytic activity of alloyed Pt nanoparticles. Focusing on the close-packed (111) surface we show how the activity per Pt atom can be increased by more than two orders of magnitude by the proper choice of particle shape and size and alloying with Au. Our methods present a general and unified stability-reactivity paradigm describing catalytic activity from the atomic- to the macro-scale.

**Grant or FWP Number: SUNCAT Center for Interface Science and Catalysis  
FWP10049**

**RECENT PROGRESS**

The SUNCAT FWP works towards developing a fundamental understanding of the factors governing catalyst phenomena at surfaces and interfaces. We focus on applying these insights or tools to processes that are of particular importance in energy transformation reactions – i.e. involving the sustainable production and use of fuels and chemicals. The SUNCAT-FWP focuses on basic principles describing events relevant for surface catalyzed chemical processes. The underlying philosophy behind the program is that by having a fundamental understanding what the catalyst structure is under different operating conditions, how durable it is, how the surface catalyzes chemical reactions, and how to engineer catalyst morphologies with higher activity and selectivity we can make a substantial leap in our ability to make predictions for new catalysts and processes. A

successful outcome requires the development of a theory that can describe phenomena in conventional temperature and pressure driven catalysis as well as reactions occurring at the complex solid-liquid interface in electrocatalysis. In the SUNCAT-FWP this work is based on a balanced approach that involves a close coupling between computational and experimental efforts where similar systems are explored in parallel to ensure that models are representative of the systems that they intend to describe and that experiments are updated or modified according to modeling results.

### ***Task 1: Catalysis Data Science and Computational Infrastructure***

We have developed a machine-learning (ML) approach to accelerate the computational screening of materials for catalysis. A challenging problem in computational catalysis is that the space of possible material configurations, including different compositions, crystal structures, and surface terminations is so large that it is impossible to sample with brute-force screening approaches. Therefore, combining DFT computation with ML techniques have a huge potential to speed up the search.

We have developed a framework for discovering new crystal polymorphs, where the generation of a diverse crystal structure space is combined with machine learning-accelerated selection of structures of interest within that space, targeting stable and metastable materials. A large set of crystal structures is generated for a given material composition, based on structures found in open crystal structure databases as well as bottom-up crystal prototype enumeration. In order to speed up the DFT computation, a machine learning model is iteratively trained on DFT data and used to select structures from the dataset for computation. This approach has recently been applied in collaboration with Task 2 to predict the existence of several new stable and metastable polymorphs of IrO<sub>3</sub> with high OER activity. A sample of active learning iterations is shown in Figure 2, where gaussian process regression was applied to predict the formation energy as well as the model uncertainty of all the IrO<sub>3</sub> polymorphs in the candidate set. The accuracy of the model improves quickly with the number of training points, leading to a significant speed up in the DFT exploration. [*Chemistry of Materials* **2020**, 32, 13, 5854–5863]

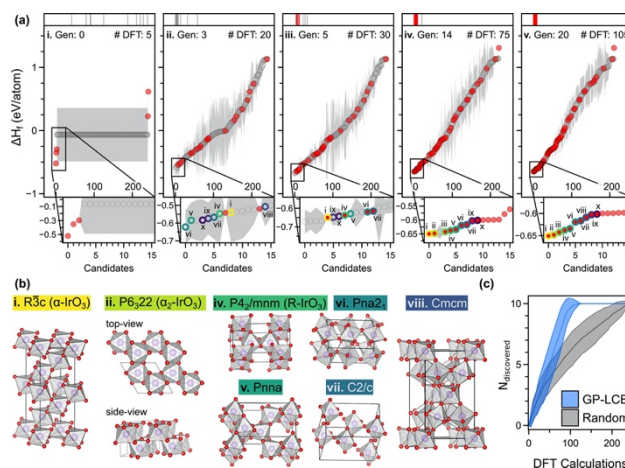


*Figure 2 Active learning model generation for the exploration of novel IrO<sub>3</sub> polymorphs, leading the discovery of several new crystal structures.*

Furthermore, we have developed a Bayesian approach for adsorption energy prediction, where we extend the single descriptor linear scaling relation to multi-descriptor linear regression models that can leverage the correlation between adsorption energy of any two

pair of adsorbates. With a large dataset of adsorption on binary alloy surfaces, we used Bayesian Information Criteria (BIC) as the model evidence to select the best linear regression model. Furthermore, Gaussian Process Regression (GPR) based on a convolution of physical properties of the metal-adsorbate complex was applied to predict the baseline residual of the selected model. This integrated Bayesian model selection and Gaussian process regression, dubbed as residual learning, can achieve performance comparable to standard DFT error (0.1 eV) for most adsorbate system.

For sparse and small datasets, we proposed an ad hoc Bayesian Model Averaging (BMA) approach to make a robust prediction. With this Bayesian framework, we significantly reduce the model uncertainty and improve the prediction accuracy. The possibilities of the framework for high-throughput catalytic materials exploration in a realistic setting is illustrated using large and small sets of both dense and sparse simulated dataset generated from a public database of bimetallic alloys available on Catalysis-Hub.org. [O. Mamun, K. T. Winther, J. R. Boes, T. Bligaard. *npj Comput Mater* 6, 177 (2020)], [Osman Mamun, Kirsten T. Winther, Jacob R. Boes, Thomas Bligaard. High-throughput calculations of catalytic properties of bimetallic alloy surfaces. *Scientific data* 6 (1), 76, (2019)]

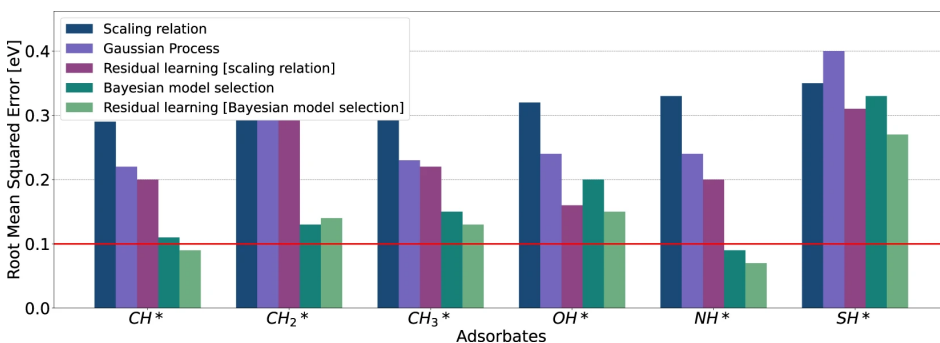


*Figure 3 Overview of model performance, demonstrating an improved adsorption energy prediction from residual learning, particularly when combined with Bayesian model selection.*

## **Task 2: Fundamentals of Electrochemistry**

We have been investigating new types of catalysts for electrochemical water oxidation, also known as the oxygen evolution reaction (OER), in both acid and alkaline environments. The OER remains a fundamental challenge as no known catalyst is able to operate near equilibrium. In acidic media, there are substantial, additional challenges involving durability; iridium oxide is the only catalyst that has been shown to drive the OER in acid in a manner sufficiently stable to cover the time-scales required for commercial technology.

To address these challenges, we took an approach combining experiment and computation to investigate ruthenium-based pyrochlores ( $A_2Ru_2O_7$ ,  $A = Y, Nd, Gd, Bi$ ) as catalysts for the OER in acid, tuning the electronic and geometric properties of the material through the nature of the A site element. The Ru-pyrochlores were synthesized via a sol-gel method and supported onto high surface area carbon for electrochemical studies. The Ru-based pyrochlores all showed significantly improved activity and stability compared to pure  $RuO_2$ , Figure 3. The reaction rates of the catalysts are dynamic over time, as are the

dissolution rates of both the A-site and Ru, depending on the particular pyrochlore formulation. Density functional theory (DFT) calculations were used to construct Pourbaix diagrams of these systems, revealing a thermodynamic driving force for dissolution, commensurate with experiments, Figure 3. The insights provided in this study help inform pathways to improved activity and durability for Ru-based OER catalysts in acid, enabling the development of improved proton exchange membrane (PEM) water electrolyzers. [M.A. Hubert, A.M. Patel, A. Gallo, Y. Liu, E. Valle, M. Ben-Naim, J. Sanchez, D. Sokaras, R. Sinclair, J.K. Nørskov, L.A. King, M. Bajdich, T.F. Jaramillo. *ACS Catal.* 2020.]

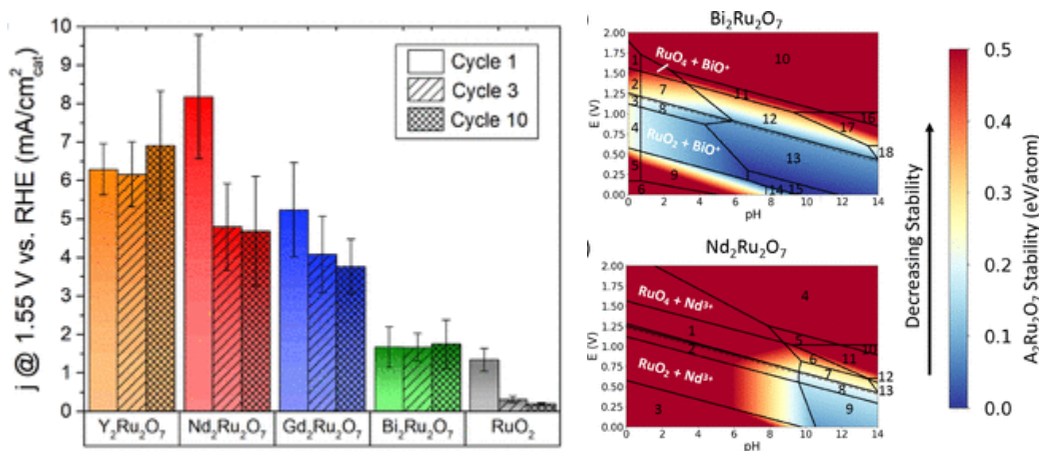


Figure 3 Activity and durability of Ru-based pyrochlore catalysts for the OER in acid, along with DFT-derived Pourbaix diagrams. [M.A. Hubert, et. al, *ACS Catalysis*, 2020]

In studying the OER in base, we have been exploring a new type of catalyst site motif based on confined transition metals. In particular, we synthesized and investigated nickel–iron electrocatalysts confined within the matrix of a layered zirconium phosphate host. We found that by confining the NiFe catalysts, mass activity could be improved by an order of magnitude compared to more conventional surface-adsorbed systems in 0.1 M KOH. The confined environments also facilitated high performance for heavily Fe-rich compositions (90%), demonstrating exceptional mass activity compared to conventionally-prepared Fe-rich OER catalysts. Density functional theory calculations provide insights into the electronic and geometric structure of the confined catalyst motif, leading to improved activity. This work reveals new approaches to enhancing catalyst activity through confinement at nanoscale dimensions. [J. Sanchez, M.B. Stevens, A.R. Young, A. Gallo, M. Zhao, Y. Liu, M.V. Ramos-Garcés, M. Ben-Naim, J.L. Colón, R. Sinclair, L.A. King, M. Bajdich, T.F. Jaramillo. *Adv. Energy Mater.*, 2003545. 2021].

### Task 3: Fundamentals of Thermal Catalysis

We have performed a systematic study that clearly identifies the geometric ensemble responsible for propene combustion on Pd and Pt catalysts. The work was a joint theory experimental collaboration where we used uniformly synthesized catalysts combined with insights from an approximative theoretical framework that enables direct assessment of site energies and surface stabilities. Catalysts with high Pt contents were shown to have high

TOFs and by explicitly studying a range of Pt/Pd catalyst particle sizes in a 1:1 ratio we identified that propene combustion is structure sensitive with the largest particles (10.2nm) showing five times higher TOF than the smallest particles (2.3nm).

Through detailed DFT calculations we identified undercoordinated step sites (211) as more active for breaking C-H, C-C, and O-O bonds and forming C-O bonds in the reaction compared to close-packed (111) surfaces. A combination of rate order measurements and a new model that can assess surface energies under operating conditions showed that a surface reconstruction caused by hydroxyl groups of water enhanced the formation of edge sites with CNs of 7–7, i.e. sites with (211)-type geometry, which were identified as the active site-ensemble for the combustion of propene. [An-Chih Yang, Tej Choksi, Verena Streibel, Hassan Aljama, Cody J Wrasman, Luke T Roling, Emmett D Goodman, Dionne Thomas, Simon R Bare, Roel S Sánchez-Carrera, Ansgar Schäfer, Yuejin Li, Frank Abild-Pedersen, Matteo Cargnello. *Proceedings of the National Academy of Sciences*, **2020**, 117, 14721-14729.]

To further elucidate the hydrocarbon chemistry on Pt/Pd nanoparticles and identify structure-property relationships, we synthesized well-defined NPs enabling us to compare variations in propane and propene combustion activity changing variables; Pt/Pd ratios, rate orders, active phase, and aging stability one parameter at a time. DFT calculations were performed to identify differences in activating the two reactants as a function of composition. The rate order results revealed the most significant differences between the two reactions. Our DFT calculations revealed that propene chemisorbs, whereas propane only physisorbs on noble metal surfaces.

This stronger binding of propene to the metal surface leads to negative rate orders for propene and oxygen, respectively. On the other hand, the weak binding of propane suggests that a higher propane partial pressure is needed to enhance propane combustion on the surface, and thus the rate orders for propane and oxygen are positive and negative, respectively. [An-Chih Yang, Verena Streibel, Tej S.Choksi, Hassan Aljama, Baraa Werghi, Simon R. Bare, Roel S. Sánchez-Carrera, Ansgar Schäfer, Yuejin Li, Frank Abild-Pedersen, Matteo Cargnello. *Journal of Catalysis*, **2021**, 401, 89-101.]

In a theory driven study of we introduced a computational framework that combined first-principle based kinetic simulations, high-throughput computations, and machine learning concepts combined with experimental verification of our catalyst candidates we investigated the dehydrogenation of propane. Our study involved many bimetallic alloys from the group of transition metals (Cu, Ag, Ag, Ni, Pt, Pd, Co, Rh, Ir, Ru, Re and Os). Our simulations identified Pt as the only pure metal catalyst with both

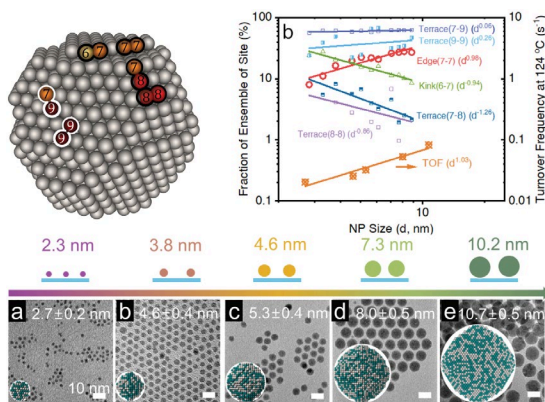


**Figure 4** Site ensembles on 4nm Pd/Pt nanoparticle, correlation between simulated site fractions and the experimental TOF at 124 °C for different size nanoparticles, and images of the size-specific synthesized nanoparticles.

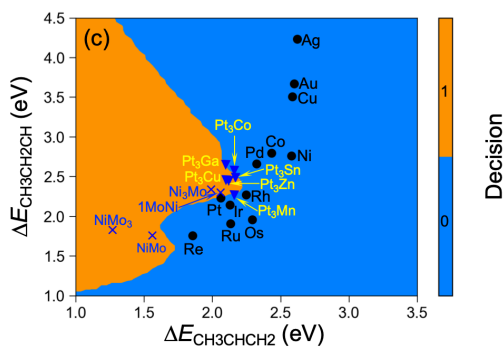


**Figure 5** Decision map for propylene production from propane as a function of energetic descriptors at 873K, 0.2bar  $C_3H_8$ ,  $C_3H_8/H_2=1/1$ , and 0.1% conversion.

reasonable propylene activity and selectivity, which explains the unique role of Pt in industrial application for propane dehydrogenation. In this study, we introduced a decision map (parameterized by two relevant  $C_3$  descriptors) based on a well-defined acquisition function enabling an effective screening of catalyst structures for the propane dehydrogenation reaction. The screening identified several interesting candidates, where many of them already had been experimentally reported as being promising catalysts for the reaction.

However, our screening also singled out NiMo as a very interesting candidate composition and our experimental collaborators verified that it has better propylene activity/selectivity than Pt. [Tao Wang, Xinjiang Cui, Kirsten T Winther, Frank Abild-Pedersen, Thomas Bligaard, Jens K Nørskov. *ACS Catalysis*, **2021**, 11, 6290-6297. ]

### Publications Acknowledging this Grant in 2018-2021

1. So Yeon Park, Hadi Abroshan, Xinjian Shi, Hyun Suk Jung, Samira Siahrostami, Xiaolin Zheng. CaSnO<sub>3</sub>: An Electrocatalyst for Two-Electron Water Oxidation Reaction to Form H<sub>2</sub>O<sub>2</sub>. *ACS Energy Letters*, **2019**, 4, 352-357.
2. Colin F. Dickens, Joseph H Montoya, Ambarish R Kulkarni, Michal Bajdich, Jens K. Nørskov . An electronic structure descriptor for oxygen reactivity at metal and metal-oxide surfaces. *Surface Science*, **2019**, 681, 122. 2019
3. Vanessa Bukas, Hyo Won Kim, Robert Sengpiel, Kristian Knudsen, Johannes Voss, Bryan McCloskey, Alan Luntz. Combining Experiment and Theory to Unravel the Mechanism of Two-Electron Oxygen Reduction at a Selective and Active Co-Catalyst. *ACS Catalysis*. **2018**
4. Elisabeth M. Dietze, Frank Abild-Pedersen, Philipp N. Plessow. Comparison of Sintering by Particle Migration and Ripening through First-Principles-Based Simulations. *The Journal of Physical Chemistry C*, **2018**, 122, 26563-26569.
5. Adam S. Hoffman , Joseph A. Singh, Stacey F. Bent, Simon R. Bare. In situ observation of phase changes of a silica-supported cobalt catalyst for the Fischer-Tropsch process by the development of a synchrotron-compatible in situ/operando powder X-ray diffraction cell. *Journal of Synchrotron Radiation*, **2018**, 25, 1673-1682.
6. Joseph A. Singh, Ang Cao, Julia Schumann, Tao Wang, Jens K. Nørskov, Frank Abild-Pedersen, Stacey F. Bent. Theoretical and Experimental Studies of CoGa Catalysts for the Hydrogenation of CO<sub>2</sub> to Methanol. *Catalysis Letters*, **2018**, 148, 3583-3591.
7. Robert Sandberg , Martin H. Hansen, Jens K. Nørskov , Frank Abild-Pedersen, Michal Bajdich. Strongly Modified Scaling of CO Hydrogenation in Metal Supported TiO Nanostripes. *ACS Catalysis*, **2018**, 8, 10555.
8. Cody J. Wrasman, Alexey Boubnov, Andrew R. Riscoe, Adam S. Hoffman, Simon R. Bare, Matteo Cargnello. Synthesis of Colloidal Pd/Au Dilute Alloy Nanocrystals and

- Their Potential for Selective Catalytic Oxidations. *Journal of American Chemical Society*, **2018**, 140, 12930-12939.
9. Ang Cao, Julia Schumann, Tao Wang, Linan Zhang, Jianping Xiao, Pallavi Bothra, Yuan Liu, Frank Abild-Pedersen, Jens K Nørskov. Mechanistic Insights into the Synthesis of Higher Alcohols from Syngas on CuCo Alloys. *ACS Catalysis*, **2018**, 8, 10148-10155.
  10. Hassan Aljama, Jens K Nørskov, Frank Abild-Pedersen. Tuning Methane Activation Chemistry on Alkaline Earth Metal Oxides by Doping. *The Journal of Physical Chemistry C*, **2018**, 122, 22544-22548.
  11. Melis S. Duyar, Charlie Tsai, Jonathan L. Snider, Joseph Singh, Alessandro Gallo, Jong Suk Yoo, Andrew J. Medford, Frank Abild-Pedersen, Felix Studt, Jakob Kibsgaard, Stacey Bent, Jens K. Nørskov, Thomas F. Jaramillo. Discovery of a highly active molybdenum phosphide catalyst for methanol synthesis from CO and CO<sub>2</sub>. *Angewandte Chemie*, **2018**, 130, 15265-15270.
  12. Emmett Goodman, Allegra A. Latimer, An-Chih Yang, Liheng Wu, Nadia Tahsini, Frank Abild-Pedersen, Matteo Cargnello. Low-Temperature Methane Partial Oxidation to Syngas with Modular Nanocrystal Catalysts. *ACS Applied Nano Materials*, **2018**, 1, 5258-5267.
  13. Leanne D. Chen, Michal Bajdich, J. Mark P. Martinez, Caroline M. Krauter, Joseph A. Gauthier, Emily A. Carter, Alan C. Luntz, Karen Chan, Jens K. Nørskov. Understanding the apparent fractional charge of protons in the aqueous electrochemical double layer. *Nature Communications*, **2018**, 9, 3202.
  14. Allegra A. Latimer, Arvin Kakekhani, Ambarish Kulkarni, Jens K. Nørskov. Direct Methane to Methanol: The Selectivity-Conversion Limit and Design Strategies. *ACS Catalysis*, **2018**, 8, 6894.
  15. Jong Suk Yoo, Julia Schumann, Felix Studt, Frank Abild-Pedersen, Jens K Nørskov. Theoretical investigation of methane oxidation on Pd (111) and other metallic surfaces. *The Journal of Physical Chemistry C*, **2018**, 122, 16023-16032.
  16. Shucheng Chen, Zhihua Chen, Samira Siahrostami, Drew Higgins, Dennis Nordlund, Dimosthenis Sokaras, Taeho Roy Kim, Yunzhi Liu, Xuzhou Yan, Elisabeth Nilsson, Robert Sinclair, Jens K. Nørskov, Thomas F. Jaramillo, Zhenan Bao. Designing Boron Nitride Islands in Carbon Materials for Efficient Electrochemical Synthesis of Hydrogen Peroxide. *Journal of the American Chemical Society*, **2018**, 140, 7851-7859.
  17. Arvin Kakekhani, Luke T. Roling, Ambarish Kulkarni, Allegra A. Latimer, Hadi Abroshan, Julia Schumann, Hassan Aljama, Samira Siahrostami, Sohrab Ismail-Beigi, Frank Abild-Pedersen, Jens K. Nørskov. On the Nature of Lone Pair–Surface Bonds and Their Scaling Relations. *Inorganic Chemistry*, **2018**, 57, 7222-7238.
  18. Joseph H. Montoya, Andrew Doyle, Jens K. Nørskov, Aleksandra Vojvodic. Trends in adsorption of electrocatalytic water splitting intermediates on cubic ABO<sub>3</sub> oxides. *Physical Chemistry Chemical Physics*, **2018**, 20, 3813-3818.
  19. Nuoya Yang, Xinyan Liu, Arun S. Asundi, Jens K. Nørskov, Stacey F. Bent. The Role of Sodium in Tuning Product Distribution in Syngas Conversion by Rh Catalysts. *Catalysis Letters*, **2018**, 148, 289
  20. Aayush Singh, Joseph H. Montoya, Brian Andrew Rohr, Charlie Tsai, Aleksandra Vojvodic, Jens K. Nørskov. Computational Design of Active Site Structures with

- Improved Transition-State Scaling for Ammonia Synthesis. *ACS Catalysis*, **2018**, *8*, 4017-4024.
21. Svante Hedström, Egon Campos Dos Santos, Chang Liu, Karen Chan, Frank Abild-Pedersen, Lars GM Pettersson. Spin Uncoupling in Chemisorbed OCCO and CO<sub>2</sub>—Two High-Energy Intermediates in Catalytic CO<sub>2</sub> Reduction. *The Journal of Physical Chemistry C*, **2018**, *122*, 12251-12258.
  22. Drew Higgins, Melissa Wette, Brenna M. Gibbons, Samira Siahrostami, Christopher Hahn, Maria Escudero-Escribano, Max Garcia-Melchor, Zachary Ulissi, Ryan C. Davis, Apurva Mehta, Bruce M. Clemens, Jens K. Nørskov, Thomas F. Jaramillo. Copper Silver Thin Films with Metastable Miscibility for Oxygen Reduction Electrocatalysis in Alkaline Electrolytes. *ACS Applied Energy Materials*, **2018**, *1*, 1990-1999.
  23. Luke T Roling, Frank Abild-Pedersen. Structure-Sensitive Scaling Relations: Adsorption Energies from Surface Site Stability. *ChemCatChem*, **2018**, *10*, 1643-1650.
  24. Julia Schumann, Andrew J Medford, Jong Suk Yoo, Zhi-Jian Zhao, Pallavi Bothra, Ang Cao, Felix Studt, Frank Abild-Pedersen, Jens K Nørskov. Selectivity of synthesis gas conversion to C<sub>2</sub>+ oxygenates on fcc (111) transition metal surfaces. *ACS Catalysis*, **2018**, *8*, 3447-3453.
  25. Liang Yu, Laia Vilella, Frank Abild-Pedersen. Generic approach to access barriers in dehydrogenation reactions. *Communications Chemistry*, **2018**, *1*, 2.
  26. Zhiyi Lu, Guangxu Chen, Samira Siahrostami, Zhihua Chen, Kai Liu, Jin Xie, Lei Liao, Tong Wu, Dingchang Lin, Yayuan Liu, Thomas F. Jaramillo, Jens K. Nørskov, Yi Cui. High-efficiency oxygen reduction to hydrogen peroxide catalysed by oxidized carbon materials. *Nature Catalysis*, **2018**, 156-162.
  27. Ariel Jackson, Alaina Strickler, Drew Higgins, Thomas F. Jaramillo. Engineering Ru@Pt Core-Shell Catalysts for Enhanced Electrochemical Oxygen Reduction Mass Activity and Stability. *Nanomaterials*, **2018**, *8*, 38.
  28. Shucheng Chen, Zhihua Chen, Samira Siahrostami, Taeho Roy Kim, Dennis Nordlund, Dimosthenis Sokaras, Stanislaw Nowak, John W. F. To, Drew Higgins, Robert Sinclair, Jens K. Nørskov, Thomas F. Jaramillo, Zhenan Bao. Defective Carbon-Based Materials for the Electrochemical Synthesis of Hydrogen Peroxide. *ACS Sustainable Chemistry & Engineering*, **2018**, *6*, 311-317.
  29. Mario V. Ramos-Garcés, Joel Sanchez, Kálery La Luz-Rivera, Daniel E. Del Toro-Pedrosa, Thomas F. Jaramillo, Jorge L. Colón. Morphology control of metal-modified zirconium phosphate support structures for the oxygen evolution reaction. *Dalton Transactions*, **2020**, *49*, 3892-3900.
  30. Arun Somayaji Asundi, Adam S. Hoffman, Pallavi Bothra, Alexey Boubnov, Fernando Vila, Nuoya Yang, Joseph A. Singh, Li Zeng, James A. Raiford, Frank Abild-Pedersen, Simon R. Bare, Stacey F. Bent. Understanding Structure-Property Relationships of MoO<sub>3</sub>-Promoted Rh Catalysts for Syngas Conversion to Alcohols. *Journal of American Chemical Society*. **2019**,
  31. Sang-Jun Lee, Charles J Titus, Roberto Alonso Mori, Michael L Baker, Douglas A Bennett, Hsiao-Mei Cho, William B Doriese, Joseph W Fowler, Kelly J Gaffney, Alessandro Gallo, Johnathon D Gard, Gene C Hilton, Hoyoung Jang, Young Il Joe, Christopher J Kenney, Jason Knight, Thomas Kroll, Jun-Sik Lee, Dale Li, Donghui Lu, Ronald Marks, Michael P Minitti, Kelsey M Morgan, Hirohito Ogasawara, Galen C O'Neil, Carl D Reintsema, Daniel R Schmidt, Dimosthenis Sokaras, Joel N Ullom,

- Tsu-Chien Weng, Christopher Williams, Betty A Young, Daniel S Swetz, Kent D Irwin, Dennis Nordlund. Soft X-ray spectroscopy with transition-edge sensors at Stanford Synchrotron Radiation Lightsource beamline 10-1. *Review of Scientific Instruments*, **2019**, 90, 113101.
32. Alessandro Gallo, Jonathan L. Snider, Dimosthenis Sokaras, Dennis Nordlund, Thomas Kroll, Hirohito Ogasawara, Libor Kovarik, Melis S. Duyar, Thomas F. Jaramillo. Ni<sub>5</sub>Ga<sub>3</sub> catalysts for CO<sub>2</sub> reduction to methanol: Exploring the role of Ga surface oxidation/reduction on catalytic activity. *Applied Catalysis B: Environmental*, **2020**, 267.
  33. Hassan Aljama, Frank Abild-Pedersen. Accessing the C–C transition state energy on transition metals. *Physical Chemistry Chemical Physics*. **2019**
  34. Laurie A. King, McKenzie A. Hubert, Christopher Capuano, Judith Manco, Nemanja Danilovic, Eduardo Valle, Thomas R. Hellstern, Katherine Ayers, Thomas F. Jaramillo. A non-precious metal hydrogen catalyst in a commercial polymer electrolyte membrane electrolyser. *Nature Nanotechnology*, **2019**, 14, 1071-1074.
  35. Joel Sanchez , Thomas R. Hellstern, Laurie A. King, Thomas F. Jaramillo. Surface Engineering of 3D Gas Diffusion Electrodes for High-Performance H<sub>2</sub> Production with Nonprecious Metal Catalysts. *Advanced Energy Materials*, **2019**, 1901824.
  36. Theis L. Skafte, Zixuan Guan, Michael L. Machala, Chirranjeevi B. Gopal, Matteo Monti, Lev Martinez, Eugen Stamate, Simone Sanna, Jose A. Garrido Torres, Ethan J. Crumlin, Max García-Melchor, Michal Bajdich, William C. Chueh, Christopher Graves. Selective high-temperature CO<sub>2</sub> electrolysis enabled by oxidized carbon intermediates. *Nature Energy*. **2019**
  37. Yecun Wu, Stefan Ringe, Chun-Lan Wu, Wei Chen, Ankun Yang, Hao Chen, Michael Tang, Guangmin Zhou, Harold Y. Hwang, Karen Chan, Yi Cui. A Two-Dimensional MoS<sub>2</sub> Catalysis Transistor by Solid-State Ion Gating Manipulation and Adjustment (SIGMA). *Nano Letters*. **2019**
  38. Sara R. Kelly, Xinjian Shi, Seoin Back, Lauren Vallez, So Yeon Park, Samira Siahrostami, Xiaolin Zheng, Jens K. Nørskov. ZnO As an Active and Selective Catalyst for Electrochemical Water Oxidation to Hydrogen Peroxide. *ACS Catalysis*, **2019**, 9, 4593-4599.
  39. Kun Jiang, Seoin Back, Austin J. Akey, Chuan Xia, Yongfeng Hu, Wentao Liang, Diane Schaak, Eli Stavitski, Jens K. Nørskov, Samira Siahrostami, Haotian Wang. Highly selective oxygen reduction to hydrogen peroxide on transition metal single atom coordination. *Nature Communications*, **2019**, 10, 3997.
  40. Alaina L. Strickler, Raul A. Flores, Laurie A. King, Jens K. Nørskov, Michal Bajdich, Thomas F. Jaramillo. Systematic Investigation of Iridium-Based Bimetallic Thin Film Catalysts for the Oxygen Evolution Reaction in Acidic Media. *ACS Applied Materials and Interfaces*. **2019**
  41. Emmett D. Goodman, Aaron C. Johnston-Peck, Elisabeth M. Dietze, Cody J. Wrasman, Adam S. Hoffman, Frank Abild-Pedersen, Simon R. Bare, Philipp N. Plessow , Matteo Cargnello . Catalyst deactivation via decomposition into single atoms and the role of metal loading. *Nature Catalysis*, **2019**, 2, 748-755.
  42. Shaama Mallikarjun Sharada, Rasmus K. B. Karlsson, Yasheng Maimaiti, Johannes Voss, Thomas Bligaard. Adsorption on transition metal surfaces: Transferability and accuracy of DFT using the ADS41 dataset. *Physical Review B*, **2019**, 100, 035439.

43. Aayush Singh, Brian Andrew Rohr, Michael Statt, Jay A Schwalbe, Matteo Cargnello , Jens K. Nørskov. Strategies toward Selective Electrochemical Ammonia Synthesis. *ACS Catalysis*, **2019**, 9, 8316-8324.
44. Michael J. Boyd, Allegra A. Latimer, Colin F. Dickens, Adam C. Nielander, Christopher Hahn, Jens K. Nørskov, Drew C. Higgins, Thomas F. Jaramillo. Electro-Oxidation of Methane on Platinum under Ambient Conditions. *ACS Catalysis*, **2019**, 9, 7578-7587.
45. Joseph A. Gauthier , Colin F. Dickens, Stefan Ringe, Karen Chan. Practical Considerations for Continuum Models Applied to Surface Electrochemistry. *ChemPhysChem*, **2019**, 20, 1-8.
46. Melissa E. Kreider, Alessandro Gallo, Seoin Back, Yunzhi Liu, Samira Siahrostami, Dennis Nordlund, Robert Sinclair, Jens K. Nørskov, Laurie A. King, Thomas F. Jaramillo. Precious Metal-Free Nickel Nitride Catalyst for the Oxygen Reduction Reaction. *ACS Applied Materials Interfaces*, **2019**, 11, 26863-26871.
47. Colin F. Dickens, Charlotte Kirk, Jens K. Nørskov. Insights into the Electrochemical Oxygen Evolution Reaction with ab Initio Calculations and Microkinetic Modeling: Beyond the Limiting Potential Volcano. *Journal of Physical Chemistry C*, **2019**, 123, 18960-18977.
48. Sokseiha Muy, Johannes Voss, Roman Schlem, Raimund Koerver, Stefan J. Sedlmaier, Filippo Maglia, Peter Lamp, Wolfgang G. Zeier, Yang Shao-Horn. High-throughput screening of solid-state Li-ion conductors using lattice-dynamics descriptors. *iScience*, **2019**, 16, 270-282.
49. Egidius W. F. Smeets, Johannes Voss, Geert-Jan Kroes. Specific Reaction Parameter Density Functional Based on the Meta-Generalized Gradient Approximation: Application to H<sub>2</sub> + Cu(111) and H<sub>2</sub> + Ag(111). *Journal of Physical Chemistry A*. **2019**
50. Philomena Schlexer Lamoureux, Aayush Singh, Karen Chan. pH effects on hydrogen evolution and oxidation over Pt(111): Insights from first principles. *ACS Catalysis*. **2019**
51. Zhenghang Zhao, Philomena Schlexer Lamoureux, Ambarish Kulkarni, Michal Bajdich. Trends in Oxygen Electrocatalysis of 3d-Layered (Oxy)(Hydro)Oxides. *ChemCatChem*. **2019**
52. Osman Mamun, Kirsten T. Winther, Jacob R. Boes, Thomas Bligaard. High-throughput calculations of catalytic properties of bimetallic alloy surfaces. *Scientific Data* , **2019**, 6, 76.
53. Kirsten T. Winther, Max J. Hoffmann, Jacob R. Boes, Osman Mamun, Michal Bajdich, Thomas Bligaard. Catalysis-Hub.org, an open electronic structure database for surface reactions. *Nature Scientific Data*, **2019**, 6, 75.
54. Wijten, Jochem H J, Riemersma, Romy L, Gauthier, Joseph, Mandemaker, Laurens D B, Verhoeven, M W G M Tiny, Hofmann, Jan P, Chan, Karen, Weckhuysen, Bert M. Electrolyte Effects on the Stability of Ni-Mo Cathodes for the Hydrogen Evolution Reaction. *ChemSusChem*, **2019**, 12, 3491-3500.
55. Philomena Schlexer Lamoureux, Kirsten Winther, Jose Antonio Garrido Torres , Verena Streibel, Meng Zhao, Michal Bajdich, Frank Abild-Pedersen, Thomas Bligaard. Machine Learning for Computational Heterogeneous Catalysis. *ChemCatChem*, **2019**, 11, 3581-3601.

56. José A. Garrido Torres, Paul C. Jennings, Martin H. Hansen, Jacob R. Boes, Thomas Bligaard. Low-Scaling Algorithm for Nudged Elastic Band Calculations Using a Surrogate Machine Learning Model. *Physical Review Letters*, **2019**, 122, 156001.
57. Hendrik H. Heenen, Johannes Voss, Christoph Scheurer, Karsten Reuter, Alan C. Luntz. Multi-ion Conduction in Li<sub>3</sub>OCl Glass Electrolytes. *Journal of Physical Chemistry Letters*, **2019**, 10, 2264-2269.
58. Jon G. Baker, Joel R Schneider, Jose Antonio Garrido Torres, Joseph A Singh, Adriaan JM Mackus, Michal Bajdich, Stacey F Bent. The Role of Aluminum in Promoting Ni–Fe–OOH Electrocatalysts for the Oxygen Evolution Reaction. *ACS Applied Energy Materials*, **2019**, 2, 3488.
59. Tej S Choksi, Luke T Roling, Verena Streibel, Frank Abild-Pedersen. Predicting Adsorption Properties of Catalytic Descriptors on Bimetallic Nanoalloys with Site-Specific Precision. *The Journal of Physical Chemistry Letters*, **2019**, 10, 1852-1859.
60. Jonathan Leon Snider, Verena Streibel, McKenzie Austin Hubert, Tej S Choksi, Eduardo Valle, David Chester Upham, Julia Schumann, Melis Seher Duyar, Alessandro Gallo, Frank Abild-Pedersen, Thomas F Jaramillo. Revealing the synergy between oxide and alloy phases on the performance of bimetallic In-Pd catalysts for CO<sub>2</sub> hydrogenation to methanol. *ACS Catalysis*, **2019**, 9, 3399-3412.
61. Jacob R. Boes, Osman Mamun, Kirsten T. Winther, Thomas Bligaard. Graph Theory Approach to High-Throughput Surface Adsorption Structure Generation. *Journal of Physical Chemistry A*, **2019**, 123, 2281-2285.
62. Luke T Roling, Tej Choksi, Frank Abild-Pedersen. A coordination-based model for transition metal alloy nanoparticles. *Nanoscale*, **2019**, 11, 4438-4452.
63. Bo You , Michael T. Tang , Charlie Tsai, Frank Abild-Pedersen, Xiaolin Zheng, Hong Li. Enhancing Electrocatalytic Water Splitting by Strain Engineering. *Advanced Materials*, **2019**, 31, 1807001.
64. Ji Hyun Baek, Thomas Mark Gill, Hadi Abroshan, Sangwook Park, Xinjian Shi, Jens K. Nørskov, Samira Siahrostami, Xiaolin Zhen. Selective and Efficient Gd-Doped BiVO<sub>4</sub> Photoanode for Two-Electron Water Oxidation to H<sub>2</sub>O<sub>2</sub>. *ACS Energy Letters*, **2019**, 4, 720-728.
65. Iris C. ten Have, Eduardo Valle, Alessandro Gallo, Jonathan L. Snider, Melis S. Duyar, Thomas F. Jaramillo. Development of MoP catalysts for higher alcohol synthesis from syngas by exploiting support and promoter effects. *Energy Technology*. **2019**
66. Yubing Lu, Jiamin Wang, Liang Yu, Libor Kovarik, Xiwen Zhang, Adam S. Hoffman, Alessandro Gallo, Simon R. Bare, Dimosthenis Sokaras, Thomas Kroll, Vanessa Dagle, Hongliang Xin, Ayman M. Karim. Identification of the active complex for CO oxidation over single-atom Ir-on-MgAl<sub>2</sub>O<sub>4</sub> catalysts. *Nature Catalysis*, **2019**, 2, 149-156.
67. Joseph A. Singh, Adam S. Hoffman, Julia Schumann, Alexey Boubnov, Arun S. Asundi, Sindhu S. Nathan, Jens Nørskov, Simon R. Bare, Stacey F. Bent. Role of Co<sub>2</sub>C in ZnO-promoted Co Catalysts for Alcohol Synthesis from Syngas. *ChemCatChem*, **2018**, 11, 799-809.
68. Janis Timoshenko, Cody J. Wrasman, Mathilde Luneau, Tanya Shirman, Matteo Cargnello, Simon R. Bare, Joanna Aizenberg, Cynthia M. Friend, Anatoly I. Frenkel. Probing Atomic Distributions in Mono- and Bimetallic Nanoparticles by Supervised Machine Learning. *Nano Letters*, **2019**, 19, 520-529.

69. Osman Mamun, Kirsten T. Winther, Jacob R. Boes, Thomas Bligaard. A Bayesian framework for adsorption energy prediction on bimetallic alloy catalysts. *npj Computational Materials*, **2020**, 6.
70. Gan Chen, Michaela Burke Stevens, Yunzhi Liu, Laurie A. King, Jihye Park, Taeho Roy Kim, Robert Sinclair, Thomas F. Jaramillo, Zhenan Bao. Nanosized Zirconium Porphyrinic Metal–Organic Frameworks that Catalyze the Oxygen Reduction Reaction in Acid. *Small Methods*, **2020**, 4, 2000085.
71. Tao Wang, Frank Abild-Pedersen. Identifying factors controlling the selective ethane dehydrogenation on Pt-based catalysts from DFT based micro-kinetic modeling. *Journal of Energy Chemistry*, **2021**, 58, 37-40.
72. McKenzie A. Hubert, Anjali M. Patel, Alessandro Gallo, Yunzhi Liu, Eduardo Valle, Micha Ben-Naim, Joel Sanchez, Dimosthenis Sokaras, Robert Sinclair, Jens K. Nørskov, Laurie A. King, Michal Bajdich, Thomas F. Jaramillo. Acidic Oxygen Evolution Reaction Activity–Stability Relationships in Ru-Based Pyrochlores. *ACS Catal.* **2020**
73. Arun S. Asundi, Adam S. Hoffman, Miaofang Chi, Sindhu S. Nathan, Alexey Boubnov, Jiyun Hong, Simon R. Bare, Stacey F. Bent. Enhanced alcohol production over binary Mo/Co carbide catalysts in syngas conversion. *Journal of Catalysis*, **2020**, 391, 446-458.
74. David M. Koshy, Alan T. Landers, David A. Cullen, Anton V. Ievlev, Harry M. Meyer III, Christopher Hahn, Zhenan Bao, Thomas F. Jaramillo. Direct Characterization of Atomically Dispersed Catalysts: Nitrogen-Coordinated Ni Sites in Carbon-Based Materials for CO<sub>2</sub> Electroreduction. *Advanced Energy Materials*, **2020**, 2001836.
75. Yuji Hamamoto, Sasfan Arman Wella, Kouji Inagaki, Frank Abild-Pedersen, Thomas Bligaard, Ikutaro Hamada, Yoshitada Morikawa. Enhanced CO tolerance of Pt clusters supported on graphene with lattice vacancies. *Physical Review B*, **2020**, 102, 075408.
76. Jihye Park, Zhihua Chen, Raul A. Flores, Gustaf Wallnerström, Ambarish Kulkarni, Jens K. Nørskov, Thomas F. Jaramillo, Zhenan Bao. Two-Dimensional Conductive Ni-HAB as a Catalyst for the Electrochemical Oxygen Reduction Reaction. *ACS Applied Materials & Interfaces*, **2020**, 12, 39074-39081.
77. Nick Gerrits, Jan Geweke, Egidius W.F. Smeets, Johannes Voss, Alec M. Wodtke, Geert-Jan Kroes. Closing the Gap Between Experiment and Theory: Reactive Scattering of HCl from Au(111). *The Journal of Physical Chemistry C*. **2020**
78. Raul A. Flores, Christopher Paolucci, Kirsten T. Winther, Ankit Jain, Jose Antonio Garrido Torres, Muratahan Aykol, Joseph H. Montoya, Jens K. Nørskov, Michal Bajdich, Thomas Bligaard. Active Learning Accelerated Discovery of Stable Iridium-oxide Polymorphs for the Oxygen Evolution Reaction. *Journal of Chemistry of Materials*. **2020**
79. An-Chih Yang, Tej Choksi, Verena Streibel, Hassan Aljama, Cody J Wrasman, Luke T Roling, Emmett D Goodman, Dionne Thomas, Simon R Bare, Roel S Sánchez-Carrera, Ansgar Schäfer, Yuejin Li, Frank Abild-Pedersen, Matteo Cargnello. Revealing the structure of a catalytic combustion active-site ensemble combining uniform nanocrystal catalysts and theory insights. *Proceedings of the National Academy of Sciences*, **2020**, 117, 14721-14729.

80. Sara R. Kelly, Charlotte Kirk, Karen Chan, Jens K. Nørskov. Electric Field Effects in Oxygen Reduction Kinetics: Rationalizing pH Dependence at the Pt(111), Au(111) and Au(100) Electrodes. *Journal of Physical Chemistry C*. **2020**
81. Simranjit Grewal, Angela Macedo Andrade, Ziqi Liu, Jose Antonio Garrido Torres, Art J. Nelson, Ambarish Kulkarni, Michal Bajdich, Min Hwan Lee. Highly Active Bifunctional Oxygen Electrocatalytic Sites Realized in Ceria-Functionalized Graphene. *Advanced Sustainable Systems*. **2020**
82. Melissa E. Kreider, Michaela Burke Stevens, Yunhzi Liu, Anjali M. Patel, Michael J. Statt, Brenna M. Gibbons, Alessandro Gallo, Micha Ben-Naim, Apurva Mehta, Ryan C. Davis, Anton V. Levlev, Jens K. Nørskov, Robert Sinclair, Laurie A. King, Thomas F. Jaramillo. Nitride or Oxynitride? Elucidating the Composition-Activity Relationships in Molybdenum Nitride Electrocatalysts for the Oxygen Reduction Reaction. *Chemistry of Materials*, **2020**, 32, 2946-2960.
83. Melis S. Duyar, Alessandro Gallo, Jonathan L. Snider, Thomas F. Jaramillo. Low-pressure methanol synthesis from CO<sub>2</sub> over metal-promoted Ni-Ga intermetallic catalysts. *Journal of CO<sub>2</sub> Utilization*, **2020**, 39.
84. Brenna M. Gibbons, Melissa Wette, Michaela Burke Stevens, Ryan C. Davis, Samira Siahrostami, Melissa E. Kreider, Apurva Mehta, Drew C. Higgins, Bruce M. Clemens, Thomas F. Jaramillo. In Situ X-Ray Absorption Spectroscopy Disentangles the Roles of Copper and Silver in a Bimetallic Catalyst for the Oxygen Reduction Reaction. *Chemistry of Materials*, **2020**, 32, 1819-1827.
85. Tej S. Choksi, Verena Streibel, Frank Abild-Pedersen. Predicting metal-metal interactions. II. Accelerating generalized schemes through physical insights. *The Journal of Chemical Physics*, **2020**, 152, 094702.
86. Verena Streibel, Tej S. Choksi, Frank Abild-Pedersen. Predicting metal-metal interactions. I. The influence of strain on nanoparticle and metal adlayer stabilities. *The Journal of Chemical Physics*, **2020**, 152, 094701.
87. Kathryn Ledbetter, Marco E Reinhard, Kristjan Kunnus, Alessandro Gallo, Alexander Britz, Elisa Biasin, James M Glowina, Silke Nelson, Tim B Van Driel, Clemens Weninger, Diana B Zederkof, Kristoffer Haldrup, Amy A Cordones, Kelly J Gaffney, Dimosthenis Sokaras, Roberto Alonso-Mori. Excited state charge distribution and bond expansion of ferrous complexes observed with femtosecond valence-to-core x-ray emission spectroscopy. *The Journal of Chemical Physics*, **2020**, 152, 074203.
88. Brian Andrew Rohr, Aayush R. Singh, Joseph A Gauthier, Michale John Statt, Jens K. Nørskov. Micro-Kinetic Model of Electrochemical Carbon Dioxide Reduction over Platinum in Non-Aqueous Solvents. *Physical Chemistry Chemical Physics*. **2020**
89. J. Tyler Mefford, Zhenghang Zhao, Michal Bajdich, William C. Chueh. Interpreting Tafel Behavior of Consecutive Electrochemical Reactions through Combined Thermodynamic and Steady State Microkinetic Approaches. *Energy & Environmental Science*, **2020**, 13, 622-634.
90. HW Kim, VJ Bukas, H Park, S Park, KM Diederichsen, J Lim, YH Cho, J Kim, W Kim, TH Han, J Voss, AC Luntz, BD McCloskey. Mechanisms of two-electron and four-electron electrochemical oxygen reduction reactions at nitrogen-doped reduced graphene oxide. *ACS Catalysis*, **2020**, 10, 852-863.
91. Chuan Xia, Seoin Back, Stefan Ringe, Kun Jiang, Fanhong Chen, Xiaoming Sun, Samira Siahrostami, Karen Chan, Haotian Wang. Confined local oxygen gas promotes

- electrochemical water oxidation to hydrogen peroxide. *Nature Catalysis*, **2020**, 3, 125-134.
92. Tao Wang, Frank Abild-Pedersen. Achieving industrial ammonia synthesis rates at near-ambient conditions through modified scaling relations on a confined dual site. *Proceedings of the National Academy of Sciences*, **2021**, 118, e2106527118.
  93. Emmett D. Goodman, Evan Z. Carlson, Elisabeth M. Dietze, Nadia Tahsini, Arun Johnson, Aisulu Aitbekova, Temy Nguyen Taylor, Philipp N. Plessow and Matteo Cargnello. Size-controlled nanocrystals reveal spatial dependence and severity of nanoparticle coalescence and Ostwald ripening in sintering phenomena. *Nanoscale*, **2021**, 13, 930-938.
  94. Tao Wang, Xinjiang Cui, Kirsten T Winther, Frank Abild-Pedersen, Thomas Bligaard, Jens K Nørskov. Theory-Aided Discovery of Metallic Catalysts for Selective Propane Dehydrogenation to Propylene. *ACS Catalysis*, **2021**, 11, 6290-6297.
  95. Upham, D. Chester, Orazov, Marat, Jaramillo, Thomas F. Phosphate-passivated mordenite for tandem-catalytic conversion of syngas to ethanol or acetic acid. *Journal of Catalysis*, **2021**, 39, 132-141.
  96. Joel Sanchez , Michaela Burke Stevens , Alexandra R. Young, Alessandro Gallo , Meng Zhao , Yunzhi Liu , Mario V. Ramos-Garcés , Micha Ben-Naim , Jorge L. Colón , Robert Sinclair, Laurie A. King, Michal Bajdich, Thomas F. Jaramillo. Isolating the Electrocatalytic Activity of a Confined NiFe Motif within Zirconium Phosphate. *Adv. Energy Mater.*, **2021**, 2003545.
  97. David M. Koshy, Sindhu Nathan, Arun Asundi, Ahmed Abdellah, Samuel Dull, David Cullen, Drew Higgins, Zhenan Bao, Stacey Bent, Thomas F. Jaramillo. Bridging thermal catalysis and electrocatalysis: Catalyzing CO<sub>2</sub> conversion with carbon-based materials. *Angewandte Chemie International Edition*. **2021**
  98. Kyuho Lee, Raul A. Flores, Yunzhi Liu, Bai Yang Wang, Yasuyuki Hikita, Robert Sinclair, Michal Bajdich, Harold Y. Hwang. Epitaxial Stabilization and Oxygen Evolution Reaction Activity of Metastable Columbite Iridium Oxide. *ACS Applied Energy Materials*, **2021**, 4, 3074-3082.
  99. Tao Wang, Guomin Li, Xinjiang Cui, Frank Abild-Pedersen. Identification of earth-abundant materials for selective dehydrogenation of light alkanes to olefins. *Proceedings of the National Academy of Sciences*, **2021**, 118, e2024666118.
  100. Sangwook Park, Angel T. Garcia-Esparza, Hadi Abroshan, Baxter Abraham, John Vinson, Alessandro Gallo, Dennis Nordlund, Joonsuk Park, Taeho Roy Kim, Lauren Vallez, Roberto Alonso-Mori, Dimosthenis Sokaras, Xiaolin Zheng. Operando Study of Thermal Oxidation of Monolayer MoS<sub>2</sub>. *Advanced Science*, **2021**, 2002768.
  101. José A. Zamora Zeledón, Michaela Burke Stevens, G. T. Kasun Kalhara Gunasooriya, Alessandro Gallo, Alan T. Landers, Melissa E. Kreider, Christopher Hahn, Jens K. Nørskov, Thomas F. Jaramillo. Tuning the electronic structure of Ag-Pd alloys to enhance performance for alkaline oxygen reduction. *Nature Communication*, **2021**, 12, 1-9.
  102. Melis S. Duyar, Alessandro Gallo , Samuel K. Regli, Jonathan L. Snider, Joseph A. Singh , Eduardo Valle, Joshua McEnaney, Stacey F. Bent , Magnus Rønning, Thomas F. Jaramillo. Understanding Selectivity in CO<sub>2</sub> Hydrogenation to Methanol for MoP Nanoparticle Catalysts Using In Situ Techniques. *Catalysts*, 11, 143. 2021

103. Anna Winiwarter, Michael J. Boyd , Soren B. Scott, Drew C. Higgins , Brian Seger, Ib Chorkendorff, Thomas F. Jaramillo. CO as a Probe Molecule to Study Surface Adsorbates during Electrochemical Oxidation of Propene. *ChemElectroChem*, **2021**, 8, 250-256.
104. Christoph Baeumer, Jiang Li, Qiyang Lu, Allen Yu-Lun Liang, Lei Jin, Henrique Perin Martins, Tomáš Duchoň, Maria Glöß, Sabrina M. Gericker, Marcus A. Wohlgemuth, Margret Giesen, Emily E. Penn, Regina Dittmann, Felix Gunkel, Rainer Waser, Michal Bajdich, Slavomír Nemšák, J. Tyler Mefford , William C. Chueh . Tuning electrochemically driven surface transformation in atomically flat LaNiO<sub>3</sub> thin films for enhanced water electrolysis. *Nature Materials* **2021**
105. An-Chih Yang Verena Streibel, Tej S.Choksi, Hassan Aljama, Baraa Werghi, Simon R. Bare, Roel S. Sánchez-Carrera, Ansgar Schäfer, Yuejin Li, Frank Abild-Pedersen, Matteo Cargnello. Insights and comparison of structure–property relationships in propane and propene catalytic combustion on Pd- and Pt-based catalysts *Journal of Catalysis*, **2021**, 401, 89-101.
106. Philomena Schlexer Lamoureux, Tej S. Choksi, Verena Streibel, Frank Abild-Pedersen Combining Artificial Intelligence and Physics-based Modeling to Directly Assess Atomic Site Stabilities: From Sub-nanometer Clusters to Extended Surfaces (*submitted*)
107. Jiang Li, Joakim Halldin Stenlid, Thomas Ludwig, Philomena Schlexer Lamoureux, Frank Abild-Pedersen. Modelling Potential-dependent Electrochemical Activation Barriers – Revisiting the Alkaline Hydrogen Evolution Reaction. (*submitted*)
108. Joakim Halldin-Stenlid, Verena Streibel, Tej S. Choksi, Frank Abild-Pedersen. Assessing Catalytic Rates with Active Site Specificity: A Case Study on NO Decomposition (*submitted*)
109. Verena Streibel, Hassan A. Aljama, Angel Yang, Tej S. Choksi, Roel S. Sánchez-Carrera, Ansgar Schäfer, Yuejin Li, Matteo Cargnello, Frank Abild-Pedersen, Microkinetic modeling of propene combustion on a stepped, metallic palladium surface and the importance of oxygen coverage (*submitted*)

**Interplay between Electroadsorption and Electrocatalysis  
on Thin-Film Oxide Surfaces**

Jin Suntivich

Cornell University, Department of Materials Science and Engineering

**Presentation Abstract**

The electrochemical conversion of water to oxygen via the oxygen evolution reaction (OER) is an enabling reaction in fuels and materials electrosynthesis. The OER rate is, however, sluggish even when facilitated by state-of-the-art Ir-oxide and Ru-oxide electrocatalysts. To improve the OER kinetics, fundamental understanding of how an electrocatalyst stabilizes the reaction intermediates (*e.g.*, OH<sub>ad</sub>, O<sub>ad</sub>, and OOH<sub>ad</sub>) during the OER is essential. In this presentation, we experimentally examine how transition-metal oxides stabilize the reaction intermediates and facilitate the OER via electroadsorption. We start by characterizing the OH<sub>ad</sub> and O<sub>ad</sub> electroadsorption on well-defined IrO<sub>2</sub>(110), RuO<sub>2</sub>(110), and Ir<sub>1-x</sub>Ti<sub>x</sub>O<sub>2</sub>(110) thin films and study how the oxygen electroadsorption affects the OER activities. Then, we examine how pH, temperature, and electronic structure influence the oxygen electroadsorption energy using ambient pressure X-ray photoelectron spectroscopy (APXPS). From these series of experiments, we have identified the nature of oxygen electroadsorption on the transition-metal-oxide electrocatalysts and validate the idea that the surface bonding of the first atom qualitatively approximates the adsorption of chemically similar adsorbates (so-called “scaling relation”) on transition-metal oxides. Taken together, our work reveals how the transition-metal oxides facilitate the OER at the molecular level and provides a roadmap on how to harness the microscopic degrees of freedom in transition-metal-oxide electrocatalysts to further improve the OER rates.

**DE-SC0018029:** Rational Selection of Transition-Metal Oxide Electrocatalysts from Structure-Electronic Structure-Activity Relations: The Role of Defects, Strain, and Sub-Surface Layering

**Students:** Austin Reese, Brady Bruno

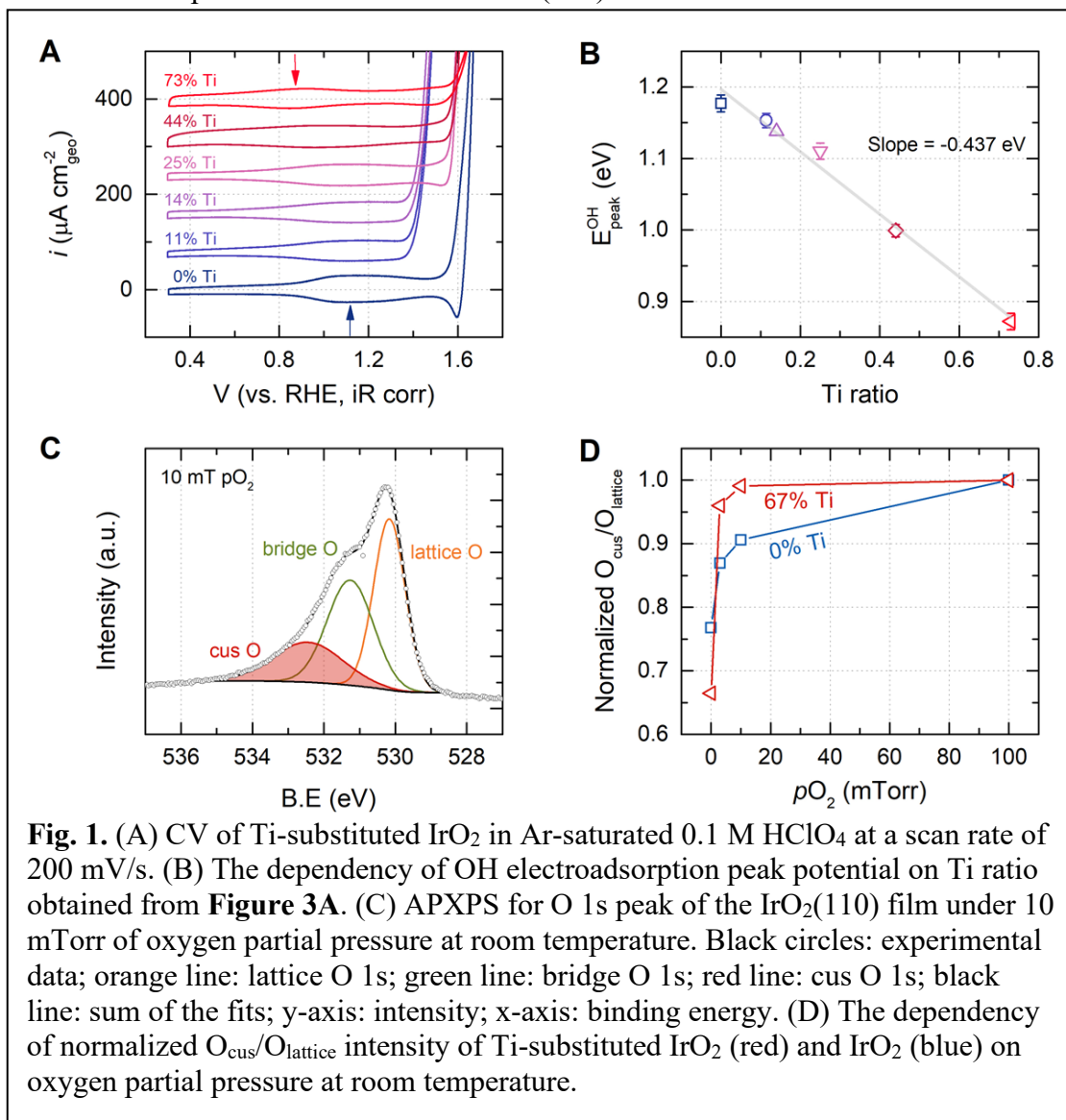
**RECENT PROGRESS**

***Influence of Ti on the Oxygen Electroadsorption and OER on IrO<sub>2</sub>(110)***

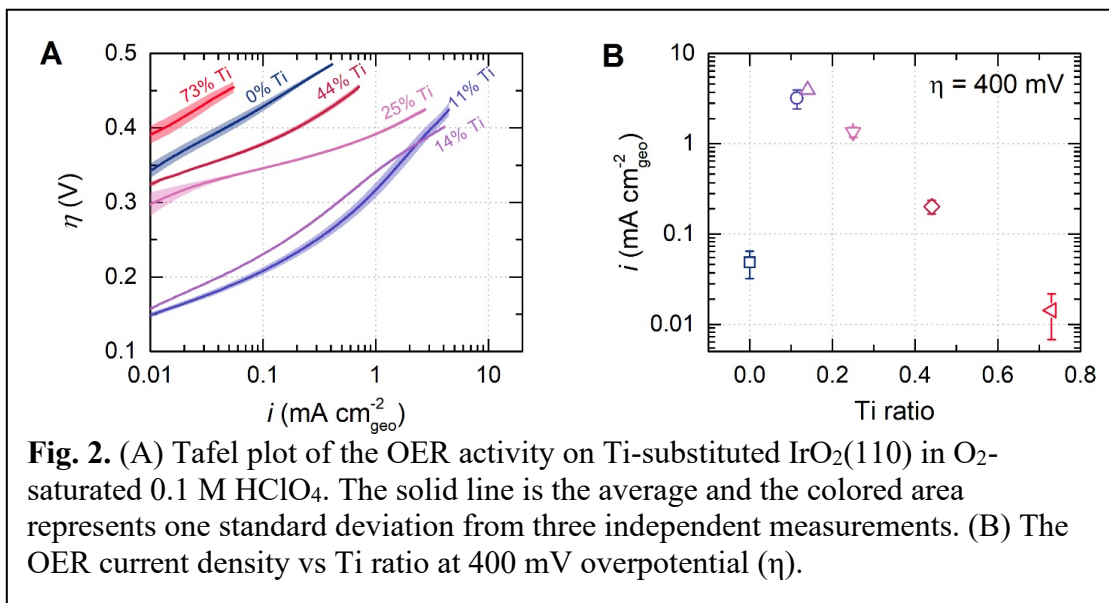
In the last two reports, we described our measurement of the oxygen electroadsorption, *e.g.*, OH<sub>ad</sub> and O<sub>ad</sub>, on well-defined IrO<sub>2</sub>(110), RuO<sub>2</sub>(110), and Ir<sub>1-x</sub>Ti<sub>x</sub>O<sub>2</sub>(110) surfaces. These well-defined oxide films were growing using molecular beam epitaxy (MBE) and characterized with X-ray diffraction (XRD) and reflective high-energy electron diffraction (RHEED). Both XRD and RHEED patterns show that all grown samples were single-crystalline transition-metal-oxide films and, in the Ir<sub>1-x</sub>Ti<sub>x</sub>O<sub>2</sub>(110) situation, behaved as a solid solution epitaxially growing along the (110) termination.

In our last report, we used cyclic voltammetry (CV) to measure the  $O_{ad}$  and  $OH_{ad}$  electroadsorption on the  $Ir_{1-x}Ti_xO_2(110)$  films (**Fig. 1A**). We evaluate the electrochemical potential where the  $OH_{ad}$  electroadsorption ( $H_2O_{ad} \rightarrow OH_{ad} + H^+ + e^-$ ) and  $O_{ad}$  ( $OH_{ad} \rightarrow O_{ad} + H^+ + e^-$ ) occur and determine the  $O_{ad}$  and  $OH_{ad}$  electroadsorption energies. We find that the inclusion of Ti strengthens the  $OH_{ad}$  electroadsorption energy on  $IrO_2(110)$  (**Fig. 1B**). Furthermore, we have verified that the  $OH_{ad}$  and  $O_{ad}$  electroadsorption energy follows the scaling relation, the idea that the first surface bond can approximate the trend of the adsorption of similar species (*i.e.*,  $\Delta G_O \propto \Delta G_{OH}$ ).

Over the past year, we have further validated the oxygen electroadsorption trend using APXPS (**Fig. 1C-D**) and *ab initio* calculations. **Fig. 1C-D** show that the O 1s APXPS result, which we use to characterize the ratio of surface oxygen adsorbed on the coordinately undersaturated sites (" $O_{cus}$ ") to the lattice oxygen (" $O_{lattice}$ "). As shown in **Fig. 1D**, the oxygen adsorption is stronger when Ti is added to  $IrO_2$  (manifested as the increased ratio of surface adsorbed to lattice oxygen signals for 67% Ti vs. 0% Ti.) This finding confirms the electroadsorption trend for the  $Ir_{1-x}Ti_xO_2(110)$  films.



We next character the OER on  $\text{Ir}_{1-x}\text{Ti}_x\text{O}_2$ . In **Fig. 2**, we observe that the OER activity (assessed using the OER current density at the constant overpotential of 400 mV) first increases with the Ti substitution. At ~15%, the OER activity increases by 80x compared with  $\text{IrO}_2$ . However, this OER enhancement decreases once the Ti concentration is more than 15%. All the Ti-substituted  $\text{IrO}_2$  films are more active than  $\text{IrO}_2$  except at 73% Ti substitution. To understand this activity trend, we use density functional theory (DFT) to assess the energies of the OER intermediates. Our DFT result shows that Ti has no preferential site on the (110) surface. Therefore, Ti atoms are likely randomly distributed on the  $\text{Ir}_{1-x}\text{Ti}_x\text{O}_2$  surface. This finding implies that there are four possible surface motifs:  $\text{Ir}_{\text{cus}}\text{-Ir}_{\text{bridge}}$ ,  $\text{Ir}_{\text{cus}}\text{-Ti}_{\text{bridge}}$ ,  $\text{Ti}_{\text{cus}}\text{-Ir}_{\text{bridge}}$ , and  $\text{Ti}_{\text{cus}}\text{-Ti}_{\text{bridge}}$ , where subscript cus and bridge denote the position of the metal sites on the (110) rutile surface. To differentiate the activities between these sites, we compute the energy of the OER intermediates on these four types of motifs. We found that, among four types of motifs,  $\text{Ir}_{\text{cus}}\text{-Ti}_{\text{bridge}}$  has the lowest OH formation energy, which supports stronger OH binding on Ti-substituted  $\text{IrO}_2$ . Thus, the  $\text{Ir}_{\text{cus}}\text{-Ir}_{\text{bridge}}$ ,  $\text{Ir}_{\text{cus}}\text{-Ti}_{\text{bridge}}$  sites likely control the electrochemistry and oxygen adsorption on the  $\text{Ir}_{1-x}\text{Ti}_x\text{O}_2$  surface.



We next consider the energy of intermediates along with the OER coordinate including the transition state where the  $\text{OOH}$  adsorbate with the H atom pointing towards up (**Fig. 3A-B**). It has been shown that the energy difference between this transition state and the  $\text{O}_{\text{ad}}$  surface linearly correlates to the activation energy of the  $\text{OOH}_{\text{ad}}$  formation. Compared to this transition state, a fully relaxed  $\text{OOH}_{\text{ad}}$  structure could dissociate as  $\text{OO}_{\text{ad}}$  on cus site metal and H on bridge site oxygen leading to an underestimation of activation energy. Our computation result shows that the formation energy of  $\text{OOH}$  transition state on  $\text{Ir}_{\text{cus}}\text{-Ti}_{\text{bri}}$  motif is smaller than the  $\text{Ir}_{\text{cus}}\text{-Ir}_{\text{bri}}$  motif at equilibrium potential (0.71 vs. 0.83 eV). The Arrhenius analysis of our temperature-dependent measurements of OER current density also reveal a lower activation energy on Ti-substituted  $\text{IrO}_2$  than pristine  $\text{IrO}_2$  (0.18 vs. 0.33 eV, **Fig. 3C**). This lowering energy barrier from the Ti substitution agrees with our DFT computation results that the  $\text{Ir}_{\text{cus}}\text{-Ti}_{\text{bri}}$  reduces the formation energy of  $\text{OOH}$  transition state by 0.12 eV compared with the  $\text{Ir}_{\text{cus}}\text{-Ir}_{\text{bri}}$  motif at 1.63 V (**Fig. 3D**).

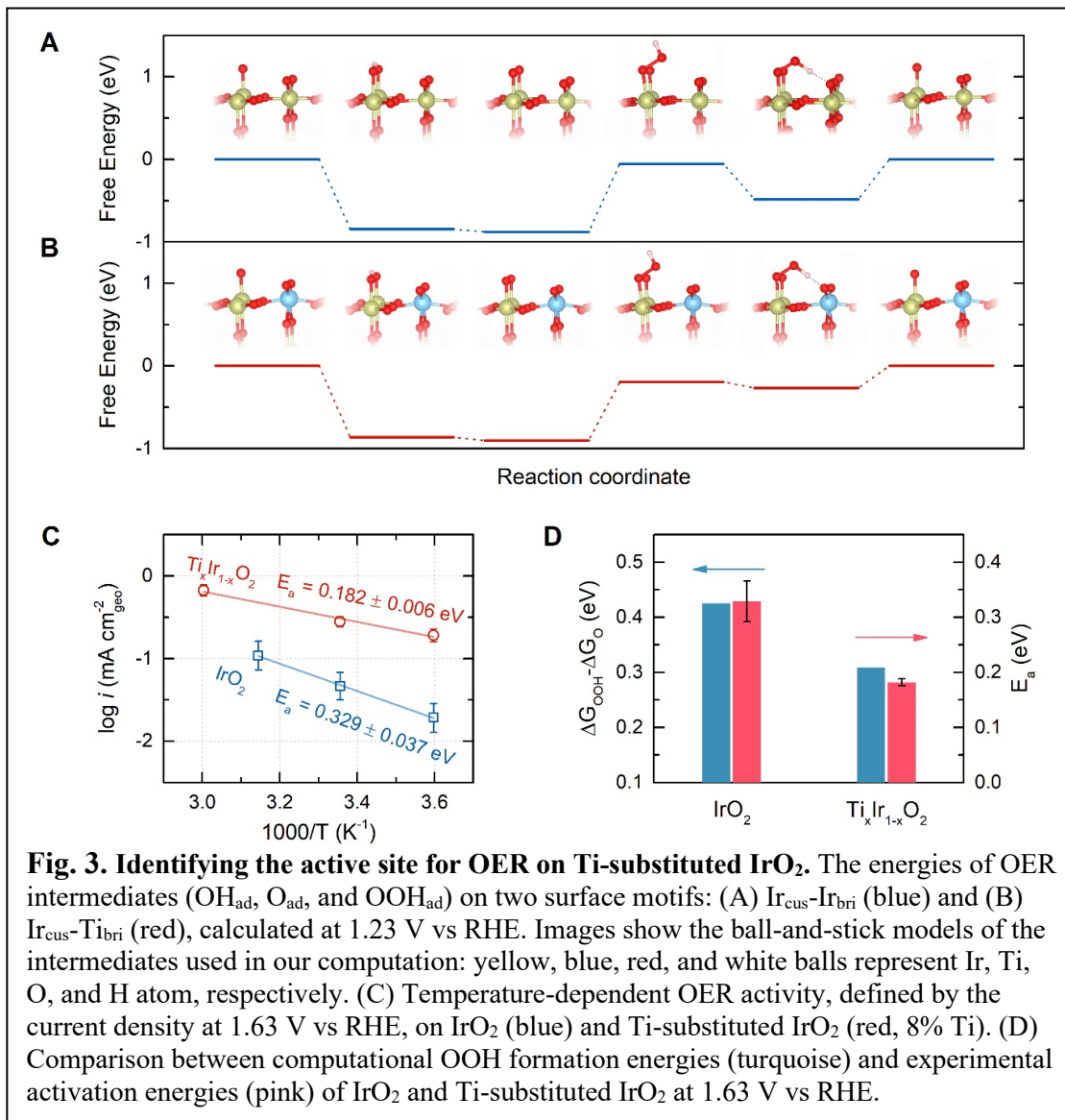


**Fig. 3. Identifying the active site for OER on Ti-substituted IrO<sub>2</sub>.** The energies of OER intermediates (OH<sub>ad</sub>, O<sub>ad</sub>, and OOH<sub>ad</sub>) on two surface motifs: (A) Ir<sub>cus</sub>-Ir<sub>bri</sub> (blue) and (B) Ir<sub>cus</sub>-Ti<sub>bri</sub> (red), calculated at 1.23 V vs RHE. Images show the ball-and-stick models of the intermediates used in our computation: yellow, blue, red, and white balls represent Ir, Ti, O, and H atom, respectively. (C) Temperature-dependent OER activity, defined by the current density at 1.63 V vs RHE, on IrO<sub>2</sub> (blue) and Ti-substituted IrO<sub>2</sub> (red, 8% Ti). (D) Comparison between computational OOH formation energies (turquoise) and experimental activation energies (pink) of IrO<sub>2</sub> and Ti-substituted IrO<sub>2</sub> at 1.63 V vs RHE.

Our results show that Ti substitution affects the OER in two ways: (i) it strengthens the OH binding, likely a result of the electronic structure modification and (ii) it generates a highly active surface motif that reduces the activation energy of the OOH<sub>ad</sub> formation. To quantify the impact of the Ti substitution, we consider that the total current density of the OER is contributed from four types of surface motifs ( $i_{total} = i_{Ir-Ir} \rho_{Ir-Ir} + i_{Ir-Ti} \rho_{Ir-Ti} + i_{Ti-Ir} \rho_{Ti-Ir} + i_{Ti-Ti} \rho_{Ti-Ti}$ , where  $i_{total}$  is the total OER current density;  $i_{A-B}$  and  $\rho_{A-B}$  represent intrinsic activity and the density of the motif; the subscript A and B denote the element located at cus and bridge sites, respectively). Since our DFT results show the Ir<sub>cus</sub> motifs are more active than Ti<sub>cus</sub> motifs for the OER catalysis, the total current density can be approximated as current density from Ir<sub>cus</sub> motifs ( $i_{total} \approx i_{Ir-Ir} \rho_{Ir-Ir} + i_{Ir-Ti} \rho_{Ir-Ti}$ ). At a given Ti ratio, the density of motifs can be obtained by assuming Ti homogeneously distributed on the surface. The total OER current density can be represented as:

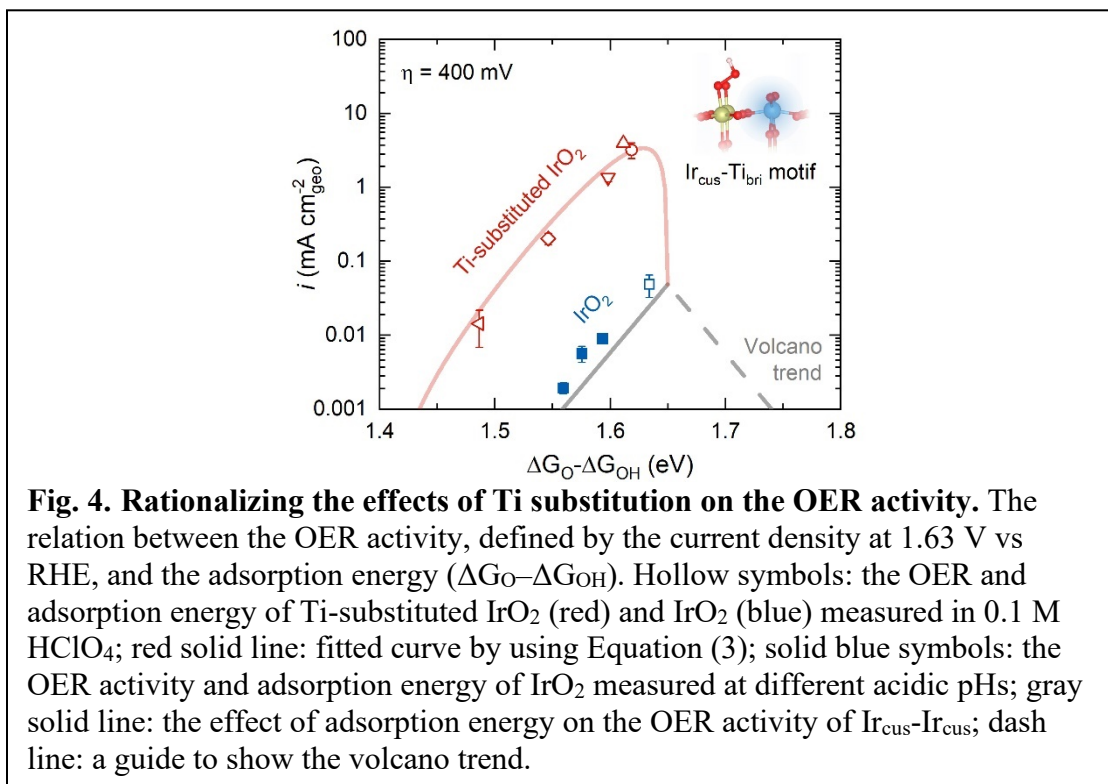
$$i_{total} \approx i_{Ir-Ir} \cdot (1-x)^2 + i_{Ir-Ti} \cdot x(1-x) = [(1-x)^2 + ax(1-x)] \cdot i_{Ir-Ir} \quad \text{Equation (1)}$$

$$i_{\text{Ir-Ir}} = k \cdot \exp[-E_a/k_bT] \quad \text{Equation (2)}$$

where  $x$ ,  $a$ ,  $k$ ,  $E_a$ ,  $k_b$ , and  $T$  are the Ti ratio, the activity enhancement of OER on the Ir<sub>cus</sub>-Ti<sub>bri</sub> motif, kinetics pre-exponential factor, activation energy barrier, Boltzmann constant, and temperature, respectively. We further used  $\Delta G_{\text{OOH}} - \Delta G_{\text{O}}$  to approximate the activation energy ( $E_a$ ) of OER on an Ir<sub>cus</sub>-Ir<sub>bri</sub> motif. This assumption is based on the Brønsted-Evans-Polanyi relation and transformed  $\Delta G_{\text{OOH}} - \Delta G_{\text{O}}$  into a function of Ti ratio ( $x$ ). The OER current can be derived as follows:

$$\log i_{\text{total}} \approx \log[(1-x)^2 + ax(1-x)] - [b/(2.303k_bT)] \cdot x + i_0 \quad \text{Equation (3)}$$

where  $b$  is the dependency of activation energy barrier on the Ti ratio, and  $i_0$  is the current density of IrO<sub>2</sub>. The first part of the equation describes how the changing concentration of the Ir<sub>cus</sub>-Ti<sub>bri</sub> motif density affects the OER activity while the second part describes how the Ti substitution modifies the oxygen adsorption energy and the OER activity on an Ir<sub>cus</sub>-Ir<sub>bri</sub> motif. We use this equation to rationalize the activity trend. We elect to show the result by comparing the OER performance to the well-known volcano plot that connects the OER activity to the oxygen binding energy (nominally,  $\Delta G_{\text{O}} - \Delta G_{\text{OH}}$ , **Fig. 4**). The best fit of the results (red line in **Fig. 4**) shows the Ir<sub>cus</sub>-Ti<sub>bri</sub> motif is three orders of magnitude more active than IrO<sub>2</sub>. Strikingly, the OER electrocatalysis of Ir<sub>1-x</sub>Ti<sub>x</sub>O<sub>2</sub> buckles the predicted volcano trend (grey line, blue data points: IrO<sub>2</sub>(110) measured in acidic pH). This trend buckling reflects how the Ir<sub>cus</sub>-Ti<sub>bri</sub> motif is able to stabilize the OOH<sub>ad</sub> species in a way that disrupts the scaling relation between  $\Delta G_{\text{OOH}}$  and  $\Delta G_{\text{O}}$  that exists on the Ir<sub>cus</sub>-Ir<sub>bri</sub> motif. Based on the fit result, the dependency of activation energy barrier is 0.26 eV revealing that the Ti inclusion affects the energy barrier of the OER on the Ir<sub>cus</sub>-Ir<sub>bri</sub> motif by 26 meV (for 10 % of Ti substitution). The consistence of our results supports that OOH formation is the limiting step for the OER.



The result of our past year's effort demonstrates that the  $O_{ad}$  and  $OH_{ad}$  electroadsorption on the Ti-substituted  $IrO_2$  obeys the scaling relations but not the  $OOH_{ad}$  electroadsorption. Thus, the experimentally measured electroadsorption energies and the OER activities of Ti-substituted  $IrO_2$  are beyond the volcano limitation. The optimum 14 % Ti-substituted  $IrO_2$  is 80 times more active than  $IrO_2$  in acidic media. Our DFT computation and Arrhenius analysis suggest that Ti substitution creates the  $Ir_{cus}-Ti_{bri}$  motif, which serves as an active site by reducing the  $OOH_{ad}$  formation energy. However, too much Ti substitution also strengthens the OH binding, which also disrupts the OER electrocatalysis. Our quantitative understandings of the Ti substitution effects point out that an advanced synthesis approach to controlling the location of substitute may further enhance the activity, paving the avenue to developing highly active OER catalysts.

### Publications Acknowledging this Grant in 2018-2021

(V) Exclusively funded by this grant;

1. Hu, B., Kuo, D.Y., Paik, H., Schlom, D.G., Suntivich, J., "Enthalpy and Entropy of Oxygen ElectroadSORption on  $RuO_2(110)$  in Alkaline Media", *J. Chem. Phys.* **152** 9 (2020), 094704.
2. Kuo, D.Y., Paik, H., Nelson, J.N., Shen, K.M., Schlom, D.G., Suntivich, J., "Chlorine Evolution Reaction Electrocatalysis on  $RuO_2(110)$  and  $IrO_2(110)$  grown using Molecular-Beam Epitaxy", *J. Chem. Phys.* **2019**, *150*, 4, 041726.
3. Kuo, D.Y., Paik, H., Kloppenburg, J., Faeth, B., Shen, K.M., Schlom, D.G., Hautier, G., Suntivich, J., "Measurements of Oxygen ElectroadSORption Energies and Oxygen Evolution Reaction on  $RuO_2(110)$ : A Discussion of the Sabatier Principle and its Role in Electrocatalysis", *J. Am. Chem. Soc.* **2018**, *140* 50, 17597-17605.

(VI) Jointly funded by this grant and other grants with leading intellectual contribution from this grant;

4. Wan, G., Freeland, J.W., Kloppenburg, J., Petretto, G., Nelson, J.N., Kuo, D.-Y., Sun, C.-J., Wen, J., Diulus, J.T., Herman, G.S., Dong, Y., Kou, R., Sun, J., Chen, S., Shen, K.M., Schlom, D.G., Rignanese, G.-M., Hautier, G., Fong, D.D., Feng, Z., Zhou, H., Suntivich, J., "Amorphization Mechanism of  $SrIrO_3$  Electrocatalyst: How Oxygen Redox Initiates Ionic Diffusion and Structural Reorganization", *Sci. Adv.* **2021**, *7*, 2, eabc7323.
5. Eom, C.J., Kuo, D.Y., Adamo, C., Moon, E.J., May, S.J., Crumlin, E.J., Schlom, D.G., Suntivich, J., "Tailoring Manganese Oxide with Atomic Precision to Increase Surface Site Availability for Oxygen Reduction Catalysis", *Nat. Commun.* **2018**, 4034.
6. Kuo, D.Y., Eom, C.J., Kawasaki, J.K., Petretto, G., Nelson, J.N., Hautier, G., Crumlin, E.J., Shen, K.M., Schlom, D.G., Suntivich, J., "Influence of Strain on the Surface-Oxygen Interaction and the Oxygen Evolution Reaction of  $SrIrO_3$ ", *J. Phys. Chem. C* **2018**, *122* 8, 4359-4364.

(VII) *Jointly funded by this grant and other grants with relatively minor intellectual contribution from this grant;*

7. Yang, Y., Zeng, R., Paik, H., Kuo, D.-Y., Schlom, D.G., DiSalvo, F.J., Muller, D.A., Suntivich, J., Abruna, H.D., “Epitaxial Thin-Film Spinel Oxides as Oxygen Reduction Electrocatalysts in Alkaline Media”, *Chem. Mater.* **2021**, 33, 11, 4006-4013.

**Awards or leadership activities during 2018-2020 calendar years**

*Awards:*

- James and Mary Tien Teaching Award, Cornell University (2020)
- Emerging Investigator in Electrochemical Energy Conversion and Storage, American Society of Mechanical Engineers (2020)
- Young Innovator Award in Nano Energy, Nano Research, Tsinghua University (2019)
- Sloan Research Fellowship, Alfred P. Sloan Foundation (2018)

*Symposium organization*

- 2019 MRS Spring (Atomic-Level Understanding of Materials in Fuel Cells & Electrolyzers)

*Editorial service (roles starting during 2018-2020 calendar years)*

- eScience, Elsevier (2020 – present)
- Cell Reports Physical Science, Cell Press (2019 – present)
- MRS Advances, Spring-Nature (2019)

## Polyketoester Synthesis via Dual Alkene Hydroesterification and Carbonylation Catalysis

Ian A. Tonks

University of Minnesota – Twin Cities, Department of Chemistry

### Presentation Abstract

Cationic *bis*(phosphine)Pd hydride catalysts are independently capable of catalyzing either alkene hydroesterification (addition of CO + ROH across the double bond) or alternating carbonylative polymerization to polyketones. Each of these reactions proceeds through a common Pd-acyl (-C(=O)OR) intermediate, indicating that the two processes could be potentially combined to make new polyketoester materials. In this project, initial discussion into catalyst effects on the rate of hydroesterification *vs.* ketone formation will be discussed, as well as the discovery of a new polyketoester platform based on the carbonylative polymerization of  $\alpha,\omega$ -enols or the terpolymerization of  $\alpha,\omega$ -enols with  $\alpha$ -olefins and CO.

### DE-SC0020214: Catalytic Alkene Hydroesterification: New Tools for Polyester Synthesis and Beyond

**Postdoc(s):** Carlton Folster

**Student(s):** Robin Harkins, Shao-Yu Lo

### RECENT PROGRESS

#### *Major Goals of the Project*

The *central hypothesis* of this project is that a common catalytic intermediate—a metal acyl—should make it possible to connect two distinct catalytic reactions, olefin/CO copolymerization and olefin hydroesterification, into a single process. By combining these reactions, it will be possible to couple inexpensive, biorenewable  $\alpha,\omega$ -enols into olefin/CO co-polymerizations, giving access to broad new classes of polyesters and polyketoesters. An additional salient outcome of this work will be a thorough, quantitative understanding of ligand effects/design for hydroesterification catalysis, which will have translational value in various conversions of commodity chemicals. There are two specific objectives to this work:

*Objective 1: Develop a quantitative understanding of alkene hydroesterification.* In order to build a rational base for innovating and improving hydroesterificative polymerizations, we need to improve our understanding of the fundamental theory and application of alkene hydroesterification, including how catalyst structure impacts the selectivity of hydroesterification *vs.* polyketone formation. We will carry out a detailed multivariate

study of hydroesterification in order to build better quantitative and predictive models for ligand and reaction design

*Objective 2: Apply hydroesterification to new carbonylative polymerization reactions of bioderived monomers like 10-undecenol.* Concurrent with and complementary to our quantitative hydroesterification model-building, we will examine the carbonylative polymerization of 10-undecenol, either on its own (to synthesize polyesters) or in terpolymerization reactions with  $\alpha$ -olefins to synthesize polyketoesters.

## RECENT PROGRESS

The majority of our work over the past 12 months has been split between objectives 1 and 2. Our initial work has focused on reaction of 1-hexene and 1-hexanol with CO, as a model for more complex bifunctional substrates that will be used for copolymerization reactions, such as 10-undecenol. In these 1-hexene/1-hexanol reactions, there is the potential for competition between 1-hexene/CO copolymerization and 1-hexene hydroesterification by 1-hexanol. By understanding ligand effects on these Pd-catalyzed reactions, we will be able to tune the microstructures of the polymers that will be later investigated. Ideally, we are interested in catalysts in which both processes occur at similar rates, getting away from the “only polyketone” or “only ester” regimes which have been previously examined. Reactions where both processes can compete will enable the synthesis of new polyketoester materials that are otherwise inaccessible.

Previously, we had developed quantitative IR methods for determining ketone to ester ratio, and begun to investigate qualitative catalysts effects in the context of the 1-hexene/1-hexanol + CO reaction. In this reporting period, we studied two main areas:

- (1) *Quantitative examination of bis(phosphine)Pd(OTf)<sub>2</sub> catalysts under identical conditions to determine which classes are promising candidates for competitive ketone and ester formation.* In our qualitative initial studies, we found that several bis(phosphine)Pd-based catalysts based off of dppp (dppp = 1,3-bis(diphenylphosphino)propane) or dppb (dppb = 1,4-bis(diphenylphosphino)butane) were capable of competitive ketone and ester formation. Based on this data, we constructed a series of 12 catalysts for each framework, varying the stereoelectronic parameters of the dpp(p/b) ligand framework. Using these new catalysts, we conducted initial rates studies to determine the relative rate of ketone and ester production, and have discovered that electron-withdrawing groups slow down both ketone and ester formation, but *significantly* disfavor ketone formation relative to ester formation. Thus, using various electron-donating and electron-withdrawing aryls on the dpp(p/b) frameworks, we can tune the ketone : ester ratio from 1 : 0 all the way to 0 : 1, with significant control in-between the extremes.
- (2) *Suppression of alkene isomerization of hydroesterification and alkene/CO copolymerization.* An ongoing challenge in the above studies is that alkene isomerization significantly impedes production of ketone and ester products (*i.e.* high starting material conversion, lower yields of products). Indeed, it appears that in most

cases, isomerization of the terminal alkene to an internal alkene results is irreversible—a significant problem when considering polymerization applications where overall molecular weight will be directly correlated to stoichiometric balance of reactive groups. Thus, in addition to the kinetic studies above, we have further invested time in optimizing reaction conditions to reduce isomerization. Conveniently, running reactions at lower temperature (25-50 °C vs > 50 °C) significantly reduces isomerization, as does incorporating electron-withdrawing substituents on the ligand backbone. These new conditions (low temperature, catalysts such as *p*-CF<sub>3</sub>-Ph modified dppp) result in closer correlations between starting material conversion and ketone/ester yield.

- (3) *Terpolymerization for the synthesis of polyketoesters*. Using our optimized catalysts described above, we have now begun to carry out terpolymerization reactions (10-undecenol, 1-hexene, and CO). Excitingly, we now have preliminary results indicating that polymers with molecular weights in excess of 30,000 g/mol can be synthesized with varying ketone/ester incorporation. We are currently deconvoluting the polymer microstructure, and examining the properties of these materials. Because of high branching content (these are most likely hyperbranched polyketoesters), the polymers are highly amorphous even at high molecular weights. Future studies into terpolymerizations with ethylene should increase polymer crystallinity.

## **Publications Acknowledging this Grant in 2018-2021**

### *(VIII) Intellectually led by this grant*

1. Folster, C. P.; Harkins, R. P.; Lo, S.-Y.; Sachs, J. D.; **Tonks, I. A.** Development and Applications of Selective Hydroesterification Reactions. *Trends in Chemistry* **2021**, 3, 469.
2. Burch, Q. J.; Butler, S. K.; **Tonks, I. A.\***, Miller, A. J. M.\* Resources for Improving Safety Culture, Training, and Awareness in the Academic Laboratory (Book Chapter) *Comprehensive Coordination Chemistry III*; Figueroa, J., Ed.; Elsevier **2021**

## **Awards or leadership activities during 2018-2020 calendar years**

### *Awards*

1. Ryerson Professorship in Chemistry (2021)
2. McKnight Land-Grant Professorship (2018)
3. ACS DCHAS Laboratory Safety Institute Graduate Research Faculty Safety Award (2021)
4. DOE Early Career Award (2019)
5. ACS Organometallics Distinguished Author Award (2019)
6. ACS Organic Division Young Academic Investigator (2018)

7. Grandpierre Lecturer, Columbia University (2018)
8. Thieme Chemistry Journals Award (2018)

*Leadership and service activities*

1. *Organometallics* Associate Editor 11/2020 – Present
2. ACS Division of Inorganic Chemistry, Alternate Councilor, 2021
3. Early Career Advisory Board, *Asian J. Org. Chem.* 11/2019 – Present
4. Editorial Advisory Board, *Organometallics* 01/2019 – 12/2020
5. Editorial Advisory Board, *The Merck Index Online* 01/2015 – Present

# **Early Career Awardees Presentations**

Charles C. L. McCrory

**Building from Discrete Molecular Catalysts to Multidimensional Architectures:  
The Effects of Charge Delocalization and Electronic Coupling on Electrocatalysis**

Charles C. L. McCrory  
University of Michigan, Department of Chemistry

**Presentation Abstract**

The electrochemical reduction of CO<sub>2</sub> is an important strategy for storing renewable energy from intermittent sources like solar and wind in the form of chemical bonds. Molecular inorganic complexes show significant promise as electrocatalysts for the selective reduction of CO<sub>2</sub> to useful chemical feedstocks and solar fuels. An outstanding challenge is incorporating these molecular catalysts into heterogeneous, multidimensional structures that reduce carbon dioxide with high activity and stability, but also maintain the selectivity of discrete, molecular catalysts. Our research focuses on determining how the complicated and interrelated effects of charge delocalization, intramolecular electrostatics, and electronic coupling influence catalytic activity and selectivity in extended multidimensional catalyst architectures. In this presentation, I will discuss some of our initial work studying how these three interrelated effects influence the CO<sub>2</sub> reduction activity of discrete molecular catalysts and multimetallic molecular assemblies. I will also introduce our plans for incorporating and studying these three effects in larger, conjugated macromolecular architectures.

**Towards a Multiscale Modeling Approach to the Electrochemical Interface with DFT Accuracy**

Craig Plaisance

Cain Department of Chemical Engineering, Louisiana State University

**Presentation Abstract**

Due to the complexity of the electrochemical environment, a multiscale approach is required to simulate the multiple length and time scales that are involved in electrocatalysis under realistic conditions. Nonetheless, the difficult and time-consuming task of parametrizing lower levels of theory from higher levels of theory has limited the use of multiscale simulations primarily to the specialized research groups that develop these methods. As a result, studies of electrocatalytic activation barriers based on an accurate energetic and statistical treatment of the electrolyte are almost nonexistent. We are developing a new type of multiscale approach centered around a low-level model that is firmly rooted in quantum mechanics so that its parameters can be directly extracted from relatively few calculations using the high-level density functional theory (DFT) method. This design avoids multivariable fitting of the low-level model, making parameterization efficient and robust so that it can be easily automated. Such a framework is enabled by employing a low level tight binding model based on an operator expansion of the wave function, rather than the traditional orbital based representation, allowing it to be applied locally to select interactions while exhibiting linear scaling with system size.

## Electrocatalytic Grafting of Polyvinylchloride

Christo S. Sevov  
Ohio State University, Department of Chemistry and Biochemistry

### Presentation Abstract

This presentation provides an introduction and overview of our group's efforts to design and implement new reaction technologies for the selective modification of chlorinated plastics, particularly polyvinylchloride (PVC). The goal of the presented research is to convert PVCs into robust materials with altered physical properties, improved lifetimes, and new end-of-life applications. Such efforts are particularly important because PVC has a narrow range of macromolecular properties, and altering these properties requires high loadings (up to 50%) of plasticizers, toxic stabilizers, and volatile impact modifiers that limit recyclability and stability. This seminar describes reductive electrocatalytic methodologies that selectively modify C–Cl bonds along the PVC backbone. The seminar will demonstrate that electrocatalysis not only provides an inexpensive and scalable way to provide electrons for these net-reductive methodologies, but also provides the ability for user control over graft density by programming the quantity of reducing equivalents. Through mechanistic study and reactions on small-molecule models, we developed redox-active catalysts that graft plasticizer mimics onto PVC resins. The macromolecular properties of the new materials are correlated to the grafting density and grafting agent in this seminar. Through this work, we demonstrate that the physical properties of PVCs can be controlled by molecular design, rather than through the reliance on formulations of non-covalent additives.

**Designing Non-Covalent Interactions at the  
Electrode-Electrolyte Interface for Nitrogen Activation**

V. Sara Thoi,\* Carter Gerke, Soumyodip Banerjee  
Johns Hopkins University, Departments of Chemistry and of Materials Science and  
Engineering

**Presentation Abstract**

Electrochemical syntheses of ammonia and its derivatives from dinitrogen are attractive alternatives to the energy-intensive Haber-Bosch process. However, most reported catalytic systems for nitrogen reduction have poor performance, underscoring the strong triple bond and non-polar nature of dinitrogen. In our work, we use non-covalent interactions at the electrode-electrolyte interface to control surface reactivity and substrate accessibility. We have previously demonstrated that cationic surfactants can not only self-assemble at a biased electrode, their presence can inhibit the hydrogen evolution reaction in favor of carbon dioxide reduction by reorganizing interfacial water molecules. Leveraging our understanding of local interactions in other electrocatalytic reactions, we tackle the selectivity challenges in nitrogen fixation by tuning the cationic interactions at the electrode-electrolyte interface and developing methods to control proton and substrate transport.

# PI Abstracts

**The Consortium for Operando and Advanced Catalyst Characterization via Electronic Spectroscopy and Structure (Co-ACCESS) at SSRL**

Simon R. Bare

Chemical Science Division, Energy Sciences Directorate, and SSRL, SLAC National Accelerator Laboratory

**Presentation Abstract**

The application of synchrotron-based techniques for catalyst characterization is an essential component of many catalysis research programs, mainly due to *in-situ/operando* methodology, which allows determination of the structure of the catalyst in the working state, and it is often the only way to determine this information. The Consortium for Operando and Advanced Catalyst Characterization via Electronic Spectroscopy and Structure (Co-ACCESS) at SSRL was formally initiated in FY19, as is based on the concept that creating a collaborative research environment in catalysis characterization at SSRL will lead to a more impactful catalysis research community. We have established ourselves as a central focal point for synchrotron-mediated operando catalysis studies. We have reached 150% over-subscription rate, with a diverse group of users and catalytic chemistry that has been enabled by the personnel, equipment, techniques, and capabilities that have been implemented.

**Grant or FWP Number: DE-AC02-76SF00515**

**Postdoc(s):** Jiyun Hong, Nirmalendu Patra

**Associate Staff Scientist:** Adam S. Hoffman (50%)

**Staff Scientist:** Fernando Vila<sup>#</sup> (37.5%)

**Student(s):** Rachita Rana\* (50%)

**Affiliations(s):** \*University of California at Davis, <sup>#</sup>University of Washington

**RECENT PROGRESS**

***Science Enabled by Co-ACCESS***

The science that has been enabled by Co-ACCESS is broad and far-reaching. The focus in this reporting period has been on *in-situ/operando* gas-phase heterogeneous catalysis. We have both an established and growing catalysis user base. We have expanded into operando electrocatalysis and recently conducted our first experiments in operando photocatalysis.

The results of the science are naturally captured in the publications, but we highlight a few studies to illustrate the science that has been conducted.

The unique catalytic activity of single atoms and single atom alloys has been the focus of many studies at Co-ACCESS. The active element in these catalysts is often present at concentrations  $\ll 0.1$  wt% and are challenging synchrotron experiments to perform.

However, the combination of high intensity wiggler based XAS beamlines with the sensitivity of the multi-element detectors and detailed XAS modeling has resulted in new understanding of these catalysts. For example, we were able to show a direct correlation of the catalytic activity with the specific binding site for isolated Pt atoms on TiO<sub>2</sub>. The bonding of an isolated Pt atom on a TiO<sub>2</sub> surface can occur in a wide range of configurations. The specific bonding location responds dynamically to the chemical environment under which the catalyst has been treated. This variation in bonding environment shows a strong influence on the chemical reactivity and catalytic performance for systems where the isolated Pt active site was adsorbed at well-defined locations on the support. This work demonstrates that to understand the behavior of atomically dispersed catalysts at the level of defining structure–function relationships, it is not sufficient to merely show that all metal species are atomically dispersed; a detailed characterization of the uniformity of the local coordination environment and how this local coordination responds to environmental conditions must be considered.

In addition to the traditional XAS studies to understand single atom catalysts, we have taken full advantage of the high-energy fluorescence detection (HERFD) XAS capability available at beamline 6-2 (now at the new undulator beamline 15-2), which has allowed characterization of highly dilute catalysts due to the inherent sensitivity of the technique, as well as the identification of the actual ligand complex of a functioning single atom catalyst. A study using Ir L<sub>3</sub>-edge HERFD-XAS of single Ir atoms on MgAl<sub>2</sub>O<sub>4</sub> allowed the identification of Ir(CO) and Ir(CO)(O) as the active complex and resting state, respectively, for CO oxidation. Such studies are critical for understanding the reaction mechanism and identifying the relationship between catalytic activity and ligand configuration on supported single atoms to help design catalysts on a molecular level.

There is an unmet need for studying long-term catalyst deactivation under conditions relevant to industry. We demonstrated the feasibility of conducting such studies at SSRL and plan to incorporate this capability as a user-accessible resource soon. The study focused on the effect of the formation of Co<sub>2</sub>C during Fischer-Tropsch synthesis at 16 bar and 220°C during 7 days' time of stream as probed by XAS at SSRL and laboratory XRD at Utrecht University. This study took full advantage of the high-pressure toxic/flammable gas delivery system at beamline 2-2. As a function of time on stream, there was an observed monotonic increase in the formation of the cobalt carbide phase at the expense of the fcc Co phase. Surprisingly, there was no decrease in catalyst activity with the increase in the formation of the cobalt carbide, indicating the need for additional research.

The ability to conduct experiments above ambient pressure is a critical capability for many catalytic studies. Co-ACCESS has prioritized this capability from the outset and can safely deliver toxic/flammable gases to the experimental hutch on several beamlines (pressures up to 80 bar). This capability has not only allowed the Fischer-Tropsch synthesis work above, but also advancements in our understanding of CO<sub>2</sub> hydrogenation and higher alcohol synthesis catalysis.

### ***Statistics – Users, Beamtime, and Publications***

There has been a continued growth in the number of publications per year (Figure 1, left), with the exception of 2020 due to the impact of COVID-19. As one of our goals is to teach and train research groups to be as independent as possible, it is also useful to see

publications resulting from beamtime where Co-ACCESS enabled the science, but the user group is sufficiently experienced to be fully independent.

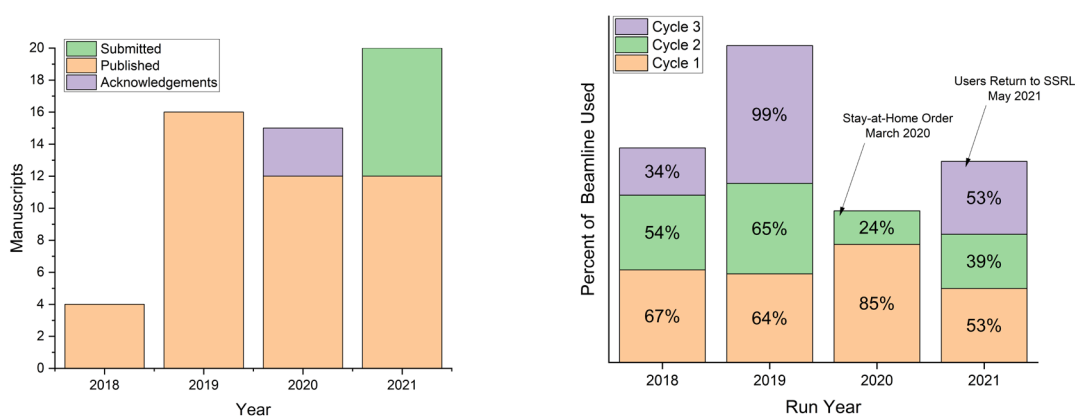


Figure 4 (left): Manuscripts submitted, published, or where Co-ACCESS was acknowledged in a given calendar year. (right): Beamtime use per cycle for each run year. Percent of a beamline used is determined by comparing the number of user-hours supported by Co-ACCESS staff and/or equipment to the user-hours of a beamline per year, approximately 1689 hours/cycle.

Users are awarded beamtime via the SSRL general user process where beamtime is allocated based on peer review and the final score of their proposal. Useful metrics to gauge success and impact of the program are the beamtime use per year, and number of proposals and beamtime in a scheduling year. Figure 1, right, summarizes the percent of a beamtime equivalent allocated to Co-ACCESS collaborator proposals in each cycle during the run year. After continued growth to 2019 we were using the equivalent of a beamline per cycle. It was these statistics, combined with the scientific impact, aligned with SSRL's strategic plan that drove the support from SSRL to invest in the transformation of beamline 10-2 into a chemistry and catalysis beamline (see section on 10-2 below). Of course, the amount of time was severely impacted in 2020 because of COVID-19.

### Equipment

The design, fabrication, and installation of the necessary equipment to allow in-situ/operando XAS studies has been a major focus. Additionally, the investment by SSRL to transform a laboratory into a functioning wet chemistry laboratory was critical. The current equipment available to users is briefly described below.

Co-ACCESS Laboratory, B130 Lab 203, is a 400 sq foot wet chemistry laboratory specifically designed for catalysis studies. The lab is equipped with a 6 ft and a 4 ft fume hood, two gas cabinets for flammable and toxic gases, an argon glove box, and ovens and furnaces. The lab is fully stocked with a diverse array of equipment necessary for the catalysis researcher and is available to collaborators. Additionally, there is a Nicolet iS50 FTIR spectrometer together with praying mantis DRIFTS cell and two transmission FTIR cells. The FTIR is directly connected to a gas manifold capable of supplying 5 different gases, a modulation excitation manifold, and isotope feed loop. There is a Hiden mass spectrometer connected to the experimental cell outlet for product analysis.

The gas cabinet at beamline 2-2 was upgraded to be able to safely deliver both high pressure (75 bar) and ambient pressure gases to the experimental hutch. This design was then duplicated for the advanced spectroscopy beamline 15-2.

Co-ACCESS has two LabView-controlled portable gas manifolds available to users. An ambient pressure manifold capable of controlling up to 6 gases, and a high-pressure (1-15 or 10-75 bar) manifold for 3 gases (typically CO, H<sub>2</sub> and He). For on-line analytics, we have two Hiden mass spectrometers and two Agilent GCs – both a full size and a micro-GC.

For in-situ reaction cells we have our workhorse capillary cell, compatible with 1 and 3 mm Kapton, borosilicate, or quartz capillary tubes. Additionally, we have more specialized cells – a high pressure tube reactor, a cell for handling air sensitive catalysts, a cell for TXM measurements, and a cell optimized for in-situ studies using tender X-rays.

In addition to the experimental laboratory equipment, Co-ACCESS (**Vila**) has obtained and maintained an allocation for supercomputing time at the National Energy Research Scientific Computing Center (NERSC), the production scientific computing center for the Office of Science of the Department of Energy. Given the complexity of the systems of interest to Co-ACCESS users, the state-of-the-art simulations associated with most of the reported results require large computational resources that are only available at high-performance computing facilities. This NERSC Co-ACCESS allocation has been crucial since simulations that would take hours or days in commodity systems can be accomplished in minutes.

### ***Developments in Data Processing***

With the implementation of continuous scanning XAS and the future install of the quick-scanning monochromator at beamline 10-2 in 2022 it is estimated that 10-100 times more XAS data will be generated in the same time period.

This increase in data allows for tracking of the evolution of species with greater resolution, elucidating the rates at which species form and disappear and identifying short-lived intermediates. In-situ experimentation also couples data containing process parameters such as temperatures, gas flow rates, and reactant product analysis, allowing for the development of structure-activity relationships. There are currently no publicly available codes or software that can handle the increase in volume of XAS data, and researchers are often required to develop their own methods for correlating the timing of the XAS spectra to other data streams. Over the past year Adam Hoffman has been working on developing scripts that correlate the asynchronous data collection of XAS, FTIR, and the flow control and mass spectrometer into one file so the researcher can quickly determine the temperature and gas feed composition when a particular spectrum was collected. Codes are also being developed to quickly normalize large numbers of XAS spectra to be used in linear combination analysis or principal component analysis.

### ***Development of Tools and Aid for Users***

Writing a proposal and then applying for beamtime can be both daunting and confusing for researchers that are new to working at SSRL. As such, we strive to lower the barrier to access, in part by having a best practice and “cheat sheet” available on our website to aid in demystifying the process.

For experimental planning, we have a template available to the users to plan their experiments to ensure that they have thought through the details of the experiment, especially from a safety perspective. Adam Hoffman has also developed a tool, “CatMass”, for the user to calculate the mass of catalyst they need for their experiment, the expected

absorption cross-section, and the absorption step height. This tool is now available for download and can be found on our website. Adam Hoffman has also developed a tool for use at the beamline for quickly screening and merging fluorescence signals from the multi-element detectors. This tool allows the researcher to quickly remove “bad” channels via visual inspection or through statistically screening the data for different criteria, creating an output file that can then be readily imported into XAS analysis software. This replaces the original go-to software, SixPack, as it allows for processing of the data in fewer steps, and the output file contains additional data needed for further processing.

### ***Outreach and Training***

Outreach and training continue to be important aspects of Co-ACCESS. At the fundamental level, extensive hands-on training occurs at the beamline where the students and postdocs receive training in all aspects of an XAS experiment. However, our training starts well before the beamtime, with mentoring in writing a beamtime proposal, and planning the actual experiment to ensure that the time is used efficiently, effectively, and in a safe manner. It is also paramount that we help the students understand both the strengths and weaknesses of the technique and ensure that they will be able to extract the necessary data to advance their research. Once the data are collected, further mentoring is provided to train the student in data processing, data analysis, data interpretation, and data reporting. These mentoring sessions span one-on-one meetings via Zoom, to group boot camp sessions to larger training sessions at national meetings.

Co-ACCESS also maintains a website on the SSRL domain. Information is posted there regarding outreach activities, and it acts as a focal point for information for collaborators.

### ***Subcontract with Prof. Fernando Vila, Univ. Washington***

Theoretical simulations of X-ray spectra are essential in aiding the interpretation of experimental measurements and play a vital role for complicated systems like catalysts. They provide insights into the structural nature of the catalyst and the way it relates to the chemical processes. However, these methodologies are, in many cases, not accessible to non-expert users, as these methods require an understanding of the theoretical foundations of spectroscopy that is critical to maximize their usefulness. To address this issue, the aim of this subcontract is to provide Co-ACCESS users with end-to-end support (**Vila**) in the use of a variety of *ab initio* codes for X-ray spectroscopies (FEFF, StoBe, etc.), and their integration to density functional theory (DFT) studies of structure using either static simulations, or more advanced techniques to account for structural disorder (DFT/MD, dynamical matrix calculations, etc.). During the past three years, this support has been deployed in a variety of ways, ranging from direct simulation support to training of users and collaborators in the use of simulation software.

### ***Subcontract with Prof. Ambarish Kulkarni, UC Davis***

This subcontract is focused on enhanced XAS modeling using DFT-based approaches. XAS modeling is typically a lengthy process in part due to the necessity of providing a user-supplied structure model, thus making data interpretation susceptible to human bias. This is further complicated as the “EXAFS fitting” procedure is cumbersome (~weeks). Generally, it requires the experimentalists to use unwieldy, decades-old

graphical user interfaces (GUIs). For example, the Demeter interface used in Athena and Artemis was developed in the mid-1990s. With the impending implementation of quick-scanning XAS, and the current implementation of continuous scanning XAS (capable of generating many thousands of XAS measurements/ hour), it is necessary to develop unbiased, theory-driven workflows to automate the data analysis. Development of such workflows will address a key bottleneck that currently limits the wider applicability of these powerful characterization techniques.

### **Publications Acknowledging this Grant in 2018-2021**

*Please classify your publications into two categories according to the source of support for the work published:*

*(IX) Intellectually led by this grant*

1. Hoffman, A.S.; Azzam, S.; Zhang, S. K.; Xu, Y.; Liu, Y.; Bare, S.R.; Simonetti, D.A. Direct Observation of the Kinetics of Gas-Solid Reactions using In-situ Kinetic and Spectroscopic Techniques. *Reaction Chemistry & Engineering* **2018**, *3*, 668 – 675.
2. Hoffman, A.S.; Singh, J.A.; Bent, S.F.; Bare, S.R. In-situ Observation of Phase Changes of a Silica Supported Cobalt Catalyst for the Fischer-Tropsch Process by the Development of a Synchrotron-Compatible In-situ/Operando Powder X-ray Diffraction Cell. *Journal of Synchrotron Radiation* **2018**, *25*, 1673-1682.
3. van Ravenhorst, I.K.; Hoffman, A.S.; Vogt, C.; Boubnov, A.; Patra, N.; Oord, R.; Akatay, C.; Meirer, F.; Bare, S.R.; Weckhuysen, B.M. On the Cobalt Carbide Formation in a Co/TiO<sub>2</sub> Fischer-Tropsch Synthesis Catalyst as Studied by High-Pressure, Long-Term Operando X-Ray Absorption Spectroscopy and Diffraction. *ACS Catalysis* **2021**, *11*, 2956-2967.

*(X) Jointly funded by this grant and other grants with intellectual leadership by other funding sources*

1. Aitbekova, A.; Wu, L.; Wrasman, C.J.; Boubnov, A.; Hoffman, A.S.; Goodman, E.D.; Bare, S.R.; Cargnello, M. Low-temperature restructuring of CeO<sub>2</sub>-supported Ru nanocrystals determines selectivity in CO<sub>2</sub> catalytic reduction. *Journal of the American Chemical Society* **2018**, *140*, 13736-13745.
2. Wrasman, C.J.; Boubnov, A.; Riscoe, A.R.; Hoffman, A.S.; Bare, S.R.; Cargnello, M. Synthesis of Colloidal Pd/Au Dilute Alloy Nanocrystals and Their Potential for Selective Catalytic Oxidations. *Journal of the American Chemical Society* **2018**, *140*, 12930-12939.
3. Schmidt, J.E.; Ye, X.; van Ravenhorst, I.K.; Oord, R.; Shapiro, D.A.; Yu, Y-S.; Bare, S.R.; Meirer, F.; Poplawsky, J.D.; Weckhuysen, B.M. Probing the location and speciation of elements in zeolites with correlated atom probe tomography and scanning transmission X-Ray microscopy. *ChemCatChem* **2018**, *10*, 1-8.

4. Y. Lu, Y. Wang, J.; Yu, L.; Kovarik, L.; Zhang, X.; Hoffman, A.S.; Gallo, A.; Bare, S.R.; Sokaras, D.; Kroll, T.; Dagle, V.; Xin, H.; Karim, A.M. Identification of the Active Complex for CO Oxidation over Single Atom Ir-on-MgAl<sub>2</sub>O<sub>4</sub> Catalysts. *Nature Catalysis* **2019**, *2*, 149-156.
5. Singh, J.A.; Hoffman, A.S.; Schumann, J.; Boubnov, A.; Asundi, A.S.; Nathan, S.S.; Nørskov, J.; Bare, S.R.; Bent, S.F. Role of Co<sub>2</sub>C in ZnO-promoted Co Catalysts for Alcohol Synthesis from Syngas. *ChemCatChem*, **2019**, *11*, 799-809.
6. Timoshenko, J.; Wrasman, C.J.; Luneau, M.; Shirman, T.; Cargnello, M.; Bare, S.R.; Aizenberg, J.; Friend, C.M.; Frenkel, A.I. Probing atomic distributions in mono- and bimetallic nanoparticles by supervised machine learning. *Nano Letters* **2019**, *19*, 520–529.
7. Babucci, M.; Fang, C-Y.; Perez-Aguilar, J.E.; Hoffman, A.S.; Boubnov, A.; Guan, E.; Bare, S.R.; Gates, B.C.; Uzun, A. Controlling catalytic activity and selectivity for partial hydrogenation by tuning the environment around active sites in iridium complexes bonded to supports. *Chemical Science* **2019**, *10*, 2623-2632
8. Asundi, A.S.; Hoffman, P. Bothra, A. Boubnov, F.D. Vila, N. Yang, J.A. Singh, L. Zheng, J.A. Raiford, F. Abild-Pedersen, S.R. Bare, S.F. Bent, S.F. Understanding Structure-Property Relationships of MoO<sub>3</sub> Promoted Rh Catalysts for Syngas Conversion to Alcohols. *Journal of the American Chemical Society* **2019**, *41*, 19655-19668.
9. DeRita, L.; Resasco, J.; Dai, S.; Boubnov, A.; Thang, H.V.; Hoffman, A.S.; I. Ro, I.; Graham, G.W.; Bare, S.R.; Pacchioni, G.; Pan, X.; Christopher, P. Structural evolution of atomically dispersed Pt catalysts dictates reactivity. *Nature Materials* **2019**, *18*, 746-751.
10. Y. Lu, Y.; Kuo, C-T.; Kovarik, L.; Hoffman, A.S.; Boubnov, A.; Driscoll, D.; Morris, J.; Bare, S.R.; Karim, A.M. Versatile approach for quantification of surface site fractions using reaction kinetics: Kinetics as a characterization tool: The case of CO oxidation on supported Ir single-atoms and nanoparticles. *J. Catalysis*, **2019**, *378*, 121-130.
11. Grosso-Giordano, N.A.; Hoffman, A.S.; Boubnov, A.; Small, D.W.; Bare, S.R.; Zones, S.I.; Katz, A. Dynamic reorganization and confinement of TiIV active sites controls olefin epoxidation catalysis on two-dimensional zeotypes. *Journal of the American Chemical Society*, (2019), **141**, 7090-7106.
12. Aitbekova, A.; Goodman, E.D.; Wu, L.; Boubnov, A.; Hoffman, A.S.; Genc, A.; Cheng, H.; Casalena, L.; Bare, S.R.; M. Cargnello, M.; Engineering of Ruthenium-Iron Oxide Colloidal Heterostructures Leads to Improved Yields in CO<sub>2</sub> Hydrogenation to Hydrocarbons. *Angewandte Chemie Int. Ed.* **2019**, *58*, 2-9.

13. Rahman, M.; Infantes-Molina, A.; Boubnov, A.; Bare, S.R.; Stavitski, E.; Sridhar, A.; Khatib, S.J. Increasing the catalytic stability by optimizing the formation of zeolite-supported Mo carbide species ex situ for methane dehydroaromatization. *J. Catalysis* **2019**, *375*, 314-328.
14. Riscoe, A.R.; Wrasman, C.J.; Herzing, A.A.; Hoffman, A.S.; Menon, A.; Boubnov, A.; Vargas, M.; Bare, S.R.; Cargnello, M. Transition State and Product Diffusion Control by Polymer-Nanocrystal Hybrid Catalysts. *Nature Catalysis* **2019**, *2*, 852-863.
15. Goodman, E.D.; Johnston-Peck, A.C.; Dietze, E.M.; Wrasman, C.J.; Hoffman, A.S.; Abild-Pedersen, F.; Bare, S.R.; Plessow, P.N.; Cargnello, M.; Catalyst deactivation via decomposition into single atoms and the role of metal loading. *Nature Catalysis* **2019**, *2*, 748-755.
16. Babucci, M.; Oztuna, F.E.S.; Debeve, L.M.; Boubnov, A.; Bare, S.R.; Gates, B.C.; Unal, A.; Uzun, A. A structurally uniform, atomically dispersed reduced graphene aerogel-supported iridium catalyst with an iridium loading of 14.8 wt%. *ACS Catalysis* **2019**, *9*, 9905-9913.
17. Simons, M.C.; Vitillo, J.G.; Babucci, M.; Hoffman, A.S.; Boubnov, A.; Beauvais, M.; Chen, Z.; Cramer, C.J.; Chapman, K.; Bare, S.R.; Gates, B.C.; Lu, C.; Gagliardi, L.; Bhan, A. Structure, dynamics, and reactivity for light alkane oxidation of Fe(II) sites situated in the nodes of a metal-organic framework. *Journal of the American Chemical Society* **2019**, *141*, 18142-18151.
18. Resasco, J.; DeRita, L.; Dai, S.; Chada, J.; Xu, M.; Yan, X.; Finzel, J.; Hanukovich, S.; Hoffman, A.S.; Graham, G.W.; Bare, S.R.; Pan, X.; Christopher, P.; Uniformity is key in defining structure-function relationships for atomically dispersed metal catalysts: the case of Pt on CeO<sub>2</sub>. *Journal of the American Chemical Society* **2019**, *142*, 169-184.
19. Goodman, E.D.; Ye, A.; Aitbekova, A.; Müller, O.; Riscoe, A.S.; Taylor, T.; Hoffman, A.S.; Boubnov, A.; Bustillo, K.C.; Nachtegaal, M.; Bare, S.R.; Cargnello, M. Palladium Oxidation Leads to Methane Combustion Activity: Effects of Particle Size and Alloying with Platinum. *Journal of Chemical Physics* **2019**, *151*, 154703.
20. Boubnov, A.; Timoshenko, J.; Wrasman, C.J.; Hoffman, A.S.; Cargnello, M.; Frenkel, A.I.; Bare, S.R. Insight into Restructuring of Pd-Au Nanoparticles using EXAFS. *Radiation Physics and Chemistry* **2020**, *175*, 108304.
21. Riley, C.; Canning, G.; De La Riva, A.; Zhou, S.; E. Peterson, A. Boubnov, A.S. Hoffman, M. Tran, S.R. Bare, S. Lin, H. Guo, A. Datye, A. Environmentally Benign Synthesis of a PGM-Free Catalyst for Low Temperature CO Oxidation. *Applied Catalysis B* **2020**, *264*, 118547.

22. Cargnello, M.; Yang, A-C.; Streibel, V.; Choksi, T.; Aljama, H.; Wrasman, C.; Roling, L.; Goodman, E.D.; Thomas, D.; Bare, S.R.; Sanchez, R.; Schaefer, A.; Li, Y.; Abild-Pedersen, F.; Revealing the Structure of a Catalytic Combustion Active Site Ensemble Combining Uniform Nanocrystal Catalysts and Theory Insights. *Proc. Nat. Acad. Sci.* **2020**, *117*, 14721-14729.
23. Babucci, M.; Hoffman, A.S.; Debeve, L.M.; Kurtoglu, S.F.; Bare, S.R.; Gates, B.C.; Uzun, A.; Unraveling the Individual Influences of Supports and Ionic Liquid Coatings on the Catalytic Properties of Supported Iridium Complexes and Iridium Clusters. *J. Catalysis* (2020), **387**, 186-195.
24. Azzam, S.A.; Boubnov, A.; Hoffman, A.S.; López-Ausen, T.; Chiang, N.; Canning, G.; Sautet, P.; Bare, S.R.; Simonetti, D.A. Insights into Copper Sulfide Formation from Cu and S K-edge XAS and DFT studies. *Inorg. Chem.* **2020**, *59*, 15276-15288.
25. Rahman, M.; Infantes-Molina, A.; Hoffman, A.S.; Bare, S.R.; Emerson, K.L.; Khatib, S.J.; Effect of Si/Al Ratio of ZSM-5 Support on Structure and Activity of Mo Species in Methane Dehydroaromatization. *Fuel*, **2020**, *278*, 118290.
26. de Lima e Freitas, L.; Puértolas, B.; Zhang, J.; Wang, B.; Hoffman, A.S.; Bare, S.R.; Pérez-Ramírez, J.; Medlin, W.J.; E. Nikolla, E. Tunable Catalytic Performance of Palladium Nanoparticles for H<sub>2</sub>O<sub>2</sub> Direct Synthesis via Surface-Bonded Ligands. *ACS Catalysis* **2020**, *10*, 5202-5207.
27. Najmi, S.; Rasmussen, M.; Innocenti, G.; Chang, C.; Stavitski, E.; Bare, S.R.; Medford, A.; Medlin, W.J.; Sievers, C. Pretreatment Effects on the Surface Chemistry of Small Oxygenates on Molybdenum Trioxide. *ACS Catalysis* **2020**, *10*, 8187-8200.
28. Qi, J.; Finzel, J.; Robotjazi, H.; Xu, M.; Hoffman, A.S.; Bare, S.R.; Pan, X.; Christopher, P. Selective Methanol Carbonylation to Acetic Acid on Heterogeneous Atomically Dispersed ReO<sub>4</sub>/SiO<sub>2</sub> Catalysts. *Journal of the American Chemical Society* **2020**, *142*, 14178-14189.
29. Guan, E.; Ciston, J.; Bare, S.R.; Runnebaum, R.; Katz, A.; Kulkarni, A.; Kronawitter, C.; Gates, B.C. Supported metal pair-site catalysts. *ACS Catalysis* **2020**, *10*, 9065-9085.
30. Kurtoglu, S.F.; Hoffman, A.S.; Akgül, D.; Babucci, M.; Aviyente, V.; Gates, B.C.; Bare, S.R.; Uzun, A. Electronic Structure of Atomically Dispersed Supported Iridium Catalyst Controls Iridium Aggregation. *ACS Catalysis* **2020**, *10*, 12354-12358.
31. Asundi, A.S.; Hoffman, A.S.; Chi, M.; Nathan, S.S.; Boubnov, A.; Hong, J.; Bare, S.R.; Bent, S.F. Enhanced Alcohol Production over Binary Mo/Co Carbide Catalysts in Syngas Conversion. *J. Catalysis* **2020**, *391*, 466-458.

32. Ouyang, M.; Papanikolaou, K.G.; Boubnov, A.; Hoffman, A.S.; Giannakakis, G.; Bare, S.R.; Stamatakis, M.; Flytzani-Stephanopoulos, M.; Sykes, E.C.H. Directing Reaction Pathways via in situ Control of Active Site Geometries in PdAu Single-Atom Alloy Catalysts. *Nature Communications* (2021), **12**, 1549.
33. Divins, N.J.; Kordus, D.; Timoshenko, J.; Sinev, I.; Zegkinoglou, I.; Widrinna, S.; Bergmann, A.; Chee, S.W.; Widrinna, S.; Karlioglu, O.; Mistry, H.; Lopez Luna, M.; Zhong, J.Q.; Hoffman, A.S.; Boubnov, A.; Boscoboinik, J.A.; Heggen, M.; Dunin-Borkowski, R.; Bare, S.R.; Roldan Cuenya, B. Operando High-Pressure investigation of Size-Controlled CuZn Catalysts for the Methanol Synthesis Reaction. *Nature Communications* **2021**, *12*, 1435.
34. Nathan, S.S.; Asundi, A.S.; Singh, J.A.; Hoffman, A.S.; Boubnov, A.; Hong, J.; Bare, S.R.; Bent, S.F. Understanding Support Effects of ZnO-Promoted Co Catalysts for Syngas Conversion to Alcohols Using Atomic Layer Deposition. *ChemCatChem* **2021**, *13*, 770-781.
35. Asundi, A.S.; Hoffman, A.S.; Nathan, S.S.; Boubnov, A.; Bare, S.R.; Bent, S.F. Impurity Control in Catalyst Design: The Role of Sodium in Promoting and Stabilizing Co and Co<sub>2</sub>C for Syngas Conversion. *ChemCatChem* **2021**, *13*, 1186–1194.
36. Luna, M.L.; Timoshenko, J.; Kordus, D.; Rettenmaier, C.; Hoffman, A.S.; Bare, S.R.; Shaikhutdinov, S.; Roldan Cuenya, B. Role of the Oxide Support on the Structural and Chemical Evolution of Fe Catalysts during the Hydrogenation of CO<sub>2</sub>. *ACS Catalysis* **2021**, *11*, 6175-6185.
37. Albrahim, M.; Thompson, C.; Leshchev, D.; Shrotri, A.; Unocic, R.; Hong, J.; Hoffman, A.S.; Meloni, M.; Runnebaum, R.; Bare, S.R.; Stavitski, E.; Karim, A. Reduction and Agglomeration of Supported Metal Clusters Induced by High Flux X-ray Absorption Spectroscopy Measurements. *J. Phys. Chem. C* **2021**, *125*, 11048-11057.
38. Yang, A.-C.; Streibel, V.; Choksi, T.S.; Aljama, H.; Werghe, B.; Bare, S.R.; Sanchez-Carrera, R.S.; Schaefer, A.; Li, Y.; Abild-Pedersen, F.; Cargnello, M. Insights and Comparison of Structure-Property Relationships in Propane and Propene Catalytic Combustion on Pd- and Pt-based Catalysts. *J. Catalysis* **2021**, *401*, 89-101.
39. Chen, L.; Unocic, R.; Hoffman, A.S.; Hong, J.; Braga, A.H.; Bao, Z.; Bare, S.R.; Szanyi, J. Unlocking the Catalytic Potential of TiO<sub>2</sub>-Supported Pt Single Atoms for the Reverse Water-Gas Shift Reaction by Altering Their Chemical Environment. *JACS Au* **2021**, *1*, 977-986.

### **Awards or leadership activities during 2018-2020 calendar years**

- Organized workshops at SSRL/LCLS Users meetings: 2018 “Catalysis by Single Metal Atoms: What is all the Fuss About?”; 2020 “Opportunities in Chemistry & Catalysis Research using Quick Scanning XAS”.
- Organized XAS short course at NAM 2019 (Invited at ICC 2020 and Denver X-ray Conference 2021 but both cancelled due to COVID-19)
- Reviewer of manuscripts for JACS, Nature, ACS Catalysis, Nature Catalysis, Journal of Physical Chemistry Letters, Applied Catalysis, Angewandte Chemie, Review of Scientific Instruments, Chemical Science, among others.
- Reviewer of proposals from Swiss National Science Foundation

Wesley H. Bernskoetter

## The Rational Design of Improved Iron Catalysts for CO<sub>2</sub> Hydrogenation and Related Processes

Nilay Hazari and Wesley H. Bernskoetter  
Yale University; University of Missouri

### Presentation Abstract

The potentially devastating consequences associated with the continued use of fossil fuels make the replacement of these finite feedstocks with sustainable energy vectors one of the most significant challenges facing society. For some applications, formic acid and methanol are prospective replacements for fossil fuels as they can be used as liquid organic hydrogen carriers, which release H<sub>2</sub> on demand, or in the case of methanol directly as a fuel. However, the utilization of these carriers in energy storage strategies requires the development of efficient catalysts for the reversible interconversion of formic acid or methanol and renewable feedstocks such as CO<sub>2</sub> and H<sub>2</sub>. This project undertakes mechanistic and computational studies of the elementary steps in proposed catalytic cycles, as well as the measurement of reaction kinetics under catalytic conditions. The guidelines and knowledge generated are used to design new catalysts and to optimize the reaction conditions. Additionally, detailed investigations of the reactivity of CO<sub>2</sub> with transition metal complexes provides information relevant to the development of catalysts for the electro- and photochemical generation of fuels and the synthesis of fine and commodity chemicals from CO<sub>2</sub>.

### DE-SC0018222: The Reversible Conversion of CO<sub>2</sub> and H<sub>2</sub> to Formic Acid and Methanol Using Iron Catalysts

**Postdoc(s):** Danielle Chirdon (Missouri)

**Student(s):** Julia Curley (Yale); Clayton Hert (Missouri); Nicholas E. Smith (Yale); Tanya Townsend (Yale)

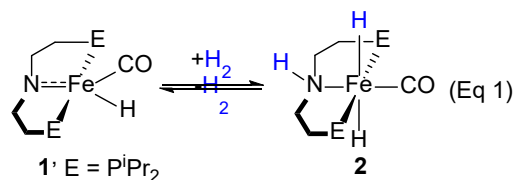
### RECENT PROGRESS

Research progress towards the design of more efficient catalysts for reversible base metal catalyzed CO<sub>2</sub> hydrogenation and related reactions is summarized below for selected areas.

#### *Understanding the Reactivity and Decomposition of a <sup>R</sup>PN<sup>H</sup>P Ligated Fe Catalyst for Hydrogenation and Dehydrogenation Reactions*

The iron pincer complex (<sup>iPr</sup>PNP)Fe(H)(CO) (**1**, <sup>iPr</sup>PNP<sup>-</sup> = N(CH<sub>2</sub>CH<sub>2</sub>P<sup>i</sup>Pr<sub>2</sub>)<sub>2</sub><sup>-</sup>) is an active (pre)catalyst for many hydrogenation and dehydrogenation reactions. This is in part

because **1** can reversibly add H<sub>2</sub> across the iron-amide bond to form (iPrPN<sup>H</sup>P)Fe(H)<sub>2</sub>(CO) (**2**, iPrPN<sup>H</sup>P = HN(CH<sub>2</sub>CH<sub>2</sub>P<sup>i</sup>Pr<sub>2</sub>)<sub>2</sub>) (Eq 1). Although **1** and related complexes typically give exceptional activity and productivity in comparison to base-metal systems, they often do not perform at the same level as precious metal catalysts. This is because rapid decomposition limits their catalytic performance. Despite the importance of understanding catalyst decomposition, there is a paucity of work exploring catalyst death for iPrPN<sup>H</sup>P ligated systems specifically and more generally for first-row transition metal catalysts. Therefore, we explored the pathways through which catalytic intermediates related to **1** and **2** undergo decomposition. This involved characterizing the unstable and previously unobserved complexes [(iPrPN<sup>H</sup>P)Fe(H)(CO)(L)]<sup>+</sup> (**3-L**; L = THF, N<sub>2</sub>, H<sub>2</sub>), which are proposed as intermediates when **1** and **2** are used as catalysts. The compound **3-H<sub>2</sub>** was synthesized through the reaction of (iPrPN<sup>H</sup>P)Fe(H)(CO)(PF<sub>6</sub>) (**4**) with H<sub>2</sub>, and the solid-state structure was established using both X-ray and neutron diffraction. This is the first example of a spectroscopically characterized H<sub>2</sub> complex for a catalyst that is proposed to operate via a Noyori-type mechanism for hydrogenation. As part of our studies understanding the reactivity of **3-L**, we determined the thermodynamic hydricity of **2**, which is valuable for predicting its reactivity as a hydride donor. Further, we showed that species such as **3-L** decompose to the same inactive species observed in catalysis using **1** and **2**, and theoretical calculations



suggest that this likely occurs via a bimolecular pathway. To provide support for this hypothesis we isolated the dimeric species [{(iPrPN<sup>H</sup>P)Fe(H)(CO)}<sub>2</sub>{μ-CN}]<sup>+</sup> (**5**) and [{(iPrPN<sup>H</sup>P)Fe(H)(CO)}<sub>2</sub>{μ-OC(H)O}]<sup>+</sup> (**6**), which shows that it is plausible for catalytic intermediates ligated by iPrPN<sup>H</sup>P can form dimeric species. Our results provide general strategies for improving catalysis using **1** and **2**, and we used this information to rationally increase the performance of **1** in formic acid dehydrogenation.

we isolated the dimeric species [{(iPrPN<sup>H</sup>P)Fe(H)(CO)}<sub>2</sub>{μ-CN}]<sup>+</sup> (**5**) and [{(iPrPN<sup>H</sup>P)Fe(H)(CO)}<sub>2</sub>{μ-OC(H)O}]<sup>+</sup> (**6**), which shows that it is plausible for catalytic intermediates ligated by iPrPN<sup>H</sup>P can form dimeric species. Our results provide general strategies for improving catalysis using **1** and **2**, and we used this information to rationally increase the performance of **1** in formic acid dehydrogenation.

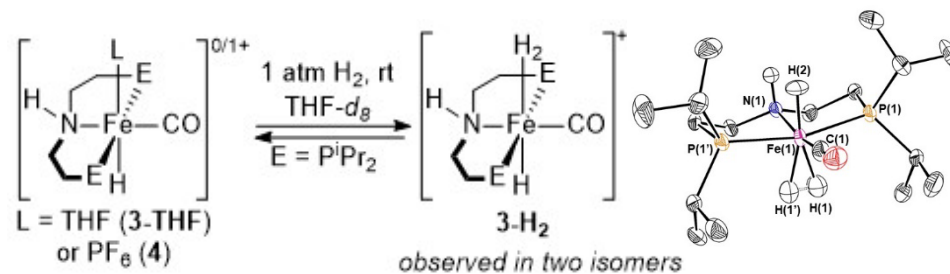


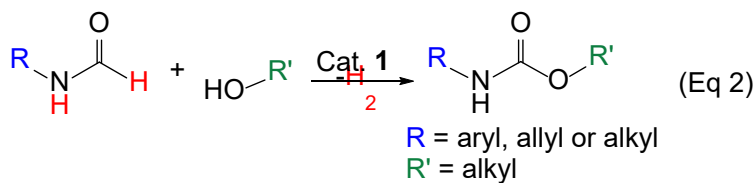
**Figure 1.** Preparation and neutron diffraction structure of the iron dihydrogen complex **3-H<sub>2</sub>**.

**Dehydrogenative Synthesis of Carbamates from Formamides and Alcohols using a Pincer-Supported Iron Catalyst**

### **Dehydrogenative Synthesis of Carbamates from Formamides and Alcohols using a Pincer-Supported Iron Catalyst**

In a continuation of our efforts to expand the application of base metal catalysis to the (de)hydrogenation of electron rich substrates containing carbonyl groups, we have utilized **1** for the dehydrogenative synthesis of carbamates from formamides and alcohols (Eq 2). This is the only example of dehydrogenative carbamate synthesis that is compatible with industrially-relevant N-alkyl formamides and the only method that uses a first-row

transition metal catalyst. The reaction is compatible with 1°, 2°, and benzylic alcohols. Mechanistic studies indicate that the first step in the reaction, Step A, is the



dehydrogenation of the formamide to a transient isocyanate by **1** (Figure 2). The isocyanate then reacts with the alcohol to generate the carbamate, Step B. However, in a competing reaction the isocyanate undergoes a reversible cycloaddition with **1** to generate an off-cycle species, **7** (Figure 2, Step ii), which is the resting state in catalysis. Stoichiometric experiments indicate that high temperatures are required in catalysis to facilitate the release of the isocyanate from the cycloaddition product. We also identified several other off-cycle processes that occur in catalysis, such as the 1,2-addition of the formamide (**8**, Step i) or alcohol (**9**, Step iii) substrate across the Fe–N bond of **1**. In general the dehydrogenation of the alcohol substrate (Step iv) to form ketones or esters is not competitive with formamide dehydrogenation and this potential side reaction does not occur to a significant extent. It has already been demonstrated that the transient isocyanate generated from dehydrogenation of the formamide can be trapped with amines to form ureas, and in principle the isocyanate could also be trapped with thiols to form thiocarbamates. Competition experiments indicate that trapping of the transient isocyanate with amines to produce ureas is faster than trapping with an alcohol to produce carbamates, and thus ureas can be formed selectively in the presence of alcohols. In contrast, thiols bind irreversibly to the iron catalyst through 1,2-addition across the Fe–N bond of **1** and it is not possible to produce thiocarbamates. Overall, our mechanistic studies provide general guidelines for facilitating dehydrogenative coupling reactions using **1** and related catalysts.

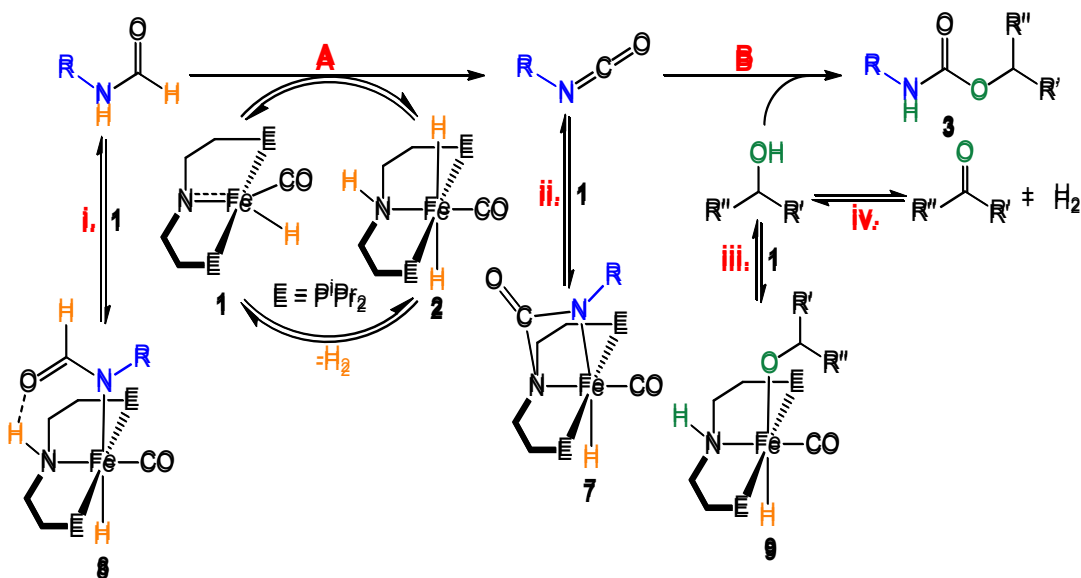


**Figure 2.** Proposed mechanism for conversion of formamides and alcohols to carbamates catalyzed by **1**.

***Influence of Metal-Ligand Cooperative in Pincer Manganese Catalyzed CO<sub>2</sub> Hydrogenation.***

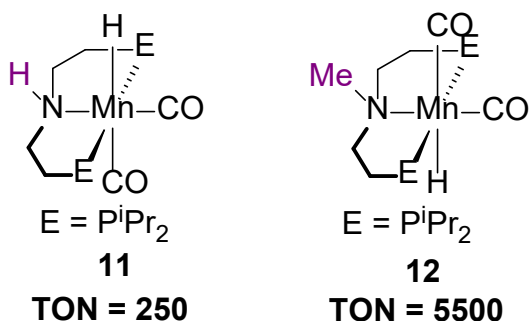
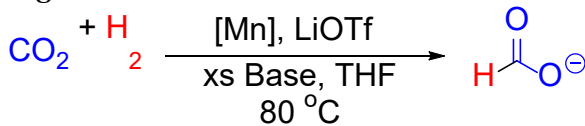


**Figure 3.** Comparison of <sup>iPr</sup>PN<sup>HP</sup> and <sup>iPr</sup>PN<sup>MeP</sup> ligated manganese catalysts for CO<sub>2</sub> hydrogenation.

Our program and others have popularized a strategy of combining earth-abundant transition metals with chemically active ligands in metal-ligand cooperation (MLC) motifs to develop catalysts for reducing electron rich carbonyls groups. While this approach has produced many state-of-the-art catalysts, the application of MLC pathways has not universally delivered superior catalysts. For example, prior work in our program compared catalyst **2** with an N-methylated congener (<sup>iPr</sup>PN<sup>MeP</sup>)Fe(H)<sub>2</sub>(CO) (**10**), which obviates MLC pathways in CO<sub>2</sub>

hydrogenation to formate. In this specific reaction, the tertiary amine supported **10** provides higher TONs than the MLC capable **2**, despite their structural similarities. Unfortunately, experimental complications related to the presence of multiple metal-hydride sites and isomeric forms complicated more in-depth comparison of the MLC and non-MLC iron catalysts. Accordingly, we sought to examine the manganese monohydride versions of these catalysts in order to more directly compare systems with and without the ability to participate in MLC as well as to test the applicability of our findings with **10** to other metals. To this end we prepared the Mn hydride species, (<sup>iPr</sup>PN<sup>HP</sup>)Mn(H)(CO)<sub>2</sub> (**11**) and (<sup>iPr</sup>PN<sup>MeP</sup>)Mn(H)(CO)<sub>2</sub> (**12**) (Figure 3). Preliminary catalytic studies indicate that once again the <sup>iPr</sup>PN<sup>MeP</sup> analog is the superior catalyst, this time producing more than an order of magnitude greater TON for formate production. However, catalytic activity is highly dependent on the presence of a Lewis acid co-catalyst with little formate production observed in the absence of lithium triflate (LiOTf). Mechanistic studies suggest that loss of formate from the metal center is rate limiting for both catalysts **11** and **12**. Kinetic studies are currently underway to directly compare the rates of this elementary reaction between the two species. These and related studies will better elucidate the influence on the MLC motif on all steps of the catalytic cycle and help determine which types of catalytic reaction will most benefit from MLC capable catalysts.

**Publications Acknowledging this Grant in 2018-2020**

(XI) *Intellectually led by this grant*

Jayarathne, U.; Hazari, N.; Bernskoetter, W. H. "Selective Iron-Catalyzed N-Formylation of Amines using Dihydrogen and Carbon Dioxide" *ACS Catal.* **2018**, *8*, 1338-1345.

Lane, E. M.; Hazari, N.; Bernskoetter, W. H. "Iron-catalyzed Urea Synthesis: Dehydrogenative Coupling of Methanol and Amines" *Chem. Sci.* **2018**, *9*, 4003-4008.

Heimann, J. E.; Bernskoetter, W.H.; Guthrie, J.A.; Hazari, N.; Mayer, J.M. "Effect of Nucleophilicity on the Kinetics of CO<sub>2</sub> Insertion into Pincer-Supported Nickel Complexes" *Organometallics*, **2018**, *37*, 3649-3653.

Lane, E. M.; Zhang, Y.; Hazari, N.; Bernskoetter, W. H. Sequential Hydrogenation of CO<sub>2</sub> to Methanol Using a Pincer Iron Catalyst.' *Organometallics* **2019**, *38*, 3084-3091.

Burkart, M. D.; Hazari, N.; Tway, C. L.; Zeitler, E. L. 'Opportunities and Challenges for Catalysis in Carbon Dioxide Utilization.' *ACS Catal.* **2019**, *9*, 7937-7956.

Heimann, J. E.; Bernskoetter; Hazari, N. "Understanding the Individual and Combined Effects of Solvent and Lewis Acid on CO<sub>2</sub> Insertion into a Metal Hydride." *J. Am. Chem. Soc.* **2019**, *141*, 10520-10529.

Smith, N. E.; Bernskoetter, W. H.; Hazari, N. "The Role of Proton Shuttles in the Reversible Activation of Hydrogen via Metal-Ligand Cooperation." *J. Am. Chem. Soc.* **2019**, *141*, 17350-17360.

Townsend, T. M.; Bernskoetter, W. H.; Brudvig, G. W.; Hazari, N.; Lant, H. M. C.; Mercado, B. Q. "Synthesis of Organometallic Pincer-Supported Cobalt(II) Complexes." *Polyhedron* **2020**, *177*, 114308.

Curley, J. B.; Bernskoetter, W. H.; Hazari, N. "Additive-Free Formic Acid Dehydrogenation Using a Pincer-Supported Iron Catalyst." *ChemCatchem* **2020**, *12*, 1934-1938.

(XII) *Jointly funded by this grant and other grants with intellectual leadership by other funding sources*

Curley, J. B.; Smith, N. E.; Bernskoetter, W. H.; Hazari, N.; Mercado, B. Q. "Catalytic Formic Acid Dehydrogenation and CO<sub>2</sub> Hydrogenation Using Iron PN<sup>R</sup>P Pincer Complexes with Isonitrile Ligands" *Organometallics*, **2018**, *37*, 3846-3853.

Suárez, L. A.; Culakova, Z.; Balcells, D.; Bernskoetter, W. H.; Eisenstein, O.; Goldberg, K.I.; Hazari, N.; Tilset, M.; Nova, A. "The Key Role of the Hemiaminal Intermediate in the Iron-Catalyzed Deaminative Hydrogenation of Amides." *ACS Catal.* **2018**, *8*, 8781-8762.

Heimann, J. E.; Bernskoetter; W.H. Hazari, N.; Mayer, J.M. "Acceleration of CO<sub>2</sub> Insertion into Metal Hydrides: Ligand, Lewis Acid and Solvent Effects on Reaction Kinetics" *Chem. Sci.* **2018**, *9*, 6629-6638.

Suárez, L. A.; Jayarathne, U.; Balcells, D.; Bernskoetter, W. H.; Hazari, N.; Jaraiz, M.; Nova, A. "Rational Selection of Co-catalysts for the Deaminative Hydrogenation of Amides" *Chem. Sci.* **2020**, *11*, 2225-2230.

### **Awards or leadership activities during 2018-2020 calendar years**

#### Wesley Bernskoetter

##### Leadership and Service Positions

2019-Present Arts & Sciences Faculty Responsibility Committee

2018-Present University Research Council

2020-Present Departmental Director of Recruiting

#### Nilay Hazari

##### Academic Awards

2020 Elected as Member of the Connecticut Academy of Science and Engineering

##### Leadership and Service Positions

##### *At Yale*

2021-Present Team Leader Carbon Dioxide Utilization in Yale Center for Natural Carbon Capture

2020-Present Poorvu Center for Teaching and Learning Advisory Board

2020-Present University Laboratory Safety Committee

2020-2021 Outside Member, Biological Sciences Area Committee and Tenure Appointments Committee

2020 Faculty of Arts and Science Instructional Support Committee for Planning a Response to COVID-19

2016-Present Director of Undergraduate Studies in Chemistry

##### *External*

2020-Present Co-Integration Team Leader, Center for Hybrid Approaches in Solar Energy to Liquid Fuels (CHASE), a DOE Energy Innovation Hub

2020 Guest Editor of Special Issue in *Organometallics* on 'Organometallic Chemistry for Enabling Carbon Dioxide Utilization'.

2018-2019 Member, National Petroleum Council Carbon Capture, Use, and Storage Study

2017-2018 Member, National Academies of Sciences Committee for Developing a Research Agenda for Utilization of Gaseous Carbon Waste Streams

## Carbenes as Powerful Transition-Metal Surrogates

Guy Bertrand

UCSD-CNRS Joint Research Chemistry Laboratory, Department of Chemistry and Biochemistry, University of California, San Diego, La Jolla, California 92093-0358

### Presentation Abstract

Our group and others have previously reported that stable electrophilic singlet carbenes, such as cyclic (alkyl)(amino)carbenes (CAACs) can activate small molecules and enthalpically strong E-H bonds. We will show that bulky CAACs not only activate CO, but also promote the catalytic carbonylation reaction of quinones into the corresponding cyclic carbonates. We will discuss the mechanism of this reaction, and show that a single electron transfer (SET) might be involved. Along this line, it was known that haloarenes could stoichiometrically be activated by super electron donors, but their functionalization was rarely reported under metal-free conditions. We will show that Breslow intermediates derived from mesoionic carbenes (BIMICs) are among the most potent organic reducing agents reported to date in the ground state (-2.49 V vs Fc/Fc<sup>+</sup>). This allows BIMICs to activate iodoarenes under mild conditions, and to promote the catalytic inter- and intramolecular arylacylation of alkenes, which affords a number of substituted ketones and even polycyclic ketones. Note that, so far, the intramolecular arylacylation reactions have only been achieved using Pd and Ni catalysts. Importantly, triazolium salts, as well as the ensuing MICs, are readily available in large quantities with a variety of N- and C-substituents allowing for a fine-tuning of their reduction potential and steric environment. The strong reduction potential of BIMICs will allow for the activation of more challenging bonds than classical NHCs such as thiazolylienes, 1,2,4-triazolylidene and imidazol(in)ylidenes can do.

### **DE-SC0009376: Novel types of stable carbene for transition metal and metal-free catalysis**

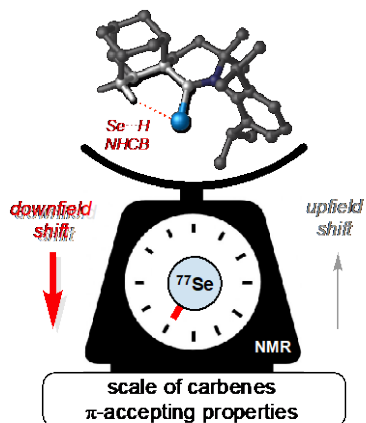
**Postdocs:** Eder Tomás-Mendivil, Rodolphe Jazzar, Mohand Melaimi, Michele Soleilhavoup

**Students:** Glen P. Junor, Francois Vermersch, Sima Yazdani, Adam Vianna, Jesse L. Peltier, Daniel A. Tolentino

## RECENT PROGRESS

### ***The influence of C(sp<sup>3</sup>)H-Selenium Interactions on the <sup>77</sup>Se NMR Quantification of the p-Accepting Properties of Carbenes***

Nowadays, a variety of stable carbenes, featuring very diverse electronic and steric properties, are known. Accordingly, choosing the best carbene for a given application is



***Non-classical hydrogen bonds (NCHB) in carbene-selenium adducts cause pronounced downfield shifts in <sup>77</sup>SeNMR spectra, perturbing the Se scale for probing π-accepting properties within a carbene family.***

selenium adducts, which cause major deviations from the expected trend in <sup>77</sup>Se NMR chemical shifts. These findings encourage caution when probing p-accepting properties within a carbene family, especially when bulky substituents are in proximity to the carbene center.

### ***Optically Pure C<sub>1</sub>-Symmetric Cyclic(alkyl)(amino)carbene Ruthenium-Complexes for Asymmetric Olefin Metathesis.***

With the discovery of the 2nd generation Grubbs catalysts, N-heterocyclic carbenes (NHCs) have become inescapable ligands in olefin metathesis, in both academic and industrial research environments. More recently, another class of carbenes namely cyclic (alkyl)(amino) carbenes (CAACs), discovered in our group, arose as a contender to NHCs. Since then, CAACs have been shown to achieve over 340000 TON in ethenolysis processes, meanwhile achieving remarkable catalytic performances in a number of other metathesis transformations. Interestingly, despite these achievements there was still no report dealing

not an easy task; it requires a thorough understanding of the carbene stereoelectronic properties. Several techniques have first been developed to evaluate the overall donor abilities of carbenes, but they failed to deconvolute the s-donating and p-accepting properties. More recently, to determine their p-accepting character, the <sup>31</sup>P{<sup>1</sup>H} NMR and <sup>77</sup>Se{<sup>1</sup>H} NMR chemical shifts of phenylphosphinidene- and selenium-carbene-adducts, respectively, have been exploited. Compared with the phosphinidene scale (~400 ppm), the selenium scale covers a wider spectral range (~1200 ppm) which should allow for a greater delineation of the π-accepting properties of closely matching carbenes. Moreover, it benefits from a simple experimental protocol *i.e.* addition of elemental selenium to an *in-situ* generated free carbene. Despite the popularity of this method, careful examination of the literature revealed several inconsistencies in <sup>77</sup>Se{<sup>1</sup>H} NMR data. We have provided experimental and computational evidence for the existence of non-classical hydrogen bonding interactions in carbene-

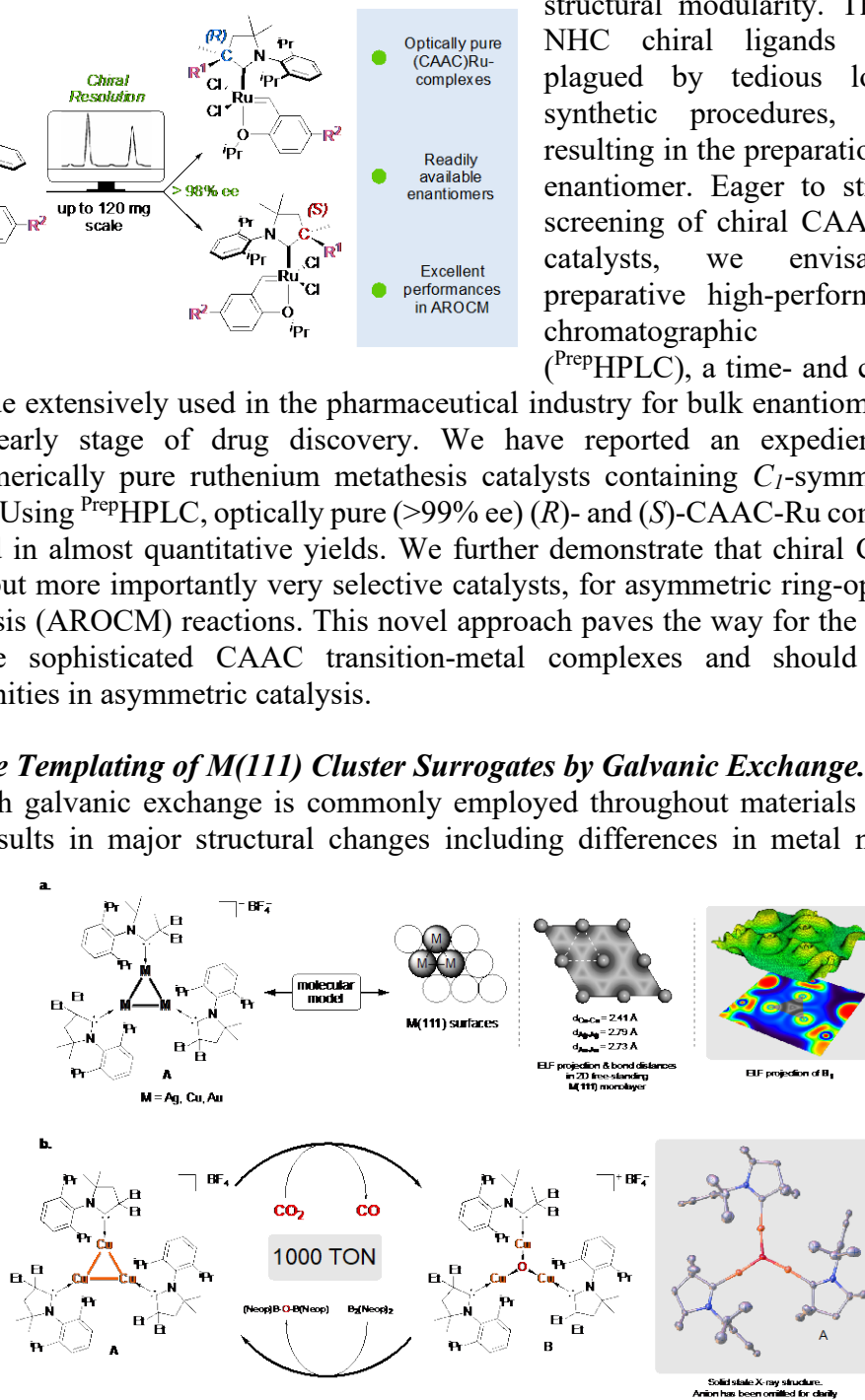
with CAAC ligands in asymmetric metathesis. In 2019, we demonstrated that a steroid derived chiral CAAC-copper complex <sup>Cholest</sup>CAAC-CuCl could induce Asymmetric Conjugate Borylation (ACB). Encouraged by these results we set to demonstrate the potency of chiral CAAC-Ru complexes in asymmetric olefin metathesis. Despite the availability of the ligand, we reasoned that the <sup>Cholest</sup>CAAC or related chiral CAAC ligands derived from naturally abundant chiral building blocks would not provide the required

structural modularity. The design of NHC chiral ligands is arguably plagued by tedious low yielding synthetic procedures, very often, resulting in the preparation of a single enantiomer. Eager to streamline the screening of chiral CAAC-ruthenium catalysts, we envisaged using preparative high-performance liquid chromatographic resolution (<sup>Prep</sup>HPLC), a time- and cost-effective

technique extensively used in the pharmaceutical industry for bulk enantiomer resolution at the early stage of drug discovery. We have reported an expedient access to enantiomerically pure ruthenium metathesis catalysts containing *C<sub>1</sub>*-symmetric CAAC ligands. Using <sup>Prep</sup>HPLC, optically pure (>99% ee) (*R*)- and (*S*)-CAAC-Ru complexes were obtained in almost quantitative yields. We further demonstrate that chiral CAACs yield active, but more importantly very selective catalysts, for asymmetric ring-opening cross-metathesis (AROCM) reactions. This novel approach paves the way for the development of more sophisticated CAAC transition-metal complexes and should create new opportunities in asymmetric catalysis.

### Absolute Templating of *M*(111) Cluster Surrogates by Galvanic Exchange.

Although galvanic exchange is commonly employed throughout materials chemistry, it often results in major structural changes including differences in metal nuclearity. In

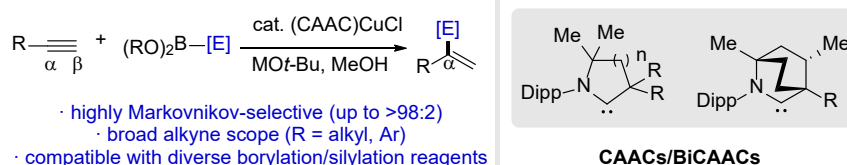


(a) *M-M* bond distances and ELF topology suggest similarities between trinuclear clusters *A* and free standing *M*(111) monolayers. (b) In contrast to the gold and silver equivalent, the trinuclear  $Cu^0_3Cu^I$  promotes the dissociative reduction of  $CO_2$  thereby affording *B*. Using bis(neopentyl glycolato)diboron to regenerate *A*, up to 1000 TON could be obtained in the reduction of  $CO_2$  to  $CO$ .

contrast, we have systematically applied galvanic exchange to trinuclear complexes of the coinage metals with maintenance of metal nuclearity throughout the series. These clusters have been synthesized in high yields using standard air-free techniques and thus provide a good platform for further study. Additionally, they feature metals in the predominantly zero oxidation state, making them reminiscent of M(111) surfaces. To further reinforce the analogy between materials and UNPs, we showed that one of our copper cluster promotes CO<sub>2</sub> reduction, a process commonly observed for Cu(111) surfaces. Additionally, the small size of these clusters allowed for the isolation and characterization of a m<sub>3</sub>-oxo copper complex, which has the potential to be occurring on Cu(111) surfaces. Error! Bookmark not defined. Our results highlight the mounting impact of  $\pi$ -acidic carbene ligands, such as CAACs, in materials science.

***Cyclic(Alkyl)(Amino)Carbene Ligands Enable Cu-Catalyzed Markovnikov Protoboration and Protosilylation of Terminal Alkynes: A Versatile Portal to Functionalized Alkenes***

Regioselective hydrofunctionalization of alkynes represents a straightforward route to access alkenyl boronate and silane building blocks. In previously reported catalytic systems, high selectivity is achieved with a limited scope of substrates and/or reagents, with general solutions lacking. This year, we described a selective copper-catalyzed Markovnikov hydrofunctionalization of terminal alkynes that is facilitated by strongly donating cyclic (alkyl)(amino)carbene (CAAC) ligands. Using this method, both alkyl- and aryl-substituted alkynes are coupled with a variety of boryl and silyl reagents with high  $\alpha$ -selectivity. The reaction is scalable, and the products are versatile intermediates that can participate in various downstream transformations. Preliminary mechanistic experiments shed light on the role of CAAC ligands in this process.



**Publications Acknowledging this Grant in 2018-2021**

*(I) Intellectually led by this grant*

- 1 Weinstein, C. M.; Junor, G. P.; Tolentino, D. R.; Jazzar, R.; Melaimi, M.; Bertrand, G. Highly Ambiphilic Room Temperature Stable Six-Membered Cyclic (Alkyl)(amino)carbenes. *J. Am. Chem. Soc.* **2018**, *140*, 9255-9260.
- 2 Romero, E. A.; Zhao, T.; Nakano, R.; Hu, X.; Wu, Y.; Jazzar, R.; Bertrand, G. Tandem Copper Hydride - Lewis Pair Catalyzed Reduction of Carbon Dioxide into Formate with Dihydrogen. *Nature Catal.* **2018**, *1*, 743-747.
- 3 Junor, G.; Romero, E. A.; Chen, X.; Jazzar, R.; Bertrand, G. Readily Available Primary Aminoboranes as Powerful Reagents for Aldimine Synthesis. *Angew. Chem. Int. Ed.* **2019**, *58*, 2875-2878.

- 4 Tolentino, D. R.; Neale, S. E.; Isaac, C. J.; Macgregor, S. A.; Whittlesey, M. K.; Jazzar, R.; Bertrand, G. Reductive Elimination at Carbon under Steric Control. *J. Am. Chem. Soc.* **2019**, *141*, 9823-9826.
- 5 Pichon, D.; Soleilhavoup, M.; Morvan, J.; Junor, G. P.; Vives, T.; Crévisy, C.; Lavallo, V.; Campagne, J. M.; Mauduit, M.; Jazzar, R.; Bertrand, G. The Debut of Chiral Cyclic (Alkyl)(amino)carbenes (CAACs) in Enantioselective Catalysis. *Chem. Sci.* **2019**, *10*, 7807-7811.
- 6 Liu, W.; Zhao, L. L.; Melaimi, M.; Cao, L.; Xu, X.; Bouffard, J.; Bertrand, G.; Yan, X. Mesoionic carbene (MIC) catalyzed H/D exchange at formyl groups. *Chem.* **2019**, *5*, 2484-2494.
- 7 Romero, E. A.; Chen, G.; Gembicky, M.; Jazzar, R.; Yu, J.-Q.; Bertrand, G. Understanding the Activity and Enantioselectivity of Acetyl-Protected Aminoethyl Quinoline ligands in Palladium-Catalyzed  $\beta$ -C(sp<sup>3</sup>)-H Bond Arylation reactions. *J. Am. Chem. Soc.* **2019**, *141*, 16726-16733.
- 8 Yazdani, S.; Junor, G. P.; Peltier, J. L.; Gembicky, M.; Jazzar, R.; Grotjahn, D. B.; Bertrand, G. Influence of Carbene and Phosphine Ligands on the Catalytic Activity of Gold Complexes in the Hydroamination and Hydrohydrazination of Alkynes. *ACS Catal.* **2020**, *10*, 5190-5201.
- 9 Sau, S. C.; Hota, P. K.; Mandal, S. K.; Soleilhavoup, M.; Bertrand, G. Stable Abnormal N-Heterocyclic Carbenes and their Applications. *Chem. Soc. Rev.* **2020**, *49*, 1233-1252.
- 10 Jazzar, R.; Soleilhavoup, M.; Bertrand, G. Cyclic (Alkyl)- and (Aryl)(amino)carbene Coinage Metal Complexes and Their Applications. *Chem. Rev.* **2020**, *120*, 4141-4168.
- 11 Junor, G. P.; Lorkowski, J.; Weinstein, C. M.; Jazzar, R.; Pietraszuk, C.; Bertrand, G. The influence of C(sp<sup>3</sup>)H-Selenium Interactions on the <sup>77</sup>Se NMR Quantification of the  $\sigma$ -Accepting Properties of Carbenes. *Angew. Chem. Int. Ed.* **2020**, *59*, 22028-22033.
- 12 Peltier, J. L.; Soleilhavoup, M.; Martin, D.; Jazzar, R.; Bertrand, G. Absolute Templating of M(111) Cluster Surrogates by Galvanic Exchange. *J. Am. Chem. Soc.* **2020**, *142*, 16479-16485.
- 13 Peltier, J. L.; Tomas-Mendivil, E.; Tolentino, D. R.; Hansmann, M. M.; Jazzar, R.; Bertrand, G. Realizing Metal-Free Carbene-Catalyzed Carbonylation Reactions with CO. *J. Am. Chem. Soc.* **2020**, *142*, 18336-18340.
- 14 Morvan, J.; Vermersch, F.; Zhang, Z.; Falivene, L.; Vives, T.; Dorcet, V.; Roisnel, T.; Crévisy, C.; Cavallo, L.; Vanthuyne, N.; Bertrand, G.; Jazzar, R.; Mauduit, M. Optically Pure C<sub>1</sub>-Symmetric Cyclic(alkyl)(amino)carbene Ruthenium-Complexes for Asymmetric Olefin Metathesis. *J. Am. Chem. Soc.* **2020**, *142*, 19895-19901.
- 15 Jazzar, R.; Soleilhavoup, M.; Bertrand, G. Cyclic (Alkyl)- and (Aryl)-(amino)carbene Coinage Metal Complexes and Their Applications, *Chem. Rev.* **2020**, *120*, 4141-4168.
- 16 Morvan, J.; Mauduit, M.; Bertrand, G.; Jazzar, R. Cyclic (Alkyl)(amino)carbenes (CAACs) in Ruthenium Olefin Metathesis. *ACS Catal.* **2021**, *11*, 1714-1748. DOI: 10.1021/acscatal.0c05508
- 17 Liu, W.; Vianna, A.; Zhang, Z.; Huang, S.; Huang, L.; Melaimi, M.; Bertrand, G.; Yan, X. Mesoionic Carbene-Breslow Intermediates as Super Electron Donors: Application to the Metal-Free Arylacylation of Alkenes. *Chem. Catalysis* **2021**, *1*, 196-206.

- 18 Gao, Y.; Yazdani, S.; Kendric, A.; Junor, G. P.; Kang, T. Grotjahn, D. B.; Bertrand, G.; Jazzar, R.; Engle, K. M. Cyclic(Alkyl)(Amino)Carbene Ligands Enable Cu-Catalyzed Markovnikov Protoboration and Protosilylation of Terminal Alkynes: A Versatile Portal to Functionalized Alkenes. *Angew. Chem. Int. Ed.* **2021**, *60*, in press.

(II) *Jointly funded by this grant and other grants with intellectual leadership by other funding sources*

- 1 Soleilhavoup, M.; Bertrand, G. Stable Carbenes, Nitrenes, Phosphinidenes, and Borylenes: Past and Future. *Chem.* **2020**, *6*, 1275-1282.

#### **Leadership activities during 2018-2020 calendar years**

Member of the Editorial Board, "Heteroatom Chemistry", 1989-present  
Member of the Editorial Board, "C. R. Acad. Sc. Paris", 1998-present  
Member of the Editorial Board, "Eur. J. Inorg. Chem.", December 2002-present  
Member of the Editorial Board, "Chemistry: an Asian Journal.", 2006-present  
Member of the Editorial Board, "Chemistry Letters", 2010-present  
Member of the Editorial Board "Chemical Science", 2010-present  
Member of the Editorial Board "Organic Chemistry Frontiers (OCF) (RSC), 2013-present  
Member of Senior Editors of Bulletin Chemical Society of Japan, 2013-present  
Member of the Editorial Board "Chem" (Cell Press), 2015-present  
Member of the Advisory Board of "Natural Sciences", 2021-present  
Associate Editor, "Chemical Reviews", 2010-present

#### **Awards during 2018-2020 calendar years**

Vilsmeier Lectureship, University of Regensburg (Germany), 2018  
Named "Distinguished Visiting Professor" at Tsinghua University (China), 2018  
Named "Honorable Professor" at Wuhan University of Technology (China), 2018  
Strem lectureship in chemical catalysis at Boston College, 2019-2020.  
Grand Prix de la Maison de la Chimie (shared with K. Matyjaszewski), 2020  
Neil Bartlett lectureship at UC Berkeley, 2021.

**Elizabeth J. Biddinger**

**Electrochemical Hydrogenation and Hydrogenolysis of Furfural over Copper Catalyst in Acid Media**

Andrew S. May<sup>1</sup>, Steven M. Watt<sup>1,2</sup>, and Elizabeth J. Biddinger<sup>1,2\*</sup>

1 Chemical Engineering, The City College of New York, CUNY, New York, NY,(USA)

2 Ph.D. Program in Chemistry, The Graduate Center of the City University of New York, New York, NY, (USA)

Electrochemical processes, when coupled with renewable energy such as solar or wind, offer a method to produce chemicals with reduced CO<sub>2</sub> emissions compared to their conventional methods. Furfural (FF) is a biomass derived species that can be converted electrochemically to furfuryl alcohol (FA), used to make furanic polymers, and 2-methylfuran (MF) which is a fuel additive. The use of electrochemical processes is a new area of interest, with the work in the past decade focusing on parameters that impact selectivity and production rate. In this work, we investigate the kinetics and the mechanism of the electrochemical hydrogenation and hydrogenolysis (ECH) reactions of FF to FA and MF.

We proved that ECH of FF is an electrochemical process using protons from the electrolyte and not a conventional thermocatalytic process that happens to use in situ generated H<sub>2</sub> gas. Mechanistically, we found that the reactions to form FA and MF both go through rate limiting steps with the same number of electrons being transferred. By modeling the reaction rates and comparing to experimental data, we significantly narrowed down the possible mechanisms of FF ECH in acidic electrolytes on copper. A non-competitive Langmuir-Hinshelwood mechanism is most likely for the reaction where FA is produced via the hydrogenation of the C<sub>4</sub>H<sub>3</sub>O-CH<sub>2</sub>O intermediate, while MF is produced via the C-O cleavage of the C<sub>4</sub>H<sub>3</sub>O-CHOH intermediate.

**Grant Number & Title**

DE-SC0019134: Reaction Mechanism and Kinetics for Electrochemical Hydrogenation and Hydrogenolysis of Biomass-Derived Species

**PI:** Elizabeth J. Biddinger

**Postdoc(s):** N/A

**Student(s):** Andrew S. May<sup>1</sup>, Steven M. Watt<sup>1,2</sup>

**Affiliations(s):** <sup>1</sup> Department of Chemical Engineering, The City College of New York; <sup>2</sup> PhD Program in Chemistry, CUNY Graduate Center

**RECENT PROGRESS**

***Understanding Kinetics and Mechanism***

To determine if ECH of furfural on copper in acidic media is truly an electrochemical process rather than a thermochemical process that utilizes hydrogen gas that has been

generated electrochemically, hydrogen gas was intentionally introduced into the electrochemical reactor during ECH. Without an applied potential, no reaction occurred over 90 minutes, showing that FF does not react with gaseous hydrogen in the reactor at 25°C (Figure 1). Once a potential was applied (-560mV vs RHE), products begin to form and the FF concentration decreased, at rates comparable to the absence of H<sub>2</sub> gas. This showed that the reactions of ECH of FF on copper in acidic electrolytes occur between FF and protons, on the surface or in the bulk solution, rather than in the gaseous form.

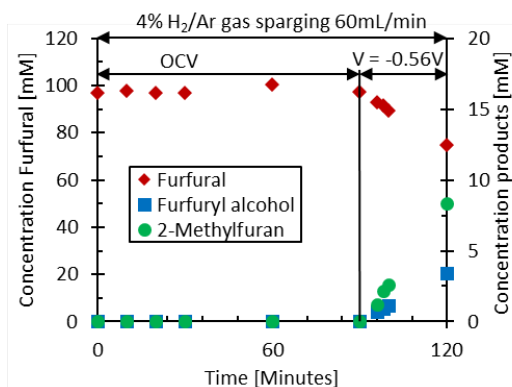


**Figure 1.** The concentration of FF, FA, and MF over time in the presence of H<sub>2</sub> gas. First 90 minutes: no applied potential. Last 30 minutes: applied potential of -560mV vs RHE. Conditions: 4%H<sub>2</sub>/Ar sparging at 60mL/minute, 100 mM FF initial concentration, 80:20 v:v DI water to acetonitrile with 0.5 M H<sub>2</sub>SO<sub>4</sub>.

To begin to analyze the rate limiting steps for the formation of FA and MF, Tafel slopes of 0.0827 and 0.0996 V/decade for FA and MF, respectively, were found (Figure 2). The similar Tafel slopes suggest that both reactions have the same number of electrons in their rate limiting steps. Since most reactions do not involve multiple electrons in a single step, it is likely that both reactions proceed via a one electron transfer rate limiting step.

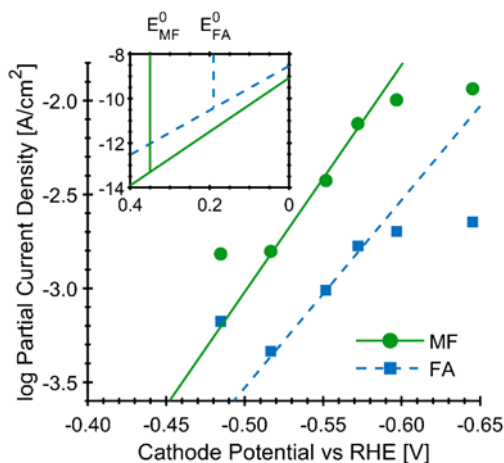


**Figure 2.** Tafel plot for the ECH of FF to FA and MF. The standard potentials are marked on the inset at 0.192V and 0.352V and labeled  $E_{FA}^0$  and  $E_{MF}^0$ . Conditions: 100 mM FF initial concentration, 25°C, 80:20 v:v DI water to acetonitrile with 0.5 M H<sub>2</sub>SO<sub>4</sub>.

To investigate the mechanisms of FF ECH to FA and MF in acidic media over copper, a schematic outlining the elementary steps was used to develop the possible rate equations (Figure 3) and compared to experimental data (Figure 4). The experimental rates of production had a first order dependence in FF at concentrations below 60 mM and a zeroth order dependence above 60 mM FF. Rates towards MF production dropped significantly with the increase in pH from 0 to 1, while rates towards FA minimally changed with the increase in pH from 0 to 1. Competitive Langmuir-Hinshelwood, non-competitive Langmuir-Hinshelwood and Eley-Rideal mechanisms were evaluated. The non-competitive Langmuir-Hinshelwood based mechanisms were the only cases in which a good fit to the experimental data was found. Additionally, it is most likely that ECH to FA has F1 or F3 (labeled on Figure 3) as the rate limiting step, due to the dependence on proton being too high with the F2 or F4 step. For MF, the likely step to be rate limiting is M7 or M4. Steps M9 and M10 are unlikely because FA was not reduced to MF in ECH over Cu in acidic media at potentials tested. Of the M4 and M7 step, the M7 step is energetically more easily performed based on the DFT results of another group. Additionally, the Tafel slopes reported above suggest the ECH to FF and ECH to MF have the same number of electrons being transferred in the rate limiting step. For these reasons, the F1 M7 mechanism is most likely, as the number of electrons in the rate limiting steps match between FA and MF, the experimental data fits well to the model, and energetically the reactions are more likely than other steps. Table 1 summarizes the reactions and parameters for the favorable non-competitive Langmuir-Hinshelwood F1-M7 ECH of FF mechanism.

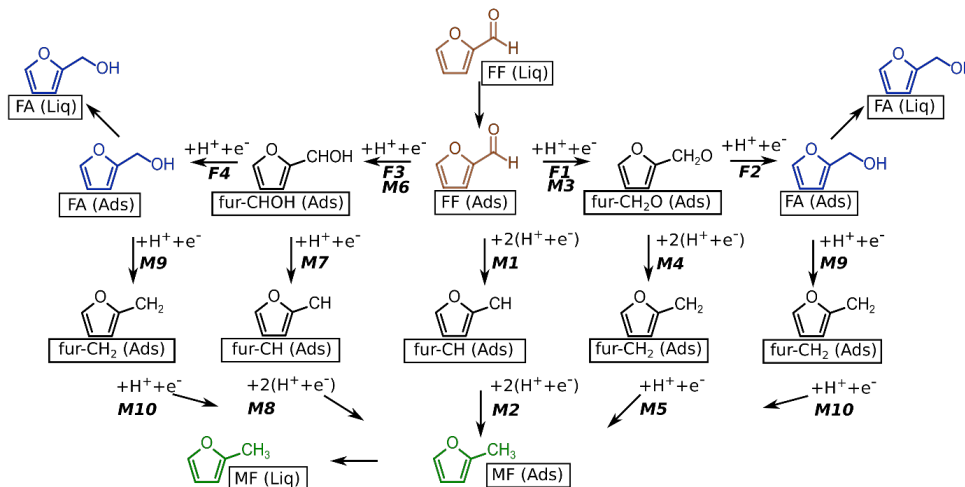


**Figure 3.** Schematic of possible elementary steps in FF ECH to FA and MF. “F” labels signify a step towards FA production while “M” labels signify a step towards MF production.

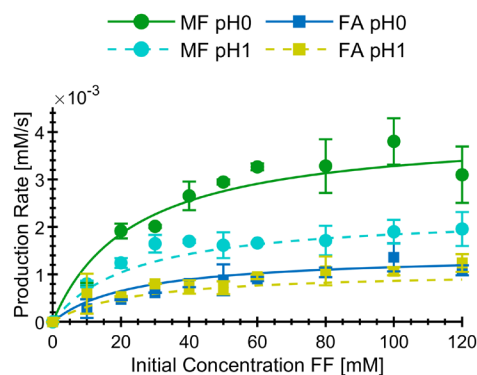


**Figure 4.** The production rate of MF and FA. Lines are models of the production rate from a non-competitive Langmuir-Hinshelwood mechanism with F1 and M7 (labeled on Figure 3) as the rate limiting steps of FF ECH.

**Table 1.** The reaction steps, rate equations, rate constants, and reduced chi square for the NCLH (F1 and M7 rate limiting steps) case shown in Figure 4.

Model	F1-NCLH M7-NCLH	
Adsorption reactions	<b>(K<sub>1</sub>):</b> H <sup>+</sup> + e <sup>-</sup> + T ⇌ H•T <b>(K<sub>2</sub>):</b> FF + S ⇌ FF•S	
Elementary Reactions FA	<b>(k<sub>rdsFA</sub>):</b> FF•S + H•T → (fur-CH <sub>2</sub> O)•S + T (fur-CH <sub>2</sub> O)•S + H•T ⇌ FA•S + T FA•S ⇌ FA + S	
Elementary Reactions MF	<b>(K<sub>3</sub>):</b> FF•S + H•T ⇌ (fur-CHOH)•S + T <b>(k<sub>rdsMF</sub>):</b> (fur-CHOH)•S + H•T → (fur-CH)•S + H <sub>2</sub> O + T (fur-CH)•S + 2H•T ⇌ MF•S + 2T MF•S ⇌ MF + S	
Rate Equations	$R_{FA} = \frac{k_{RDSFA} K_2 [FF] K_1 \alpha_H}{(1+K_2[FF])(1+K_1 \alpha_H)} \quad R_{MF} = \frac{k_{RDSMF} K_2 [FF] K_3 (K_1)^2 (\alpha_H)^2}{(1+K_2[FF]) * (1+K_1 \alpha_H)^2}$	
Reduced chi-square	FA= 134 MF= 17.5	* FA <sub>14.2</sub> = 2.95 * MF <sub>14.2</sub> = 1.32
Rate Constants	K <sub>1</sub> = 25.9 ± 6 K <sub>2</sub> = (0.042 ± 0.02) 1/mM k <sub>RDSFA</sub> = (0.00148 ± 0.0003) mM/s K <sub>3</sub> k <sub>RDSMF</sub> = (0.00438 ± 0.0005) mM/s	

\*The reduced chi-square with a subscript 14.2 is found assuming a hypothetical standard deviation of 14.2%, which is the average standard deviation found in experimental data.

### Publications Acknowledging this Grant in 2018-2021

*Intellectually led by this grant*

May, A. S.; Biddinger, E. J., Strategies to control electrochemical hydrogenation and hydrogenolysis of furfural and minimize undesired side reactions. *ACS Catal.* **2020**, *10*, 3212-3221.

## **Awards or leadership activities during 2018-2020 calendar years**

### **Awards**

- **2019 CCNY Grove School of Engineering Dean's Award for Excellence** for outstanding research, teaching & service
- **2018 US Department of Energy Early Career Award** for biomass electroreduction research

### **Leadership Activities**

#### **Guest Edited Special Issues**

- “Electrochemical Routes for Biomass Conversion,” Special Issue of *Journal of Applied Electrochemistry*, Guest Editors: E.J. Biddinger, J. Holladay, O. Gutierrez, 2020, January 2021, Volume 51, issue 1, pages 1-130.
- “Special Issue Honoring Umit S. Ozkan: 2017 ACS Henry H. Storch Award Winner,” Special Volume of *Catalysis Today*. Guest Editors: E.J. Biddinger, N. Brunelli, Volume 323, 15 February 2019, pages 1-270.
- “Molten Salts and Ionic Liquids 21,” Issue of *ECS Transactions*, AiMES 2018/234<sup>th</sup> ECS Meeting, Editors: W.M. Reichert, R.A. Mantz, P.C. Trulove, L.M. Haverhals, E.J. Biddinger, H.C. De Long, A.H. Suroviec, M. Mizuhata, M. Ueda, A. Ispas, A. Bund, D.P. Durkin, Volume 86, Issue 14, 30 September 2018, pages 1-387.

#### **Society Engagement**

- Industrial Electrochemistry and Electrochemical Engineering Division of The Electrochemical Society; Student & Earl Career Awards Chair, 2014-Present; Member-At-Large, 2018-Present
- The Electrochemical Society; Publications Subcommittee Member, 2017-2020; Alternate Teller of Election, 2016 – 2018
- Catalysis and Reaction Engineering Division of the American Institute of Chemical Engineers; Director, 2017 – 2019

#### **Conference Organization**

- 22<sup>nd</sup> North American Meeting of the North American Catalysis Society, New York City, NY, May 2021 (*postponed to May 2022*); Member of organizing committee; Kokes Student Travel Awards Chair
- 17<sup>th</sup> International Congress on Catalysis, San Diego, CA, June 2020 (*cancelled May 15, 2020 due to COVID-19*); Member of organizing committee; Member of “Posters, Workshops and Satellite Conferences” sub-committee

#### **Center Leadership**

- Center for Decarbonizing Chemical Manufacturing Using Sustainable Electrification (DC-MUSE); Deputy Director; 2021 – Present.

**Engineering Host-Guest Catalysts for the Tandem Catalytic Hydrogenation of CO<sub>2</sub> to Methanol**

Jeffery A Byers, Chia-Kuang "Frank" Tsung, Natalia Shustova\*, Thomas M. Rayder, Banruo Li, Abhijai Mather\*, William Thompson, and Enric H. Adillon  
Boston College, Department of Chemistry  
University of South Carolina

**Presentation Abstract**

The industrial hydrogenation of carbon dioxide to methanol is carried out using a Cu/Zn heterogeneous catalyst that is not well defined and difficult to systematically modify to improve performance. In this presentation, a tandem host-guest catalyst system is described that enables the hydrogenation of carbon dioxide to methanol. The system relies on encapsulating homogeneous molecular ruthenium-based hydrogenation catalysts in metal-organic frameworks (MOFs) derived from the robust MOF UiO-66. The host-guest catalyst system enables the hydrogenation of carbon dioxide with high turnover at relatively low temperatures. The catalyst system is readily recycled and, unlike the commercial catalysts used for carbon dioxide hydrogenation, the catalyst can be easily modified by altering the identity of the homogeneous guest catalyst precursor or the MOF host. Modifications made to the linkers of the MOF host led to a two-fold increase in catalytic activity. Mechanistic investigations revealed that catalyst confinement is critical to catalytic performance. Further experimentation revealed that second-sphere interactions are most beneficial for aiding in the first step of the reaction, the hydrogenation of carbon dioxide to formic acid. Further investigations revealed the importance of water removal in these reactions: dynamic removal of water resulted in a nearly five-fold increase in catalyst activity. As a result of the modularity in the host-guest catalyst system, the highest reported turnover number (TON) (19,000) and turnover frequency (TOF) (9100 h<sup>-1</sup>) in the conversion of carbon dioxide to methanol was achieved. Moreover, the reaction was readily recyclable, leading to an extremely high cumulative TON (>100,000) after ten reaction cycles. In addition to catalyst modifications, efforts to locate guest molecules encapsulated in metal-organic frameworks so as to better engineer tandem catalysts so that they mimic biological multi-component catalyst systems will be discussed.

**Grant or FWP Number: DOE-BES DE-SC0019055**  
**Organometallic Catalysis from Molecular Catalysts Non-Covalently Confined in Metal-Organic Frameworks**

**co-PI:** Chia-Kuang "Frank" Tsung (2017-2020), Natalia Shustova\* (2021-present)

**Postdoc(s):** none

**Student(s):** Adam T. Benselah, Banruo Li, Abhijai Mather\*, Thomas R. Rayder, William Thompson, Enric H. Adillon, Noella D'Souza, Trevor Hale, Lucy Hanson

**Affiliations(s):** \*University of South Carolina

## RECENT PROGRESS

### Goal 1. Develop a tandem catalyst system that benefits from the cooperation of multiple catalytically active species for the hydrogenation of CO<sub>2</sub> to methanol.

This goal was completed in the previous funding period, and a publication describing this work recently was accepted for publication in *Chem* in 2020 (*see below*).

### Goal 2. Utilize non-covalent interactions between the host and guest to modulate chemical reactivity.

The first part of this funding period was devoted to completing this goal. In the last funding period, we discovered that second-sphere interactions may be important in altering the local environments for guests encapsulated in metal-organic framework hosts through encapsulation of the fluorescent dye Rhodamine-6G in the metal-organic framework UiO-66 (and derivatives of UiO-66). Analysis of these host-guest materials by fluorescence spectroscopy revealed an intimate connection between the identity of functionality installed in the ligand of the MOF, the identity of the solvent that spectra were acquired in, and the degree of confinement from the guest. We had prepared an article that described this study prior to the last DOE meeting, but we determined further analysis of the data was necessary before we could submit the article. We have now completed the analysis of these data and plan to submit an article describing this work in the coming months.

In parallel with these investigations, we were carrying out CO<sub>2</sub> hydrogenation reactions using the tandem catalyst system developed in Goal 1 and various functionalized UiO-66-X derivatives. Last year, we reported that UiO-66-NH<sub>3</sub><sup>+</sup> led to enhanced turnover number relative to catalysis carried out using UiO-66 (Figure 1). The effect was only noticeable with the CO<sub>2</sub> to formic acid catalyst, (t<sup>Bu</sup>PNP)RuHCICO (i.e., **1**), encapsulated in the MOF. When the ester hydrogenation catalyst, (t<sup>Bu</sup>PNN)RuHCICO (i.e., **2**), was encapsulated in the MOF or when UiO-66-NH<sub>3</sub><sup>+</sup> was added to a reaction in addition to the normal cascade reaction conditions, no increase in turnover number was observed. These results suggested that there was a specific interaction between the linkers on UiO-66-NH<sub>3</sub><sup>+</sup> and the encapsulated CO<sub>2</sub> to formic acid catalyst that was resulting in the higher catalytic turnover. Reactions carried out using UiO-66-NMe<sub>x</sub>H<sub>y</sub><sup>+</sup> hosts (x = 0-2, y = 3-1, respectively) suggested

**Figure 1.** Effect of substituents installed in the linker of UiO-66 on the tandem catalytic hydrogenation of CO<sub>2</sub> to methanol.

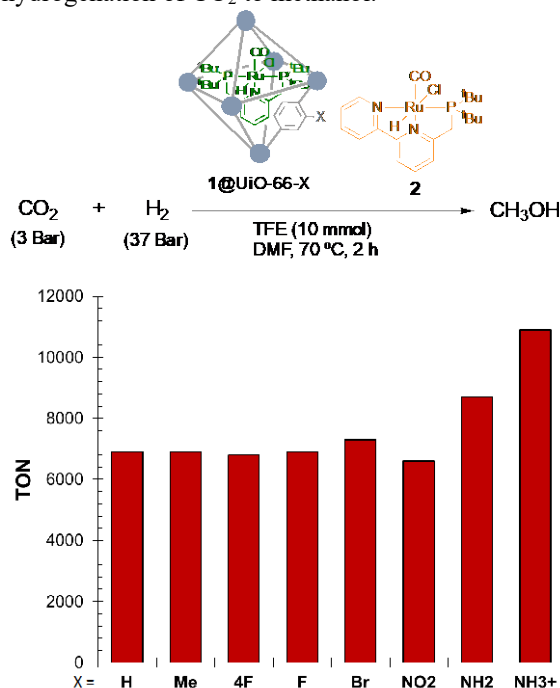


**Table 1.** Effect of amine substituents on the activity of hydrogenation of CO<sub>2</sub> to methanol.

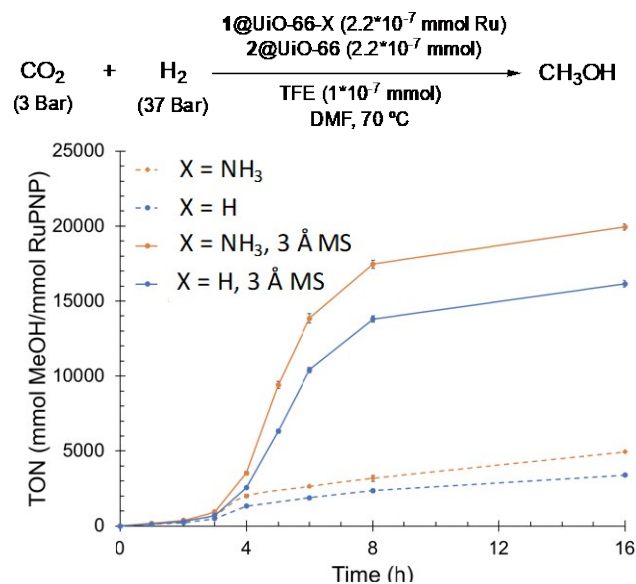
Entry	X	pK <sub>a</sub> /pK <sub>b</sub> of Ph-X	TON
1	NH <sub>2</sub>	9.42	6200 ± 500
2	NHMe	9.15	6100 ± 400
3	NMe <sub>2</sub>	8.94	6000 ± 350
4	H	-	6000 ± 400
5	NH <sub>3</sub> <sup>+</sup>	4.58	8900 ± 350
6	NH <sub>2</sub> Me <sup>+</sup>	4.85	7200 ± 300
7	NHMe <sub>2</sub> <sup>+</sup>	5.06	6600 ± 400
8	ND <sub>3</sub> <sup>+</sup>	4.70	6100 ± 400

In an effort to extend the autocatalytic regime that the catalyst system benefits from, time course experiments revealed that the difference between catalysis run with **1**@UiO-66 and **1**@UiO-66-NH<sub>3</sub><sup>+</sup> occurred at intermediate times. We hypothesized that after a certain reaction period, water builds up in the reaction, which stifles the overall transformation. To illustrate the importance of water removal in these reactions, we carried out the reactions in the presence of molecular sieves, which resulted in a nearly 5-fold increase in catalyst activity (Figure 2). Moreover, the period where the functionalized MOF outperformed the unfunctionalized MOF was extended, thereby increasing the beneficial effects from the second-sphere interactions that resulted for the NH<sub>3</sub><sup>+</sup>.

With the optimal catalyst system in hand, the robustness of the fully heterogeneous catalyst system (i.e. with **1** and **2** encapsulated in the MOF) was demonstrated by recycling the catalyst. Recycling was successful over ten reactions without any loss in catalyst activity or evidence for catalyst leaching. A publication describing this research was published in *JACS* earlier this year (*see below*).

that the functionality was most likely serving as a specific Bronsted acid catalyst, which we hypothesize help aide with protonation of a ruthenium-formate species that is the known resting state of the catalyst (Table 1). Additionally, the cooperative effect was effective only when the functional group (-NH<sub>3</sub><sup>+</sup>) was in close proximity to the encapsulated catalyst: When the catalyst was encapsulated in UiO-67-NH<sub>3</sub><sup>+</sup> an isomorph of UiO-66-NH<sub>3</sub><sup>+</sup> with larger cages or encapsulated in native UiO-66 with the addition of high concentration of exogenous ammonium chloride in the solution, the cooperative effect was not significant.

**Figure 2.** The effect of 3 Å molecular sieves on the cascade hydrogenation of CO<sub>2</sub> to methanol.



### **Goal 3: Stabilize reactive intermediates through their encapsulation in the confined structures in MOFs.**

Although we are still interested in further exploring the tandem catalytic properties of the system mentioned in Goals 1 and 2, an advantage of the aperture opening method that we use to encapsulate transition metal complexes in MOFs is that it affords us the opportunity to encapsulate organometallic precursors that can be transformed into reactive intermediates that would otherwise be too unstable to observe. In the last reporting period, we disclosed a method to improve guest molecule loading in MOFs by using acetonitrile as the solvent for the aperture-opening encapsulation method. Using this method, we were successful in encapsulating  $\square$ -diketiminato iron complexes that have been used to split nitrogen. Characterization of these complexes was possible using a combination of Mössbauer spectroscopy, infrared spectroscopy, and ICP-OES. Unfortunately, progress on this goal was significantly impacted by the COVID-19 pandemic with the death of PI Tsung and the subsequent impact that this tragedy had on the researchers carrying out this part of the project. Fortunately, we have begun a new collaboration with Natalia Shustova (University of South Carolina), who is an expert in MOF synthesis and characterization. With this new team in place, we are currently exploring the reduction of the encapsulated iron complexes as well as developing methods for the encapsulation of organometallic complexes in molecular cages that are structurally similar to the UiO-66 MOFs that we have been using. These cages will serve as molecular models for supramolecular host materials that we ultimately will use as catalysts. These models will enable us to use x-ray crystallography to characterize guest molecules in hosts.

### **Publications Acknowledging this Grant in 2018-2021**

*(XIII) Intellectually led by this grant*

1. Rayder, Thomas M.; Adillon, Enric H.; Byers, Jeffery A.; Tsung, Chia-Kuang A Bioinspired Multicomponent Catalytic System for Converting Carbon Dioxide into Methanol Autocatalytically *Chem*, **2020**, *6*, 1742-1754.
2. Rayder, Thomas M.; Bensalah, Adam T.; Li, Banruo; Byers, Jeffery A. \*, Tsung, Chia-Kuang\* "Engineering Second Sphere Interactions in a Host-Guest Multicomponent Catalyst System for the Hydrogenation of Carbon Dioxide to Methanol" *Journal of the American Chemical Society*, **2021**, *143*, 3, 1630-1640.

### **Awards and Leadership Activities**

**PI: Jeffery A. Byers**

2018-2019

1. Organizer of the "Paper to Plastics" summer outreach program for high school students (2018-2019).
2. Boston College Beckman Scholars Steering Committee Member (2018-2019).

## 2018

1. McCarthy Prize Committee Member, 2018
2. Organizing Committee Member for BORAM XVI (Chestnut Hill, MA on June 26-30, 2018).

## 2019

1. Organizer of the 48th Boston Regional Inorganic Colloquium (Chestnut Hill, MA on March 2, 2019).
2. Participant in the Department of Energy Basic Energy Science Roundtable on Chemical Upcycling of Polymers (Washington DC on April 30-May 1, 2019).
3. Department of Chemistry Chair's Steering Committee (2019-present).

## 2020

1. Serving as a Co-PI for an NSF-CCI Center for Integrated Catalysis.
2. Participated in the program review for DOE-BES LBNL Catalysis program.
3. Established the "Catalyzing eXploration in Chemistry" remote outreach program for high school students.

## **Co-PI: Chia-Kuang "Frank" Tsung**

### 2018

1. Organizer of a catalysis symposium in the Division of Catalysis Science and Technology for the 2018 256th ACS National Meeting & Exposition (Boston, MA on August 19-23, 2018).
2. Organizing Committee of ACS Publications Symposium: Innovation in Materials Science (Shanghai, China on July 29-31, 2018).

### 2019

1. Organizer of Materials Chemistry Mini-Symposium (Berkeley, CA on June 28-29, 2019)
2. Discussion Leader of Gordon Research Conference: Nanoporous Materials and Their Applications (Andover, NH on August 4-9, 2019).
3. Organizer of 2019 International Symposium on Hollow Nanostructured Materials (Beijing, China on August 18th 2019).
4. Session Chair of 18th Asian Chemical Congress 18th ACC (Taipei, Taiwan, on December 10th 2019).

Charles T. Campbell

**Supported Metal Nanoparticle Catalysts and Electrocatalysts:  
Correlating Structure with Function through Energetics**

Charles T. Campbell  
University of Washington, Department of Chemistry

**Presentation Abstract**

Metal adsorption calorimetry measurements have revealed systematic relationships between the energy of a catalytic surface metal atom and (1) the size of the metal nanoparticle on which it resides, and (2) the support surface to which this metal particle is anchored. We have shown that the metal atom's energy (or chemical potential) increases strongly with decreasing particle size below ~6 nm but remains nearly constant near the bulk metal value above ~6 nm. For particles below 6 nm, it decreases with increasing metal/support adhesion energy ( $E_{adh}$ ). We discovered an equation that accurately predicts these dependences on size and  $E_{adh}$ . We made progress in understanding how  $E_{adh}$  depends upon the metal and the support material. We also developed a new method for studying metal adsorption and adhesion energies on clean surfaces of powdered support particles.

We also applied Degree of Rate Control (DRC) analysis (a concept invented by the PI) in a variety of important new ways, most importantly by proving that the apparent activation energy equals a weighted average of the standard-state enthalpies (relative to reactants) of all the species (intermediates, transition states and products) in the reaction mechanism, each weighted by its DRC.

In collaborations with PNNL, we have also elucidated the mechanism of aqueous-phase catalytic and electrocatalytic hydrogenation of phenol and benzaldehyde (model biomass conversions) over Pt-group metals. This led us to discover important new ways to estimate the effects of solvents on the adsorption energies of catalytic reaction intermediates and the adhesion energies of solvents to clean metal surfaces.

**DE-FG02-96ER14630: Supported Metal Nanoparticle Catalysts and  
Electrocatalysts: Correlating Structure with Function through Energetics**

**Postdoc(s):** Kun Zhao, PhD

**Student(s):** John R. Rumptz

**RECENT PROGRESS**

***Overview***

Nanoparticles of late transition metals are used as catalysts and electrocatalysts for industrial chemical reactions that produce fuels, convert them to electricity and clean up pollution associated with the generation and use of fuels. For such applications, they usually are bonded onto the surfaces of oxide or carbon support materials. To provide the energy needed for sustained economic development, we must develop new and improved solid catalysts and electrocatalysts for a variety of reactions that take better advantage of traditional and alternate energy sources (solar, wind, biomass or nuclear) and avoid serious

environmental problems. This experimental research program is aimed to provide the basic understanding needed to develop new and improved catalysts and electrocatalysts for a variety of reactions that involve nanoparticles of late transition metals supported on oxide and carbon materials. Specifically, we study well-defined model catalysts consisting of metal and bimetallic nanoparticles supported on single-crystalline oxide, mixed-oxide and carbon surfaces, structurally characterized using a variety of ultrahigh vacuum surface science techniques. We use calorimetry techniques invented here and available nowhere else in the world to measure the energies of the metal atoms in these particles, the metal/support adhesion energies and the energy of adsorbed intermediates on these particles. Our prior results showed that the chemical potential of the metal atoms in the particles, which we measure directly by metal adsorption calorimetry, is an important descriptor for catalytic performance. For particles smaller than 6 nm, it depends strongly on their size and the nature of the oxide or carbon support upon which the particles sit, and it correlates with their catalytic performance (resistance to sintering, bond energies to adsorbed catalytic reaction intermediates, catalytic activity and selectivity). Our prior results led us to a quantitative relationship that accurately predicts metal chemical potential versus particle size and the metal / support adhesion energy ( $E_{adh}$ ). Thus, knowing how  $E_{adh}$  varies with the metal and support material is crucial to predicting metal chemical potential for different catalyst materials, and thus their catalytic performance. We also discovered how to predict  $E_{adh}$  for different metals on a given oxide support, once  $E_{adh}$  is known for one metal. One of our main goals now it to refine these relationships, extending them to other oxides and carbon supports, thus enabling predictions of adhesion energies for new metal/support combinations without measurement. The second goal is to measure quantitative relationships between metal chemical potential and catalytic properties for metals in model structures where their chemical potential is tuned by independently varying the particle size and the support strength, and by alloying with other metals. Another goal is to measure adsorption energies of two important and ubiquitous adsorbed catalytic intermediates ( $-CH_3$ ,  $-OCH_3$ ) on these nanoparticles, and the particles sintering rates, and to correlate these with metal chemical potential. We also aim to measure the adsorption energies of metal monomers on these supports, which are crucial parameters in kinetic models for sintering rates. This work thus aims to provide the basic understanding needed to develop better catalyst materials for clean, sustainable energy technologies. Finally, we aim to measure these energies with sufficient accuracy that they will serve as the key benchmarks (that cannot be provided by any other laboratory, nor by any theoretical methods currently available) needed for developing more accurate computational tools for heterogeneous catalysis and surface science. A marked improvement in such computational tools would revolutionize research in many areas.

### ***Metal adsorption and adhesion energies to catalyst support materials***

We continued our calorimetric studies of the adsorption energies of metal atoms as they grow nanoparticles on oxide supports. This provides the metal adhesion energy to the support ( $E_{adh}$ ) and also the metal atom's chemical potential ( $\square_M$ ) versus particle size. We had previously discovered a trend in how  $E_{adh}$  varies with the metal for a give support oxide. For a given oxide,  $E_{adh}$  increases linearly from metal to metal with increasing heat of formation of the most stable oxide of the metal (per mole metal), or metal oxophilicity. Our new results for Ni on MgO(100) and on CeO<sub>2</sub>(111) validated this linear correlation by

doubling the range of oxophilicities studied for both oxides. We also measured Ag on rutile  $\text{TiO}_2(100)$ .

In collaboration with Tom Mallouk's group at Penn State, we measured heats of adsorption of Ag atoms onto the basal plane of calcium niobate nanosheets. This required major modifications to one of our calorimeters to allow colloidal-dispersed nanosheets of the type provided by Mallouk's group to be deposited directly on a heat detector and outgassed at high temperatures in ultrahigh vacuum before calorimetry measurements of metal adsorption energies. We extended this to prove that we can measure metal adsorption energies of powdered support materials deposited from liquid dispersions, with accurate measurements of Ag adsorption energy versus coverage on clean surfaces of 5 nm spherical nanoparticles of anatase  $\text{TiO}_2$ .

### ***Developing tools for microkinetic modelling and catalyst optimization***

The "degree of rate control" (DRC) is a mathematical approach for analysing multi-step reaction mechanisms that has proven very useful in catalysis research. It was invented by the PI to identify the "rate-controlling transition states and intermediates" (i.e., those whose DRCs are large in magnitude). Kinetic isotope effects (KIEs) have been used for decades in catalysis research as a tool for clarifying reaction mechanisms. Significant primary kinetic isotope effects have usually been interpreted as being a result of isotope substitution at a site of bond breaking (or forming) in the rate-determining step in the reaction mechanism. However, quantitative analysis of the magnitude of the KIE in complex multistep reaction mechanisms is seldom reported. We recently prove that the logarithm of the KIE (i.e., the rate ratio for two isotopes) is the weighted average over all species in the mechanism of their standard-state free-energy difference between the two isotopes, divided by  $RT$ . The weighting factor is the DRC for that species (i.e., transition state, intermediate, reactant).

### ***Aqueous phase catalysis and electrocatalysis***

In collaboration with Johannes Lercher's team at PNNL, we studied both electrocatalytic hydrogenation (ECH) and thermal catalytic hydrogenation (TCH) of phenol by carbon-supported Pt, Rh and Pd particles. We characterized the mechanism and surface intermediates in the TCH and ECH reaction using kinetics and in situ spectroscopies.

### ***Impact on the development of human resources***

During this year, this research grant provided strong interdisciplinary, research-based education for one graduate student and one postdoc, as well as intensive research experience for 2 undergraduate students. An undergraduate who previously worked on this project was a coauthor on resulting publication that appeared this year. It also provided opportunities for the graduate student and postdoc to get experience with training and mentoring undergraduate researchers.

## Publications Acknowledging this Grant in 2018-2021

### (I). Publications Resulting from this DOE Grant Support with the largest intellectual contribution from this grant.

1. Energetics of Au adsorption and film growth on Pt(111) by single-crystal adsorption calorimetry, Gabriel M. Feeley, Stephanie L. Hemmingson and Charles T. Campbell, *Journal of Physical Chemistry C* 123, 5557-5561 (2019). DOI: 10.1021/acs.jpcc.9b00018.
2. A Simple Bond-Additivity Model Explains Large Decreases in Heats of Adsorption in Solvents Versus Gas Phase: A Case Study with Phenol on Pt(111) in Water, Nirala Singh and Charles T. Campbell, *ACS Catalysis* 9, 8116–8127 (2019). DOI: 10.1021/acscatal.9b01870.
3. Adhesion Energies of Solvent Films to Pt(111) and Ni(111) Surfaces by Adsorption Calorimetry, John R. Rumpitz and Charles T. Campbell, *ACS Catalysis* 9, 11819–11825 (2019). DOI: 10.1021/acscatal.9b03591.
4. Apparent Activation Energies in Complex Reaction Mechanisms: A Simple Relationship via Degrees of Rate Control, Zhongtian Mao and Charles T. Campbell, *ACS Catalysis* 9, 9465–9473 (2019). DOI: 10.1021/acscatal.9b02761.
5. The Degree of Rate Control of Catalyst-Bound Intermediates in Catalytic Reaction Mechanisms: Relationship to Site Coverage, Zhongtian Mao and Charles T. Campbell, *Journal of Catalysis* 381, 53–62 (2020). DOI: 10.1016/j.jcat.2019.09.044.
6. Kinetic Isotope Effects: Interpretation and Prediction Using Degrees of Rate Control, Zhongtian Mao and Charles T. Campbell, *ACS Catalysis* 10, 4181–4192 (2020). (Also selected for inclusion in the *ACS Catalysis* Virtual Issue: Blurring the Lines between Catalysis Subdisciplines.) DOI: 10.1021/acscatal.9b05637
7. Energetics and Structure of Ni Atoms and Nanoparticles on MgO(100), Zhongtian Mao, Wei Zhao, Ziareena Al-Mualem and Charles T. Campbell, *Journal of Physical Chemistry C* 124, 14685–14695 (2020). DOI: 10.1021/acs.jpcc.0c03468.
8. Calorimetric Metal Vapor Adsorption Energies for Characterizing Industrial Catalyst Support Materials, Wei Zhang and Charles T. Campbell, *J. Catalysis* 392, 209–216 (2020). DOI: 10.1016/j.jcat.2020.09.022
9. Ni Nanoparticles on CeO<sub>2</sub>(111): Energetics, Electron Transfer and Structure by Ni Adsorption Calorimetry, Spectroscopies and DFT, Zhongtian Mao, Pablo G. Lustemberg, John R. Rumpitz, M. Verónica Ganduglia-Pirovano and Charles T. Campbell, *ACS Catalysis* 10, 5101–5114 (2020). DOI: 10.1021/acscatal.0c00333
10. Catalytic Properties of Model Supported Nanoparticles, Charles T. Campbell, Nuria Lopez, and Stefan Vajda, *Journal of Chemical Physics* 152, 140401 (2020) (3 pages). <https://doi.org/10.1063/5.0007579>
11. Silver Adsorption on Calcium Niobate(001) Nanosheets: Calorimetric Energies Explain Sinter-Resistant Support, Wei Zhang, Ritesh Uppuluri, Thomas E. Mallouk and Charles T. Campbell, *J. Am. Chem. Soc.* 142, 15751–15763 (2020). DOI: 10.1021/jacs.0c05044
12. Energetics of Ag Adsorption on and Adhesion to Rutile TiO<sub>2</sub>(100) Studied by Microcalorimetry, Zhongtian Mao, John R. Rumpitz, and Charles T. Campbell, *Journal of Physical Chemistry C* 125, 3036–3046 (2021). DOI: 10.1021/acs.jpcc.0c10504.

13. Predicting a key catalyst-performance descriptor for supported metal nanoparticles: metal chemical potential, Zhongtian Mao and Charles T. Campbell, *ACS Catalysis* **11**, 8284–8291 (2021).
14. The nature of the active sites on Ni/CeO<sub>2</sub> catalysts for methane conversions, Pablo G. Lustemberg, Zhongtian Mao, Agustín Salcedo, Beatriz Irigoyen, M. Verónica Ganduglia-Pirovano and Charles T. Campbell, *ACS Catalysis* (submitted).
15. Analysis and prediction of reaction kinetics using the degree of rate control, Charles T. Campbell & Zhongtian Mao, *Journal of Catalysis* (invited, for special issue in honor of Michel Boudart), submitted.

**(II). Publications jointly funded by this DOE grant and other grants of the PI and/or his co-authors, with a larger intellectual contribution from another grant.**

16. The physical chemistry and materials science behind sinter-resistant catalysts, Yunqian Dai, Ping Lu, Charles T. Campbell and Younan Xia, *Chemical Society Reviews* **47**, 4314-4331 (2018).
17. Impact of pH on Aqueous-Phase Phenol Hydrogenation Catalyzed by Carbon-Supported Pt and Rh, Nirala Singh, Mal-Soon Lee, Sneha A. Akhade, Guanhua Cheng, Donald M. Camaioni, Oliver Y. Gutiérrez, Vassiliki-Alexandra Glezakou, Roger Rousseau, Johannes A. Lercher and Charles T. Campbell, *ACS Catalysis* **9**, 1120-1128 (2019). DOI: 10.1021/acscatal.8b04039.
18. Heats of Adsorption of N<sub>2</sub>, CO, Ar and CH<sub>4</sub> versus Coverage on the Zr-Based MOF NU-1000: Measurements and DFT Calculations, Graeme O. Vissers, Wei Zhang, Oscar E. Vilches, Wei-Guang Liu, Haoyu S. Yu, Donald G. Truhlar and Charles T. Campbell, *Journal of Physical Chemistry C* **123**, 6586–6591 (2019). DOI: 10.1021/acs.jpcc.8b12263.
19. Quantifying adsorption of organic molecules on platinum in aqueous phase by hydrogen site blocking and in situ X-ray absorption spectroscopy, Nirala Singh, Udishnu Sanyal, John L. Fulton, Oliver Y. Gutiérrez, Johannes A. Lercher and Charles T. Campbell, *ACS Catalysis* **9**, 6869–6881 (2019). DOI: 10.1021/acscatal.9b01415.
20. Aqueous phase catalytic and electrocatalytic hydrogenation of phenol and benzaldehyde over platinum group metals, Nirala Singh; Udishnu Sanyal; Griffin Ruehl; Kelsey Stoerzinger; Oliver Y Gutiérrez; Donald M Camaioni; John L Fulton; Johannes A Lercher and Charles T Campbell, *Journal of Catalysis* **382**, 372–384 (2020) DOI: 10.1016/j.jcat.2019.12.034 .

**Awards or leadership activities during 2018-2020 calendar years: C. T. Campbell**

HONORS / AWARDS

Elected Honorary Fellow of the Chinese Chemical Society, 2020.  
 American Chemical Society Catalysis Division Award for Exceptional Achievements in Catalysis, 2020.

EDITORIAL RESPONSIBILITIES

Editor-in-Chief of the journal *Surface Science Reports* (2013-present).

Guest Co-Editor with Beatriz Roldan, Manos Mavrikakis and Younan Xia: *Chemical Reviews*, Thematic Issue on Advanced Materials and Methods for Catalysis / Electrocatalysis by Transition Metals, 2021.

Guest Co-Editor with Štefan Vajda and Núria López: *Journal of Chemical Physics* special issue on Catalytic Properties of Model Supported Nanoparticles, 2019.

#### SCIENTIFIC ADVISORY BOARDS

Exascale Catalytic Chemistry (ECC) Project, Sandia National Laboratory, Livermore, CA, 2021-present

Idaho National Laboratory, Energy and Environment Science and Technology Directorate Strategic Advisory Committee, 2010-2020.

Pacific Northwest National Lab Institute for Integrated Catalysis Advisory Board, 2013-present.

Founding Member of the Scientific Advisory Board for Northwestern University's Center for Catalysis and Surface Science (CCSS), 2017 – 2019.

#### OUTREACH and INVITED TALKS

This grant also enabled much scientific outreach that favorably impacts the development of future scientists and engineers. Since May 15, 2020, the PI gave (virtually/remotely) or accepted future invited talks at 3 scientific meetings (including 1 international conference) and 10 at universities (including 2 in Europe and a very prestigious lectureship in China (the Forum of Great Minds, USTC), almost all of which included (or will include) results from this grant. In addition, he had 5 other invited talks at major national and international scientific meetings scheduled, but they were cancelled due to COVID.

**Chemical Imaging of Single-Particle Photoelectrocatalysis:  
Inter-facet junction effects on particulate photoelectrodes**

Peng Chen, Xianwen Mao  
Department of Chemistry and Chemical Biology, Cornell University

**Presentation Abstract**

Particulate semiconductor photocatalysts are paramount for many solar energy conversion technologies. In anisotropically-shaped photocatalyst particles, the different constituent facets may form inter-facet junctions at their adjoining edges, analogous to lateral two-dimensional (2D) heterojunctions or pseudo-2D junctions made of few-layer 2D materials. Using subfacet-level multimodal functional imaging, we uncover inter-facet junction effects on anisotropically-shaped bismuth vanadate particles and identify the characteristics of near-edge transition zones on the particle surface, which underpin the whole-particle photoelectrochemistry. We further show that chemical doping modulates the widths of such near-edge surface transition zones, consequently altering particles' performance. Decoupled facet-size scaling laws further translate inter-facet junction effects into quantitative particle-size-engineering principles, revealing surprising multiphase size dependences of whole-particle photoelectrode performance. The imaging tools, the analytic framework, and the inter-facet junction concept pave new avenues toward understanding, predicting, and engineering (opto)electronic and photoelectrochemical properties of faceted semiconducting materials, with broad implications in energy science and semiconductor technology.

**DE-SC0004911: Chemical Imaging of Single-Particle Photoelectrocatalysis**

**PI:** Peng Chen

**Postdoc(s):** Xianwen Mao, Ming Zhao, Wenjie Li

**Student(s):** Zhiheng Zhao

**RECENT PROGRESS**

**Background.** Particulate semiconductor photocatalysts are promising systems for solar-to-fuel technologies. In such catalytic systems, one critical factor for attaining high energy conversion efficiencies is the effective separation of photogenerated electrons and holes within individual particles to prevent charge carrier recombination. Recent studies show that charge carrier separation can be facilitated using anisotropically-shaped semiconductor particles exposing facets with different work functions. While previous studies of anisotropically-shaped semiconductor particles recognize the differences in work function and the associated charge carrier activities among *different* facets, they all assume no variations of these properties within the *same* facet.

We hypothesize that within each anisotropically-shaped photocatalyst particle, the different constituent facets may form inter-facet junctions at their adjoining edges (Fig. 1a) analogous to lateral two-dimensional (2D) heterojunctions or pseudo-2D junctions made of few-layer 2D materials, and that these inter-facet junctions should lead to spatial

variations of electronic and photoelectrochemical properties along the particle surface even within the *same* facet at near-edge regions. These inter-facet edges resemble one-dimensional (1D) interfaces of lateral 2D junctions (Fig. 1b); the valence and conduction band levels at the surface ( $E_V^{\text{surf}}$ ,  $E_C^{\text{surf}}$ ) would bend near these edges, forming near-edge transition zones along the facet surface (Fig. 1b, red lines). We further hypothesize that, if the surface transition zone width becomes comparable to the overall particle size (which is likely considering that lateral 2D junctions are known to have broad depletion zones), such surface band bending should significantly influence the overall (opto)electronic properties and performance of the whole particle toward applications such as (photo)electrocatalysis, important for renewable energy technologies. Whether these hypotheses are true is completely unknown, however.

Using subfacet-level multimodal functional imaging, we uncover inter-facet junction effects and associated intra-facet variations of photoelectrochemical properties in anisotropically-shaped bismuth vanadate ( $\text{BiVO}_4$ ) particles under photocatalyst working conditions (i.e., under illumination and electrochemical control, in an aqueous electrolyte, and with water oxidation occurring). Our major results are summarized below.

**Visualizing inter-facet junction effects.** We chose to study  $\text{BiVO}_4$  because of its promise as a high-performance photoanode material for water oxidation (bandgap  $\sim 2.4$  eV; valence band edge  $\sim 2.4$  V vs. reversible hydrogen electrode, RHE). We synthesized anisotropically-shaped  $\text{BiVO}_4$  particles with a truncated bipyramidal morphology, exposing  $\{010\}$  and  $\{110\}$  facets with tunable facet sizes ( $L_{\{010\}}$ ,  $L_{\{110\}}$ :  $\sim 100$  nm to tens of microns; Fig. 1a). The  $\{010\}$  facet is lower in electron energy (i.e., larger work function) and richer in  $\text{O}^{2-}$  (which can act as an electron donor); the  $\{110\}$  facet is higher in electron energy (i.e., smaller work function) and richer in  $\text{Bi}^{5+}$  (which can act as an electron acceptor). The  $\{010\}|\{110\}$  edge therefore constitutes a 1D interface, giving rise to an inter-facet junction, which should in turn lead to intra-facet variations of  $E_C^{\text{surf}}$  and  $E_V^{\text{surf}}$  along the particle surface (Fig. 1b, red lines). Importantly, upon contacting electrolytes, this inter-facet junction should give rise to location-dependent band bending degree ( $\Delta\phi_{\text{SEI}}$ ) across the solid-electrolyte interface (SEI) perpendicular to the facet: shallower bending on the donor-richer  $\{010\}$  facet, steeper bending on the acceptor-richer  $\{110\}$  facet, and varying continuously across the inter-facet edge (Fig. 1b, blue lines). We envisioned that this  $\Delta\phi_{\text{SEI}}$  variation should lead to subfacet position ( $x$ )-dependent photoelectrochemical currents, a key photoelectrode performance metric.

We therefore focused a 405-nm laser to probe photoelectrochemical currents locally, and systematically scan the focused laser spot along the  $x$ -direction across the inter-facet edge on a single  $\text{BiVO}_4$  particle (Fig. 1c, left). Correlated with scanning electron microscopy (SEM) (Fig. 1d), we measured, at a subfacet resolution ( $\sim 380$  nm), the local steady-state anodic photoelectrochemical current ( $i_{\text{ph}}$ ) associated with water oxidation at various potentials (all referenced to RHE), which show striking spatial pattern (Fig 1g) that agree qualitatively with our hypotheses (Fig. 1b), suggests that inter-facet junction effects exist on anisotropically-shaped semiconducting particles and influence particles' photoelectrochemistry.

To probe local photoelectrochemical properties beyond the diffraction-limited resolution, we performed single-molecule super-resolution microscopy with redox-

selective fluorogenic probes to map surface reactions induced by photogenerated holes ( $h^+$ ) or electrons ( $e^-$ ) at  $\sim 40$  nm resolution (Fig. 1c, middle). Here we reveal, for the first time, a spatial variation of surface hole activities even within the *same* facet (also for surface electron activities; Fig 1e-f): the specific rate of  $h^+$ -induced reaction ( $v_h$ ) shows a striking *s*-like, micron-sized spatial trend along the *x*-direction (Fig. 1h, red), which parallels that of the local anodic photoelectrochemical current (dominated by  $h^+$ -induced water oxidation reaction; Fig. 1g) but possesses  $\sim 10$ -times higher spatial resolution.

A modified Reichman model allowed us to analyze and fit satisfactorily the potential dependences of local photoelectrochemical currents and  $h^+/e^-$ -induced reaction rates. And we obtained intrinsic, potential-independent, parameters that govern photoelectrochemical water oxidation performance at the solid-electrolyte interface, including: the flat-band potential ( $V_{FB}$ ), the electron-hole separation efficiency in the depletion zone at the SEI ( $\eta_{sep}$ ), and the effective rate constant  $k_h$  ( $k_e$ ) reflecting the surface hole (electron) activity. All these parameters show *s*-like transitions along the *x*-direction across the  $\{010\}|\{110\}$  edge (Fig. 1i-j), as we hypothesized for the inter-facet transition zones on a particle's surface (Fig. 1b, purple line). These observations are the *first* direct mapping of inter-facet junction effects within an anisotropically-shaped semiconductor particle.

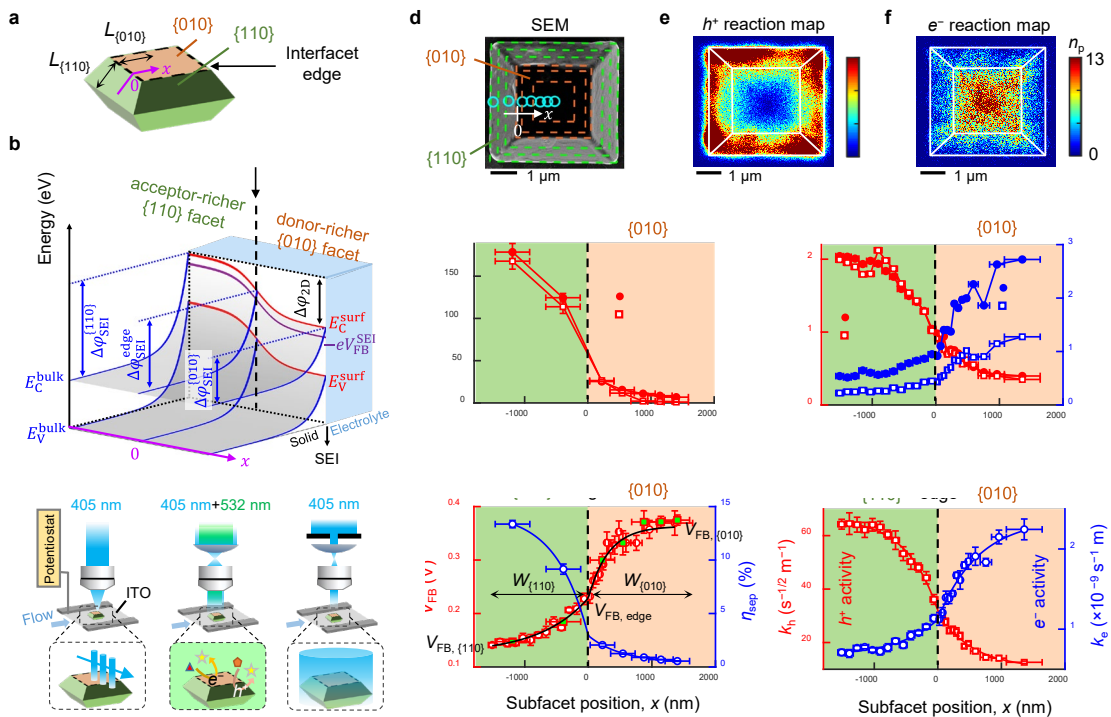


**Figure 1. Visualizing inter-facet junction effects in anisotropically-shaped semiconductor particles.** (a) Schematic illustration of an anisotropically-shaped  $\text{BiVO}_4$  particle with exposed  $\{010\}$  and  $\{110\}$  facets.  $L_{\{010\}}$  ( $L_{\{110\}}$ ) quantifies the  $\{010\}$  ( $\{110\}$ ) facet size. The *x*-axis is defined to be along the facet surface ( $x = 0$ : inter-facet edge.  $x > 0$ :  $\{010\}$  facet.  $x < 0$ :  $\{110\}$  facet.) (b) Envisioned energy diagram demonstrating inter-facet junction effects in an anisotropically-shaped  $\text{BiVO}_4$  particle in contact with an electrolyte. SEI: solid-electrolyte interface. (c) Multimodal functional imaging set-up comprising a microfluidic photoelectrochemical cell with individual particles dispersed on an indium-doped tin oxide (ITO) electrode, under three different laser illumination configurations. Left: focused 405-nm laser excitation for subfacet-level photoelectrochemical current mapping. Middle: wide-field epifluorescence illumination for super-resolution charge-carrier reaction imaging; 532-nm laser excites the reaction product fluorescence. Right: iris-confined illumination for single-whole-particle photoelectrochemical current measurement. (d) SEM image of a representative  $\text{BiVO}_4$  particle examined in e-j. Dashed lines: facet dissections. Circles: size and position of focused 405-nm laser. (e, f) Super-resolution images of  $h^+$  (potential  $\geq 0.93$  V) (e) and  $e^-$  (potential  $\leq 0.63$  V) (f) induced reactions.  $n_p$ : number of

detected product molecules. Bin size:  $37.1^2 \text{ nm}^2$ . White lines: structural contours from SEM (d). Imaging duration (each potential): 22.5 min. (g, h) Subfacet-position dependences of  $i_{\text{ph}}$  (g),  $v_{\text{h}}$  and  $v_{\text{e}}$  (h) at selected potentials. Solid lines connect points. (i, j) Subfacet-position dependences of  $V_{\text{FB}}$  (green-filled red squares: determined from  $i_{\text{ph}}$  in g; white-filled red circles: determined from  $v_{\text{h}}$  and  $v_{\text{e}}$  in h),  $\eta_{\text{sep}}$  (i),  $k_{\text{h}}$  and  $k_{\text{e}}$  (j). Solid lines: fits with Eq. 1.  $y$  error bars: s.d.  $x$  error bars: measurement resolution or size of dissected region.

**Other major results.** Capitalizing on the above results, we have expanded the experiments to achieve/show the following (now shown here due to limited space):

1)  $V_{\text{FB}}$  at the edge or intrinsic to the two facets show clear facet-size dependences: smaller facets exhibit more negative  $V_{\text{FB}}$ , consistent with higher surface energies of smaller particles.

2) The SEI charge separation efficiencies show opposite facet-size dependences to  $V_{\text{FB}}$ , since steeper SEI band bending renders more efficient charge separation in the SEI depletion zone.

3) Determination of the near-edge transition zone width,  $W_{\{010\}}$  and  $W_{\{110\}}$ , from the inter-facet junction effect. Both show no facet-size dependence, possibly because they only depend on the surface chemical compositions of respective facets, analogous to the observation that the depletion zone widths of lateral 2D junctions are solely determined by the chemical compositions (e.g., dopant densities) of their constituent 2D materials.

4) The determination and quantitative prediction of photoelectrochemical current densities ( $j_{\text{ph}}$ ) for whole particles of any facet sizes at any potential, a key photoanode performance metric.

5) The determination of the maximally achievable applied-bias photon-to-current efficiency ( $\text{ABPCE}_{\text{max}}$ ), another key photoelectrode performance metric, and the corresponding optimal potential ( $E_{\text{opt}}$ ), for particles with any facet sizes.

6) Tuning of the inter-facet junction effect by chemical doping. Here both the near-edge surface transition zone widths and the whole particle photoelectrochemistry properties are altered in a quantitatively predictable way.

7) The determination of 2D surface dopant densities on  $\{110\}$  vs.  $\{010\}$  facets, a *first-of-its-kind* information made accessible by our subfacet-level functional imaging.

8) Determination of quantitative size and shape engineering relationships to improve the performance of photoelectrochemical water oxidation.

**Publication up coming.** The above results have been included in a manuscript submitted to *Nature Materials*. It received three positive reviews. We are currently revising the manuscript to address the reviewers' specific comments. We expect to submit the revised version within the next few weeks.

## Publications Acknowledging this Grant in 2018-2021

(XIV) *Intellectually led by this grant*

- Mao, X.; Liu, C.; Hesari, M.; Zou, N.; Chen, P.\*, Super-resolution imaging of non-fluorescent reactions via competition. *Nature Chem.* **2019**, *11*, 687-694.
- Sambur, J. B.\*; Shepherd, D. P.; Hesari, M.; Erdewyk, M. V.; Choudhary, E.; Chen, P.\*, Correlated Single-Molecule Reaction Imaging and Photocurrent Measurements Reveal Underlying Rate Processes in Photoelectrochemical Water Splitting. *J. Electrochem. Soc.* **2019**, *166*, H3286.

- Hesari, M.; Sambur, J. B.; Mao, X.; Jung, W.; Chen, P.\*, Quantifying Photocurrent Loss of a Single Particle–Particle Interface in Nanostructured Photoelectrodes. *Nano Lett.* **2019**, *19*, 958-962.
- Hesari, M.; Mao, X.; Chen, P.\*, Charge Carrier Activity on Single-Particle Photo(electro)catalysts: Toward Function in Solar Energy Conversion. *J. Am. Chem. Soc.* **2018**, *140*, 6729-6740.

(XV) *Jointly funded by this grant and other grants with intellectual leadership by other funding sources*

- Sarkar, S.; Wang, X.; Hesari, M.; Chen, P.; Mirkin, M. V.\*, Scanning electrochemical and photo-electrochemical microscopy on finder grids: toward correlative multi-technique imaging of surfaces. *Anal. Chem.* **2021**, *93*, 5377–5382.
- Kang, J.; Park, S. J.; Chen, P.\*; Sung, J.\*, Stochastic kinetics of nanocatalytic systems. *Phys. Rev. Lett.* **2021**, *126*, 126001.
- Mao, X.; R. Ye, R.; Chen, P.\*, Single-molecule fluorescence microscopy for characterizations of heterogeneous catalysts” In Springer Handbook of Advanced Catalyst Characterization, edited by Israel Wachs and Miguel A. Bañares. Accepted. Invited contribution.
- Zhao, M.; Chen, P.\*, Exploring Plasmonic Photocatalysis via Single-Molecule Reaction Imaging. *Nano Lett.* **2020**, *20*, 2939-2940.
- Ye, R.; Mao, X.; Sun, X.; Chen, P.\*, Analogy between Enzyme and Nanoparticle Catalysis: A Single-Molecule Perspective. *ACS Catal.* **2019**, *9*, 1985-1992.
- Zou, N.; Chen, G.; Mao, X.; Shen, H.; Choudhary, E.; Zhou, X.; Chen, P.\*, Imaging Catalytic Hotspots on Single Plasmonic Nanostructures via Correlated Super-Resolution and Electron Microscopy. *ACS Nano* **2018**, *12*, 5570-5579.
- Zou, N.; Zhou, X.; Chen, G.; Andoy, N. M.; Jung, W.; Liu, G.; Chen, P.\*, Cooperative Communication within and between Single Nanocatalysts. *Nature Chem.* **2018**, *20*, 607-614.

## **Awards or leadership activities during 2018-2020 calendar years**

### **Honors and Awards**

2020 Best Editor Award, *Nano Research*

2019 Chemical Pioneer Award

2018 Fellow, American Association for the Advancement of Science

2018 Bau Family Award in Inorganic Chemistry

### **Named Lectureships**

2019 Joan Van der Waals Lecturer, University of Leiden

2019 Brian Bent Lecturer, Columbia University

2018 Sessler Distinguished Alumni Lecturer, Stanford University

### **Special Invitation Conference Lectures**

2020 Keynote Lecture, 71st Annual Meeting of the International Society of Electrochemistry

- 2019 Keynote Lecture, 18th Beijing Conference and Exhibition on Instrumental Analysis
- 2019 Keynote Lecture, 16th Conference on Methods and Applications of Fluorescence (MAF 2019)
- 2019 Keynote Lecture, 5th International Conference on Energy Conversion and Storage (5th ICECS)
- 2019 Opening Keynote Lecture, International Bunsen Discussion Meeting on Probing Chemical Reactions by Single-molecule Spectroscopy
- 2018 Keynote Lecture, 14th European Biological Inorganic Chemistry Conference (EuroBIC-14)
- 2018 Plenary Lecture, IBS Symposium on Nanomaterials and Spectroscopy, Korean Advanced Institute of Science and Technology, South Korea
- 2018 Plenary Lecture, Symposium of the Center for Chemical Dynamics in Living Cells, Chung-Ang University, South Korea
- 2018 Plenary Lecture, 6th International Congress on Operando Spectroscopy

### **Professional Activities**

#### ***Editorial Services***

- *ACS Chem. Biol.* (Editorial Advisory Board, 1/2016-12/2018)
- *Analysis & Sensing* (Editorial Advisory Board, 2020-2024)
- *Chem. Phys. Lett.* (Editorial Advisory Board, 2014-2020)
- *Coord. Chem. Rev.* (Co-Guest Editor, Special issue in honor of E. I. Solomon's 65<sup>th</sup> Birthday, 2011)
- *J. Biol. Inorg. Chem.* (Editorial Advisory Board, 1/2019-12/2021)
- *Nano Research* (Young Star Editor, 5/2019-5/2023)
- *Natural Sciences* (Associate Editor for Chemistry, 2021-2023)

#### ***Conference Organizations***

- Co-organizer, Symposium on "Single-molecule fluorescence imaging", PacifiChem, December 2020

Phillip Christopher

**Exploring and Exploiting the Oxidation State Void between Single Atom Catalysts and Single Atom Alloys - a Combined Model and Real Catalyst Approach**

Phillip Christopher<sup>1</sup>, Charles H. Sykes<sup>2</sup>

1. Department of Chemical Engineering, University of California, Santa Barbara, Santa Barbara, CA 93106
2. Department of Chemistry, Tufts University, 62 Talbot Ave, Medford, MA 02155

**Postdoc(s):** Jaeha Lee

**Student(s):** Anika Jalil, Rosadriana Zelaya, Alex Schilling, Audrey Dannar, Volkan Cinar

**RECENT PROGRESS**

**Recent Progress A: Developing Single-Site Pt Catalysts for the Preferential Oxidation of CO: A Surface Science and First Principles-Guided Approach**

Preferential CO oxidation (PrOX) catalysts are important in industry and are critical for technologies such as polymer-electrolyte membrane fuel cells that require elimination of CO from H<sub>2</sub> streams because CO is a potent poison which can limit the efficiency of the catalysts and fuel cells.

We report a comprehensive study combining surface science, DFT calculations, and real catalyst synthesis, characterization, and testing to investigate the preferential oxidation of CO in the presence of H<sub>2</sub> over single-site Pt<sub>1</sub>/Cu<sub>x</sub>O catalysts. Surface science studies show that while Pt<sub>1</sub>/Cu<sub>x</sub>O model surfaces enable low-temperature CO oxidation via a Mars-van Krevelen mechanism (Figure 1), there was no evidence for H<sub>2</sub> activation or oxidation. DFT-based calculations explain these results and demonstrate that the H<sub>2</sub> oxidation barrier is high as compared to H<sub>2</sub> desorption from Pt<sub>1</sub>/Cu<sub>x</sub>O. Inspired by these model catalyst studies, nanoporous Pt<sub>1</sub>/Cu<sub>x</sub>O catalysts were synthesized and demonstrated to be active and highly selective for the preferential oxidation of CO (Figure 2). This work highlights the potential of combined surface science, theory, and catalyst studies for identifying new catalytic materials, which in this case led to the development of a novel single-site Pt<sub>1</sub>/Cu<sub>x</sub>O catalyst for the preferential oxidation of CO.

We plan to continue using this integrated approach for understanding catalytic sites and reaction mechanisms and our future model studies will move beyond the “29” Cu<sub>x</sub>O and focus on Pt atoms on Cu<sub>2</sub>O(111) thereby allowing us to interrogate how the charge state of Pt affects reaction pathway.

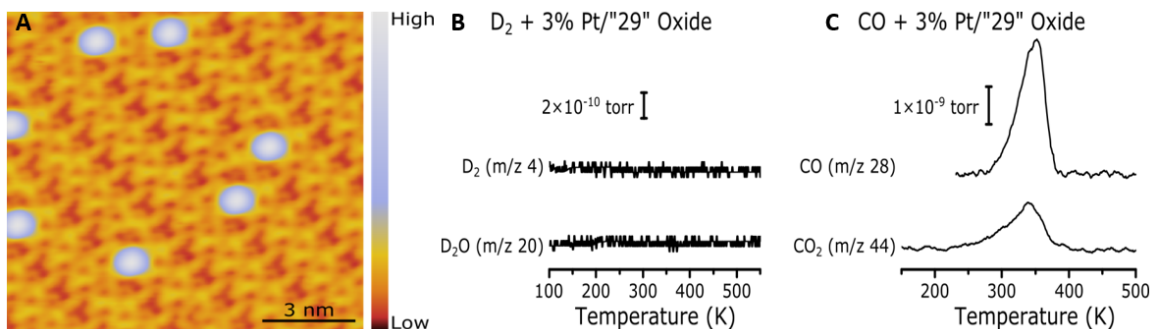


**Figure 1.** Model study investigation of 3% ML of Pt supported on the “29” Cu surface oxide toward CO and hydrogen oxidation. A) STM image of single Pt atoms supported on the “29” oxide  $\text{Cu}_2\text{O}$  surface following a 250 K anneal. Imaging conducted at 5 K at conditions of -0.45 V, 1 nA. TPD results following exposure to B) 100 L  $\text{D}_2$  and C) 10 L CO. TPD traces are offset for clarity.

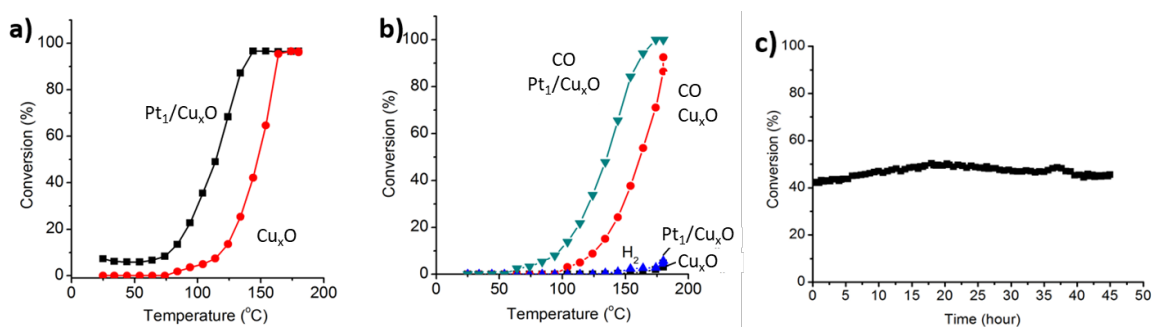


**Figure 2.** a) Second cycle TPSR data for CO oxidation over  $\text{Pt}_1/\text{Cu}_x\text{O}$  and  $\text{Cu}_x\text{O}$  catalysts, flow rate: 50 mL/min, 2%  $\text{O}_2$ , 2% CO, bal. He, 500 mg samples b) Temperature Programmed PrOX reaction on  $\text{Pt}_1/\text{Cu}_x\text{O}$  and  $\text{Cu}_x\text{O}$  catalysts, flow rate: 50 mL/min, 2%  $\text{O}_2$ , 2% CO, 40%  $\text{H}_2$ , bal. He, 500 mg sample c) Steady-state PrOX at 130°C over  $\text{Pt}_1/\text{Cu}_x\text{O}$ , flow rate: 50 mL/min, 2%  $\text{O}_2$ , 2% CO, 40%  $\text{H}_2$ , bal. He, 250 mg sample.

## Recent Progress B: Understanding the surface structure of $\text{Cu}_2\text{O}(111)$ and $\text{CuO}_x$ nanoparticles as model supports for single atom catalysts.

To develop the field of single atom catalysts beyond reports of promising catalytic properties, the atomic-scale structure of active sites must be understood and correlated with their chemical reactivity. Using both a model and nanoparticle approach we have begun studying the surface chemistry of  $\text{Cu}_2\text{O}$  before we add metal atom sites. The surface structure of  $\text{Cu}_2\text{O}$  is dynamic, complex and far less understood than bulk structure and properties. The (111) surface of  $\text{Cu}_2\text{O}$  is the most experimentally studied and considered the most stable through a range of conditions. However, Wulff reconstructions of  $\text{Cu}_2\text{O}$  nanoparticles reveal that the (111) facet becomes less stable as oxygen chemical potential is increased.

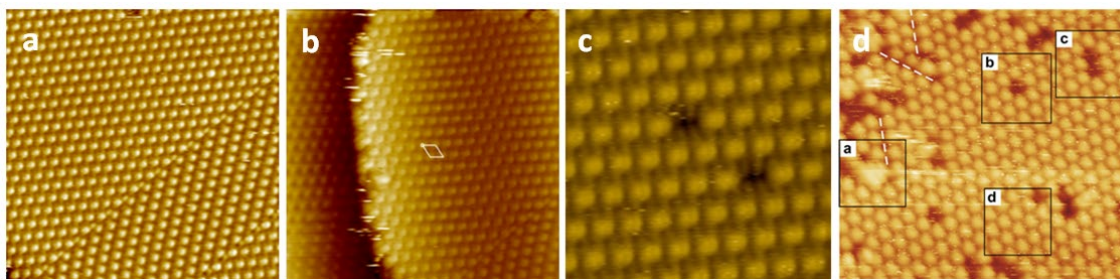


**Figure 3:** A: Atomically resolved  $\text{Cu}_2\text{O}(111)$  surface. Total image size:  $13.2 \text{ nm}^2$  and the unit cell of the 111 surface is  $6.15 \text{ \AA} \times 5.60 \text{ \AA}$  (shown in B). B: Step edge nearby the line feature shown in A, same image size and unit cell. C: Two Cu vacancies in the  $\text{Cu}_2\text{O}(111)$  surface. D:  $23 \times 21.6 \text{ nm}$  STM image of the  $(\sqrt{3} \times \sqrt{3}) \text{ R}30^\circ$  reconstruction reported by Onsten et al using  $-1.0 \text{ V}$ ,  $0.015 \text{ nA}$  scanning conditions. 3 dislocations are shown with dashed lines. Cu vacancy highlighted in box b.

We have acquired  $\text{Cu}_2\text{O}$  bulk crystals cut to exhibit the (111) surface facet and begun to study their atomic-scale surface structure (Figure 3). We have on occasion observed the  $1 \times 1$  surface termination consistent with literature reports but further work to correlate the cleaning to the surface structure is required, because we often observe an unreported 1D surface structure that is epitaxial with one of the high symmetry directions of the bulk  $\text{Cu}_2\text{O}$  structure. We are now working to perform a more complete study of how the preparation conditions affect the surface structure of the  $\text{Cu}_2\text{O}$  single crystal before advancing to the investigation of dispersed Pt and Rh atoms and their catalytic chemistry.

Corollary to the surface science studies, we have initiated experiments examining the surface structure of  $\text{CuO}$  and  $\text{Cu}_2\text{O}$  nanoparticles. Because direct imaging of the surface structure is not feasible for nanoparticles, as it is for single crystals, we utilize CO probe molecule FTIR measurements to probe the surface sites present on the surface of the  $\text{CuO}_x$  particles as a function of pre-treatment conditions. These studies will be correlated to similar studies on single crystals and also inform differences in  $\text{CuO}_x$  surface chemistry induced by deposition of atomically dispersed metals. CO IR experiments at  $-130^\circ\text{C}$  exhibited no signals associated with CO adsorbing onto the sample that had been oxidized at  $400^\circ\text{C}$  for 1 hour, consistent with literature data that CO does not adsorb on  $\text{Cu}^{2+}$ . An hour reduction of the  $\text{CuO}$  sample at  $150^\circ\text{C}$  in  $\text{H}_2$  followed by CO exposure at cryogenic temperature enabled CO adsorption with stretching frequencies at  $2135 \text{ cm}^{-1}$  and  $2110 \text{ cm}^{-1}$ , associated with CO on  $\text{Cu}^+$  ions (Figure 4). Increasing  $\text{H}_2$  reduction temperature to  $250^\circ\text{C}$  followed by CO adsorption again resulted in CO adsorption on  $\text{Cu}^+$  which were located at  $2135 \text{ cm}^{-1}$  and  $2115 \text{ cm}^{-1}$  (modified

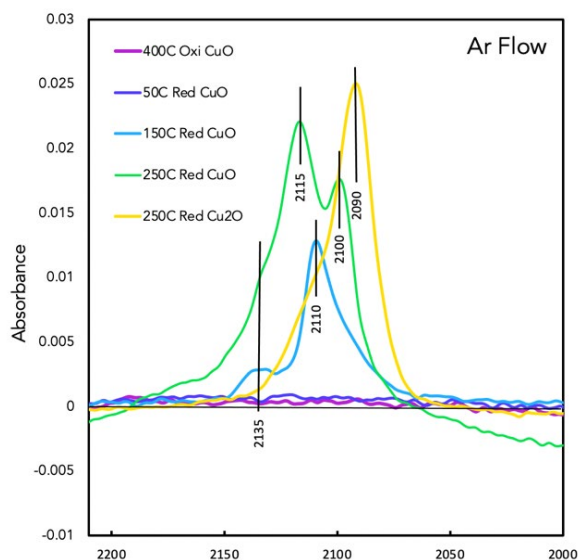


**Figure 4:** COIR spectra taken at  $\sim -130 \text{ C}$  while purging with Ar for 5%  $\text{CuO}$  nanoparticles mixed with  $\text{Al}_2\text{O}_3$ . Samples were pretreated for 1 hour at indicated temperature under  $\text{O}_2$  or  $\text{H}_2$  flow.

from the behavior of 150°C reduction) and band at 2100 cm<sup>-1</sup>, likely corresponding to CO adsorbed on metallic copper sites located at a step edge. When a Cu<sub>2</sub>O sample is subjected to the same reducing pretreatment at 250°C, there is a clear shift towards the metallic species with the most prominent CO band being observed at 2090 cm<sup>-1</sup> and a small shoulder located at 2110 cm<sup>-1</sup>. These results give a preliminary idea of how the surface sites on these copper oxides change under different conditions and serve as a reference point to compare to surface science studies and future studies on CuO<sub>x</sub> nanoparticles containing atomically dispersed metals.

Moving forward, our continued efforts will focus on comparing insights obtained from analyses of the surface structure of CuO<sub>x</sub> materials on single crystals and nanoparticles and begin to explore the influence of atomically dispersed metals on CuO<sub>x</sub> reducibility and reactivity for catalytically important elementary steps such as H<sub>2</sub> and CO<sub>2</sub> activation.

#### **Publications Acknowledging this Grant in 2018-2021 (This grant started 9/1/20)**

*(XVI) Intellectually led by this grant*

- 1) ["Developing Single-Site Pt Catalysts for the Preferential Oxidation of CO: A Surface Science and First Principles-Guided Approach"](#) J. Liu, A. J. R. Hensley, G. Giannakakis, A. J. Therrien, A. Sukkar, A. C. Schilling, K. Groden, N. Ulumuddin, R. T. Hannagan, M. Ouyang, M. Flytzani-Stephanopoulos, J. McEwen, E. C. H. Sykes *Applied Catalysis B: Environmental* **2020**, 284 119716 *The experimental parts of this manuscript were funded solely by DOE/BES under Grant # DE-SC0021196. Theory collaborator McEwen was funded by his NSF CAREER award.*

*(XVII) Jointly funded by this grant and other grants with intellectual leadership by other funding sources*

- 2) ["Atomically Dispersed Pt-group Catalysts: Reactivity, Uniformity, Structural Evolution, and Paths to Increased Functionality"](#) J. Resasco, P. Christopher *J Phys Chem Lett* **2020**, *11*, **23**, 10114-1023. *This is an invited perspective paper that highlighted the potential bifunctional behavior created by single metal atoms on reducible oxide supports, which was credited to DOE/BES under Grant# DE-SC0021124.*
- 3) ["First-principles design of a single-atom-alloy propane dehydrogenation catalyst"](#), Ryan T. Hannagan, Georgios Giannakakis, Romain Reocreux, Julia Schumann, Jordan Finzel, Yicheng Wang, Angelos Michaelides, Prashant Deshlahra, Phillip Christopher, Maria Flytzani-Stephanopoulos, Michail Stamatakis, E. Charles H. Sykes, *Science*, 2021, 372, 1444-1447. *The work done at UCSB on catalyst characterization was credited to DOE/BES under Grant# DE-SC0021124.*

## **Awards or leadership activities during 2018-2020 calendar years**

### **Phillip Christopher**

#### ***Awards***

2020 AIChE CRE Division Young Investigator Award

2020 ACS CATL Division Early Career in Catalysis Award

2019 Presidential Early Career Award for Scientists and Engineers (PECASE)

#### ***Leadership***

Guest Editor for a special issue in Journal of Chemical Physics in 2020 entitled “Heterogeneous Single-Atom Catalysts”.

Chair, 17<sup>th</sup> meeting on Dynamics, Interactions, and Electronic Transitions at Surfaces (DIET). Planning of this meeting has started but is on hold due to the COVID-19 pandemic.

Chair, 3<sup>rd</sup> International Symposium of Single Atom Catalysis (ISSAC-3), Asilomar, CA, June 10-13 2020. (This was an official satellite meeting for the International Congress on Catalysis that had ~70 registered attendees from 13 countries before it was cancelled due to the COVID-19 pandemic.)

Senior Editor, ACS Energy Letters, 2018 - Present.

### **E. Charles H. Sykes**

#### ***Awards***

ACS Catalysis Lectureship with M. Flytzani-Stephanopoulos

#### ***Leadership***

Guest Editor for a special issue in Journal of Chemical Physics in 2020 entitled “Heterogeneous Single-Atom Catalysts”.

Editor, Surface Science Reports, 2021-present

## Electrocatalytic Oxidation of Carbon Monoxide on Metal Nanoparticles in the Presence and Absence of Interactions with Metal-Oxide Supports

Richard M. Crooks, Graeme Henkelman, Kihyun Shin, and Aigerim Galyamova  
The University of Texas at Austin, Department of Chemistry

### Presentation Abstract

In our previously reported oxygen reduction reaction (ORR) study, we showed that fully passivating, ultra-thin (2.8 nm-thick),  $\text{TiO}_x$  ( $x = 1.9; 2.0$ ) films can be deposited onto carbon electrodes via atomic layer deposition (ALD). More importantly, subsequent adsorption of Au DENs ( $\text{G6NH}_2(\text{Au}_{147})$ , average diameter:  $1.8 \pm 0.2$  nm) onto the oxide surface leads to an electrocatalytically active interface. Additionally, a UV/ $\text{O}_3$  treatment (Scheme 1) can be used to almost completely remove the dendrimer surrounding the surface-confined Au DENs without changing their size, shape, or electrocatalytic properties. Experimental electrocatalysis studies indicated improvement in the ORR kinetics and positive shifts in the onset potential by 0.10 V and by 0.05 V when the AuNPs were in direct contact with the underlying  $\text{TiO}_{1.9}$  and  $\text{TiO}_{2.0}$  supports, respectively. These experimental results were in good agreement with the density functional theory (DFT)-predicted onset potential shift of 0.10 V. We now continue to use the same workflow and electrocatalyst configurations ( $\text{PPF}/\text{TiO}_x/\text{G6NH}_2(\text{Au}_{147})$  and  $\text{PPF}/\text{TiO}_x/\text{Au}_{147}$  for our new carbon monoxide oxidation (COO) study.

Theoretical calculations investigated several different COO reaction pathways. Specifically, the direct mechanism indicate improvement in the COO *onset potential* by 0.18 V when the Au rod in direct contact with the underlying  $\text{TiO}_2(110)$  support compared to isolated  $\text{Au}_{147}$  NP. According to DFT, this activity enhancement is attributed to the increased stability of  $\text{COOH}^*$  intermediate at the  $\text{TiO}_2(110)/\text{Au}$  interface. More experiments are currently on the way to confirm or deny this observation.

### DE-SC0010576: Testing the Predictive Power of Theory for Determining the Structure and Activity of Nanoparticle Electrocatalysts

**Co-PI:** Graeme Henkelman

**Postdoc:** Kihyun Shin

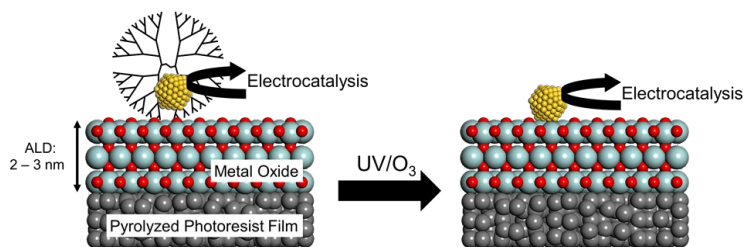
**Graduate Student:** Aigerim Galyamova

### RECENT PROGRESS

#### *Introduction*

The objective of this project is to develop an in-depth understanding of nanoparticle (NP) and metal oxide support interactions using the synergy between predictive theory and confirming experiments to carry out both simple and complex electrocatalytic reactions. We accomplished this goal using the model shown in Scheme 1, where the catalysts are well-defined 1-2 nm metallic or bimetallic NPs atop an ultrathin metal oxide support deposited on a conductive electrode using ALD. This construct is electroactive and can be

used to study electrocatalytic reactions taking place at the NP surface. The right frame of Scheme 1 shows that a UV/O<sub>3</sub> treatment can be used to remove the encapsulating dendrimer without changing the NP composition or morphology. In this case, the NP is in direct contact with the oxide surface. Hence, it is possible to study electrocatalytic reactions at the NP surface in the absence or presence of substrate effects. This study is focused specifically on electro-catalytic reactions that are of critical importance for the production and use of



**Scheme 1.** Deposition of metal NP on ultrathin metal oxide support by removing the encapsulating dendrimer via UV/O<sub>3</sub> treatment.

chemical fuels. These include the COO, alcohol oxidation, formic acid oxidation, and the ORR.

This abstract is focused specifically on the effect of TiO<sub>2</sub>/Au interactions on the COO. The research was conducted in two parts. The first part involved using DFT to understand interactions between AuNPs and TiO<sub>2</sub> supports. The second part involved testing the theoretical prediction experimentally. This consisted of immobilizing dendrimer-encapsulated AuNPs (Au DENs) onto thin TiO<sub>x</sub> support layers deposited by ALD, subsequent removal of the dendrimers, and electrocatalytic testing of both constructs (non-direct and direct) shown in Scheme 1.

### Theoretical Findings

AuNPs having 147 atoms having an icosahedron structure (Au<sub>147</sub> Ih) and Au rod supported on the stoichiometric rutile TiO<sub>2</sub>(110) system (TiO<sub>2</sub>/Au) were used to calculate the reaction energy diagrams for the COO. These structures were identical to the ones that we studied in our previously reported ORR work, where the theoretical calculations closely matched the experimental results.

We considered several possible reaction mechanisms to thoroughly characterize the reactivity of the electrocatalysts. Those are the direct, Eley-Rideal (ER), Langmuir-Hinshelwood (LH), and Mars van Krevelen (MvK) mechanisms. It is important to note that MvK itself can proceed via direct, ER or LH pathways, but with TiO<sub>2</sub>(110) lattice oxygen playing an active role during the oxidation. Therefore, we incorporated the MvK mechanism into our calculations by

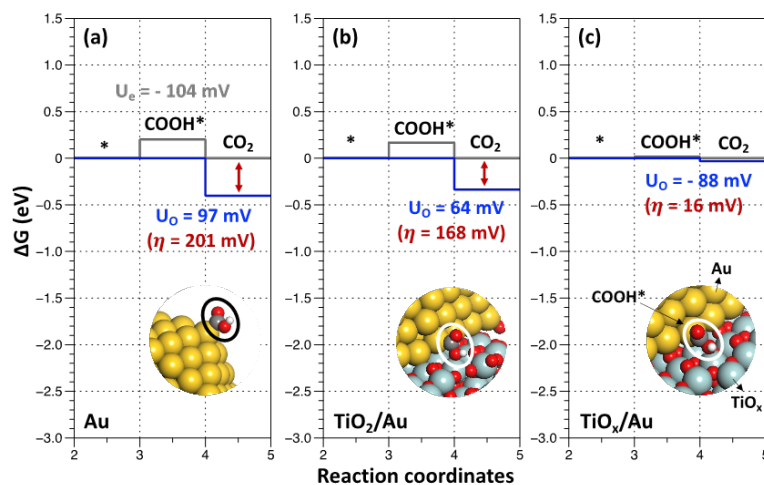


**Figure 1.** Gibbs free energy diagram for the COO via direct mechanism at: (a) isolated AuNPs, (b) Au/TiO<sub>2</sub>, and (c) Au/TiO<sub>x</sub>

including  $\text{TiO}_x/\text{Au}$  having an oxygen vacancy as a reaction site for each reaction mechanism. In all the considered reaction pathways, the rate determining step is the  $\text{COOH}^*$  intermediate instability. Here, we will specifically discuss the direct mechanism because this reaction pathway exhibits the lowest overpotential among other possible mechanisms.

The direct mechanism is the simplest pathway for the COO because only electron transfer needs to be taken into the account during the simulations. In Figure 1, Gibbs free energy diagrams at equilibrium potentials ( $U_e$ , grey line) are shown for  $\text{Au}_{147}$  Ih (left),  $\text{TiO}_2/\text{Au}$  (middle), and  $\text{TiO}_x/\text{Au}$  having an oxygen vacancy (right). We found that the first step of the reaction, formation of  $\text{COOH}^*$ , is the limiting step at all reaction sites. Specifically, the instability of the  $\text{COOH}^*$  intermediate limits the reactivity of isolated  $\text{Au}_{147}$  Ih. In contrast,  $\text{COOH}^*$  stability increases at the Au and  $\text{TiO}_x$  interface. Specifically,  $\text{TiO}_x/\text{Au}$  exhibited a 185 mV smaller overpotential ( $\eta$ ) than isolated  $\text{Au}_{147}$  Ih ( $\eta = 201$  mV) due to the stronger  $\text{COOH}^*$  binding at the  $\text{TiO}_x/\text{Au}$  interface.

In conclusion, we found that  $\text{COOH}^*$  stability at the reaction site is a rate-determining step of the COO. Specifically, for the discussed mechanisms pathways, the interface between Au and  $\text{TiO}_2$  had higher activity than isolated  $\text{Au}_{147}$  Ih. Furthermore, the MvK mechanism ( $\text{TiO}_x/\text{Au}$  with an oxygen vacancy) exhibits highest COO activity compared to isolated  $\text{Au}_{147}$  Ih.

### Experimental Findings

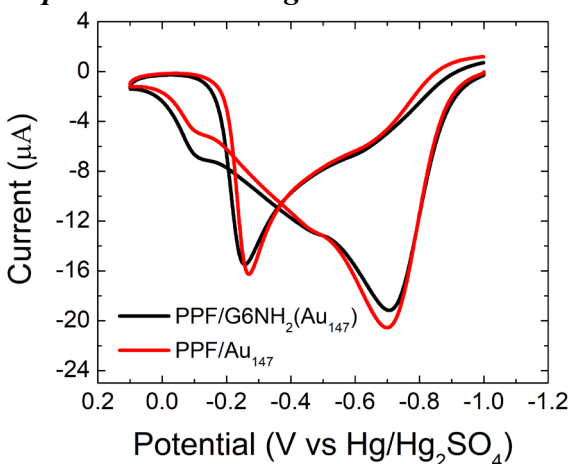


**Figure 2.** Cyclic voltammograms for COO at pH 13 on PPF supported AuNPs with (black) and without (red) dendrimers

supported Au DENs before and after the UV/ $\text{O}_3$  dendrimer removal procedure. The results from these experiments are shown in Figure 2. The key finding of these experiments is that there is no significant difference in the COO peak positions (during both positive and negative sweeps) on AuNPs with and without the dendrimers present in the system. This means that our experimental conditions and UV/ $\text{O}_3$  dendrimer removal procedure do not artificially alter Au DENs COO activity. This is an important result because the COO is well known to be highly sensitive to changes in NPs size and structure. We are now proceeding to studying the COO on PPF/ $\text{TiO}_x/\text{G6NH}_2$  ( $\text{Au}_{147}$ ) and PPF/ $\text{TiO}_x/\text{Au}_{147}$  supports.

The COO is an electrocatalytic probe reaction that has not previously been characterized or studied in our system (Scheme 1). Therefore, we first confirmed that our experimental conditions and treatments do not artificially alter the Au DENs activity towards the COO. This was accomplished by studying the Au DENs COO activity on Pyrolyzed Photoresist Film (PPF) electrodes.

PPF is a glassy carbon-like conductive material that is known to be an inert electrode material. This means that PPF does not change the electrocatalytic performance of the supported NPs by itself. Thus, we performed the COO on PPF

Early preliminary results indicate that thin  $\text{TiO}_x$  ALD layers prevents tunneling between the underlying PPF electrode and the Au DENs, but only in the case of oxidation reactions (like the COO). Reduction reactions, like the ORR, are not inhibited. This is a very surprising result, as our model, which has been verified for other metal oxides, like  $\text{SnO}_x$  and  $\text{Al}_2\text{O}_3$ , exhibit normal tunneling behavior. We have confirmed this finding through extensive control experiments, and we are currently working toward a theoretical understanding of this unanticipated phenomenon.

### ***Summary and Conclusions***

We used DFT calculations to predict the nature of  $\text{TiO}_2/\text{Au}$  interactions and the effect of these interactions on COO activity at  $\text{TiO}_2/\text{Au}$  compared to  $\text{Au}_{147}$  Ih. We considered several reaction mechanisms for the COO. The calculations indicate that the  $\text{COOH}^*$  intermediate instability is the rate determining step for all considered reaction pathways. Specifically for the direct mechanism, the  $\text{TiO}_2/\text{Au}$  construct exhibits a 185 mV lower COO overpotential compared to isolated  $\text{Au}_{147}$  Ih due to the increased  $\text{COOH}^*$  stability. *The enhanced  $\text{COOH}^*$  intermediate stability at the  $\text{TiO}_2/\text{Au}$  interface increases COO activity due to electron accumulation at interface. Experimentally, we confirmed that the UV/ $\text{O}_3$  dendrimer removal treatment and experimental conditions themselves do not artificially alter Au DENs COO activity. However, the presence of the thin  $\text{TiO}_x$  ALD layer inhibits electron tunneling from the support Au DENs into the underlying PPF electrode. We are presently working toward a theoretical understanding of this surprising result.*

### **Publications Acknowledging this Grant in the period 2018-2021**

*Category I Publications (note that some of these publications cite funding from student fellowships, our endowments from the Robert A. Welch Foundation, and collaborators' grants)*

1. Strasser, J. W.; Hersbach, T. J. P.; Liu J.; Lapp, A. S.; Frenkel, A. I.; Crooks, R. M. Electrochemical Cleaning Stability and Oxygen Reduction Reaction Activity of 1-2 nm Dendrimer-Encapsulated Au Nanoparticles. *ChemElectroChem* **2021**, *8*, 2545–2555.
2. Kim, S. K.; Shin, K.; Henkelman, G. Stability of Pt Skin Intermetallic Core Catalysts and Adsorption Properties for the Oxygen Reduction Reaction. **2021**, *125*, 3527-3534.
3. Galyamova, A.; Shin, K.; Henkelman, G.; Crooks, R. M. Effect of  $\text{TiO}_x$  Substrate Interactions on the Electrocatalytic Oxygen Reduction Reaction at Au Nanoparticles. *J. Phys. Chem. C* **2020**, *124*, 10045-10056.
4. Guo, H.; Trindell, J. A.; Li, H.; Fernandez, D.; Humphrey, S. M.; Henkelman, G.; Crooks, R. M. Testing the Predictive Power of Theory for  $\text{Pd}_x\text{Ir}_{(100-x)}$  Alloy Nanoparticles for the Oxygen Reduction Reaction. *J. Mater. Chem. A* **2020**, *8*, 8421-8429.

5. Ciufu, R. A.; Han, S.; Floto, M. A.; Henkelman, G.; Mullins, C. B. Low Temperature Dissociation of CO on Manganese Promoted Cobalt(poly). *Chem. Commun.* **2020**, *56*, 2865-2868.
6. Kawashima, K.; Shin, K.; Wygant, B. R.; Kim, J-H.; Cao, C. L.; Lin, J.; Son, Y. J.; Liu, Y.; Henkelman, G.; Mullins, C. B. Cobalt Metal–Cobalt Carbide Composite Microspheres for Water Reduction Electrocatalysis. *ACS Appl. Energy Mater.* **2020**, *3*, 3909-3918.
7. Timoshenko, J.; Duan, Z.; Henkelman, G.; Crooks, R. M.; Frenkel A. I. Solving the Structure and Dynamics of Metal Nanoparticles by Combining X-Ray Absorption Fine Structure Spectroscopy and Atomistic Structure Simulations. *Annual Rev. Anal. Chem.* **2019**, *12:1*, 501-522.
8. Liu, Y.; Duan, Z.; Henkelman, G. Computational Design of CO-tolerant Pt<sub>3</sub>M Anode Electrocatalysts for Proton-Exchange Membrane Fuel Cell. *Phys. Chem. Chem. Phys.* **2019**, *21*, 4046-4052.
9. Duan, Z.; Henkelman, G. Theoretical Resolution of the Exceptional Oxygen Reduction Activity of Au(100) in Alkaline Media. *ACS Catalysis* **2019**, *9*, 5567-5573.
10. Li, H.; Shin, K.; Henkelman, G. Effects of Ensembles, Ligand, and Strain on Adsorbate Binding to Alloy Surfaces. *J. Chem. Phys.* **2018**, *149*, 174705.
11. Duan, Z.; Henkelman, G. Calculations of the pH-Dependent Onset Potential for CO Electrooxidation on Au(111). *Langmuir* **2018**, *34*, 15268-15275.
12. Lapp, A. S.; Duan, Z.; Marcella, N.; Luo, L.; Genc, A.; Ringnalda, J.; Frenkel, A. I.; Henkelman, G.; Crooks, R. M. Experimental and Theoretical Structural Investigation of AuPt Nanoparticles Synthesized Using a Direct Electrochemical Method. *J. Am. Chem. Soc.* **2018**, *140*, 6249-6259.
13. Ostojic, N.; Duan, Z.; Galyamova, A.; Henkelman, G.; Crooks, R. M. Electrocatalytic Study of the Oxygen Reduction Reaction at Gold Nanoparticles in the Absence and Presence of Interactions with SnO<sub>x</sub> Supports. *J. Am. Chem. Soc.* **2018**, *140*, 13775-13785.

### Category II Publications

none

**Awards or leadership activities during 2018-2021 calendar years**

Richard M. Crooks (PI)

2021- Scientific advisor board: Lantha Sensors  
2021- Scientific advisor board: Stoicea, LLC  
2020- Co-founder: Galvanix, LLC  
2017- Robert A. Welch Chair in Materials Chemistry  
2017-2019 Executive Editor of the ACS journal *Langmuir*

Graeme Henkelman (co-PI)

2019- Scientific advisory board: Lantha Sensors  
2019- George W. Watt Centennial Professor, Department of Chemistry  
2017- Editorial board: Surface Science

## Sub Nanometer Sized Clusters for Heterogeneous Catalysis

Abhaya Datye<sup>1</sup> and Yong Wang<sup>2</sup>

<sup>1</sup>University of New Mexico and <sup>2</sup>Washington State University

### Presentation Abstract

The focus of this project is the synthesis, characterization and reactivity of transition metal moieties ranging from single atoms to clusters of about 1 nm in diameter that are present on high surface area supports. A major barrier in the utilization of sub-nm clusters is that they are subject to Ostwald ripening, leading to growth in size to form nanoparticles. Our recent work suggests that trapping single atoms on the support could help to slow the rates of ripening. Hence, one of the goals of this project is the understanding of anchoring sites on high surface area catalyst supports. Conventional (non-reducible) oxide supports provide only limited number of sites to anchor ionic species. Reducible oxides, such as ceria provide many more sites for anchoring due to the presence of defects. But reducible oxides are often not available in high surface area form, and they may not be as robust (can react to form carbonates, for example, or sinter easily) compared to the commonly-used high surface area supports such as silica, alumina, or carbon. Increasing atomic trapping sites on conventional catalyst supports is therefore important for improving the stability of sub-nm metal clusters on a supported catalyst. Another goal of this project is to expand the applicability of single atom catalysts to a broader class of catalyzed reactions. Transition metals in ionic form are perfectly situated for further manipulation of their catalytic activity by use of ligands, as in homogeneous catalysis. Understanding the principles that help in the design and application of robust single atom catalysts is one of the research challenges that is addressed in this project.

### DOE grant # DE-FG02-05ER15712

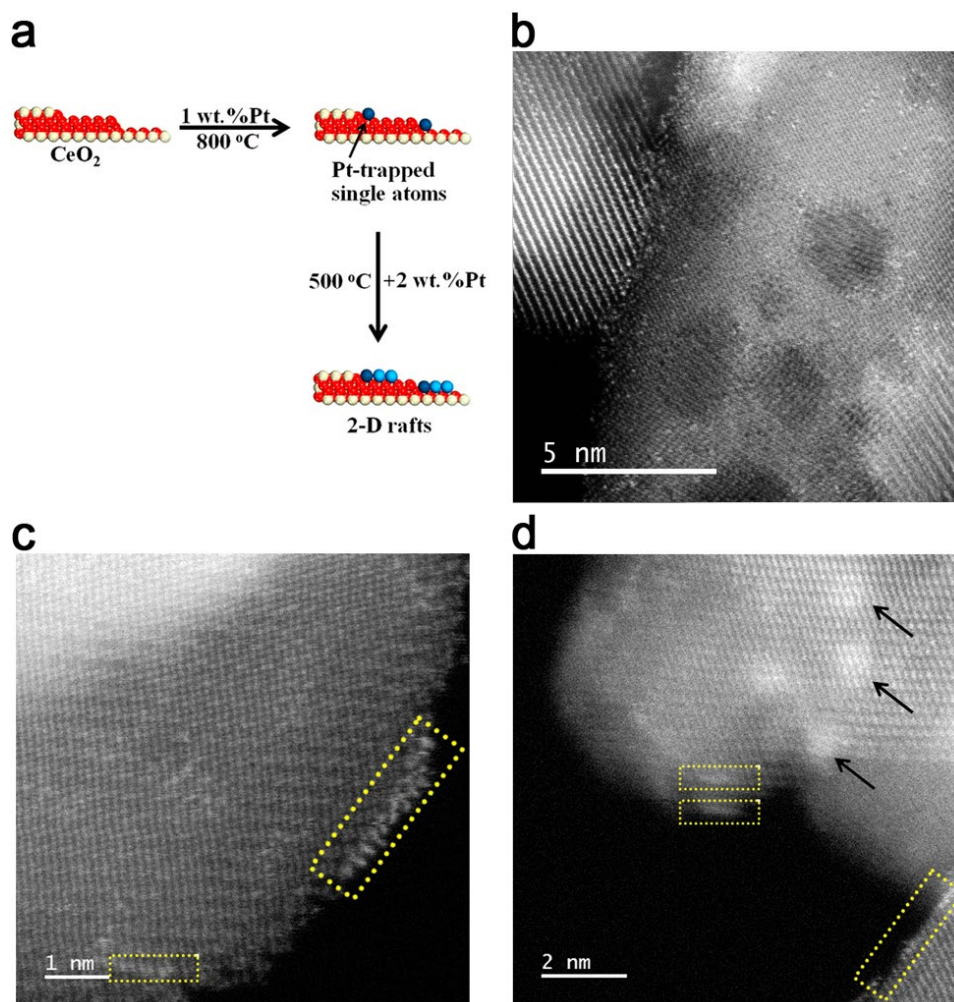
#### Sub Nanometer Sized Clusters for Heterogeneous Catalysis

Post-docs: Andrew DeLaRiva (UNM), Dong Jiang (WSU)  
Graduate Students: Stephen Porter (UNM), Carlos Vargas and Jianghao Zhang (WSU)  
Collaborators: Hua Guo (UNM), Ayman Karim (VT), Jean Sabin McEven (WSU), L. Hu (U. Maryland), Haifeng Xiong (Xiamen)

### RECENT PROGRESS

#### *Controlling nucleation & growth of clusters via atom trapping*

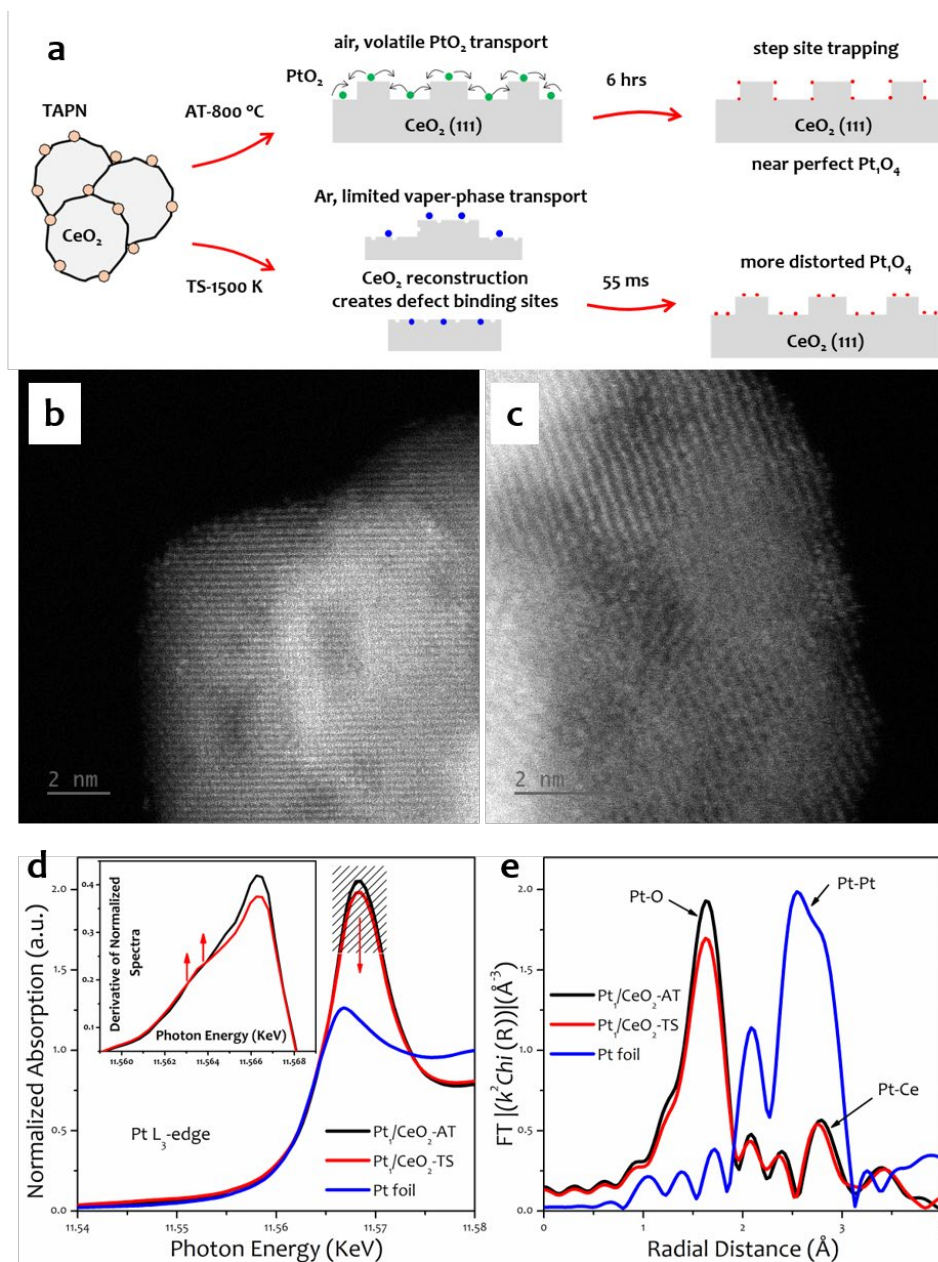
In previous work (Jones et al., Science, 2016), we demonstrated that Pt atoms can be trapped on ceria in thermally stable form by simply heating the Pt/ceria catalyst to 800 °C in air. We have now explored the ability of these stable single atoms to control the nucleation and growth of metal and metal oxide clusters on the ceria support. In a manuscript that has been accepted for publication in Nature Catalysis, we show how 2-D rafts of Pt and Pd oxides can be stabilized on this engineered ceria support. These novel structures provide improved water tolerance for low temperature methane oxidation.



**Fig. 1 | Scanning transmission electron microscope images of 2D rafts of Pt on Pt@CeO<sub>2</sub>.** **a**, Schematic illustration showing the morphologies of Pt catalysts supported on ceria prepared by depositing Pt on a Pt-trapped ceria. The Pt atoms were labelled with different colors for the purpose of emphasizing the two steps in preparation. **b**, AC-STEM image of 1 wt.%Pt@CeO<sub>2</sub> prepared by atom trapping showing atomically dispersed Pt indicated by white dots. **c,d**, AC-STEM images of the catalyst prepared by depositing 2 wt% Pt on atom trapped 1wt% Pt@CeO<sub>2</sub>. Edge-on views (**c,d**) indicated by rectangles show that Pt forms 2D rafts which are approximately 1.5 nm in diameter as seen in top-down views indicated by arrows in (**d**). The uniform contrast of the particles in (**d**) confirms that these are not three-dimensional nanoparticles, which is a result of the modification of the catalyst support via atom trapping.

### *Single atom sites created by shock wave synthesis*

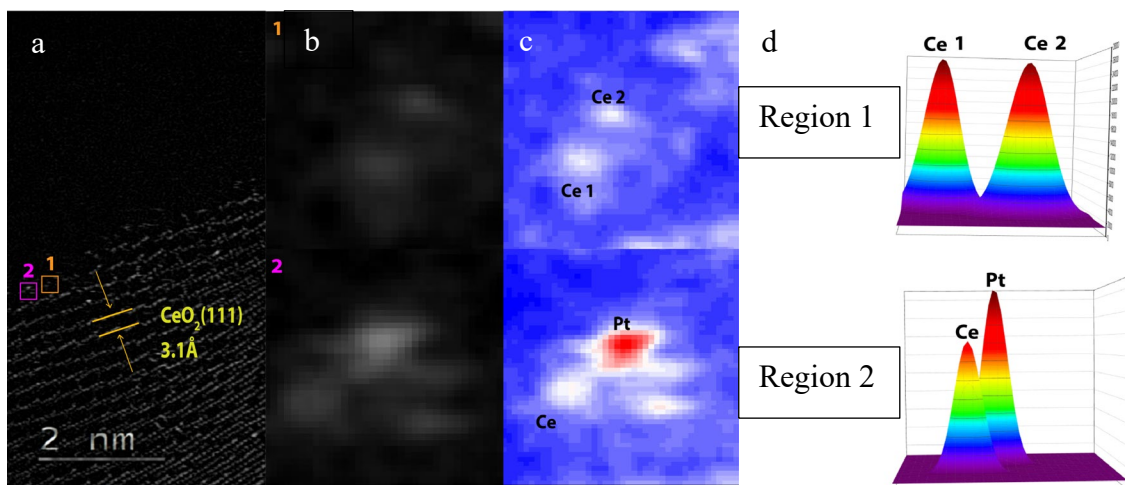
Our initial work on atom trapping demonstrated the ability to create stable single atoms of Pt on ceria. However, these Pt atoms are present in the form of ionic Pt(2+) and adsorb CO weakly and are not able to activate oxygen. The CO oxidation activity of these Pt sites is not any better than on metallic Pt. We collaborated with Prof. Hu at the University of Maryland to explore the potential of shock wave synthesis. In a manuscript accepted for publication in *Angew. Chemie*, we show that with this approach, we are able to create ionic Pt sites whose environment is distorted, enhancing the reactivity for CO oxidation.



**Figure 2.** (a) Schematic of AT (atom trapping) and TS (thermal shock) synthesis of single-atom 1wt % Pt<sub>1</sub>/CeO<sub>2</sub> catalysts with near-perfect and distorted Pt<sub>1</sub>O<sub>4</sub> coordination, respectively. HAADF-STEM images of as-synthesized Pt<sub>1</sub>/CeO<sub>2</sub>\_AT (b) and Pt<sub>1</sub>/CeO<sub>2</sub>\_TS (c). Pt L<sub>3</sub>-edge XANES (d) and the Fourier transform of *k*<sup>2</sup>-weighted EXAFS (e) of as-synthesized Pt<sub>1</sub>/CeO<sub>2</sub>\_AT and Pt<sub>1</sub>/CeO<sub>2</sub>-TS as well as Pt foil. Inset of (d) is the 1<sup>st</sup> derivative of the normalized XANES.

### Identifying individual atoms in single atom catalysts

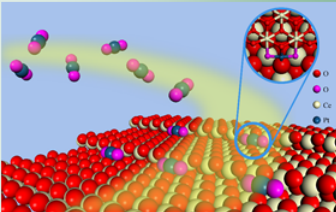
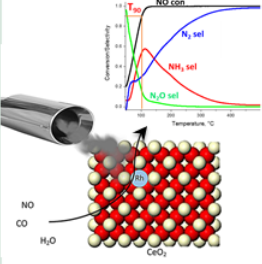
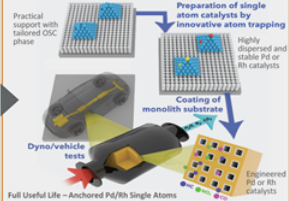
At UNM, we recently acquired an electron microscope that provides resolution of 0.71 Å which is ideally suited for single atom imaging. We are now working on methods to improve the characterization of these catalysts, specifically our ability to locate and identify individual atoms on catalyst supports. The initial work was presented at the Microscopy and Microanalysis meeting in 2021 showing the ability to use the contrast from individual Ce atoms from the support to normalize the intensity of the catalytically active phase. Future work will focus on applying this approach to better define where these atoms are located on the oxide supports and to relate these structures to catalytic performance.



**Figure 3.** (a) Annular dark field image of 1 wt% Pt/CeO<sub>2</sub>. (b) Two regions in this image were selected for further study. (c) After background subtraction and image processing, the single atoms are clearly visible. (d) 2-D Gaussian fits to the intensity profile are shown for each region. The ratio of integrated intensity of the Ce atoms ( $Z=58$ ) to the Pt atoms ( $Z=78$ ) is 0.55 which agrees with the expected ratio based on atomic number (Intensity varies  $\sim Z^2$ ), confirming these bright atoms to be Pt single atoms.

*Translation of BES supported fundamental research to industrial practice*

## Atom Trapping For Single Atom Catalysts

BES Basic Science	EERE/VTO Applied Research	Industrial Collaboration Toward Deployment
 <p>Catalysts based on single atoms of scarce precious metals can lead to more efficient use through enhanced reactivity and selectivity. Research supported at WSU and UNM led to the discovery of thermally stable single atom catalysts by atom trapping.</p>  <p><i>Science</i>, 2016. DOI: 10.1126/science.aaf8800</p>	 <p>Work supported at PNNL demonstrated highly active and thermally stable 0.1 wt% Rh<sub>1</sub>/CeO<sub>2</sub> single atom catalysts achieving 90% NO conversion at 100°C, exceeding the US DRIVE 150°C T90 Challenge</p>  <p><i>Angew. Chem. Int. Ed.</i>, 2020 DOI: 10.1002/anie.202010815</p>	 <p>Jointly working with FCA and BASF to demonstrate advanced TWC technologies to address the PGM shortage while enabling efficient combustion engines to meet stringent CAFE and emission standards</p> 

This slide presents an overview of our recently funded program to develop the application of single atom catalysts to exhaust emission control.

## Publications Acknowledging this Grant in 2018-2021

(XVIII) Intellectually led by this grant (25)

1. D. Jiang, Y. Yao, T. Li, G. Wan, X.I. Pereira-Hernández, Y. Lu, J. Tian, K. Khivantsev, M.H. Engelhard, C. Sun, C.E. García-Vargas, A.S. Hoffman, S.R. Bare, A.K. Datye, L. Hu, and Y. Wang, Tailoring the Local Environment of Platinum in Single-Atom Pt<sub>1</sub>/CeO<sub>2</sub> Catalysts for Robust Low-Temperature CO Oxidation. *Angewandte Chemie International Edition*. 2021, accepted, in press, <https://doi.org/10.1002/anie.202108585>
2. Haifeng Xiong, Deepak Kunwar, Dong Jiang, Carlos E. García-Vargas, Hengyu Li, Congcong Du, Griffin Canning, Xavier Isidro Pereira-Hernandez, Qiang Wan, Sen Lin, Stephen C. Purdy, Jeffrey T. Miller, Kevin Leung, Stanley S. Chou, Hidde H. Brongersma, Rik ter Veen, Jianyu Huang, Hua Guo, Yong Wang, Abhaya K. Datye, Engineering catalyst supports to stabilize PdOx two-dimensional rafts for water-tolerant methane oxidation, *Nature Catalysis*, 2021, accepted, in press. Preprint available at Research Square of the submitted manuscript - <https://doi.org/10.21203/rs.3.rs-113744/v1>
3. R. Alcala, A. DeLaRiva, E.J. Peterson, A. Benavidez, C.E. Garcia-Vargas, D. Jiang, X.I. Pereira-Hernández, H.H. Brongersma, R.t. Veen, J. Staněk, J.T. Miller, Y. Wang, and A. Datye, Atomically Dispersed Dopants for Stabilizing Ceria Surface Area. *Applied Catalysis B: Environmental*, 2021. 284: p. 119722.
4. A.K. Datye and H. Guo, Single atom catalysis poised to transition from an academic curiosity to an industrially relevant technology. *Nature Communications*, 2021. 12(1): p. 1-3.
5. H. Xiong, A.K. Datye, and Y. Wang, Thermally Stable Single-Atom Heterogeneous Catalysts. *Advanced Materials*, 2021: p. 2004319.
6. S. Porter and A. Datye, Identifying Individual Atoms in Single Atom Pt/CeO<sub>2</sub> Catalysts. *Microscopy and Microanalysis*, 2021. 27(S1): p. 2608-2610.
7. B.Qian, J.Zhang, S.Zhou, J.Lu, Y.Liu, B.Dai, C.Liu, Y.Wang, H.Wang, L.Zhang, "Synthesis of (111) facet-engineered MgO nanosheet from coal fly ash and its superior catalytic performance for high-temperature water gas shift reaction", *Appl.Catal.A, General*, 2021, doi: 10.1016/j.apcata.2021.118132.
9. D.Jiang, G. Wan, C. Garcia, L. Li, X.I.P.Hernandez, C. Wang, Y.Wang, "Elucidation of the Active Sites in Single-Atom Pd<sub>1</sub>/CeO<sub>2</sub> Catalysts for Low-Temperature CO Oxidation", *ACS Catalysis*, 2020, DOI: 10.1021/acscatal.0c02480 (cover)
10. B.Qian, J.Zhang, S.Zhou, J.Lu, Y.Liu, B.Dai, C.Liu, Y.Wang, H.Wang, L.Zhang, "Synthesis of (111) facet-engineered MgO nanosheet from coal fly ash and its superior catalytic performance for high-temperature water gas shift reaction", *Appl.Catal.A, General*, 2021, doi: 10.1016/j.apcata.2021.118132.
11. Zhang, J.; Sun, J.; Wang, Y., Recent advances in the selective catalytic hydrodeoxygenation of lignin-derived oxygenates to arenes. *Green Chemistry* **2020**, 22 (4), 1072-1098.



12. Zhang, J.; Sun, J.; Sudduth, B.; Pereira Hernandez, X.; Wang, Y., Liquid-phase hydrodeoxygenation of lignin-derived phenolics on Pd/Fe: A mechanistic study. *Catalysis Today* **2020**, *339*, 305-311.
13. J.Dong, K.Konstantin, Y.Wang, “Low-temperature methane oxidation for efficient emission control in natural gas vehicles: Pd and beyond”, *ACS Catal.*, 2020, doi:10.1021/acscatal.0c03338. **(cover)**
14. Zhang, J.; Sun, J.; Kovarik, L.; Engelhard, M. H.; Du, L.; Sudduth, B.; Li, H.; Wang, Y., Surface engineering of earth-abundant Fe catalysts for selective hydrodeoxygenation of phenolics in liquid phase. *Chemical Science* **2020**, *11* (23), 5874-5880. **(cover)**
15. Riley, C.; Canning, G.; De La Riva, A.; Zhou, S.; Peterson, E.; Boubnov, A.; Hoffman, A.; Tran, M.; Bare, S. R.; Lin, S.; Guo, H.; Datye, A., Environmentally benign synthesis of a PGM-free catalyst for low temperature CO oxidation. *Applied Catalysis B: Environmental* **2020**, *264*, 118547.
16. Spezzati, G.; Benavidez, A. D.; DeLaRiva, A. T.; Su, Y. Q.; Hofmann, J. P.; Asahina, S.; Olivier, E. J.; Neethling, J. H.; Miller, J. T.; Datye, A. K.; Hensen, E. J. M., CO oxidation by Pd supported on CeO<sub>2</sub>(100) and CeO<sub>2</sub>(111) facets. *Applied Catalysis B-Environmental* **2019**, *243*, 36-46.
17. Riley, C.; De La Riva, A.; Zhou, S.; Wan, Q.; Peterson, E.; Artyushkova, K.; Farahani, M. D.; Friedrich, H. B.; Burkemper, L.; Atudorei, N.-V.; Lin, S.; Guo, H.; Datye, A., Synthesis of Nickel-Doped Ceria Catalysts for Selective Acetylene Hydrogenation. *ChemCatChem* **2019**, *11* (5), 1526-1533.
18. Pereira-Hernández, X. I.; DeLaRiva, A.; Muravev, V.; Kunwar, D.; Xiong, H.; Sudduth, B.; Engelhard, M.; Kovarik, L.; Hensen, E. J. M.; Wang, Y.; Datye, A. K., Tuning Pt-CeO<sub>2</sub> interactions by high-temperature vapor-phase synthesis for improved reducibility of lattice oxygen. *Nature Communications* **2019**, *10* (1), 1358.
19. Kunwar, D.; Zhou, S.; DeLaRiva, A.; Peterson, E. J.; Xiong, H.; Pereira-Hernández, X. I.; Purdy, S. C.; ter Veen, R.; Brongersma, H. H.; Miller, J. T.; Hashiguchi, H.; Kovarik, L.; Lin, S.; Guo, H.; Wang, Y.; Datye, A. K., Stabilizing High Metal Loadings of Thermally Stable Platinum Single Atoms on an Industrial Catalyst Support. *ACS Catalysis* **2019**, *9*, 3978-3990. **(cover)**
20. Yu, N.; Rahman, M. M.; Chen, J.; Sun, J.; Engelhard, M.; Hernandez, X. I. P.; Wang, Y., Steam reforming of simulated bio-oil on K-Ni-Cu-Mg-Ce-O/Al<sub>2</sub>O<sub>3</sub>: The effect of K. *Catalysis Today* **2018**.
21. Xiong, H. F.; Wiebenga, M. H.; Carrillo, C.; Gaudet, J. R.; Pham, H. N.; Kunwar, D.; Oh, S. H.; Qi, G. S.; Kim, C. H.; Datye, A. K., Design considerations for low-



- temperature hydrocarbon oxidation reactions on Pd based catalysts. *Applied Catalysis B-Environmental* **2018**, *236*, 436-444.
22. Riley, C.; Zhou, S.; Kunwar, D.; De La Riva, A.; Peterson, E.; Payne, R.; Gao, L.; Lin, S.; Guo, H.; Datye, A., Design of Effective Catalysts for Selective Alkyne Hydrogenation by Doping of Ceria with a Single-Atom Promotor. *Journal of the American Chemical Society* **2018**, *140* (40), 12964-12973.
  23. Hensley, A. J. R.; Zhang, J. H.; Vincon, I.; Hernandez, X. P.; Tranca, D.; Seifert, G.; McEwen, J. S.; Wang, Y., Mechanistic understanding of methanol carbonylation: Interfacing homogeneous and heterogeneous catalysis via carbon supported Ir-La. *Journal of Catalysis* **2018**, *361*, 414-422.
  24. Feng, Y. X.; Wang, Q.; Xiong, H. F.; Zhou, S. L.; Chen, X.; Hernandez, X. I. P.; Wang, Y.; Lin, S.; Datye, A. K.; Guo, H., Correlating DFT Calculations with CO Oxidation Reactivity on Ga-Doped Pt/CeO<sub>2</sub> Single-Atom Catalysts. *Journal of Physical Chemistry C* **2018**, *122* (39), 22460-22468.
  25. Datye, A.; Wang, Y., Atom trapping: a novel approach to generate thermally stable and regenerable single-atom catalysts. *National Science Review* **2018**, *5* (5), 630-632.

(XIX) *Jointly funded by this grant and other grants with intellectual leadership by other funding sources (11)*

1. Y.B. Lu, C. Thompson, D. Kunwar, A.K. Datye, and A.M. Karim, Origin of the High CO Oxidation Activity on CeO<sub>2</sub> Supported Pt Nanoparticles: Weaker Binding of CO or Facile Oxygen Transfer from the Support? *ChemCatChem*, 2020. 12(6): p. 1726-1733.
2. D. Kunwar, C. Carrillo, H. Xiong, E. Peterson, A. DeLaRiva, A. Ghosh, G. Qi, M. Yang, M. Wiebenga, S. Oh, W. Li, and A.K. Datye, Investigating anomalous growth of platinum particles during accelerated aging of diesel oxidation catalysts. *Applied Catalysis B: Environmental*, 2020. 266: p. 118598.
3. Datye, A. and Votsmeier, M., Advanced Materials for Emission Control – Opportunities and Challenges, *Nature Materials*, **2020**, p1-11.
4. Hensley, A. J. R.; Collinge, G.; Wang, Y.; McEwen, J.-S., Coverage-Dependent Adsorption of Hydrogen on Fe(100): Determining Catalytically Relevant Surface Structures via Lattice Gas Models. *The Journal of Physical Chemistry C* **2020**, *124* (13), 7254-7266.
5. Du, L.; Prabhakaran, V.; Xie, X.; Park, S.; Wang, Y.; Shao, Y., Low-PGM and PGM-Free Catalysts for Proton Exchange Membrane Fuel Cells: Stability Challenges and Material Solutions. *Advanced Materials* **2020**.
6. Chaudhary, N.; Hensley, A.; Collinge, G.; Wang, Y.; McEwen, J.-S., Coverage-Dependent Adsorption of Phenol on Pt(111) from First Principles. *The Journal of Physical Chemistry C* **2019**.
7. Pham, H. N.; Howe, J. Y.; Ghosh, A.; Melton, M.; Kunwar, D.; Peterson, E. J.; Datye, A. K., Using a Combination of HAADF and SE Imaging to Locate Pt Nanoparticles within a Mesoporous Silica Diesel Oxidation Catalyst. *Microscopy and Microanalysis* **2018**, *24* (S1), 1700-1701.

8. Hensley, A. J. R.; Wang, Y.; Mei, D. H.; McEwen, J. S., Mechanistic Effects of Water on the Fe-Catalyzed Hydrodeoxygenation of Phenol. The Role of Bronsted Acid Sites. *ACS Catalysis* **2018**, *8* (3), 2200-2208.
9. Bray, J.; Hensley, A. J. R.; Collinge, G.; Che, F.; Wang, Y.; McEwen, J.-S., Modeling the adsorbate coverage distribution over a multi-faceted catalytic grain in the presence of an electric field: O/Fe from first principles. *Catalysis Today* **2018**, *312*, 92-104.
10. A.J.R.Hensley, G.Collinge, Y.Wang, J.S.McEwen, “Guiding the design of oxidation-resistant Fe-based single atom alloy catalysts with insights from configurational space”, *J.Chem.Phys.*, 2021, doi:10.1063/5.00048698.
11. A.J.R. Hensley, I.deJoode, Y.Wang, J.S.McEwen, “Identifying Trends in the Field Ionization of Diatomic Molecules over Adsorbate Covered Pd(331) Surfaces”, *Topics in Catalysis*, 2020, doi: 10.1007/s11244-020-01392-y.

### **Awards or Leadership Activities (2018-2021)**

#### **Abhaya Datye**

- Robert L Burwell award from the North American Catalysis Society, 2019.
- Vice Chair of the International Congress of Catalysis, San Diego, June 2020 (cancelled due to the pandemic)
- Elected as Director at Large of the North American Catalysis Society (2019-2023)
- ACS Petroleum Research Fund, advisory board member 2015-2020
- Editorial board of Catalysis Letters
- Co-organizer of symposium in honor of Johannes Schwank, AIChE meeting, Boston, MA, November 2021

#### **Yong Wang**

- 2021 ACS E.V. Murphree Industrial and Engineering Chemistry Award (2021)
- 2019 AIChE Catalysis and Reaction Engineering Practice Award (2019)
- 2018 ACS I&EC Division Fellow Award (2017)
- 2019 ACS National Award committee chair
- co-organizer of symposium in honor of Chuck Peden Research, 257th ACS National Meeting in Orlando, March 30-31, 2019.
- Editorial board ACS Catalysis, JACS Au, and Catalysis Today (2010 – present)

## Role of the Reaction Environment on the Catalytic Activation of Cellulose

Paul Dauenhauer and Matthew Neurock

Department of Chemical Engineering and Materials Science, University of Minnesota

### Presentation Abstract

The dynamic reaction environment that forms during the thermal conversion of cellulose, the most abundant biopolymer in lignocellulosic biomass can significantly influence its conversion to value-added chemical intermediates. The presence of hydroxyl groups and naturally occurring metals such as calcium and magnesium within biomass can catalytically activate specific C-O, C-H and O-H bonds initiating the decomposition and conversion of cellulose into Levoglucosan and volatile oxygenates products. In this work, we combine millisecond kinetic studies using the PHASR (Pulse-Heated Analysis of Solid/Surface Reactions) reactor together with in-situ analytical methods and detailed ab initio calculations and integrated kinetic Monte Carlo/molecular dynamics simulations to track the molecular transformations of cellulose and determine intrinsic reaction kinetics. We examine the reactions within the complex solid and liquid environments that form during pyrolysis and show how the local environment can significantly promote the reactivity by catalyzing particular reactions. More specifically, we examine the influence of local hydroxyl groups on transglycosylation of the C-O bonds of cellulose to form levoglucosan as well paths that lead to light oxygenates. These reactions dominate at lower temperatures where hydroxyl nests can form an aid in proton transfer steps promote transglycosylation, dehydration, ring opening and cracking. In addition, we examine the role of Ca and Mg ions on the catalytic activation of the intermonomer  $\beta$ -glycosidic bonds in long chains of cellulose. Millisecond kinetics measured for calcium-catalyzed reactions at temperatures from 370–430 °C reveal accelerated glycosidic ether scission with a second-order rate dependence on the  $\text{Ca}^{2+}$  ions. First-principles density functional theory calculations identify specific  $\text{Ca}^{2+}$  ion configurations that demonstrate accelerated transglycosylation kinetics with an apparent activation barrier of 50 kcal mol<sup>-1</sup> for a cooperative calcium-catalyzed cycle which agrees well with the experimental barrier of  $48.7 \pm 2.8$  kcal mol<sup>-1</sup>. Calcium enhances the reactivity through a primary role of stabilizing charged transition states and a secondary role of disrupting native H-bonding. Mg ions show similar behavior to that of Ca.

### Grant or FWP Number: Grant Title

DE-SC0012659: Catalytic Activation of Pyran Ethers in Self-Solvating Saccharides with Alkaline Earth Metals

**Student(s):** Vineet Maliekkal, Gregory Facas, Jimmy Soeherman, and Ziwei Wang

### RECENT PROGRESS

#### *1. Experimental Kinetics of Cellulose Activation*

The catalyzed rate of cellulose activation via glycosidic cleavage was measured for 20 milliseconds up to 2.0 seconds using the method of pulse-heated analysis of solid reactions (PHASR) with thin films of cellulose between 350 – 500 °C. Using the surrogate of  $\alpha$ -

cyclodextrin, the rate of disappearance of the reactant was measured by rapidly heating (~20 ms) and cooling (~40 ms) the sample and quantifying the remaining amount of cyclodextrin. This approach permitted the determination of the kinetics (**Figure 1-1**) of transport-free (no heat or diffusion limitations) of molten carbohydrates at millisecond time-scale with varying loadings of alkaline earth metal catalysts (both  $\text{Mg}^{2+}$  and  $\text{Ca}^{2+}$ ) that naturally occur in lignocellulosic materials.

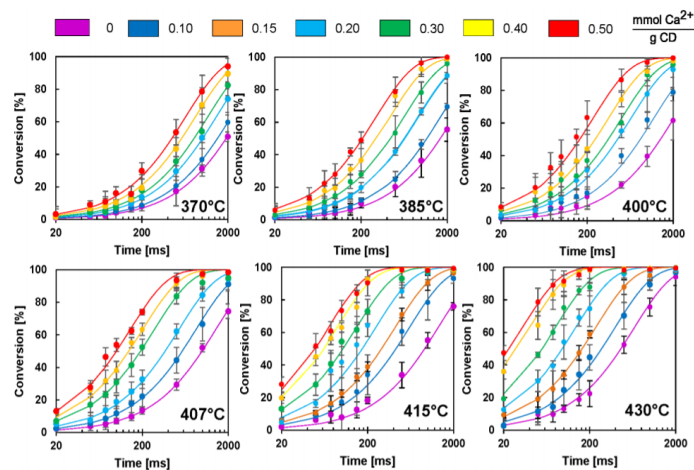


**Figure 1-1.** Kinetics of the cellulose surrogate,  $\alpha$ -cyclodextrin, with a calcium catalyst. The thermal activation of cyclodextrin was measured by determining conversion of cyclodextrin with various loadings of the  $\text{Ca}^{2+}$  catalyst ( $0\text{--}0.50\text{ mmol Ca}^{2+}\text{ gCD}^{-1}$ ) and at various temperatures ( $370\text{--}430\text{ }^\circ\text{C}$ ) using the pulse-heated analysis of solid and surface reactions (PHASR). All

experimental conditions exhibited first-order kinetics in cyclodextrin, and the conversion ( $\bullet$ ) fit to a first-order model ( $-$ ). Error bars represent 95% confidence intervals based on triplicate runs

## 2. Computed Catalytic Mechanisms.

In previous efforts we integrated detailed PHASR experiments together with theoretical calculations to elucidate the pathways, kinetics and mechanisms that govern the initial cellulose decomposition pathways involving the transglycosylation of C-O bonds to form levoglucosan. Subsequent experiments, however, showed intriguing results where  $\alpha$ -linked cyclodextrin followed kinetics that were similar to those for the  $\beta$ -linked cellulose.<sup>1</sup> The structural differences in  $\alpha$  and  $\beta$  stereoisomers, however, would prevent them from following the same transglycosylation mechanism. As such, we carried out detailed kinetic studies along with first-principles Density Functional theory (DFT) simulations to examine (1) the influence of stereochemical structure on the glycosidic C-O bond activation and (2) the dynamics of catalytic hydroxyl nests that form within cellulose under reaction conditions and their effects on mediating catalytic paths that drive the kinetics. The work was published in *ACS Catal.* 2019, 9, 1943-1955. Detailed DFT calculations showed that the  $\alpha$ - and  $\beta$ - isomers indeed proceed via different mechanism. The elementary steps however are similar and as such lead to very similar kinetic behavior which is fully consistent with the experimental findings. The activation of  $\alpha$  stereochemical glycosidic bonds proceeds through an epoxide mechanism rather than the direct O6 attack of the hydroxymethyl at the C1 site and coupled proton transfer in the transglycosylation mechanism but follows the same elementary C-O bond making and breaking and intramolecular proton transfer steps. The difference between two is simply the intramolecular hydroxyl group ( $\text{O}_2\text{H}$  vs  $\text{O}_6\text{H}$ ) that carries out the reaction. The calculated kinetics for the activation of the  $\alpha$ -linked cyclodextrin via the epoxide mechanism were directly comparable to those found for transglycosylation of the  $\beta$ -linked cellulose thus

indicating that differences in stereochemistry lead to no observable differences in kinetics of glycosidic activation. In addition, we showed the dynamic behavior of hydroxyl nests present in cellulose at reaction conditions helped to catalyze glycosidic bond activation. Ab initio molecular dynamic (AIMD) simulations were used along with explicit molecular models of the detailed cellulose environment to sample numerous configurations along the reaction coordinate and to reliably estimate the free energies of activation. The increased size and complexity of the models along with the rigorous sampling of many configurations in the AIMD simulations provides higher fidelity system by which to compare with the experimental results. These simulations established free energies of activation of 33-36 kcal mol<sup>-1</sup> which is significantly lower than the free energy of activation for the simulated thermal activation of glycosidic bonds (~54 kcal mol<sup>-1</sup>). Snapshots of the transition state along the trajectory (**Fig. 2-1**) show the formation of catalytic hydroxyl nests that stabilize

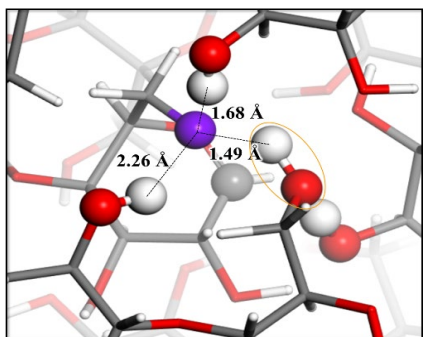


**Figure 2-1:** Snapshot of transition state for hydroxyl catalyzed glycosidic activation reveals formation of catalytic nest with 3 hydroxyl groups.

the transition state via the formation of between 2 to 3 hydrogen bonds. While this anchoring leads to a small loss in entropy, this is offset by the significant enthalpic gains thus lowering the free energy of activation. The results show that non-reducing chain ends have a greater flexibility to interact with such catalytic hydroxyl nests than those at mid-chain sites, thus making them more susceptible to hydroxyl-catalyzed activation. This is supported by the nearly 3 kcal mol<sup>-1</sup> difference in the free energy of activation for reaction at these two positions along the cellulose chain. More generally, we show that vicinal hydroxyl groups are able to self-organize to form such regions of high reactivity. These findings were discussed in *ACS*

*Catal.* 2020, 10, 8454-8464 (**Fig. 2-1** is adapted from this publication).

We have extended our efforts on elucidating the mechanisms that control cellulose pyrolysis by examining the pathways and kinetics to form light oxygenates. Glycolaldehyde which is one of the major light gas products that forms during pyrolysis of biomass is thought to form via ring opening and fragmentation reactions.<sup>2</sup> Ab initio simulations were carried out to examine in detail the elementary steps and kinetics that control the conversion of: 1) non-reducing sites, 2) levoglucosan chain ends of anhydro-oligomers and 3) reducing glucose sites to glycolaldehyde formation.

Elementary mid-chain dehydration, retro-Diels-Alder, bicyclic ring opening, glucose ring opening, and retro-aldol C-C cracking steps are all possible in the mechanisms that drive the formation of glycolaldehyde (or its tautomer ethenediol). DFT calculations show that in the absence of any assistance from hydroxyl groups, glucose ring opening followed by retro-aldol C-C cracking is the most favorable pathway to light oxygenates. This suggests that the reducing glucose chain end is most susceptible to transform to light oxygenate species. The presence of hydroxyl groups can catalyze several of these elementary steps. The presence

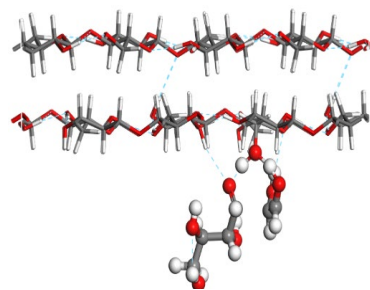


**Figure 2-2:** Optimized transition state for vicinal hydroxyl catalyzed retro-aldol C-C rupture.

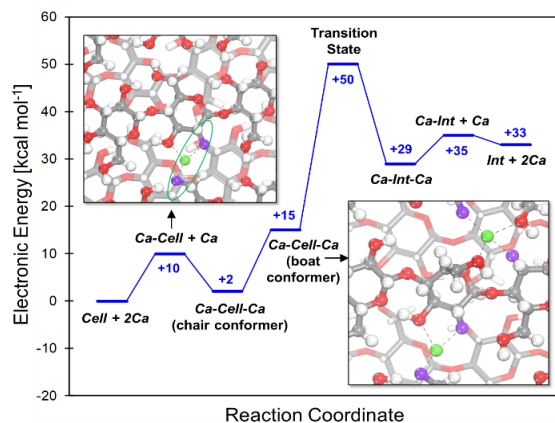


**Figure 2-3:** Reaction energy profile for dual Ca catalyzed cellulose activation.

barrier for bicyclic ring opening of levoglucosan from 56 to 43 kcal mol<sup>-1</sup>. Such findings indicate that vicinal hydroxyl groups can have a more general and pervasive effect on the reactions of cellulose pyrolysis beyond catalyzing only its initial activation. Further experimental validation of these findings are ongoing and will be an interesting addition to this work.

Significant effort has also been invested into understanding the effect of alkaline earth metal ions, specifically calcium (Ca), on the activation of cellulose. Alkaline earth metal ions naturally present within biomass are known to significantly affect pyrolysis chemistry, kinetics and the final distribution of products.<sup>3,4</sup> Therefore, understanding their influence on the governing pathways, kinetics and mechanisms is of great importance. Experiments carried out with Ca loaded  $\alpha$ -cyclodextrin, a cellulose surrogate, reveal accelerated rates of activation as compared to experiments carried out in the absence of Ca<sup>5</sup>. Experimental kinetics show a near second order dependence on the calcium concentration. Experimental results suggest that the active site is comprised of a *Lewis base-Lewis acid-Lewis base* bridge wherein the deprotonated hydroxyl groups serve as the Lewis base sites while the Ca ion is the Lewis acid. Having identified the active site, it was proposed that two catalytic cycles – a single Ca and dual Ca cycle – occur in conjunction during Ca-catalyzed cellulose activation. The single Ca cycle was found to have a calculated activation energy of 53 kcal mol<sup>-1</sup> with Ca playing a primary catalytic role of stabilizing the transition state. The dual Ca cycle involves the participation of two Ca ions wherein the second Ca ion plays a secondary role of destabilizing the reactant by disrupting native hydrogen bonding environments that act to “lock up” protons. This dual catalytic cycle was shown to have an activation energy of 50 kcal mol<sup>-1</sup> which is lower than that for the single Ca cycle (Fig. 2-3 for reaction energy profile). Such a lowering of around ~3 kcal mol<sup>-1</sup> is not unexpected as the typical energy of hydrogen bonds is 3-5 kcal mol<sup>-1</sup>. The calculated activation energy for the dual Ca cycle is

of hydroxyl groups can promote intramolecular proton transfer and catalyze reactions very similar to what we showed for transglycosylation. Our calculations show that vicinal hydroxyl groups within cellulose help to promote dehydration, glucose ring opening, and retro-aldol C-C cracking reactions by lowering their barriers from 68 to 54 kcal mol<sup>-1</sup> for dehydration, from 46 to 21 kcal mol<sup>-1</sup> for ring opening and from 27 to 19 kcal mol<sup>-1</sup> for retro-aldol C-C cracking (transition state shown in Fig. 2). These vicinal hydroxyl groups can also serve as weak Brønsted acid sites that also lower the

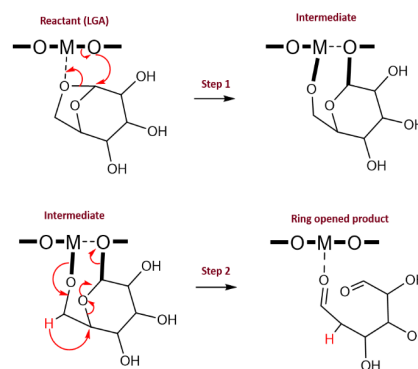


**Figure 2-4:** Proposed mechanism for metal (or Ca) catalyzed bicyclic ring opening of levoglucosan.

also in good agreement with the experimentally observed barrier ( $48.7 \pm 2.8$  kcal mol<sup>-1</sup>). Furthermore, such cooperative dual cycles are able to explain the the near second order dependence of rates on calcium concentration. These findings were summarized in a recent publication *JACS Au* 2021, 1, 272-281 (**Fig. 2-3** is adapted from this publication). More generally, this investigation has provided a framework for performing combined experimental and theoretical studies in the area of metal catalyzed cellulose pyrolysis. This same framework has been extended to understand the effect of Mg on cellulose activation with current results of this collaboration indicating that there are no significant differences in observed kinetics for Ca and Mg. As part of ongoing work to publish these results, efforts are being made to gain a deeper understanding and establish important descriptors that can explain and predict the observed behavior of different metals.

Previous literature show that the yields of levoglucosan significantly drop while those of light oxygenates and char increase when the reactions carried out in the presence of alkaline earth metal ions such as calcium.<sup>4</sup> In order to gain a mechanistic understanding of how calcium influences these pathways we examined the formation of glycolaldehyde from glucose and levoglucosan. Our DFT simulations show that the activation energy for glucose ring opening and retro-aldol C-C cracking carried out in the presence of Ca are 37 and 19 kcal mol<sup>-1</sup> respectively. The barriers are significantly lower than the barriers calculated for those carried out thermally in absence of the metal. They are also significantly lower than the barrier for Ca catalyzed transglycosylation thus suggesting that the glucose chain ends will primarily convert to glycolaldehyde in the presence of Ca. The proclivity of levoglucosan to undergo bicyclic ring opening in the presence of calcium was also examined. A new two-step mechanism was suggested for this reaction (**Fig. 2-4**), wherein the first step consists of opening the first C-O bond in levoglucosan such that the C center is stabilized by the Lewis basic O<sup>-</sup> site while the O center is stabilized by the Lewis acidic Ca ion. The second step consists of opening the second C-O bond to form the final open chain structure. The second step is calculated to be the rate determining step with a barrier of 35 kcal mol<sup>-1</sup>. This finding therefore shows that levoglucosan can readily undergo bicyclic ring opening in the presence of Ca thus leading to enhanced production of light oxygenates at the cost of levoglucosan yields. This proposed mechanism is in agreement with previous experiments carried out directly on levoglucosan that show conversion of levoglucosan to light oxygenates in the presence of Ca.<sup>3</sup> Further validation of the calculated kinetics by PHASR studies are being carried out currently.

In addition to elucidating the mechanisms and establishing the elementary step kinetics involved in the selective conversion of biomass, we have utilized this intrinsic kinetic information to establish more faithful and reliable kinetic models that can be used to predict the conversion of biomass and other feedstocks. We have combined the pathways and the elementary step intrinsic kinetics derived from DFT simulations to establish a fundamental kinetic database that is used in atom-explicit kinetic Monte Carlo simulations to simulate the conversion of cellulose and other biomass feedstocks and to compare with the PHASR experimental results. We note from the theoretical results described above that the kinetics depend on the explicit reaction environment which changes during the course of reaction. In order to appropriately capture the dynamic changes during reaction, we carry out in-situ molecular dynamics simulations within the kinetic Monte Carlo simulations. This kMC/MD model is the first of its kind that allows one to not only follow the intrinsic kinetic transformation but also track the influence and dynamics of the

changing reaction environment. In very recent efforts, we have incorporated all of the new pathways and DFT-calculated kinetics for the formation of glycoaldehyde and other light oxygenates into the kMC/MD code. The simulations are now able to track the kinetics for cellulose pyrolysis to form LGA as well as light oxygenate products and show how the dynamics within the cellulose during reaction conditions promotes the formation of hydroxyl catalyzed reactions.

### **Publications Acknowledging this Grant in 2018-2021**

Facas, G.G.; Maliekkal, V.; Neurock, M.; Dauenhauer, P. J., Activation of Cellulose with Alkaline Earth Metals. *Green Chem. Submitted August 2021*. (*Intellectually led by this grant*)

Facas, G. G., Maliekkal, V.; Zhu, C.; Neurock, M.; Dauenhauer, P. J. Cooperative Activation of Cellulose with Natural Calcium. *J. Am. Chem. Soc. Au 2021*, 1, 3, 272–281. (*Intellectually led by this grant*)

Maliekkal, V.; Dauenhauer, P.; Neurock M. Glycosidic C-O Bond Activation in Cellulose Pyrolysis: Alpha Verses Beta and Condensed Phase Hydroxyl-Catalytic Scission. *ACS Catal. 2020*, 10, 15, 8454-8464. (*Intellectually led by this grant*)

Maliekkal, S.; Maduskar, S.; Saxon, D. J., Nasiri, M.; Reineke, T. R.; Neurock M.; and Dauenhauer, P.; Activation of Cellulose via Cooperative Hydroxyl-Catalyzed Transglycosylation of Glycosidic Bonds. *ACS Catal. 2019*, 9, 3, 1943-1955 (*Intellectually led by this grant*)

Maduskar, S.; Maliekkal, V.; Neurock, M.; Dauenhauer, P. J. On the Yield of Levoglucosan from Cellulose Pyrolysis. *ACS Sustainable Chem. and Eng. 2018*, 6, 5, 7017-7025. (*Intellectually led by this grant*)

Zhu, C.; Krumm, C.; Facas, G.; Neurock, M.; Dauenhauer, P. J. Energetics of cellulose and cyclodextrin glycosidic bond cleavage *Reaction Chem. and Eng. 2017*, 2, 2, 201-214. (*Intellectually led by this grant*)

### **Awards or leadership activities during 2018-2020 calendar years**

#### **Paul Dauenhauer**

- Co-Director, Catalysis Center for Energy Innovation, a U.S. Department of Energy, Energy Frontiers Research Center
- Herman Pines Award, 2021
- Blavatnik Finalist, 2021
- MacArthur Fellow, 2020 – 2025
- 2019: Department of Energy, Top Ten EFRC Invention Award
- 2019: University of Minnesota, Outstanding Advisor Award
- 2019: ACS Sustainable Chemistry & Engineering Lectureship

- 2018: AIChE Catalysis & Reaction Engineering CRE Young Investigator Award
- Co-Founder: Lakril Technologies, 2020

**Matthew Neurock**

- 2020: Thrust Leader NSF CCI Center for Synthetic Organic Electrochemistry
- 2019: Executive Board of the DOE Energy Frontier Research Center: Inorganometallic Catalyst Design Center.
- Robert Burwell Lectureship in Catalysis, North American Catalysis Society, 2015-2017

Massimiliano Delferro

**Electronic Cooperativity in Supported Single- and Multinuclear-Sites for Catalytic C-C and C-H Bonds Functionalization**

Massimiliano Delferro, David M. Kaphan, Cong Liu, A. Jeremy Kropf  
Chemical Sciences and Engineering Division, Argonne National Laboratory, Lemont, IL  
60439

**Presentation Abstract**

Our group has achieved success in each of our three cross-cutting core scientific areas—experimentation, computation, and X-ray characterization—in the past triennial research period (FY19-21). Our experimental efforts have focused on two sub-thrusts, the understanding of complex, multi-component active sites (including multi-metallic catalysts and functionalized surfaces) and the investigation of Li-ion battery cathodes as tunable, “redox non-innocent” catalyst supports. For the first task, we designed well-defined, bimetallic-single-site catalysts on high-surface area metal oxides for selective hydrocarbon transformations such as alkene metathesis. In this work, the reactivity of supported dimers may be explained either by the lowering of the activation barrier of the complex through the electronic influence of the surface or by site isolation of catalytically active sites. We have also shed light on the operant mechanism for the hydrogenation of olefins catalyzed by supported low-valent, earth-abundant complexes on silica, such as those of vanadium and iron, and we have investigated the role of highly Brønsted acidic surfaces on iridium-mediated hydrocarbon functionalization. Furthermore, we have shown that battery materials such as lithium manganese oxide ( $\text{Li}_x\text{Mn}_2\text{O}_4$ ) and lithium titanium oxide ( $\text{Li}_x\text{TiO}_2$ ), which access a wide range of surface potential as a function of lithiation state, can function as dynamically tunable catalyst supports, a strategy that we believe will prove general to the rational design of dynamic catalysts for a variety of applications. In addition, we are advancing computational methods for the prediction of X-ray absorption near-edge spectroscopy (XANES) features for supported and unsupported earth-abundant vanadium catalysts. Lastly, we have upgraded the X-ray emission spectrometer at Sector 10 of the Advanced Photon Source (APS) to extend and improve our high-resolution X-ray absorption and emission capabilities and advance X-ray analysis of supported single- and multi-site catalysts for the scientific community.

**FWP59066: Electronic Cooperativity in Supported Single- and Multinuclear-Sites for Catalytic C-C and C-H Bonds Functionalization**

**Principal Investigators:** Massimiliano Delferro (Lead PI), David M. Kaphan, Cong Liu, A. Jeremy Kropf

**Additional Argonne Staff:** Magali Ferrandon

**Postdocs:** Alon Chapovetsky, Prajay Patel, Ryan Witzke

**Affiliations:** Chemical Sciences and Engineering Division, Argonne National Laboratory, Lemont, IL 60439

## RECENT PROGRESS

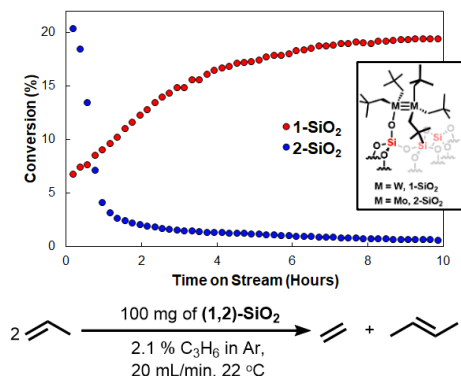


**Figure 1.** Metathesis of propylene to ethylene and butenes catalyzed by supported  $W_2$  and  $Mo_2$  on  $SiO_2$ .

### Electronic Cooperativity in Supported Organometallic Catalysts for Low Temperature Upgrading of Light Alkenes.

Multi-metallic complexes bearing multiply bonded metal ions play a major role in both biogenic and anthropogenic chemistries, with diverse applications in catalysis. While the close-proximity of multiple metal centers, coupled with the electron reservoir in the metal-metal bond, has been shown to impart interesting reactivity to these species, there is a paucity of examples of supported systems bearing multi-metallic motifs. Encouraged by the promise of these complexes as pre-catalysts for olefin metathesis, dimers of the form  $M_2X_6$  (where  $M = W$  and  $Mo$ ;  $X =$  neopentyl,

*tert*-butoxide, and dimethylamide) were grafted onto partially dehydroxylated silica (Figure 1). A combination of advanced characterization techniques and density functional theory (DFT) calculations were leveraged to elucidate the binding modes of the dimers on the surface and probe their catalytic reactivity. The chemisorption reactions the alkyl dimers  $M_2(CH_2CCMe_3)_6$  ( $M = W$  (**1**) and  $Mo$  (**2**)) on  $SiO_2$  were monitored using  $^1H$  NMR spectroscopy to show the disappearance of the parent alkyl complexes over the course of 16 hours and the appearance of roughly one equivalent (per dimer) of neopentane (the protonated ligand) suggesting that grafting occurs via a protonolysis reaction between the metal complex and a silanol on the surface to yield **1-SiO<sub>2</sub>** (W-neopentyl) and **2-SiO<sub>2</sub>** (Mo-neopentyl) and their related heteroatom substituted derivatives. This was further corroborated by a suite of characterization tools including diffuse reflectance infrared Fourier transform spectroscopy (DRIFTS), UV resonance Raman spectroscopy, XAS, high-angle annular dark field scanning transmission electron microscopy (HAADF-STEM), and dynamic nuclear polarization-enhanced solid-state nuclear magnetic resonance spectroscopy (DNP SS NMR). The activity of the resultant materials towards the disproportionative self-metathesis of propylene to ethylene and 2-butene was evaluated in a plug flow reactor. While the unsupported complexes were catalytically inactive, upon chemisorption, the alkyl dimers  $M_2(CH_2CCMe_3)_6$  ( $M = W$  (**1**) and  $Mo$  (**2**)) became active towards olefin metathesis, albeit with differing reaction profiles. The supported tungsten species (**1-SiO<sub>2</sub>**) exhibited an induction period over the first five hours on stream, likely due to the formation of the active alkylidene-W dimer species, with conversion gradually increasing from 6.6 to 20.0% followed by a slow deactivation (16.0% conversion at 30 h on stream). Similar profiles have been observed for other supported tungsten alkyl systems and is often associated with the formation of a tungsten alkylidene moiety. Post-catalysis characterization using DRIFT, Raman, and  $^{13}C$  SSNMR spectroscopies confirmed the persistence of the dimer on the surface. In contrast, the supported molybdenum homologue (**2-SiO<sub>2</sub>**), showcased a maximum conversion of 20.3% at the onset of the experiment, followed by a rapid deactivation in the first 5 h (conversion rate of 1.0%), likely due to sintering and/or decomposition.

## Mechanistic Investigations of Surface Organometallic Catalysts for Hydrocarbon Hydrogenation and Dehydrogenation.

Understanding the mechanisms of action for base

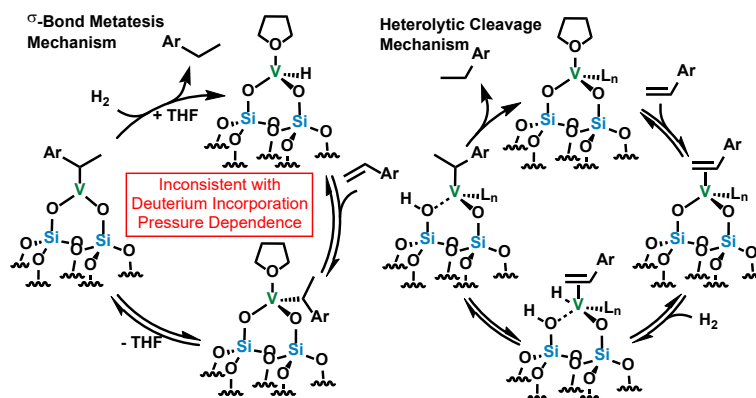


**Figure 2.** Plausible  $\sigma$ -bond metathesis mechanism (left) or heterolytic bond activation mechanism (right) for the hydrogenation of styrene catalyzed by **V(III)/SiO<sub>2</sub>**.

metal catalysis for transformations typically associated with precious metals is essential for the design of new technologies for a sustainable energy economy. Isolated transition metal and post-transition metal catalysts on oxides such as silica are generally proposed to effect hydrogenation and dehydrogenation by a mechanism featuring a key bond activation step of

either  $\sigma$ -bond metathesis (characteristic of the early transition metals) or heterolytic bond cleavage (observed for mid- and late-transition metal catalysts) (Figure 2). We previously reported a silica-supported organovanadium(III) complex (**V(Mes)(THF)/SiO<sub>2</sub>**, Mes = mesityl; **V(III)/SiO<sub>2</sub>**), which was an efficient catalyst for olefin hydrogenation. It was not clear *a priori*, however, if the isolated organovanadium catalyst would mechanistically emulate early transition metal reactivity ( $\sigma$ -bond metathesis) or would be more similar to its later transition metal congeners (heterolytic bond activation). The hydrogenation reaction was targeted for a detailed mechanistic study through a combination of reaction kinetics and deuterium labeling and incorporation experiments. Upon exposure to dihydrogen, spectroscopic evidence, including EPR and X-ray absorption spectroscopy, was consistent with the formation of a persistent surface vanadium(III) hydride. This structural assignment is further supported by study of ethylene oligomerization activity for both the hydrogenolyzed (**V-H**) and as-prepared material. The putative vanadium hydride was highly active for oligomerization at room temperature. Unexpectedly, the as-prepared material also effected this transformation, after ethylene insertion into the vanadium-mesityl bond and  $\beta$ -hydride elimination to generate the vanadium hydride *in situ*. The kinetic dependencies of the reaction components of the hydrogenation process were potentially consistent with both the  $\sigma$ -bond metathesis and the heterolytic bond activation mechanisms; however, in a key deuterium incorporation experiment it was found the degree of deuterium incorporation was independent of **D<sub>2</sub>** pressure, which excludes the  $\sigma$ -bond metathesis mechanism. Alternatively, a two-electron redox cycle, rarely invoked for homologous supported catalyst systems, is also consistent with the experimental observations. In addition to the experimental kinetic study, DFT calculations and kinetic Monte Carlo (kMC) simulations were carried out to study the active sites and reaction mechanism of styrene hydrogenation using the surface vanadium catalyst. A crucial consideration for surface organometallic catalysts is the non-uniformity of the active sites. To understand the role of active site non-uniformity, computational models were developed for a series of potentially active sites of **V(III)/SiO<sub>2</sub>** with different coordination

environments and structural parameters (e.g., the V-O(siloxane) distance). The reaction pathways computed via DFT identified a tripodal vanadium structure, generated after hydride transfer to the surface as a likely active catalytic resting state. The calculated lowest energy mechanism for styrene hydrogenation proceeds via the heterolytic cleavage of H<sub>2</sub> on the V-O bond, consistent with experimental observations. Based on these results, we hypothesized that the structural non-uniformity of the amorphous surface might manifest itself in the strain induced elongation or contraction of the V-O(siloxane) bond, which is integral to the barrier to heterolytic bond activation. Indeed, the calculated reaction energetics follow a trend as a function of the V-O (siloxane) distance, with an inverse relationship between the V-O (siloxane) distance and the barrier of the reaction. The kMC simulations of varying reactant concentrations indicated that a linear combination of the profiles for all three V-O(siloxane) bond lengths considered (2.1, 2.3, and 2.5 Å) were required to gain a qualitative understanding of the experimental kinetics, further emphasizing the importance to model surface heterogeneity.

**Predicting K-edge XANES for Single-Site Heterogeneous Vanadium Catalysts.** X-ray Absorption Near-Edge Structure (XANES) and Extended X-ray Absorption Fine Structure (EXAFS) spectroscopy are powerful tools to reveal key structural and electronic features of isolated catalytic sites, yet theoretical insight is necessary for accurate interpretation of the spectra, especially when there exists significant heterogeneity among the catalytic sites. To obtain a general understanding of how these spectra can be simulated, we endeavored to develop a general model for accurately simulating the XANES spectra of vanadium as a representative element due to its interesting catalytic properties (*vide supra*) and pronounced pre-edge features. Using a diverse calibration set of the XANES spectra for 39 vanadium complexes with a wide variety of oxidation states and coordination environments, a model that predicted pre-edge energies to within 0.4 eV accuracy was generated. With this calibration model, we examined hydride interactions and second-shell interactions, both of which are challenging to characterize solely based on experimental XAS data. For the hydride interactions, two degrees of surface heterogeneity were investigated: V-O (siloxane) bond distance (metal center and donor siloxane group on the support) and O-O bond distance (two Si-O ligands on the support). The computed XANES spectra (Figure 3b-d) highlight the broadening of the experimental pre-edge features in the H<sub>2</sub>-treated catalyst (**V(III)-H/SiO<sub>2</sub>**, Figure 3a) by visualizing the orbital contributions of the V-O, V-C, and V-H bonds, which emphasizes the importance of ligand geometry and substitution. By measuring the dominant contributions for the lowest and highest O-O distances, the peak width increased from 0.62 eV for the (b) pre-catalyst **V(III)/SiO<sub>2</sub>** to 1.01 eV when (c) THF is bound and 0.73 eV when (d) THF is not bound to the **V(III)-H/SiO<sub>2</sub>** catalyst. The observed increase in broadening between the **V(III)-H/SiO<sub>2</sub>** models relative to the **V(III)/SiO<sub>2</sub>** pre-catalyst indicates that the V-H interactions are responsible for the observed

broadening of the pre-edge peak upon H<sub>2</sub> treatment and correlates with the weakening of the metal-support interaction due to the distortion of the grafting site. To further investigate second-shell coordination effects and their role in multi-metallic systems, two groups of complexes, characterized by V-O and V-N coordination spheres (from Prof. D. Mendiola, UPenn) were studied computationally. Through extensive analysis into the computed XANES spectra and natural transition orbitals, an effect of second-shell coordination on XANES was identified. For the divanadium V-O complex, the V-O-V second shell interaction leads to a larger difference of the two dominant transitions that resulted in the calculated pre-edge energy increasing by 0.81 eV, which is consistent with the experimental observation (0.8 eV). A multi-metallic V-N complex with two unique V environments represented an opportunity to gauge the effects of second-shell coordination. The computed XANES showed that the interactions between V and the backbone ligand created a subtle shoulder feature; yet the interaction between the V and bridging nitride was imposed onto the transitions dominated by V-N-V second-shell interactions. These techniques can be used to characterize SOMC in terms of metal-oxide cluster formation and grafting onto nitride supports, which further guides computational approaches for modeling SOMC.

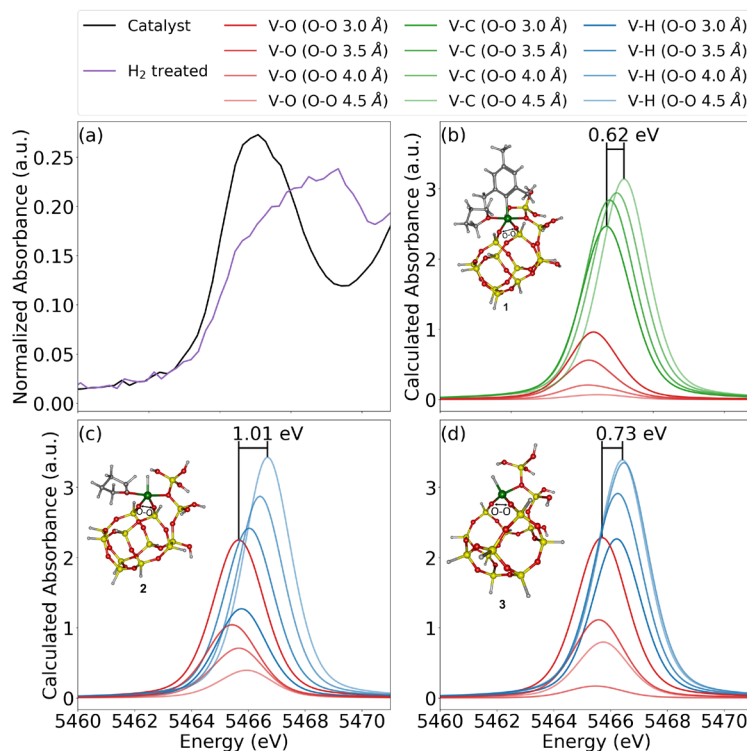


**Figure 3.** a) Experimental XANES of **V(III)/SiO<sub>2</sub>** and **V(III)-H/SiO<sub>2</sub>**. b) Computed XANES of **V(III)/SiO<sub>2</sub>**, c) d) Computed XANES of **V(III)-H/SiO<sub>2</sub>**. In b), c) and d), V-O, V-C and V-H (presented in different colors) represent individual orbital contributions involved in the XANES spectra. For each individual contribution, the spectra were mapped across different O-O distances, shown from darker lines to lighter lines as the O-O distance increased from 3.0 to 4.5 Å.

## Lithium-Ion Battery Materials as Tunable, Redox Non-Innocent Catalyst Supports.

The treatment of inorganic catalyst supports as chemically dynamic ligands represents an underexplored mechanism space in the design and investigation of heterogenized catalysts.

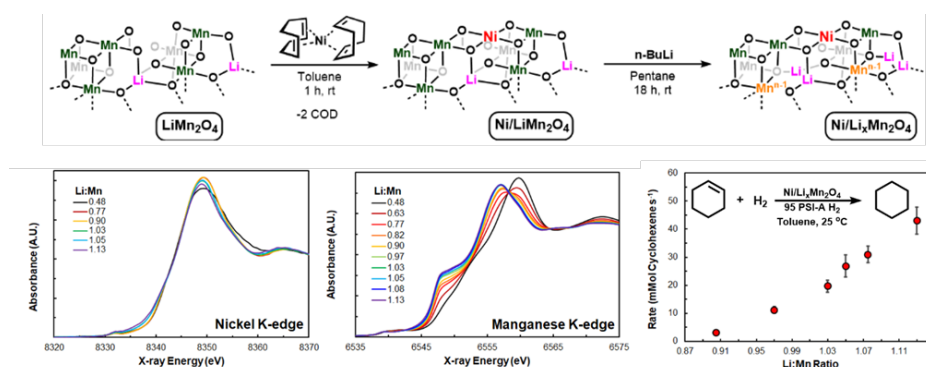


**Figure 4.** (Top) synthesis of  $\text{Ni/Li}_x\text{Mn}_2\text{O}_4$  by oxidative grafting of  $\text{Ni(COD)}_2$  followed by reduction with BuLi. (Bottom, left) nickel and manganese K-edge XANES of  $\text{Ni/Li}_x\text{Mn}_2\text{O}_4$  as a function of lithiation state. (Bottom, right) rate of cyclohexene hydrogenation catalyzed by  $\text{Ni/Li}_x\text{Mn}_2\text{O}_4$  as a function of lithiation state.

homogeneous catalysis, reversibly storing electrons in the supporting ligand to facilitate multi-electron catalytic cycles. To test the hypothesis that the support redox state could be used to finely tune catalyst activity, single Ni atoms on  $\text{Li}_x\text{Mn}_2\text{O}_4$  were targeted with the intention of lowering the barrier to the oxidative process of bond insertion in the elementary step of hydrogen activation (Figure 4). Addition of  $\text{LiMn}_2\text{O}_4$  to a solution of bis(1,5-cyclooctadiene)nickel(0) in  $\text{C}_6\text{D}_6$ , monitored by  $^1\text{H}$  NMR spectroscopy, resulted in a sharp decrease in the nickel precursor concentration and the appearance of free cyclooctadiene ligand over the first hour, and saturation was reached in 24 hours. The same experiment with partially dehydroxylated silica as the support resulted in no reaction, suggesting that the chemisorption of the nickel precursor onto  $\text{LiMn}_2\text{O}_4$  is driven by an oxidative process. XAS and X-ray Photoelectron Spectra (XPS) of the resultant material,  $\text{Ni/LiMn}_2\text{O}_4$ , confirmed that upon grafting nickel is oxidized to the +2-oxidation state. Transmission Electron Microscopy (TEM), along with Energy Dispersive X-ray spectroscopy (EDS) maps of  $\text{Ni/LiMn}_2\text{O}_4$  corroborated the dispersity of nickel on the surface with no agglomeration to clusters or nanoparticles. Addition of varying amounts of n-butyllithium to a suspension of  $\text{Ni/LiMn}_2\text{O}_4$  in pentane and subsequent workup resulted in the formation of variably reduced lithiated materials of the form  $\text{Ni/Li}_x\text{Mn}_2\text{O}_4$  ( $x = 1.26 - 2.26$ ). The XAS spectra of the reduced materials showed that addition of nBuLi results in the reduction of the average oxidation state of Mn from +3.5 to +3, with the bulk of the nickel remaining in the +2-oxidation state. EDS maps of the fully reduced material  $\text{Ni/Li}_{2.26}\text{Mn}_2\text{O}_4$  show that upon reduction nickel remains site-isolated and dispersed on the surface of the support. Kinetic measurements on the hydrogenation of cyclohexene catalyzed by a range of lithiated materials showed an onset of activity was observed for the material with Li:Mn ratio of 0.90, and catalytic rates increased monotonically with the degree of further support lithiation, suggesting that the extent of reduction plays a critical role in facilitating catalytic activity. Computational efforts suggest that hydrogenation goes through a heterolytic  $\text{H}_2$  cleavage pathway across a nickel tripodal surface site and an oxygen atom. While lithiation induces only a minor change in the charge on the nickel atoms, the oxygen atoms undergo

The redox activity of materials such as Li-ion battery cathodes suggests the possibility that they may function in a manner analogous to “redox non-innocent” ligands in

a significant charge buildup, rendering them more reactive toward heterolytic bond cleavage. The generality of catalyst control through support lithiation was also established by demonstrating a similar process wherein an organotantalum complex on titania was found to affect a similar hydrogenation process only upon reduction of the support with lithium naphthalenide.

**5.3.5 X-ray Absorption and X-ray Emission Spectroscopies (XAS and XES).** These spectroscopic techniques are crucially important for identifying the oxidation state of the active metal site in surface-grafted molecules. Several examples have already been given where XAS has contributed to understanding the catalyst structure and oxidation state. We have made significant progress in other areas of X-ray spectroscopy. Silicon crystal “Laue” analyzers at X-ray emission energies above 9 keV offer higher integrated intensity than Bragg analyzers. This energy range is appropriate for the 4d K edges and 5d L edges which was the focus of our work through FY19. Our focus has now shifted to include 3d transition metals that, along with the lanthanides, emit hard X-rays below 10 keV, where the absorption from the silicon wafer increases quickly. At lower energies Bragg analyzers are much more attractive. To avoid aberrations and improve the energy resolution, XES Bragg spectrometers typically employ symmetric reflecting planes parallel to the surface and analyzers are exchanged to cover all emission lines. We have demonstrated complete coverage from 4.5 – 10 keV using a single Ge(022) cylindrically bent Bragg analyzer crystal. In our spectrometer off-axis, or asymmetric (h l l) reflections and larger angular ranges cover the gaps between the symmetric (h l l) reflections. Chromatic aberration is essentially eliminated using a pixel array detector to collect 2D maps of X-rays, which are converted to a histogram of counts vs. energy by calibrating the array detector field. This method, which we have used with Laue analyzers for a long time, preserves the intrinsic resolution of the X-ray optic. Two analyzers, one Bragg and one Laue, can cover the entire

range of the beam line; therefore, we can switch rapidly between emission lines and absorption edges.

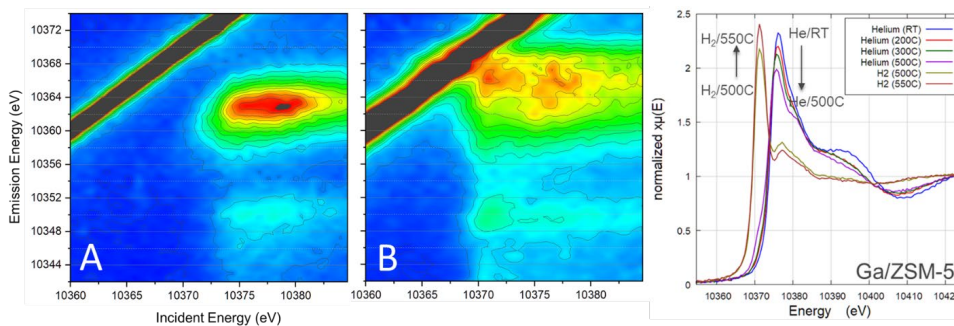


**Figure 5.** In situ Ga-ZSM VRXES: (A) In helium at T = 500°C, (B) in H<sub>2</sub> at T = 500 °C. (Right) In situ XANES: in helium increase from RT to 500 °C, switch to H<sub>2</sub> and increase to T = 500 °C.

We previously reported that the large shift in the XANES of gallium(III)-zeolite at high temperature in H<sub>2</sub> may not, in fact, be due to reduction to Ga(I). The large absorption may instead be a bound state transition to an empty p state. We are extending that work and have measured the resonant XES spectra for the K $\alpha_{1,2}$  and K $\beta_{1,3}$  main lines and the valence band. These spectra can be compared in detail to predictions based on computational spectroscopy. In the meantime, qualitative analysis of VRXES supports the view that the Ga(III) state persists. The closing of the band gap in H<sub>2</sub> at high temperature is expected

(Figure 5), indicated by the emission peak closing the gap to the elastic scattered X-rays (grey diagonal bar), while the weaker  $K\beta_5$  peak does not appear to shift significantly.

### **Publications Acknowledging this Grant in 2018-2021**

#### **Work at Argonne funded solely by this FWP with Argonne as the lead institution**

- 1) Chapovetsky, A.; Witzke, R.; Kennedy, R. M.; Wegener, E. C.; Dogan, F.; Patel, P.; Ferrandon, M.; Niklas, J.; Poluektov, O. G.; Rui, N.; Senanayake, S. D.; Rodriguez, J. A.; Johnson, C.; Jenks, C. J.; Kropf, A. J.; Liu, C.; Delferro, M.; Kaphan, D. M., Lithium ion battery materials as tunable, redox non-innocent catalyst supports. *ChemRxiv* **2021**, 1-19. [https://chemrxiv.org/articles/preprint/Lithium\\_Ion\\_Battery\\_Materials\\_as\\_Tunable\\_Redox\\_Non-Innocent\\_Catalyst\\_Supports/13828901/1](https://chemrxiv.org/articles/preprint/Lithium_Ion_Battery_Materials_as_Tunable_Redox_Non-Innocent_Catalyst_Supports/13828901/1)
- 2) Patel, P.; Wells, R. H.; Kaphan, D. M.; Delferro, M.; Skodje, R. T.; Liu, C., Computational investigation of the role of active site heterogeneity for a supported organovanadium(III) hydrogenation catalyst. *ACS Catal.* **2021**, 11, 1-16 (DOI: 10.1021/acscatal.1c00688).
- 3) Mindiola, D. J.; Delferro, M.; Humphrey, S. M., Organometallic Chemistry at Various Length Scales: More Than Just Metal–Carbon Bonds Bring Chemists Together. *Organometallics* **2020**, 39, 881-882 (DOI: 10.1021/acs.organomet.0c00198).
- 4) Witzke, R. J.; Chapovetsky, A.; Conley, M. P.; Kaphan, D. M.; Delferro, M., Nontraditional Catalyst Supports in Surface Organometallic Chemistry. *ACS Catal.* **2020**, 10, 11822-11840 (DOI: 10.1021/acscatal.0c03350).
- 5) Chapovetsky, A.; Patel, P.; Liu, C.; Sattelberger, A. P.; Kaphan, D. M.; Delferro, M., Electrochemical Investigation of Low-Valent Multiply  $M\equiv M$  Bonded Group VI Dimers: A Standard Chemical Reduction Leads to an Unexpected Product. *Organometallics* **2020**, 39, 4430-4436 (DOI: 10.1021/acs.organomet.0c00533).
- 6) Chapovetsky, A.; Langeslay, R. R.; Celik, G.; Perras, F. A.; Pruski, M.; Ferrandon, M. S.; Wegener, E. C.; Kim, H.; Dogan, F.; Wen, J.; Khetrapal, N.; Sharma, P.; White, J.; Kropf, A. J.; Sattelberger, A. P.; Kaphan, D. M.; Delferro, M., Activation of Low-Valent, Multiply  $M-M$  Bonded Group VI Dimers toward Catalytic Olefin Metathesis via Surface Organometallic Chemistry. *Organometallics* **2020**, 39, 1035–1045 (DOI: 10.1021/acs.organomet.9b00787).
- 7) Kaphan, D. M.; Ferrandon, M. S.; Langeslay, R. R.; Celik, G.; Wegener, E. C.; Liu, C.; Niklas, J.; Poluektov, O. G.; Delferro, M., Mechanistic Aspects of a Surface Organovanadium(III) Catalyst for Hydrocarbon Hydrogenation and Dehydrogenation. *ACS Catal.* **2019**, 9, 11055-11066 (DOI: 10.1021/acscatal.9b02800).
- 8) Syed, Z. H.; Kaphan, D. M.; Perras, F. A.; Pruski, M.; Ferrandon, M. S.; Wegener, E. C.; Celik, G.; Wen, J.; Liu, C.; Dogan, F.; Goldberg, K. I.; Delferro, M., Electrophilic

Organoiridium(III) Pincer Complexes on Sulfated Zirconia for Hydrocarbon Activation and Functionalization. *J. Am. Chem. Soc.* **2019**, *141*, 6325-6337 (DOI: 10.1021/jacs.9b00896).

- 9) Langeslay, R. R.; Kaphan, D. M.; Marshall, C. L.; Stair, P. C.; Sattelberger, A. P.; Delferro, M., Catalytic Applications of Vanadium: A Mechanistic Perspective. *Chem. Rev.* **2019**, *119*, 2128-2191 (DOI: 10.1021/acs.chemrev.8b00245).
- 10) Plascencia, C.; Curtiss, L. A.; Liu, C., Hydrogen Activation by Silica-Supported Metal Ion Catalysts: Catalytic Properties of Metals and Performance of DFT Functionals. *J. Phys. Chem. A* **2019**, *123*, 171-186 (DOI: 10.1021/acs.jpca.8b08340).

### **Work at Argonne funded by this FWP with Argonne not the lead institution**

- 11) Kaphan, D. M.; Brereton, K. R.; Klet, R. C.; Witzke, R. J.; Miller, A. J. M.; Mulfort, K. L.; Delferro, M.; Tiede, D. M., Photocatalytic Transfer Hydrogenation in Water: Insight into Mechanism and Catalyst Speciation. *Organometallics* **2021**, *40*, 1482-1491 (DOI: 10.1021/acs.organomet.1c00133).
- 12) Liu, P.; Zhang, Y.; Liu, C.; Emery, J. D.; Das, A.; Bedzyk, M. J.; Hock, A. S.; Martinson, A. B. F. Thermal Atomic Layer Deposition of Gold: Mechanistic Insights, Nucleation, and Epitaxy. *ACS Appl. Mater. Interfaces* **2021**, *13*(7), 9091–9100 (DOI: 10.1021/acsami.0c17943).
- 13) Perras, F. A.; Paterson, A. L.; Syed, Z. H.; Kropf, A. J.; Kaphan, D. M.; Delferro, M.; Pruski, M., Revealing the Configuration and Conformation of Surface Organometallic Catalysts with DNP-Enhanced NMR. *J. Phys. Chem. C* **2021**, *125*, 13433-13442 (DOI: 10.1021/acs.jpcc.1c03176).
- 14) Wang, J.; Lu, Y.; Liu, L.; Yu, L.; Yang, C.; Delferro, M.; Hoffman, A. S.; Bare, S. R.; Karim, A. M.; Xin, H., Catalytic CO Oxidation on MgAl<sub>2</sub>O<sub>4</sub>-Supported Iridium Single Atoms: Ligand Configuration and Site Geometry. *J. Phys. Chem. C* **2021**, *125*, 11380-11390. (DOI: 10.1021/acs.jpcc.1c02287),
- 15) Robison, L.; Gong, X.; Evans, A. M.; Son, F. A.; Wang, X.; Redfern, L. R.; Wasson, M. C.; Syed, Z. H.; Chen, Z.; Idrees, K. B.; Islamoglu, T.; Delferro, M.; Dichtel, W. R.; Coudert, F.-X.; Gianneschi, N. C.; Farha, O. K., Transient Catenation in a Zirconium-Based Metal-Organic Framework and Its Effect on Mechanical Stability and Sorption Properties. *J. Am. Chem. Soc.* **2021**, *143*, 1503-1512 (DOI: 10.1021/jacs.0c11266).
- 16) Sheludko, B.; Wegener, E. C.; Celik, G.; Kropf, A. J.; Castro, C. F.; Delferro, M.; Goldman, A. S.; Kaphan, D. M.; Celik, F. E., In situ formation of a sub-nanometer iridium phosphide catalyst from supported organometallic species. *ChemRxiv* **2020**, 1-9. [https://chemrxiv.org/articles/preprint/In\\_Situ\\_Formation\\_of\\_a\\_Sub-Nanometer\\_Iridium\\_Phosphide\\_Catalyst\\_from\\_Supported\\_Organometallic\\_Species/12935585/1](https://chemrxiv.org/articles/preprint/In_Situ_Formation_of_a_Sub-Nanometer_Iridium_Phosphide_Catalyst_from_Supported_Organometallic_Species/12935585/1)

- 17) Fagiolari, L.; Bini, M.; Costantino, F.; Gatto, G.; Kropf, A. J.; Marmottini, F.; Nocchetti, M.; Wegener, E. C.; Zaccaria, F.; Delferro, M.; Vivani, R.; Macchioni, A., Iridium-Doped Nanosized Zn–Al Layered Double Hydroxides as Efficient Water Oxidation Catalysts. *ACS Appl. Mater. Interfaces* **2020**, *12*, 32736–32745 (DOI: 10.1021/acscami.0c07925).
- 18) Wegener, E. C.; Bukowski, B. C.; Yang, D.; Wu, Z.; Kropf, A. J.; Delgass, W. N.; Greeley, J.; Zhang, G.; Miller, J. T., Intermetallic Compounds as an Alternative to Single-atom Alloy Catalysts: Geometric and Electronic Structures from Advanced X-ray Spectroscopies and Computational Studies. *ChemCatChem* **2020**, *12*, 1325-1333 (DOI: 10.1002/cctc.201901869).
- 19) Purdy, S. C.; Ghanekar, P.; Mitchell, G.; Kropf, A. J.; Zemlyanov, D. Y.; Ren, Y.; Ribeiro, F.; Delgass, W. N.; Greeley, J.; Miller, J. T., Origin of Electronic Modification of Platinum in a Pt<sub>3</sub>V Alloy and Its Consequences for Propane Dehydrogenation Catalysis. *ACS Appl. Energy Mater.* **2020**, *3*, 1410-1422 (DOI: 10.1021/acsaem.9b01373).
- 20) ZhuChen, J.; Gao, J.; Probus, P. R.; Liu, W.; Wu, X.; Wegener, E. C.; Kropf, A. J.; Zemlyanov, D.; Zhang, G.; Yang, X.; Miller, J., The Effect of Strong Metal-Support Interaction (SMSI) on Pt-Ti/SiO<sub>2</sub> and Pt-Nb/SiO<sub>2</sub> Catalysts for Propane Dehydrogenation. *Catal. Sci. Technol.* **2020**, ASAP (DOI: 10.1039/D0CY00897D).
- 21) Choudhury, D.; Mandia, D. J.; Langeslay, R. R.; Yanguas-Gil, A.; Letourneau, S.; Sattelberger, A. P.; Balasubramaniam, M.; Mane, A. U.; Delferro, M.; Elam, J. W., Atomic layer deposition of HfO<sub>2</sub> films using carbon-free tetrakis(tetrahydroborato)hafnium and water. *J. Vac. Sci. Technol. A* **2020**, *38*, 042407 (DOI: 10.1116/6.0000053).
- 22) Pei, Y.; Chen, M.; Zhong, X.; Zhao, T. Y.; Ferrer, M.-J.; Maligal-Ganesh, R. V.; Ma, T.; Zhang, B.; Qi, Z.; Zhou, L.; Bowers, C. R.; Liu, C.; Huang, W., Pairwise semi-hydrogenation of alkyne to cis-alkene on platinum-tin intermetallic compounds. *Nanoscale* **2020**, *12*, 8519-8524 (DOI: 10.1039/D0NR00920B).
- 23) H. Xu, D. Rebollar, H. He, L. Chong, Y. Liu, C. Liu, C.-J. Sun, T. Li, J. V. Muntean, R. E. Winans, D.-J. Liu, T. Xu. Highly Selective Electrocatalytic CO<sub>2</sub> Reduction to Ethanol by Metallic Clusters Dynamically Formed from Atomically Dispersed Copper. *Nat. Energy* **2020**, *5*, 623–632 (DOI: 10.1038/s41560-020-0666-x)
- 24) Wu, Y. A.; McNulty, I.; Liu, C.; Lau, K. C.; Liu, Q.; Paulikas, A. P.; Sun, C.-J.; Cai, Z.; Guest, J. R.; Ren, Y.; Stamenkovic, V.; Curtiss, L. A.; Liu, Y.; Rajh, T. Facet-Dependent Active Sites of a Single Cu<sub>2</sub>O Particle Photocatalyst for CO<sub>2</sub> Reduction to Methanol. *Nat. Ener.* **2019**, *4*, 957-968 (DOI: 10.1038/s41560-019-0523-y).
- 25) Liu, F.; Liu, C.; Zhong, X. Enhancing Electrocatalysis for Hydrogen Production over CoP Catalyst by Strain: A Density Functional Theory Study. *Phys. Chem. Chem. Phys.* **2019**, *21*, 9137 (DOI: 10.1039/C9CP00128J).

- 26) Asadi, M.; Motevaselian, M. H.; Sun, T. V.; Liu, C.; Abbasi, P.; Moradzadeh, A.; Zapol, P.; Khodadoust, A.; Curtiss, L. A.; Aluru, N. R.; Salehi-Khojin, A. CO<sub>2</sub> Photo-reduction at 23% Efficiency Using Inexpensive and Earth Abundant Catalytic System. *Adv. Energy Mater.* **2019**, *9*, 1803536 (DOI: 10.1002/aenm.201803536).
- 27) Jang, J. H.; Sohn, H.; Camacho-Bunquin, J.; Yang, D.; Park, C. Y.; Delferro, M.; Abu-Omar, M. M., Deoxydehydration of Biomass-Derived Polyols with a Reusable Unsupported Rhenium Nanoparticles Catalyst. *ACS Sustainable Chem. Eng.* **2019**, *7*, 11438-11447 (DOI: 10.1021/acssuschemeng.9b01253).
- 28) Zhong, H.; Friedfeld, M. R.; Camacho-Bunquin, J.; Sohn, H.; Yang, C.; Delferro, M.; Chirik, P. J., Exploring the Alcohol Stability of Bis(phosphine) Cobalt Dialkyl Precatalysts in Asymmetric Alkene Hydrogenation. *Organometallics* **2019**, *38*, 149-156 (DOI: 10.1021/acs.organomet.8b00516).

### **Awards or leadership activities during 2018-2020 calendar years**

#### **Massimiliano Delferro**

- Science for a Circular Economy, Leader, Argonne National Laboratory Initiative 2021
- Physical Sciences and Engineering (PSE) Excellence Award 2021 - Programmatic Scientific Achievement for development of a new catalyst for upcycling polyethylene plastic wastes into higher-value products
- Argonne Impact Award for Innovation 2020
- Guest Editor, Special Issue " Organometallic Chemistry at Various Length Scales: More Than Just Metal–Carbon Bonds Bring Chemists Together" of the journal *Organometallics*, 2020

#### **David M. Kaphan**

- North American Catalysis Society programing committee for the 2021 national meeting
- Catalysis Club of Chicago Secretary 2020-2021
- Argonne pyrophoric safety committee member
- Impact Argonne award for Extraordinary Effort in support of the COVID-19 pandemic 2020

#### **Cong Liu**

- Guest Editor, Special Issue "Computational Catalysts and Materials Design for Energy Conversion and Storage " of the journal *Processes*, 2021
- Editorial Board Member, Scientific Reports, Nature, 2021 – present
- Associate editor, Frontiers in Catalysis-Modelling, Theory and Computational Catalysis, 2020 – present
- Review editor, Frontiers in Chemistry-Theoretical and Computational Chemistry, 2019 – present
- Review panel, Center for Functional Nanomaterials, Brookhaven National Laboratory, 2019 – present

**A. Jeremy Kropf**

- Member of Materials Research Collaborative Access Team (@APS) Beamline Advisory Committee

## Modeling and Design of Main-Group Metal Catalyzed Alkane C-H Functionalization Reactions

Daniel H. Ess

Department of Chemistry and Biochemistry, Brigham Young University, Provo, UT 84602

### Presentation Abstract

This presentation will describe our efforts using density functional theory (DFT) calculations to model and predict main-group and transition-metal catalysts for methane C-H activation and functionalization. This presentation will focus on: i) Our prediction and subsequent experimental validation of an  $\text{Sb}^{\text{V}}$  complex that quantitatively converts methane to methyl bisulfate. ii) Our development and proof-of-principle implementation of software that automates building and location of transition states as well as uses machine learning to maximize the yield of successful optimizations.

**Grant Number:** DE-SC0018329

**PI:** Daniel H. Ess

**Postdocs:** Shusen Chen

**Students:** Taylor Nielson (undergraduate), Elayna Zalit (undergraduate), Bradon Borough (undergraduate), Zack Meyer (undergraduate), Spencer Yu (undergraduate), William Hirschi (undergraduate).

### RECENT PROGRESS

#### *Theory and Experiment Demonstrate that Sb(V)-Catalyzed Methane C-H Activation and Functionalization Outcompetes Superacid Protonolysis*

Abundant light alkanes, especially methane, are extremely unreactive because they have strong, nonpolar covalent C-H bonds. There are four general strategies to induce functionalization of strong methane C-H bonds. The first involves superacid protonolysis, which generally results in alkane oligomerization and formation of products with new C-C bonds (carbo-functionalization). This is perhaps best illustrated by  $\text{Sb}^{\text{V}}\text{F}_5$  in the presence of a Brønsted acids, such as  $\text{HSO}_3\text{F}$ . This main-group metal-Brønsted acid combination is generally proposed to facilitate protonation of methane to methanium ( $[\text{CH}_5]^+$ ) that is subsequently transformed into methyl cation, which then induces carbo-functionalization to generate larger carbocation intermediates (e.g. *tert*-butyl cation). While this superacid-type strategy is useful, especially if employed in ZSM type solid-state catalysts, it does not generally produce oxy-functionalization products, such as methanol derivatives.

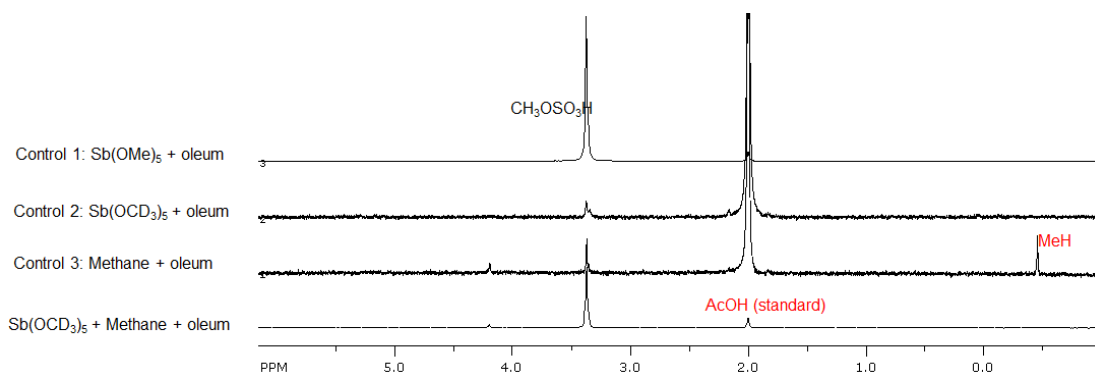
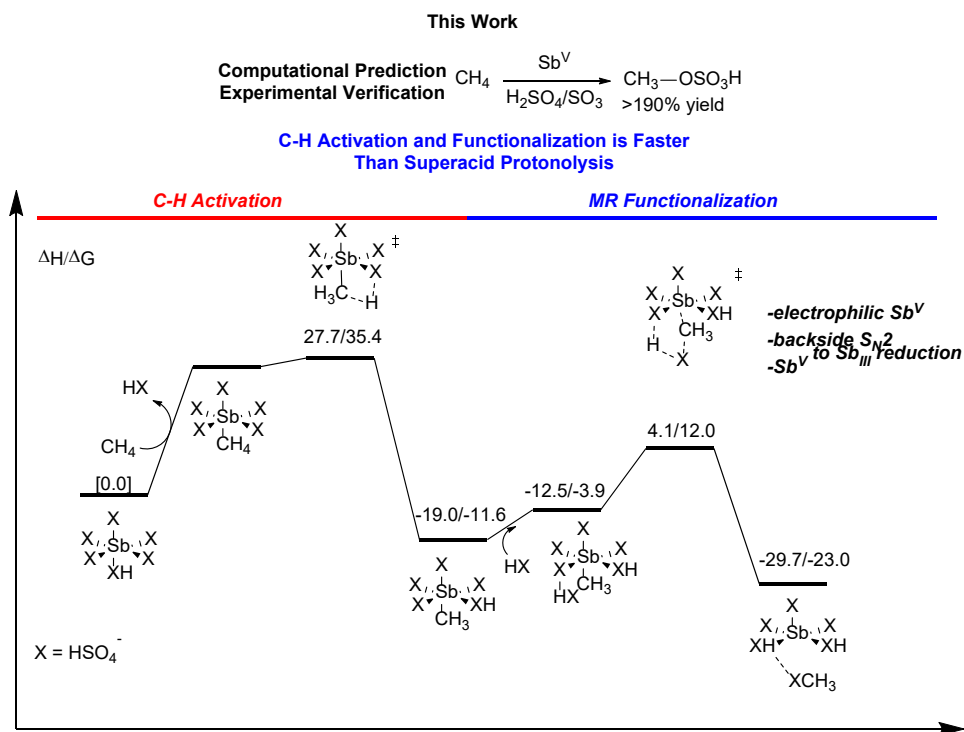
In contrast to the carbo-functionalization often proposed to proceed through methane protonolysis, the other general methane functionalization strategies involve either metal-mediated C-H activation, metal oxo direct functionalization, or radical mediated functionalization, and each of these strategies can potentially generate C-O bonds. The metal-mediated C-H activation strategy is where a metal-methyl intermediate is generated followed by two-electron reductive functionalization. Under catalytic conditions or batch

reoxidation conditions the metal is reoxidized. For this C-H activation strategy to be successful, the resulting functionalized product must be significantly less reactive than methane to obtain high selectivity. The most well-known examples of methane functionalization catalysis by this C-H activation strategy are the  $\text{Hg}^{\text{II}}$  and (bipyrimidine) $\text{Pt}^{\text{II}}\text{Cl}_2$  catalysts that operate in sulfuric acid, which generate high yields of methyl bisulfate that is significantly less reactive than methane.

Given the well-established precedent for protonolysis reactivity that occurs with the main-group metal  $\text{Sb}^{\text{V}}$  in superacids, it is perhaps in retrospect not extremely surprising that  $\text{Sb}^{\text{V}}$ , and related  $\text{Tl}^{\text{III}}$  and  $\text{Pb}^{\text{IV}}$ ,  $d^{10}s^0$  main-group metals induced stoichiometric methane C-O functionalization to methyl oxy-esters in relatively weak carboxylic acid solvents. However, the reaction of methane with  $\text{Sb}^{\text{V}}(\text{TFA})_5$  (TFA = trifluoroacetate) in trifluoroacetic acid after 3 hours at 180 °C yielded only a 6% of the methyl ester (based on added Sb). However, our calculations and experimental isotopolog studies did provide relatively strong evidence that this methane functionalization proceed by  $\text{Sb}^{\text{V}}$  mediated C-H activation and a  $\text{Sb}^{\text{V}}\text{-CH}_3$  intermediate followed by functionalization.

With our calculations indicating  $\text{Sb}^{\text{V}}(\text{TFA})_5$  in non-superacid solvent functionalizing methane through a C-H activation pathway we wondered if  $\text{Sb}^{\text{V}}$  in superacids would also preferentially functionalize  $\text{CH}_4$  via a C-H activation pathway or whether the dominant pathway for functionalization would proceed via expected protonolysis. Evidence for the possibility of a more facile C-H activation pathway came from predictive density functional theory (DFT) calculations where we found accessible barriers for C-H activation and functionalization between methane and  $\text{Sb}^{\text{V}}(\text{HSO}_4)_5$  and our previous work showed that generation of functionalized products by dissociation of  $\text{H}_2$  from  $[\text{CH}_5]^+$  produced by protonolysis of  $\text{CH}_4$  by in an Sb superacid system has a barrier >40 kcal/mol.

Overall, we used DFT calculations that showed  $\text{Sb}^{\text{V}}(\text{HSO}_4)_5$  in the superacid solvent  $\text{H}_2\text{SO}_4$  containing  $\text{SO}_3$  can functionalize methane to methyl bisulfate via a C-H activation pathway that is lower in energy than methane functionalization via protonolysis (see the pathway energy surface below). The concept that  $\text{Sb}^{\text{V}}$  induces C-H activation to generate a  $\text{Sb}\text{-Me}$  intermediate even in superacids provides a new mechanistic pattern for p-block, main-group metals that is generally only found with transition metals. Previous work only demonstrated the possibility C-H activation in non-superacid carboxylic acid solvents. In confirmation of our calculations, reactions of  $\text{Sb}^{\text{V}}(\text{HSO}_4)_5$  with methane in sulfuric acid containing  $\text{SO}_3$  at 180 °C for 3 hours resulted in super-stoichiometric yields of methyl bisulfate (>190%), see NMR spectra below.

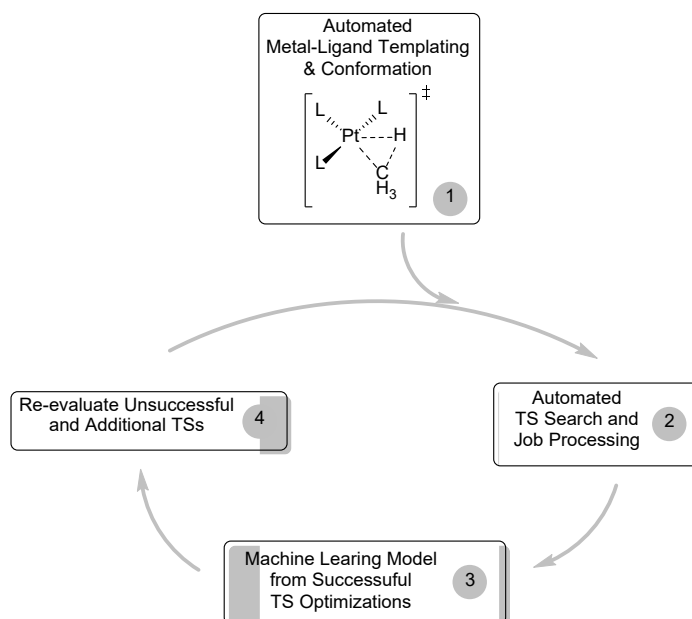


### ***Automated Construction and Optimization Combined with Machine Learning to Generate Pt(II) Methane C-H Activation Transition States***

While quantum-mechanical calculations can aid in the identification and design of C-H activation catalysts, this process is relatively slow, and to date only a limited amount of the vast chemical space has been computationally evaluated. A major limitation that governs the evaluation of C-H activation transition states (and all other types of transition states) is that new structures are generally located by manually building new combinations of metals and coordinating ligands as well as using chemical intuition for guesses of partial bond distances (i.e. bonds that are being formed or broken). Very good guesses of transition-state partial bond distances are critical for fast and successful saddle point optimization. In addition to time consuming manual building, this process is often prolonged by the necessity to review and manipulate electronic structure input and output files.

We developed a workflow and programs for automated construction of ligand combinations on a transition-state core structure (program called Mason;

<https://github.com/DanielEss-lab/>), transition-state searching, and job control and review (program called Taylor; <https://github.com/DanielEss-lab/>). Additionally, because a critical aspect of locating a transition-state structure is the guess of forming and breaking bonds, we combined this automated workflow with machine learning in a feedback loop to generate guess structures to enhance the overall yield of fully optimized C-H activation transition-state structures. As proof of concept, we chose the Pt<sup>II</sup> metal center not only because of the known (bpym)Pt<sup>II</sup>Cl<sub>2</sub> catalyst, but also because oxidative addition transition-state geometries are sensitive to the ligand chassis. Using our workflow, we targeted rapid generation of nearly 1000 transition states with Pt<sup>II</sup> using a diverse ligand library (in just 3 days). Using our new programs, the first pass yield of fully optimized transition states was >300 transition states. Using a rapidly generated autocorrelation-type machine learning model, along with other easy and fast improvement techniques, re-evaluation of failed transition states resulted in nearly 600 fully optimized transition states. Overall, this automated, machine-learning enhanced approach provides a pathway to computationally examine a large and diverse chemical space for C-H activation.



### Publications Acknowledging this Grant in 2018-2021

- (XX) a) Gustafson, S. J.; Konnick, M. M.; Periana, R. A.; Ess, D. H. Mechanisms and Reactivity of Tl(III) Main-Group Metal-Alkyl Functionalization in Water. *Organometallics*, **2018**, *37*, 2723-2731.
- b) King, C. R.; Rollins, N.; Holdaway, A.; Konnick, M. M.; Periana, R. A.; Ess, D. H. Electrophilic Impact of High-Oxidation State Main-Group Metal and Ligands on Methane C-H Activation and Functionalization Reactions. *Organometallics*, **2018**, *37*, 3045-3054.
- c) Koppaka, A.; Park, S. H.; Hashiguchi, B. G.; Gunsalus, N. J.; King, C. R.; Konnick, M. M.; Ess, D. H.; Periana, R. A. Selective C-H Functionalization of Methane and Ethane by a Molecular Sb(V) Complex. *Angew. Chem. Int. Ed.* **2019**, *58*, 2241-2245.

- d) Gunsalus, N. J.; Park, S. H.; Hashiguchi, B. G.; Koppaka, A.; Smith, S. J.; Ess, D. H.; Periana, R. A. Selective N Functionalization of Methane and Ethane to Aminated Derivatives by Main-Group-Directed C-H Activation. *Organometallics* **2019**, *38*, 2319-2322.
- e) King, C. R.; Holdaway, A.; Durrant, G.; Wheeler, J.; Suaava, L.; Konnick, M. M.; Periana, R. A.; Ess, D. H. Supermetal: SbF<sub>5</sub>-Mediated Methane Oxidation Occurs by C-H Activation and Isobutane Oxidation Occurs by Hydride Transfer. *Dalton Trans.* **2019**, *48*, 17029-17036.
- f) Ess, D. H.; Gagliardi, L.; Hammes-Schiffer, S. Introduction: Computational Design of Catalysts from Molecules to Materials. *Chem. Rev.* **2019**, *119*, 6507-6508
- g) Ahn, S.; Hong, M.; Sundararajan, M.; Ess, D. H.; Baik, M-H. Design and Optimization of Catalysts Based on Mechanistic Insights Derived from Quantum Chemical Reaction Modeling. *Chem. Rev.* **2019**, *119*, 6509-6560.
- h) Rollins, N.; Pugh, S. L.; Maley, S. M.; Grant, B. O.; Hamilton, S. R.; Teynor, M. S.; Carlsen, R.; Jenkins, J. R., Ess, D. H. Machine Learning Analysis of Direct Dynamics Trajectory Outcomes for Thermal Deazetization of 2,3-Diazabicyclo[2.2.1]hept-2-ene. *J. Phys. Chem. A* **2020**, *124*, 4813-4826.
- (XXI) a) Gunsalus, N.; Koppaka, A.; Hashiguchi, B.; Konnick, M.; Park, S. H.; Ess, D. H.; Periana, R. S<sub>N</sub>2 and E2 Branching of Main-Group Metal Alkyl Intermediate in Alkane CH Oxidation: A Mechanistic Investigation using Isotopically Labelled Main-Group Metal Alkyls. *Organometallics*, **2020**, *39*, 1907-1916.

#### Awards or leadership activities during 2018-2020 calendar years

- PI and director of the NSF-funded Chemistry and Biochemistry Research Experiences for Undergraduates REU program “*Chemistry and Biochemistry REU Site to Prepare Students for Graduate School and an Industrial Career*”. Established 2018, the goal of this program is to provide a pathway to graduate school. This site hosts 10 visiting undergraduate students each year and 2 high school teachers (RET).
- Guest editor for *Chemical Reviews* Volume 119, Issue 11 on “Computational Design of Catalysts from Molecules to Materials”. Authored editorial: <https://doi.org/10.1021/acs.chemrev.9b00296>.
- Cofounder of monthly Zoom conference computational chemistry conference (2020-present). Currently attended by >20 international research groups.

## Selenium Oxyanion Reduction

Alison R. Fout, Kelly L. Gullett, Tabitha J. Miller, Courtney L. Ford  
University of Illinois at Urbana-Champaign, Department of Chemistry

### Presentation Abstract

Seleniferous oxyanions, selenate ( $\text{SeO}_4^{2-}$ ) and selenite ( $\text{SeO}_3^{2-}$ ), are of interest due to their bioavailability and toxicity as well as the usefulness of the reduced product, red  $\text{Se}^0$ . Selenium is an essential micronutrient to living organisms on Earth, but only one order of magnitude separates healthy and toxic concentrations of selenium in aquatic environments. There is a noticeable dearth of information in the literature with regards to synthetic inorganic complexes reducing seleniferous oxyanions. Recently we have shown successful stoichiometric reduction of seleniferous oxyanions to red  $\text{Se}^0$  through the use of  $[\text{N}(\text{afa}^{\text{Cy}})_3\text{FeOTf}]\text{OTf}$  ( $\text{L}^{\text{Cy}}\text{FeOTf}_2$ ).  $\text{Se}^0$  can be readily reduced to  $\text{Se}^{2-}$  in the presence of  $\text{PPh}_3$ , yielding  $\text{Se}=\text{PPh}_3$ , allowing for a simple method of quantification of the  $\text{Se}^0$  product by  $^{31}\text{P}$  NMR spectroscopy. The red selenium nanoparticles were characterized using UV-Vis and  $^{77}\text{Se}$  NMR spectroscopies in addition to TEM imaging. Within this work we seek to address the following: 1) the mechanism of selenate and selenite reduction in our system; 2) to expand the scope of iron complexes able to reduce seleniferous oxyanions; and 3) accomplish catalytic selenate reduction.

### Grant or FWP Number: Bio-inspired Catalysts Featuring Earth Abundant Metals and Secondary Coordination Sphere Interactions for the Reduction of Oxyanions

Student(s): Tabitha Miller, Kelly Gullett, Courtney Ford

### Publications Acknowledging this Grant in 2018-2021

*(XXII) Intellectually led by this grant*

1. Ford, C. L.; Miller, T. J.; Park, Y.; Iranmanesh, N.; Gray, D. L. "Varying the Secondary Coordination Sphere: Synthesis of Cobalt and Iron Complexes of a Tripodal Ligand Featuring Two Hydrogen Bond Donors or Acceptors." *J. Coord. Chem.*, **2020**, *73*, 2195-2208.
2. Drummond, M. J.; Miller, T. J.; Ford, C. L.; Fout, A. R. "Catalytic Perchlorate Reduction Using Iron: Mechanistic Insights and Improved Catalyst Turnover." *ACS Catalysis*, **2020**, *10*, 3175-3182.
3. Gordon, Z.; Matson, E. M.; Burgess, M.; Miller, T. J.; Drummond, M. J.; Lord, R. L.; Popescu, C. V.; Rodríguez López, J.; Fout, A. R. "Characterization of Terminal Fe(III)-Oxo and Fe(III)-Hydroxo Complexes Derived from  $\text{O}_2$ ." *Inorganic Chemistry* **2019**, *58*, 15801-15811.

4. Drummond, M. J.; Ford, C. L.; Gray, D. L.; Popescu, C. V.; Fout, A. R. "Radical Rebound Hydroxylation Versus H-atom Transfer in Non-Heme Iron(III)-hydroxo Complexes: Reactivity and Structural Differentiation." *J. Am. Chem Soc.* **2019**, *141*, 6639-6650

**Awards or leadership activities during 2018-2020 calendar years**

**Awards**

- 2018            **Helen Corley Petit Scholar**, UIUC  
2018            **Ed Stiefel Young Investigator Award**, Metals in Biology GRC  
2018            **Emergent Investigator in Bioinorganic Chemistry**, ACS Division of  
                    Inorganic Chemistry  
2019            **Building Pathways for Emerging Leaders Fellow**, UIUC  
2019            **Thieme Chemistry Journals Award**

**Leadership Activities**

- 2018 – Present            Editorial Advisory Board for Inorganic Chemistry  
2018 – Present            Editorial Advisory Board for Organometallics

## Site Selective Deoxygenation of Cellulosic Biorenewables With Boron Catalysts

Michel R. Gagné  
University of North Carolina at Chapel Hill

### Presentation Abstract

This presentation will outline progress to the generic goal of developing new catalysts for the deoxygenation of C–O bonds. The last reporting period has focused on a fascinating set of catalysts generated by the hydroboration of the octa-vinyl silsesquioxane core. These catalysts are significantly more active than expected and required the development of a kinetic protocol with 2 minute quenches. The per Boron activity of these catalysts increases with an increase in the number of boron centers per cube. Experiments to source this unique reactivity sought to establish a role for steric, electronic, and neighboring group effects.

### DE-FG02-05ER15630: Catalytic Approaches to C–O Bond Activation in Biorenewable Feedstocks

**Student(s):** Hannah E. Starr (4<sup>th</sup> year), William Hearne (1<sup>st</sup> year), and Nathan DeSousa (1<sup>st</sup> year)

### RECENT PROGRESS

**Piers Borane Hydroborations.** Previous work in our lab uncovered the ability of various heteroleptic fluoroarylborane catalysts to selectively reduce tertiary amides.<sup>1</sup> The hydroboration of alkenes with Piers borane ( $\text{HB}(\text{C}_6\text{F}_5)_2$ ) is a rapid process that occurs at room temperature without the need for any other reagents.<sup>2</sup> We opted to extend this work to alkene-containing silsesquioxanes (Figure 1), namely the octavinyl silsesquioxane (OV,  $\text{R} = \text{R}_1 = \text{vinyl}$ ), the monovinylheptaisobutyl silsesquioxane (MVHIB,  $\text{R} = \text{vinyl}$ ,  $\text{R}_1 = \text{isobutyl}$ ), the monoallylheptaisobutyl silsesquioxane (MAHIB,  $\text{R} = \text{allyl}$ ,  $\text{R}_1 = \text{isobutyl}$ ), and the monoallylheptacyclopentyl silsesquioxane (MAHCP,  $\text{R} = \text{allyl}$ ,  $\text{R}_1 = \text{cyclopentyl}$ ). We then tested these compounds as catalysts for C–O bond reduction.

**Exceptional Reactivity of the Octavinyl Catalyst.** Reactions with the catalyst generated using OV and Piers borane, when at loadings of  $>5$  borons/silsesquioxane, had exceptional reactivity. For example, The TMS-protected linear hexitol, galactitol was fully reduced to a mixture of hexane isomers in 5 hours using the reductant 1,1,3,3-tetramethyldisiloxane (TMDS). This reactivity surprised us given that it was more similar to the reactivity of tris(pentafluorophenyl)borane than it was to other heteroleptic fluoroarylboranes, including those generated via hydroboration of

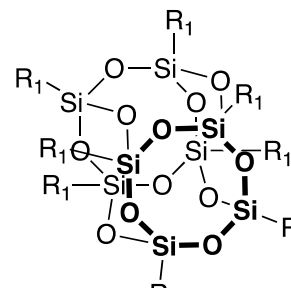


**Figure 5.** General structure of a fully condensed T8 silsesquioxane.

the mono-alkene silsesquioxanes. Unfortunately, the catalysts generated with OV are complex given the rapid hydroboration and the

varying symmetries that arise when there are 2-6 borons per silsesquioxane and both linear and branched isomers result. Because of this, we turned to the mono-alkene silsesquioxanes to better understand the enhanced reactivity in the OV catalyst.

**Table 1.** Isomerization of Allyl Catalysts

	% linear	% branched
TMS-allyl	12	88
MAHCP	28	72
MAHIB	26	74

**Quenching Reactions with Isochroman.** Isochroman was selected as an ideal test substrate since it is affordable and does not require any silyl protections like the sugar molecules we have previously tested. We found that we could effectively quench these catalysts with triethylamine (TEA), and we chose a time point of 2 minutes because these catalysts were unable to fully reduce isochroman to the single reduction product during that amount of time. This allowed us to use <sup>1</sup>H NMR spectroscopy to quantify the ratio of

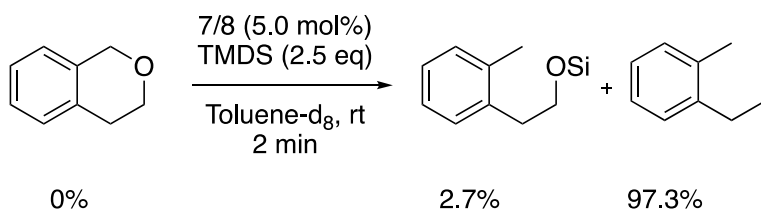


**Figure 6.** Reduction of isochroman with the OV catalyst produced almost exclusively 2-ethyltoluene within 2 minutes.

starting material to reduced product at various catalyst loadings using each of the various catalysts. It is important to note that the reaction of the catalyst generated with 7 equivalents of boron and OV actually proceeded

almost completely to the fully reduced 2-ethyltoluene in the 2 minutes used for our test reactions (Figure 2). This reactivity was not observed with the other catalysts (catalyst loadings are all scaled to amount of boron), so a measure starting material and the single reduction product was sufficient in those cases.

**Catalyst Isomerization Informs on Reactivity.** The well-established b-silicon effect has implications on this chemistry. Specifically, boron has the potential to migrate to the same carbon as silicon where it benefits from electron donation into the empty p<sub>z</sub> orbital, and this has been reported by Piers for molecules generated using Piers borane.<sup>2,3</sup> In the case of OV and MVHIB, hydroboration initially produces a mixture of linear and branched borane with the ratio heavily favoring linear (81% linear for OV and 82% linear for MVHIB). Heating these catalysts will cause minor isomerization to the more branched product, but the ratio still favors linear.

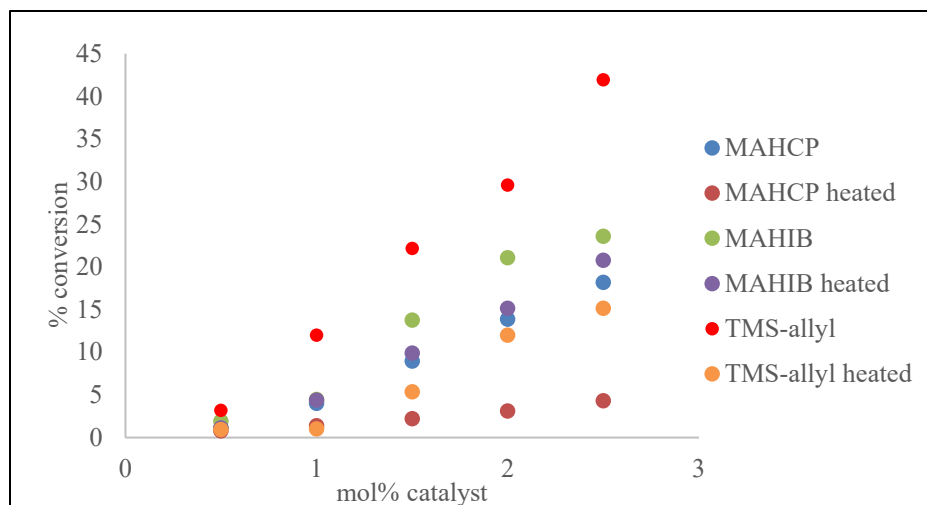


**Figure 3.** Reactivity of allyl catalysts before and after isomerization to the more branched isomer. All three catalysts were more reactive prior to isomerization.

MVHIB, MAHCP, and our non-silsesquioxane control of TMS-allyl have a much more dramatic change when subjected to heat. For each of these catalysts, initial hydroboration produces exclusively the linear catalyst. Heating to 100 °C overnight causes a series of retrohydroboration/rehydroboration that shifts the ratio to favor the branched product (Table 1). We then tested both the fully linear and the isomerized catalysts to determine how the position of the boron impacted the reactivity of the catalyst. As shown in Figure 3 the linear to branched isomerization decreases the reactivity and indicates that moving boron to the same carbon as silicon has a negative impact on reactivity. We hypothesized that this could be both a steric and an electronic effect. In the case of the silsesquioxanes, isomerization moves boron closer to the congested core. In the case of TMS-allyl, where sterics are less likely to play a detrimental role in catalyst activity, the stronger electron donating ability of the Si–C bond in TMS-allyl (c.f. the silsesquioxane core) could further reduce the boron’s electrophilicity due to the b-Si effect; we have previously hypothesized that Boron’s Lewis acidity correlates directly to catalytic activity. The notion that increased Lewis acidity benefits the reactivity of the catalyst is consistent with results showing that increasing the loading of boron on the OV catalyst increases reactivity. The bis(pentafluorophenyl) borane moieties are expected to be more electron deficient than the initial vinyl group, and increasing the electron-withdrawing ability of the loaded silsesquioxane will increase the Lewis acidity at boron.

**Future Work.** As we wrap up this silsesquioxane work, we will continue to explore other plausible explanations for the enhanced reactivity of the OV catalyst. One area we still need to explore is the possibility of cooperativity between neighboring borons in the OV catalyst. Preliminary experiments suggest that cooperativity could be at play. Additionally, we are working to generate a vinylated silica surface with protected hydroxyls (Figure 4) so that we can transition this work to heterogeneous catalysts.

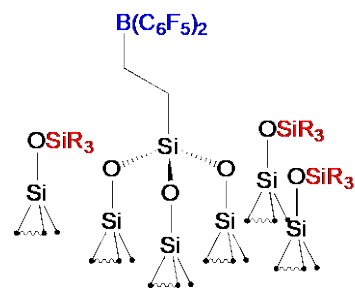


**Figure 4.** Heterogeneous catalyst using the Piers borane hydroboration on vinylated silica.

## References.

1. Peruzzi, M. T., Mei, Q. Q., Lee, S. J. & Gagné, M. R. Chemoselective amide reductions by heteroleptic fluoroaryl boron Lewis acids. *Chem. Commun.* **54**, 5855–5858 (2018).
2. Parks, D. J., Rupert, R. E. & Piers, W. E. Bis(pentafluorophenyl)borane: Synthesis, Properties, and Hydroboration Chemistry of a Highly Electrophilic Borane Reagent. *Angew. Chemie Int. Ed. English* **34**, 809–811 (1995).
3. Parks, D. J. & Piers, W. E. Hydroboration of vinyl silanes with bis-(pentafluorophenyl)borane: Ground state  $\beta$ -silicon effects. *Tetrahedron* **54**, 15469–15488 (1998).

## Publications Acknowledging this Grant in 2018-2021

1. Unfortunately, no publications in 2020-2021.

## Awards and Memberships

- Fellow, Royal Society of Chemistry (2016); RSC “Catalysis in Organic Chemistry” Award (2016); Fellow, American Association for the Advancement of Science (2012), University of Alberta Alumni Honour Award (2011), “Excellent” Poster Award (2004, ICOS, Nagoya Japan), Camille Dreyfus Teacher Scholar Award (2000), Union Carbide Innovation Recognition Faculty Research Award (2000), 3M Untenured Faculty Award (1999-2000), NSF CAREER Award (1996-2000), Fred H. Irwin Memorial Prize in Organic Chemistry, 1986.
- EastChem Visiting Professor (University of St. Andrews, and University of Edinburgh Aug 2014), Visiting Professor (Duke University, Spring 2011), CaRLa Fellow, University of Heidelberg (June 2008), W.R. Kenan Jr. UNC Leave (2005-2006); Visiting Fellow, Exeter College; SCR Member Wadham College (Oxford University 2005-2006)
- NSERC Funding task force (2011-2012), NSERC Banting Fellows Selection Committee (2010-2013), EPSRC College (2006-2009), GSC-24 NSERC Grants Selection Committee (2005-2008), NIH SBCB ad hoc 10/05
- Board of Editors, Canadian Journal of Chemistry (2002-2005), International Advisory Board of *ChemCatChem* (2016-2021)
- NSERC of Canada postdoctoral fellowship, 1992-1994
- American Chemical Society (Inorganic and Organic Divisions), Canadian Institute of Chemistry, Royal Society of Chemistry

**Supported Molecular Metal Catalysts:  
Single-Sites to Pair-Sites to Metal Clusters**

Bruce C. Gates  
University of California, Davis

**Presentation Abstract**

Isolated single-atom species on supports have new catalytic properties and afford maximum efficiency in the use of the often-expensive metals. We have investigated the precise synthesis of these materials and characterized them in depth, focusing on methods including atomic-resolution scanning transmission electron microscopy, X-ray absorption and IR spectroscopies, and DFT, determining structures that include the support sites where the metals are bonded and determining relationships between structure and catalyst performance, using reactions of small probe molecules with distinctive spectroscopic signatures. The reactions include hydrogenation of small olefins and CO oxidation. The catalysts have been made primarily from platinum and iridium precursors, opening the way to understanding and control of the metal–support bonding and ligands on the metal, including catalytic reaction intermediates. In a wide range of collaborations, we have also investigated supports other than conventional ones, an increasing range of metals, and methods of catalyst stabilization, including encapsulation within supports.

**DE-FG02-04ER15513: Atomically Dispersed Supported Metal Catalysts:  
Understanding Fundamentals and Extending to New Catalyst Classes**

**Postdoc:** Yizhen Chen. **Students:** Yizhen Chen, Louise Debeve, Chia-Yu Fang, Erjia Guan, Adam Hoffman, Andrew Palermo, Jorge Perez-Aguilar, Ounjit Sodpiban, Hanlei Sun, University of California, Davis, Departments of Chemical Engineering and Materials Science & Engineering + **colleagues**, Anastassia Alexandrova, UCLA; Ilke Arslan, ANL; Simon R. Bare, Co-ACCESS, SSRL, SLAC; J.-M. Basset, Catalysis Center, KAUST; Pedro Castaño, KAUST; C.-Y. Chen, Chevron; Miaofang Chi, ORNL; Valerio D’Elia, Vistec Institute of Science and Technology; David A. Dixon, University of Alabama; Maria Flytzani-Stephanopoulos, Tufts University; J. Hughes, Zeolyst; Alexander Katz, University of California, Berkeley; Sibudjing Kawi, National University of Singapore; Coleman Kronawitter, University of California, Davis; Ambarish Kulkarni, University of California, Davis; Jingyue Liu, Arizona State University; David Osborn, Sandia National Laboratory, Javier Pérez-Ramírez, ETH Zurich; Ryan Richards, Colorado School of Mines; Alper Uzun, Koç University; Yang Wong, Washington State University and PNNL; Feng-Shou Xiao, Zhejiang University.

## RECENT PROGRESS

Atomically dispersed supported metal catalysts offer new properties and the benefits of maximized metal accessibility and utilization. We wrote an extensive review in *Small* of the field with a focus on supported platinum and supported iridium.

We reported such a catalyst for CO oxidation, Pt/MgO, with the crystalline MgO support chosen for its stable, well-defined bonding sites to host platinum. The catalyst has been characterized by atomic-resolution imaging, IR spectroscopy of adsorbed CO, EXAFS spectroscopy, and HERFD-XANES spectroscopy, including in-operando characterization. We show how high-throughput density functional theory calculations (for assessing all the potentially stable MgO binding sites for platinum) combined with automated EXAFS analysis can lead to unbiased identification of isolated, surface-enveloped platinum cations as the catalytic species, in agreement with experiment. The data demonstrate that Pt cations are embedded in the MgO. This theory-guided workflow leads to rigorously determined structural models and provides a more detailed picture of catalytic sites than what is currently possible with conventional EXAFS analysis. As this approach is efficient and agnostic to the metal, support, and catalytic reaction, we posit that it will be of broad interest to the catalysis community.

Atomically dispersed supported platinum catalysts were synthesized by the reaction of Pt(acac)<sub>2</sub> (acac = acetylacetonato) with the silicoaluminophosphate molecular sieve SAPO-37. Extended X-ray absorption fine structure (EXAFS) spectra show that, after heating in air to 623 K, each platinum atom on average was bonded to approximately two oxygen atoms of the SAPO, with no evidence of platinum clusters. X-ray absorption near edge spectra (XANES) indicate a platinum formal oxidation state of +2. Infrared spectra characterizing support OH groups show that Pt(acac)<sub>2</sub> reacted with them. The supported species catalyzed ethylene hydrogenation at 1 bar and room temperature in a once-through flow reactor. The EXAFS-determined Pt–Pt coordination number (CN) increased from essentially zero to  $1.8 \pm 0.4$  as the XANES white line intensity decreased, all within minutes after the start of reactant flow, before recording of the first catalyst performance data. After 2 h of continuous reactant flow and catalysis, the Pt–Pt CN had increased to  $2.7 \pm 0.5$ . The data indicate the almost instantaneous formation of platinum clusters of only a few atoms each (with average diameters of about 0.4–0.8 nm). Subsequent exposure of the catalyst to ethylene led to a decrease in the Pt–Pt coordination number to  $1.6 \pm 0.3$  and an increase in the white line intensity, indicating partial oxidative fragmentation of the clusters by ethylene. Platinum clusters in SAPO-37 formed in separate experiments by exposure to H<sub>2</sub> prior to catalysis were also catalytically active for ethylene hydrogenation. The data all support the conclusion that platinum clusters are the catalytically active species, with no evidence of catalysis by atomically dispersed platinum.

### Publications Acknowledging this Grant in 2018-2021

1. (I) Guan, E.; Gates, B. C. Stable Rhodium Pair Sites on MgO: Influence of Ligands and Rhodium Nuclearity on Catalysis of Ethylene Hydrogenation and H-D Exchange in the Reaction of H<sub>2</sub> with D<sub>2</sub> *ACS Catal.*, **2018**, *8*, 482.

2. (II) Maity, N.; Barman, S.; Minenkov, Y.; Ould-Chikh, S.; Abou-Hamad, E.; Ma, T.; Qureschi, Z. S.; Cavallo, L.; D'Elia, V.; Gates, B. C.; Basset, J.-M. A Silica-Supported Monoalkylated Tungsten Dioxo Complex Catalyst for Olefin Metathesis. *ACS Catal.* **2018**, *8*, 2715.
3. (I) Hoffman, A. S.; Debeve, L. M.; Zhang, S.; Perez-Aguilar, J. E.; Conley, E. T.; Justl, K. R.; Arslan, I.; Dixon, D. A.; Gates, B. C. Beating Heterogeneity of Single-Site Catalysts: MgO-Supported Iridium Complexes. *ACS Catal.*, **2018**, *8*, 3489.
4. (II) Wang, L.; Guan, E.; Zhang, J.; Yang, J.; Zhu, Y.; Han, Y.; Yang, M.; Cen, C.; Fu G.; Gates, B. C.; Xiao F.-S. Single-site catalyst promoters accelerate metal-catalyzed nitroarene hydrogenation *Nat. Commun.* **2018**, *9*, 1362.
5. (I) Guan, E.; Fang, C.-Y.; Yang, D.; Wang, L.; Xiao, F.-S.; Gates, B. C. Supported cluster catalysts synthesized to be small, simple, selective, and stable. *Faraday Disc.* **2018**, *28*, 9.
6. (II) Zhang, J.; Wang, L.; Zhang, B.; Zhao, H.; Kolb, H.U.; Zhu, Y.; Liu, L.; Han, Y. Wang, G.; Wang, C.; Su, D. S.; Gates, B. C.; Xiao, F.-S. Sinter-Resistant Metal Nanoparticle Catalysts Achieved by Immobilization within Zeolite Crystals via Seed-Directed Growth. *Nat. Catal.* **2018**, *1*, 540.
7. (II) Palermo, A. P.; Zhang, S. J.; Hwang, S.-J.; Dixon, D. A.; Gates, B. C.; Katz, A. Weakly Interacting Solvation Spheres Surrounding a Calixarene-Protected Tetrairidium Carbonyl Cluster: Contrasting Effects on Reactivity of Alkane Solvent and Silica Support. *Dalton Trans* **2018**, *47*, 13550.
8. (II) Aljuhani, M. A.; Barman, S.; Abou-Hamad, E.; Gurinov, A.; Ould-Chikh, S.; Guan, E.; Jedidi, A.; Cavallo, L.; Gates, B. C.; Pelletier, J. D. A.; Basset, J.-M. Imine Metathesis Catalyzed by a Silica-Supported Hafnium Imido Complex. *ACS Catal.* **2018**, *8*, 9440.
9. (II) Babucci, M.; Fang, C.-Y.; Perez-Aguilar, J. E.; Hoffman, A. S.; Boubnov, A.; Guan, E.; Bare, S. R. Catalysis by Design: a Tungsten Catalyst incorporating a Well-Defined Lewis Acidic Surface Ligand for Selective Metathesis of Propane,  $[(\equiv\text{Si}-\text{O}-\text{Si}\equiv)(\equiv\text{Si}-\text{O}-)_2\text{Al}-\text{O}-\text{W}(\equiv\text{CtBu})(\text{H})_2]$  Gates, B. C.; Uzun, A. Controlling Catalytic Activity and Selectivity for Partial Hydrogenation by Tuning Environment around Active Sites in Iridium Complexes Bonded to Supports. *Chem. Sci.* **2019**, *10*, 2623.
10. (II) Werghi, B.; Bendjeriou-Sedjerari, A.; Jedidi, A.; Morlanes, N.; Abou-Hamad, E.; Bhatte, K.; Guan, E.; Ma, T.; Aguilar, A.; Ould Chikh, S.; Cavallo, L.; Gates, B. C.; Basset, J.-M. *ChemCatChem*, **2019**, *11*, 614.
11. (II) Schöttle, C.; Guan, E.; Okrut, A.; Grosso-Giordano, N. A.; Palermo, A.; Solovyov, A.; Gates, B. C.; Katz, A. Bulky Calixarene Ligands Stabilize Supported Iridium Pair-Site Catalysts. *J. Am. Chem. Soc.* **2019**, *141*, 4010.
12. (I) Fang, C.-Y.; Zhang, S.; Hu, Y.; Vasiliu, M.; Perez-Aguilar, J.; Conley, E.; Dixon, D. A.; Chen, C. Y.; Gates, B. C. Reversible Metal Aggregation and Redispersion Driven by the Catalytic Water Gas Shift Half Reactions: Interconversion of Single-Site

Rhodium Complexes and Tetra-rhodium Clusters in Zeolite HY. *ACS Catal.* **2019**, *9*, 3311.

13. (I) Gates, B. C. Atomically Dispersed Supported Metal Catalysts: Seeing is Believing. *Trend Chem.* **2019**, *1*, 99.

14. (II) Jimenez-Izal, E.; Gates, B. C.; Alexandrova, A. N. Designing clusters for Heterogeneous Catalysis. *Phys. Today*, July 2019, p. 38.

15. (II) Wang, C.; Guan, E.; Wang, L.; Chu, X.; Wu, Z.; Zhang, J.; Yang, Z.; Jiang, Y.; Zhang, L.; Meng, X.; Gates, B. C.; Xiao, F.-S. Product Selectivity Controlled by Nanoporous Environments in Zeolite Crystals Enveloping Rhodium Nanoparticle Catalysts for CO<sub>2</sub> Hydrogenation. *J. Am. Chem. Soc.* **2019**, *141*, 8482.

16. (II) Aljuhani, M. A.; Zhang, Z.; Barman, S.; El Eter, M.; Failvene, L.; Ould-Chikh, S.; Guan, E.; Abou-Hamad, E.; Emwas, A.-H.; Pelletier, J. D. A.; Gates, B. C.; Cavallo, L.; Basset, J.-M. Mechanistic Study of Hydroamination of Alkyne through Tantalum-Based Silica-Supported Surface Species. *ACS Catal.* **2019**, *9*, 8719.

17. (I) Guan, E.; Debeve, L.; Vasiliu, M.; Zhang, S.; Dixon, D. A.; Gates, B. C. MgO-Supported Iridium Pair-Site Catalysts are More Active and Resistant to CO Poisoning than Analogous Single-Site Catalysts for Ethylene Hydrogenation and H-D Exchange. *ACS Catal.* **2019**, *9*, 9545.

18. (I) Palermo, A. P.; Schöttle, C.; Zhang, S.; Grosso-Giordano, N.; Okrut, A.; Dixon, D. A.; Frei, H.; Gates, B. C.; Katz, A. Spectroscopic Characterization of  $\mu$ - $\eta^1$ : $\eta^1$ -Peroxo Ligands Formed by Reaction of Dioxygen with Electron-Rich Iridium Clusters. *Inorg. Chem.* **2019**, *58*, 14338.

19. (II) Babucci, M.; Sarac Oztuna, F. E.; Debeve, L. M.; Boubnov, A.; Bare, S. R.; Gates, B. C.; Unal, U.; Uzun A. Atomically Dispersed Reduced Graphene Aerogel-Supported Iridium Catalyst with an Iridium Loading of 14.8 wt %. *ACS Catal.* **2019**, *9*, 9905.

20. (I) Debeve, L. M.; Hoffman, A. S.; Yeh, A.; Runnebaum, R. C.; Shulda, S.; Richards, R.; Arslan, I.; Gates, B. C. Iridium Atoms Bonded to Crystalline Powder MgO: Characterization by Imaging and Spectroscopy. *J. Phys. Chem. C*, **2020**, *124*, 459.

21. (I) Fang, C.-Y.; Valecillos-Diaz, J.; Conley, E. T.; Chen, C.-Y.; Castaño, P.; Gates, B. C. Synthesis of Rh<sub>6</sub>(CO)<sub>16</sub> in Supercages of Zeolite HY: Reaction Network and Kinetics of Formation from Mononuclear Rhodium Precursors via Rh<sub>4</sub>(CO)<sub>12</sub> Facilitated by the Water Gas Shift Half-Reaction. *J. Phys. Chem. C*, **2020**, *124*, 2513.

22. (II) Wang, L.; Guan, E.; Wang, Y.; Wang, L.; Gong, Z.; Cui, Y.; Meng, X.; Gates, B. C.; Xiao, F.-S. Silica accelerates the selective hydrogenation of CO<sub>2</sub> to methanol on cobalt catalysts. *Nat. Commun.* **2020**, *11*:1033.

23. (II) Saidi, A.; Samantaray, M.; Abou-Hamad, E.; Poater, A.; Ould-Chikh, S.; Guo, X.; Guan, E.; Ma, T.; Gates, B. C.; Basset, J.-M. Docking of Tetra-methyl Zirconium to the Surface of Silica A Well-Defined Pre-catalyst for Conversion of CO<sub>2</sub> to Cyclic Carbonates, W. Almaksoud. *Chem Commun* **2020**, *56*, 3528.

24. (II) Das, S.; Pérez-Ramírez, J.; Gong, J.; Dewangan, N.; Hidajat, K.; Gates, B. C.; Kawi, S. Core-shell structured catalysts for thermocatalytic, photocatalytic, and electrocatalytic conversion of CO<sub>2</sub>. *Chem. Soc. Rev.* **2020**, *49*, 2937.
25. (II) Babucci, M.; Hoffman, A. S.; Debeve, L. M.; Kurtoglu, S. F.; Bare, S. R.; Gates, B. C., Uzun, A. Unraveling the individual influences of supports and ionic liquid coatings on the catalytic properties of supported iridium complexes and iridium clusters. *J. Catal.* **2020**, *387*, 186.
26. (II) Wang, H.; Xu, D.; Guan, E.; Wang, L.; Zhang, J.; Wang, C.; Wang, S.; Xu, H.; Meng, X.; Yang, B.; Gates, B. C.; Xiao F.-S. Atomically Dispersed Ru on Manganese Oxide Catalyst Boosts Oxidative Cyanation. *ACS Catal.*, **2020**, *10*, 6299.
27. (I) Perez-Aguilar, J. E.; Chen, C.-Y.; Hughes, J. T.; Fang, C.-Y.; Gates, B. C. Isostructural Atomically Dispersed Rhodium Catalysts Supported on SAPO-37 and on HY Zeolite. *J. Am. Chem. Soc.* **2020**, *142*, 11474.
28. (I) Guan, E.; Ciston, J.; Bare, S. R.; Runnebaum, R. C.; Katz, A.; Kulkarni, A.; Kronawitter, C. X.; Gates, B. C. Supported Metal Pair-Site Catalysts. *ACS Catal.* **2020**, *10*, 9065.
29. (II) Wang, L.; Guan, E.; Wang, Z.; Wang, L.; Gong, Z.; Cui, Y.; Yang, Z.; Wang, C.; Zhang, J.; Meng, X.; Hu, P.; Gong, X.-Q.; Gates, B. C.; Xiao, F.-S. Dispersed Nickel Boosts Catalysis by Copper in CO<sub>2</sub> Hydrogenation. *ACS Catal.* **2020**, *10*, 9261.
30. (II) Kurtoğlu, S. F.; Hoffman, A. S.; Akgül, D.; Babucci, M.; Aviyente, V.; Gates, B. C.; Bare, S. R.; Uzun, A. Electronic Structure of Atomically Dispersed Supported Iridium Catalyst Controls Iridium Aggregation. *ACS Catal.*, **2020**, *10*, 12354.
31. (II) Chen-Wiegert, Y. C. K.; Walu, I.; Kiss, A.; Campbell, S.; Yang, L.; Dooryhee, E.; Trelewicz, J. R.; Li, Y.; Gates, B.; Rivers, M.; Yager, K. G. Multimodal Synchrotron Approach: Research Needs and Scientific Vision. *Synchrotron Rad. News* **2020**, *33*, 44.
32. (I) Chen, Y.; Sun, H.; Gates, B. C. Prototype Atomically Dispersed Supported Metal Catalysts: Iridium and Platinum. *Small* **2021**, *17*, 2004665.
33. (I) Perez-Aguilar, J. E.; Hughes, J. T.; Chen, C.-Y.; Gates, B. C. Transformation of Atomically Dispersed Platinum in SAPO-37 into Platinum Clusters: Catalyst for Ethylene Hydrogenation. *Catal. Sci. Technol.* **2021**, in press, <https://doi.org/10.1039/D1CY01216A>.

#### Awards or leadership activities during 2018-2020 calendar years

Catalysis Society of North America, member of Board of Directors (at large), 1997–2021.

Scientific Advisory Committees, SSRL, 2010–present; NSLS-II, 2016–2021.

International Congress on Catalysis 2020, Vice Chair, 2018–2021 [meeting was cancelled, COVID]

Co-chair 3<sup>rd</sup> International Conference on Single Atom Catalysts 2020 [meeting was cancelled, COVID].

Editorial Boards/Scientific Boards, *Catalysis Letters*; *Journal of Catalysis*; *Topics in Catalysis*; *Catalysis, Structure and Reactivity*.

**Activation of Alkyl C-H Bonds and Dehydrogenation of Alkanes Achieved through Proton-Coupled Electron Transfer. High- and Low-Oxidation State Iridium**

Alan S. Goldman

Rutgers – The State University of New Jersey, Department of Chemistry

**Presentation Abstract**

The dehydrogenation of alkanes to give olefins offers almost unlimited potential as a route to their catalytic conversion to commodity chemicals or to alkanes of higher fuel value. Molecular (homogeneous) catalysts offer promising selectivity in this context, with great progress having been made in the development of transition-metal-based molecular catalysts for alkane dehydrogenation. However, sacrificial acceptors are commonly employed which are costly and introduce complications for the development of practical systems. Alternatively, acceptorless alkane dehydrogenation systems are feasible but tend to give slow rates and relatively low turnovers. An approach very distinct from the transfer of hydrogen to an olefin or purging H<sub>2</sub> from the solution would be the separate removal of electrons and protons. In principle, the transfer of electrons and protons could proceed as in a fuel cell to yield useful energy or, in the absence of O<sub>2</sub> at the cathode, the protons could be reduced to give H<sub>2</sub>.

We have found that electron-acceptors and bases can replace sacrificial hydrogen acceptors. (pincer)IrH<sub>2</sub> (pincer = PCP, POCOP) complexes are found to react readily with a strong base and two equiv electron acceptor to generate (pincer)IrH<sup>+</sup>. A slower reaction with base generates the fragment “(pincer)Ir” which reacts with alkane to give alkene and regenerate (pincer)IrH<sub>2</sub>. This reaction can be conducted catalytically to give good yields of olefin based on oxidant and base. Of course in order for any such system to be of practical value, the base and oxidant must be regenerated, electrochemically and/or with O<sub>2</sub>; work to develop such systems is in progress.

In a project begun more serendipitously, we find that the *p*-pyridyl derivative of (<sup>t</sup>BuPCP)IrHCl (pN-PCP)IrHCl, with N at the position para to Ir) is easily oxidized. This results from an equilibrium with a tautomeric Ir(I) complex in which the hydride has shifted (as H<sup>+</sup>) to the pN-PCP N atom. A second oxidation gives a cationic Ir(III) intermediate which undergoes addition of a *t*-butyl (sp<sup>3</sup>) C-H bond. Likewise, oxidation of (<sup>t</sup>BuPCP)IrH(OAc) gives an analogous cyclometalation. Thus while the (<sup>t</sup>BuPCP)Ir(I) fragment undergoes intermolecular C-H addition, Ir(III) complexes (<sup>t</sup>BuPCP)IrX<sup>+</sup> undergo intramolecular addition. Development of ligand architectures resistant to cyclometalation should allow intermolecular C-H activation leading to dehydrogenation or other functionalizations.

**DE-SC0020139: Alkane Transformations based on Dehydrogenation and Related Reactions: A Tandem Approach**

**Student(s):** Tariq Bhatti, Santanu Malakar, Benjamin Gordon, Ariella Askew, Jessica Malcolm, Soumyadipa Das, Ashish Parihar.

## RECENT PROGRESS

As noted in the Presentation Abstract, the dehydrogenation of alkanes to give olefins offers almost unlimited potential as a route to their catalytic conversion to commodity chemicals or to alkanes of higher fuel value. Molecular (homogeneous) catalysts offer promising selectivity in this context, with great progress having been made in the development of transition-metal-based molecular catalysts for alkane dehydrogenation. However, sacrificial acceptors are commonly employed which are costly and introduce complications for the development of practical systems. Further, most systems to date are based upon low-oxidation-state species which limits their ability to act in tandem with functionalized reagents or to dehydrogenate functionalized hydrocarbons.

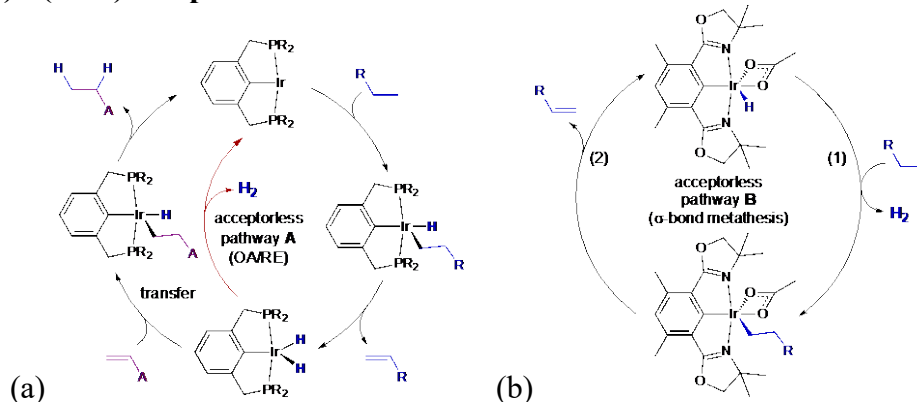
Under the auspices of this project we are developing dehydrogenation systems based on new paradigms and approaches. An approach very distinct from the transfer of hydrogen to an olefin or purging H<sub>2</sub> from solution would be the separate removal of electrons and protons. In principle, the transfer of electrons and protons could proceed as in a fuel cell to yield useful energy or, in the absence of O<sub>2</sub> at the cathode, the protons could be reduced to give H<sub>2</sub>.

In a complementary approach we are developing systems based on high oxidation state species, which operate via “heterolytic dehydrogenation”. There is reason to believe that these are more promising than conventional systems for acceptorless dehydrogenation.

**Alkane dehydrogenation driven by electron and proton acceptors.** We have found that electron- and proton acceptors can replace sacrificial hydrogen acceptors for alkane dehydrogenation. (pincer)IrH<sub>2</sub> (pincer = PCP, POCOP) complexes are found to react readily with a strong base and two equiv electron acceptor, such as Ag<sup>+</sup> or Cp<sub>2</sub>Fe<sup>+</sup>, to generate (pincer)IrH<sup>+</sup>. A slower reaction with a second equivalent of base generates the fragment “(pincer)Ir” which reacts with alkane to give alkene and regenerate (pincer)IrH<sub>2</sub>. This reaction can be conducted catalytically to give good yields of olefin based on oxidant and base. Remarkably even the very weak oxidant Cp<sub>2</sub>Co (E° = -1.33 V) is quite effective. This highlights that a very low driving force would be needed. Of course in order for any such system to be of practical value the base and oxidant must be regenerated, electrochemically and/or with O<sub>2</sub>; work to develop such systems is in progress.

**High-Oxidation State Alkane Dehydrogenation Catalysts.** It has previously been reported that pincer-ligated iridium complexes of the general type (PCP)Ir and isoelectronic congeners can effect acceptorless alkane dehydrogenation, but much more slowly than dehydrogenation achieved with the use of sacrificial olefinic hydrogen acceptors. This can be easily rationalized in terms of the mechanisms that have been proposed for acceptorless and transfer-dehydrogenation, respectively. In particular, the acceptorless reaction requires loss of H<sub>2</sub> from (pincer)IrH<sub>2</sub>, to generate the reactive 14e fragment (pincer)Ir (Scheme 1a, pathway A). Given that the (pincer)Ir fragment must abstract H<sub>2</sub> from alkane, and the enthalpy of alkane dehydrogenation is ca. +30 kcal/mol, this reaction is inevitably very endothermic. A much more thermodynamically favorable reaction is the hydrogenation of olefin by (pincer)IrH<sub>2</sub>, which can follow a kinetically facile pathway that is the microscopic reverse of the actual alkane dehydrogenation reaction (Scheme 1a).

**Scheme 1. Dehydrogenation pathways proposed for (a) (PCP)Ir, and (b) (Phebox)Ir(OAc) complexes**



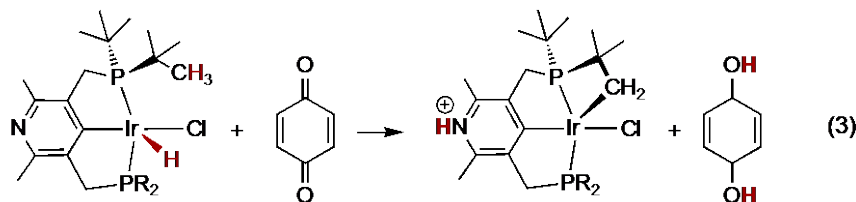
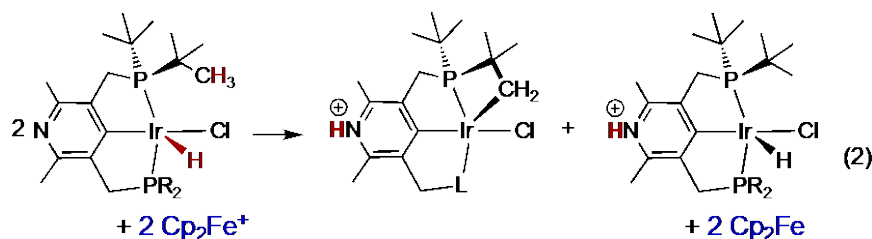
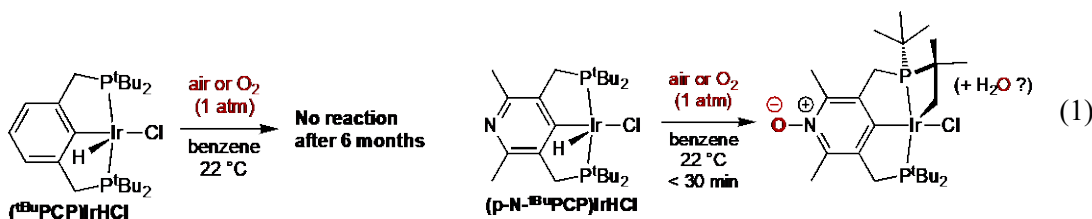
An alternative pathway for acceptorless dehydrogenation comprises two net reactions, as shown in Scheme 1b (pathway **B**): Ir-H/C-H  $\sigma$ -bond metathesis (step 1) and  $\beta$ -H elimination (step 2). (For step 1 we refer only to the net reaction and not to the mechanistic connotations often associated with the term “s-bond metathesis”; indeed we find several possible pathways, none of which include the classic mechanism for s-bond metathesis originally reported for  $d^0$  transition metal complexes.) Pathway **B** may be viewed as the microscopic reverse of a “Heterolytic H<sub>2</sub> Activation” pathway for olefin hydrogenation as defined by Crabtree. We have shown that in contrast with complexes of PCP-pincer ligands, (dimethyl-Phebox)Ir(OAc)H can effect dehydrogenation through such a pathway. The thermodynamics of the overall reaction are highly endothermic and highly endergonic under standard conditions and are of course independent of the catalytic cycle. For the reaction to proceed, conditions must be such that  $\Delta G$  is negative for the overall reaction, which in practice means high temperatures and, especially, maintaining an extremely low concentration of H<sub>2</sub> by removing it in some way from solution. We consider that Pathway **B** offers an advantage over Pathway **A** in that step 1 is likely to be moderately endothermic - but significantly less so than the overall enthalpy of dehydrogenation - and highly entropically favorable due to the formation of free H<sub>2</sub> under such conditions. This realization of a very large entropic gain under these reaction conditions could allow the build-up of a substantial concentration of the alkyl complex shown in Scheme 1b. If step 2 is also moderately endothermic, the barrier highest in free energy for the overall catalytic cycle may be modest. Thus the overall free energy barrier, under properly chosen reaction conditions, can be significantly less than either  $\Delta H^\circ$  or even  $\Delta G^\circ$  for the overall reaction.

Pathways such as **B** also potentially offer another advantage over those like pathway **A**. Because they do not involve low oxidation state intermediates such as Ir(I), pathways like **B** may prove to be much more tolerant of reagents or catalysts that can be used to effect reactions in tandem with dehydrogenation. They may also be more effective for the dehydrogenation of substrates with functional groups not tolerated by low-oxidation-state intermediates.

A bis-trifluoromethyl-substituted (Phebox)Ir complex has been prepared and investigated as a catalyst for the acceptorless dehydrogenation of alkanes. TONs over 1000 have been obtained within 24 h. However, even these high observed values appear to understate the actual catalytic activity since the observed rates appear to be limited,

remarkably, by the rate at which H<sub>2</sub>, which is present in solution in an extremely low steady-state concentration, is expelled from solution.

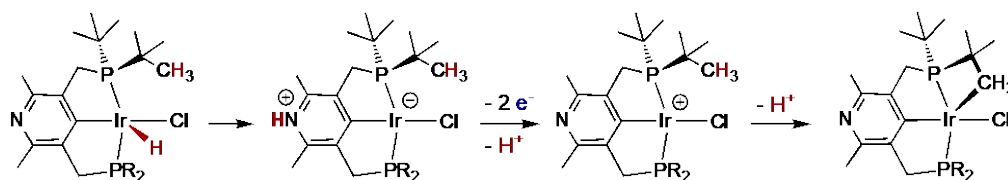
**MLC-based dehydrogenation and C-H activation by oxidized species.** The *p*-pyridyl derivative of (PCP)Ir, (p-N-PCP)Ir has proven to have chemistry remarkably different from its unsubstituted parent. Fascinating results were obtained even before we reduced the typical synthetic precursor i.e. the hydrido chloride (in this case (p-N-PCP)IrHCl). It was found that this Ir(III) precursor reacts with O<sub>2</sub> (eq 1) and even simple oxidants like Cp<sub>2</sub>Fe (eq 2), much more readily than does the parent PCP catalyst. This was quite unexpected since a pyridine derivative is expected to be *less* easily oxidized. The resulting oxidized species are found to have undergone addition of a phosphino t-butyl (primary sp<sup>3</sup>) C-H bond.



Benzoquinone is readily hydrogenated by (p-N-PCP)IrHCl, stoichiometrically (eq 3). The cyclometalated species are rapidly regenerated by H<sub>2</sub> so the hydrogenation can also be conducted catalytically. Unlike the hydrogenation of olefins, the hydrogenation of benzoquinone generally operates via proton-coupled electron transfer; for the same reason, unlike olefins, benzoquinone can be easily electrochemically regenerated from the hydroquinone product.

We have shown that the key to the high reactivity of (p-N-PCP)IrHCl is a low energy zwitterionic tautomer, in which a proton has transferred from the Ir center to the ligand N atom (Scheme 2). This affords a complex with a formally anionic iridium(I) center which is easily oxidized.

### Scheme 2. Mechanism of reaction of (pN-PCP)IrHCl with electron acceptors



A second oxidation leads to a cationic Ir(III) center which activates the  $sp^3$  C-H bond of a ligand *t*-butyl group. If it were to instead react intermolecularly and add an *n*-alkane C-H bond the resulting alkyl iridium chloride would undergo  $\beta$ -H elimination, thereby completing a catalytic cycle for dehydrogenation. Both the surprising ease of oxidation and the reactivity of the cationic center toward C-H bonds have very direct implications for the themes of PCET-driven dehydrogenation and high-oxidation-state catalysts above.

The overlap that has emerged between these projects has been quite remarkable. In an effort to explore PCP derivatives of the Phebox acetate, we find that  $(t^{\text{Bu}}\text{PCP})\text{Ir}(\text{OAc})\text{H}$  also reacts with oxidants to undergo  $sp^3$  C-H bond cyclometalation of the phosphino *t*-butyl groups. A common theme thus appears to be that the cationic  $(t^{\text{Bu}}\text{PCP})\text{Ir}^{\text{III}}\text{X}$  complexes, unlike  $(t^{\text{Bu}}\text{PCP})\text{Ir}^{\text{I}}$  complexes, undergo cyclometalation in preference to intermolecular reaction with an alkane C-H bond. We believe this can be circumvented through modification of the ligand architecture and particularly reduced steric crowding. If so, we expect that intermolecular C-H activation would lead to  $\beta$ -H elimination which would complete a high-oxidation-state catalytic cycle driven by PCET.

### Publications Acknowledging this Grant in 2018-2021

Please classify your publications into two categories according to the source of support for the work published:

- (I) Intellectually led by this grant
- (II) Jointly funded by this grant and other grants with intellectual leadership by other funding sources

(I) Publications intellectually led by this grant.:

Sheludko, B.; Castro, C. F.; Goldman, A. S.; Celik, F. E., Poison or Promoter? Investigating the Dual-Role of Carbon Monoxide in Pincer-Iridium-Based Alkane Dehydrogenation Systems via Operando Diffuse Reflectance Infrared Fourier Transform Spectroscopy. *ACS Catal.* **2020**, *10*, 12425-12436.

Sheludko, B.; Castro, C. F.; Khalap, C. A.; Emge, T. J.; Goldman, A. S.; Celik, F. E., Regioselective Gas-Phase *n*-Butane Transfer Dehydrogenation via Silica-Supported Pincer-Iridium Complexes. *ChemCatChem* **2021**, *13*, 407-415.

Shada, A. D. R.; Miller, A. J. M.; Emge, T. J.; Goldman, A. S., Catalytic Dehydrogenation of Alkanes by PCP-Pincer Iridium Complexes Using Proton and Electron Acceptors. *ACS Catal.* **2021**, *11*, 3009-3016.

Biswas, S.; Blessent, M.; Gordon, B. M.; Zhou, T.; Malakar, S.; Wang, D. Y.; Jespersen, K. K.; Goldman, A. S., Regioselective Dehydrogenation of Alkanes by Pincer-Iridium Complexes. A Combined Experimental and Computational Study. **2021**, submitted for publication.

Zhou, X.; Malakar, S.; Dugan, T.; Wang, K.; Sattler, A.; Marler, D. O.; Emge, T. J.; Krogh-Jespersen, K.; Goldman, A. S., Alkane Dehydrogenation Catalyzed by a Fluorinated Phebox Iridium Complex. **2021**, submitted for publication.

(II) Publication jointly funded by this grant and other grants with intellectual leadership by other funding sources

Sheludko, B.; Wegener, E. C.; Celik, G.; Kropf, A. J.; Castro, C. F.; Delferro, M.; Goldman, A. S.; Kaphan, D. M.; Celik, F. E., In situ formation of a sub-nanometer iridium phosphide catalyst from supported organometallic species. ChemRxiv 2020, 1-9. (Also submitted for peer-reviewed publication.)

#### **Awards or leadership activities during 2018-2020 calendar years**

Royal Society of Chemistry Sir Geoffrey Wilkinson Award, 2020

American Chemical Society Award in Organometallic Chemistry, 2019

Japan Society for the Promotion of Science Invitational Fellowship, 2018

Vice Chair for Graduate Program, Rutgers Department of Chemistry and Chemical Biology, July, 2019 – June, 2021

**Support Effect Studied on Thin-Film Perovskites.**

R. J. Gorte  
Chemical & Biomolecular Engineering  
University of Pennsylvania  
Philadelphia, PA 19104

Sintering of metal catalysts is a serious problem in some high-temperature applications because it leads to the loss of active surface area. A possible solution to this problem involves supporting the metals on oxides which have the perovskite structure. The idea is that the metals can be redispersed by incorporation into the oxide lattice under oxidizing conditions and brought back to the surface by ex-solution under reducing conditions. However, the surface areas of typical perovskites are too low and the length scales for ingress and egress are too long to take practical advantage of this effect. The present work is addressing these issues by depositing very thin perovskite films onto high-surface-area supports by Atomic Layer Deposition (ALD). After adding the metal catalyst, the physical and thermodynamic properties of the supported catalysts are being characterized in order to understand the effects of perovskite composition and film thickness. The catalytic properties are being evaluated for reactions of interest to emissions-control catalysis.

**DE-FG02-13ER16380: Support Effect Studied on Thin-Film Perovskites**

**P.I.:** Raymond J. Gorte

**Postdoc:** Ohhun Kwon

**Students:** Ching-Yu Wang, Chao Lin, Xinyu Mao

**RECENT PROGRESS**

***Dry Reforming of Methane Over Ni Supported on LaMnO<sub>3</sub> Thin Films:***

Thin films of LaMnO<sub>3</sub> were deposited onto MgAl<sub>2</sub>O<sub>4</sub> by Atomic Layer Deposition (ALD) and studied as supports for Ni Dry Reforming of Methane (DRM) catalysts. Scanning Transmission Electron Microscopy (STEM) with Energy-Dispersive X-ray Spectroscopy (EDS) demonstrated that LaMnO<sub>3</sub> covered the support uniformly, and X-ray diffraction (XRD) showed that the LaMnO<sub>3</sub> films maintained their perovskite structure after 5 redox cycles at 1073 K. The Ni also remained well dispersed after 5 redox cycles at 1073 K. The LaMnO<sub>3</sub>-supported catalyst was more active than Ni on the unmodified MgAl<sub>2</sub>O<sub>4</sub> and showed superior resistance against coke formation. Finally, the results for Ni on the LaMnO<sub>3</sub> films are compared to previous results for Ni on LaFeO<sub>3</sub>, CaTiO<sub>3</sub>, SrTiO<sub>3</sub>, and BaTiO<sub>3</sub> films.

### ***Changes in Ni-NiO Equilibrium Due to LaFeO<sub>3</sub> and the Effect on Dry Reforming of CH<sub>4</sub>:***

The interactions between Ni and LaFeO<sub>3</sub> were studied on catalysts prepared by Atomic Layer Deposition (ALD) of 0.5-nm films of LaFeO<sub>3</sub> on MgAl<sub>2</sub>O<sub>4</sub>. Scanning Transmission Electron Microscopy showed that the films covered the support uniformly, even after 5 redox cycles at 1073 K, and X-Ray Diffraction showed that the films had the perovskite structure. Equilibrium between Ni and NiO was studied using coulometric-titration and flow-titration measurements on 5-wt% Ni catalysts, with and without LaFeO<sub>3</sub>. While equilibrium constants for Ni/MgAl<sub>2</sub>O<sub>4</sub> were similar to that expected for bulk Ni, equilibrium  $P_{O_2}$  were shifted to significantly lower values in the presence of LaFeO<sub>3</sub>. In studies of Methane Dry Reforming, the shift in equilibrium resulted in catalyst deactivation due to Ni oxidation at low CO:CO<sub>2</sub> ratios, even though Ni/LaFeO<sub>3</sub>/MgAl<sub>2</sub>O<sub>4</sub> otherwise showed a high reaction rate and excellent tolerance against coking.

### ***Investigation of Rh-titanate (ATiO<sub>3</sub>) interactions on high-surface-area perovskites thin films prepared by atomic layer deposition:***

Thin, ~1-nm films of CaTiO<sub>3</sub>, SrTiO<sub>3</sub>, and BaTiO<sub>3</sub> were deposited onto MgAl<sub>2</sub>O<sub>4</sub> by Atomic Layer Deposition (ALD) and studied as catalyst supports for Rh. Scanning Transmission Electron Microscopy (STEM) and X-Ray Diffraction (XRD) demonstrated that the films had the perovskite structure and formed uniform coatings stable to 1073 K. Rh, added by ALD, interacted strongly with CaTiO<sub>3</sub> and somewhat less strongly with SrTiO<sub>3</sub>, while Rh on BaTiO<sub>3</sub> was similar to Rh on unmodified MgAl<sub>2</sub>O<sub>4</sub>. STEM measurements of Rh on CaTiO<sub>3</sub> films showed Rh remained well dispersed after repeated oxidations and reductions at 1073 K; however, the Rh was inactive for CO-oxidation. Rh formed small particles on SrTiO<sub>3</sub> films and was active for CO oxidation after reduction at 1073 K. The reducibility and catalytic activity of Rh/BaTiO<sub>3</sub>/MgAl<sub>2</sub>O<sub>4</sub> were similar to that of Rh/MgAl<sub>2</sub>O<sub>4</sub>. Evidence from CO-TPR, FTIR, and XPS all indicated that the degree of interaction between Rh and the three perovskite films can be ranked in the following order: Rh/CaTiO<sub>3</sub>/MgAl<sub>2</sub>O<sub>4</sub> > Rh/SrTiO<sub>3</sub>/MgAl<sub>2</sub>O<sub>4</sub> > Rh/BaTiO<sub>3</sub>/MgAl<sub>2</sub>O<sub>4</sub>. Bulk ex-solution catalysts, synthesized by reduction of ATi<sub>0.98</sub>Rh<sub>0.02</sub>O<sub>3</sub> (A=Ca, Sr, and Ba), were also examined for comparison.

### ***A Thermodynamic Investigation of Ni on Thin-Film Titanates (ATiO<sub>3</sub>):***

Thin, ~1-nm films of CaTiO<sub>3</sub>, SrTiO<sub>3</sub>, and BaTiO<sub>3</sub> were deposited onto MgAl<sub>2</sub>O<sub>4</sub> by Atomic Layer Deposition (ALD) and then studied as catalyst supports for ~5 wt % of Ni that was added to the perovskite thin films by Atomic Layer Deposition. Scanning Transmission Electron Microscopy demonstrated that both the Ni and the perovskites uniformly covered the surface of the support following oxidation at 1073 K, even after redox cycling, but large Ni particles formed following a reduction at 1073 K. When compared to Ni/MgAl<sub>2</sub>O<sub>4</sub>, the perovskite-containing catalysts required significantly higher temperatures for Ni reduction. Equilibrium constants for Ni oxidation, as determined from Coulometric Titration, indicated that the oxidation of Ni shifted to lower  $P_{O_2}$  on the perovskite-containing materials. Based on Ni equilibrium constants, Ni interactions are strongest with CaTiO<sub>3</sub>, followed by SrTiO<sub>3</sub> and BaTiO<sub>3</sub>. The shift in the equilibrium constant was shown to cause reversible deactivation of the Ni/CaTiO<sub>3</sub>/MgAl<sub>2</sub>O<sub>4</sub> catalyst for CO<sub>2</sub> reforming of CH<sub>4</sub> at high CO<sub>2</sub> pressures, due to the oxidation of the Ni.

## Publications Acknowledging this Grant in 2018-2021

*Exclusively funded by this grant (for RJG)*

1. Kwon, O.; Huang, R.; Cao, T.; Vohs, J. M.; Gorte, R. J. Dry Reforming of Methane Over Ni Supported on LaMnO<sub>3</sub> Thin Films, *Catalysis Today*, accepted.
2. Lin, C.; Foucher, A. C.; Mao, X.; Stach, E. A.; Gorte, R. J. A Thermodynamic Investigation of Ni on Thin-Film Titanates (ATiO<sub>3</sub>), *Inorganics*, **2020**, *8*, 69
3. Mao, X.; Lin, C.; Graham, G. W.; Gorte, R. J. A Perspective on Thin-Film Perovskites as Supports for Metal Catalysts, *ACS Catalysis*, **2020**, *10*, 8840–8849
4. Lin, C.; Foucher, A. C.; Ji, Y.; Stach, E. A.; Gorte, R. J. Investigation of Rh-titanate (ATiO<sub>3</sub>) interactions on high-surface-area perovskites thin films prepared by atomic layer deposition, *Journal of Materials Chemistry A*, **2020**, *8* 16973-16984.
5. Mao, X.; Foucher, A. C.; Montini, T.; Stach, E. A.; Fornasiero, P.; Gorte, R. J. Epitaxial and Strong Support Interactions between Pt and LaFeO<sub>3</sub> Films Stabilize Pt Dispersion, *Journal of the American Chemical Society*, **2020**, *142*, 10373-82.
6. Mao, X.; Foucher, A. C.; Stach, E. A.; Gorte R. J. Changes in Ni-NiO Equilibrium Due to LaFeO<sub>3</sub> and the Effect on Dry Reforming of CH<sub>4</sub>, *Journal of Catalysis*, **2020**, *381*, 561-69.
7. Mao, X.; Foucher, A.; Stach, E. A.; Gorte, R. J. “Intelligent” Pt Catalysts Based on Thin LaCoO<sub>3</sub> Films Prepared by Atomic Layer Deposition, *Inorganics*, **2019**, *7*, 113.
8. Lin, C.; Foucher, A. C.; Ji, Y.; Stach, E. A.; Gorte, R. J. “Intelligent” Pt Catalysts Prepared by Atomic Layer Deposition, *ACS Catalysis*, **2019**, *9*, 7318-27.
9. Mao, X.; Foucher, A.; Stach, E.; and Gorte, R. J. A Study of Support Effects for CH<sub>4</sub> and CO Oxidation Over Pd Catalysts on ALD-Modified Al<sub>2</sub>O<sub>3</sub>, *Catalysis Letters*, **2019**, *149*, 905-15.
10. Lin, C.; Jang, J.-B.; Zhang, L.; Stach, E. A.; Gorte, R. J. Improved Coking Resistance of “Intelligent” Ni Catalysts Prepared by Atomic Layer Deposition, *ACS Catalysis*, **2018**, *8*, 7679-87.
11. Onn, T. M.; Küngas, R.; Fornasiero, P.; Huang, K.; Gorte, R. J. Atomic Layer Deposition on Porous Materials: Problems with Conventional Approaches to Catalyst and Fuel Cell Electrode Preparation, *Inorganics*, **2018**, *6*, 34.
12. Onn, T. M.; Monai, M.; Dai, S.; Fonda, E. Montini, T.; Pan, X.Q.; Graham, G. W.; Fornasiero, P.; Gorte, R. J. Smart Pd Catalyst with Improved Thermal Stability Supported on High-Surface-Area LaFeO<sub>3</sub> Prepared by Atomic Layer Deposition, *J. Amer. Chem. Soc.*, **2018**, *140*, 4841-48.

**Electrocatalytic activity of Fe(IV) model compounds  $\text{La}_{1-x}\text{Sr}_x\text{FeO}_{3-\delta}$  for oxygen evolution reaction in alkaline solution**

Lauren F. Greenlee,<sup>1,2</sup> Clemens Heske,<sup>3,4</sup> Jingyi Chen,<sup>5</sup> Tadashi Ogitsu,<sup>6</sup> Lothar Weinhardt,<sup>3,4</sup> Monika Blum,<sup>7</sup> Geletu Qing,<sup>1</sup> Nan Jiang,<sup>3</sup> Sergio I. Perez Bakovic,<sup>1</sup> Stephen Faussett,<sup>3</sup> Jennifer Napoles<sup>3</sup>

<sup>1</sup>Ralph E. Martin Department of Chemical Engineering, University of Arkansas

<sup>2</sup>Department of Chemical Engineering, Pennsylvania State University

<sup>3</sup>Department of Chemistry and Biochemistry, University of Nevada, Las Vegas

<sup>4</sup>Institute for Photon Science and Synchrotron Radiation, Karlsruhe Institute of Technology

<sup>5</sup>Department of Chemistry and Biochemistry, University of Arkansas

<sup>6</sup>Quantum Simulations Group, Lawrence Livermore National Laboratory

<sup>7</sup>Advanced Light Source, Lawrence Berkeley National Laboratory

**Presentation Abstract**

Electrochemical water splitting provides a potential route to the scalable storage of renewable energy in the form of hydrogen chemical bonds. While the hydrogen and oxygen evolution reactions (HER and OER) are the two half reactions in water splitting, the latter is the main bottleneck in the process. Among various OER catalysts, Fe-doped  $\text{Fe}_x\text{Ni}_{100-x}\text{O}(\text{H})_y$  is considered as the benchmark experimental catalyst in alkaline media due to its high catalytic activity and low anticipated cost. The mechanism of OER on  $\text{Fe}_x\text{Ni}_{100-x}\text{O}(\text{H})_y$  catalysts is, however, far from fully understood. Recent density functional theory (DFT) calculations implicate Fe(IV) as part of a synergistic dual catalyst site (Fe(IV)-Ni(IV)) (Xiao *et al.*, *PNAS*, 2018). However, experimental evidence for Fe(IV) remains ambiguous. The major objective of this project is to determine Fe and O electronic and chemical structure in Fe(II), Fe(III), and Fe(IV) reference compounds and  $\text{Fe}_x\text{Ni}_{100-x}\text{O}(\text{H})_y$  electrocatalyst materials using cutting-edge soft x-ray spectroscopy, and also to develop a computational framework to describe the  $\text{Fe}_x\text{Ni}_{100-x}\text{O}(\text{H})_y$  electrocatalyst electronic structure. In this presentation, we report our preliminary results on the synthesis, characterization, and OER activity of a series of Fe(IV) reference compounds,  $\text{La}_{1-x}\text{Sr}_x\text{FeO}_{3-\delta}$ , in alkaline media. The  $\text{La}_{1-x}\text{Sr}_x\text{FeO}_{3-\delta}$  compounds were synthesized using a combustion method, and their crystalline structures were determined using x-ray diffraction and Rietveld refinement. The percentages of Fe(IV) and oxygen vacancies in the samples were determined using redox titration. The OER activity was evaluated in 1 M KOH, and a subset of the sample series was characterized with soft x-ray absorption spectroscopy (XAS) at the Advanced Light Source in Berkeley. The experimental electronic structure results have been discussed and transferred to enable DFT calculations of reference materials and catalysts.

**Grant or FWP Number: DE-SC0021308: In Pursuit of Unambiguous Determination of Fe(III) versus Fe(IV) in Transition Metal Oxide Electrocatalysts**

**PI:** Lauren F. Greenlee

**Co-PI(s):** Clemens Heske, Jingyi Chen

**Postdoc(s):** Geletu Qing, Nan Jiang

**Student(s):** Sergio I. Perez Bakovic, Stephen Faussett, Jennifer Napoles

## RECENT PROGRESS

### *Synthesis of $\text{La}_{1-x}\text{Sr}_x\text{FeO}_{3-\delta}$*

A sample series of  $\text{La}_{1-x}\text{Sr}_x\text{FeO}_{3-\delta}$  ( $x = 0.0, 0.2, 0.4, 0.6, 0.8, \text{ and } 1.0$ ) was synthesized using a combustion method.<sup>1</sup> Briefly, stoichiometric amounts of  $\text{La}(\text{NO}_3)_3 \cdot 6\text{H}_2\text{O}$ ,  $\text{Sr}(\text{NO}_3)_2$ , and  $\text{Fe}(\text{NO}_3)_3 \cdot 9\text{H}_2\text{O}$  were mixed with ethylenediaminetetraacetic acid and citric acid in 1 M  $\text{NH}_4\text{OH}$ , and then the solution pH was adjusted to 8.0 by adding 1 M  $\text{NH}_4\text{OH}$ . The solution mixture was stirred and heated on a hotplate until forming a gel, which was then calcined sequentially at 200 °C for 6 h, 900 °C for 5 h, and 1,300 °C for 4 h in air. The samples were cooled down at a rate of 5 °C/min after the last calcination step. The slow cooling rate allows the samples to take up oxygen from the atmosphere, leading to a (partial) filling of oxygen vacancies.<sup>2</sup>

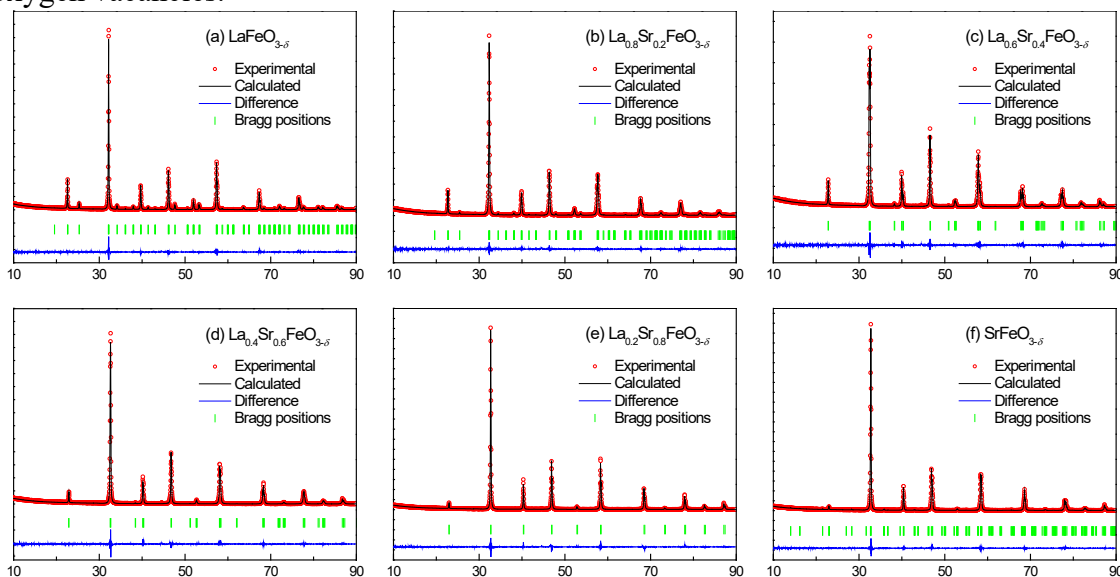


**Figure 1.** Rietveld refinement of the structural model for a series of  $\text{La}_{1-x}\text{Sr}_x\text{FeO}_{3-\delta}$  compounds. The red dots are the experimental data points, and the black curves are the calculated XRD patterns. The difference between the experimental data points and the calculated XRD patterns is shown in blue. Bragg reflections are indicated using green vertical lines.

### *Crystalline structure of $\text{La}_{1-x}\text{Sr}_x\text{FeO}_{3-\delta}$*

The XRD patterns of the  $\text{La}_{1-x}\text{Sr}_x\text{FeO}_{3-\delta}$  compounds match very well with those reported in the literature.<sup>2</sup> We used Rietveld refinement to extract structural parameters from the XRD patterns. The Rietveld refinement fits of the XRD patterns are shown in Figure 1, and the extracted structural parameters are listed in Table 1. All experimental patterns were fitted with reasonable accuracy, as indicated by  $\chi^2$  values between one and two (see Table 1). For Sr contents of 0.8 and 1.0, oxygen vacancies must be included in the model (*i.e.*,  $\delta > 0$ ) to achieve reasonable fit results. The amount of oxygen vacancies in the Rietveld refinement model was taken from reference patterns available in the Crystallography Open

Database. We also determined the exact amount of oxygen vacancies in the samples using titration, which will be introduced in the following section. The data in Table 1 show that the distance between Fe and O atoms decreases when  $x$  increases from 0.0 to 1.0. This trend indicates a gradual increase in the oxidation state of Fe,<sup>2</sup> which is also quantified using titration.

**Table 1.** Selected structural parameters (model, space group, lattice constants, and cell volume), goodness-of-fit ( $\chi^2$ ), and Fe-O bond lengths obtained from the Rietveld refinement of the  $\text{La}_{1-x}\text{Sr}_x\text{Fe(III)}_{1-y}\text{Fe(IV)}_y\text{O}_{3-\delta}$  sample series. The values of  $y$  and  $\delta$  obtained by titration are given in the last two rows.

Sample ( $x$ )	0.0	0.2	0.4	0.6	0.8	1.0
Model	$\text{LaFeO}_3$	$\text{La}_{0.8}\text{Sr}_{0.2}\text{FeO}_3$	$\text{La}_{0.6}\text{Sr}_{0.4}\text{FeO}_3$	$\text{La}_{0.4}\text{Sr}_{0.6}\text{FeO}_3$	$\text{La}_{0.2}\text{Sr}_{0.8}\text{FeO}_{2.94}$	$\text{SrFeO}_{2.75}$
Space group	$Pbnm$	$Pbnm$	$R-3c$	$R-3c$	$Pm-3m$	$Cmmm$
$a$ (Å)	5.5560	5.5521	5.5301	5.4989	3.8725	10.9596
$b$ (Å)	5.5666	5.5249				7.7144
$c$ (Å)	7.8558	7.8196	13.4294	13.4221		5.4743
$V$ (Å <sup>3</sup> )	242.96	239.87	355.67	351.48	58.07	462.84
$\chi^2$	1.41	1.29	1.56	1.64	1.85	1.59
<Fe-O> (Å)	Fe-O1: 2.0235 Fe-O1: 1.9849 Fe-O2: 2.0174	Fe-O1: 1.9986 Fe-O1: 1.9641 Fe-O2: 1.9915	Fe-O: 1.9660	Fe-O: 1.9484	Fe-O: 1.9362	Fe1-O1: 1.9346 Fe1-O3: 1.8824 Fe2-O2: 1.9383 Fe2-O3: 2.0002
$y$	$0.012 \pm 0.003$	$0.204 \pm 0.001$	$0.395 \pm 0.002$	$0.588 \pm 0.003$	$0.667 \pm 0.003$	$0.611 \pm 0.002$
$\delta$	$-0.006 \pm 0.002$	$-0.002 \pm 0.001$	$0.002 \pm 0.001$	$0.006 \pm 0.002$	$0.066 \pm 0.002$	$0.195 \pm 0.001$

#### ***Titrimetric determination of the values of $y$ and $\delta$ in $\text{La}_{1-x}\text{Sr}_x\text{Fe(III)}_{1-y}\text{Fe(IV)}_y\text{O}_{3-\delta}$***

The amounts of Fe(IV) and oxygen vacancies in the  $\text{La}_{1-x}\text{Sr}_x\text{Fe(III)}_{1-y}\text{Fe(IV)}_y\text{O}_{3-\delta}$  compounds are indicated by  $y$  and  $\delta$ , respectively. To obtain the values of  $y$  and  $\delta$ , we used the method of redox titration with Mohr's salt and cerium (IV) sulfate.<sup>3,4</sup> Each sample was measured three times, and the mean value of the data and the error bars were reported. The values of  $y$  and  $\delta$  obtained by titration are listed in the last two rows in Table 1. The titration results are highly reproducible since the standard errors are less than 0.004. We find an almost linear increase in  $y$  until  $x = 0.6$ . When  $x$  was further increased from 0.6 to 1.0,  $y$  first increased and then decreased. The amount of oxygen vacancies in the samples, indicated by  $\delta$ , first increased slowly when  $x$  was increased from 0.0 to 0.6 and then increased rapidly when  $x$  further increased from 0.6 to 1.0. These results demonstrate that, for Sr doping levels between 0.0 and 0.6, the content of Fe(IV) in the samples increases linearly with  $x$ , while the amount of oxygen vacancies in the samples remains close to zero. However, when the Sr doping level is further increased (i.e., from 0.6 to 1.0), significant amounts of oxygen vacancies were observed and, as a result, the content of Fe(IV) in the sample leveled off. The  $\text{La}_{1-x}\text{Sr}_x\text{FeO}_{3-\delta}$  compounds thus provide a series of reference materials containing different percentages of Fe(IV). Among them,  $\text{La}_{0.2}\text{Sr}_{0.8}\text{O}_{2.93}$  has the highest percentage of Fe(IV), reaching 67%.

## Electrochemical oxygen evolution activities of $\text{La}_{1-x}\text{Sr}_x\text{FeO}_{3-\delta}$ compounds

The electrochemical oxygen evolution activities of the  $\text{La}_{1-x}\text{Sr}_x\text{FeO}_{3-\delta}$  compounds were investigated in 1 M KOH solution using a three-electrode configuration. The working electrode was prepared by drop casting a catalyst ink composed of the  $\text{La}_{1-x}\text{Sr}_x\text{FeO}_{3-\delta}$  catalyst, water, isopropanol, and Nafion ionomer on a glassy carbon rotating disk electrode (catalyst loading  $0.25 \text{ mg/cm}^2$ ). A

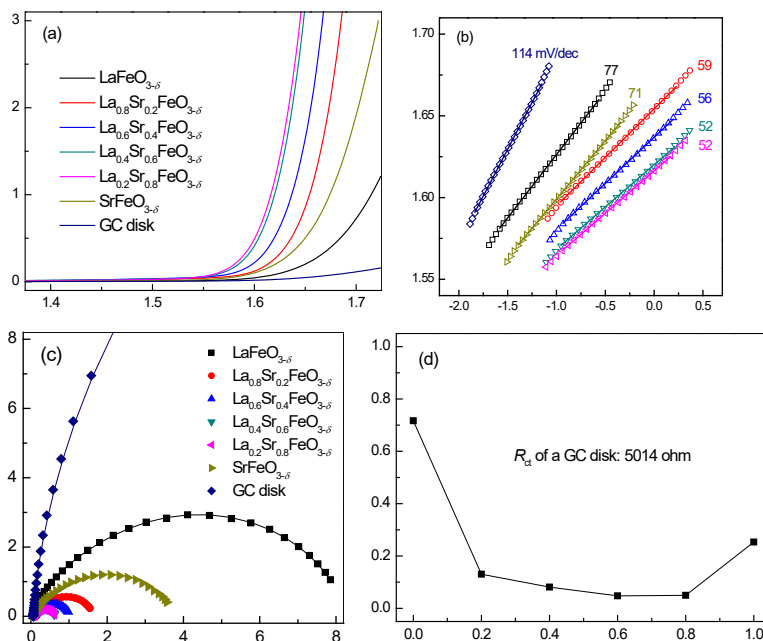


**Figure 2.** Oxygen evolution activities of the  $\text{La}_{1-x}\text{Sr}_x\text{FeO}_{3-\delta}$  catalysts in 1 M KOH. (a) Linear sweep voltammograms at 10 mV/s scan rate and 1,600 rpm rotation rate. (b) Tafel plots obtained from the LSV curves. (c) Electrochemical impedance spectra recorded at 0.73 V vs Hg/HgO and 1,600 rpm rotation rate. (d) The charge transfer resistances ( $R_{ct}$ ) obtained from the equivalent circuit fitting of the impedance data.

Hg/HgO (4.24 M KOH) electrode was used as the reference electrode and a graphite rod as the counter electrode. The electrolyte solution was purged with high-purity Ar for 10 min before the experiments, and the Ar flow was maintained above the electrolyte solution throughout. The Linear Sweep Voltammograms (LSVs) in Figure 2a demonstrate a swift increase in the oxygen evolution activity of the  $\text{La}_{1-x}\text{Sr}_x\text{FeO}_{3-\delta}$  catalysts when increasing the Sr content from 0.0 to 0.6. However, when the Sr content was further increased from 0.6 to 1.0, the oxygen evolution activity first increased slightly and then decreased significantly. The Tafel plots in Figure 2b show a similar trend: the Tafel slope first decreased when the Sr content increased from 0.0 to 0.6, and then increased when the Sr content increased from 0.8 to 1.0. The impedance spectra are shown in Figure 2c. The filled shapes are the experimental data points, and the curves are the calculated spectra using the equivalent circuit of  $R_s + Q_1/R_{ct} + Q_2/R_1$ , where  $R_s$  represents the solution resistance,  $Q_1/R_{ct}$  represents the double-layer capacitance and charge transfer processes, and  $Q_2/R_1$  represents the diffusion/adsorption of reaction intermediates in the porous structures between the catalyst particles.<sup>5</sup> Figure 2d shows the charge transfer resistances obtained from the equivalent circuit fitting. Like the LSV curves in Figure 2a and the Tafel plots in Figure 2b, the charge transfer resistance first decreased and then increased with the increase of Sr content from 0.0 to 1.0. These results demonstrate a strong correlation between the oxygen evolution activity and electronic structure (oxidation state, covalency, etc.) of Fe in  $\text{La}_{1-x}\text{Sr}_x\text{FeO}_{3-\delta}$ .

$x\text{Sr}_x\text{FeO}_{3-\delta}$ , prompting further experimental and theoretical investigations, in particular using soft x-ray absorption spectroscopy and DFT calculations.

### *Fe L-edge x-ray absorption spectroscopy of selected $\text{La}_{1-x}\text{Sr}_x\text{FeO}_{3-\delta}$ compounds*

The Fe oxidation state in the  $\text{La}_{1-x}\text{Sr}_x\text{FeO}_{3-\delta}$  compounds was examined by Fe L-edge x-ray absorption spectroscopy (XAS), as shown in Figure 3. The Fe L-edge XAS measurements were performed at the undulator beamline 8.0.1 of the Advanced Light Source (ALS) at Lawrence Berkeley National Laboratory (LBNL). Due to the ongoing COVID-19 pandemic, only one researcher (N. Jiang) was allowed at the beamline at any given time, and beamtime access was substantially limited, such that only a subset of the full  $\text{La}_{1-x}\text{Sr}_x\text{FeO}_{3-\delta}$  series could be analyzed. The Fe L-edge spectra were collected in total electron yield (TEY, Fig. 3) and fluorescence yield mode (FY, not shown) mode.

The spectra in Fig. 3 were normalized to the maximum of the  $L_3$  absorption edge. The spectra can be separated into two regions ( $L_3$  edge around 707 eV and  $L_2$  edge around 720 eV), resulting from the core-hole spin-orbit interaction. The Fe  $L_{2,3}$  lines are further split by atomic multiplet and crystal field effects.<sup>6</sup> The overall line shape of the Fe L-edge spectrum of  $\text{LaFeO}_{3-\delta}$  is consistent with Fe(III), i.e., with a  $t_{2g}^3e_g^2$  high-spin configuration.<sup>7</sup> As the Sr content is increased, the line shape of the Fe L-edges systematically changes, owing to an increase of the Fe oxidation state, from Fe(III) to Fe(IV). A distinct change of the resonance at  $\sim 708$  eV, in particular a shift and broadening, is observed for both  $\text{La}_{0.2}\text{Sr}_{0.8}\text{FeO}_{3-\delta}$  and  $\text{SrFeO}_{3-\delta}$  (marked by a vertical arrow in Fig. 3). This indicates that Fe(IV) is likely in a high spin state with a  $t_{2g}^3e_g^1$  configuration.<sup>8</sup> Overall, the spectra of  $\text{La}_{0.2}\text{Sr}_{0.8}\text{FeO}_{3-\delta}$  and  $\text{SrFeO}_{3-\delta}$  are broader than that of  $\text{LaFeO}_{3-\delta}$ , which is attributed to a superposition of the two oxidation states and an increasing covalency, implying the presence of Fe(IV) as well. Future experiments after the current ALS shutdown, likely to be scheduled at the end of 2021, will focus on additional members of the  $\text{La}_{1-x}\text{Sr}_x\text{FeO}_{3-\delta}$  sample series, as well as selected reference compounds to further allow for an experimental description of the electronic structure. In parallel, the existing data will be used to initiate DFT-based studies of the electronic structure of the  $\text{La}_{1-x}\text{Sr}_x\text{FeO}_{3-\delta}$  surfaces and their impact on the oxygen evolution reaction of these catalyst materials.

### References

1. Jung, J. I.; Risch, M.; Park, S., et al., *Energy & Environmental Science* **2016**, 9 (1), 176-183.
2. Haas, O.; Vogt, U. F.; Soltmann, C., et al., *Mater. Res. Bull.* **2009**, 44 (6), 1397-1404.
3. Blasco, J.; Aznar, B.; Garcia, J., et al., *Phys Rev B* **2008**, 77 (5).
4. Haavik, C.; Atake, T.; Stolen, S., *Physical Chemistry Chemical Physics* **2002**, 4 (6), 1082-1087.
5. Li, G. F.; Anderson, L.; Chen, Y. N., et al., *Sustain Energ Fuels* **2018**, 2 (1), 237-251.

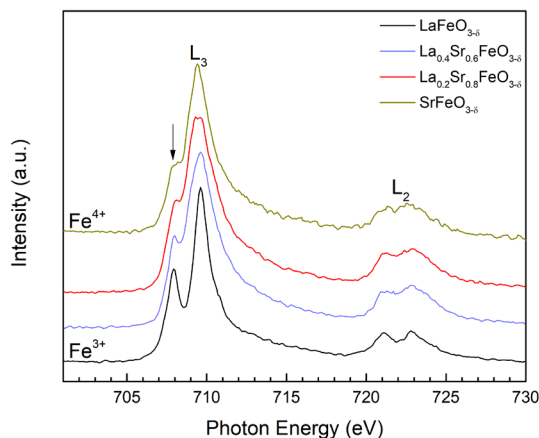


**Figure 3.** Fe  $L_{2,3}$ -edge soft x-ray absorption (XAS) spectra of selected samples from the  $\text{La}_{1-x}\text{Sr}_x\text{FeO}_{3-\delta}$  series (measured in total electron yield – TEY).

6. Abbate, M.; Zampieri, G.; Okamoto, J., et al., *Phys. Rev. B* **2002**, *65*, 165120.
7. Jana, S.; Panda, S. K.; Phuyal, D., et al., *Phys. Rev. B* **2019**, *99*, 075106.
8. Galakhov, V. R.; Kurmaev, E. Z.; Kuepper, K., et al., *J. Phys. Chem. C* **2010**, *114* (11), 5154-5159.

### **Publications Acknowledging this Grant in 2018-2021**

*No publications to date.*

### **Awards or leadership activities during 2018-2020 calendar years**

#### PI Greenlee

- Proposal Review Board, Catalysis Panel, Stanford Synchrotron Radiation Lightsource, 2020 - present
- International Conference on Catalysis, Session Co-Organizer & Co-Chair, Environmental Catalysis, June 2020
- Electrochemical Society, Programming/Planning Committee Member, Energy Technology Division
- Electrochemical Society, Symposium Chair/Organizer, Electrochemical Nitrogen Conversion & First Row Transition Metal Electrocatalysts for the OER
- Editorial Board, Chemical Engineering Journal
- 2020 Ralph E. Martin Dept. of Chemical Engineering Research Award
- 2019 Ralph E. Martin Leadership Chair, University of Arkansas
- 2018 University of Arkansas Dept. of Chemical Engineering research award

#### Co-PI Heske

- Founding Editor, IEEE Journal of Photovoltaics (JPV), Subject Area Characterization
- Chair, New Meetings Subcommittee, Materials Research Society (MRS)
- Member, Meetings Committee, Materials Research Society (MRS)
- Member, Users' Executive Committee, Advanced Light Source, Lawrence Berkeley National Lab

#### Co-PI Chen

- Member of Editorial Board of Nanoscale and Nanoscale Advances (RSC journals).
- Co-Organizer for Symposium: "Surface Chemistry of Colloidal Nanocrystals" at ACS Meeting, Orlando, Florida, 2019
- Spring 2020 Electrochemical Society meeting symposium focused on metal oxide electrocatalysts
- 2021 Nolan Faculty Award, Fulbright College of Arts and Sciences, University of Arkansas

T. Brent Gunnoe

**Development of Transition Metal Catalysts for the Functionalization of Carbon-Hydrogen Bonds: Fundamental Studies of Catalytic Hydroarylation of Olefins**

T. Brent Gunnoe<sup>a</sup>, Weihao Zhu<sup>a</sup>, Xiaofan Jia<sup>a</sup>, Marc T. Bennett<sup>a</sup>, Lucas I. Frye<sup>a</sup>, Junqi Chen<sup>a</sup>, Hannah E. Ketcham,<sup>a</sup> Charles B. Musgrave III<sup>b</sup>, William A. Goddard III<sup>b</sup>

<sup>a</sup> Department of Chemistry, University of Virginia

<sup>b</sup> Materials & Process Simulation Center, California Institute of Technology

**Presentation Abstract**

The ability to selectively manipulate C–H bonds of arenes, alkanes and more complex organic molecules would open the door to a wide range of useful synthetic transformations. For example, the addition of aromatic C–H bonds across olefin C=C bonds, olefin hydroarylation, provides an atom economical reaction with broad potential including applications in both commodity scale processes as well as fine chemical synthesis. We have been studying olefin hydroarylation (to produce alkyl aromatics) and oxidative olefin hydroarylation (to produce alkenyl aromatics) catalyzed by well-defined Ru, Rh, Pd, Pt and Ir catalysts. The research effort is focused on four objectives: **Objective 1.** Mechanistic studies of Rh catalyzed arene alkenylation. **Objective 2.** With the success of Rh catalysis with "capping arene" ligands, we have extended studies of catalysis with ligated Rh catalysts. **Objective 3.** We have observed arene alkenylation using simple Pd(II) catalyst precursors. We are comparing features of Rh and Pd catalysis in order to understand differences in rates, selectivity and catalyst longevities. **Objective 4.** We have extended our studies of C–H functionalization reactions in three directions, including a) catalytic production of stilbenes, b) alkenylation of toluene using substituted olefins, and c) development of catalytic arene alkenylation with only air as the oxidant.

**Grant Number:** DE-SC0000776

**Grant Title:** Development of Transition Metal Catalysts for the Functionalization of Carbon-Hydrogen Bonds: Fundamental Studies of Catalytic Hydroarylation of Olefins

**PI:** T. Brent Gunnoe

**Postdocs:** N/A

**Students:** Weihao Zhu (G), Xiaofan Jia (G), Junqi Chen (G), Zhongwen Luo (G), Lucas Frye (U), Hannah Ketcham (G), Marc Bennett (G)

**Collaborators:** William Goddard III (California Institute of Technology), Robert Davis (University of Virginia), Sen Zhang (University of Virginia)

## RECENT PROGRESS

**Objective 1.** Continue mechanistic studies of Rh catalyzed arene alkenylation using  $[Rh(\mu-OAc)(\eta^2\text{-ethylene})_2]_2$  as catalyst precursor. Here, we will focus on understanding the early stages of the reaction, delineating the factors that control initial reduction of Rh followed by re-dissolving, and identifying catalyst intermediates. In our most recent studies, we have used a combined experimental and computational study focused on the mechanism

of oxidative conversion of benzene and ethylene to styrene using  $[(\eta^2\text{-C}_2\text{H}_4)_2Rh(\mu-OAc)]_2$  as the catalyst precursor in the presence of  $Cu(OPiv)_2$  (OPiv = pivalate). Using  $[(\eta^2\text{-C}_2\text{H}_4)_2Rh(\mu-OAc)]_2$  as the catalyst precursor, ~411 turnovers of styrene are observed after 1 hour, giving an apparent turnover frequency of  $\sim 0.11\text{ s}^{-1}$  (calculated assuming the binuclear structure is maintained in the active catalyst). We identified the catalyst resting state to be  $[(\eta^2\text{-C}_2\text{H}_4)_2Rh^I(\mu-OPiv)_2]_2(\mu-Cu)$  (Figure 1), which is a molecular complex in which a central  $Cu^{II}$  atom bridges two Rh moieties. At high Rh concentration in the presence of  $Cu(OPiv)_2$  and pivalic acid (HOPiv), the trinuclear complex  $[(\eta^2\text{-C}_2\text{H}_4)_2Rh^I(\mu-OPiv)_2]_2(\mu-Cu)$  converts to the binuclear Rh(II) complex  $[(HOPiv)Rh^{II}(\mu-OPiv)_2]_2$ ,

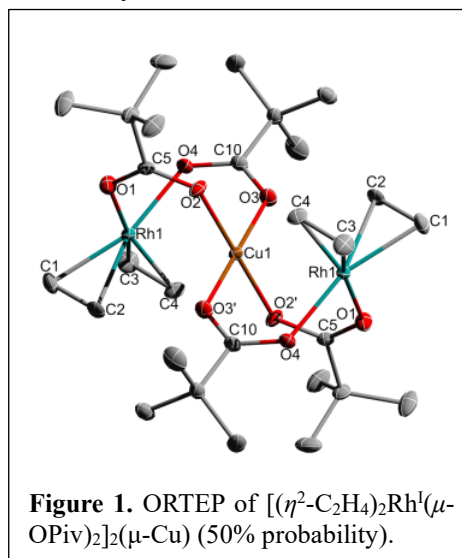


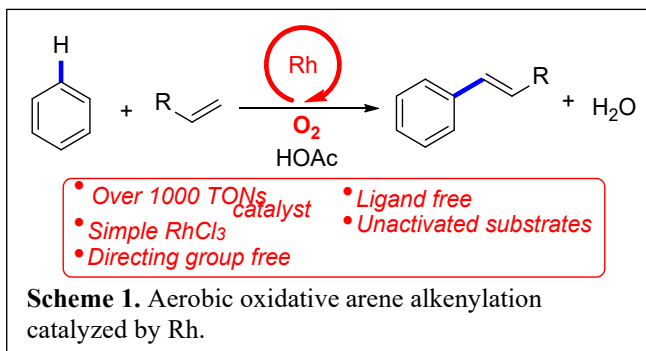
**Figure 1.** ORTEP of  $[(\eta^2\text{-C}_2\text{H}_4)_2Rh^I(\mu-OPiv)_2]_2(\mu-Cu)$  (50% probability).

which has been identified by  $^1H$  NMR spectroscopy and single crystal X-ray diffraction. The binuclear Rh(II)  $[(HOPiv)Rh^{II}(\mu-OPiv)_2]_2$  is not a catalyst for styrene production, but under catalytic conditions  $[(HOPiv)Rh^{II}(\mu-OPiv)_2]_2$  can be *partially* converted to the active catalyst, the Rh-Cu-Rh complex  $[(\eta^2\text{-C}_2\text{H}_4)_2Rh^I(\mu-OPiv)_2]_2(\mu-Cu)$ , following an induction period of ~6 hours. Using quantum chemical calculations (Goddard group), we sampled possible mononuclear and binuclear Rh species, finding that the binuclear Rh(II)  $[(HOPiv)Rh^{II}(\mu-OPiv)_2]_2$  paddle-wheel is a low energy global minimum, which is consistent with experimental observations that  $[(HOPiv)Rh^{II}(\mu-OPiv)_2]_2$  is not a catalyst for styrene formation. Further, we investigated the mechanism of styrene production starting from  $[(\eta^2\text{-C}_2\text{H}_4)_2Rh^I(\mu-OAc)]_2(\mu-Cu)$ ,  $[(\eta^2\text{-C}_2\text{H}_4)_2Rh(\mu-OAc)]_2$ , and  $(\eta^2\text{-C}_2\text{H}_4)_2Rh(\kappa^2\text{-OAc})$ . For all reaction pathways studied, the predicted activation barriers for styrene formation from  $[(\eta^2\text{-C}_2\text{H}_4)_2Rh(\mu-OAc)]_2$  and  $(\eta^2\text{-C}_2\text{H}_4)_2Rh(\kappa^2\text{-OAc})$  are too high compared to experimental kinetics. In contrast, the overall activation barrier for styrene formation predicted by DFT from the Rh-Cu-Rh complex  $[(\eta^2\text{-C}_2\text{H}_4)_2Rh^I(\mu-OPiv)_2]_2(\mu-Cu)$  is in agreement with experimentally determined rates of catalysis. Based on these results, we conclude that incorporation of Cu(II) into the active Rh-Cu-Rh catalyst reduces the activation barrier for benzene C–H activation, O–H reductive elimination, and ethylene insertion into the Rh–Ph bond.

In collaboration with the Davis group (UVA, Chemical Engineering), we focused on the synthesis of supported Rh materials and study of their efficacy as pre-catalysts for the oxidative alkenylation of arenes. Rhodium particles supported on silica (Rh/SiO<sub>2</sub>; ~3.6 wt% Rh) and on nitrogen-doped carbon (Rh/NC; ~1.0 wt% Rh) were synthesized and tested. Heating mixtures of Rh/SiO<sub>2</sub> or Rh/NC with benzene and ethylene or  $\alpha$ -olefins and CuX<sub>2</sub>

{X = OPiv (trimethylacetate) or OHex (2-ethyl hexanoate)} to 150 °C results in the production of alkenyl arenes. When using Rh/SiO<sub>2</sub> or Rh/NC as catalyst precursor, the conversion of benzene and propylene or toluene and 1-pentene yields a ratio of anti-Markovnikov to Markovnikov products that is nearly identical to the same ratios as the molecular catalyst precursor [Rh(μ-OAc)(η<sup>2</sup>-C<sub>2</sub>H<sub>4</sub>)<sub>2</sub>]<sub>2</sub>. These results and other observations are consistent with the formation of active catalysts by leaching of soluble Rh from the supported Rh materials.

We studied oxidative conversion of unactivated arenes and alkenes to alkenyl arenes using unpurified air or purified dioxygen as the only oxidant (Scheme 1). This method uses RhCl<sub>3</sub> salt as the catalyst precursor and avoids the use



of co-oxidants such as Cu(II). The use of dioxygen as the *in situ* oxidant gives water as the only by-product of the alkenylation reaction. Conditions to achieve > 1000 turnovers of alkenyl benzene products have been developed. As the catalysis progresses, oxidation of styrene product to form benzaldehyde becomes competitive. Compared to the Rh catalysis using Cu(II) oxidants, the aerobic reactions give decreased reaction rate and reduced anti-Markovnikov/Markovnikov selectivity when using α-olefins. For styrene formation, the reaction rate shows a first-order dependence on catalyst concentration, ethylene concentration (with saturation at higher ethylene concentrations), and dioxygen. An intermolecular kinetic isotope effect value of 2.7(6) was determined from parallel reactions with C<sub>6</sub>H<sub>6</sub> versus C<sub>6</sub>D<sub>6</sub>. Synthesis of trans-stilbene and pentenyltoluenes have been demonstrated using this Rh-catalyzed aerobic alkenylation reaction.

**Objective 3.** *We have observed arene alkenylation using simple Pd(II) catalyst precursors. In the next funding period, we propose to study and compare the Rh and Pd catalysis in order to begin to understand the differences in rates, selectivity and catalyst longevities.*

[M]	Allylbenzene (TOs)	β-transmethylstyrene (TOs)	β-cismethylstyrene (TOs)	α-methylstyrene (TOs)	Linear: Branched Ratio
Pd(OAc) <sub>2</sub>	3.4(3)	59(4)	0.3(1)	13(2)	5:1
[Rh(η <sup>2</sup> -C <sub>2</sub> H <sub>4</sub> ) <sub>2</sub> (μ-OAc)] <sub>2</sub>	32(3)	26(1)	4.8(1)	6.6(1)	10:1

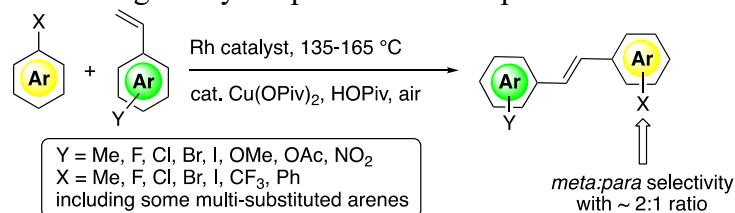
**Table 1.** Selectivity for catalytic conversion of benzene and propylene (25 psig) using [Rh(μ-OAc)(η<sup>2</sup>-C<sub>2</sub>H<sub>4</sub>)<sub>2</sub>]<sub>2</sub> or Pd(OAc)<sub>2</sub> (0.001 mol %) at 150 °C with 240 equivalents of Cu(OPiv)<sub>2</sub>.

We expanded our studies of oxidative ethylene hydrophenylation to include the use of Pd(OAc)<sub>2</sub> as catalyst precursor. A newly discovered Pd(OAc)<sub>2</sub>-catalyzed process converts the byproduct vinyl ester and benzene to styrene, which allows catalytic styrene formation with > 85% selectivity and with > 2400 TOs. We have investigated the differences in

alkenylation of benzene using propylene. Four alkenylated products are observed: allylbenzene,  $\beta$ -trans-methylstyrene,  $\beta$ -cis-methylstyrene and  $\alpha$ -methylstyrene. There are two primary differences for Pd vs. Rh catalysis. First, the L:B ratio (L = anti-Markovnikov products, B = Markovnikov product) for Rh catalyzed reactions is greater than the Pd catalyzed process. Representative data from a reaction with 25 psig propylene at 150 °C are shown in Table 1. Also, the ratio of allylbenzene to  $\beta$ -trans-methylstyrene varies greatly for Rh (1.2) and Pd (0.06).

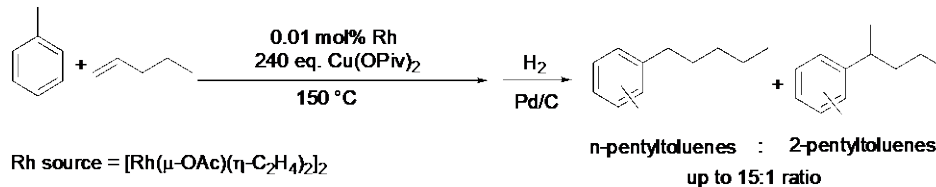
**Objective 4.** We will extend our studies of C–H functionalization reactions in three directions, including a) catalytic production of stilbenes, b) alkenylation of toluene using  $\alpha$ -olefins, and c) development of catalytic arene alkenylation with only air as the oxidant.

We have developed a method based on our Rh-catalyzed arene alkenylation chemistry to convert arenes and vinyl arenes to stilbene and stilbene derivatives (Scheme 3). The synthesis involves direct C–H activation, eliminating the need for additional steps to install leaving or directing groups, thereby reducing stoichiometric waste. A sub-stoichiometric amount of Cu(II) carboxylate is used as a direct oxidant, which is regenerated by dioxygen from air, making dioxygen the terminal oxidant. We have also investigated catalysis using a wide range of arenes with different functional groups. This catalysis shows tolerance to functionalities including fluorine, chlorine, trifluoromethyl, ester, nitro, acetoxy, cyano and ether groups. We compared Rh catalysis with Pd and found that Rh catalysis has better halo group tolerance and higher selectivity for *meta* functionalization. Resveratrol and DMU-212 [(*E*)-1,2,3-trimethoxy-5-(4-methoxystyryl)benzene] were synthesized from this single-step approach, and it has been demonstrated that this synthetic method can be used in gram-scale synthesis using a very simple reaction setup.



**Scheme 3.** Stilbene and derivatives production by aerobic Rh-catalyzed alkenylation reaction.

We demonstrated successful alkenylation of toluene with 1-pentene to form pentenyltoluenes using  $[\text{Rh}(\mu\text{-OAc})(\eta^2\text{-C}_2\text{H}_4)_2]_2$ . The process is selective for anti-Markovnikov products in a ratio up to 11:1 for 1-pentenyltoluenes:2-pentenyltoluenes. The process favors the production of *meta*- and *para* substituted pentenyltoluenes with a *meta*:*para* ratio of  $\sim$ 7:3. These results are significant in terms of potential applications as 1-pentenyltoluenes and 2-pentenyltoluenes can undergo a ring-closure reaction to form bicyclic products, while the 3-pentenyltoluenes are susceptible to fragmentation under ring closing conditions.



**Scheme 4.** Alkenylation of toluene with 1-pentene to form *n*-pentenyltoluenes and 2-pentenyltoluenes (Rh =  $[\text{Rh}(\mu\text{-OAc})(\eta^2\text{-C}_2\text{H}_4)_2]_2$ ). For clarity, substitution is presented as variable; *m*-, *p*-, and *o*-*n*-pentenyltoluenes form as do *m*- and *p*-2-pentenyltoluenes.

## Publications Acknowledging this Grant in 2018-2021

### I. Intellectually led by this grant

1. Chen, J., Nielsen, R. J.\*, Goddard III, W. A., McKeown, B. A., Dickie, D. A., Gunnoe, T. B.\* "Catalytic Synthesis of Super Linear Alkenyl Arenes Using a Rh(I) Catalyst Supported by a "Capping Arene" Ligand: Access to Aerobic Catalysis" *J. Am. Chem. Soc.* **2018**, *140*, 17007-17018. DOI: 10.1021/jacs.8b07728
2. Zhu, W., Luo, Z., Chen, J., Liu, C., Yang, L., Dickie, D. A., Liu, N., Zhang, S., Davis, R. J., Gunnoe, T. B.\* "Mechanistic Studies of Single-Step Styrene Production Catalyzed by Rh Complexes with Diimine Ligands: An Evaluation of the Role of Ligands and Induction Period" *ACS Catalysis* **2019**, *9*, 7457-7475. DOI: 10.1021/acscatal.9b01480
3. Jia, X., Foley, A. M., Liu, C., Vaughan, B. A., McKeown, B. A., Zhang, S., Gunnoe, T. B.\* "Styrene Production from Benzene and Ethylene Catalyzed by Palladium(II): Enhancement of Selectivity towards Styrene via Temperature Dependent Vinyl Ester Consumption" *Organometallics* **2019**, *38*, 3532-3541. DOI: 10.1021/acs.organomet.9b00349 (manuscript was selected for the issue cover)
4. Liebov, N. S., Zhu, W., Chen, J., Webster-Gardiner, M. S., Schinski, W. L., Gunnoe, T. B.\* "Rhodium-Catalyzed Alkenylation of Toluene using 1-Pentene: Regioselectivity to Generate Precursors for Bicyclic Compounds" *Organometallics* **2019**, *38*, 3860-3870. DOI: 10.1021/acs.organomet.9b00535
5. Zhu, W., Gunnoe, T. B.\* "Advances in Rhodium Catalyzed Oxidative Arene Alkenylation" *Acc. Chem. Res.* **2020**, *53*, 920-936. DOI: 10.1021/acs.accounts.0c00036
6. Jia, X., Frye, L. I., Zhu, W., Gu S., Gunnoe, T. B.\* "Synthesis of Stilbenes by Rhodium-Catalyzed Aerobic Alkenylation of Arenes via C-H Activation" *J. Am. Chem. Soc.* **2020**, *142*, 10534-10543. DOI: 10.1021/jacs.0c03935
7. 151. "Rhodium-Catalyzed Arene Alkenylation Using Only Dioxygen as Oxidant" Zhu, W., Gunnoe, T. B.\* *ACS Catal.* **2020**, *10*, 11519-11531. DOI: 10.1021/acscatal.0c03439
8. "Transition Metal-Catalyzed Arene Alkylation and Alkenylation: Catalytic Processes for the Generation of Chemical Intermediates" Gunnoe, T. B.\*, Schinski, W. L.\*, Jia, X. *ACS Catal.* **2020**, *10*, 14080-14092. DOI: 10.1021/acscatal.0c03494
9. "Oxidative Alkenylation of Arenes Using Supported Rh Materials: Evidence that Active Catalysts are Formed by Rh Leaching" Luo, Z., Whitcomb, C., Kaylor, N., Zhang, Y., Zhang, S., Davis, R. J.\*, Gunnoe, T. B.\* *ChemCatChem* **2021**, *13*, 260-270. DOI: 10.1002/cctc.202001526

10. "Advances in Group 10 Transition Metal-Catalyzed Arene Alkylation and Alkenylation" Zhu, W., Gunnoe, T. B.\* *J. Am. Chem. Soc.* **2021**, *143*, 6746-6766. DOI: 10.1021/jacs.1c01810
11. "Mechanistic Studies of Styrene Production from Benzene and Ethylene using [Rh( $\mu$ -OAc)( $\eta^2$ -C<sub>2</sub>H<sub>4</sub>)<sub>2</sub>]<sub>2</sub> as Catalyst Precursor: Identification of a Bis-Rh<sup>I</sup> Mono-Cu<sup>II</sup> Complex as Catalyst" Musgrave III, C. B., Zhu, W., Coutard, N., Ellena, J. F., Dickie, D. A., Gunnoe, T. B.\*, Goddard III\*, W. A. *ACS Catal.* **2021**, *11*, 5688-5702. DOI: 10.1021/acscatal.1c01203

**II. Jointly funded by this grant and other grants with intellectual leadership by other funding sources**

None

**Awards or leadership activities during 2018-2020 calendar years**

Leadership Activities

Co-chair, BES/Catalysis Science PI meeting	9/21
Executive Editor, <i>ACS Catalysis</i>	3/21 – present
Interim Editor in Chief, <i>ACS Catalysis</i>	8/20 – 2/21
Management Review Panel for the U.S. Department of Energy Office of Basic Energy Sciences Energy Frontier Research Center	3/19
Inaugural Associate Editor, <i>ACS Catalysis</i>	12/10 – 8/20

Awards/recognition

Invited Speaker Catalysis Gordon Conference	2018
Keynote lecture in the Unconventional Catalysis – Target Stable Molecules symposium, 255 <sup>th</sup> ACS National Meeting	2018
Commonwealth Professor of Chemistry	8/17 – present

**John F. Hartwig**

**Catalysis Program at Lawrence Berkeley National Laboratory:  
Harnessing Complexity for Catalytic Efficiency**

John F. Hartwig-Program Leader, Polly L. Arnold, Alexis T. Bell, Robert G. Bergman (affiliate), Christopher J. Chang, Michelle C. Chang, Kenneth N. Raymond (affiliate), Miquel B. Salmeron, Gabor A. Somorjai (affiliate), T. Don Tilley, F. Dean Toste, Peidong Yang  
Chemical Sciences Division, Lawrence Berkeley National Laboratory

**Presentation Abstract**

The LBNL Catalysis Program seeks to reveal foundational principles for the creation of new catalysts, realization of new processes, and creation of new approaches to learn how catalysts operate. The overarching theme of the current research is to reveal and exploit complexity inherent in, or designed to be a part of, catalytic systems that operate with high rates and selectivity. The types of catalysts and catalytic reactions studied in the current Catalysis Program, and the classes of mechanisms by which the catalysts react, are broad in scope, but converge on several themes that constitute the three subtasks. These three subtasks are organized by layers of complexity. The first subtask reveals and creates multiple functionality in a single active site; the second reveals and creates new catalytic systems that involve multiple catalytic sites that work cooperatively or that convert from one to another; the third subtask focuses on catalytic systems in which two components, one the active site and one the supramolecular confines of that site, work cooperatively to change the course of the catalytic transformation. Each of these subtasks directly addresses PROs in workshop reports on catalysis and cross-cutting themes of the BES CSGB division.

**FWP Number: CH030201**

**FWP Title: Program in Catalysis and Chemical Transformations – Harnessing Complexity for Catalytic Efficiency**

**Postdoc(s):** Eva Jingjing Ge, Mina Narouz, Hao Chen, Addison N. Desnoyer, Dustin Bornemann, Stefan Alexander Kuenzi, Laurent Severy, Mufan Li,

**Student(s):** Lance Bettinson, Branden Leonhardt, Patricia Lizeth De La Torre, Jeffrey Derrick, Jason Fang, Elijah Kissman, Jeremy Nicolai, Brandon Bloomer, Steven Hanna, Yehao Qiu, Alex Wheeler, Mathew See, Jose Martinez, Stephen Bierschenk, Elizabeth Dawn Heafner, Kelly Xia, Banruo Huang, Sheena Louisia, Shouping Chen, Wesley Chuang, Chubai Chen, Sunmoon Yu

**Staff Scientists(s):** Miao Zhang, Chithra Asokan, Ji Su, Liang Qi, Ji Yang

**RECENT PROGRESS**

**Subtask 1. Multifunctional Catalyst Systems for Selective Transformations**

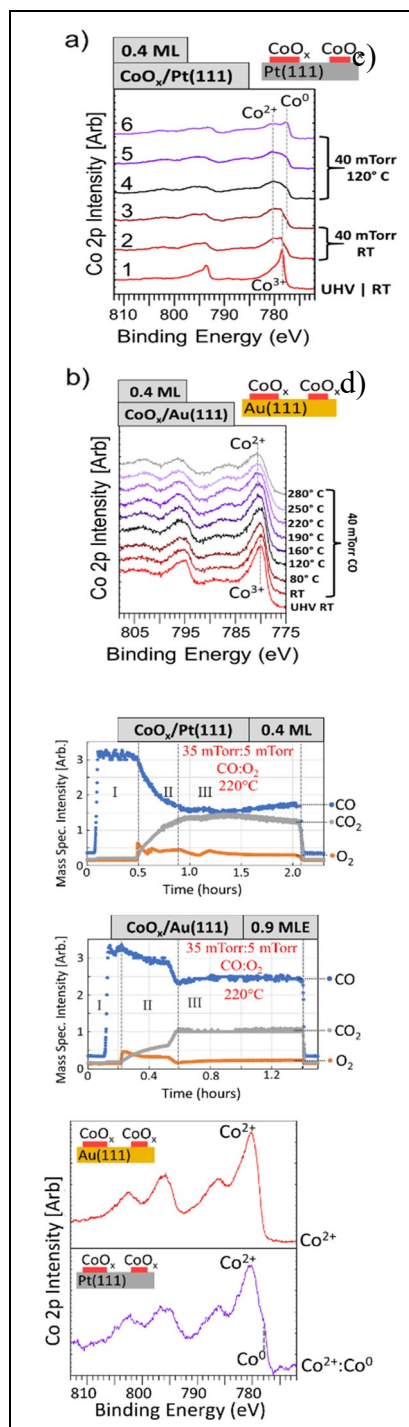
Subtask 1 focuses on the creation of multi-functional catalysts in which multiple interactions in the second coordination sphere or multiple metal centers within the coordination sphere impart a major influence on the activity and selectivity of the system.

Such control includes the influence of secondary, non-covalent interactions on catalyst activity and selectivity, the effect of a second (or more) metal center on the electronic properties of the active site, or multimetallic interactions that enable transformations that would be difficult or impossible to achieve with a simple active site. These catalysts are being applied to transformations such as additions to alkenes, isomerization of alkenes, reductions of carbon dioxide, and functionalization of hydrocarbons, which are crucial to efficient use of multiple feedstocks. Novel spectroscopic methods and reactor systems are being applied to monitor these processes as they are occurring, and modern theoretical methods are being used to interpret spectral data, to help elucidate reaction mechanisms, and to understand data on rates and selectivities. A selection of projects and recent results are described in the next sections.

### 1.1 Strong Metal-Support Interaction (Salmeron/Somorjai)

Salmeron has continued studies of the  $\text{CoO}_x$ -Au and  $\text{CoO}_x$ -Pt SMSI using an inverse support catalyst system to determine the identity and properties of the active site. Literature studies have assigned the active site to the interface periphery of the active noble metal and the support oxide. By comparing the activities for the catalytic oxidation of CO to  $\text{CO}_2$  on Pt and Au, the role of the noble metal separates from that of the support. To do so, Salmeron used a system in which small islands of  $\text{CoO}_x$  ( $x=1, 1.33, 2$ ) deposited on Pt and Au, provide interfaces between the noble metal and the oxide. The islands (atomic layer thick) were found to be more active on Pt than on Au, but the reactivity of the Au- $\text{CoO}_x$  remains substantial, corroborating the hypothesis that the  $\text{Co}^{n+}$  in  $\text{CoO}_x$  is activated by contact with the electronegative Au and Pt noble metal. Figure 1.1 a&b shows the evolution of the Pt&Au/ $\text{CoO}_x$  catalysts (APXPS) during the reaction. Figure 1.1 c&d shows the reactants and products detected by mass-spectroscopy,

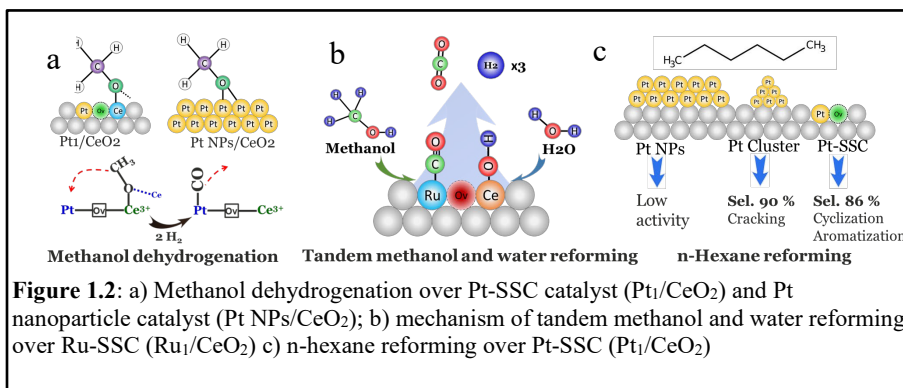
simultaneously with detection of the catalyst chemical state by APXPS (*in operando*). These experiments, interrupted during the pandemic shut-down, are now being resumed at NSLS-II (Brookhaven), SSRL (SLAC, Stanford), and the ALS.



## 1.2 Single Metal Atom-Support Interaction Create “Ensemble Reaction Pool” (Somorjai/Salmeron)

Somorjai’s group demonstrated an ensemble S1-Vo-S2 site with incorporated single metal(S1), neighboring oxygen vacancy(Vo), and unsaturated support metal ion(S2) can be prepared on reducible metal oxide supported single site catalyst. The S1-Vo-S2 as an “ensemble reaction pool” (ERP) create synergistic effects and favor the adsorption, activation, reaction and desorption of the reactant, intermediate and product.

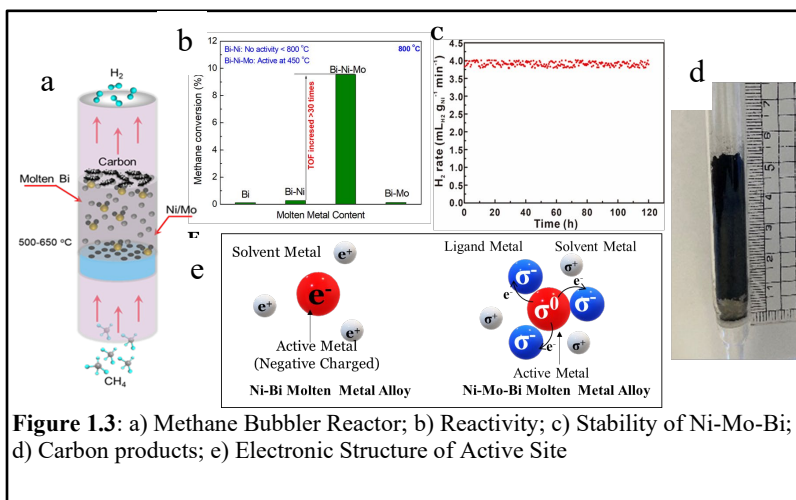
For example, the synergistic effect between single Pt-O vacancy-unsaturated Ce atom promoted the dissociation rate of methanol for 40 to 800 times higher than Pt nanoparticle catalysts (Figure 1.2a). They also demonstrated the “ERP” created by the single Ru-O vacancy-unsaturated Ce atom enhanced the activity and selectivity (up to 9360 mol H<sub>2</sub> per



mol Ru per hour with 99.5 % CO<sub>2</sub> selectivity) in tandem methanol and water reforming (methanol decomposition and subsequent water gas shift reaction), Figure 1.2b. Likewise, the synergy of the Pt ion and O vacancy could also modify the reaction pathway and catalyze the cyclization and aromatization of linear hydrocarbons with high selectivity (>86 %) (Figure 1.2c). That provide new knowledge for hydrocarbon refinery and polyethylene upcycling. This study paves the way for the further rational design of single site catalysts at the atomic scale.

## 1.3 Developing Catalysis System in Molten Metal for Methane Pyrolysis (Somorjai)

Study of molten metal for methane pyrolysis has demonstrated that the ternary molten metal catalyst (Ni-Mo in Bi solution) can drive down initial reaction temperature of methane pyrolysis from 1000 °C to 450 °C, Figure 1.3. With the same reaction conditions, our ternary molten metal catalyst (Ni-Mo-Bi) is 30 times faster than the previous study with molten Ni-Bi as catalyst. Results showing that, the Ni-Mo-

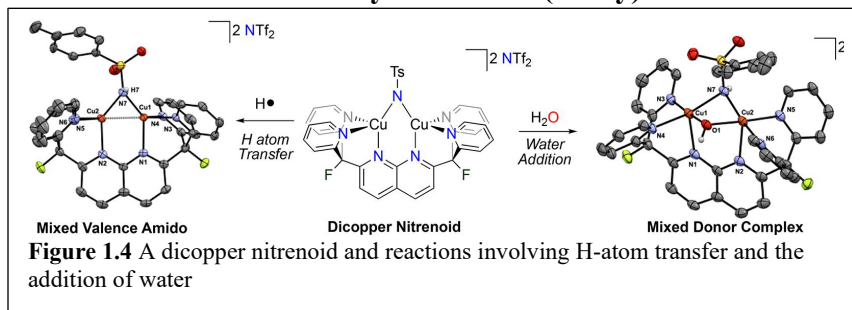


Bi solution) can drive down initial reaction temperature of methane pyrolysis from 1000 °C to 450 °C, Figure 1.3. With the same reaction conditions, our ternary molten metal catalyst (Ni-Mo-Bi) is 30 times faster than the previous study with molten Ni-Bi as catalyst. Results showing that, the Ni-Mo-

Bi molten metal alloys created a uniform catalysis system with Ni as the active metal, Mo as the ligand metal and Bi as the solution metal. The interaction of Mo with Ni distributed the negative charge among the Ni-Mo complex and created a highly active site for methane pyrolysis at low temperature.

#### 1.4 Studies on Well-Defined Multimetallic Catalytic Centers (Tilley)

Tilley has prepared well-defined models for multimetallic catalysts to gain insights into the influence of multiple metals on the reaction

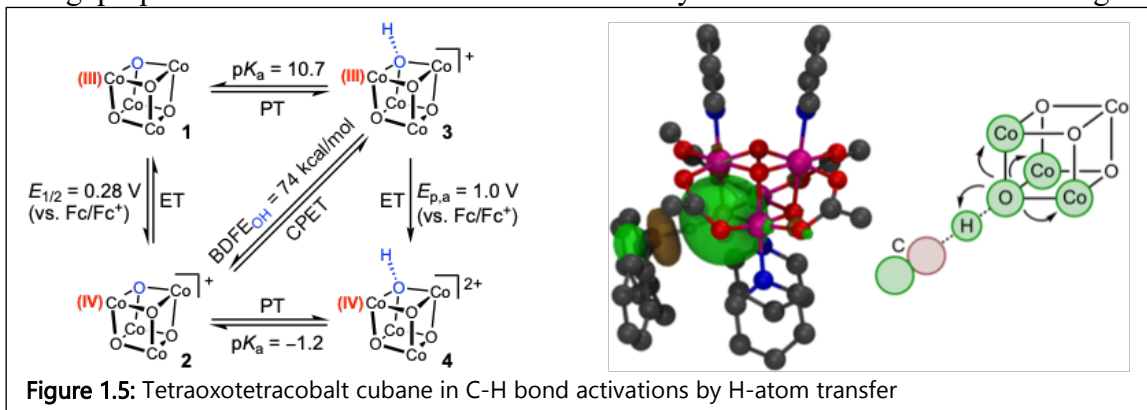


mechanisms. In one

direction toward this goal, they have prepared and investigated the reactivity of well-defined bimetallic systems supported by binucleating naphthyridine-based ligands. This work has led to synthesis of a dicopper nitrenoid complex, formed *via* oxidation of an acetonitrile-bridged dicopper(I) precursor with an iminoiodinane (Figure 1.4). Copper nitrenoids are often invoked as intermediates in copper-catalyzed amination and aziridination reactions, but have rarely been experimentally observed. The complex they prepared is highly reactive, readily abstracting hydrogen atoms from a variety of sources to form a mixed valence Cu(I)/Cu(II) dicopper amido complex. Reactivity studies demonstrate that the source of H atoms can be either solvent (such as THF) or the acetonitrile that acts as a bridging ligand in the starting material. They have found that use of a CO-bridged dicopper(I) complex as starting material (*i.e.* where the bridging ligand does not contain C-H bonds) allows for facile generation of this nitrenoid complex *in situ*. NMR methods demonstrate that the nitrenoid has a triplet configuration, and density function theory calculations (with Tom Cundari) were performed to examine the electronic structure of this unusual species. Spin localization calculations reveal that the complex is best described as an iminyl (NR radical anion) moiety coupled to a mixed valence Cu(I)/Cu(II) core. Notably, the nitrenoid was found to react rapidly with water at low temperatures to form a mixed donor hydroxo/amido dicopper(II) complex, which was characterized by standard methods, including X-ray crystallography iminoiodinane (Figure 1.4). As the mixed donor complex resembles intermediates proposed in Chan-Evans-Lam coupling, they explored reactivity with a variety of transmetalation reagents, and found that treating the mixed donor complex with the Grignard reagent  $\text{MgPh}_2(\text{THF})_2$  resulted in the formation of a number of organic products consistent with successful C-X coupling (X = O or N), illustrating that both reduction of dicopper(II) to dicopper(I) and concomitant C-X bond formation are feasible.

### 1.5 Stabilization of Reactive Co<sub>4</sub>O<sub>4</sub> Cubane Catalysts (Tilley)

Simultaneous proton- and electron-transfer mechanisms (concerted proton-electron transfer, CPET) facilitate key biological and synthetic oxidation processes. These catalytic processes have inspired significant advances in the rich chemistry of high-valent oxo complexes of manganese, iron, and copper in the last few decades. In contrast, a dearth of CPET reactivity with oxocobalt complexes has been established, especially for highly oxidized complexes with formal oxidation states greater than three and despite such species being proposed as reactive intermediates in catalytic oxidation of water and organic



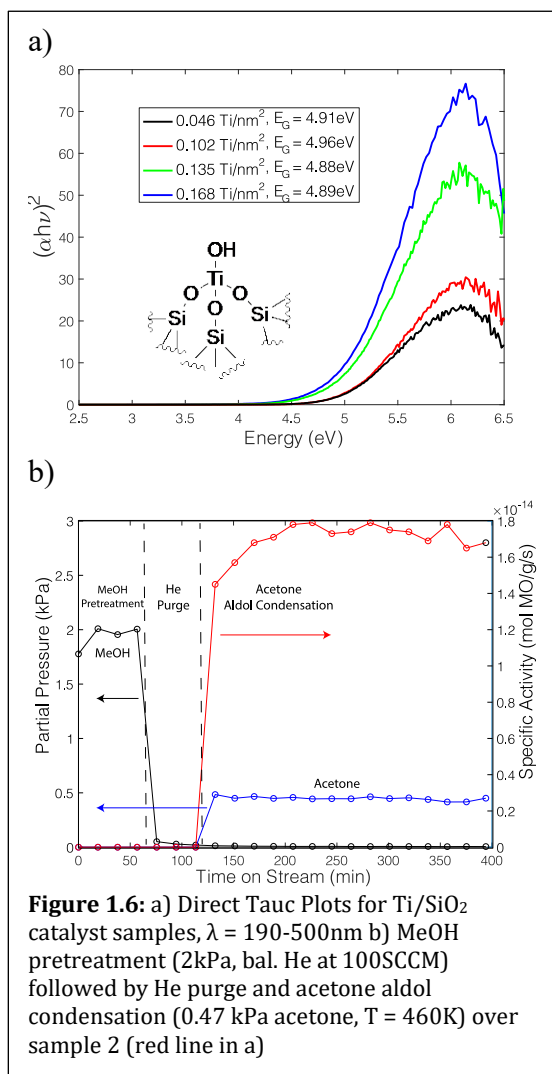
substrates.

The mechanistic steps of H-atom abstraction reactivity for an established water oxidation catalyst, the [Co<sub>4</sub>O<sub>4</sub>(OAc)<sub>4</sub>(py)<sub>4</sub>][PF<sub>6</sub>]<sup>-</sup> cubane were studied (Figure 1.5), with organic substrates. Mechanistic analyses corroborated with theoretical studies support a concerted proton-electron transfer (CPET) reaction at the multimetallic oxocobalt(IV) cluster. The observed stoichiometric and catalytic reactivity of the cubane offers promising implications towards biomimetic catalysis in which CPET facilitates challenging oxidation reactions at high-valent multimetallic-oxo active sites. In addition, computational studies (with David Balcells, U. Oslo) provide insights into cooperative effects of multimetallic centers and the reactive oxo ligand in C-H bond activation, which may be of substantial importance for C-H activation catalysis with Co oxide materials. Shown in 1.2.2, since oxidation reactions with **2** are well behaved with clean formation of **3** as evidenced by NMR spectroscopy, the catalytic reactivity of **2** was investigated by incorporation of a sacrificial base and oxidant to regenerate **2** from **3**. As an initial proof of concept, a slight excess of Ag<sub>2</sub>O (0.6:1; Ag<sub>2</sub>O: reactive C-H bond) proved to provide catalytic behavior. With 5 mol% of **2**, H-atom abstraction of CHD resulted in the formation of benzene (99% yield) in dichloromethane-*d*<sub>2</sub> after 20 h at 23 °C, along with concurrent generation of visible Ag(0) particles and water (by <sup>1</sup>H NMR spectroscopy).

## 1.6 Conferring stability to isolated Ti sites for acetone aldol condensation by methanol pretreatment (Bell/ Head-Gordon (MSD))

Biomass derived alcohols and ketones present an attractive, green alternative to petroleum as a source of carbon for chemicals. Catalytic upgrading of acetone into longer chain ketones can occur through the aldol condensation reaction in the gas phase. This reaction can be catalyzed by metal oxides, but this makes the control of product selectivity difficult. Single-site heterogenous catalysts (SSHCs) consisting of well-defined tetrahedrally coordinated metal oxide cations anchored to high surface area silica supports also catalyze this reaction and are much more amenable to control of activity and selectivity by placement of groups for secondary interactions and the surrounding support to control the active site. To this end, four titanium SSHCs were synthesized via air-free grafting of fumed, dehydroxylated silica utilizing  $\text{Cp}_2\text{TiCl}_2$  as the Ti precursor. A primary means for determining site-isolation is through the ligand-to-metal charge-transfer energy, measured by UV/Vis spectroscopy. Figure 1.6a displays direct Tauc plots used to determine the LMCT gaps ( $E_G$ ) for each catalyst. The high and nearly identical edge energies observed for all Ti loadings indicates that the Ti speciation is consistent with site-isolation independent of Ti loading.

Aldol condensation is often plagued by rapid and sometimes persistent deactivation caused by subsequent aldol condensation reactions of products ( $\alpha$ - $\beta$  unsaturated ketones) with acetone into highly condensable oligomers that block active sites. Deactivation can be curbed by two approaches: 1. hydrogenating  $\alpha$ - $\beta$  unsaturated products before they react further by cofeeding hydrogen and utilizing a Cu or Pd/SiO<sub>2</sub> cocatalyst and 2. cofeeding an alcohol to lower acetone surface coverages and limit reactions causing deactivation. Since continuous feed of alcohol also inhibits the desired aldol condensation, Bell has explored a strategy of selective poisoning of the highly active sights causing deactivation by pre-adsorbing methanol on the catalyst and then flushing the catalyst of any gas before the introduction of acetone. Figure 1.6b demonstrates that this procedure leads to stable activity for 3.5 h for the production of mesityl oxide and water. Without pretreatment in methanol, rapid deactivation occurs within 15 min. Measurements of the reaction kinetics revealed that the reaction is 0.5-0.8 order in acetone, suggesting C-C coupling is not rate determining under these conditions, and possibly enolization of

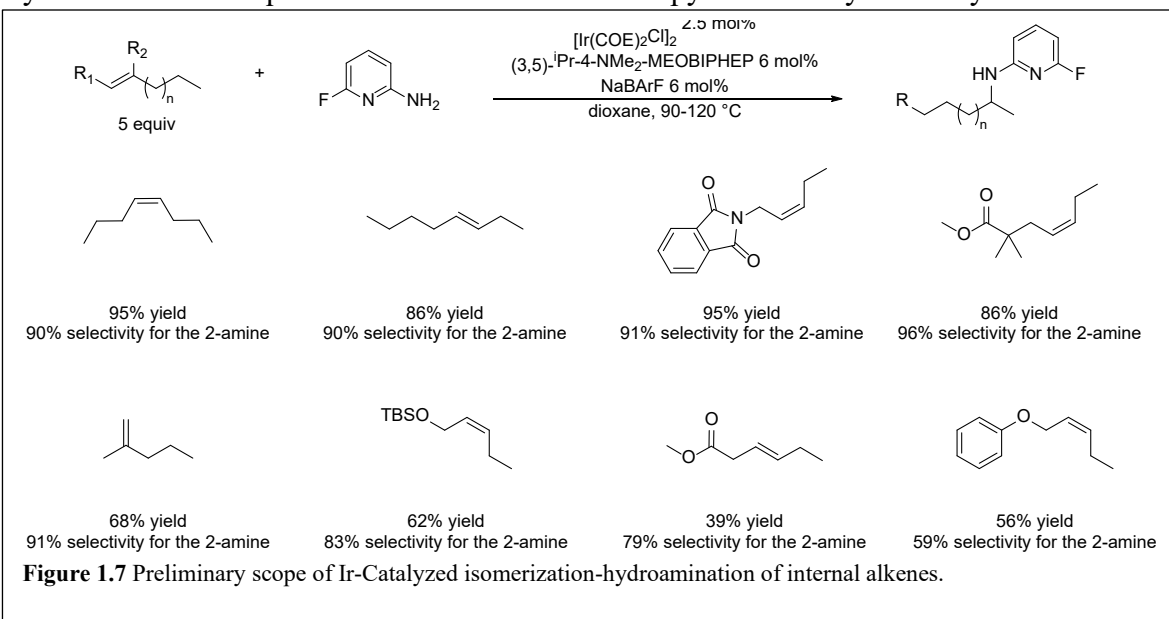


adsorbed acetone is rate determining. The apparent activation energy measured over a 40K range is 18-25 kJ/mol. DFT analysis of the free energy landscape for this reaction is being conducted to identify the origins of this low apparent activation energy. Future work will interrogate the mechanism of acetone aldol condensation on Ti SSHCs utilizing H/D isotopic labelling and application of a recently developed first principles microkinetic model.

### 1.7 Chain-Walking Hydrofunctionalization of Alkenes (Hartwig/Head-Gordon (MSD))

To understand how secondary interactions inside and outside of the primary coordination sphere influence reactivity, researchers in the program have been investigating reactions catalyzed by complexes of ligands and reagents that benefit from attractive secondary interactions. These studies have led to a combination of reagent and catalyst that led to a multistep, chain-walking hydroarylation in published work and to chain-walking hydroamination in new unpublished work. Chain-walking hydrofunctionalization of alkenes is a transformation that converts a mixture of isomeric alkenes into a single functionalized product. This process occurs by the isomerization of secondary and tertiary alkyl-metal intermediates into primary alkyl-metal intermediates before the reductive elimination to form the functionalized product. Although chain-walking hydrosilylation and hydroboration to add Si-H and B-H bonds are well-known, similar processes that involve addition of X-H bonds in which X is an electronegative element are unknown. The development of a sequential isomerization-hydroamination of alkenes could lead to efficient methods for the synthesis of aliphatic amines from readily available alkenes in an atom-economic manner.

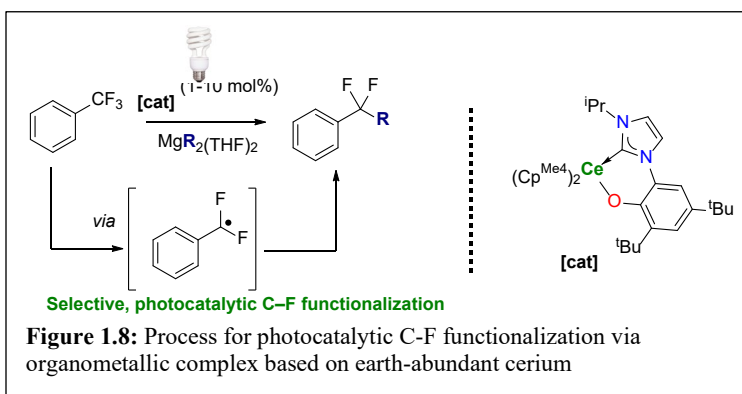
The chain-walking hydroamination discovered comprises an Ir catalyst and amino pyridine to give 2-amines as the major product by the isomerization of the internal alkenes to give a mixture of isomeric alkenes, followed by the selective Markovnikov hydroamination of the most reactive terminal alkene. More specifically the combination of  $[\text{Ir}(\text{COE})_2\text{Cl}]_2$ , (3,5)- $^i\text{Pr}$ -4-NMe<sub>2</sub>-MEOBIPHEP, and NaBARF catalyzes this isomerization-hydroamination sequence with 6-fluoro-2-aminopyridine to yield alkylamines. For



example, the reaction of cis-4-octene with this catalyst and amine occurred in 95% yield with 90% regioselectivity for the 2-aminoalkyl product (Figure 1.7). In addition to cis, internal alkenes, trans-alkenes and 1,1-disubstituted alkenes underwent isomerization-hydroamination to afford amines with moderate to good yield with high regioselectivity. Preliminary investigation of the scope the reaction showed that this reaction was compatible with a variety of functional groups, including protected amines, esters, protected alcohols and ethers. Future work will focus on developing ligands that enhance secondary interactions, such as dispersion interactions to improve the rate and regioselectivity of this transformation and expanding the compatibility of the reaction to a range of functional groups.

### 1.8 Selective Photocatalytic C-F Functionalization (Arnold/Wilson (CPIMS)/ Alpha N'Diaye (ALS))

Compounds containing C-F bonds can have unique properties and find application in many important areas of chemistry from materials to biomedicine. Some of the most important arise from the almost complete lack of natural sources of C-F bonds. However, a ramification of this is that



nature has virtually no ways to mediate their breakdown in the environment. The very strong C-F bond contributes to the moniker of fluorinated compounds as “forever chemicals” whose environmental persistence can have deleterious effects on ecosystem biodiversity and human health. The activation of C-F bonds typically requires harsh, energy-intensive, unselective conditions.

Arnold’s group has studied application of tunable, organic-soluble, lanthanide complexes as selective, homogeneous catalysts for a variety of reactions related to a sustainable future chemical economy. Based on our previous work, they hypothesized that the high halophilicity of lanthanides, offers an opportunity for controllable C-F bond activation and functionalization. Most recently a protocol has been developed for photocatalytic C-F bond functionalization using a new organometallic complex based on earth-abundant cerium (see Figure 1.8,  $\text{Cp}^{\text{Me}4} = \text{C}_5\text{Me}_4\text{H}$ ), and using visible light, at room temperature and pressure. Selective mono-defluorination of a  $\text{CF}_3$  group is possible with catalyst loadings as low as 1 %. Selective cross-coupling of trifluoromethyl arenes with magnesium dialkyls  $\text{MgR}_2$  is also possible, yielding difluoroalkanes, with a range of R groups. Our mechanistic studies, and DFT calculations with collaborators, agree on a radical pathway, and show the essential interplay between the lanthanide complex and magnesium cross-coupling partner in the steps involving Lewis acid – control of the C-F activation and stabilization of radicals in the C-C bond-forming step. Work is in progress within the LBL program to develop electrochemical methodologies to turn over the catalysts.

## Subtask 2. Cooperative and Evolving Multi-Catalytic Systems

Subtask 2 focuses on catalytic systems that comprise multiple catalysts. It encompasses systems in which multiple catalysts work together and systems in which multiple structures and compositions dynamically interconvert under operating conditions. Examples include multiple soluble metal complexes that operate synergistically in the same system to enable mild conditions for traditionally high temperature and pressure processes, multiple catalysts cooperatively disassembling long hydrocarbons by cleavage of C-C bonds or catenating components of biomass to form longer carbon chains, and nano-scale electrocatalysts that reduce CO<sub>2</sub> by changing shape, composition, and oxidation state during catalysis to generate environments that are highly active to form products containing C-C bonds. Again, new methods for *in situ* and *operando* spectroscopic and structural characterization are being developed to reveal these catalyst dynamics under operating conditions. This theme of catalysis with multiple and evolving catalysts has gained increased prominence during the past three years to become a dedicated subtask in the current review document.

### 2.1 Ethanol Conversion to Butadiene over Isolated Zinc and Yttrium Sites Grafted onto Dealuminated Beta Zeolite (Bell)

Studies during the past year introduced zinc and yttrium single sites into the silanol nests of dealuminated zeolite BEA to produce Zn-DeAlBEA and Y-DeAlBEA. These materials were then investigated for the conversion of ethanol to 1,3-butadiene. XAS together with FTIR demonstrated that the structure of Zn and Y sites are  $\equiv\text{Si}-\text{O}-\text{Zn}-\text{O}-\text{Si}\equiv$  and  $\equiv\text{Si}-\text{O}-\text{Y}(\text{OH})-\text{O}-\text{Si}\equiv$ . Zn-DeAlBEA was found to be highly active for ethanol dehydrogenation to acetaldehyde and exhibited low activity for the generation of 1,3-butadiene, Figure 2.1 a and b. By contrast, Y-DeAlBEA was highly active for the formation of 1,3-butadiene but exhibited no activity for ethanol dehydrogenation.

It is theorized C-C bond coupling in Y-DeAlBEA proceeds by the reaction of coadsorbed acetaldehyde and ethanol to form crotyl alcohol and water. The active centers for this process are  $\equiv\text{Si}-\text{O}-\text{Y}(\text{OH})-\text{O}-\text{Si}\equiv$  groups closely associated with adjacent silanol groups. The active sites in Y-DeAlBEA are 70 times more active than the Y sites supported on silica, for which the Y site is similar to that in Y-SiO<sub>2</sub> but lacks adjacent hydroxyl groups. The dehydration of crotyl alcohol to

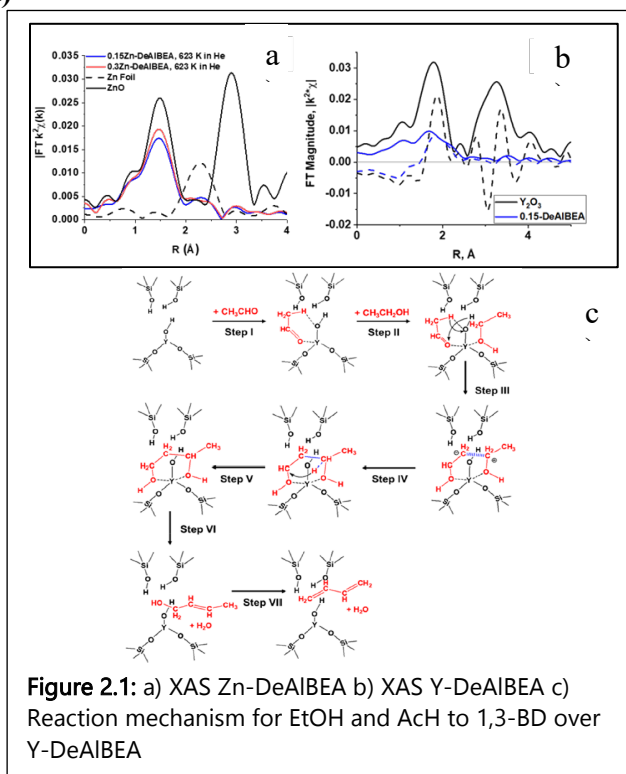


Figure 2.1: a) XAS Zn-DeAlBEA b) XAS Y-DeAlBEA c) Reaction mechanism for EtOH and AcH to 1,3-BD over Y-DeAlBEA

1,3-butadiene is facile and occurs over the mildly Brønsted acidic  $\equiv\text{Si}-\text{OH}$  groups present in the silanol nest of DeAlBEA.

The single sites catalysts developed in this study also formed 1,3-BD through both one-step and two-step processes, Figure 2.1c. The reaction of 5.3 kPa EtOH fed at a WHSV of 12.24 g/g<sub>cat</sub>/h over 0.15Zn-0.225Y-DeAlBEA occurred with an EtOH conversion of 94% at 673 K. The selectivity to all C<sub>4</sub> olefins was 61.6%, and the corresponding 1,3-BD productivity was 3.6 g/g<sub>cat</sub>/h. The reaction of 4.1 kPa EtOH and 2.5 kPa AcH over 0.375Y-DeAlBEA at 673 K produced 1,3-BD at the rate of 6.6 g/g<sub>cat</sub>/h with a selectivity of 66.4%. To the best of our knowledge, this productivity of 1,3-BD over 0.15Zn-0.225Y-DeAlBEA and 0.375Y-DeAlBEA for the one-step and two-step EtOH-to-1,3-BD process are the highest values reported. Future work will focus on identifying the C-C bond formation mechanism and investigating 1,3-BD formation over other isolated Lewis acid sites.

## 2.2 Optimizing the Catalytic Environment for CO<sub>2</sub> Reduction (Yang/ Somorjai/ Salmeron)

Creating optimal nanoscopic reaction environments around active sites of catalysts is key to achieving high selectivity for the electroreduction of CO<sub>2</sub>. An emerging strategy for this goal is to synthesize catalyst surfaces with tethered organic ligands, intended to tune the energetics of the catalyst itself, the bound CO<sub>2</sub>, or bound intermediates.

However, at present it is challenging to control the nanoscale reaction environment, due to the intricate and dynamic electrochemical interface.

The Yang team has recently discovered a new class of nanoparticle catalyst containing a Nanoparticle/Ordered-Ligand Interlayer (NOLI). This unique interlayer is created between the metal nanoparticle surface and an ordered layer of alkylphosphonic ligands from the reductive bias during evolution of densely assembled noble metal nanoparticles (such as

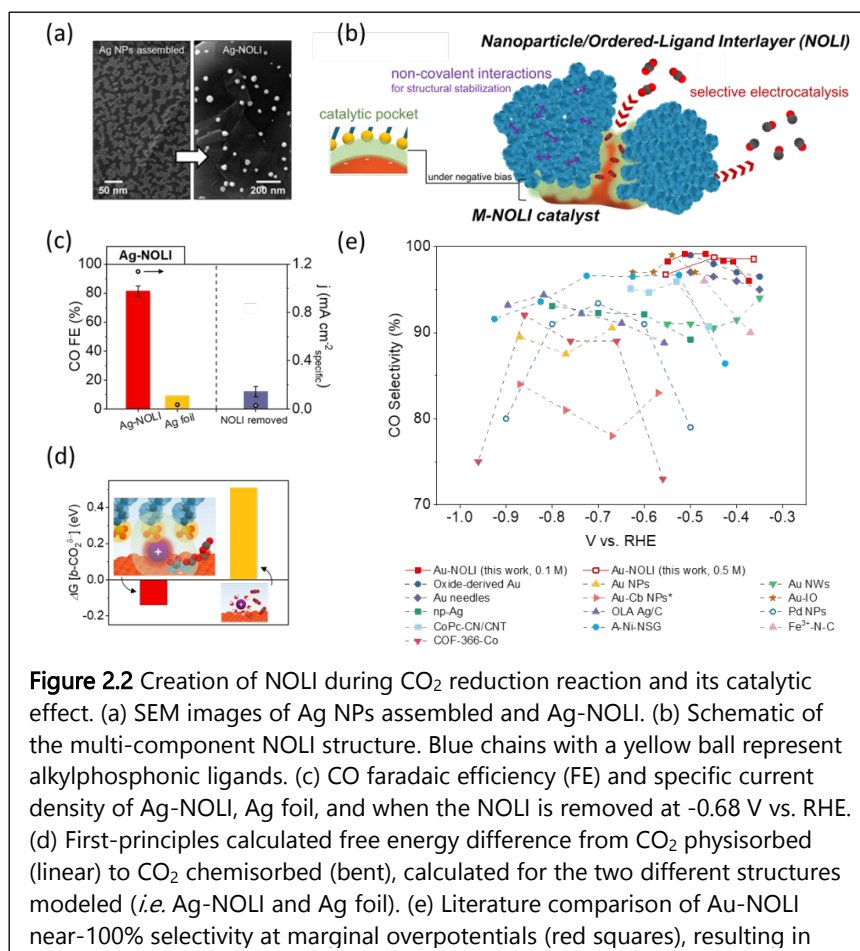


**Figure 2.2** Creation of NOLI during CO<sub>2</sub> reduction reaction and its catalytic effect. (a) SEM images of Ag NPs assembled and Ag-NOLI. (b) Schematic of the multi-component NOLI structure. Blue chains with a yellow ball represent alkylphosphonic ligands. (c) CO faradaic efficiency (FE) and specific current density of Ag-NOLI, Ag foil, and when the NOLI is removed at -0.68 V vs. RHE. (d) First-principles calculated free energy difference from CO<sub>2</sub> physisorbed (linear) to CO<sub>2</sub> chemisorbed (bent), calculated for the two different structures modeled (*i.e.* Ag-NOLI and Ag foil). (e) Literature comparison of Au-NOLI near-100% selectivity at marginal overpotentials (red squares), resulting in

Ag, Figure 2.2a). Through electrochemical and spectroscopic analysis (*i.e.* XPS and FTIR), they found that the ligands are collectively detached once a negative bias is applied, but remain in the vicinity of the particle surface, due to the strong non-covalent hydrophobic interactions among the tails of the ligands (Figure 2.2b). The NOLI acts as a catalytic pocket in which selective conversion of CO<sub>2</sub> to CO can be achieved, resulting in Ag-NOLI exhibiting strongly enhanced selectivity and specific activity over that of bare Ag structures without a NOLI (Figure 2.2c).

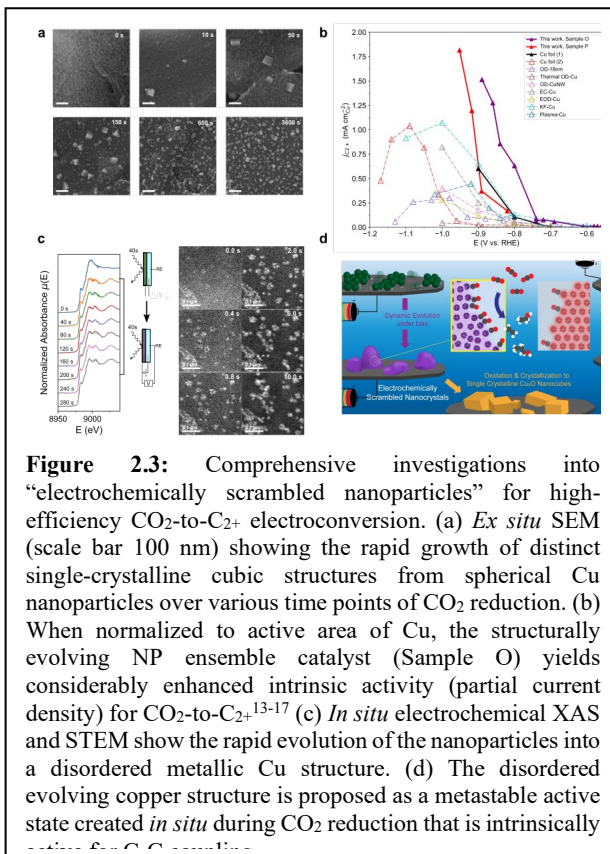
Electrochemical impedance spectroscopy and XAS analyses obtained at the Advanced Light Source (Beamline 10.3.2) show that the NOLI possesses striking pseudocapacitive characteristics where dehydrated cations are interposed between the metal and organic layers. They hypothesize that dehydrated cations intercalated in the interlayer can stabilize the intermediates during CO<sub>2</sub> reduction better than fully solvated cations, due to strong electrostatic interactions, confirmed by free energy calculations (Figure 2.2d). Considering this multi-faceted organic/inorganic hybrid structure that was created *in situ* in response to bias, this team is investigating how the NOLI concept can be applied across a diversity of metal compositions. Specifically, they seek to connect the elemental composition of the metal nanoparticle (M) with catalytic activity of the ensuing M-NOLI catalyst. For example, using gold nanoparticles with the same ligand chemistry, the *in situ* formed Au-NOLI catalysts achieve nearly unit selectivity (~99%) for formation of CO at marginal overpotentials (Figure 2.2e), allowing CO<sub>2</sub> reduction to approach the enzymatic ideal.

This rigorous investigation will create a better understanding and control of the dynamic nanoscale environment of this previously unrecognized interlayer between metal nanoparticles and their capping ligands under bias. In addition to these fundamental studies in traditional H-cells electrocatalysis, their translation to high-current-density gas diffusion environments will be investigated. This translation is challenging, due to the change in local reaction environment (*e.g.* local pH, concentration gradient, etc.) and consequently catalytic behavior. The Yang group has developed and are closely studying various nanoparticle-based catalysts, including the electrochemically scrambled Cu nanocrystals with superior intrinsic activity for CO<sub>2</sub>-to-C<sub>2+</sub> conversion and the M-NOLI catalysts with 99% selectivity at low over potentials

### 2.3 Optimizing Cu Catalysts for CO<sub>2</sub> Reduction (Yang/Salmeron/Fakra (ALS)/Ercius (Molecular Foundry)/L. Wang (MSD))

Because copper is the only known material to catalyze CO<sub>2</sub> reduction to products beyond CO (e.g. methane and multi-carbons) with reasonable efficiency and selectivity, Yang's team has spent significant effort to understand the structural transformations of copper nanocatalysts during electroreduction of CO<sub>2</sub>. Previously, they observed a remarkable structural transformation in which an ensemble of spherical copper nanoparticles evolved into cuboidal features that seemed to correlate with enhanced activity of the catalyst for CO<sub>2</sub> reduction to multi-carbon products at reduced overpotentials. These results led the team to pursue two fundamental questions underlying CO<sub>2</sub> electrocatalysts: what is the structure of the active surface for C-C formation and what is the nature of copper's structural evolution under electrochemically reducing conditions? To answer these questions, they embarked on a multi-faceted study of the copper nanoparticle (NP) ensemble system, in which they used *ex situ*, passivated *ex situ*, and *in situ* characterization techniques in concert to reveal the evolution process and the resultant active state of copper.

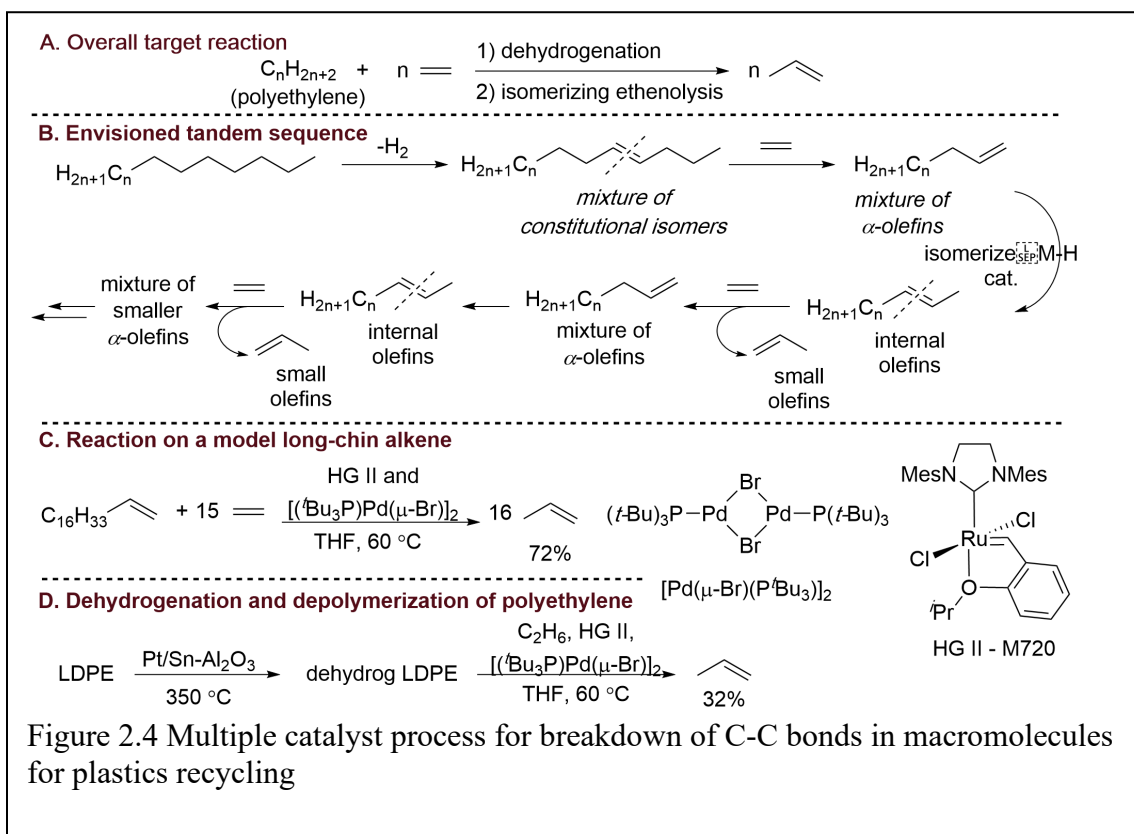
They systematically studied this platform that catalyzes aqueous CO<sub>2</sub> electroreduction at low overpotential to multi-carbon products in concert with unique structural dynamics. *Ex situ* characterization revealed a surprisingly rapid transition into a distinct structural signature, single-crystalline cuprous oxide cubes and cuboids (Figure 2.3 a). Ambient chemical passivation techniques revealed low crystallinity (increased disorder) in the active state. Remarkably, this disorder was observed to account for a 7-fold enhancement in the activity for formation of multi-carbon products over crystalline Cu and high-activity oxidized polycrystalline copper at moderate overpotentials (e.g. -0.8 V vs. RHE) (Figure 2.3 b). They further probed this transformation by *in situ* electrochemical X-ray Absorption Spectroscopy (XAS) in collaboration with scientists at the Advanced Light Source and *in situ* electrochemical Transmission Electron Microscopy (TEM) at the Molecular Foundry (Figure 2.3c). This work is the first use of electrochemical TEM to illuminate a CO<sub>2</sub> electrocatalyst *in situ*. Through such techniques, it was observed that the disordered active structure results from the high mobility and rapid fusion of the initial nanoparticles, resulting in structural transformation on the order of seconds. In conjunction with *ex situ* results, these *in situ* observations illustrate a phenomenon denoted "electrochemical



scrambling,” characterized by the rapid fusion of nanocrystals into a disordered state induced by a reducing bias, with a signature rapid oxidation to single crystal oxides on release of bias (Figure 2.3d). By combining a multitude of state-of-the-art *ex situ* and *in situ* techniques for characterization of materials, this study revealed the critical role of structural changes to create the active site that forms C-C bonds. These results will launch an array of future studies centered around disordered Cu structures for enhanced intrinsic activity towards CO<sub>2</sub> electroconversion to products containing multiple carbons.

#### 2.4. Multicatalytic Depolymerization of Polyethylene to Propene (Hartwig/Bell)

An additional study that involves multiple catalyst sites operating simultaneously focuses on the breakdown of C-C bonds in macromolecules, rather than the formation of C-C bonds



in small feedstocks, like CO<sub>2</sub>. Approximately 9% of plastics produced since 1950 have been recycled, yet approximately half of all plastics are designated for short-term use. This disparity originates from the high cost of recycling single-use plastics relative to that of producing virgin plastics from crude oil, which can be extracted and refined exceedingly cheaply. Polyethylene is the single most commonly produced plastic. Thermal depolymerization of PE to ethylene is not economically viable, as this reaction requires very high temperatures, nor are catalytic cracking, hydrocracking, and alkane metathesis, as these processes produce low-value mixtures. For a method of chemical recycling to contribute significantly to the development of a closed-loop economy (Figure 2.4), the products must be valuable commodity chemicals for which demand approaches the supply of PE waste. Hartwig and Bell are following an approach for the selective chemical recycling of polyethylene through dehydrogenation and isomerizing ethenolysis. This

process produces a single gaseous product, propene, which is easily separated from the solid starting materials and liquid solvent.

To achieve this process, polyethylene was dehydrogenated over a Pt/Sn/Al<sub>2</sub>O<sub>3</sub> catalyst to produce a polymer with up to 0.2% double bonds, and this polymer was converted to propene in 33% yield and butenes in 8% yield through olefin metathesis with ethylene in the presence of an isomerization catalyst. Our results demonstrate that propene forms in moderate yields and good selectivities from polyethylene. They anticipate that the yield of propene can be increased through optimization of the dehydrogenation and isomerizing ethenolysis steps and that this method could help create a closed-loop plastics economy in which polyethylene is upcycled rather than downcycled.

As an initial proof of concept, they isomerized octadecene with the M720 Hoveyda-Grubbs catalyst (HG II) as the metathesis catalyst (6 mol%) and [Pd(P<sup>t</sup>Bu<sub>3</sub>)(μ-Br)]<sub>2</sub> as the isomerization catalyst (2 mol%). Under these conditions, propene formed in up to 72% yield, and butenes formed in 6% yield. Control experiments revealed that a significant amount of butenes formed by ethylene dimerization in the absence of octadecene or another alkene, and a small amount of propene formed by ethylene dimerization, followed by ethylene-butene conproportionation. To improve the yield of the dehydrogenation, they are investigating heterogeneous catalysts, homogeneous catalysts, and tandem processes involving iodination and base-promoted elimination. To improve the yield of the isomerizing ethenolysis, they are currently investigating the effects of increasing the pressure of ethylene, altering the identities of the catalysts, and altering solvents and temperatures to promote solubility.

### **Subtask 3. Catalysis in Confined Spaces**

The third subtask focuses on conducting catalysis in confined environments. This theme was initiated by work on catalysis within a supramolecular nanovessel and has been a long-standing component of this Catalysis Program. Now, this work on confined environments has motivated research on catalysis in a broader range of confined spaces, including new supramolecular cages, the pores of metal-organic frameworks (MOFs), boxes with metal-porphyrins as sides, and active sites of artificial and natural metalloenzymes. Recent highlights of these new directions that illustrate the broadened scope include the use of supramolecular hosts to achieve enzyme-like regioselectivity from reactions of polyunsaturated molecules, the use of new types of cages to reveal the role of charge on the rates of reactions promoted by these anionic assemblies, the use of a porous, 3-dimensional coordination network to stabilize an active form of the Co<sub>4</sub>O<sub>4</sub> oxo cubane for prolonged electrocatalytic water splitting, regioselective C-H bond functionalizations by evolved artificial metalloenzymes, monomeric metal hydrides as new classes of abiotic enzyme intermediates, and new non-heme iron enzymes that catalyze halogenation reactions by control over the trajectory of the rebound step by the protein surroundings.

#### **3.1. The Effect of Metal Vertex Modification in Supramolecular Catalysis (Toste/Bergman/Raymond)**

Over the last few decades, the field of supramolecular catalysis has undergone tremendous growth, both in the diversity of synthetic host molecules and in the complexity of the reactions these assemblies catalyze. Supramolecular hosts emulate properties of enzymes, serving as simplified model systems to advance our understanding of the underlying

principles of enzymatic catalysis. Both synthetic and biological systems depend intimately on catalyst structure, which gives rise to important attributes including charge, cavity size, the degree of solvent exclusion, and other non-covalent interactions. Metal ions often play a critical role in enzyme catalysis, either as co-factors that directly activate the substrate toward catalysis, or as structural components that aid in self-assembly and impart an overall charge. Similarly, many supramolecular hosts contain metals that aid the assembly of their ligands; however, the role of these metals in catalysis remains ambiguous. In this study, a suite of four isostructural, catalytically active, anionic  $M_4L_6$  hosts, composed of identical ligands but differing metal centers were prepared. The structural diversification of the hosts was enabled by a guest-templated synthesis procedure. Comprehensive experimental studies were conducted to determine the contribution of their coordinatively saturated metal centers to supramolecular catalytic activity and showed changing the metal center had little effect on the hosts' catalytic performance when the overall charge of the host was held constant. These results provide evidence that supramolecular hosts can tolerate systematic structural modifications without significant loss of catalytic activity.

The ability of supramolecular hosts to exert simultaneous control over multiple stereocenters renders them not only synthetically valuable, but worthy targets for mechanistic analysis to rationalize microenvironment selectivity. Supramolecular host in figure 3.1 (1) is characterized by a hydrophobic interior and a highly charged, dodecanionic framework. This structure stabilizes cationic intermediates, enabling efficient acid catalysis within its core. The ability of host in figure 3.1 (1) to stabilize iminium ions motivated us to develop a 1-catalyzed aza-Darzens condensation to generate substituted aziridines. The host in figure 3.1 (1) provides high *trans* selectivity while the background process provides the *cis* diastereomer in poor yields, indicating the host overrides the intrinsic diastereoselectivity of the reaction. Subjecting enantiopure host in figure 3.1 (2), which self-assembles as a single diastereomer, to the aza-Darzens conditions gave excellent enantioselectivity and reactivity. Inspired by this result, a library of six new enantiopure supramolecular hosts was developed via substitution of the external chiral amide, in order to gain a better understanding on the role of this auxiliary on active site speciation. Subjecting these new hosts to the reaction conditions provided disparate reactivity and enantioselectivity across the catalyst series. Further investigation of this effect revealed that differing host encapsulation dynamics plays a role in reaction

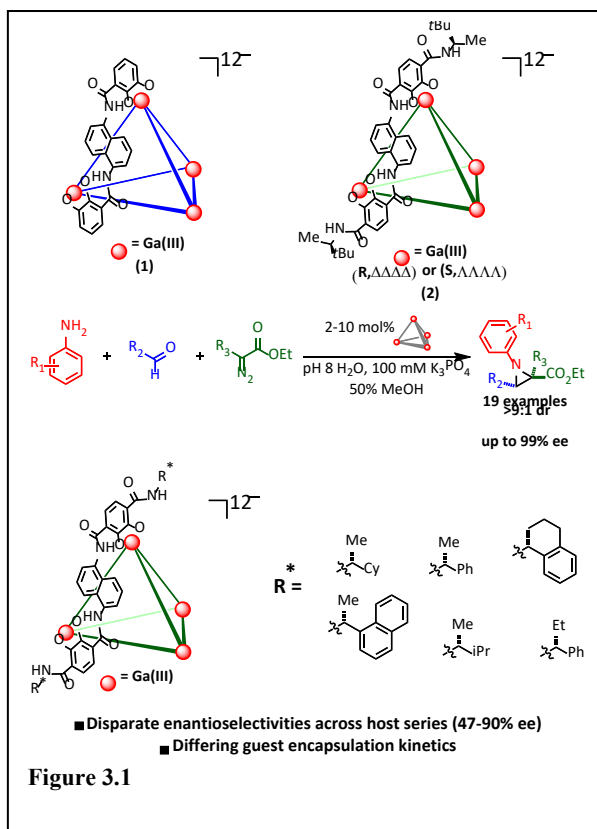
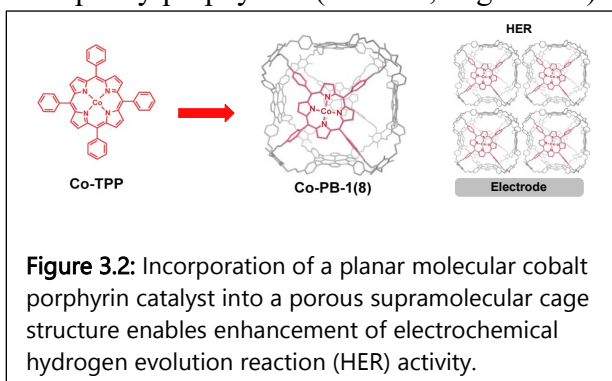


Figure 3.1

selectivity, with the most flexible hosts being the most enantioselective catalysts for the transformation.

### 3.2 Cobalt Porphyrin Based Supramolecular Catalyst for Electrochemical Hydrogen Evolution from Water (C. Chang)

Researchers in the program have also created caged structures from porphyrins to influence the association between catalyst active sites. A porous organic cage composed of six cobalt tetraphenylporphyrins (Co-TPP, Figure 3.2) was used as a supramolecular catalyst for



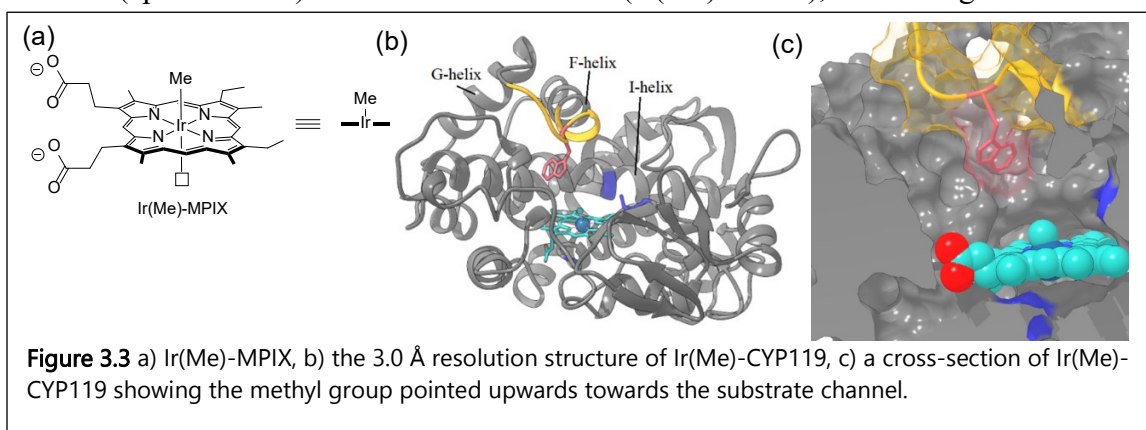
**Figure 3.2:** Incorporation of a planar molecular cobalt porphyrin catalyst into a porous supramolecular cage structure enables enhancement of electrochemical hydrogen evolution reaction (HER) activity.

electrochemical hydrogen evolution reaction (HER) from water at neutral pH. The supramolecular structure was constructed by condensing six tetraformylphenylporphyrins and eight triamine linkers. A Brunauer–Emmett–Teller surface area of 519 m<sup>2</sup>/g was measured by gas sorption, which confirmed the permanent porosity of Co-PB-1(8). This porous structure enables Co-PB-1(8) to yield a catalyst film with a

5-fold increase in the number of electrochemically active cobalt atoms than Co-TPP, as determined by measuring the scan rate dependence of the reversible Co<sup>III</sup>/Co<sup>II</sup> redox couple. The structural porosity of Co-PB-1(8) also accelerates the rate-limiting step in HER by facilitating the delivery of both electrons and protons to the active Co centers, thereby leading to an improvement in the Tafel slope from 170 mV/decade to 119 mV/decade compared to a planar cobalt porphyrin analog. Controlled potential electrolysis in 1 M pH 7 phosphate buffer at a potential of -0.6 V vs. RHE for 24 hours showed Co-PB-1(8) produced more than twice the amount of H<sub>2</sub> with 100% Faradaic efficiency than did Co-TPP, corresponding to a turnover number (TON) of 19,030 and an average turnover frequency (TOF) of 0.22 s<sup>-1</sup>. These data demonstrate that embedding small molecular catalyst into a supramolecular architecture is an effective strategy to enhance catalytic activity.

### 3.3. Mechanistic and Structural Characterization of an Iridium-Containing Cytochrome Reveals Kinetically Relevant Cofactor Dynamics (Hartwig/ Clark (MBIB)/ Adams (MBIB))

Studies on artificial metalloenzymes bridge synthetic supramolecular systems and natural enzymatic systems. These enzymes contain unnatural metal active sites within a natural (often mutant) protein and have been generated in multiple ways by multiple groups. While studies to observe new reactions and assess reaction scope have been conducted, detailed mechanistic studies that reveal the influence of the artificial cofactor have not. Enzymes and synthetic catalysts have been studied independently, but there are no such kinetic studies on reactions catalyzed by artificial metalloenzymes (ArMs). Hartwig in collaboration with Doug Clark in the MBIB division have conducted a detailed mechanistic study on the ArM, Ir(Me)-CYP119, which consists of a cytochrome P450 scaffold (apo-CYP119) and an iridium cofactor (Ir(Me)-MPIX), seen in Figure 3.3.



They studied the mechanism of the cyclopropanation of the terpene carvone by ethyldiazoacetate (EDA) catalyzed by Ir(Me)-CYP119. In collaboration with Paul Adams and his coworkers in the MBIB division, they determined the structure of Ir(Me)-CYP119 and found that the cofactor resides in the enzyme active site with the open coordination site on iridium facing away from the enzyme substrate channel (Figure 3.3). This orientation of the cofactor suggests that a majority of the enzyme is inactive in solution or that the cofactor flips to the opposite orientation prior to catalysis. The latter hypothesis was corroborated by the observation of an induction period during kinetics studies on the enzyme-catalyzed reaction, but not on the reaction catalyzed by the free cofactor. Studies on the effect of substrate concentration on the rate showed that the induction period was not due the substrates, that EDA binds to the enzyme before the terpene substrate, and that carbene formation is rate-determining. Furthermore, they determined that the rate constant for dissociation of the cofactor and the rate constant for binding of an exogenous fluorescent ligand were nearly identical. These data imply that a flip of the synthetic iridium cofactor by dissociation of the cofactor from the active site occurs prior to the catalytic reaction. This study will guide in efforts to develop more active and selective ArMs by improving the specificity of cofactor-protein interactions.

### 3.4. Enzyme Controlled Reactivity of Metal Centers (M. Chang)

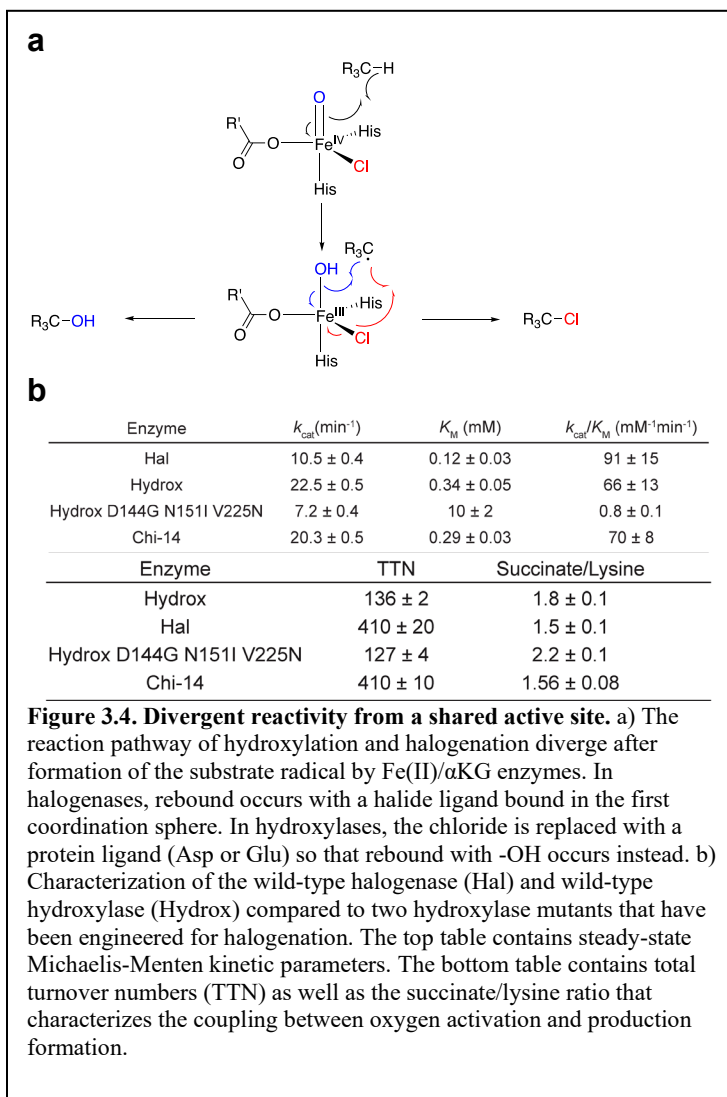
Studies on the origins of reactivity and selectivity in a natural enzymatic system for C-H

bond functionalization also have been conducted. M. Chang's team has been exploring how enzymes control the reactivity of metal centers in non-heme iron  $\alpha$ -ketoglutarate-dependent enzymes. Diverse reactions are possible in this family despite conservation of the first-sphere

ligand environment of the iron center. They are currently studying how the reaction partitions between related Fe/ $\alpha$ KG hydroxylases and halogenases.

Radical rebound occurs between either the -OH or -Cl group to form products from hydroxylation or halogenation, respectively (Figure 3.4). They had reported the use of directed evolution and the development of a high-throughput fluorescent screen for halogenation that identified 14 mutations that are key to enabling the conversion of a hydroxylase to a halogenase with wild-type activity for the first time. They have now fully

characterized these mutants to show that their steady-state parameters are indeed indistinguishable from wild-type (Figure 3.4). In these experiments, they compare the wild-type halogenase (Hal) and hydroxylase (Hydrox) as well as two mutants of Hydrox that catalyze halogenation (Hydrox D144G N141I V225N and Hydrox Chi-14). They observe that the steady-state Michaelis-Menten parameters, as well as the stability and coupling, of the evolved Chi-14 mutant mimic those of the wild-type Hal within the Hydrox scaffold. They have further shown that the stereochemical selectivity of the wild-type and engineered halogenases are the same.



## LBNL Catalysis Program Publications 2018–2021

### *(I.) Intellectually led by this Program*

- Dombrowski, J. P.; Ziegler, M. S.; Phadke, N. M.; Mansoor, E.; Levine, D. S.; Witzke, R. J.; Head-Gordon M.; Bell A. T.; and Tilley, T. D., "Siloxaluminates and siloxogallate complexes as models for framework and partially hydrolyzed framework sites in zeolites and zeotypes." *Chemistry – A European Journal* 27 (2021) DOI 307-15. 10.1002/chem.202002926.
- Qi, L.; Zhang Y.; Conrad, M. A.; Russell, C. K.; Miller J.; and Bell, A. T., "Ethanol conversion to butadiene over isolated zinc and yttrium sites grafted onto dealuminated beta zeolite." *Journal of the American Chemical Society* 142 (2020) DOI 14674-87. 10.1021/jacs.0c06906.
- Zhang, Y.; Qi, L.; Lund, A.; Lu, P.; and Bell, A. T., "Mechanism and kinetics of acetone conversion to isobutene over isolated hf sites grafted to silicalite-1 and sio2." *Journal of the American Chemical Society* 143 (2021) 8352-66. DOI 10.1021/jacs.1c01315.
- Derrick, J. S.; Loipersberger, M.; Chatterjee, R.; Iovan, D. A.; Smith, P. T.; Chakarawet, K.; Yano, J.; Long, J. R.; Head-Gordon, M. and Chang C. J., "Metal–ligand cooperativity via exchange coupling promotes iron- catalyzed electrochemical CO2 reduction at low overpotentials." *Journal of the American Chemical Society* 142 (2020) 20489-501. DOI 10.1021/jacs.0c10664.
- Smith, P. T.; Kim, Y.; Benke, B. P.; Kim K.; and Chang, C. J., "Supramolecular tuning enables selective oxygen reduction catalyzed by cobalt porphyrins for direct electrosynthesis of hydrogen peroxide." *Angewandte Chemie International Edition* 59 (2020) 4902-07. DOI 10.1002/anie.201916131.
- Smith, P. T.; Nichols, E. M.; Cao, Z.; and Chang, C. J., "Hybrid catalysts for artificial photosynthesis: Merging approaches from molecular, materials, and biological catalysis." *Accounts of Chemical Research* 53 (2020) 575-87. DOI 10.1021/acs.accounts.9b00619.
- Smith, P. T.; Weng S.; and Chang C. J., "An nadh-inspired redox mediator strategy to promote second-sphere electron and proton transfer for cooperative electrochemical co2 reduction catalyzed by iron porphyrin." *Inorganic Chemistry* 59 (2020) 9270-78. DOI 10.1021/acs.inorgchem.0c01162.
- Wuttig, A.; Derrick, J. S.; Loipersberger, M.; Snider, A.; Head-Gordon, M.; Chang, C. J.; and Toste, F. D., "Controlled single-electron transfer via metal–ligand cooperativity drives divergent nickel-electrocatalyzed radical pathways." *Journal of the American Chemical Society* 143 (2021) 6990-7001. DOI 10.1021/jacs.1c01487.
- Zee, D. Z.; Nippe, M.; King, A. E.; Chang, C. J.; and Long, J. R., "Tuning second coordination sphere interactions in polypyridyl–iron complexes to achieve selective electrocatalytic reduction of carbon dioxide to carbon monoxide." *Inorganic Chemistry* 59 (2020) 5206-17. DOI 10.1021/acs.inorgchem.0c00455.
- Chen, L.; Malollari, K. G.; Uliana, A.; Sanchez, D.; Messersmith, P. B.; and Hartwig, J. F., "Selective, catalytic oxidations of c–h bonds in polyethylenes produce functional materials with enhanced adhesion." *Chem* 7 (2021) 137-45. DOI 10.1016/j.chempr.2020.11.020.

- Hanna, S.; Wills, T.; Butcher, T. W.; and Hartwig, J. F., "Palladium-catalyzed oxidative dehydrosilylation for contra-thermodynamic olefin isomerization." *ACS Catalysis* 10 (2020): 8736-41. DOI 10.1021/acscatal.0c02697.
- Qiu, Y.; and Hartwig, J. F., "Mechanism of ni-catalyzed oxidations of unactivated c(sp<sup>3</sup>)-h bonds." *Journal of the American Chemical Society* 142 (2020) 19239-48. DOI 10.1021/jacs.0c09157.
- Xi, Y.; Ma, S.; and Hartwig J. F., "Catalytic asymmetric addition of an amine n-h bond across internal alkenes." *Nature* 588 (2020) 254-60. DOI 10.1038/s41586-020-2919-z.
- Xi, Y.; Su, B.; Qi, X.; Pedram, S.; Liu P.; and Hartwig, J. F.; "Application of trimethylgermyl-substituted bisphosphine ligands with enhanced dispersion interactions to copper-catalyzed hydroboration of disubstituted alkenes." *Journal of the American Chemical Society* 142 (2020) 18213-22. DOI 10.1021/jacs.0c08746.
- Chen, L.; Qi, Z.; Zhang, S.; Su, J.; Somorjai, G.A., Application of Single-Site Catalysts in the Hydrogen Economy. *Trends in Chemistry* 2 (2020) 1114–1125. DOI 10.1016/j.trechm.2020.09.009
- Chen, L.; Qi, Z.; Zhang, S.; Su, J.; and Somorjai, G. A., "Catalytic hydrogen production from methane: A review on recent progress and prospect." *Catalysts* 10 (2020) 858. DOI 10.3390/catal10080858.
- Chen, S.; Liu, X.-Y.; Jin, J.; Gao, M.; Chen, C.; Kong, Q.; Ji, Z.; Somorjai, G. A.; Yaghi, O. M.; and Yang, P. , "Individually encapsulated frame-in-frame structure." *ACS Materials Letters* 2 (2020) 685-90. DOI 10.1021/acsmaterialslett.0c00161.
- Qi, Z.; Chen, L.; Zhang, S.; Su, J.; and Somorjai, G. A., "A mini review of cobalt-based nanocatalyst in fischer-tropsch synthesis." *Applied Catalysis A: General* 602 (2020) 117701. DOI 10.1016/j.apcata.2020.117701
- Qi, Z.; Chen, L.; Zhang, S.; Su, J.; and Somorjai, G. A., "Integrating the fields of catalysis: Active site engineering in metal cluster, metal organic framework and metal single site." *Topics in Catalysis* 63 (2020) 628-34. DOI 10.1007/s11244-020-01248-5.
- Qi, Z.; Chen, L.; Zhang, S.; Su, J.; and Somorjai, G. A., "Mechanism of methanol decomposition over single-site pt1/ceo2 catalyst: A drifts study." *Journal of the American Chemical Society* 143 (2021) 60-64. DOI 10.1021/jacs.0c10728.
- Zhang, S.; Chen, L.; Qi, Z.; Zhuo, L.; Chen, J.-L.; Pao, C.-W.; Su, J.; and Somorjai, G. A., "Insights into the mechanism of n-hexane reforming over a single-site platinum catalyst." *Journal of the American Chemical Society* 142 (2020) 16533-37. DOI 10.1021/jacs.0c07911.
- Amtawong, J.; Skjelstad, B. B.; Balcells, D.; and Tilley, T. D., "Concerted proton–electron transfer reactivity at a multimetallic co<sub>4</sub>o<sub>4</sub> cubane cluster." *Inorganic Chemistry* 59 (2020) 15553-60. DOI 10.1021/acs.inorgchem.0c02625.
- Amtawong, J.; Skjelstad, B. B.; Handford, R. C.; Suslick, B. A.; Balcells, D.; and Tilley, T. D., "C-H activation by RuCo<sub>3</sub>O<sub>4</sub> oxo cubanes: Effects of oxyl radical character and metal–metal cooperativity." *Journal of the American Chemical Society* (2021) DOI 10.1021/jacs.1c04069.
- Desnoyer, A. N.; Nicolay, A.; Rios, P.; Ziegler, M. S.; and Tilley, T. D., "Bimetallics in a nutshell: Complexes supported by chelating naphthyridine-based ligands." *Accounts of Chemical Research* 53 (2020) 1944-56. DOI 10.1021/acs.accounts.0c00382.

- Desnoyer, A. N.; Nicolay, A.; Ziegler, M. S.; Lakshmi, K. V.; Cundari, T. R.; and Tilley T. D., "A dicopper nitrenoid by oxidation of a cuicui core: Synthesis, electronic structure, and reactivity." *Journal of the American Chemical Society* 143 (2021) 7135-43. DOI 10.1021/jacs.1c02235.
- Desnoyer, A. N.; Nicolay, A.; Ziegler, M. S.; Torquato, N. A.; and Tilley, T. D., "A dicopper platform that stabilizes the formation of pentanuclear coinage metal hydride complexes." *Angewandte Chemie International Edition* 59 (2020) 12769-73. DOI 10.1002/anie.202004346.
- Nicolay, A.; Ziegler, M. S.; Rochlitz, L.; and Tilley, T. D., "Low-valent iron and cobalt complexes supported by a rigid xanthene-based disilylamido ligand." *Polyhedron* 180 (2020) 114420. DOI 10.1016/j.poly.2020.114420.
- Nicolay, A.; Héron, J.; Shin, C.; Kuramarohit, S.; Ziegler, M. S.; Balcells, D.; and Tilley, T. D., "Unsymmetrical naphthyridine-based dicopper(i) complexes: Synthesis, stability, and carbon–hydrogen bond activations." *Organometallics* 40 (2021) 1866-73. DOI 10.1021/acs.organomet.1c00188.
- Nicolay, A.; Ziegler, M. S.; Small, D. W.; Grünbauer, R.; Scheer, M.; and Tilley, T. D., "Isomerism and dynamic behavior of bridging phosphalkynes bound to a dicopper complex." *Chemical Science* 11 (2020) 1607-16. DOI 10.1039/c9sc05835d.
- Suslick, B. A. and Tilley T. D., "Mechanistic interrogation of alkyne hydroarylations catalyzed by highly reduced, single-component cobalt complexes." *Journal of the American Chemical Society* 142 (2020) 11203-18. DOI 10.1021/jacs.0c04072.
- Suslick, B. A.; and Tilley T. D., "Olefin hydroarylation catalyzed by a single-component cobalt(-i) complex." *Organic Letters* 23 (2021) 1495-99. DOI 10.1021/acs.orglett.1c00258.
- Witzke, R. J.; Hait, D.; Head-Gordon, M.; and Tilley T. D., "Two-coordinate iron(i) complexes on the edge of stability DOI Influence of dispersion and steric effects." *Organometallics* 40 (2021) 1758-64. DOI 10.1021/acs.organomet.1c00218.
- Bierschenk, S. M.; Bergman, R. G.; Raymond, K. N.; and Toste, F. D., "A nanovessel-catalyzed three-component aza-darzens reaction." *Journal of the American Chemical Society* 142 (2020) 733-37. DOI 10.1021/jacs.9b13177.
- Lee, J. S.; Kapustin, E. A.; Pei, X.; Llopis, S.; Yaghi, O. M.; and Toste, F. D., "Architectural stabilization of a gold(iii) catalyst in metal-organic frameworks." *Chem* 6 (2020) 142-52. DOI 10.1016/j.chempr.2019.10.022.
- Wuttig, A.; Derrick, J. S.; Loipersberger, M.; Snider, A.; Head-Gordon, M.; Chang, C. J.; and Toste, F. D., "Controlled single-electron transfer via metal–ligand cooperativity drives divergent nickel-electrocatalyzed radical pathways." *Journal of the American Chemical Society* 143 (2021) 6990-7001. DOI 10.1021/jacs.1c01487.
- Chen, C.; Li, Y.; and Yang, P. "Address the “alkalinity problem” in co2 electrolysis with catalyst design and translation." *Joule* 5 (2021) 737-42. DOI 10.1016/j.joule.2021.02.008.
- Chen, C.; Li, Y.; Yu, S.; Louisia, S.; Jin, J.; Li, M.; Ross, M. B.; and Yang, P., "Cu-ag tandem catalysts for high-rate CO<sub>2</sub> electrolysis toward multicarbons." *Joule* 4 (2020) 1688-99. DOI 10.1016/j.joule.2020.07.009.
- Chen, P.-C.; Gao, M.; Yu, S.; Jin, J.; Song, C.; Salmeron, M.; Scott, M. C.; and Yang, P., "Revealing the phase separation behavior of thermodynamically immiscible elements in a nanoparticle." *Nano Letters* (2021) DOI 10.1021/acs.nanolett.1c02225.

- Chen, S.; Li, M.; Gao, M.; Jin, J.; Van Spronsen, M. A.; Salmeron, M. B.; and Yang, P., "High-performance pt-co nanoframes for fuel-cell electrocatalysis." *Nano Letters* 20 (2020) 1974-79. DOI 10.1021/acs.nanolett.9b05251.
- Kim, D.; Yu, S.; Zheng, F.; Roh, I.; Li, Y.; Louisia, S.; Qi, Z.; Somorjai, G.A.; Frei, H.; Wang, L.-W.; and Yang, P., Selective CO<sub>2</sub> electrocatalysis at the pseudocapacitive nanoparticle/ordered-ligand interlayer. *Nature Energy* 5, (2020) 1032-1042. DOI 10.1038/s41560-020-00730-4.
- Li, M.; Zhang, B.; Cheng, T.; Yu, S.; Louisia, S.; Chen, C.; Chen, S.; Cestellos-Blanco, S.; Goddard, W. A.; and Yang, P., "Sulfur-doped graphene anchoring of ultrafine Au<sub>25</sub> nanoclusters for electrocatalysis." *Nano Research* (2021) DOI 10.1007/s12274-021-3561-2.
- Li, Y.; Kim, D.; Louisia, S.; Xie, C.; Kong, Q.; Yu, S.; Lin, T.; Aloni, S.; Fakra, S. C.; and Yang, P., "Electrochemically scrambled nanocrystals are catalytically active for CO<sub>2</sub>-to-multicarbon." *Proceedings of the National Academy of Sciences* 117 (2020) 9194-201. DOI 10.1073/pnas.1918602117.
- Xie, C.; Niu, Z.; Kim, D.; Li, M.; and Yang, P., "Surface and interface control in nanoparticle catalysis." *Chemical Reviews* 120 (2020) 1184-249. DOI 10.1021/acs.chemrev.9b00220
- Zhang, B.; Chen, C.; Chuang, W.; Chen, S.; and Yang, P., "Size transformation of the Au<sub>22</sub>(sg)<sub>18</sub> nanocluster and its surface-sensitive kinetics." *Journal of the American Chemical Society* 142 (2020) 11514-20. DOI 10.1021/jacs.0c03919.
- Kersell, H.; Hooshmand, Z.; Yan, G.; Le, D.; Nguyen, H.; Eren, B.; Wu, C. H.; Waluyo, I.; Hunt, A.; Nemšák, S.; Somorjai, G.; Rahman, T. S.; Sautet, P.; and Salmeron, M., CO Oxidation Mechanisms on CoOx-Pt Thin Films. *J. Am. Chem. Soc.* 142 (18), (2020) 8312-8322. DOI 10.1021/jacs.0c01139.
- Bierschenk, S. M.; Bergman, R. G.; Raymond, K. N.; and Toste, F. D., A Nanovessel-Catalyzed Three Component Aza-Darzens Reaction. *J. Am. Chem. Soc.*, 142 (2), (2020) 733-737. DOI 10.1021/jacs.9b13177.
- Desnoyer, A. N.; Nicolay, A.; Rios, P.; Ziegler, M. S.; and Tilley, T. D., Bimetallics in a Nutshell: Complexes Supported by Chelating Naphthyridine-Based Ligands. *Acc. Chem. Res.* 53 (9), (2020) 1944-1956. DOI 10.1021/acs.accounts.0c00382.
- Desnoyer, A. N.; Nicolay, A.; Ziegler, M. S.; and Tilley, T. D., A Dicopper Platform that Stabilizes the Formation of Pentanuclear Coinage Metal Hydride Complexes. *Angew. Chem. Int. Ed.* 59 (31), (2020) 12769-12773. DOI 10.1002/anie.202004346.
- Dombrowski, J.P.; Ziegler, M.S.; Phadke, N.M.; Mansoor, E.; Levine, D.S.; Witzke, R.J.; Head-Gordon, M.; Bell, A.T.; Tilley, T.D. Siloxyaluminate and Siloxygallate Complexes as Models for Framework and Partially Hydrolyzed Framework Sites in Zeolites and Zeotypes. *Chemistry: A European Journal.* 27 (2021). DOI: 10.1002/chem.202002926
- Hanna, S.; Wills, T.; Butcher, T. W.; and Hartwig, J. F., Palladium-Catalyzed Oxidative Dehydrosilylation for Contra-Thermodynamic Olefin Isomerization. *ACS Catal.* 10 (15), (2020) 8736-8741. DOI 10.1021/acscatal.0c02697.
- Li, Y.; Kim, D.; Louisia, S.; Xie, C.; Kong, Q.; Yu, S.; Lin, T.; Aloni, S.; Fakra, S. C.; and Yang, P., Electrochemically Scrambled Nanocrystals are Catalytically Active

- for CO<sub>2</sub>-to-Multicarbon. *Proc. Natl. Acad. Sci.* 117 (17), (2020) 9194-9201. DOI 10.1073/pnas.1918602117.
- Nicolay, A.; Ziegler, M. S.; Small, D. W.; Grünbauer, R.; Scheer, M.; and Tilley, T. D., Isomerism and Dynamic Behavior of Bridging Phosphaalkynes Bound to a Dicopper Complex. *Chem. Sci.* 11, (2020) 1607-1616. DOI 10.1039/C9SC05835D.
- Qi, Z.; Chen, L.; Zhang, S.; Su, J.; and Somorjai, G. A., Integrating the Fields of Catalysis: Active Site Engineering in Metal Cluster, Metal Organic Framework and Metal Single Site. *Top. Catal.* 2020, 63 (7-8 SI), 628-634. DOI 10.1007/s11244-020-01248-5.
- Salmeron, M., and Eren, B. High-Pressure Scanning Tunneling Microscopy. *Chemical Reviews* 121, (2021) 962–1006. DOI 10.1021/acs.chemrev.0c00429
- Saper, N. I.; Ohgi, A.; Small, D.; Semba, K.; Nakao, Y.; and Hartwig, J. F., Nickel-Catalyzed Anti-Markovnikov Hydroarylation of Unactivated Alkenes with Unactivated Arenes Facilitated by non-Covalent Interactions. *Nat. Chem.* 12, (2020) 276-283. DOI 10.1038/s41557-019-0409-4.
- Shylesh, S.; Bettinson, L. A.; Aljahri, A.; Head-Gordon, M.; and Bell, A. T., Experimental and Computational Studies of Carbon–Carbon Bond Formation via Ketonization and Aldol Condensation over Site Isolated Zirconium Catalysts. *ACS Catal.* 10, (2020) 4566-4579. DOI 10.1021/acscatal.9b05176.
- Smith, P. T.; Nichols, E. M.; Cao, Z.; and Chang, C. J., Hybrid Catalysts for Artificial Photosynthesis: Merging Approaches from Molecular, Materials, and Biological Catalysis. *Acc. Chem. Res.* 53, (2020) 575-587. DOI 10.1021/acs.accounts.9b00619.
- Smith, P. T.; Weng, S.; and Chang, C., An NADH-Inspired Redox Mediator Strategy to Promote Second-Sphere Electron and Proton Transfer for Cooperative Electrochemical CO<sub>2</sub> Reduction Catalyzed by Iron Porphyrin. *Inorg. Chem.* 2020, 59 (13), 9270–9278, DOI 10.26434/chemrxiv.12159207.v1.
- Suslick, B. A.; and Tilley, T. D., Mechanistic Interrogations of Hydroarylations Catalyzed by Highly Reduced, Single Component Cobalt Complexes. *J. Am. Chem. Soc.* 142 (25), (2020) 11203-11218. DOI 10.1021/jacs.0c04072.
- Zhang, B.; Chen, C.; Chuang, W.; Chen, S.; and Yang, P., Size Transformation of the Au<sub>22</sub>(SG)<sub>18</sub> Nanocluster and its Surface Sensitive Dynamics. *J. Am. Chem. Soc.* 142 (26), (2020) 11514-11520. DOI 10.1021/jacs.0c03919.
- Hartwig, J. F.; and Ward, T. R., New ‘Cats’ in the House: Chemistry Meets Biology in Artificial Metalloenzymes and Repurposed Metalloenzymes. *Acc. Chem. Res.* 52, (2019) 1145–1145. DOI 10.1021/acs.accounts.9b00154.
- Ho C. R.; Bettinson L. A.; Choi J.; Head-Gordon M.; and Bell A. T., Zeolite-Catalyzed Isobutene Amination: Mechanism and Kinetics. *ACS Catal.* 9, (2019) 7012–7022. DOI 10.1021/acscatal.9b01799.
- Ho, C. R.; Defalque, V.; Zheng S.; and Bell A. T., Propanol Amination over Supported Nickel Catalysts: Reaction Mechanism and Role of the Support. *ACS Catal.* 9, (2019) 2931–2939. DOI 10.1021/acscatal.8b04612.
- Li Y.; and Yang, P. Co-Feeding Copper Catalysts Couple Carbon. *Nat. Nanotech.* 14, (2019) 1002–1003, DOI 10.1038/s41565-019-0575-y.
- F. Liu, H.-L. Han, L. M. Carl, D. Zherebetsky, K. An, L.-W. Wan and G. A. Somorjai, Catalytic 1-Propanol Oxidation on Size-Controlled Platinum Nanoparticles at Solid-

- Gas and Solid-Liquid Interfaces: Significant Differences in Kinetics and Mechanisms. *J. Phys. Chem. C* 123 (13), (2019) 7577–7583. DOI 10.1021/acs.jpcc.8b00405.
- M. W. Mara, D. S. Tatum, A. M. March, G. Doumy, E. G. Moore and K. N. Raymond, Energy Transfer from Antenna Ligand to Europium(III) Followed Using Ultrafast Optical and X-ray Spectroscopy. *J. Am. Chem. Soc.* 141, (2019) 11071–11081, DOI 10.1021/jacs.9b02792.
- S. N. Natoli and J. F. Hartwig, Noble-Metal Substitution in Hemoproteins: An Emerging Strategy for Abiological Catalysis. *Acc. Chem. Res.* 52 (2), (2019) 326–335. DOI 10.1021/acs.accounts.8b00586.
- A. I. Nguyen, K. M. Van Allsburg, M. W. Terban, M. Bajdich, J. Oktawiec, M. S. Ziegler, J. P. Dombrowski, K. V. Lakshmi, W. S. Drisdell, J. Yano, S. J. L. Billinge and T. D. Tilley, Stabilization of Reactive Co<sub>4</sub>O<sub>4</sub> Cubane Oxygen-Evolution Catalysts within Porous Frameworks. *Proc. Nat. Acad. Sci.* 116 (24), (2019) 11630–11639, DOI 10.1073/pnas.1815013116.
- E. M. Nichols and C. J. Chang, Urea-Based Multipoint Hydrogen-Bond Donor Additive Promotes Electrochemical CO<sub>2</sub> Reduction Catalyzed by Nickel Cyclam. *Organometallics*. 38 (6), (2019) 1213–1218. DOI 10.1021/acs.organomet.8b00308.
- J. E. Rorrer, A. T. Bell and F. D., Toste, Synthesis of Biomass-Derived Ethers for Use as Fuels and Lubricants. *ChemSusChem* 12, (2019) 2835–2858. DOI 10.1002/cssc.201900535.
- Rorrer, J. E.; Toste F. D.; and Bell A. T.; Mechanism and Kinetics of Isobutene Formation from Ethanol and Acetone over Zn<sub>x</sub>Zr<sub>y</sub>O<sub>z</sub>. *ACS Catal.* 9, (2019) 10588–10604. DOI 10.1021/acscatal.9b03045.
- Ross, M. B.; Li, Y.; De Luna P.; Kim D.; Sargent E. H.; and Yang P., Electrocatalytic Rate Alignment Enhances Syngas Generation. *Joule*. 3 (1), (2019) 257–264. DOI 10.1016/j.joule.2018.09.013.
- Wu C. H.; Zhang S.; Su D.; Xin H.; Fang H.; Eren B.; Murray C. B.; and Salmeron M. B., Bimetallic Synergy in CoPd Alloy Nanocatalysts for CO Oxidation. *Nat. Catal.* 2 (1), (2019) 78–85. DOI 10.1038/s41929-018-0190-6.

(II.) *Jointly funded by this Program and other agencies with intellectual leadership by other funding sources*

- Arnold, P. L.; Halliday, C. J. V.; Puig-Urrea, L.; and Nichol, G. S., "Instantaneous and phosphine-catalyzed arene binding and reduction by U(iii) complexes." *Inorganic Chemistry* 60 (2021) 4162-70. DOI 10.1021/acs.inorgchem.1c00327.
- Arnold, P. L.; Ochiai, T.; Lam, F. Y. T.; Kelly, R. P.; Seymour, M. L.; and Maron, L., "Metallacyclic actinide catalysts for dinitrogen conversion to ammonia and secondary amines." *Nature Chemistry* 12 (2020) 654-59. DOI 10.1038/s41557-020-0457-9.
- Cowie, B. E.; Douair, I.; Maron, L.; Love, J. B.; and Arnold, P. L., "Selective oxo ligand functionalisation and substitution reactivity in an oxo/catecholate-bridged uiv/uiv pacman complex." *Chemical Science* 11 (2020) 7144-57. DOI 10.1039/d0sc02297g.
- Dejesus, J. F., R.; Kerr, W. F.; Penchoff, D. A.; Carroll, X. B.; Peterson, C. C.; Arnold, P. L.; and Jenkins, D. M., "Actinide tetra-n-heterocyclic carbene 'sandwiches'." *Chemical Science* 12 (2021) 7882-87. DOI 10.1039/d1sc01007g.

- Gray, S. J.; Brown, K.; Francis, L. Y. T.; Garden, J. A.; and Arnold, P. L., "Dinuclear ce(iv) aryloxides: Highly active catalysts for anhydride/epoxide ring-opening copolymerization." *Organometallics* 40 (2021) 948-58. DOI 10.1021/acs.organomet.1c00055.
- Kerr, R. W. F.; Ewing, P. M. D. A.; Raman, S. K.; Smith, A. D.; Williams, C. K.; and Arnold, P. L., "Ultraprapid cerium(iii)-nhc catalysts for high molar mass cyclic polylactide." *ACS Catalysis* 11 (2021) 1563-69. DOI 10.1021/acscatal.0c04858.
- Tsapatsis, M.; Lu, P.; Ghosh, S.; Dorneles De Mello, M.; Kamaluddin, H.S.; Li, X.; Kumar, G.; Duan, X.; Abeykoon, M.; Boscoboinik, J.A.; Qi, L.; Dai, H.; Luo, T.; Al-Thabaiti, S.; Narasimharao, K.; Khan, Z.; Rimer, J.D.; Bell, A.T.; Dauenhauer, P.; Mkhoyan, K.A., Few-unit-cell MFI zeolite synthesized using a simple di-quaternary ammonium structure-directing agent. *Angewandte Chemie*. (2021) DOI 10.1002/ange.202104574
- Mao, Y.; Loipersberger, M.; Kron, K. J.; Derrick, J. S.; Chang, C. J.; Sharada, S. M.; and Head-Gordon, M. "Consistent inclusion of continuum solvation in energy decomposition analysis: Theory and application to molecular CO<sub>2</sub> reduction catalysts." *Chemical Science* 12 (2021) 1398-414. DOI 10.1039/d0sc05327a.
- Fuentes, M. A.; Gava, R.; Saper, N. I.; Romero, E.; Caballero, A.; Hartwig, J. F.; and Pérez, P. J. "Copper-catalyzed dehydrogenative amidation of light alkanes." *Angewandte Chemie* (2021). DOI 10.1002/ange.202104737.
- Dover, C. M.; Grinter, D. C.; Yim, C. M.; Murn, C. A.; Bluhm, H.; Salmeron, M.; and Thornton, G., "Orientation of acetic acid hydrogen bonded to acetate terminated TiO<sub>2</sub>(110)." *Surface Science* 699 (2020) 121628. DOI 10.1016/j.susc.2020.121628.
- Lorenzon, M.; Jurow, M.; Hong, M. J.; Lu, Y. H.; Barnard, E. S.; Salmeron, M.; Liu, Y.; Penzo, E.; Schwartzberg, A. M.; and Weber-Bargioni A., "Improved stability and exciton diffusion of self-assembled 2d lattices of inorganic perovskite nanocrystals by atomic layer deposition." *Advanced Optical Materials* 8 (2020) 2000900. DOI 10.1002/adom.202000900.
- Lu, Y.-H.; Morales, C.; Zhao, X.; Van Spronsen, M.A.; Baskin, A.; Prendergast, D.; Yang, P.; Bechtel, H.A.; Barnard, E.S.; Ogletree, D.F.; Altoe, V.; Soriano, L.; Schwartzberg, A.M.; Salmeron, M., "Ulthathin free-standing oxide membranes for electron and photon spectroscopy studies of solid-gas and solid-liquid interfaces." *Nano Letters* 20 (2020) 6364-71. DOI 10.1021/acs.nanolett.0c01801.
- Snider, J.L.; Su, J.; Verma, P.; El Gabaly, F.; Sugar, J.D.; Chen, L.; Chames, J.M.; Talin, A.A.; Dun, C., Urban, J.J., Stavila, V., Prendergast, D., Somorjai, G.A., Allendorf, M.D., Stabilized open metal sites in bimetallic metal-organic framework catalysts for hydrogen production from alcohols. *Journal of Materials Chemistry A* 9, (2021) 10869-10881. DOI 10.1039/d1ta00222h
- Buchwald, S. L.; and Hartwig, J. F., In Praise of Basic Research as a Vehicle to Practical Applications: Palladium-Catalyzed Coupling to Form Carbon-Nitrogen Bonds. *Isr. J. Chem.* 60, (2020) 177-179. DOI 10.1002/ijch.201900167.
- Dery, S.; Berg, I.; Kim, S.; Cossaro, A.; Verdini, A.; Floreano, L.; Toste, F. D.; and Gross, E., Strong Metal-Absorbate Interactions Increase the Reactivity and Decrease the Orientational Order of OH-Functionalized N-Heterocyclic Carbene Monolayers. *Langmuir* 36 (3), (2020) 697-703. DOI 10.1021/acs.langmuir.9b02401.

- Dery, S.; Kim, S.; Feferman, D.; Mehlman, H.; Toste, F. D.; and Gross, E., Site-Dependent Selectivity in Oxidation Reaction on Single Pt Nanoparticles. *Phys. Chem. Chem. Phys.* 22, (2020) 18765-18769. DOI 10.1039/d0cp00642d.
- Smith, P. T.; Kim, Y.; Benke, B. P.; Kim, K.; and Chang, C. J., Supramolecular Tuning Enables Selective Oxygen Reduction Catalyzed by Cobalt Porphyrins for Direct Electrosynthesis of Hydrogen Peroxide. *Angew. Chem. Int. Ed.*, 59, (2020) 4902-4907. DOI 10.1002/anie.201916131.
- Xi, Y., Ma, S., and Hartwig, J.F., Catalytic asymmetric addition of an amine N–H bond across internal alkenes. *Nature* 588, (2020) 254–260. DOI 10.1038/s41586-020-2919-z
- Baek J.; Rungtaweivoranit, B.; Pei, X.; Park, M.; Fakra, S. C.; Liu, Y.-S.; Matheu, R.; Alshimri, S. A.; Alshehri, S.; Trickett, C. A.; Somorjai G. A.; and Yaghi, O., M.; Bioinspired Metal-Organic Framework Catalysts for Selective Methane Oxidation to Methanol. *J. Am. Chem. Soc.* 140 (51), (2018) 18208–18216. DOI 10.1021/jacs.8b11525.
- Cao, Z. ; Derrick, J. S.; Xu, J.; Gao, R.; Gong, M.; Nichols, E. M.; Smith, P. T.; Liu, X.; Wen, X.; Copéret, C.; and Chang, C. J., Chelating N-Heterocyclic Carbene Ligands Enable Tuning of Electrocatalytic CO<sub>2</sub> Reduction to Formate and Carbon Monoxide: Surface Organometallic Chemistry. *Angew. Chem. Int. Ed.* 57 (18), (2018) 4981–4985. DOI 10.1002/anie.201800367.
- Diercks, C. S.; Lin, S.; Kornienko, N.; Kapustin, E. A.; Nichols, E. M.; Zhu, C.; Zhao, Y.; Chang C. J.; and Yaghi O. M., Reticular Electronic Tuning of Porphyrin Active Sites in Covalent Organic Frameworks for Electrocatalytic Carbon Dioxide Reduction. *J. Am. Chem. Soc.* 140 (3), (2018) 1116–1122. DOI 10.1021/jacs.7b11940.
- Eren, B.; Torres, D.; Karshoğlu, O.; Liu, Z.; Wu, C. H.; Stacchiola, D. ; Bluhm, H.; Somorjai, G.; and Salmeron, M., Structure of Copper-Cobalt Surface Alloys in Equilibrium with Carbon Monoxide Gas. *J. Am. Chem. Soc.* 140 (21), (2018) 6575–6581, DOI 10.1021/jacs.7b13621.
- Goulas, K. A.; Song, Y.; Johnson, G. R.; Chen, J. P.; Gohkale, A. A.; Grabow, L. C.; and Toste, F. D., Selectivity Tuning over Monometallic and Bimetallic Dehydrogenation Catalysts: Effects of Support and Particle Size. *Catal. Sci. Technol.* 8 (1), (2018) 314–327. DOI 10.1039/c7cy01306j.
- Horowitz, Y.; Han, H.-L.; Soto, F. A.; Ralston, W. T.; Balbuena P. B.; and Somorjai, G. A., Fluoroethylene Carbonate as a Directing Agent in Amorphous Silicon Anodes – Electrolyte Interface Structure Probed by Sum Frequency Vibrational Spectroscopy and *Ab Initio* Molecular Dynamics. *Nano Lett.* 18 (2), (2018) 1145–1151. DOI 10.1021/acs.nanolett.7b04688.
- Horowitz, Y.; Steinrück, H.-G.; Han, H.-L.; Cao, C.; Abate, I. I.; Tsao, Y.; Toney M. F.; and Somorjai G. A., Fluoroethylene Carbonate Induces Ordered Electrolyte Interface on Silicon and Sapphire Surfaces as Revealed by Sum Frequency Generation Vibrational Spectroscopy and X-ray Reflectivity. *Nano Lett.* 18 (3), (2018) 2105–2111.
- Kim H. W.; Ross M.; Kornienko, N.; Zhang, L.; Guo, J.; Yang P.; and McCloskey, B., Efficient Hydrogen Peroxide Generation Using Reduced Graphene Oxide-based

- Oxygen Reduction Electrocatalysts. *Nat. Catal.* 2018, 1 (4), 282–290, DOI 10.1038/s41929-018-0044-2.
- Luna, P. D.; Quintero-Bermudez, R.; Dinh, C.-T.; Ross, M. B.; Bushuyev, O.; Todorovic, P.; Regier, T.; Yang P.; and Sargent, E. H. Catalyst Electro-Redeposition Controls Morphology and Oxidation State for Selective Carbon Dioxide Reduction. *Nat. Catal.* 1 (2), (2018) 103–110, DOI 10.1038/s41929-017-0018-9.
- Melaet, G.; Stavila, V.; Klebanoff L.; and Somorjai, G. A., The Effect of Aluminum and Platinum Additives on Hydrogen Adsorption on Mesoporous Silicates. *Phys. Chem. Chem. Phys.* 20 (17), (2018) 12075–12083. DOI 10.1039/C7CP07015B.
- Olshansky, L.; Huerta-Lavorie, R.; Nguyen, A. I.; Vallapurackal, J.; Furst, A., Tilley, T. D., and Borovik, A. S., Artificial Metalloproteins Containing Co<sub>4</sub>O<sub>4</sub> Active Sites. *J. Am. Chem. Soc.* 140 (8), (2018) 2739–2742. DOI 10.1021/jacs.7b13052.
- Sahar, D.; Kim, S.; Haddad, D.; Cossaro, A.; Alberto, V.; Floreano, L.; Toste, F. D.; and Gross, E., Identifying Site Dependent Reactivity in Oxidation Reactions on Single Pt Particles. *Chem. Sci.* 9 (31), (2018) 6523–6531. DOI 10.1039/c8sc01956h.
- Smith, P. T; Benke, B. P.; Cao, Z.; Kim, Y.; Nichols, E. M.; Kim, K.; and Chang C. J.; Iron Porphyrins Embedded into a Supramolecular Porous Organic Cage for Electrochemical CO<sub>2</sub> Reduction in Water. *Angew Chem Int Ed Engl* 57 (31), (2018) 9684–9688. DOI 10.1002/anie.201803873
- Wang, J. Y.; Strom, A. E.; and Hartwig, J. F., Mechanistic Studies of Palladium-Catalyzed Aminocarbonylation of Aryl Chlorides with Carbon Monoxide and Ammonia. *J. Am. Chem. Soc.* 140 (25), (2018) 7979–7993. DOI 10.1021/jacs.8b04073.
- Wu, L.; Gokhale, A.; Goulas, K. A.; Myers, J. E.; Toste, F. D.; and Scown, C. D., A Hybrid Biological-Chemical Approach Offers Flexibility and Reduces the Carbon Footprint of Bio-based Plastics, Rubbers, and Fuels. *ACS Sus. Chem. Eng.* 6 (11), (2018) 14523–14532. DOI 10.1021/acssuschemeng.8b03158.
- Yang, E.; Jang, E. J.; Lee, J. G.; Yoon, S.; Lee, J.; Musselwhite, N.; Somorjai, G. A.; Kwak, J. H., and An. K., Acidic Effect of Porous Alumina as Supports for Pt Nanoparticle Catalysts in n-Hexane Reforming. *Catal. Sci. Technol.* 8 (13), (2018) 3295–3303. DOI 10.1039/c8cy00776d.
- Yim, C. M.; Chen, J.; Zhang, Y.; Shaw, B.-J.; Pang, C.; Grinter, D.; Bluhm, H.; Salmeron, M.; Murny, C.; Michaelides, A.; and Thornton, G., Visualization of Water-Induced Surface Segregation of Polarons on Rutile TiO<sub>2</sub>(110). *J. Phys. Chem. Lett.* 9 (17), (2018) 4865–4871. DOI 10.1021/acs.jpcclett.8b01904.
- Yoon, S.; Oh, K.; Liu, F.; Seo, J. H.; Somorjai, G. A.; Lee, J. H.; and An, K. Specific Metal-Support Interactions between Nanoparticle Layers for Catalysts with Enhanced Methanol Oxidation Activity. *ACS Catal.* 8 (6), (2018) 5391–5398. DOI 10.1021/acscatal.8b00276.
- Balan, A. D.; Olshansky, J. H.; Horowitz, Y.; Han, H. L.; O'Brien, E. A.; Tang, L.; Somorjai, G. A. and Alivisatos, A. P., Unsaturated Ligands Seed an Order to Disorder Transition in Mixed Ligand Shells of CdSe/CdS Quantum Dots. *ACS Nano* 13 (12), (2019) 13784–13796. DOI 10.1021/acsnano.9b03054.
- Dery, S.; Kim, S.; Tomschun, G.; Berg, I.; Feferman, D.; Cossaro, A.; Verdini, A.; Floreano, L.; Kluener, T.; Toste, F. D.; and Gross, E. Elucidating the Influence of Anchoring Geometry on the Reactivity of NO-Functionalized N-Heterocyclic Carbene

- Monolayers. *J. Phys. Chem. Lett.* 10, (2019) 5099–5104. DOI 10.1021/acs.jpcllett.9b01808.
- Dery, S.; Kim, S.; Tomschun, G.; Hannad, D.; Cossaro, A.; Verdini, A.; Floreano, L.; Kluener, T.; Toste, F. D.; and Gross, E., Flexible NO<sub>2</sub>-Functionalized N-Heterocyclic Carbene Monolayers on Au(111) Surface. *Chem. Eur. J.* 25, (2019) 15067–15072. DOI 10.1002/chem.201903434.
- Jia, S.; He, D.; and Chang, C. J., Bioinspired Thiophosphorodichloridate Reagents for Chemoselective Histidine Bioconjugation. *J. Am. Chem. Soc.* 141, (2019) 7294–7301. DOI 10.1021/jacs.8b11912.
- Lee, S.; Uliana, A.; Taylor, M. K.; Chakarawet, K.; Bandaru, S. R. S.; Gul, S.; Xu, J.; Ackerman, C. M.; Chatterjee, R.; Furukawa, H.; Reimer, J. A.; Yano, J.; Gadgil, A.; Long, G. J.; Grandjean, F.; Long, J. R.; and Chang, C. J., Iron Detection and Remediation with a Functionalized Porous Polymer Applied to Environmental Water Samples. *Chem. Sci.* 10, (2019) 6651–6660. DOI 10.1039/C9SC01441A.
- Neugebauer, M. E.; Sumida, K. H.; Pelton, J. G.; McMurry, J. L.; Marchand, J. A.; and Chang, M. C. Y., A Family of Radical Halogenases for the Engineering of Amino Acid-Based Products. *Nat. Chem. Biol.* 15, (2019) 1009–1016. DOI 10.1038/s41589-019-0355-x.
- Ross, M. B.; De Luna, P.; Li, Y.; Dinh, C. T.; Kim, D.; Yang, P.; and Sargent, E. H., Designing Materials for Electrochemical Carbon Dioxide Recycling. *Nat. Catal.* 2 (8), (2019) 648–658. DOI 10.1038/s41929-019-0306-7.
- Stelson, A. C.; Hong, C. M.; Groenenboom, M. C.; Little, C. A. E.; Booth, J. C.; Orloff, N. D.; Bergman, R. G.; Raymond, K. N.; Toste, F. D.; and Long, C. J., Measuring Ion-Pairing and Hydration in Variable Charge Supramolecular Cages with Microwave Microfluidics. *Commun. Chem.* 2, (2019) 54. DOI 10.1038/s42004-019-0157-9.
- Trickett, C. A.; Popp, T. M. O.; Su, J.; Yan, C.; Weisberg, J.; Huq, A.; Urban, P.; Jiang, J.; Kalmutzki, M. J.; Liu, Q.; Baek, J.; Head-Gordon, M. P.; Somorjai, G. A.; Reimer, J. A.; and Yaghi, O. M., Identification of the Strong Bronsted Acid Site in a Metal-Organic Framework Solid Acid Catalyst. *Nat. Chem.* 11 (2), (2019) 170–176. DOI 10.1038/s41557-018-0171-z.

## Surface and Gas Phase Chemistry of Boron-Catalyzed Oxidative Dehydrogenations

Ive Hermans

Department of Chemistry & Department of Chemical and Biological Engineering  
University of Wisconsin-Madison, 1101 University Ave, Madison, Wisconsin 53706

### Presentation Abstract

Aerobic alkane oxidation with minimal production of CO<sub>x</sub> is a desirable alternative to naphtha cracking and direct dehydrogenation for ethylene and propylene production. For years, supported vanadium oxide was determined to be the state-of-the-art catalyst for oxidative dehydrogenation (ODH) despite that it is subject to over-oxidation to CO and CO<sub>2</sub>. Recently, boron-containing catalysts have been identified as high performing materials for ODH of propane with low CO<sub>x</sub> selectivity. During this presentation I will highlight the insights we obtained in the ODH of propane over boron-containing catalysts. Product formation takes place both on the surface of the catalyst and, unlike on metal oxides, as well in the gas phase. All relevant elementary reaction steps, the proposed active sites, and insights into the enhanced selectivity of boron materials will be discussed.

### DE-SC0017918 - *Controlled Activation of Molecular Oxygen on Boron Nitride Materials for Selective Oxidation Catalysis*

**Postdoc(s):** Lesli O. Mark

**Student(s):** William P. McDermott

### RECENT PROGRESS

For reporting period 09/2020-2021, our objectives were to: (1) characterize the surface reactivity of bulk and supported boron catalysts, (2) decouple the contributions of molecular oxygen in boron-based catalyst to better understand its role in surface-mediated radical reactions, and (3) develop improved supported materials that incorporate the knowledge generated thus far.

Using temperature programmed isopropanol (IPA) decomposition as a molecular probe reaction, we studied the different surface reactivities of the adsorbate over spent bulk BN and B/SiO<sub>2</sub> catalysts via *in-situ DRIFTS* with online-MS for product analysis under oxidative conditions. Surface reactions of IPA may yield propylene over acidic sites via dehydration, and acetone *via* a concerted dehydrogenation mechanism over adjacent acid-base sites, or redox active sites (Scheme 1). IPA adsorption on BN results in the irreversible consumption of B-OH groups and the formation of bridged and terminally bonded isopropoxide species *via* respective dissociative adsorption modes, (Fig. 1A).

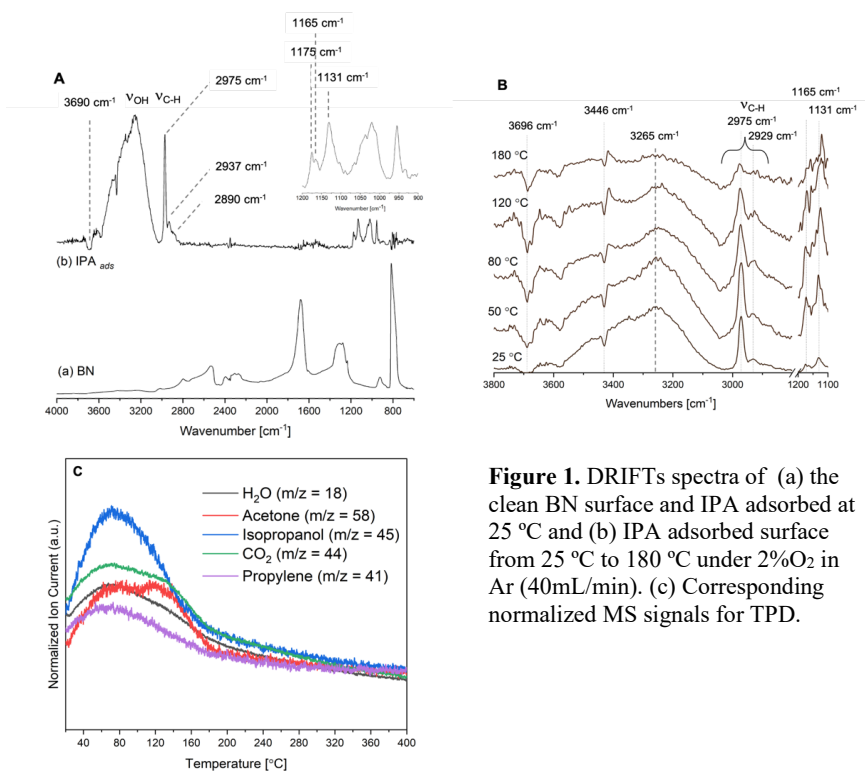


**Figure 1.** DRIFTS spectra of (a) the clean BN surface and IPA adsorbed at 25 °C and (b) IPA adsorbed surface from 25 °C to 180 °C under 2%O<sub>2</sub> in Ar (40mL/min). (c) Corresponding normalized MS signals for TPD.

The band assigned to the  $\alpha$ -C-H bond on BN is profoundly weaker than on B/SiO<sub>2</sub>, suggesting that the oxidized boron surface layer on BN breaks the  $\alpha$ -C-H bond more readily. Terminally bonded isopropoxide species, remain stable up to 180 °C, well beyond the observed product signals in MS, suggesting that the bridge bonded isopropoxide species are reactive intermediates for BN (Fig. 1B). This

provides further evidence that proximity and mobility requirements are principal criterion for reactivity on the BN surface. Major products observed were reversibly adsorbed IPA, propylene, acetone, CO<sub>2</sub>, and water, with an onset temperature of 40 °C, (Fig. 1C). 6.4 wt % B/SiO<sub>2</sub> was similarly studied. The surface exhibited isolated Si-OH and B-OH features. This is notable because no isolated B-OH modes were detected on BN, but rather a low broad signal in the OH region. The B/SiO<sub>2</sub> surface therefore presented a higher degree of hydroxylation and different surface acidity. No bridge or terminally bonded IPA was detected, and all C-H stretching bands assigned to the adsorbed IPA persist up to 400 °C, which was very dissimilar to BN. Major products observed were reversibly adsorbed IPA, propylene, acetone, CO<sub>2</sub> and water, with an onset temperature of 40 °C and at 240 °C. While the two-feature product distribution profile mirrors our previous TGA-DSC-MS study of adsorbed IPA on the plane SiO<sub>2</sub> support, the appearance of propylene and acetone at both onset temperatures is new. This may be attributed to the presence of the oxidized boron surface layer, given that no acetone was observed on the plane support and only H<sub>2</sub>O and CO<sub>2</sub> was observed at the second onset—owing to the combustion of surface isopropoxide groups. Our next steps involve further analysis of the SiO<sub>2</sub> support to understand whether the presence of the support or the synthetic protocol result in increased Brønsted acidity and how this influences the observed oxidative dehydrogenation pathways. It has been shown that the adsorbed alcohol likely participates in the dehydration pathway to propylene. Comparison between the BN and 6.4 wt % B/SiO<sub>2</sub> provides early evidence that the oxidized boron surface exhibits primarily redox reactivity to acetone.

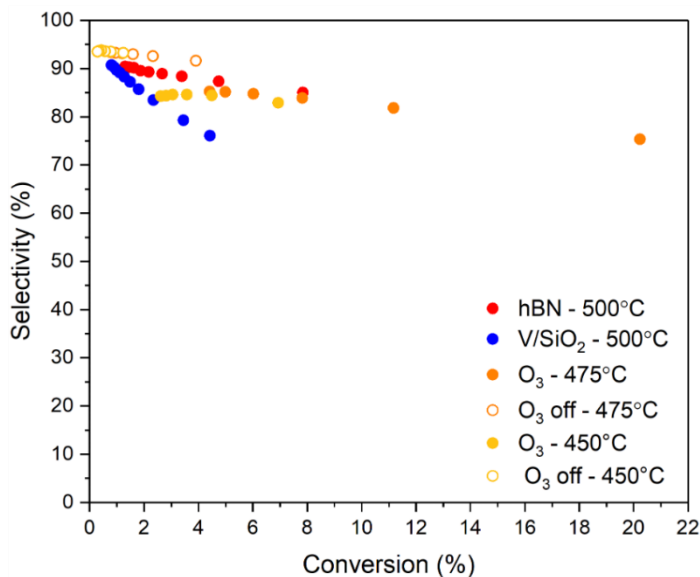


**Figure 2.** Comparison of propylene selectivity as a function of conversion for O<sub>3</sub>, h-BN, and V/SiO<sub>2</sub>. O<sub>3</sub>-mediated ODH conditions:  $P_{C_3H_8} = 0.30$  atm,  $P_{O_2} = 0.149$  atm,  $P_{N_2} = 0.55$  atm, 730 ppm O<sub>3</sub>. h-BN and V/SiO<sub>2</sub> conditions:  $P_{C_3H_8} = 0.30$  atm,  $P_{O_2} = 0.15$  atm,  $P_{N_2} = 0.55$  atm.

selectivity trends between O<sub>3</sub> and h-BN appear coherent to one another (Fig. 3A). The O<sub>3</sub>/O<sub>2</sub> exhibits significantly more CO<sub>x</sub> species, which warrants further study. Additionally, we find that increasing O<sub>3</sub> in the feed decreases propylene selectivity while concurrently increasing CO selectivity (Fig. 3B). Product selectivity at isoconversion across various O<sub>3</sub> concentrations suggests that lower concentrations of O<sub>3</sub> enhance the overall selectivity to the desired propylene product.

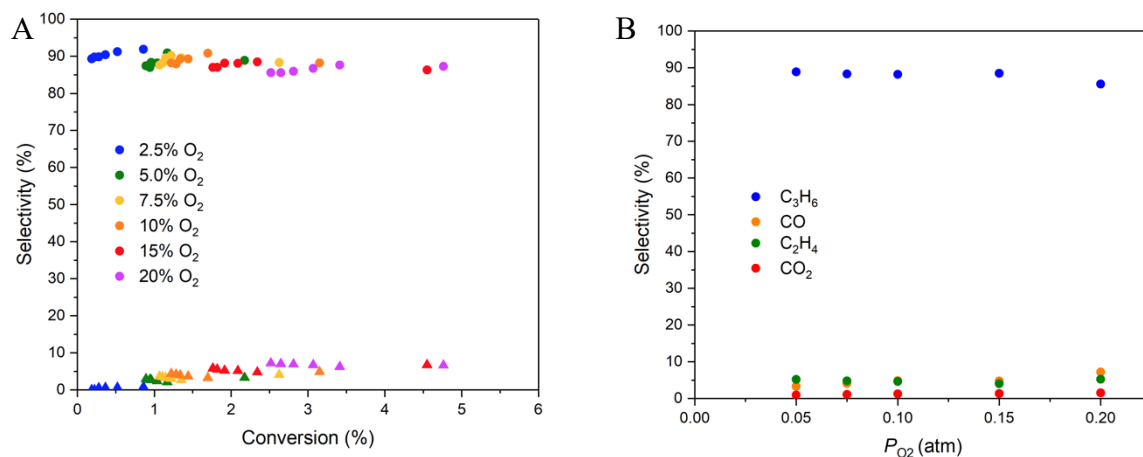


**Figure 3.** (A) Propylene (circles) and CO (triangles) selectivity as a function of conversion at variable concentrations of O<sub>2</sub> and constant O<sub>3</sub>. (B) Propylene selectivity as a function of O<sub>3</sub> concentration at  $X_{C_3H_8} = 4.5\text{-}5.4\%$ .  $P_{C_3H_8} = 0.30$  atm, 120 ppm O<sub>3</sub>, balance N<sub>2</sub>.  $F_{tot} = 40 - 140$  mL min<sup>-1</sup>.  $T = 450^\circ\text{C}$ .

By examining whether ozone might initiate gas phase reactions with propane in a homogeneously catalyzed system, we aimed to decouple the individual contributions of the surface reactions and the subsequent gas radical reactions involving molecular oxygen. Ozone, O<sub>3</sub>, is well known for its decomposition to O<sub>2</sub> and O•, the latter being a highly reactive species capable of abstracting H-atoms from alkanes.<sup>1</sup> Catalytic studies in trace amounts of O<sub>3</sub> offer key insights into the difference between surface mediated gas-phase and solely homogeneous gas-phase reactive pathways while offering potential opportunities for scale up. Our key findings show that while background conversion of C<sub>3</sub>H<sub>8</sub> and O<sub>2</sub> in the empty reactor is limited, the introduction of 730 ppm of O<sub>3</sub> increases the conversion of C<sub>3</sub>H<sub>8</sub> from 1.2 % to 6.9 % and from 3.9% to 20.2% at 450°C and 475°C, respectively (Fig. 2). Conversion-

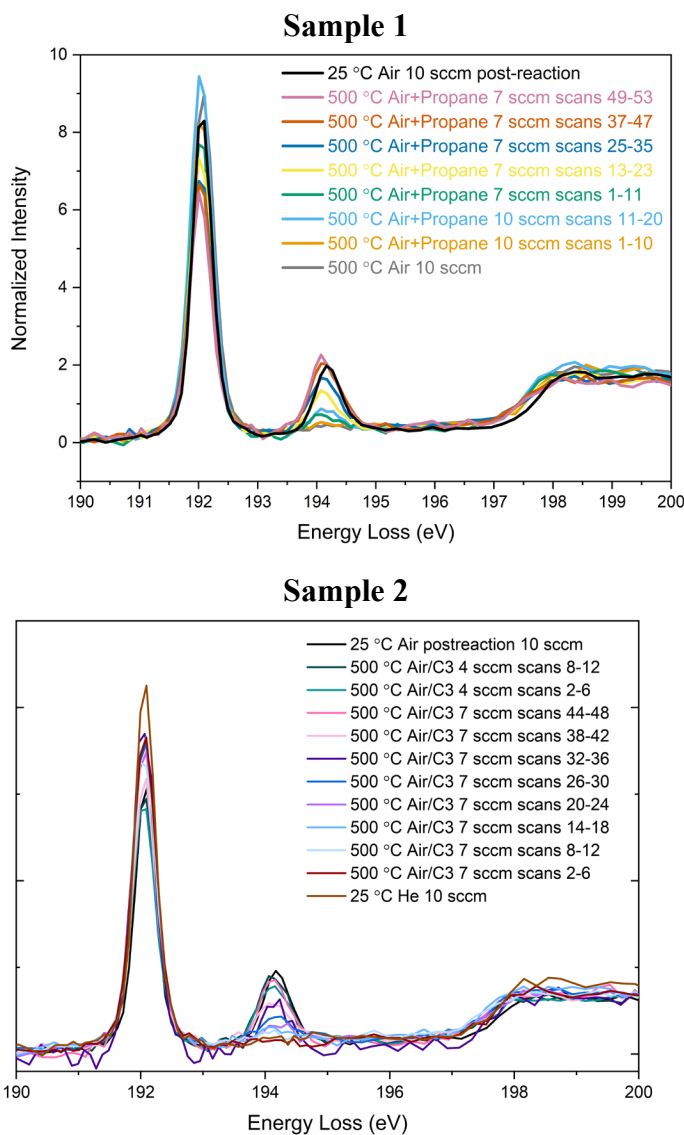


**Figure 4.** Normalized X-ray Raman spectra showing the boron K-edge region measured under reaction conditions. Each individual line is an average of several scans, as indicated in the legend. Sample 1 and 2 were two different capillary tubes. Spectra are labelled in chronological

area of the  $\text{BO}_3$  species increases gradually, while the  $\text{BN}_3$  species peak area decreases, before levelling off. Decreasing the gas flow rate (e.g., 10 mL/min to 7 mL/min), in turn increasing the contact time, leads to an increased rate of oxide formation, suggesting that conversion is correlated with oxide formation, at least during the induction period. These results provide the foundation for future operando XRS that explore surfacer changes under different kinetic regimes as well as using other boron catalysts.

### Publications Acknowledging this Grant in 2018-2021

1. Mark, L. O.; Dorn, R. W.; Mcdermott, W. P.; Agbi, T. O.; Altvater, N. R.; Jansen, J.; Lebrón-Rodríguez, E. A.; Cendejas, M. C.; Rossini, A. J.; Hermans, I. Highly

We performed operando X-ray Raman spectroscopy (XRS) of exfoliated h-BN at beamline 15-2 of the Stanford Synchrotron Radiation Lightsource (SSRL) at the Stanford Linear Accelerator National Lab (SLAC). XRS is a hard X-ray technique that provides soft XAS data. This photon-in/photon-out method measures the energy loss of an incident high energy X-ray ( $\sim 6.5$  keV), enabling the collection of soft XAS information without the experimental conditions required for soft x-rays. Our goal with these experiments was first to simply observe the fresh catalyst surface as it becomes oxidized during the induction period, as this dynamic behavior had not yet been directly observed. In two separate experimental runs, we were able to track the growth of a peak indicative of  $\text{BO}_3$ -types species concomitant with a decrease of  $\text{BN}_3$ -type species (Fig 4). **This is the first direct observation of oxide formation during ODH.** The integrated peak

- Selective Carbon-Supported Boron for Oxidative Dehydrogenation of Propane. *ChemCatChem*. **2021**, selected for cover.
2. McDermott, W. P. Development of Boron-based Catalysts for the Oxidation of Light Alkanes to Olefins. PhD Thesis, University of Wisconsin – Madison, April 2021.
  3. McDermott, W. P.; Cendejas, M. C.; Hermans, I. Recent Advances in the Understanding of Boron-Containing Catalysts for the Selective Oxidation of Alkanes to Olefins. *Top. Catal.* **2020**, *63*, 1700–1707.
  4. Venegas, J. M.; Zhang, Z.; Agbi, T. O.; McDermott, W. P.; Alexandrova, A.; Hermans, I. Why Boron Nitride is such a Selective Catalyst for Oxidative Dehydrogenation of Propane. *Angew. Chem., Int. Ed.* **2020**, *59*, 16527-16535.
  5. Love, A. M.; Cendejas, M. C.; Thomas, B.; McDermott, W. P.; Uchupalanun, P.; Kruszynski, C.; Burt, S. P.; Agbi, T.O.; Rossini, A. J.; Hermans, I. Synthesis and Characterization of Silica-Supported Boron Oxide Catalysts for the Oxidative Dehydrogenation of Propane. *J. Phys. Chem. C*, **2019**, *123*, 27000-27011.
  6. McDermott, W. P.; Venegas, J. M.; Hermans, I. Selective Oxidative Cracking of n-Butane to Light Olefins over Hexagonal Boron Nitride with Limited Formation of Cox. *ChemSusChem*. **2019**, *13*, 152-158.

#### **Awards or leadership activities during 2018-2020 calendar years**

- 2020 Alexander von Humboldt Professorship, von Humboldt Foundation (Berlin, 2020), declined.
- 2019 Finalist Blavatnik Award, New York Academy of Sciences and the Blavatnik Family Foundation (New York, 09/23/2019).
- Inducted as a Member of *Sigma Xi, The Scientific Research Honor Society* (2019).
- 2019 Ipatieff Prize, American Chemical Society (citation: “For innovative contributions and industrial impact in catalytic oxidations and other chemical transformations”; Orlando, 3/31-4/4/2019).
- 2018 Inaugural Robert Augustine Award, the Organic Reactions Catalysis Society (citation: “For contributions to catalysis of organic reactions of industrial importance”; San Diego, 04/2018).
- Member of the International Scientific Advisory board of the Inorganometallic Catalyst Design Center (ICDC), an Energy Frontier Research Center
- Member of the editorial board of *Journal of Catalysis* (Elsevier; 2021-)
- Member of the editorial Advisory board of *Reaction Chemistry and Engineering* (RSC; 2016-)
- Member of the International Advisory Board of *ChemCatChem* (Wiley-VCH; 2020-)
- Member of the International Advisory Board of *ChemSusChem* (Wiley-VCH; 2015-)
- Member of the editorial Advisory board of *ACS Sustainable Chemistry & Engineering* (ACS; 2019-)

**Theoretical Investigation of Heterogeneous Catalysis at the Solid-Liquid Interface for the Conversion of Lignocellulosic Biomass Model Molecules**

Andreas Heyden  
University of South Carolina, Department of Chemical Engineering

**Presentation Abstract**

The objective of this research program is to develop and validate a hierarchy of multi-scale methods for computing rates of elementary processes occurring at metal-water interfaces. Next, we extend these methods to enable solvation effect studies in porous media such as zeolites. Furthermore, we apply these methods to the rational design of novel heterogeneous catalysts with exceptional activity and selectivity for the liquid-phase conversion of lignocellulosic biomass into transportation fuels or commodity and specialty chemicals. Selectivity issues in the reductive deoxygenation of glycerol, guaiacol, and organic acids such as propionic acid and levulinic acid are investigated over Pt-group metal catalysts and zeolite-supported metal catalysts under aqueous-phase processing conditions. Glycerol is a model molecule for polyols and a major by-product of the biodiesel production from transesterification of vegetable oils, and the diversification of products derived from glycerol has been identified as a key issue in the biodiesel production. Next, guaiacol is a model for lignin building blocks in the phenolic fraction of bio-oils. Valorization of this phenolic fraction by conversion into hydrocarbon fuels or aromatic chemicals has the potential to improve the viability of a future bio-refinery. Finally, propanoic acid is a model organic acid of importance for upgrading of bio-oils from pyrolysis of lignocellulosic biomass and levulinic acid is a biomass platform chemical that can be produced inexpensively but that needs to be deoxygenated to facilitate its separation from its aqueous broth that levulinic acid is produced in.

**DE-SC0007167: Theoretical Investigation of Heterogeneous Catalysis at the Solid-Liquid Interface for the Conversion of Lignocellulosic Biomass Model Molecules**

**Postdoc(s):** Biplab Rajbanshi, Wenqiang Yang, Md. Saleheen

**Student(s):** Subrata Kundu, Mehdi Zare

**RECENT PROGRESS**

***Liquid phase effects on adsorption processes in heterogeneous catalysis***

Aqueous solvation free energies of adsorption have recently been measured for phenol adsorption on Pt(111) surfaces. Endergonic solvent effects of >1.4 eV suggest solvents dramatically influence a metal catalysts activity with significant implications for catalyst design. However, measurements are indirect and involve adsorption isotherm models which potentially reduces the reliability of the measurements. Computational, implicit solvation models predict exergonic solvation effects for phenol adsorption, failing to agree with measurements even qualitatively. In this study, an explicit, hybrid QM/MM approach

for computing solvation free energies of adsorption is developed, solvation free energies of phenol adsorption are computed, and experimental data for solvation free energies of phenol adsorption are reanalyzed using multiple adsorption isotherm models. Explicit solvation calculations predict an endergonic solvation free energy of  $1.48 \pm 0.04 \text{ eV}$  for phenol adsorption on Pt(111), that agrees with measurements to within the experimental uncertainty. Computed adsorption free energies of solvation of carbon monoxide, ethylene glycol, and phenol over the (111) facet of Pt and Cu suggests that liquid water destabilizes all adsorbed species, with the largest impact on the largest adsorbates. Figure 1 displays an Arrhenius plot of the solvation effect for phenol adsorption on Pt(111). The solvent effect on the enthalpy and entropy of adsorption is  $0.71 \text{ eV}$  and  $-2.6 \text{ meV/K}$ , demonstrating that the strong endergonic solvation effect on phenol adsorption originates from both enthalpic and entropic contributions that both reduce the amount of phenol adsorption under catalytic conditions.

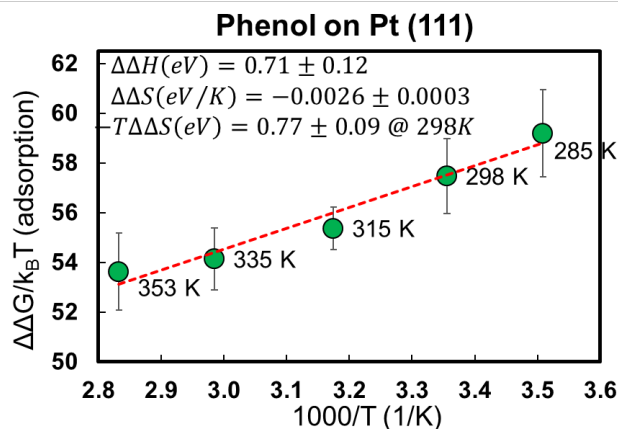


**Fig. 1:** Temperature dependence of the aqueous-phase effect on the free energy of low coverage adsorption of phenol over a Pt(111) surface ( $\Delta\Delta G = \Delta\Delta G_{\text{Adsorbate}}^{\text{gas} \rightarrow \text{liq}}(\theta_{\text{Adsorbate}} = 0)$ ). Error bars indicate 95% confidence intervals based on limited water sampling and multiple (three) independent simulations.

### ***Investigation of the deoxygenation of lignocellulosic biomass model molecules over transition metal surfaces***

The effects of an aqueous phase on the ethanol decomposition for hydrogen production over a Ru(0001) catalyst surface model have been investigated from first principles. Solvent effects on the reaction mechanism and kinetic parameters have been quantified with the help of a microkinetic reactor model, density functional theory, and an implicit solvation scheme (*iSMS*). Our calculations indicate that in both vapor- and aqueous-phase reaction environments, the ethanol decomposition starts with acetaldehyde formation on the surface, some of which further dehydrogenates to ketylenyl species (CHCO), where the C-C bond cleaves to form methylidyne (CH) and CO. In the vapor phase, adsorbed CH gets hydrogenated to methane, and CO desorbs or undergoes methanation reducing the amount of hydrogen produced. In contrast, under aqueous phase reaction conditions, the methanation is inhibited, and the water-gas shift (WGS) reaction is accelerated, leading to complete conversion of CO to CO<sub>2</sub> and H<sub>2</sub>. Despite a one order of magnitude higher overall turnover frequency and higher selectivity for C-C bond cleavage at low conversion in the vapor phase (~70%) relative to the aqueous phase (~50%), the fast conversion of CO to CO<sub>2</sub> via WGS and the suppression of the methanation reaction leads to a higher hydrogen yield in an aqueous reaction environment.

Next, Cu-based alloy catalysts have recently been investigated experimentally for the hydrodeoxygenation (HDO) of biomass derived organic acids. Here, we studied the HDO of propanoic acid (PAC) over Cu(111) by mean-field microkinetic modeling based on parameters obtained from first-principles calculations. Models were developed for the gas- and liquid-phase HDO in condensed water and 1,4-dioxane. In agreement with experimental observations, the gas-phase PAC conversion rate is low at 573 K and increases in liquid water by one order of magnitude. In all reaction environments, the decarboxylation mechanism is dominant at low hydrogen partial pressures less than 0.1 bar, and the C-COO bond dissociation is the rate-controlling elementary step. This observation contrasts with the rate-controlling step identified over most Group VIII metal surfaces, which is the C-OH bond dissociation in the decarbonylation mechanism. At high hydrogen (H<sub>2</sub>) partial pressures greater than 10 bar, the HDO of PAC produces propionaldehyde that can re-adsorb and further react through decarbonylation to produce C<sub>2</sub> alkane products, which is conceptually different to the low H<sub>2</sub> partial pressure scenario. At high H<sub>2</sub> partial pressure, the initial hydrogenation at the carbonyl carbon of PAC becomes the rate controlling elementary step.

Finally, first-principles periodic density functional theory calculations, continuum solvation models, and mean-field microkinetic reactor modeling have been employed to study the effect of a condensed phase reaction environment for the hydrodeoxygenation of guaiacol over Pt catalysts. Our calculations indicate that the presence of a solvent reaction medium does not alter the reaction mechanism or promote deoxygenation activity of guaiacol over Pt terrace sites. Catechol was found to be the major aromatic product across all reaction environments. Our analysis invalidates the possibility of unsaturated monooxygenates production from catechol. Here, we also observed that liquid water promotes the hydrogenation activity of phenol over Pt(111) sites, the kinetics however, remains challenging. We conclude that Pt terrace sites are not active deoxygenation sites for guaiacol hydrodeoxygenation and a solvent reaction medium does not alter the catalytic activity of the surface despite significant solvation effects.

### **Publications Acknowledging this Grant in 2018-2021**

*(XXIII) Intellectually led by this grant*

1. Zare, M., Saleheen, Md., Kundu, S.K., Heyden, A. Dependency of solvation effects on metal identity in surface reactions. *Commun. Chem.* 3, 187, **2020**, <https://doi.org/10.1038/s42004-020-00428-4>
2. Yang, W., Solomon, R.V., Mamun, O., Bond, J.Q., Heyden, A. Investigation of the reaction mechanism of the hydrodeoxygenation of propionic acid over a Rh(111) surface: A first principles study. *J. Catal.*, 391, 98-110, **2020**. <https://doi.org/10.1016/j.jcat.2020.08.015>
3. Zare, M.; Solomon, R.V.; Yang, W.; Yonge, A.; Heyden, A. Theoretical investigation of solvent effects on the hydrodeoxygenation of propionic acid over a Ni(111) catalyst model. *J. Phys. Chem. C*, 124, 16488-16500 **2020**. Emily Carter Festschrift issue. <https://doi.org/10.1021/acs.jpcc.0c04437>
4. Rajbanshi, B.; Saha, S.; Fricke, C; Ammal, S.C.; Heyden, A. Oxidative Dehydrogenation of Propane on the Oxygen Adsorbed Edges of Boron Nitride

- Nanoribbons. *Catal. Sci. Tech.* **10**, 5181-5195 **2020**.  
<https://doi.org/10.1039/D0CY01031F>
5. Xi, Y.; Heyden, A. Selective Activation of Methane C-H bond in the presence of Methanol on Metal Oxide-Supported Single Atoms. *J. Catal.* **2020**, 386, 12-18.  
<https://doi.org/10.1016/j.jcat.2020.03.036>
  6. Yang, W.; Solomon, R.V.; Lu, J.; Mamun, O.; Bond, J.Q.; Heyden, A. Unraveling the Mechanism of the Hydrodeoxygenation of Propionic Acid over a Pt(111) Surface in Vapor and Liquid Phases. *J. Catal.* **2020**, 381, 547-560.  
<https://doi.org/10.1016/j.jcat.2019.11.036>
  7. Saleheen, M.; Verma, A.M.; Mamun, O.; Lu, J.; Heyden, A. Investigation of Solvent Effects on the Hydrodeoxygenation of Guaiacol over Ru Catalysts. *Catal. Sci. Technol.* **2019**, 8, 6253-6273. Selected as 2019 HOT Catalysis Science & Technology article. <https://doi.org/10.1039/c9cy01763a>
  8. Saleheen, M.; Zare, M.; Faheem, M.; Heyden, A. Computational Investigation of Aqueous-Phase Effects on the Dehydrogenation and Dehydroxylation of Polyols over Pt(111). *J. Phys. Chem. C* **2019**, 123, 19052-19065.  
<https://doi.org/10.1021/acs.jpcc.9b04994>
  9. Mamun, O.; Saleheen, M.; Bond, J.Q.; Heyden, A. Investigation of Solvent Effects in the Hydrodeoxygenation of Levulinic Acid to  $\gamma$ -Valerolactone over Ru catalysts. *J. Catal.* **2019**, 379, 164-179. <https://doi.org/10.1016/j.jcat.2019.09.026>
  10. Saleheen, M.; Heyden, A. Liquid-Phase Modeling in Heterogeneous Catalysis. *ACS Catal.* **2018**, 8, 2188-2194. <https://dx.doi.org/10.1021/acscatal.7b04367>
- II. *Jointly funded by this grant and other grants with intellectual leadership by other funding sources*
11. Chowdhury, A.J.; Yang, W.; Abdelfatah, K.E.; Zare, M.; Heyden, A.; Terejanu, G. A Multiple Filter Based Neural Network Approach to the Extrapolation of Adsorption Energies on Metal Surfaces for Catalysis Applications. *J. Chem. Theory Comput.* **2020**, 16, 2, 1105-1114. <https://dx.doi.org/10.1021/acs.jctc.9b00986>
  12. Abdelfatah, K.; Yang, W.; Solomon, R.V.; Rajbanshi, B.; Chowdhury, A.J.; Zare, M.; Kundu, S.K.; Yonge, A.; Heyden, A.; Terejanu, G.A. Prediction of Transition-State Energies of Hydrodeoxygenation Reactions on Transition-Metal Surfaces Based on Machine Learning. *J. Phys. Chem. C* **2019**, 123, 49, 29804-29810.  
<https://dx.doi.org/10.1021/acs.jpcc.9b10507>
  13. Chowdhury, A.J.; Yang, W.; Walker, E.; Mamun, O.; Heyden, A.; Terejanu, G. Prediction of Adsorption Energies for Chemical Species on Metal Catalyst Surfaces Using Machine Learning. *J. Phys. Chem. C* **2018**, 122, 28142-28150. ACS Editors' Choice. <https://dx.doi.org/10.1021/acs.jpcc.8b09284>

Simon M. Humphrey

**Insights into the Behavior of Classical Catalysts in Non-Classical Environments:  
Rh(I) and Pt(II) Single-Site Catalysts in Phosphine MOFs as Solid-State Ligands**

Stephanie L. White, Samuel Emslie, Benjamin Siu, Naman Katyal, Simon M. Humphrey,  
Graeme Henkelman, Craig Brown (NIST), Jong-San Chang (KRICT, Korea)

Department of Chemistry, University of Texas at Austin, Austin TX 78712

**Abstract**

**Goals.** The objectives of this project are to utilize a unique class of metal-organic frameworks (MOFs) based on triarylphosphines and the corresponding arsines as ‘solid-state ligands’ to support low-valent metal complexes in unusual (*i.e.*, coordinatively strained and/or sterically encumbered) environments. We seek to study the structures of such novel hybrid catalysts with atomic-level scrutiny, and then to utilize the materials in model catalytic studies that can provide previously inaccessible structure-function insights. Further, we aim to employ density functional theory (DFT) to help elucidate the origins of observed reactivity in comparison to molecular catalyst analogues, and to better understand how to design other new MOF-catalyst materials with further-improved properties. Here, we present unusual structural revelations arising from the single crystal X-ray structures of two new catalyst materials prepared with Rh(I) and Pt(II) centers, and their reactivity in hydroformylation and Suzuki coupling, respectively.

**DOE Catalysis Sciences Interest.** Our research directly addresses relevant fundamental questions concerning how critical catalytic reactions performed by established low-valent coordination complexes can be conducted in environments that are energetically significantly perturbed (*i.e.*, beyond the traditional active site). Further, we aim to prepare stable and isolable catalytic intermediates that can be interrogated in detail, but that are transient or otherwise inaccessible under classical solution-phase reaction conditions.

**Grant or FWP Number: DE-SC00250630**

**Insights into the Behavior of Classical Catalysts in Non-Classical Environments:  
Rh(I) and Pt(II) Single-Site Catalysts in Phosphine MOFs as Solid-State Ligands**

**Student(s):** Stephanie L. White, Samuel Emslie, Benjamin Siu, Naman Katyal

**RECENT PROGRESS**

The recently reported modular MOF solid-state ligand, PCM-101<sup>1</sup> (PCM = Phosphine Coordination Material), which contains defined *trans*-P<sub>2</sub> coordination pockets within the micropores, has been exploited to support unusual Rh<sub>2</sub>Cl(CO)<sub>2</sub>L<sub>2</sub> dimeric catalyst moieties. The material (Figure 1) was remarkably prepared by the direct treatment of PCM-101 crystals with a solution of [Rh(CO)<sub>2</sub>Cl]<sub>2</sub> at room temperature. The resulting material retains full crystallinity, enabling an atomic level of scrutiny over the products (Figure 1). Most remarkably, PCM-101 supports neutral P–Rh–Cl–Rh–P dimers that cannot be

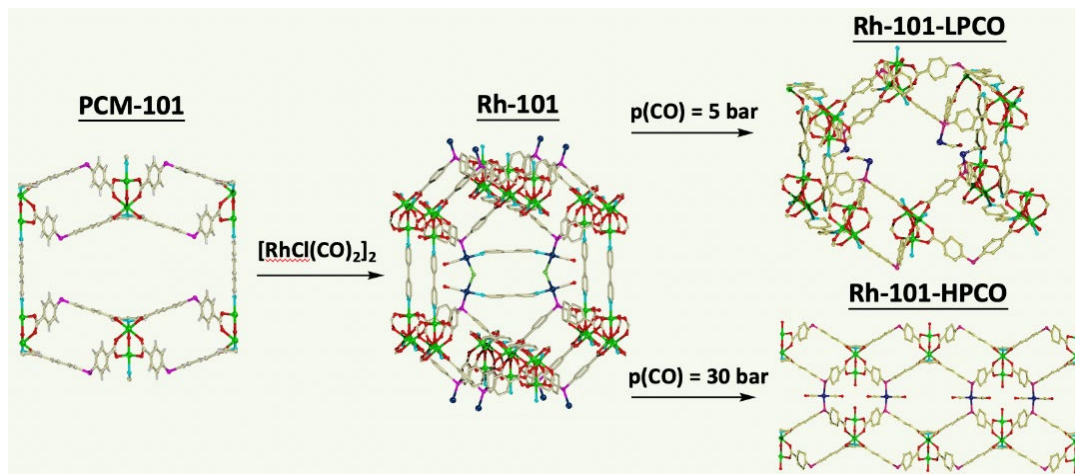
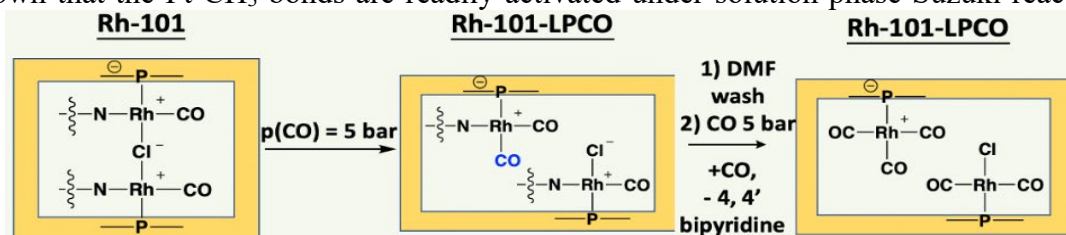


**Figure 1.** **Left:** Crystal structure of PCM-101. **Center:** Crystal structure of post-synthetically modified PCM-101 containing Rh(CO)Cl(bipy)<sub>2</sub> dimers. Color code: Rh = navy; Cl = light green; N = cyan. **Right:** new crystal structures obtained by exposure to different CO pressures; LP = low pressure, HP = high pressure.

accessed by conventional solution coordination chemistry, since the motif would be mono-cationic and would require a counterion to achieve charge-balance. Here, the MOF scaffold can act as the counterion, thus providing access to counterion-free catalysts. We have initially interrogated this system in liquid-phased hydroformylation reactions under 5-30 bar of CO and H<sub>2</sub>. Interestingly, there is a clear reaction selectivity for *n* vs. *iso* products as a function of the CO pressure employed. Through treatment of crystals with CO gas only, we have obtained rare insights into catalyst reorganization. Specifically, at intermediate CO pressure, the Rh–Cl–Rh bond is split to generate two new, asymmetric species (see Scheme 1). At significantly higher CO pressures, the catalyst is irreversibly transformed to a new material, containing only square-planar P<sub>2</sub>Rh(CO)<sup>+</sup> sites.

Concomitantly, we have discovered that when PCM-101 (shown in Figure 1 above) is exposed to a solution of (COD)PtMe<sub>2</sub>, a more unusual rearrangement occurs spontaneously, whereby the 4,4-bipyridine MOF structural elements are removed from between the MOF layers and directly re-incorporated in situ to give Me<sub>2</sub>Pt<sub>4</sub>(bipy)<sub>4</sub> squares that are supported between P: sites (Figure 2). This material is presently being tested for C-C coupling reactions that may be sensitive to the steric environment of the pores. Initial studies have shown that the Pt-CH<sub>3</sub> bonds are readily activated under solution-phase Suzuki reaction



**Scheme 1.** Observed solid-state structural transitions in Rh(I)-PCM-101 as a function of exposure to 5 atm CO gas, resulting in asymmetric bond cleavage to generate two distinct Rh(I) catalyst sites in the same micropore environment.

conditions (1 atm) to yield active species that are proficient in hetero-couplings between a variety of small aryl iodides and aryl boronic acids. However, there is a stark difference in observed reactivity as a function of aryl group substituent patterns, which we believe is due to the pore environment and could be exploited to achieve product selectivity from crude reagent mixtures.

**Current Work.** We are presently performing final studies on the Rh(I)-PCM-101 system described above, including DFT calculations to better understand the driving forces behind the observed single crystal-to single crystal structural transformations. Meanwhile, catalysis studies with Pt(II)-PCM-XXX are nearing completion, providing structure-selectivity insights into the origins of hetero- and homocoupling of products as a function of reactants and catalyst activation conditions.

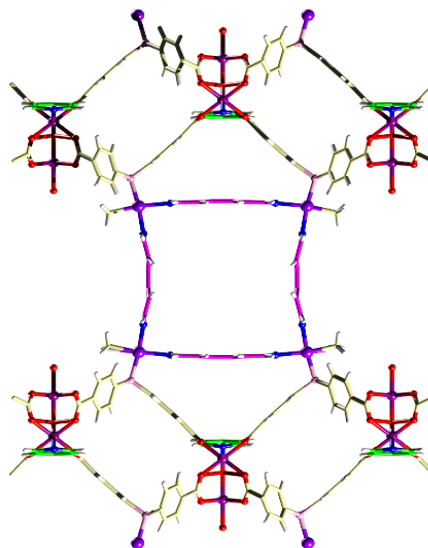


**Figure 2.** Resulting structure when PCM-101 is treated with (COD)PtMe<sub>2</sub>, yielding a tethered molecular square. The Pt(II) atoms are drawn in purple and the 4,4'-bipy groups (viewed side-on) are drawn in pink for clarity.

Michael J. Janik

**Data-driven discovery of intermetallic catalysts with controlled active site nuclearity**

Michael J. Janik,<sup>1</sup> Robert M. Rioux<sup>1</sup>, Zi-Kui Liu,<sup>2</sup> Zachary W. Ulissi<sup>3</sup>

1 - Department of Chemical Engineering, Pennsylvania State University

2- Department of Materials Science and Engineering, Pennsylvania State University

3 – Department of Chemical Engineering, Carnegie Mellon University

**Presentation Abstract**

Binary and ternary intermetallic materials can offer enhanced selectivity in heterogeneous catalysis, and offer a complex and broad composition space. Combining minority active late transition metals (M) with a majority host component (Zn, Cd, or p-block Al, Ga, In, Ge, Sn) within intermetallic structures can provide active sites of controlled nuclearity in the form of  $M_x$  ( $x=1-6$ ) surface exposed clusters separated from each other by host atoms. This project is developing computational tools and a workflow to guide selective intermetallic catalyst design for hydrogenation reactions. The computational workflow begins by mining materials databases (MaterialsProject, AFlowLib) for intermetallic structures within the targeted compositional space. For compositional spaces missing from these databases, the Liu lab has developed the CrystALL approach to generate candidate structures, and this is paired with the SIPFENN (Structure-Informed Prediction of Formation Energy using Neural Networks) to rapidly generate additional candidate intermetallic structures not yet in these databases. All low-index surfaces are then generated for candidate structures, and the nuclearity of all active-metal clusters is enumerated. A subset of surfaces exposing desired nuclearity is then selected for adsorption energy calculations, using automated placement of adsorbates. This method has been used to generate adsorption energies of ethylene, C, and ethyl over ~1000 surfaces that expose isolated active metal atom sites of varying nuclearity. Correlations among adsorbates are explored, and machine learning algorithms are being trained to predict adsorbate binding energies across the wider database of structures. Collaboration with experimental efforts is helping to elucidate active site requirements for selective acetylene hydrogenation and benzene semi-hydrogenation to cyclohexane. We have used  $\gamma$ -brass materials to combine experimental kinetics, DFT, and microkinetic modeling to elucidate active site requirements, including both binary (Pd-Zn) and ternary (Pd-M-Zn, M=Cu, Ag, Au) materials.

**Grant or FWP Number: DE-SC0020147**

**Data-driven discovery of intermetallic catalysts with controlled active site nuclearity**

**Postdoc(s):** Griffin Canning

**Student(s):** Haoran He, Angela Nguyen, Rushi Gong, Unnatti Sharma

## RECENT PROGRESS

### *CrystALL, SIFPENN, and cluster expansion approaches to search for stable Ru-Zn intermetallics*

Ru-Zn bimetallics have shown selectivity for hydrogenation of benzene to cyclohexane. The experimental phase diagram has a paucity of stable structures, showing only a  $\text{RuZn}_5$  stable structure. The CrystALL approach was used to generate candidate structures for Ru-Zn stoichiometries ranging from  $\text{Ru}_3\text{Zn}$  to  $\text{RuZn}_{22}$ . This approach mines available databases of bimetallic structures for similar materials (Fe, Ru, Os – Zn, Cd, Hg binary materials, for this system), and generated  $\sim 500,000$  possible structures. The SIFPENN

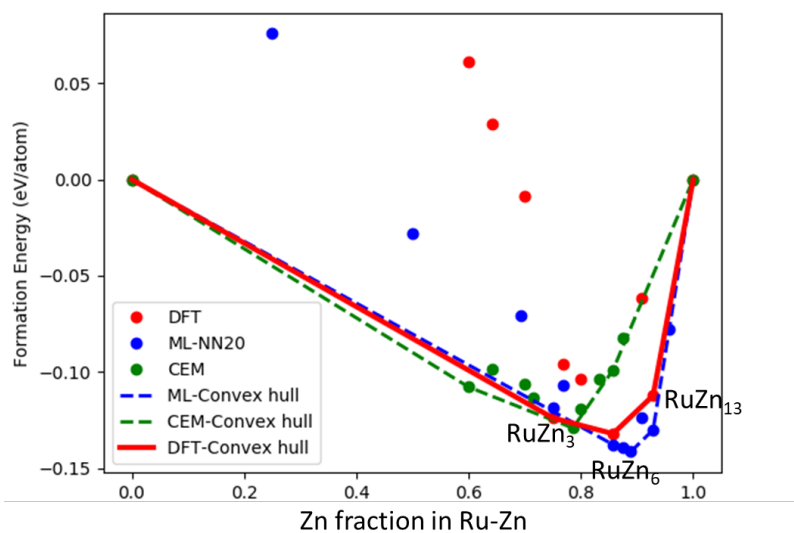


Figure 7. Ru-Zn formation energies for structures near the convex hull in Ru-Zn. Formation energies are shown from the neural network approach (ML-NN20), cluster expansion method (CEM) and direct DFT calculations. NN and CEM approaches considered many more structures, and formation energies are only shown for those structures close enough to the convex hull to motivate DFT refinement.

method then uses a trained neural network to predict the formation energy of Ru-Zn intermetallics in each structure. Structures with formation energies near the convex hull are then examined using direct DFT calculations to generate possible stable intermetallic structures along with the cluster expansion methods (CEM) for the hcp lattice structure (Figure 1). These structures can then be added to our database of potential intermetallic catalysts for screening, or further evaluated computationally for their stability using CALPHAD approaches.  $\text{RuZn}_3$ ,  $\text{RuZn}_6$ , and  $\text{RuZn}_{13}$  appear on the convex hull based on DFT calculations along with a potential hcp-based phase around  $\text{Ru}_2\text{Zn}_3$ .

### *“Nuclearity zoo” utility developed to search intermetallic sites for nuclearity and shape*

During last project year, we reported on a tool developed in the Ulissi group to determine the nuclearity of exposed clusters of active metal atoms on an intermetallic surface (<https://github.com/ulissigroup/NuclearityCalculation>). A new tool was developed to also classify the shape of active metal atom arrangements for nuclearities of 3 or more. A web-based searchable database has been generated (<https://nuclearity-zoo.herokuapp.com/>) to allow researchers to search for intermetallic surfaces that expose active sites of defined nuclearity and shape (see Figure 2).

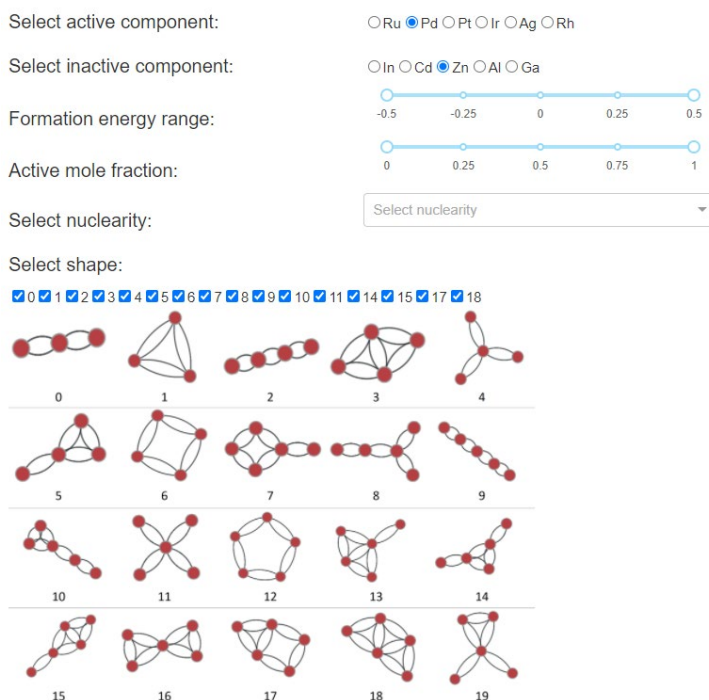


Figure 2. Screenshot of the user interface portion of the web tool to search the database for surface facets of active-host intermetallics for sites of defined nuclearity and shape. <https://nuclearity-zoo.herokuapp.com/>.

### ***Automated evaluation of adsorption energies of unsaturated hydrocarbons on intermetallics***

Following enumeration of nuclearity of low-index surfaces of active-host intermetallics, we chose ~1000 surfaces offering a distribution of different nuclearities to calculate adsorption energies. As a first adsorbate, we automated the placement of ethylene on atop sites and evaluated adsorption energies. We have also evaluated the adsorption energy of atomic C on the same sites, and are currently running the adsorption of ethyl across these sites. Initial analysis shows little correlation of ethylene binding energy and C binding energy. Expecting poor adherence to scaling relationships across this wide assortment of surface compositions and structures, we are training a series of machine learning approaches on this adsorption energy data and assessing their ability to predict binding on other intermetallic surfaces.

### **Publications Acknowledging this Grant in 2018-2021**

*Publications from this grant are currently under review.*

**Awards or leadership activities during 2018-2020 calendar years**

- Outstanding Advising Award from the Penn State Engineering Alumni Society (Spring 2021)
- George W. Atherton Award for Excellence in Teaching from the PSU Schreyer Institute for Teaching Excellence (Spring 2018)
- Associate Department Head of Chemical Engineering, Pennsylvania State University (Sept 2020-current)
- Managing Guest Editor, Catalysis Today special issue in honor of Chunshan Song's receipt of the George Olah award from ACS. (2020-2021).

## Spectroscopic Signatures and Shape-Selective Synthesis of Cyclopentenyl Cations

Friederike C. Jentoft, Eric D. Hernandez, Babgen Manookian, Scott M. Auerbach  
University of Massachusetts Amherst  
Department of Chemical Engineering & Department of Chemistry

### Presentation Abstract

Methanol-to-olefins conversion is known to proceed through long-lived intermediates in the pores of zeolites or zeotypes. The exact constitution and role of these species for formation of select olefins or coke is under debate. Through experiment and DFT, we have found spectra of unsaturated carbocations to be largely independent of the environment, which allows us to use computed gas phase vibrational spectra and measured solution phase UV-vis or IR spectra for the interpretation of respective spectra of cations located inside zeolite pores. Trends known from solution chemistry pertain to species adsorbed on surfaces; that is, the UV-vis absorption wavelength is a linear function of the size of an unsaturated cation (expressed as number of carbon atoms), while the constitution and the number of conjugated double bonds are additional parameters. We have resolved controversies around the allylic  $C=C-C^+$  stretching mode, which is indicative of an acyclic or cyclic nature and of the number of substituents on the allylic system. We apply this knowledge to monitor cyclization of dienyl species and formation of differently substituted cyclopentenyl cations in zeolites with different framework (TON, MFI, MOR). In the pores of TON, the ends of the allylic system of the cyclopentenyl cation are alkyl-substituted, whereas in MOR, all carbons of the allylic system bear alkyl substituents. We propose that the observed cyclization products are the result of kinetic rather than thermodynamic control.

**Grant or FWP Number: DE-SC0021041 Acid Catalysis Design Guided by Spectroscopic Analysis of Reaction Networks**

**Student(s):** Eric D. Hernandez, Dipti M. Bhave

### RECENT PROGRESS

#### *Brief description of scientific problem and approach*

Methanol-to-olefins (MTO) conversion is emerging as an advantageous pathway for the manufacture of small olefins. Catalysts in use for MTO are microporous solid acids, that is, zeolites and zeotypes, with the key materials being HZSM-5 and SAPO-34. In MTO conversion, long-lived surface species (“hydrocarbon pool”) are believed to be essential for product formation. Reported species include methylbenzenium ions and cyclopentenyl cations. Because of the complex mixture present, the exact nature of these species and the role of individual species for product formation are not resolved. At the same time, the selectivity towards specific products can only be partially controlled, while coke formation

is a permanent risk. We hypothesize that selectivity towards desired products can be enhanced if the acid site and its environment are tailored to favor specific intermediates rather than to have an adventitiously formed “pool”. The first stage of this project focuses on the spectroscopic identification of long-lived surface species, study of their reactivity, and elucidation of their contribution to MTO conversion.

### **Identification of surface species by UV-vis and IR spectroscopy**

In the past years (including prior to the start of this project in 2020), we have sought to spectroscopically identify the exact nature of the surface species present during MTO catalysis. A significant fraction of these species are unsaturated carbocations. To progress beyond the first level of assignment of bands, which is the distinction of monoenylic, dienylic, and trienylic cations, a refined spectral interpretation is needed. A major advance was the observation that the spectra are largely independent of the environment, and therefore, DFT-computed gas phase spectra, solution phase spectra, and “in pore”-spectra of the same unsaturated cation are alike. The similarity between the spectra in solution with those of the same cation in zeolite pores is illustrated by the experimental UV-vis and IR spectra of cyclopentenyl cations in Figure 1.

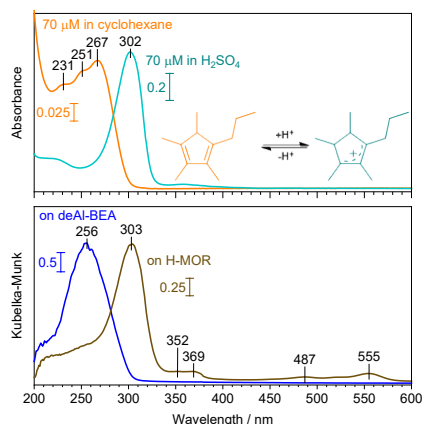


Figure 1a: UV-vis spectra of propyltetramethyl cyclopentadiene and the respective cyclopentenyl cation. Diene in cyclohexane or on dealuminated BEA; cation in sulfuric acid or on H-mordenite.

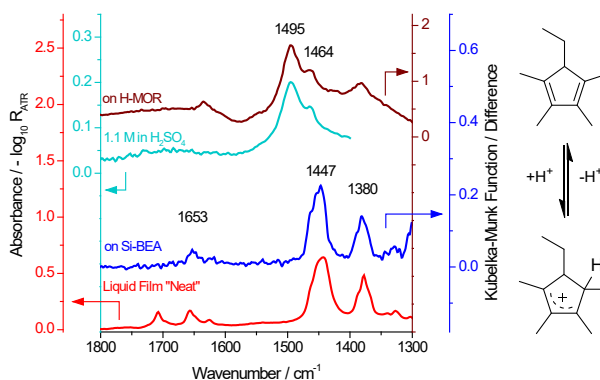


Figure 1b: IR spectra of ethyltetramethyl cyclopentadiene and the respective cyclopentenyl cation. Diene neat or on non-acidic BEA; cation in sulfuric acid or on H-mordenite.

As a result, the vast number of UV-vis spectra of carbocations in liquid acids that are available in the literature can be used as reference, and additional spectra (both UV-vis and IR) can easily be measured. UV-vis spectra are known to obey so-called increment rules with respect to substituents on chromophores; these are well documented for neutral species and can be found in textbooks. Very similar trends have been described in the literature for cations in solution; and we find the spectra of cations in zeolite pores to obey the same rules, with the positions of the maxima falling onto the correlations generated for solution phase cations. We had already published a linear trend in band position with size for methylbenzenium ions in 2014 (Wulfers and Jentoft, ACS Catalysis) and reported a similar trend for acyclic and cyclic cations (Figure 2) in 2020 (Hernandez and Jentoft, ACS Catalysis). To ensure fidelity of the measured spectra, we typically use an immediate

precursor, that is, a diene or triene, and a large pore zeolite, to directly adsorb even large species. The most recent spectroscopic advance is the distinction of the substitution pattern at the allylic system, specifically, 1,3-dialkyl substitution vs. 1,2,3-trialkyl substitution, as can be seen by the two different trendlines for these ions in Figure 2. Because of the overlap of some species regarding their UV–vis absorption, some a priori knowledge of the structure and its stability is needed, or additional information from another method such as IR spectroscopy.

The key vibration of olefins and unsaturated carbocations is the carbon–carbon vibration. Principally, upon protonation of a double bond, the associated carbon–carbon vibration shifts to lower frequency since the bond order decreases. However, the positions of allylic C=C–C<sup>+</sup> stretching vibrations are debated in the literature, and the effects of certain structural elements, acyclic vs. cyclic, larger vs. smaller rings, and of additional conjugated double bonds were not clear. For comparable species, we have now asserted that the allylic stretch (i) of acyclic monoenylic ions occurs at higher frequencies than that of cyclic monoenylic ions, (ii) of cyclic cations decreases with decreasing ring size, and (iii) of dienylic cations is observed at higher frequency than that of monoenylic cations. Moreover, we discovered that the C=C–C<sup>+</sup> stretching vibration is sensitive to the substitution pattern at the allylic unit; specifically 1,2,3-trialkyl-substituted species absorb at lower frequencies than 1,3-dialkyl-substituted species, which, on a simple level, can be understood as an effect of difference in reduced mass. A second criterion for distinction of the substitution patterns is the presence or absence of an allylic C–H stretch. Used in concert, the two spectroscopies and the associated correlations and trends provide powerful means to identify hydrocarbon surface species.

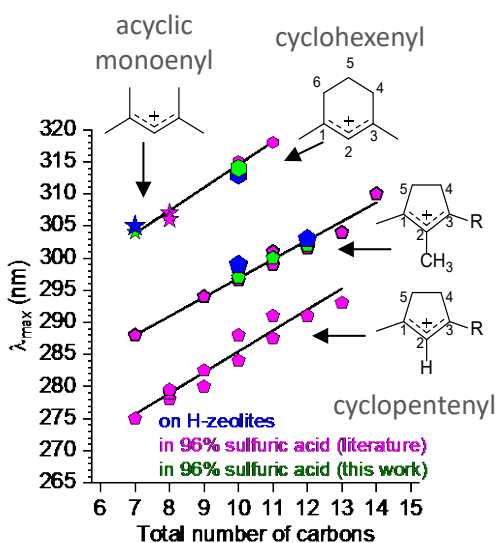


Figure 2: Correlation between wavelength of maximum absorption and total number of carbons for acyclic and cyclic monoenylic cations.

### ***Effect of zeolite pore size on constitution of cations formed through cyclization***

During MTO catalysis, the “hydrocarbon pool” is formed from methanol, implying that numerous C–C bond forming reactions, presumably oligomerizations involving olefins, and cyclization must take place. We determined the influence of the zeolite framework on the structure of cyclopentenyl cations formed via cyclization.

We chose H-ZSM-5 with MFI framework as a commercially relevant MTO catalyst. The MFI framework is characterized by 10-membered rings and a three-dimensional channel network. The TON framework of H-ZSM-22 also has 10-membered rings, but the channel system is one-dimensional and lacks the intersections that provide larger spaces in the MFI framework. Finally, we used BEA and MOR as large-pore zeolites with 12-membered rings and three-dimensional and one-dimensional channel network, respectively.

A straightforward path to a cyclic allylic cation is from a triene precursor, which is protonated to a dienylic cation and cyclizes to a monoenylic cation. We chose 2,6-dimethyl-2,4,6-octatriene.

Adsorption of the dimethyloctatriene at 20 °C on H-MOR, H-ZSM-5, or H-ZSM-22 produced a single strong electronic absorption band at about 400 nm. This band is assigned to the  $\pi \rightarrow \pi^*$  transition of the conjugated allylic system of the 2,6-dimethyloctadienyl cation. The  $\lambda_{\text{max}}$  exhibited very little variation across the three different zeolite frameworks ( $\Delta\lambda_{\text{max}} \approx 2\text{--}4$  nm). In the corresponding IR spectra, a strong, sharp band at about 1568–1567  $\text{cm}^{-1}$  was observed and assigned to the  $\nu_{\text{as}}(\text{C}=\text{C}-\text{C}^+)$  of the octadienyl cation. The band appears to be characteristic of the specific cation, and the position is found to be almost the same in the three different zeolites and (from the literature) also in liquid acid. Cyclization was initiated by heating and occurred in all investigated zeolites. In the UV-vis spectra, the band at 400 nm decreased, indicating conversion of the octadienyl cations, and new bands formed concomitantly, at 298 nm for H-MOR, at 290 nm for H-ZSM-5, and at 287 nm for HZSM-22. The bands at 298 nm and 287 nm cleanly fall onto the known correlations (Figure 3a). The corresponding IR spectra show the  $\nu_{\text{as}}(\text{C}=\text{C}-\text{C}^+)$  band at 1494  $\text{cm}^{-1}$  (H-MOR), 1515  $\text{cm}^{-1}$  (H-ZSM-5), and 1511  $\text{cm}^{-1}$  (H-ZSM-22). These vibrations shift to lower frequency with increasing temperature (Figure 3b). The spectra of the species on H-ZSM-5 and H-ZSM-22 also exhibit the allylic C–H vibration.

We deduce from these data that in large-pore zeolites like H-MOR (and H-BEA), cyclopentenyl cations with an alkyl substituent in the 2-position of the allylic system form. In the medium-pore zeolite H-ZSM-22, cyclopentenyl cations with a hydrogen in the 2-position of the allylic system form. In H-ZSM-5, both types of cations appear to be present.

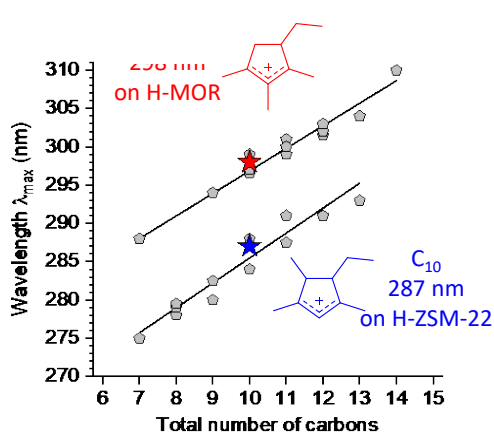


Figure 3a: Interpretation of UV-vis spectra obtained after cyclization of 2,6-dimethyl-2,4,6-octatriene in the pores of H-MOR and H-ZSM-22.

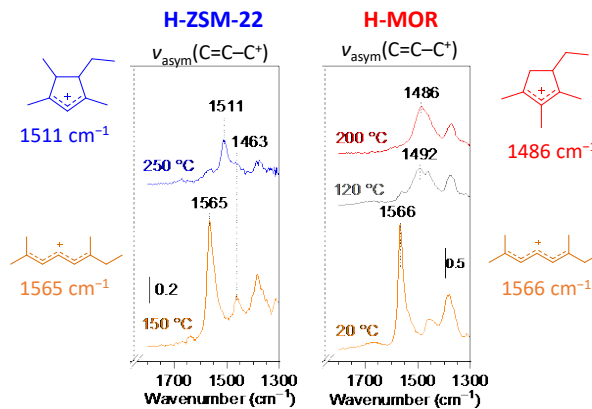


Figure 3b: IR spectra of the 2,6-dimethyl-2,4,6-octadienyl cation and its cyclization product in the pores of H-MOR or H-ZSM-22.

Our collaborators, the Auerbach group in the Department of Chemistry at UMass, found through DFT that the 1,2,3-trialkyl-substituted cyclopentenyl cations principally fit into the pores of all three investigated frameworks. In addition, the 1,2,3-trialkyl-substituted cyclopentenyl cations are always thermodynamically more stable than the 1,3-dialkyl-substituted cyclopentenyl cations, in the gas phase and also in the zeolite, which is consistent with the observations in liquid acids reported in the literature. Hence, the spatial

restrictions during the cyclization presumably lead to the formation of different types of cations depending on pore size.

***Relevance to MTO conversion: Formation of cyclopentenyl cations from ethylene***

We investigated the formation of cyclopentenyl cations from ethylene, which is an early product in MTO conversion and was also used by Haw and co-workers in NMR investigations of hydrocarbon species in zeolite pores.

Ethylene was reacted at a temperature of 200 °C. A single strong electronic band developed at 297, 293, and 286 nm in the UV–vis spectra of the H-MOR, H-ZSM-5, and H-ZSM-22 exposed to ethylene. The corresponding IR spectra contained bands at 1485 cm<sup>-1</sup>, 1507 cm<sup>-1</sup> and 1509 cm<sup>-1</sup>. The band positions match well those appearing following the cyclization of the dimethyloctatriene and are accordingly assigned to cyclopentenyl cations with alkyl substitution (MOR, MFI) or hydrogen substitution (TON, MFI) in the 2-position of the allylic system.

We conclude that cyclopentenyl cations can be considered common and stable intermediates in zeolite pores, and that the zeolite pore topology determines the substitution of the allylic system. In stable species, the 1 and 3 positions of the allylic system are always alkyl-substituted, whereas the 2-position is preferably alkyl-substituted but may be hydrogen-substituted if the cation is formed under spatial constraints.

**Publications Acknowledging this Grant in 2018-2021**

*(XXIV) Jointly funded by this grant and other grants with intellectual leadership by other funding sources*

3. Hernandez, E. D.; Manookian, B.; Auerbach, S. M.; Jentoft, F. C. Shape-Selective Synthesis of Alkylcyclopentenyl Cations in Zeolites and Spectroscopic Distinction of Constitutional Isomers, *ACS Catal.*, revision in preparation.

**Awards or leadership activities during 2018-2020 calendar years**

*Awards*

- ◆ Excellence in Catalysis Award, Catalysis Society of Metropolitan New York (2018)

*Conference organization*

- ◆ Member, Technical Program Committee, North American Catalysis Society Meeting, New York, NY, USA, May 22–27, 2022.
- ◆ Co-organizing symposium “In Honor of Bruce Gates’ 80<sup>th</sup> Birthday”, originally planned for 2020 AIChE (cancelled), now planned for the ACS National Meeting and Exposition, San Diego, CA, USA, 2022.
- ◆ Scientific Committee of the 5<sup>th</sup> International Congress on Catalysis for Biorefineries, Turku, Finland, Sept. 23–27, 2019.
- ◆ Co-organized ACS Symposium “Frontiers in Catalysis for Energy and Sustainability” on behalf of ACS Catalysis Division (CATL), 257<sup>th</sup> ACS National Meeting and Exposition, Orlando, FL, USA, March 31–April 4, 2019.

*Offices in societies*

- ◆ Elected Member at Large, ACS Catalysis Division Executive Committee, 2019-2021 and Chair of ACS CATL Division Educational Committee (2020); launched inaugural ACS CATL Division Educational Seminar Series in fall 2020

## Cascade Catalysis in Tunable Multicompartment Nanoreactors

Eman Ahmed (NYU), Jinwon Cho (GT), Jacob Cleveland (GT), Seung Soon Jang (GT), Christopher W. Jones (GT), Michael Küpfert (NYU), Robin Lawler (GT), Fangbei Liu (NYU), Peiyuan Qu (NYU), Cornelia Rosu (GT), and Marcus Weck (NYU) (NYU) Department of Chemistry and Molecular Design Institute, New York University, New York, NY 10003; (GT) School of Chemical & Biomolecular Engineering, School of Materials Science & Engineering, Georgia Institute of Technology, Atlanta, GA 30332

### Presentation Abstract

Spatial confinement of multiple catalysts presents an effective strategy for performing sequential or tandem chemical transformations in a one-pot reaction. Nature is capable of shuttling reactants and products through individual compartments, allowing for cascade or tandem reaction pathways combining (non-orthogonal) transformations for the synthesis of complex molecules. To date, synthetic analogs to such chemical reaction diversity do not exist, though there is significant interest in one-pot, multistep strategies to supersede intermediate work-up procedures. Spatial catalyst separation may be used to catalyze numerous reactions in conditions that are otherwise incompatible between catalyst and solvent, different catalysts, or reagents. Appropriate site isolation or support structure design will lead to significant advantages in atom economy, purification, and costs; the development of the interface between a catalyst and its confined microenvironment is paramount for realizing the next generation of nanoreactors. Polymer and inorganic scaffolds can create tailor-made microenvironments resulting in catalyst compartmentalization. Through the optimization of several variables such as size, solubility, functionality, and morphology of the nanoreactor, catalyst activity and selectivity can be tuned.

### **DE-FG02-03ER15459: Multi Compartment Nanoreactors as Supports for Incompatible Molecular Catalysts**

**PI:** Seung Soon Jang, Christopher W. Jones, Marcus Weck

**Postdoc(s):** Cornelia Rosu

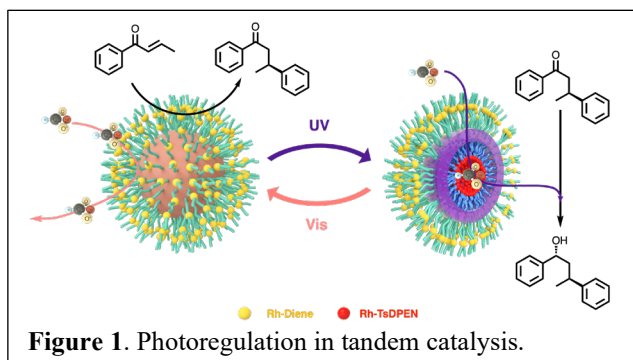
**Student(s):** Eman Ahmed, Jacob Cleveland, Jinwon Cho, Robin Lawler Fangbei Liu, Michael Küpfert, Peiyuan Qu

### RECENT PROGRESS

#### *Compartmentalization and Photo-Regulation for Incompatible Tandem Catalysis*

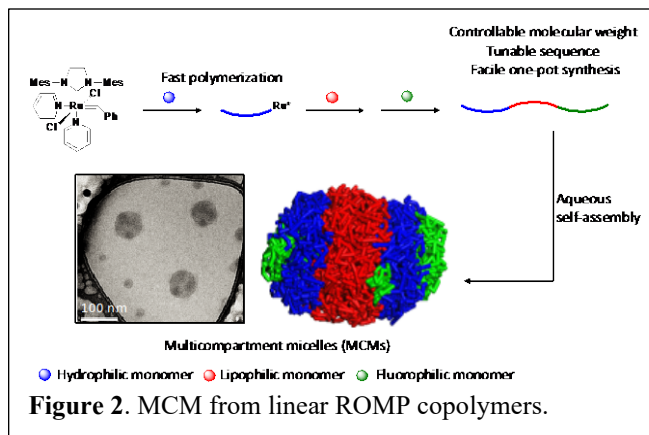
The research team has reported an advanced compartmentalized micellar nanoreactor that possesses a reversible photo-responsive feature and its application towards photo-regulating reaction pathways for incompatible tandem catalysis (Figure 1). Our smart nanoreactor is based on multi-functional amphiphilic poly(2-oxazoline)s and covalently cross-linked with spiropyran upon micelle formation in water. It responds to light irradiation in a wavelength-selective manner, switching its morphology as confirmed by

dynamic light scattering and cryo-transition electron microscopy. The compartmental structure renders distinct nanoconfinements for two incompatible enantioselective transformations: a rhodium-diene complex-catalyzed asymmetric 1,4-addition occurs in the hydrophilic corona while a Rh-TsDPEN-catalyzed asymmetric transfer hydrogenation proceeds in the hydrophobic core. Control experiments and kinetic studies showed that the gated behavior induced by the photo-triggered reversible spiropyran to merocyanine transition in the cross-linking layer is the key to discriminating among substrates/reagents during the catalysis. The smart nanoreactor realized photo-regulation to direct the reaction pathway to give a multi-chiral products with high conversions and ideal enantioselectivities. Our SCM catalytic system, on a basic level, mimics the concepts of compartmentalization and responsiveness that Nature uses to coordinate thousands of incompatible chemical transformations into streamlined metabolic processes.



### *Multicompartment Copolymer Nanoreactors*

The research team is developing multicompartment (MCM) copolymers as catalytic scaffolds for non-orthogonal tandem reactions. We have prepared compartmentalized micelles through the self-assembly of linear triblock terpolymers containing hydrophilic, lipophilic, and fluorophilic domains (Figure 2). The triblock copolymers were synthesized via living ring-opening metathesis polymerization of norbornene-based monomers. Our terpolymer design offers a facile approach for the synthesis of the target materials with fast polymerization kinetics, complete block incorporation and control over block sequence. A range of triblock terpolymers are prepared with variations in block sequence and block ratio and self-assembled in aqueous media. Interaction parameter ( $\chi$ ) values between each block are determined using a Flory-Huggins based computational model. “Core-shell-corona,” “disk-like,” “raspberry-like” and “worm-like” morphologies are observed through cryogenic transmission electron microscopy and dissipative particle dynamics simulations.



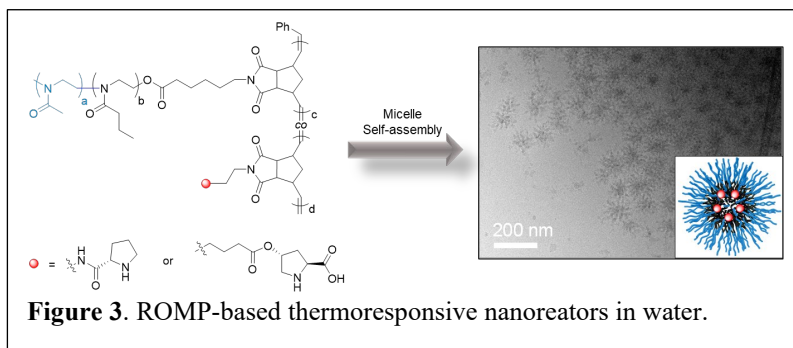
### *Thermoresponsive Nanoreactors for Asymmetric Aldol Addition in Water*

The manipulation and tunability of self-assembled block copolymers through external stimuli presents an attractive strategy to develop smart polymer-based nanoreactors as supports for non-orthogonal tandem catalysis. We synthesized thermoresponsive core-shell micelles based on poly[norbornene-poly(2-methyl-2-oxazoline-block-2-propyl-2-

oxazoline)]-graft-poly[norbornene L-proline] (P[NB-P(MeOx-b-PropOx)]-graft-P[NB-L-proline]) as catalyst supports for L-proline (Figure 3). These

molecular brushes exhibit large differences in lower critical solution temperature behavior and nanostructure size in water depending on the chain-lengths and proline connectivity. L-Proline-

mediated aldol reactions expose the efficiency by which the molecular brushes self-assemble into micelles. Molecular brushes with an extended backbone show higher activity and selectivity, suggesting better core-shell segregation of the micelles and exclusion of water from the catalytic site. We envision that the combination of triggerable units and self-assembled polymers will be increasingly important to create catalysts with specified activities, similar to the biological cell.



### *Azobenzene Cross-linked SCMs as Photoresponsive Nanoreactors*

Shell cross-linked micelles (SCMs) are fascinating catalytic systems to provide unique compartmentalization and responsiveness to mimic Nature's cells. Responsive catalytic systems can externally modulate catalytic reactivities and direct reaction pathways for multistep synthesis. We synthesized photoresponsive SCMs cross-linked by bifunctionalized photoswitchable azobenzene ( $N_3$ -AB- $N_3$ ). The azobenzene (AB) cross-linked SCMs were based on the assembly of amphiphilic triblock copolymers of poly(2-oxazoline)s with orthogonal functionalities at various locations. The photoresponsive SCMs respond to different wavelengths of light and switch their physicochemical properties. A micelle size change of 25 nm upon irradiation under visible light to UV light was confirmed by dynamic light scattering (DLS). Alkene-functionalized chiral rhodium-based *N*-tosylated 1,2 diphenyl-1,2-ethylenediamine (Rh-TsDPEN) catalyst for asymmetric transfer hydrogenation (ATH) was immobilized at the core of the photoresponsive SCMs. Control experiments and kinetic studies on ATH reaction using AB cross-linked SCMs as catalyst demonstrate that the reversible photochromic transition of *trans*-AB to *cis*-AB in the cross-linking layer results in the gated behavior to SCMs. The photoinduced change in micellar morphology is the key to discriminating among substrate/reagents during single-step catalysis.

### *Mesoporous silica – polymer composite materials for cascade catalysis*

Using atom transfer radical polymerization (ATRP), thiol-ene chemistry, and surface functionalization reactions, a variety of bifunctional acid-base materials were prepared for the purposes of cascade catalysis. The probe reaction studied is the well-known deacetalization of benzaldehyde dimethyl acetal followed by the Knoevenagel condensation with malononitrile to form benzylidene malononitrile. Emphasis was placed on understanding the role of polymer molecular weight and silica pore diameter and its effect on compartmentalization of silica grafted sulfonic acids and polymer supported benzylamines. Olefin end-group copolymers of styrene and poly(styrene-co 2-(4-

vinylbenzyl)isoindoline-1,3-dione) were tethered to the supports MCM41 and SBA15 using thiol-ene chemistry. Experimental results found the lowest molecular weight (6100 g/mol) SBA15 and MCM41 systems showed the most effective bifunctionality, resulting in quantitative conversion to the cascade product in around 7 hours. Significant reduction in activity of polymer supported benzylamines was found with molecular weights of 16,000 g/mol and above, as well as with the MCM41 support, due to non-ideal domain confinement or mass transfer limitations.

### ***Simulations of Oligomeric Catalysis in a Nanoporous System.***

Connecting to the above experiments, the radius of gyration ( $R_g$ ) of poly(st-co-NPhth) chain in dichloromethane was investigated as a function of molecular weight (MW) using molecular dynamics (MD) simulations. It was found that  $R_g$  of the polymer chain was 1.31 and 1.78 nm at MW of 6100 and 16000 g/mol, respectively. Both polymer chains can diffuse into the mesopores of SBA15 with a pore diameter of 7 nm, whereas the diffusion of these polymer chains would incur resistance due to steric effects with the smaller pore MCM41 (3 nm pore diameter). From the experimental results, the larger molecular weight polymers result in significantly reduced activity in the base-catalyzed reaction. The effect was more pronounced in MCM41 compared to SBA15. We discovered that polymer swelling at an elevated temperature hinders the diffusion of reactant molecules in the pore and the accessibility of the active sites (Figure 4b). From this result, we expect that the longer chains will block the porous tunnels, resulting in low amine accessibility. Shorter chains would be preferential due to greater solubility and flexibility when confined into narrow domains.

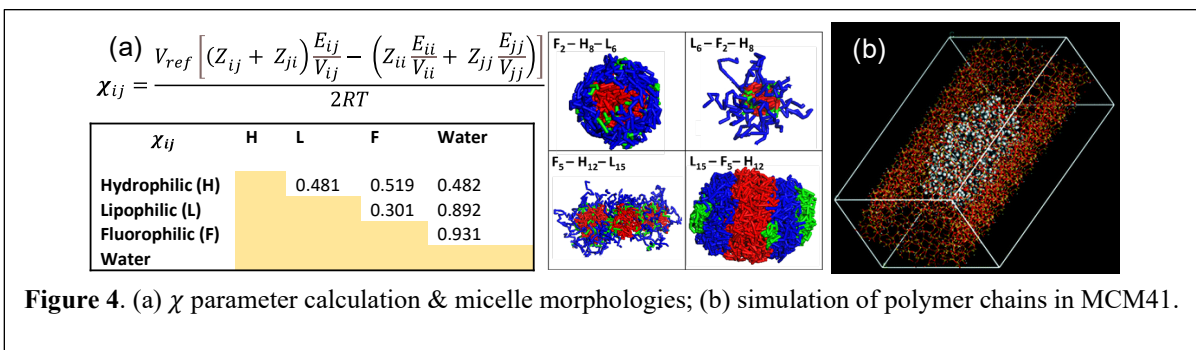
### ***Nature-inspired Polypeptide Composites for Tandem Catalysis***

Polypeptide-based heterogeneous catalysts were prepared by grafting from and ring-opening polymerization approaches. The monomers were sequentially and randomly distributed along the backbone of the polymers containing pair combinations of poly(L-glutamic acid) (PLGA), poly(L-tyrosine) (PTYR) [acidic sites] and poly(L-lysine) (PLYS) [basic sites] grafted from the mesoporous SBA-15 particles. The random polymers had a ratio of 10:90 and 30:70 monomers of PTYR and PLYS. The resulting co-polymers had high molecular weights in the 30 – 60 kDa range. The catalysts were also designed with slightly different grafting densities. The majority of these catalysts used in the model Knoevenagel tandem reaction led to over 90% yield of the main product. They showed good efficiency during the recovery reactions as well, with no significant decrease in catalytic activity (and in some cases, increased rates, as later runs already had polypeptide chains self-assembled into proper conformations). The random polypeptide-based catalysts listed in the table had higher initial rates and TOF numbers than the control catalysts consisting of SBA-15-NH<sub>2</sub> and SBA-15-COOH (small molecule active sites). The control catalysts matched the basic (NH<sub>2</sub>) and the acidic (COOH) sites of the polypeptide-based homologues. The results of the investigations acquired so far indicate that polypeptide-based composites that mimic closely the structure of natural tandem catalysts show potential for use in heterogeneous catalysis.

### ***Models and Simulations of Multicompartment Micelles***

We have developed multiscale computational models to predict (i) Flory-Huggins  $\chi$  parameters using density functional theory (DFT) and statistical mechanics calculations,

and (ii) the micelle morphologies via dissipated particle dynamics (DPD) simulations. The  $\chi$ -parameter is defined based on the Gibbs free energy of mixing, which considers the molecular volume, the coordination number of the species  $j$  around the species  $i$ , and the interaction energy between individual molecules. It was found that  $\chi$  parameters for structures shown in Figure 2 are in the order of H-F pair ( $\chi=0.519$ ), L-H pair ( $\chi=0.481$ ), and L-F pair ( $\chi=0.301$ ), in which F, L, and H consist of  $C_{11}H_{13}F_9$ ,  $C_{15}H_{25}NO_2$ , and  $C_{16}H_{28}N_2O_5$ , respectively. Among polymer-solvent (water) pairs, the  $\chi$  parameter is the highest for F-water, followed by L-water and H-water. Using these  $\chi$  parameters, DPD simulations were performed to investigate various micelle morphologies such as core-shell, worm-like and disk-like structures shown in Figure 4, which closely match the experimental results in Figure 2.



### Publications Acknowledging this Grant in 2018-2021

(XXV) *Intellectually led by this grant*

1. Qu, P.; Kuepfert, M.; Ahmed, E.; Liu, F.; Weck, M., Cross-Linked Polymeric Micelles as Catalytic Nanoreactors. *European Journal of Inorganic Chemistry* 2021, 2021 (15), 1420-1427.
2. Kuepfert, M.; Ahmed, E.; Weck, M., Self-Assembled Thermoresponsive Molecular Brushes as Nanoreactors for Asymmetric Aldol Addition in Water. *Macromolecules* 2021, 54 (8), 3845-3853.
3. Cleveland, J. W.; Kumar, D. R.; Cho, J.; Jang, S. S.; Jones, C. W., Creation of discrete active site domains via mesoporous silica poly(styrene) composite materials for incompatible acid-base cascade reactions. *Catalysis Science & Technology* 2021, 11 (4), 1311-1322.
4. Qu, P.; Kuepfert, M.; Hashmi, M.; Weck, M., Compartmentalization and Photoregulating Pathways for Incompatible Tandem Catalysis. *Journal of the American Chemical Society* 2021, 143 (12), 4705-4713.5.
5. Ahmed, E.; Womble, C. T.; Cho, J.; Dancel-Manning, K.; Rice, W. J.; Jang, S. S.; Weck, M., One-pot synthesis of linear triblock terpolymers and their aqueous self-assembly. *Polymer Chemistry* 2021, 12 (13), 1967-1974.
6. Ahmed, E.; Womble, C. T.; Weck, M., Synthesis and Aqueous Self-Assembly of ABCD Bottlebrush Block Copolymers. *Macromolecules* 2020, 53 (20), 9018-9025.

7. De Vylder, A.; Lauwaert, J.; De Clercq, J.; Van Der Voort, P.; Jones, C. W.; Thybaut, J. W., Aminated poly(ethylene glycol) methacrylate resins as stable heterogeneous catalysts for the aldol reaction in water. *Journal of Catalysis* 2020, 381, 540-546.
8. Xie, J.; Ellebracht, N. C.; Jones, C. W., Inter- and Intramolecular Cooperativity Effects in Alkanolamine-Based Acid–Base Heterogeneous Organocatalysts. *ACS Omega* 2019, 4 (1), 1110-1117.
9. Hoyt, C. B.; Sarazen, M. L.; Jones, C. W., Hydroboration of substituted alkynes using a solid polymeric carboxylic acid catalyst. *Journal of Catalysis* 2019, 369, 493-500.10.
10. Callaway, C. P.; Lee, S. M.; Mallard, M.; Clark, B.; Jang, S. S., Effect of Block Length and Side Chain Length Ratios on Determining a Multicompartment Micelle Structure. *The Journal of Physical Chemistry B* 2019, 123 (22), 4784-4791.11.
11. Callaway, C. P.; Bond, N.; Hendrickson, K.; Lee, S. M.; Jang, S. S., Structural Tunability of Multicompartment Micelles as a Function of Lipophilic–Fluorophilic Block Length Ratio. *The Journal of Physical Chemistry B* 2018, 122 (50), 12164-12172.
12. Kuepfert, M.; Qu, P.; Cohen, A. E.; Hoyt, C. B.; Jones, C. W.; Weck, M., Reversible Photoswitching in Poly(2-oxazoline) Nanoreactors. *Chemistry – A European Journal* 2020, 26 (51), 11776-11781.
13. Qu, P.; Kuepfert, M.; Jockusch, S.; Weck, M., Compartmentalized Nanoreactors for One-Pot Redox-Driven Transformations. *ACS Catalysis* 2019, 9 (4), 2701-2706.
14. Womble, C. T.; Kuepfert, M.; Weck, M., Multicompartment Polymeric Nanoreactors for Non-Orthogonal Cascade Catalysis. *Macromolecular Rapid Communications* 2019, 40 (1), 1800580.
15. Kuepfert, M.; Cohen, A. E.; Cullen, O.; Weck, M., Shell Cross-Linked Micelles as Nanoreactors for Enantioselective Three-Step Tandem Catalysis. *Chemistry – A European Journal* 2018, 24 (70), 18648-18652.

*(XXVI) Jointly funded by this grant and other grants with intellectual leadership by other funding sources*

#### **Awards or leadership activities during 2018-2020 calendar years**

##### Christopher Jones

2018 William H. Schwarz Lecture, Johns Hopkins University

2019 Global Distinguished Lectureship, KAIST

2019 Ensor Lectureship, Washington State University

2020 Dreyfus Foundation Chemistry Shorts Film, <https://chemistryshorts.org/>

2020 Founding Editor in Chief, *JACS Au*

2021 Georgia Tech Award for Outstanding Achievement in Research Innovation

2021 Kwang-Yu and Lee-Chien Wang Lecture, University of Rochester  
Vice-President, North American Catalysis Society, 2017-present  
Member Governing Board for Publishing, American Chemical Society 2021-present,  
Program Co-Chair, International Congress on Catalysis, June 2020 (cancelled)

Marcus Weck

2019 Chair, Scientific Advisory Board, Excellence Cluster 3D Matter Made to Order,  
Karlsruhe Institute of Technology, Germany  
2018-2021 Member, ACS National Award Selection Committee (2019 – 2021 award  
cycle)

## Catalytic Activation of C-H and O-H Bonds for the Upgrading of Alcohols

William D. Jones  
Department of Chemistry, University of Rochester

### Presentation Abstract

This project is directed towards fundamental investigations of the reactions of homogeneous transition metal complexes with C-H and O-H bonds for the upgrading of alcohols via the Guerbet reaction. The Guerbet reaction combines two alcohols to produce a larger alcohol plus water. Our studies will provide fundamental information about the mechanisms and energetics of reactions of metal complexes with alcohols and related substrates, and will also examine new tandem catalyst systems for the upgrading of alcohols to higher products. We have also discovered a novel catalyst for the *dehydration* of phenylethanol to make styrene. The development of first-row transition metal complexes with tetradentate fused-bisoxazolidine ligands has proven to be most fruitful.

**Grant or FWP Number:** DE-SC0020230

**PI:** William D. Jones

**Postdoc(s):** Olaf Nachtigall

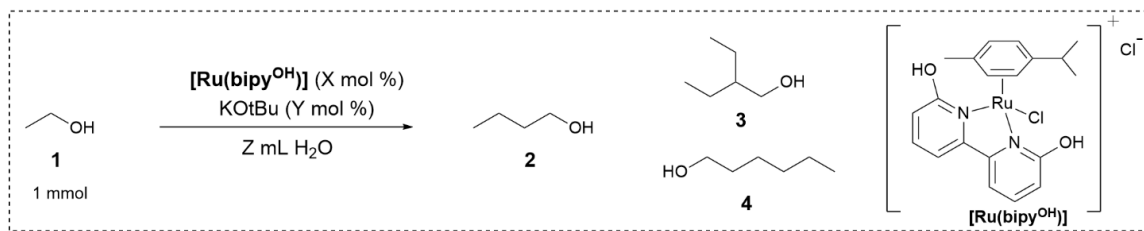
**Student(s):** Tarah Dibenedetto (GS), John Clay (UG), Ignacio Camarero Temino (GS)

### RECENT PROGRESS

In the first two years of this new project, we targeted three specific areas: (1) the synthesis and evaluation of transition metal complexes that have been demonstrated to operate in aqueous solution, (2) the synthesis of new catalysts with redox active ligands that can be used for the dehydrogenation/hydrogenation catalysis, and (3) discovery of a new catalytic process, the dehydration of alcohols to give olefins, specifically, styrene.

#### 1. Water Soluble Catalysts for the Guerbet Reaction

Focusing our efforts towards catalysis, we sought to investigate a system that could operate in water, *as none of the modern catalytic systems can perform the Guerbet reaction under aqueous conditions*. Below are selected results highlighting the potential of this catalytic system (Table 1). Notably, we have been able to run these reactions in water without additional co-solvents, and the ethanol to water ratio approaches the aforementioned feedstock ratio (10% ethanol to 90% water). Upgrading ethanol in water removes the need for the prior distillation of the fermentation broth, which would be required for most other systems. It also makes this a more environmentally friendly process as it forgoes the use of any additional organic co-solvents. Another important factor that contributes to the overall cost of this process is the heat required by the reaction. Typical Guerbet reactions run at very high temperatures, upwards of 150 °C. Our system is able to run at 80 °C, achieving up to a 16% yield of butanol, and we have been able to operate at temperatures as low as 75 °C, albeit with a corresponding decrease in yield and conversion. To the best of our knowledge this is the lowest reported temperature at which this process has been run.

**Table 1.** Selected results in aqueous media

Entry	X (mol %)	Y (mol %)	H <sub>2</sub> O:EtOH (v/v)	Time, h	T, °C	1 <sup>a</sup>	2 <sup>b</sup>	3 <sup>b</sup>	4 <sup>b</sup>	Selectivity <sup>c</sup>	TON <sup>d</sup>
1	1.5	50	84:16	24	80	58	24	6	2.2	57	28
2	2	60	84:16	24	85	43	29	8	3	51	29
8	2	60	84:16	18	80	51	28	7	3	57	25
9	2	55	84:16	18	80	52	22	5	2	46	24
12	2.5	70	91:9	24	80	58	20	6	2	48	17

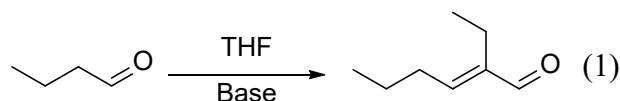
All reactions conducted on a 1 mmol scale, ethanol (1 mmol, 1 equiv). <sup>a</sup> amount of ethanol recovered, GC yield (%) vs. *n*-propanol as the internal standard. <sup>b</sup> GC yield (%)<sup>§</sup> vs. *n*-propanol as the internal standard. <sup>c</sup> selectivity (%) is reported for the formation of *n*-butanol vs. conversion of ethanol. <sup>d</sup> TON based upon EtOH consumed.

Further work on this system is needed to improve the conversion and yield of the reaction. In particular, to work in aqueous solution with concentrations of ethanol relevant to fermentation (<10%), we need to work with more active water-soluble catalysts. We are currently beginning investigations with a Cp\*Ir(bipy(OH)<sub>2</sub>) complex that has high activity in water.

## 2. Bulky Transition Metal Bases for the Selective Aldol Reaction

One goal of this project is to determine if bulky transition metal complexes can be found that will catalyze the Aldol condensation with a high selectivity for acetaldehyde, the product of ethanol dehydrogenation. The idea here is to have acetaldehyde react ~100x faster than butyraldehyde, since both will be present during the Guerbet reaction. A selectivity for acetaldehyde will result in only *n*-butanol being formed, but no higher alcohols.

Preliminary studies have been carried out in which butyraldehyde reactivity was examined (eq 1). Three bulky metal hydroxides were used as catalysts and compared with KOH as base (Figure 1). KOH gives the condensation product in good yield. Nacnac-zinc complex **1** catalyzes condensation, and appears to give the hydrated intermediate of the Aldol condensation. Both **1** and **2** give less product than KOH. However, the NHC Cu hydroxide complex **3** did not catalyze the reaction at all. It is a good candidate for moving forward with selective Aldol condensation of acetaldehyde.



We have now made a number of other bulky metal-hydroxide catalysts with Zn and Cu and will investigate their reactivity with aldehydes.

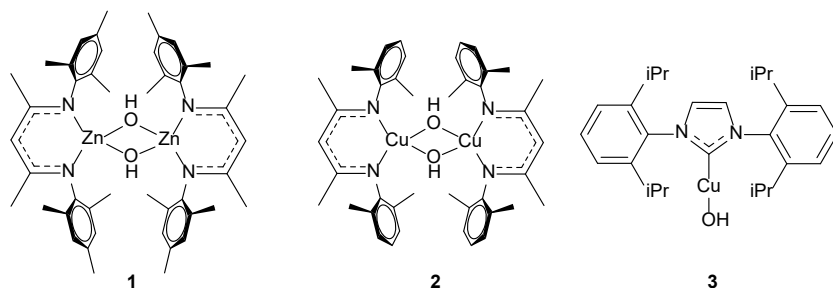


**Figure 1.** Bulky transition metal bases for Aldol studies.

### 3. Coordination Chemistry and Catalysis of Fused Oxazolidine (FOX) Ligands

We are currently investigating the chiral 5-hydroxymethyl-2,8-dipyridyl-3,7-dioxo-1-aza-bicyclo[3.3.0]octane and its achiral *meso* isomer (Figure 2). This ligand is synthesized from inexpensive starting materials in one step, and we have found that  $\text{AlCl}_3$  can isomerize it to the *meso* form.

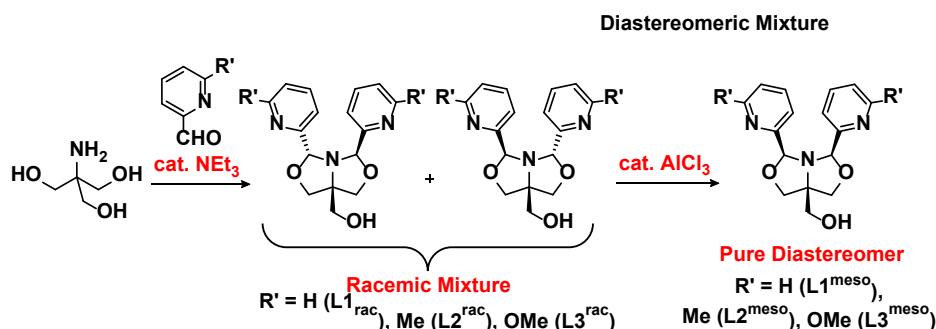


**Figure 2.** Synthesis of chiral (*rac*) and achiral (*meso*) fused bisoxazolidine (FOX) ligands.

The heteroatoms in its skeleton as well as its substituents in the *rac* are heterofacial (Figure 2, center). Therefore, a *fac*- $\kappa^3$ -binding mode was expected. The *meso* isomer has both pyridyl groups on the same side of the bicycle, and can coordinate in a  $\kappa^4$ -binding mode. Indeed, the reaction of the ligand with stoichiometric amounts of first row transition metals has led to the synthesis of 22 new complexes with these ligands. Several examples of complexes of the *rac* and *meso* ligands are shown below

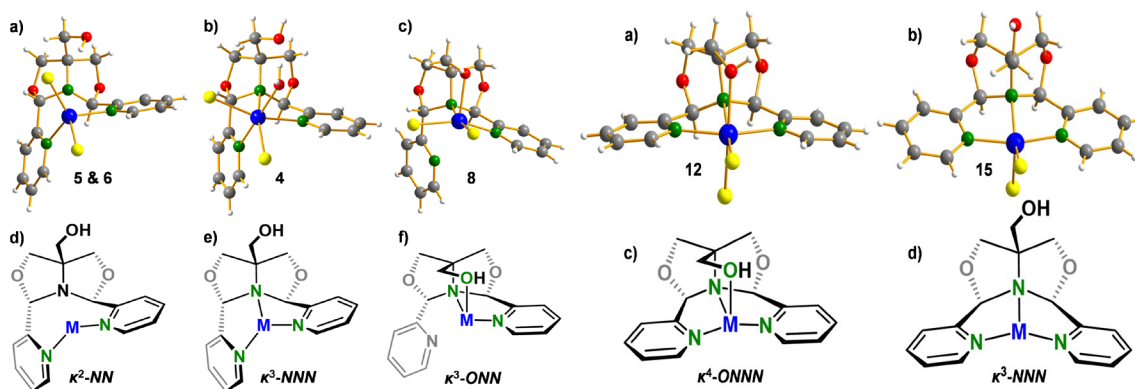
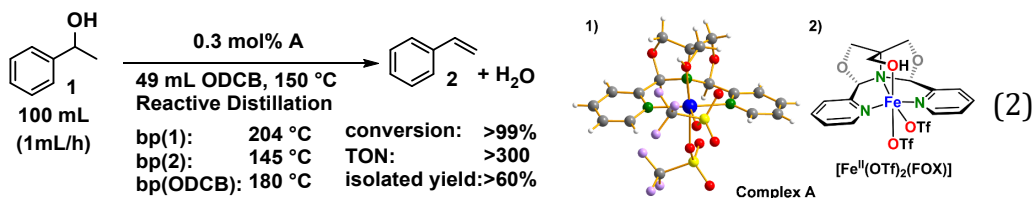


**Figure 3.** Different coordination modes of fused bisoxazolidine (FOX) ligands. Left:  $\kappa^2$ - and  $\kappa^3$ -binding mode of *rac* FOX ligand. Right:  $\kappa^2$ - and  $\kappa^4$ -binding mode of the *meso* FOX ligand. M =  $\text{Mn}^{\text{II}}$ ,  $\text{Fe}^{\text{II}}$ ,  $\text{Co}^{\text{II}}$ ,  $\text{Ni}^{\text{II}}$ ,  $\text{Cu}^{\text{II}}$ .

We have discovered that one of these complexes, (<sup>meso</sup>FOX)Fe(OTf)<sub>2</sub> (**A**), is an efficient catalyst for the dehydration of 1-phenylethanol to produce styrene plus water (eq 2). This reaction is carried out on the ~1 mole scale in a reactive distillation setup. The high-boiling *o*-dichlorobenzene solvent (ODCB) allows the styrene and water products to distill out as more alcohol is continuously added. Further development of alcohol dehydrogenations will be the target of future studies.



#### 4. Additional Accomplishments

We have also published a topical review on carbon capture and conversion in *J. Am. Chem. Soc.* We completed and published our work on amine, ketone, and ester C-H activation using tris-pyrazolylborate rhodium complexes. We have also published work using a chiral bisoxazoline-pincer cobalt catalyst for alkene hydrogenation. We also reported a copper NHC complex that catalyzes Markovnikov hydroboration of alkenes.

#### Publications Acknowledging this Grant in 2019-2021

1. Yuwen, J.; Brennessel, W. W.; Jones, W. D. Coordination or Oxidative Addition? Activation of N–H with [Tp’Rh(PMe<sub>3</sub>)], *Inorg. Chem.*, **2019**, *58*, 557–566. (DOE) #264 doi: <https://doi.org/10.1021/acs.inorgchem.8b02752> (I)
2. Parsons, A. M.; Jones, W. D. Photolysis of Tp’Rh(CNneopentyl)(PhNCNneopentyl) in the Presence of Ketones and Esters: Kinetic and Thermodynamic Selectivity for Activation of Different Aliphatic C-H Bonds. *Dalton Trans.* **2019**, *48*, 10945–10952. (DOE) #266 doi: [10.1039/C9DT01802F](https://doi.org/10.1039/C9DT01802F) (I)
3. DiBenedetto, T. A.; Parsons, A. M.; Jones, W. D. Markovnikov Selective Hydroboration of Olefins Catalyzed by a Copper N-Heterocyclic Carbene Complex. *Organometallics*, **2019**, *38*, 3322–3326. (DOE) #267 doi: [10.1021/acs.organomet.9b00394](https://doi.org/10.1021/acs.organomet.9b00394) (I)
4. Ritz, M. D.; Parsons, A. M.; Palermo, P. N.; Jones, W. D. Bisoxazoline-Pincer Ligated Cobalt-Catalyzed Hydrogenation of Alkenes. *Polyhedron*, **2020**, *180*, 114416. (DOE, NSF, Xray) #269 doi: [10.1016/j.poly.2020.114416](https://doi.org/10.1016/j.poly.2020.114416) #269 (I)
5. Jones, W. D. Carbon Capture and Conversion. *J. Am. Chem. Soc.* **2020**, *142*, 4955–4957. (DOE) #270 doi: [10.1021/jacs.0c02356](https://doi.org/10.1021/jacs.0c02356) (I)
6. Vetter, A. J.; DiBenedetto, T. A.; Ritz, M. D.; Jones, W. D. The functionalization of benzene by boranes using trispyrazolylborate complexes, *Polyhedron*, **2021**, *197*, 115042. (DOE, NSF) doi: [10.1016/j.poly.2021.115042](https://doi.org/10.1016/j.poly.2021.115042) (I)
7. Nachtigall, O.; VanderWeide, A. I.; Brennessel, W. W.; Jones, W. D. First-Row Transition Metals Complexes with Fused Oxazolidine (FOX) Ligands, *Z. Anorg. Alleg. Chem.* **2021**, *647*, 1442–1448. doi: [10.1002/zaac.202100056](https://doi.org/10.1002/zaac.202100056) (DOE). (I)
8. DiBenedetto, T. A.; Jones, W. D. Upgrading of Ethanol to n-Butanol via a Ruthenium Catalyst in Aqueous Solution, *Organometallics*. **2021**, *40*, 1884–1888. doi: [10.1021/acs.organomet.1c00217](https://doi.org/10.1021/acs.organomet.1c00217) (DOE) (I)

9. Reshma, G.; Kumar, M.; Kulkarni, N. V.; Jones, W. D. Dehydrogenation of 1-Phenylethanol Catalyzed by Nickel (II)-Diphosphine Complexes, *Acta Chim. Slov.*, **2021**, *68*, in press. (DOE) (II)
10. Nachtigall, O.; VanderWeide, A. I.; Brennessel, W. W.; Jones, W. D. Iron-Based Dehydration Catalyst for Selective Formation of Styrene, *ACS Catal.* **2021**, submitted, revision requested. (DOE) (I)

*Classification:*

(I) *Intellectually led by this grant*

(II) *Jointly funded by this grant and other grants with intellectual leadership by other funding sources*

**Awards or leadership activities during 2018-2020 calendar years**

Member of the American Academy of Arts & Sciences, 2021

William H. Riker Award for Excellence in Graduate Teaching, U. Rochester, 2019

Alexander von Humboldt Foundation Research Award, 2018

Associate Editor, *J. Am. Chem. Soc.*, 2003-

Charles F. Houghton Professor of Chemistry, 2000-

Dow Lecturer, Berkeley, CA 2018

Keynote Lecturer, 26<sup>th</sup> Symposium on Chemistry Postgraduate Research in Hong Kong, 2019

## Investigating Novel Approaches for Synthesizing Supported Molecular Catalysts

Alexander Katz, Michael A. Boreen, Franck Ulm  
Department of Chemical and Biomolecular Engineering, University of California,  
Berkeley

Sonjong Hwang  
Division of Chemistry, California Institute of Technology, Pasadena, California

### Presentation Abstract

Establishing control in the design of supported molecular catalysts by understanding how the structure of the support and the molecular site affect catalyst activity and stability is critical for applications using these materials. In addition, new approaches for synthesizing robust and leach-resistant catalysts for liquid-phase reactions is a continuing grand challenge. We report a two-pronged approach for controlling (i) the catalytic hydrogenation activity of a cationic iridium(I) complex (Crabtree's catalyst) supported on different crystalline and amorphous silicate and aluminosilicate supports as a function of time under flow conditions; and (ii) investigate the immobilization of supported molecular catalysts in the liquid phase via surface polymerization. Our results demonstrate that the shape and composition of the support affects both initial catalytic rates and the rate of catalyst deactivation in area (i). Future work will focus on how ligand sterics influence rates of deactivation of supported catalysts and how this effect may differ depending on the nature of the support. In area (ii), initial results point to a role of surface polymerization in rigidifying and permanently anchoring grafted Ti-calixarene sites on silica.

### DE-FG02-05ER15696: Controlling Partial Confinement and Environment in Supported Molecular Catalysts

Postdoc(s): Michael A. Boreen, Franck Ulm

### RECENT PROGRESS

#### *Electrostatic and Partial Confinement Effects in Supported Molecular Catalysis*

Effects of support external-surface pockets and electrostatic exchange sites on catalyst activity and stability were investigated by measuring ethylene hydrogenation activity versus time on stream for Crabtree's catalyst ( $[\text{Ir}(\text{PCy}_3)(\text{Py})(\text{COD})][\text{PF}_6]$ , Cy = cyclohexyl, Py = pyridine, COD = 1,5-cyclooctadiene) anchored onto a series of comparative, different supports (the resulting catalyst is denoted as Crabtree@Support, see Scheme 1A for synthetic procedure). Comparing Crabtree@(H)-Al-SSZ-70 (Al-SSZ-70 is a crystalline MWW-type zeolite) to Crabtree@(H)-Al-MCM-41 (Al-MCM-41 is a non-crystalline mesoporous aluminosilicate, which, like H-Al-SSZ-70 possesses ion-exchange sites), similar initial rates of ethylene hydrogenation were observed, but the latter catalyst

rapidly deactivated, while the former experienced an initial incubation period of increasing catalytic rate before beginning to deactivate gradually. We hypothesize that the partially confining environment of the hemispherical pockets on the MWW-type zeolite surface contributed to increased catalyst stability when this material was used as support.

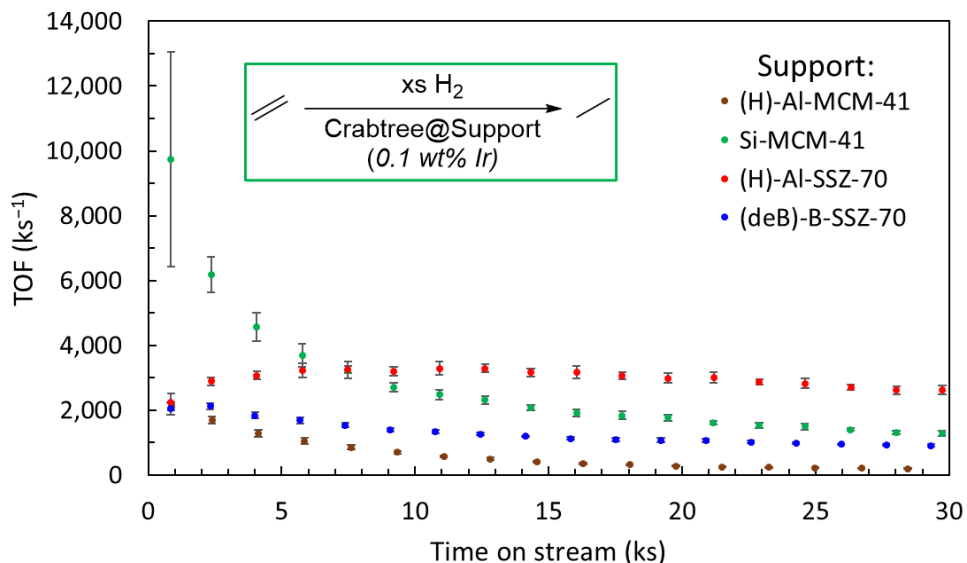
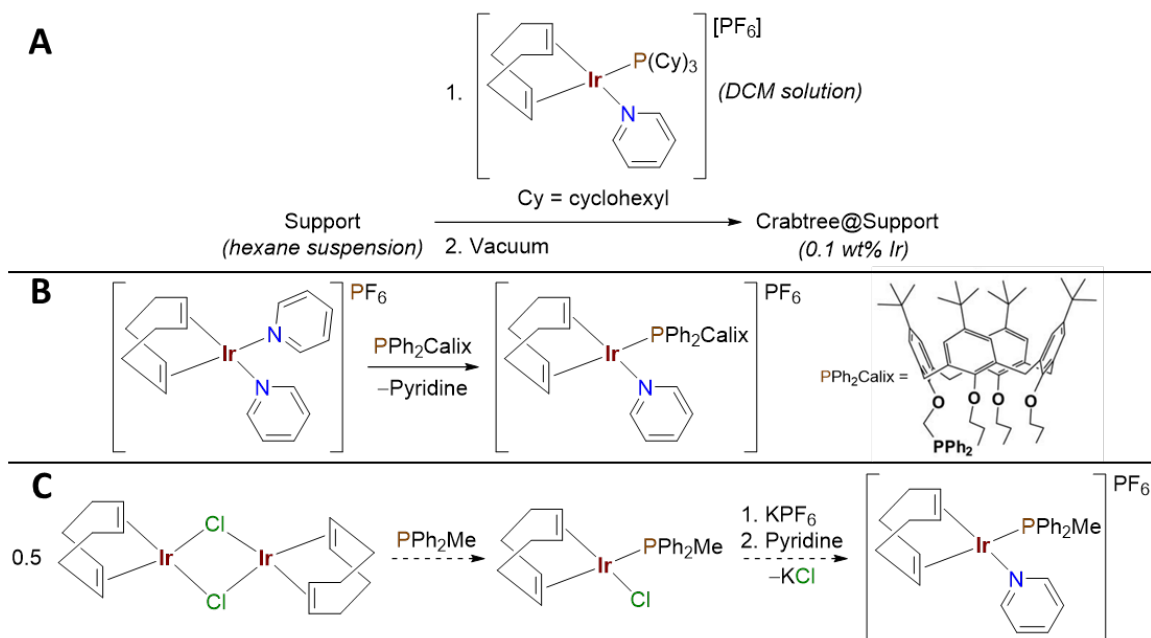


**Figure 1.** Ethylene hydrogenation activity data for three catalysts consisting of Crabtree's catalyst anchored onto different supports. Catalysis was performed in a gas-flow reactor, and data are plotted as turnover frequency (TOF,  $\text{ks}^{-1}$ ) as a function of time on stream (ks). Error bars show the standard deviation of the TOF over each set of four measurements. Conditions for catalysis:  $-14 \pm 1$  °C, 3/50/10 ml/min flow rate for  $\text{C}_2\text{H}_4/\text{He}/\text{H}_2$ .

Considering Crabtree@(deB)-B-SSZ-70 (deboronated B-SSZ-70, an all-silica analog to (H)-Al-SSZ-70 with the same structure), a similar initial rate was also observed, but a short incubation period was followed by deactivation at much earlier times than was recorded for Crabtree@(H)-Al-SSZ-70. This suggests that the anionic electrostatic anchoring sites present only in the aluminosilicate material are responsible for an increase in stability of the cationic catalyst, and suggests a synergistic effect of external-surface pockets in achieving partial confinement as well as electrostatic anchoring of the sites, for achieving greater site stability. Either one of these alone is insufficient. Notably, Crabtree@Si-MCM-41 exhibited high initial rates of catalysis, but rapid deactivation quickly reduced the activity using this amorphous, all-silica support to below that of Crabtree@(H)-Al-SSZ-70. Previously, our results have indicated Ir aggregation as being responsible for this rapid deactivation on silica.

X-ray absorption spectroscopy (XAS) experiments are planned to compare the coordination environment of the iridium centers in Crabtree@Support before and after ethylene hydrogenation catalyst and will provide insight toward the deactivation mechanism for the various supports above. We are particularly interested in determining any differences in XAS results between supports, as this may indicate distinct deactivation mechanisms. Future work on this project also involves testing the effect of ligand sterics on catalyst activity and stability and how support effects vary depending on ligand sterics. To this end, we have developed the synthesis of a novel analog to Crabtree's catalyst,

$[\text{Ir}(\text{PPh}_2\text{Calix})(\text{Py})(\text{COD})][\text{PF}_6]$ , containing a bulky calixarene phosphine ligand ( $\text{PPh}_2\text{Calix}$ ) in place of  $\text{PCy}_3$  (Figure 1B). Synthesis of the related complex  $[\text{Ir}(\text{PPh}_2\text{Me})(\text{Py})(\text{COD})][\text{PF}_6]$  containing a methyl group instead of the calixarene is in progress and will provide access to two electronically similar species with drastically different steric environments (Figure 1C).

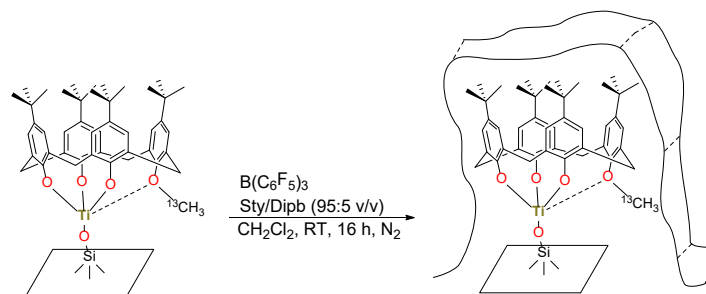


**Scheme 1.** (A) Anchoring procedure to prepare supported molecular catalysts Crabtree@Support, (B) synthesis of  $[\text{Ir}(\text{PPh}_2\text{Calix})(\text{Py})(\text{COD})][\text{PF}_6]$ , and (C) proposed synthesis of  $[\text{Ir}(\text{PPh}_2\text{Me})(\text{Py})(\text{COD})][\text{PF}_6]$ .

Comparing the results of ethylene hydrogenation experiments with each of these catalysts anchored onto a similar variety of supports as used for the experiments shown in Figure 1 will enable us to determine how this change in sterics affects the rate of catalysis and catalyst deactivation (for the same support) as well as whether changing the support has a greater or lesser effect on catalyst activity and stability for the two different sites.

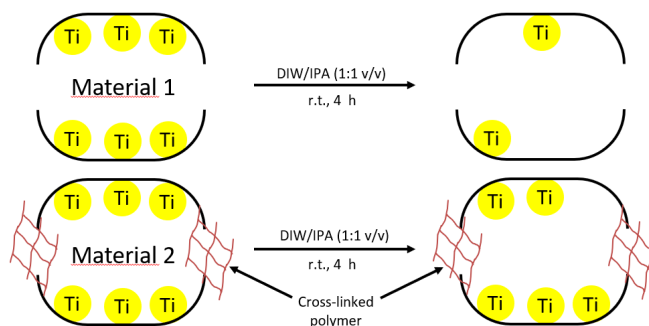
### ***Permanent Anchoring of Grafted Ti-calixarene Sites in Liquid-Phase***

The mechanical encapsulation of a catalyst inside a nanocage-like reactor has previously been demonstrated as a robust method to maintain high activity and enable recyclability for homogeneous catalysts in a heterogeneous environment, in the liquid phase. Herein, we leverage on a previously developed surface polymerization approach to entrap a  $^{13}\text{C}$ -labeled Ti(IV)-calixarene complex, which is grafted onto a silica support, as shown in Scheme 2. The  $^{13}\text{C}$ -labeled methoxy group on the calixarene ligand was synthetically incorporated in order to answer a central question of whether the surface polymer is wrapped around individual Ti(IV)-calixarene complexes within a pore (depicted in Scheme 1) or whether the polymer plays the role of a gatekeeper, blocking complexes from escaping the pore (depicted in Scheme 3).



**Scheme 1.** Polymerization process of Ti(IV)-Calixarene. Sty = styrene, Dipb = Diisopropenylbenzene.

To evaluate the robustness of entrapment using this protective surface polymer layer, we conducted a liquid-phase leaching stress test by treating the unpolymerized and polymerized materials (Materials 1 and 2, respectively) with a mixture of deionized water (DIW) and Isopropanol (IPA) (1:1 v/v) for 4 h at room temperature, as shown in Scheme 2. TGA analysis showed that nearly all of the organic content in Material 2 remained, while the organic content in Material 1 drastically decreased after leaching, suggesting that the polymerization technique prevents the Ti(IV)-calixarene complexes from leaching into solution.



**Scheme 2.** Leaching stress test of the unpolymerized and polymerized materials (Materials 1 and 2, respectively).

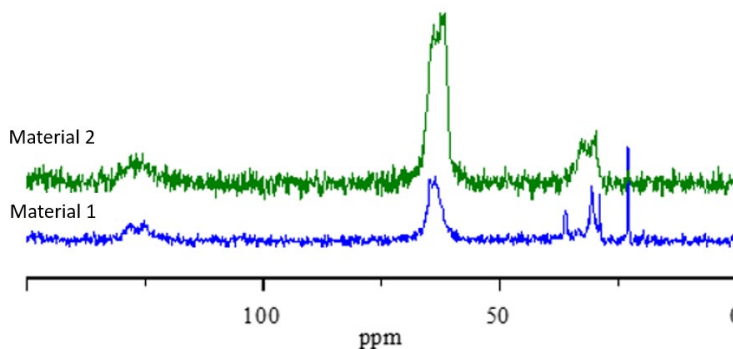


**Figure 2.**  $^{13}\text{C}$  CP/MAS NMR spectrum of Material 1 and Material 2 after leaching tests.

To gain further insight into the nature of this protective layer,  $^{13}\text{C}$  MAS NMR spectroscopy was used to characterize the two materials after the leaching test, with results shown in Figure 2. The resonance around 60 ppm is assigned to the  $^{13}\text{C}$ -methoxy substituent on the calixarene ligand. After leaching, the spectrum of Material 1 exhibited low intensity, while the spectrum of Material 2 displayed a relatively high intensity. The NMR data therefore show that, after exposure to the protic conditions of the leaching test, the Ti(IV)-calixarene complex is present in considerably higher concentration in the sample containing the protective polymer layer, which is consistent with the TGA analysis mentioned above. This result motivates us to analyze a “wet sample” (i.e., a polymerized material after the leaching test but not dried) by  $^{13}\text{C}$  solid-state NMR to gain more insight into the role of the polymer and see if a labile Ti(IV)-calixarene can be observed during the stress test. In these conditions, labile complexes within pores are expected if the polymer acts as a gatekeeper, while immobile complexes are expected if the polymer is tightly wrapped around each complex. Finally, we are in the process of using this construct, once a better understanding of its function is achieved, in order to immobilize homogeneous catalytic active sites for liquid-phase reactions.

### **Publications Acknowledging this Grant in 2018-2021**

#### *(I) Exclusively funded by this grant*

1. N. A. Grosso-Giordano, S. I. Zones and A. Katz. Opportunities for controlling catalysis by designing molecular environments around active sites: cations supported on amorphous versus crystalline zeolitic silicate supports. *Catalysis (published by RSC; edited by J. Spivey, Y.-F. Han, D. Shekhawat)* **2019**, *31*, 72–126.
2. M. Yabushita, G. Papa, P. Li, A. Fukuoka, O. K. Farha, B. A. Simmons, A. Katz. Effect of ionic liquid on sugar-aromatic separation selectivity by metal-organic framework NU-1000 in aqueous solution. *Fuel Processing Technology* **2020**, *197*, 106189. <https://doi.org/10.1016/j.fuproc.2019.106189>
3. Y. Xie, C. Schöttle, Y. Li, Carraro, C, X. Y. Zhang, A. Katz, R. Maboudian. Synthesis and Electrochemical Stability of Ultrahigh Aspect Ratio Nanoporous Gold after Calixarene-Phosphine Ligand Removal. *ACS Appl. Mater. Interfaces* **2019**, *11*, 15189 – 15194.
4. A. Solovyov, M. Yabushita, A. Katz. Mechanical Control of Rate Processes: Effect of Ligand Steric Bulk on CO Exchange in Trisubstituted Tetrairidium Cluster Catalysts. *J. Phys. Chem. C* **2020**, *124*, 26279 – 26286.
5. N. A. Grosso-Giordano, C. Schroeder, L. Xu, A. Solovyov, D. W. Small, H. Koller, S. I. Zones, A. Katz. Characterization of a Molecule Partially Confined at the Pore Mouth of a Zeotype. *Angew. Chem. Int. Ed. Engl.* **2021**, *60*, 10239 – 10246.

#### *(II) Jointly funded by this grant and other grants with leading intellectual contribution from this grant*

- 1 A. Solovyov, M. Yabushita, A. Katz. Sterically Bulky Calixarene Phosphine Ligands Freeze CO Exchange Processes in Trisubstituted Tetrairidium Clusters, *submitted*.

- 2 A. P. Palermo, C. Schöttle, S. Zhang, N. A. Grosso-Giordano, A. Okrut, D. A. Dixon, H. Frei, B. C. Gates, A. Katz. Spectroscopic Characterization of  $\mu$ - $\eta^1$ : $\eta^1$ -Peroxo Ligands Formed by Reaction of Dioxygen with Electron-Rich Iridium Clusters. *Inorg. Chem.* **2019**, *58*, 14338-14348.
- 3 Y. Guo, S.-J. Hwang, A. Katz. Hydrothermally robust Ti/SiO<sub>2</sub> epoxidation catalysts via surface modification with oligomeric PMHS. *Molecular Catalysis* **2019**, *477*, 110509.
- 4 N. A. Grosso-Giordano, A. S. Hoffman, A. Boubnov, D. W. Small, S. R. Bare, S. I. Zones, A. Katz. Dynamic reorganization and confinement of Ti(IV) active sites controls olefin epoxidation catalysis on two-dimensional zeotypes. *J. Am. Chem. Soc.*, **2019**, *141*, 7090–7106.
- 5 A. Okrut, N. A. Grosso-Giordano, C. Schöttle, S. Zones, A. Katz. Understanding the role of Zn(II) in surfactant-free layered silicate delamination: exfoliation of magadiite. *Microporous Mesoporous Mater.*, **2019**, *283*, 55–63.
- 6 C. Schöttle, E. Guan, A. Okrut, N. A. Grosso-Giordano, A. Palermo, A. Solovyov, B. C. Gates, A. Katz. Bulky Calixarene Ligands Stabilize Supported Iridium Pair-Site Catalysts. *J. Am. Chem. Soc.*, **2019**, *149*, 4010–4015.
- 7 A. Okrut, M. Aigner, C. Schöttle, N. A. Grosso-Giordano, S.-J. Hwang, X. Ouyang, S. Zones, A. Katz. SSZ-70 borosilicate delamination without sonication: effect of framework topology on olefin epoxidation catalysis. *Dalt. Trans.*, **2018**, *47*, 15082–15090.
- 8 M. Yabushita, N. A. Grosso-Giordano, A. Fukuoka, A. Katz. Selective sequestration of aromatics from aqueous mixtures with sugars by hydrophobic molecular calixarene cavities grafted on silica. *ACS Appl. Mater. Interfaces*, **2018**, *10*, 39670–39678.
- 9 A. Palermo, S. Zhang, S.-J. Hwang, D.A. Dixon, B.C. Gates, A. Katz. Weakly interacting solvation spheres surrounding a calixarene-protected tetrairidium carbonyl cluster: contrasting effects on reactivity of alkane solvent and silica support. *Dalton Trans.*, **2018**, *47*, 13550-13558.
- 10 N. A. Grosso-Giordano, C. Schroeder, A. Okrut, A. Solovyov, C. Schöttle, W. Chassé, N. Marinković, H. Koller, S. I. Zones, A. Katz. Outer-sphere control of catalysis on surfaces: a comparative study of Ti(IV) single-sites grafted on amorphous versus crystalline silicates for alkene epoxidation. *J. Am. Chem. Soc.*, **2018**, *140*, 4956–4960.
- 11 E. Guan, J. Ciston, S. R. Bare, R. C. Runnebaum, A. Katz, A. Kulkarni, C. X. Kronawitter, B. C. Gates. Supported Metal Pair-Site Catalysts. *ACS Catalysis* **2020**, *10*, 9065 – 9085.
- 12 “Effect of ionic liquid on sugar-aromatic separation selectivity by metal-organic framework NU-1000 in aqueous solution” by M. Yabushita, G. Papa, P. Li, A. Fukuoka, O. K. Farha, B. A. Simmons, A. Katz, *Fuel Processing Technology* **2020**, *197*, 106189.
- 13 M. Ramamurthy, N. A. Grosso-Giordano, S.-J. Hwang, L. Xu, D. Xie, M. Mishra, A. Okrut, S. I. Zones, Alexander Katz. Substitution of Cetyltrimethylammonium for OSDA Cations During B-SSZ-70 Zeotype Synthesis and Its Influence on Delamination. *Microporous and Mesoporous Materials* **2021**, *319*, 111042.

**Awards or leadership activities during 2018-2020 calendar years**

Co-director UC Davis/Berkeley NSF IUCRC Center for Rational Catalyst Synthesis (CeRCaS).

Award for Excellence in Catalysis from the Catalysis Society of Metropolitan New York (2020)

**Transdisciplinary Approaches to Realize Novel Catalytic Pathways to Energy Carriers**

Johannes Lercher

Pacific Northwest National Laboratory

**Presentation Abstract**

The central goal of this BES Catalysis Sciences research program is to develop overarching insight into novel approaches for designing catalytic centers and their environment with a focus on C-C and C-H bond formation and C-O bond cleavage reactions on acid-base and hydrogenation sites. The program is organized into two thrusts centered on tailoring acid-base sites for controlled C-C bond formation and enhancing H<sub>2</sub> addition rates by designing the metal center and its environment. Further molecular insight into the catalytic activity of these types of sites is achieved by coupling the experimental investigations with cross-cutting computational studies. In the first thrust, we focus on the impact of geometric and electronic properties of Lewis and Brønsted acid-base sites on the C-C bond formation reactions. Advanced synthesis of homotopic active sites of chosen nuclearity and the stabilization of such sites on faceted oxides, mesoporous solids, and zeolites allowed us to make progress in this area. Spectroscopic signatures of the active sites and reaction intermediates in the catalytic transformations we investigated were determined to obtain an unprecedented level of insights. The second thrust addressed the fundamentals of hydrogen addition to CO groups in molecules such as CO<sub>2</sub> and other oxygenates. The activity of single metal atoms and small clusters of defined nuclearity supported on uniform molecular scaffolds of increasing complexity and stabilized on heterogeneous supports such as faceted oxides and in nanopores were exploited as novel, highly active sites.

**FWP 47319: Transdisciplinary Approaches to Realize Novel Catalytic Pathways to Energy Carriers**

**PI:** Johannes Lercher

**Subtask PIs:** Aaron M. Appel, Zdenek Dohnálek, Johannes A. Lercher, Roger Rousseau, János Szanyi

**Co-PIs and Key Personnel:** S. Thomas Autrey, R. Morris Bullock, David A. Dixon, John L. Fulton, Feng Gao, Bojana Ginovska, Vassiliki-Alexandra Glezakou, Oliver Gutiérrez-Tinoco, Jian Zhi Hu, Enrique Iglesia, Andreas Jentys, Abhijeet Karkamkar, Bruce D. Kay, Greg A. Kimmel, Libor Kovarik, Joseph Laureanti, Mal-Soon Lee, John C. Linehan, Gregory K. Schenter, Wendy J. Shaw, Ba Tran, Huamin Wang, Yong Wang, Eric S. Wiedner

## RECENT PROGRESS

***Fundamental aspects of adsorption and reactions on anatase TiO<sub>2</sub>(101).*** In these studies, we correlate the reaction mechanisms on well-defined, faceted nano-crystalline (FNC) and planar single-crystalline (PSC) anatase TiO<sub>2</sub>(101) surfaces by combining high-resolution imaging, vibrational spectroscopies, reaction kinetics, and theoretical calculations for small oxygenates (Figure 1). For formic acid (FA), a prototypical probe molecule for acid-base and redox properties, we followed the temperature-dependent evolution of surface intermediates with unprecedented detail. Understanding the behavior of resulting formate species is germane for the C-C coupling and CO<sub>2</sub> hydrogenation studied within this program. We have revealed a complex molecular view of the adsorption configurations as a function of coverage and temperature. At low temperatures (<150 K), we find the coexistence of monodentate (MD) and bidentate (BD) species and identified their spectroscopic signatures (Figure 1). The stability of MD species increases dramatically at high coverage where they become isoenergetic with BD species. Under the reaction conditions, oxygen vacancies form due to water production, yielding new types of formate intermediates, with one of their oxygens being a part of the lattice. On PSC TiO<sub>2</sub>(101), CO and H<sub>2</sub>CO are the main reaction products suggesting a disproportionation of neighboring surface formate species. Comparative infrared spectroscopy studies on PSC and FNC TiO<sub>2</sub>(101) show identical surface intermediates illustrating the power of this synergistic approach.

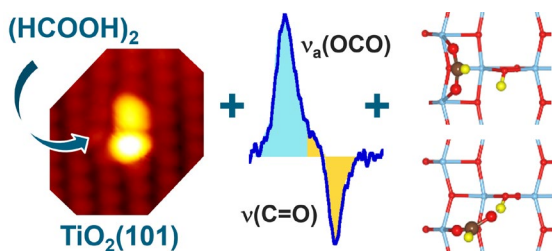
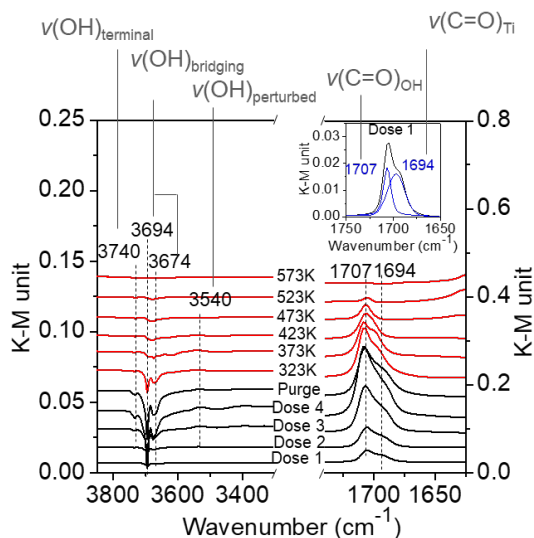


Figure 8. A combination of scanning tunneling microscopy (STM) imaging, infrared reflection absorption spectroscopy (IRAS), and density functional theory (DFT) calculations reveal the complex behavior of MD and BD formate species on TiO<sub>2</sub>(101). Left: High-resolution STM image of BD and MD formate resulting from the adsorption of FA dimer at 80 K. Middle: OCO and C=O IRAS bands due to BD and MD species observed after the adsorption. Right: DFT structures of BD (top) and MD (bottom) species.

**Comparing and contrasting catalytic chemistry on faceted TiO<sub>2</sub>(101) and (001).** To provide a fundamental understanding of how the geometric and electronic structure of complex Lewis and Brønsted acid-base centers on oxides control reaction mechanisms and energy landscapes of O eliminations and C-C bond formation, two anatase TiO<sub>2</sub> high surface area model catalysts, with preferential exposure of (101) and (001) facets, were synthesized. We have studied the site requirements and elementary steps of acetone aldol condensation on these two types of anatase TiO<sub>2</sub> nanocrystals. Temperature-dependent diffuse reflectance infrared Fourier transform spectroscopy (DRIFTS) experiments showed the existence of abundant acetone bonded to surface hydroxyl groups (acetone-O<sub>s</sub>H) and acetone bonded to Lewis acid sites (acetone-Ti<sub>5c</sub>) on both (101) and (001) TiO<sub>2</sub> (Figure 2). We find that the rate-limiting step is the condensation between an enolate formed on the Lewis acidic Ti<sub>5c</sub> site and acetone hydrogen-bonded to a vicinal surface O<sub>s</sub>H group is the kinetically relevant step. The TiO<sub>2</sub> (001) facet has a lower apparent activation energy of acetone aldol condensation. Two possible reasons are proposed for the higher activity on the (001) facet. First, the kinetically relevant C-C coupling step requires proton transfer from O<sub>s</sub>H to the aldol precursor and then partial desorption to form the adsorbed aldol. The weaker Lewis acid and Brønsted base strengths of the (001) facet favors the proton transfer and desorption, making the C-C coupling step more exothermic on the (001) facets and results in an earlier transition state with a lower activation barrier. The second reason is that the (001) facet has a smaller surface corrugation and therefore less hindrance for intermolecular C-C bond formation, meaning that transition state is better stabilized on the (001) facet.



**Figure 9.** DRIFTS spectra for acetone adsorption (black lines, 303 K, acetone vapor dose in He) and temperature-programmed desorption (red lines, desorption in flowing He) on TiO<sub>2</sub>(101) (inserted figure shows the examples of peak deconvolution for the  $\nu(\text{C}=\text{O})$  band).

**Molecular shuttles: Formic acid decomposition routes and their possible involvement in catalytic CI chemistry.** Oxides that catalyze HCOOH dehydration (TiO<sub>2</sub>, ZnO, CeO<sub>2</sub>) promote the water-gas shift (WGS) reaction and CH<sub>3</sub>OH synthesis (and their reverse reactions) on metals that dehydrogenate HCOOH (Cu, Pt, Au), even as physical mixtures. This project addresses whether such synergies require atomic contact, the mechanism of HCOOH dehydration (on TiO<sub>2</sub>) and dehydrogenation (on Cu), and HCOOH as a plausible molecular shuttle. We find that at low temperatures, HCOOH dehydration occurs on TiO<sub>2</sub> via interactions with refractory bidentate formate adlayers. At the lower coverages that prevail at higher temperatures, spectroscopic, desorption-reaction, kinetic, isotopic, and theoretical methods show that acid-base pairs directly mediate dehydration turnover rates via concurrent C-O and C-H activation in molecularly-bound HCOOH at Ti<sub>5c</sub>-O<sub>2c</sub> acid-base pairs. On Cu, bound HCOOH-derived bidentate formates decompose

monomolecularly via kinetically-relevant C-H activation steps, but experiments and theory demonstrate that when  $\text{HCOOH}(\text{g})$  is present during catalysis, turnovers occur at interstices in adlayers of bidentate formate spectators, via concurrent C-H and O-H activation at  $\text{HCOOH} \cdot \text{HCOO}^*$  complexes, with the O-atom in  $\text{HCOO}^*$  acting as the base in Cu-O site pairs.  $\text{TiO}_2$  and  $\text{CeO}_2$  as powders mixed with a metal function (Cu, Pt) as nanoparticles on inert supports ( $\text{SiO}_2$ ,  $\text{Al}_2\text{O}_3$ ) (or on  $\text{ZnO}/\text{Al}_2\text{O}_3$ ) exhibit WGS rate enhancements that become stronger as such physical mixtures become more intimate (Figure 3). These effects could reflect the involvement of gaseous  $\text{HCOOH}$  or  $\text{HCOCOOH}$  (formic anhydride) formed on oxides from  $\text{CO}/\text{H}_2\text{O}$  reactants via the reverse of  $\text{HCOOH}$  dehydration and their dehydrogenation on Cu or Pt nanoparticles. They may also arise from atomic contact caused by  $\text{H}_2\text{O}$ -induced atomic migration during thermal treatment or catalysis.

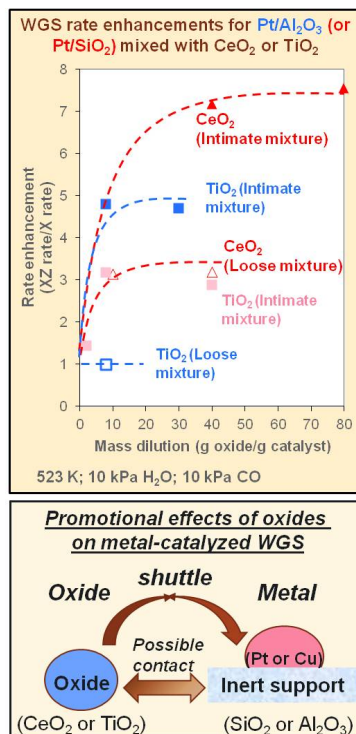


Figure 10. Water-gas shift rate enhancements (over monofunctional catalyst) for intimate (filled symbols) and loose (open symbols) dilutions of Pt/SiO<sub>2</sub> and Pt/Al<sub>2</sub>O<sub>3</sub> catalysts with CeO<sub>2</sub> or TiO<sub>2</sub> as diluents (5-80 diluent:catalyst mass ratio) with dashed curves showing trends (He balance) and schematic depicting potential bifunctional routes involving atomic contact or gaseous molecular shuttles.

**Enabling high activity in CO<sub>2</sub> reduction on single metal atoms and supported nanoparticles by designing the environment of metal-O-Fe bonds.** We show that single atoms of Pt-group metals embedded into the surface of Fe<sub>3</sub>O<sub>4</sub> greatly enhance interactions with CO<sub>2</sub> relative to the bare Fe<sub>3</sub>O<sub>4</sub>. The strong CO<sub>2</sub> adsorption on single Rh atoms and corresponding low activation energies lead to two orders of magnitude higher conversion rates of CO<sub>2</sub> compared to Rh nanoparticles (Figure 4). This high activity of single atoms stems from the partially oxidic state imposed by their coordination to the support. Fe<sub>3</sub>O<sub>4</sub>-supported Rh nanoparticles follow the behavior of single atoms for CO<sub>2</sub> interaction and reduction, which is attributed to the dominating role of partially oxidic sites at the Fe<sub>3</sub>O<sub>4</sub>-Rh interface. Thus, we show a likely common catalytic chemistry for two kinds of materials thought to be

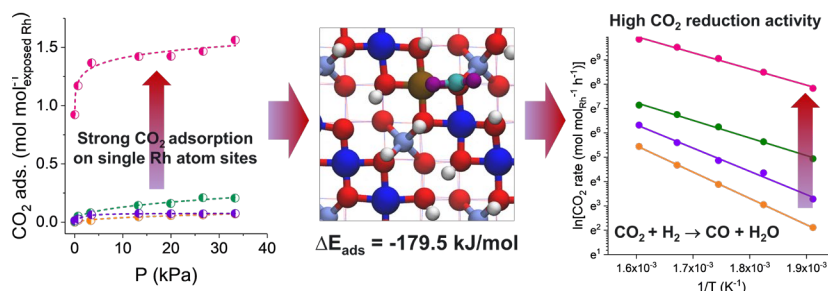


Figure 11. Sites containing single atoms (Rh in this case) supported of Fe<sub>3</sub>O<sub>4</sub> adsorb CO<sub>2</sub> stronger than metal nanoparticles and have lower activation energies. This gives the Rh-O-Fe sites high intrinsic activity in the reverse water-gas shift reaction.

different, and we demonstrate that single atoms of Pt-group metals on  $\text{Fe}_3\text{O}_4$  are especially successful catalysts for reactions that depend primarily upon sites with the metal–O–Fe environment.

**The organization of solvents and alkanols in nanoscopic confinements determines the rates for dehydration.** Rates of acid-catalyzed dehydration of alcohols strongly depend on the solvent and the environment of the acid sites. Brønsted acid sites in large-pore zeolites, but not in medium-pore zeolites, catalyze cyclohexanol dehydration in decalin at significantly higher rates than hydrated hydronium ions in the aqueous phase. The difference in turnover rates between the two solvents amounts to 2–3 orders of magnitude on H-BEA and H-FAU, while being modest for H-MFI. Combining kinetic, isotopic tracer, and  $^2\text{H}$  nuclear magnetic resonance (NMR) measurements, we concluded that cyclohexanol dehydration generally follows an E1-elimination pathway in decalin. A notable exception is the monomer dehydration route on H-MFI, which exhibits much lower activation energy and a substantially negative activation entropy that is associated with an E2-type mechanism. The C–O bond cleavage displays a dominant degree of rate control in decalin, which stands in contrast to deprotonation (C–H cleavage) being rate-limiting in aqueous-phase dehydration (Figure 5).

Dehydration rates catalyzed by hydronium ions in zeolite pores are also influenced by intermolecular interactions among alcohol molecules. The higher dehydration rates in MFI zeolite with pores smaller than BEA zeolites for dehydration of secondary alkanols, 3-heptanol and 2-methyl-3-hexanol, is caused by a lower activation enthalpy in the tighter confines that offsets a less positive activation entropy. The higher activity in BEA than in MFI for dehydration of a tertiary alkanol, 2-methyl-2-hexanol, is caused by lowering the activation enthalpy through stabilizing intraporous interactions of the  $\text{C}_\beta\text{-H}$  transition state with alcohol molecules in the BEA pore, which has a higher intrapore alcohol concentration than MFI. The stabilizing interaction results from the low charge density on the alkyl groups connected to the stabilized tertiary carbenium ion in the E1 elimination pathway.

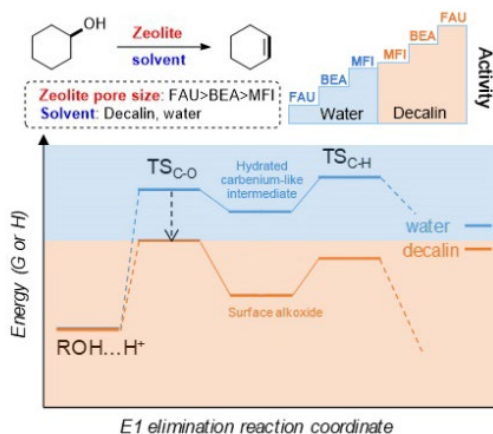


Figure 12. Dehydration rates in micropores depend on both size of the confined space and molecular organization in such confines. Changes in solvent, from water to decalin, for instance, lead to changes in reactivity trends among the studied zeolites (top) and changes in the rate-controlling step (bottom).

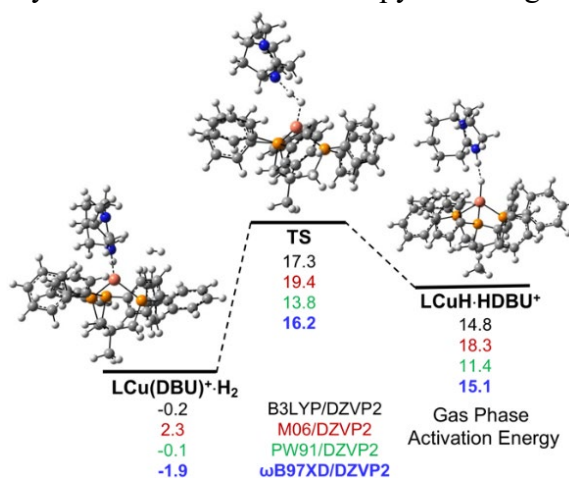
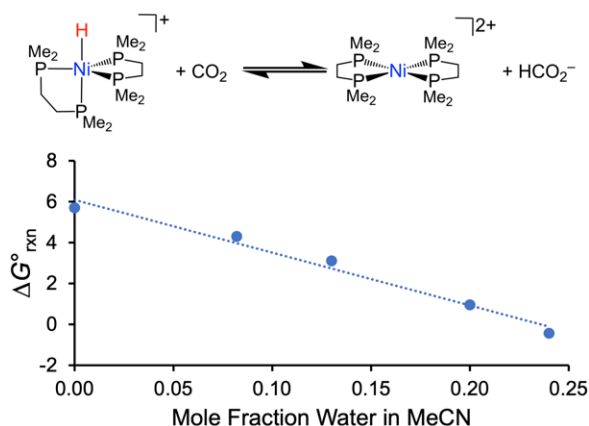


Figure 13. In the molecular copper catalyst,  $\text{H}_2$  inserts between the metal center and an equivalent of bound base. The proposed transition state was identified and quantified through computational studies.

**Hydrogenation of CO<sub>2</sub> by molecular ruthenium and copper catalysts.** Molecular Cu complexes have rarely been demonstrated to be catalytic for the reduction of CO<sub>2</sub>, in spite of the prevalence of heterogeneous catalysts based on Cu. This likely results from the general inability to regenerate the active hydride species from H<sub>2</sub> using mild conditions and reagents. We have demonstrated well-defined Cu hydride complexes can catalytically hydrogenate CO<sub>2</sub> to formate. Based on experimental and computational studies, the heterolysis of H<sub>2</sub> is a critical step that occurs through the insertion of H<sub>2</sub> between the metal center and an equivalent of the base that is bound to the metal (Figure 6). This route for heterolysis of H<sub>2</sub> is atypical for the formation of transition metal hydrides and has an analogy to mechanisms proposed for frustrated Lewis pairs. We have studied a Ru complex that catalyzes the hydrogenation of CO<sub>2</sub> to formate at room temperature without phosphine ligands. [CpRu(CH<sub>3</sub>CN)<sub>3</sub>]<sup>+</sup> hydrogenates CO<sub>2</sub> to formate in the presence of DBU (1,8-diazabicyclo[5.4.0]undec-7-ene). No other base, either weaker or stronger, gave catalysis. Thermodynamic and kinetic studies reveal two DBUs must bind to the Ru center before an active catalyst is produced. Just as in the Cu catalysis described above, the binding of DBU is critical to the activity of the Ru catalyst, even though most researchers consider DBU a very poor ligand.

**Binary solvent mixtures to control hydride transfer and regeneration.**

The transfer of hydride (H<sup>-</sup>) to a reactant, such as CO<sub>2</sub>, is greatly impacted by choice of the solvent. In recent studies, we have extended the use of the effects of solvent through investigations of binary solvent mixtures. The free energy for transfer of a hydride from HNi(dmpe)<sub>2</sub><sup>+</sup> to CO<sub>2</sub> to generate formate and Ni(dmpe)<sub>2</sub><sup>2+</sup> is known to be unfavorable by 6 kcal/mol in MeCN and favorable by 8 kcal/mol in water. By studying this complex in solutions containing both of these solvents, we have shown that at 0.24-mole fraction of water, hydride transfer becomes thermoneutral (Figure 7). Building upon this result, we have demonstrated that HNi(dmpe)<sub>2</sub><sup>+</sup>, which is not catalytically active in either MeCN or water, is indeed catalytically active in mixtures of these solvents. These results demonstrate that by using a combination of MeCN and water, we were able to achieve not only hydride transfer to generate formate, but also the regeneration of the catalytically active metal hydride under these conditions.



**Figure 14.**  $\Delta G^{\circ}_{\text{rxn}}$  reaches thermoneutrality at 0.24 mole fraction of water and enables catalytic hydrogenation using HNi(dmpe)<sub>2</sub><sup>+</sup>, which is inactive in either pure solvent.

**Use of extended environment in controlling formation of active species.** Interest in copper hydrides has grown rapidly in catalysis because they can readily functionalize alkenes, ketones, and aldehydes under mild reaction conditions. Notwithstanding the increasing recognition of their widespread value in catalysis, it is not well established how Cu-H breaks  $\pi$ -bonds, largely because mononuclear copper hydrides are notoriously unstable. We determined two distinct pathways for insertion reactions of  $[(\text{NHC})\text{Cu}(\mu\text{-H})_2]$  complexes with carbonyl substrates (Figure 8), using a combination of spectroscopic kinetic studies, H/D isotopic labeling, and X-ray crystallography. The rate of insertion of more active substrates is controlled by the formation of  $(\text{NHC})\text{Cu-H}$  monomer from  $[(\text{NHC})\text{Cu}(\mu\text{-H})_2]$ . In contrast, for less active substrates, the rate of insertion depends on the rate of hydride transfer from the transiently formed Cu-H monomer to the substrate. The overall rate in both kinetic regimes is highly dependent on the formation of the Cu-H monomer, which is strongly dependent on the size of the NHC ligand, even when the substitution is on the periphery of the NHC ligand.

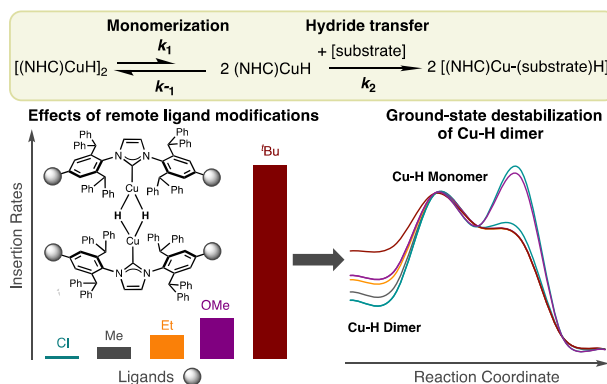


**Figure 15.** Two major kinetic regimes of rate-limiting monomerization or hydride transfer were established for insertion reactions of Cu-H complexes. The relative insertion rate in both regimes is dependent on the steric properties of the remote substitutions on the ligands to promote monomer formation.

**Modeling collective dynamics and its impact on catalysis.** Some of the most critical challenges in representing reactivity in structured media, such as in non-ideal solvents or interfaces at high density, is the need to account for global anharmonicity and collective dynamics. In this context, traditional models of reactivity that rely on idealized models fail, and it becomes necessary to perform detailed sampling of the free energy surfaces. This approach requires the use of variables that describe the collective motions of molecules, particularly at transition states.

We investigated the development and use of advanced collective variables (CVs) that capture the appreciable effects on the reaction free energy emanating from complex chemical environments such as flexible extended coordination spheres and confined spaces. As an example, combining reactivity studies, thermochemistry, NMR spectroscopy and extensive ab initio molecular dynamics simulations, we showed that water in HZSM-5 adsorbs through clustering in units of up to eight molecules adjacent to the Brønsted acid site. To explore the ubiquity of this phenomenon, we have adopted a set of CVs able to access the acid-

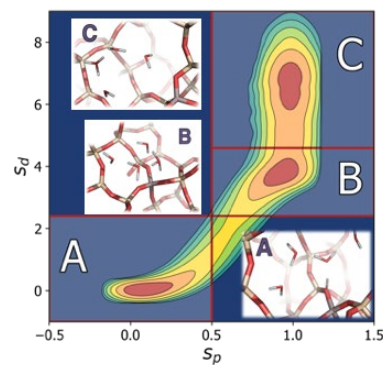


**Figure 16.** Relative free energy of three protonation states in water-filled zeolites: (A) Undissociated state; (B) Contact ion pair; and (C) Solvated proton state.

base properties of complex catalysts independent of the number of acid-base species simultaneously present, nature of reactants, and the kind of solvent. This has allowed us to understand the evolution of acid/base properties inside the zeolite pores as a function of the pore size/shape and number of water molecules present (Figure 9). We find that it is a delicate balance between enthalpic and entropic drivers that determine the protonation state in zeolites with the preferred state being a protonated water cluster whose size is dependent upon that of the zeolite pore in which it is confined. Moving forward, this allows us to understand how interactions between these clusters and organic molecules in these anisotropic confined spaces impact catalysis. Moreover, this capability will enable us to reliably sample free energy surfaces and transition states in complex environments far from ideality and access the role of collective dynamics upon reaction kinetics.

## Publications Acknowledging this Grant in 2018-2021

*Publications exclusively funded by this grant*

### 2018

1. Baxter, A. F.; Schaab, J.; Hegge, J.; Saal, T.; Vasiliu, M.; Dixon, D. A.; Haiges, R.; Christe, K. O.,  $\alpha$ -Fluoroalcohols: Synthesis and Characterization of Perfluorinated Methanol, Ethanol and n-Propanol, and their Oxonium Salts. *Chem. Eur. J.* **2018**, *24*, 16737-16742. <http://dx.doi.org/10.1002/chem.201804306>. (DA Dixon and M. Vasiliu supported by this proposal for all of the computational work and writing the manuscript. Solely funded.)
2. Baylon, R. A. L.; Sun, J.; Kovarik, L.; Engelhard, M.; Li, H.; Winkelman, A. D.; Martin, K. J.; Wang, Y., Structural Identification of  $Zn_xZr_yO_z$  Catalysts for Cascade Aldolization and Self-Deoxygenation Reactions. *Appl. Catal. B* **2018**, *234*, 337-346. <http://dx.doi.org/10.1016/j.apcatb.2018.04.051>. (Solely funded by the financial support of this program.)
3. Dahal, A.; Mu, R.; Lyubinetsky, I.; Dohnálek, Z., Hydrogen Adsorption and Reaction on  $RuO_2(110)$ . *Surf. Sci.* **2018**, *677*, 264-270. <http://dx.doi.org/10.1016/j.susc.2018.07.014>. (This work was solely funded by this program.)
4. Glezakou, V.-A.; Rousseau, R., Shedding Light on Black Titania. *Nat. Mater.* **2018**, *17*, 856-857. <http://dx.doi.org/10.1038/s41563-018-0150-1>. (Authors were solely funded on this program.)
5. Kwon, S.; Deshlahra, P.; Iglesia, E., Dioxygen Activation Routes in Mars-Van Krevelen Redox Cycles Catalyzed by Metal Oxides. *J. Catal.* **2018**, *364*, 228-247. <http://dx.doi.org/https://doi.org/10.1016/j.jcat.2018.05.016>. (Solely supported by this program.)
6. Maestri, M.; Iglesia, E., First-Principles Theoretical Assessment of Catalysis by Confinement:  $NO-O_2$  Reactions within Voids of Molecular Dimensions in Siliceous Crystalline Frameworks. *Phys. Chem. Chem. Phys.* **2018**, *20*, 15725-15735. <http://dx.doi.org/10.1039/C8CP01615A>. (This publication is based on previous work

supported by this grant. Iglesia's contributions were exclusively funded by this grant. Maestri contributions were supported by his own funding at the Politecnico of Milano.)

7. Novotny, Z.; Nguyen, M.-T.; Netzer, F. P.; Glezakou, V.-A.; Rousseau, R.; Dohnálek, Z., Formation of Supported Graphene Oxide: Evidence for Enolate Species. *J. Am. Chem. Soc.* **2018**, *140*, 5102-5109. <http://dx.doi.org/10.1021/jacs.7b12791>. (This work was solely funded by this program. Z.N. performed experimental work and analysis of the data. Z.D. designed the experiments. Z.D. and F.N. guided the data analysis. M.T.N., V.A.G., and R.R. performed DFT simulations. The manuscript was written by all the authors.)
8. Petrik, N. G.; Mu, R.; Dahal, A.; Wang, Z.; Lyubinetsky, I.; Kimmel, G. A., Diffusion and Photon-Stimulated Desorption of CO on TiO<sub>2</sub>(110). *J. Phys. Chem. C* **2018**, *122*, 15382-15389. <http://dx.doi.org/10.1021/acs.jpcc.8b03418>. (Sole Contribution.)
9. Shi, D.; Wang, H.; Kovarik, L.; Gao, F.; Wan, C.; Hu, J. Z.; Wang, Y., WO<sub>x</sub> Supported on  $\gamma$ -Al<sub>2</sub>O<sub>3</sub> with Different Morphologies as Model Catalysts for Alkanol Dehydration. *J. Catal.* **2018**, *363*, 1-8. <http://dx.doi.org/10.1016/j.jcat.2018.04.004>. (This work was solely funded by this program.)
10. Tran, B. L.; Fulton, J. L.; Linehan, J. C.; Lercher, J. A.; Bullock, R. M., Rh(CAAC)-Catalyzed Arene Hydrogenation: Evidence for Nanocatalysis and Sterically Controlled Site-Selective Hydrogenation. *ACS Catal.* **2018**, *8*, 8441-8449. <http://dx.doi.org/10.1021/acscatal.8b02589>. (Solely funded.)
11. Wang, M.; Gutierrez, O. Y.; Camaioni, D. M.; Lercher, J. A., Palladium Catalyzed Reductive Insertion of Alcohols in Aryl Ether Bonds. *Angew. Chem. Int. Ed.* **2018**, *57*, 3747-3751. <http://dx.doi.org/10.1002/anie.201709445>. (Solely funded by this program.)
12. Wiedner, E. S.; Linehan, J. C., Making a Splash in Homogeneous CO<sub>2</sub> Hydrogenation: Elucidating the Impact of Solvent on Catalytic Mechanisms. *Chem. Eur. J.* **2018**, *24*, 16964-16971. <http://dx.doi.org/doi:10.1002/chem.201801759>. (Authors were solely funded on this program.)

## 2019

13. Dahal, A.; Petrik, N. G.; Wu, Y.; Kimmel, G. A.; Gao, F.; Wang, Y.; Dohnálek, Z., Adsorption and Reaction of Methanol on Anatase TiO<sub>2</sub>(101) Single Crystals and Faceted Nanoparticles. *J. Phys. Chem. C* **2019**, *123*, 24133-24145. <http://dx.doi.org/10.1021/acs.jpcc.9b07080>. (Solely Funded.)
14. Dutta, A.; Shaw, W. J., Chemical Method for Evaluating Catalytic Turnover Frequencies (TOF) of Moderate to Slow H<sub>2</sub> Oxidation Electrocatalysts. *Organometallics* **2019**, *38*, 1311-1316. <http://dx.doi.org/10.1021/acs.organomet.8b00580>. (Sole.)
15. Eckstein, S.; Hintermeier, P. H.; Zhao, R.; Barath, E.; Shi, H.; Liu, Y.; Lercher, J. A., Influence of Hydronium Ions in Zeolites on Sorption. *Angew. Chem. Int. Ed. Engl.* **2019**, *58*, 3450-3455. <http://dx.doi.org/10.1002/anie.201812184>. (J.A.L. and H.S. acknowledge support by this program. Solely funded.)

16. Kumar, R.; Karkamkar, A.; Bowden, M.; Autrey, T., Solid-State Hydrogen Rich Boron–Nitrogen Compounds for Energy Storage. *Chem. Soc. Rev.* **2019**, *48*, 5350-5380. <http://dx.doi.org/10.1039/C9CS00442D>. (The BES program was the sole source for the authors to write the review.)
17. Kwon, S.; Deshlahra, P.; Iglesia, E., Reactivity and Selectivity Descriptors of Dioxygen Activation Routes on Metal Oxides. *J. Catal.* **2019**, *377*, 692-710. <http://dx.doi.org/https://doi.org/10.1016/j.jcat.2019.07.048>. (S.K., E.I, exclusively funded.)
18. Laureanti, J. A.; O'Hagan, M.; Shaw, W. J., Chicken Fat for Catalysis: A Scaffold Is as Important for Molecular Complexes for Energy Transformations as It Is for Enzymes in Catalytic Function. *Sustain. Energy Fuels* **2019**, *3*, 3260-3278. <http://dx.doi.org/10.1039/C9SE00229D>. (Sole)
19. Li, H.; Sun, J.; Wang, Y., Surface Acetone Reactions on  $Zn_xZr_yO_z$ : A DRIFTS-MS Study. *Appl. Catal. A* **2019**, *573*, 22-31. <http://dx.doi.org/10.1016/j.apcata.2019.01.007>. (Solely funded.)
20. Marcinkowski, M. D.; Yuk, S. F.; Doudin, N.; Smith, R. S.; Nguyen, M.-T.; Kay, B. D.; Glezakou, V.-A.; Rousseau, R.; Dohnálek, Z., Low-Temperature Oxidation of Methanol to Formaldehyde on a Model Single-Atom Catalyst: Pd Atoms on  $Fe_3O_4(001)$ . *ACS Catal.* **2019**, *9*, 10977-10982. <http://dx.doi.org/10.1021/acscatal.9b03891>. (Solely Funded.)
21. Mei, D.; Lercher, J. A., Effects of Local Water Concentrations on Cyclohexanol Dehydration in H-BEA Zeolites. *J. Phys. Chem. C* **2019**, *123*, 25255-25266. <http://dx.doi.org/10.1021/acs.jpcc.9b07738>. (Exclusively funded by this grant.)
22. Nelson, N. C.; Nguyen, M.-T.; Glezakou, V.-A.; Rousseau, R.; Szanyi, J., Carboxyl Intermediate Formation Via an in Situ-Generated Metastable Active Site During Water-Gas Shift Catalysis. *Nat. Catal.* **2019**, *2*, 916-924. <http://dx.doi.org/10.1038/s41929-019-0343-2>. (Solely funded.)
23. Persaud, R. R.; Chen, M.; Peterson, K. A.; Dixon, D. A., Potential Energy Surface of Group 11 Trimers (Cu, Ag, Au): Bond Angle Isomerism in  $Au_3$ . *J. Phys. Chem. A* **2019**, *123*, 1198-1207. <http://dx.doi.org/10.1021/acs.jpca.8b11219>. (Solely Funded.)
24. Tran, B. L.; Fulton, J. L.; Linehan, J. C.; Balasubramanian, M.; Lercher, J. A.; Bullock, R. M., Operando XAFS Studies on Rh(CAAC)-Catalyzed Arene Hydrogenation. *ACS Catal.* **2019**, *9*, 4106-4114. <http://dx.doi.org/10.1021/acscatal.8b04929>. (Solely funded.)
25. Wang, M.; Jaegers, N. R.; Lee, M.-S.; Wan, C.; Hu, J. Z.; Shi, H.; Mei, D.; Burton, S. D.; Camaioni, D. M.; Gutierrez, O. Y.; Glezakou, V. A.; Rousseau, R.; Wang, Y.; Lercher, J. A., Genesis and Stability of Hydronium Ions in Zeolite Channels. *J. Am. Ceram. Soc.* **2019**, *141*, 3444-3455. <http://dx.doi.org/10.1021/jacs.8b07969>. (Solely funded.)

**2020**

26. Collinge, G.; Yuk, S. F.; Nguyen, M.-T.; Lee, M.-S.; Glezakou, V.-A.; Rousseau, R., Effect of Collective Dynamics and Anharmonicity on Entropy in Heterogenous Catalysis: Building the Case for Advanced Molecular Simulations. *ACS Catal.* **2020**, *10*, 9236-9260. <http://dx.doi.org/10.1021/acscatal.0c01501>. (This work was solely funded by this program.)
27. Confer, M. P.; Outlaw, D. A.; Dixon, D. A., Potential Main Group Amine Borane-Based Chemical Hydrogen Storage Molecular Systems. *Comput. Theor. Chem.* **2020**, *1189*, 112953. <http://dx.doi.org/10.1016/j.comptc.2020.112953>. (Solely funded by this program.)
28. Deshlahra, P.; Iglesia, E., Reactivity Descriptors in Acid Catalysis: Acid Strength, Proton Affinity and Host–Guest Interactions. *Chem. Commun.* **2020**, *56*, 7371-7398. <http://dx.doi.org/10.1039/D0CC02593C>. (Exclusively funded by this program.)
29. Erickson, J. D.; Preston, A. Z.; Linehan, J. C.; Wiedner, E. S., Enhanced Hydrogenation of Carbon Dioxide to Methanol by a Ruthenium Complex with a Charged Outer-Coordination Sphere. *ACS Catal.* **2020**, *10*, 7419-7423. <http://dx.doi.org/10.1021/acscatal.0c02268>. (Sole Contribution.)
30. Jaegers, N. R.; Hu, W.; Wang, Y.; Hu, J. Z., High-Temperature and High-Pressure in Situ Magic Angle Spinning Nuclear Magnetic Resonance Spectroscopy. *JoVE* **2020**, e61794. <http://dx.doi.org/doi:10.3791/61794>. (Solely funded by this program.)
31. Jaegers, N. R.; Wang, Y.; Hu, J. Z., Thermal Perturbation of NMR Properties in Small Polar and Non-Polar Molecules. *Sci. Rep.* **2020**, *10*, 6097. <http://dx.doi.org/10.1038/s41598-020-63174-6>. (Sole supported.)
32. Kovarik, L.; Bowden, M.; Andersen, A.; Jaegers, N. R.; Washton, N.; Szanyi, J., Quantification of High-Temperature Transition Al<sub>2</sub>O<sub>3</sub> and Their Phase Transformations. *Angew. Chem. Int. Ed.* **2020**, 2-11. <http://dx.doi.org/10.1002/anie.202009520>. (Solely Funded.)
33. Kwon, S.; Lin, T. C.; Iglesia, E., Elementary Steps and Site Requirements in Formic Acid Dehydration Reactions on Anatase and Rutile TiO<sub>2</sub> Surfaces. *J. Catal.* **2020**, *383*, 60-76. <http://dx.doi.org/10.1016/j.jcat.2019.12.043>. (Sole Contribution.)
34. Kwon, S.; Lin, T. C.; Iglesia, E., Formic Acid Dehydration Rates and Elementary Steps on Lewis Acid–Base Site Pairs at Anatase and Rutile TiO<sub>2</sub> Surfaces. *J. Phys. Chem. C* **2020**, *124*, 20161-20174. <http://dx.doi.org/10.1021/acs.jpcc.0c05721>. (Solely funded.)
35. Li, H.; Sun, J.; Li, G.; Wu, D.; Wang, Y., Real-Time Monitoring of Surface Acetone Enolization and Aldolization. *Catal. Sci. Technol.* **2020**, *10*, 935-939. <http://dx.doi.org/10.1039/C9CY02339A>. (HL, JS, GL, DW funded by BES. DW funded by Alexandra Navrotsky Institute.)
36. Lin, F.; Chen, Y.; Zhang, L.; Mei, D.; Kovarik, L.; Sudduth, B.; Wang, H.; Gao, F.; Wang, Y., Single-Facet Dominant Anatase TiO<sub>2</sub> (101) and (001) Model Catalysts to Elucidate the Active Sites for Alkanol Dehydration. *ACS Catal.* **2020**, *10*, 4268-4279. <http://dx.doi.org/10.1021/acscatal.9b04654>. (Solely Funded.)

37. McNeill, A. S.; Zhan, C.-G.; Appel, A. M.; Stanbury, D. M.; Dixon, D. A., The H•/H-Redox Couple and Absolute Hydration Energy of H. *J. Phys. Chem. A* **2020**, *124*, 6084-6095. <http://dx.doi.org/10.1021/acs.jpca.0c03833>. (Solely supported.)
38. Milakovic, L.; Hintermeier, P. H.; Liu, Q.; Shi, H.; Liu, Y.; Barath, E.; Lercher, J. A., Towards Understanding and Predicting the Hydronium Ion Catalyzed Dehydration of Cyclic-Primary, Secondary and Tertiary Alcohols. *J. Catal.* **2020**, *390*, 237-243. <http://dx.doi.org/10.1016/j.jcat.2020.08.009>. (Solely funded by this program.)
39. Nelson, N. C.; Chen, L.; Meira, D.; Kovarik, L.; Szanyi, J., In Situ Dispersion of Palladium on TiO<sub>2</sub> During Reverse Water–Gas Shift Reaction: Formation of Atomically Dispersed Palladium. *Angew. Chem. Int. Ed.* **2020**, *59*, 17657-17663. <http://dx.doi.org/https://doi.org/10.1002/anie.202007576>. (Solely Funded.)
40. Nelson, N. C.; Szanyi, J., Heterolytic Hydrogen Activation: Understanding Support Effects in Water-Gas Shift, Hydrodeoxygenation, and CO Oxidation Catalysis. *ACS Catal.* **2020**, *10*, 5663-5671. <http://dx.doi.org/10.1021/acscatal.0c01059>. (N.C.N and J.S. were exclusively funded by this program for all the experiment work and writing the manuscript.)
41. Persaud, R. R.; Chen, M.; Dixon, D. A., Prediction of Structures and Atomization Energies of Coinage Metals, (M)<sub>N</sub>, n < 20: Extrapolation of Normalized Clustering Energies to Predict the Cohesive Energy. *J. Phys. Chem. A* **2020**, *124*, 1775-1786. <http://dx.doi.org/10.1021/acs.jpca.9b11801>. (Sole support by this program.)
42. Stein, T. H.; Vasiliu, M.; Arduengo, A. J.; Dixon, D. A., Lewis Acidity and Basicity: Another Measure of Carbene Reactivity. *J. Phys. Chem. A* **2020**, *124*, 6096-6103. <http://dx.doi.org/10.1021/acs.jpca.0c03877>. (Solely supported.)
43. Wang, M.; Zhao, Y.; Mei, D.; Bullock, R. M.; Gutiérrez, O. Y.; Camaioni, D. M.; Lercher, J. A., The Critical Role of Reductive Steps in the Nickel-Catalyzed Hydrogenolysis and Hydrolysis of Aryl Ether C–O Bonds. *Angew. Chem. Int. Ed.* **2020**, *59*, 1445-1449. <http://dx.doi.org/10.1002/anie.201909551>. (All exclusively funded by this grant.)
44. Yuk, S. F.; Collinge, G.; Nguyen, M.-T.; Lee, M.-S.; Glezakou, V.-A.; Rousseau, R., Selective Acetylene Hydrogenation over Single Metal Atoms Supported on Fe<sub>3</sub>O<sub>4</sub>(001): A First-Principle Study. *J. Chem. Phys.* **2020**, *152*, 154703. <http://dx.doi.org/10.1063/1.5142748>. (Sole funding.)
45. Yuk, S. F.; Collinge, G.; Nguyen, M.-T.; Lee, M.-S.; Glezakou, V.-A.; Rousseau, R. *Single-Atom Catalysis: An Analogy between Heterogeneous and Homogeneous Catalysts in Advanced Heterogeneous Catalysts Volume 2: Applications at the Single-Atom Scale*; American Chemical Society, **2020**; Vol. 1360; pp 1-15. (Solely Funded.)
46. Zhang, J.; Sun, J.; Wang, Y., Recent Advances in the Selective Catalytic Hydrodeoxygenation of Lignin-Derived Oxygenates to Arenes. *Green Chem.* **2020**, *22*, 1072-1098. <http://dx.doi.org/10.1039/C9GC02762A>. (Solely funded.)
47. Zhang, W.; Cheng, G.; Haller, G. L.; Liu, Y.; Lercher, J. A., Rate Enhancement of Acid-Catalyzed Alcohol Dehydration by Supramolecular Organic Capsules. *ACS Catal.* **2020**, *10*, 13371-13376. <http://dx.doi.org/10.1021/acscatal.0c03625>. (Solely funded by this program.)

**2021**

48. Chen, F.; Shetty, M.; Wang, M.; Shi, H.; Liu, Y. S.; Camaioni, D. M.; Gutierrez, O. Y.; Lercher, J. A., Differences in Mechanism and Rate of Zeolite-Catalyzed Cyclohexanol Dehydration in Apolar and Aqueous Phase. *ACS Catal.* **2021**, *11*, 2879-2888. <http://dx.doi.org/10.1021/acscatal.0c05674>. (Solely Funded.)
49. Chen, L.; Smith, R. S.; Kay, B. D.; Dohnalek, Z., Formation of Gas-Phase Allyl Radicals from Glycerol on Rutile TiO<sub>2</sub>(110). *J. Phys. Chem. C* **2021**, *125*, 7227-7239. <http://dx.doi.org/10.1021/acs.jpcc.1c00991>. (Sole funding.)
50. Chen, L.; Unocic, R. R.; Hoffman, A. S.; Hong, J.; Braga, A. H.; Bao, Z.; Bare, S. R.; Szanyi, J., Unlocking the Catalytic Potential of TiO<sub>2</sub>-Supported Pt Single Atoms for the Reverse Water–Gas Shift Reaction by Altering Their Chemical Environment. *JACS Au* **2021**. <http://dx.doi.org/10.1021/jacsau.1c00111>. (Solely supported by the BES Catalysis Program.)
51. Doudin, N.; Collinge, G.; Gurunathan, P. K.; Lee, M.-S.; Glezakou, V.-A.; Rousseau, R.; Dohnálek, Z., Creating Self-Assembled Arrays of Mono-Oxo (MoO<sub>3</sub>)<sub>1</sub> Species on TiO<sub>2</sub>(101) Via Deposition and Decomposition of (MoO<sub>3</sub>)<sub>N</sub> Oligomers. *Proc. Natl. Acad. Sci. U.S.A.* **2021**, *118*, e2017703118. <http://dx.doi.org/10.1073/pnas.2017703118>. (This work was solely funded by this program.)
52. Doudin, N.; Collinge, G.; Persaud, R. R.; Gurunathan, P. K.; Lee, M.-S.; Glezakou, V. A.; Dixon, D. A.; Rousseau, R.; Dohnalek, Z., Binding and Stability of MgO Monomers on Anatase TiO<sub>2</sub>(101). *J. Chem. Phys.* **2021**, *154*, 204703. <http://dx.doi.org/10.1063/5.0047521>. (Solely funded.)
53. Grifoni, E.; Piccini, G.; Lercher, J. A.; Glezakou, V.-A.; Rousseau, R.; Parrinello, M., Confinement Effects and Acid Strength in Zeolites. *Nat. Commun.* **2021**, *12*, 2630. <http://dx.doi.org/10.1038/s41467-021-22936-0>. (Solely funded.)
54. Khivantsev, K.; Jaegers, N. R.; Kwak, J.-H.; Szanyi, J.; Kovarik, L., Precise Identification and Characterization of Catalytically Active Sites on the Surface of  $\gamma$ -Alumina. *Angew. Chem. Int. Ed.* **2021**. <http://dx.doi.org/https://doi.org/10.1002/anie.202102106>. (Solely funded.)
55. Lin, F.; Wang, H.; Zhao, Y.; Fu, J.; Mei, D.; Jaegers, N. R.; Gao, F.; Wang, Y., Elucidation of Active Sites in Aldol Condensation of Acetone over Single-Facet Dominant Anatase TiO<sub>2</sub> (101) and (001) Catalysts. *JACS Au* **2021**, *1*, 41-52. <http://dx.doi.org/10.1021/jacsau.0c00028>. (Solely Funded.)
56. Liu, Y.; Cheng, G.; Baráth, E.; Shi, H.; Lercher, J. A., Alkylation of Lignin-Derived Aromatic Oxygenates with Cyclic Alcohols on Acidic Zeolites. *Appl. Catal. B* **2021**, *281*, 119424. <http://dx.doi.org/https://doi.org/10.1016/j.apcatb.2020.119424>. (Solely funded by this program.)
57. Peng, G.; Xu, L.; Glezakou, V.-A.; Mavrikakis, M., Mechanism of Methanol Synthesis on Ni(110). *Catal. Sci. Technol.* **2021**. <http://dx.doi.org/10.1039/D1CY00107H>. (Sole support. V.-A. G. acknowledges support by this program.)

58. Wiedner, E. S.; Preston, A. Z.; Helm, M. L.; Appel, A. M., Thermodynamic Trends for Reduction of CO by Molecular Complexes. *Organometallics* **2021**. <http://dx.doi.org/10.1021/acs.organomet.1c00178>. (Solely Funded.)
59. Wu, Y.; Gao, F.; Wang, H.; Kovarik, L.; Sudduth, B.; Wang, Y., Probing Acid–Base Properties of Anatase TiO<sub>2</sub> Nanoparticles with Dominant {001} and {101} Facets Using Methanol Chemisorption and Surface Reactions. *J. Phys. Chem. C* **2021**, *125*, 3988-4000. <http://dx.doi.org/10.1021/acs.jpcc.0c11107>. (Solely funded.)
60. Xu, S.; Jaegers, N. R.; Hu, W.; Kwak, J. H.; Bao, X.; Sun, J.; Wang, Y.; Hu, J. Z., High-Field One-Dimensional and Two-Dimensional <sup>27</sup>Al Magic-Angle Spinning Nuclear Magnetic Resonance Study of  $\Theta$ -,  $\delta$ -, and  $\gamma$ -Al<sub>2</sub>O<sub>3</sub> Dominated Aluminum Oxides: Toward Understanding the Al Sites in  $\gamma$ -Al<sub>2</sub>O<sub>3</sub>. *ACS Omega* **2021**, *6*, 4090-4099. <http://dx.doi.org/10.1021/acsomega.0c06163>. (Solely funded.)
61. Zhu, Y. F.; Yuk, S. F.; Zheng, J.; Nguyen, M. T.; Lee, M. S.; Szanyi, J.; Kovarik, L.; Zhu, Z. H.; Balasubramanian, M.; Glezakou, V. A.; Fulton, J. L.; Lercher, J. A.; Rousseau, R.; Gutierrez, O. Y., Environment of Metal-O-Fe Bonds Enabling High Activity in CO<sub>2</sub> Reduction on Single Metal Atoms and on Supported Nanoparticles. *J. Am. Chem. Soc.* **2021**, *143*, 5540-5549. <http://dx.doi.org/10.1021/jacs.1c02276>. (Solely Funded.)

*Publications jointly funded by this grant and other grants with leading intellectual contribution from this grant*

## 2018

62. Andrella, N. O.; Liu, K.; Gabidullin, B.; Vasiliu, M.; Dixon, D. A.; Baker, R. T., Metal Heptafluoroisopropyl (M-hfip) Complexes for Use as Hfip Transfer Agents. *Organometallics* **2018**, *37*, 422-432. <http://dx.doi.org/10.1021/acs.organomet.7b00837>. (DA Dixon and M. Vasiliu supported by this program for all of the computational work and writing the manuscript.)
63. Andrews, L.; Cho, H.-G.; Fang, Z.; Vasiliu, M.; Dixon, D. A., Tungsten Hydride Phosphorus- and Arsenic-Bearing Molecules with Double and Triple W–P and W–As Bonds. *Inorg. Chem.* **2018**, *57*, 5320-5332. <http://dx.doi.org/10.1021/acs.inorgchem.8b00348>. (DA Dixon, Z. Fang, and M. Vasiliu supported by this proposal for all of the computational work and writing and writing the manuscript.)
64. Burks, D. B.; Vasiliu, M.; Dixon, D. A.; Papish, E. T., Thermodynamic Acidity Studies of 6,6'-Dihydroxy-2,2'-Bipyridine: A Combined Experimental and Computational Approach. *J. Phys. Chem. A* **2018**, *122*, 2221-2231. <http://dx.doi.org/10.1021/acs.jpca.7b11441>. (DA Dixon and M. Vasiliu supported by this program for all of the computational work and writing the manuscript.)
65. Cassidy, S. J.; Brettell-Adams, I.; McNamara, L. E.; Smith, M. F.; Bautista, M.; Cao, H.; Vasiliu, M.; Gerlach, D. L.; Qu, F.; Hammer, N. I.; Dixon, D. A.; Rugar, P. A., Boranes with Ultra-High Stokes Shift Fluorescence. *Organometallics* **2018**, *37*, 3732-3741. <http://dx.doi.org/10.1021/acs.organomet.8b00460>. (DA Dixon and M.

Vasiliu supported by this proposal for all of the computational work and writing the manuscript.)

66. Dutta, A.; Appel, A. M.; Shaw, W. J., Designing Electrochemically Reversible H<sub>2</sub> Oxidation and Production Catalysts. *Nat. Rev. Chem.* **2018**, *2*, 244-252. <http://dx.doi.org/10.1038/s41570-018-0032-8>. (All authors contributed equally to the preparation of this review which was supported by both EFRC (Appel) and BES (Shaw) funding.)
67. Fang, Z.; Vasiliu, M.; Peterson, K. A.; Dixon, D. A., Computational Study of Molecular Hydrogen Adsorption over Small (Mo<sub>2</sub>)N Nanoclusters (M = Ti, Zr, Hf; n = 1 to 4). *J. Phys. Chem. A* **2018**, *122*, 4338-4349. <http://dx.doi.org/10.1021/acs.jpca.7b12634>. (DA Dixon, Z. Fang, and M. Vasiliu supported by this proposal for all of the computational work and writing the manuscript.)
68. Feller, D.; Dixon, D. A., Density Functional Theory and the Basis Set Truncation Problem with Correlation Consistent Basis Sets: Elephant in the Room or Mouse in the Closet? *J. Phys. Chem. A* **2018**, *122*, 2598-2603. <http://dx.doi.org/10.1021/acs.jpca.8b00392>. (DA Dixon supported by this program for writing the manuscript.)
69. Frederick, R. T.; Novotny, Z.; Netzer, F. P.; Herman, G. S.; Dohnálek, Z., Growth and Stability of Titanium Dioxide Nanoclusters on Graphene/Ru(0001). *J. Phys. Chem. B* **2018**, *122*, 640-648. <http://dx.doi.org/10.1021/acs.jpcc.7b05518>. (Z Novotny and Z Dohnalek were funded by this FWP. ZN took part in the STM measurements, ZD guided the experiments and contributed to the manuscript preparation.)
70. Hoffman, A. S.; Debeve, L. M.; Zhang, S.; Perez-Aguilar, J. E.; Conley, E. T.; Justl, K. R.; Arslan, I.; Dixon, D. A.; Gates, B. C., Beating Heterogeneity of Single-Site Catalysts: MgO-Supported Iridium Complexes. *ACS Catal.* **2018**, *8*, 3489-3498. <http://dx.doi.org/10.1021/acscatal.8b00143>. (DA Dixon and S. Zhang supported by this proposal for all of the computational work and writing the manuscript.)
71. Junk, C. P.; He, Y.; Zhang, Y.; Smith, J. R.; Dixon, D. A.; Vasiliu, M.; Lemal, D. M., Chemistry of the Highly Strained Alkene Perfluorobicyclo[2.2.0]hex-1(4)-ene. *Eur. J. Org. Chem.* **2018**, *2018*, 3167-3179. <http://dx.doi.org/10.1002/ejoc.201800058>. (DA Dixon and M. Vasiliu supported by this proposal for all of the computational work and writing the manuscript.)
72. Liu, Y.; Baráth, E.; Shi, H.; Hu, J.; Camaioni, D. M.; Lercher, J. A., Solvent-Determined Mechanistic Pathways in Zeolite-H-BEA-Catalysed Phenol Alkylation. *Nat. Catal.* **2018**, *1*, 141-147. <http://dx.doi.org/10.1038/s41929-017-0015-z>. (J. Z. Hu was supported by this program for the in situ <sup>13</sup>C MAS NMR experiments and the results (Figure 3) in this work.)
73. Novotny, Z.; Zhang, Z.; Dohnálek, Z., Imaging Chemical Reactions One Molecule at a Time. *Encyclopedia of Interfacial Chemistry* **2018**, 220-240. <http://dx.doi.org/10.1016/B978-0-12-409547-2.12844-6>. (ZN and ZD writing contributions were funded by this program.)

74. Oughli, A. A.; Ruff, A.; Boralugodage, N. P.; Rodríguez-Maciá, P.; Plumeré, N.; Lubitz, W.; Shaw, W. J.; Schuhmann, W.; Rüdiger, O., Dual Properties of a Hydrogen Oxidation Ni-catalyst Entrapped within a Polymer Promote Self-Defense against Oxygen. *Nat. Commun.* **2018**, *9*, 864. <http://dx.doi.org/10.1038/s41467-018-03011-7>. (Shaw was funded by this FWP to help design experiments, interpret data, and write the manuscript. Boralugodage was funded by this FWP to provide complexes.)
75. Palermo, A. P.; Zhang, S.; Hwang, S.-J.; Dixon, D. A.; Gates, B. C.; Katz, A., Weakly Interacting Solvation Spheres Surrounding a Calixarene-Protected Tetrairidium Carbonyl Cluster: Contrasting Effects on Reactivity of Alkane Solvent and Silica Support. *Dalton Trans.* **2018**, *47*, 13550-13558. <http://dx.doi.org/10.1039/C8DT01371C>. (DA Dixon and S. Zhang supported by this proposal for all of the computational work and writing the manuscript.)
76. Prodinge, S.; Shi, H.; Wang, H.; Derewinski, M. A.; Lercher, J. A., Impact of Structural Defects and Hydronium Ion Concentration on the Stability of Zeolite BEA in Aqueous Phase. *Appl. Catal. B* **2018**, *237*, 996-1002. <http://dx.doi.org/10.1016/j.apcatb.2018.06.065>. (JA Lercher was supported by this program as science lead and for writing the manuscript.)
77. Prodinge, S.; Vjunov, A.; Hu, J. Z.; Fulton, J. L.; Camaioni, D. M.; Derewinski, M. A.; Lercher, J. A., Elementary Steps of Faujasite Formation Followed by in Situ Spectroscopy. *Chem. Mater.* **2018**, *30*, 888-897. <http://dx.doi.org/10.1021/acs.chemmater.7b04554>. (A Vjunov and JL Fulton were supported by this program to perform XAFS measurements and contributed to the interpretation of the data, JZ Hu participated in NMR measurements and data evaluation, JL Camaioni and JA Lercher were supported by this program and participated in the evaluation of the data and manuscript preparation.)
78. Sanwald, K. E.; Berto, T. F.; Jentys, A.; Camaioni, D. M.; Gutiérrez, O. Y.; Lercher, J. A., Kinetic Coupling of Water Splitting and Photoreforming on SrTiO<sub>3</sub>-Based Photocatalysts. *ACS Catal.* **2018**, *8*, 2902-2913. <http://dx.doi.org/10.1021/acscatal.7b03192>. (D.M.C., O.Y.G., and J.A.L. acknowledge support for their contribution by this program.)
79. Xue, N.; Vjunov, A.; Schallmoser, S.; Fulton, J. L.; Sanchez-Sanchez, M.; Hu, J. Z.; Mei, D.; Lercher, J. A., Hydrolysis of Zeolite Framework Aluminum and Its Impact on Acid Catalyzed Alkane Reactions. *J. Catal.* **2018**, *365*, 359-366. <http://dx.doi.org/10.1016/j.jcat.2018.07.015>. (A Vjunov, JL Fulton, JZ Hu, D Mei and JA Lercher were funded by this FWP. A Vjunov, JL Fulton, and JZ Hu perform experimental, X-ray and NMR experiments, respectively. D Mei was supported by this program for the computational work. JA Lercher was supported by this program as science lead and for writing the manuscript.)
80. Yu, Z.; Wang, Y.; Liu, S.; Yao, Y.; Sun, Z.; Li, X.; Liu, Y.; Wang, W.; Wang, A.; Camaioni, D. M.; Lercher, J. A., Aqueous Phase Hydrodeoxygenation of Phenol over Ni<sub>3</sub>P-CePO<sub>4</sub> Catalysts. *Ind. Eng. Chem. Res.* **2018**, *57*, 10216-10225. <http://dx.doi.org/10.1021/acs.iecr.8b01606>. (DM Camaioni and JA Lercher were funded by this FWP. DM Camaioni was supported by this program for writing the

manuscript and scientific advisor. JA Lercher was supported by this program as science lead and for writing the manuscript.)

81. Yu, Z.; Wang, Y.; Sun, Z.; Li, X.; Wang, A.; Camaioni, D. M.; Lercher, J. A., Ni<sub>3</sub>P as a High-Performance Catalytic Phase for the Hydrodeoxygenation of Phenolic Compounds. *Green Chem.* **2018**, *20*, 609-619. <http://dx.doi.org/10.1039/C7GC03262E>. (Supported by this project to explore nonoxidic supports for deoxygenation, J A Lercher and DM Camaioni participated in the interpretation of the results, in the postulation of hypotheses, and in the drafting of the manuscript.)
82. Yun, D.; Wang, Y.; Herrera, J., Ethanol Partial Oxidation over VO<sub>x</sub>/TiO<sub>2</sub> Catalysts: The Role of Titania Surface Oxygen on the Vanadia Reoxidation in the Mars-Van Krevelen Mechanism. *ACS Catal.* **2018**, *8*, 4681-4693. <http://dx.doi.org/10.1021/acscatal.7b03327>. (Y. Wang was supported by this program for the interpretation of results and writing the manuscript.)

## 2019

83. Arduengo, A. J.; Uchiyama, Y.; Dixon, D. A.; Vasiliu, M., Crystal Structure of Burgess Inner Salts and Their Hydrolyzed Ammonium Sulfaminates. *Aust. J. Chem.* **2019**, *72*, 867-873. <http://dx.doi.org/https://doi.org/10.1071/CH19338>. (DA Dixon and M. Vasiliu supported by this proposal for all of the computational work and writing the manuscript.)
84. Christe, K. O.; Dixon, D. A.; Vasiliu, M.; Haiges, R.; Hu, B., How Energetic are cyclo-Pentazoles? *Propellants Explos. Pyrotech.* **2019**, *44*, 263-266. <http://dx.doi.org/10.1002/prop.201800351>. (DA Dixon and M. Vasiliu supported by this proposal for all of the computational work and writing the manuscript.)
85. Denk, C.; Foraita, S.; Kovarik, L.; Stoerzinger, K. A.; Liu, Y.; Barath, E.; Lercher, J. A., Rate Enhancement by Cu in Ni<sub>x</sub>Cu<sub>1-x</sub>/ZrO<sub>2</sub> Bimetallic Catalysts for Hydrodeoxygenation of Stearic Acid. *Catal. Sci. Technol.* **2019**, *9*, 2620-2629. <http://dx.doi.org/10.1039/C9CY00181F>. (C Denk was supported for experimental work. L Kovarik was supported for microscopy characterization. KA Stoerzinger was supported for XPS characterization. JA Lercher was supported as science lead and for writing the manuscript.)
86. Doudin, N.; Yuk, S. F.; Marcinkowski, M. D.; Nguyen, M.-T.; Liu, J.-C.; Wang, Y.; Novotny, Z.; Kay, B. D.; Li, J.; Glezakou, V.-A.; Parkinson, G.; Rousseau, R.; Dohnálek, Z., Understanding Heterolytic H<sub>2</sub> Cleavage and Water-Assisted Hydrogen Spillover on Fe<sub>3</sub>O<sub>4</sub>(001)-Supported Single Palladium Atoms. *ACS Catal.* **2019**, *9*, 7876-7887. <http://dx.doi.org/10.1021/acscatal.9b01425>. (ND, SFY, MDM, MTN, YW, BDK, VAG, RR, and ZD were funded by this program. ND, MDM, and YW acquired the data, carried out the analysis, and participated in the preparation of the manuscript. SFY and MTN carried out calculations and participated in the preparation of the manuscript. BDK, VAG, RR, and ZD conceived the study, contributed to data analysis and interpretation, and manuscript preparation.)
87. Falbo, L.; Visconti, C. G.; Lietti, L.; Szanyi, J., The Effect of CO on CO<sub>2</sub> Methanation over Ru/Al<sub>2</sub>O<sub>3</sub> Catalysts: A Combined Steady-State Reactivity and Transient Drift

- Spectroscopy Study. *Appl. Catal. B* **2019**, *256*, 117791. <http://dx.doi.org/https://doi.org/10.1016/j.apcatb.2019.117791>. (Lead, J. Szanyi hosted/supervised visiting student (L. Falbo) with the DRIFTS experiments; participated in experimental design, data interpretation and MS preparation.)
88. Fang, C.-Y.; Zhang, S.; Hu, Y.; Vasiliu, M.; Perez-Aguilar, J. E.; Conley, E. T.; Dixon, D. A.; Chen, C.-Y.; Gates, B. C., Reversible Metal Aggregation and Redispersion Driven by the Catalytic Water Gas Shift Half-Reactions: Interconversion of Single-Site Rhodium Complexes and Tetra-rhodium Clusters in Zeolite HY. *ACS Catal.* **2019**, *9*, 3311-3321. <http://dx.doi.org/10.1021/acscatal.8b04798>. (DA Dixon, S. Zhang and M. Vasiliu supported by this FWP for all of the computational work and writing the manuscript.)
  89. Fourmond, V.; Wiedner, E. S.; Shaw, W. J.; Léger, C., Understanding and Design of Bidirectional and Reversible Catalysts of Multielectron, Multistep Reactions. *J. Am. Chem. Soc.* **2019**, *141*, 11269-11285. <http://dx.doi.org/10.1021/jacs.9b04854>. (Lead. The work discussed here was originally supported for W.J.S. by the Office of Science Early Career Research Program through the USDOE, with current funding from the USDOE, BES, Chemical Sciences, Geosciences, and Biosciences program.)
  90. Guan, E.; Debeve, L.; Vasiliu, M.; Zhang, S.; Dixon, D. A.; Gates, B. C., MgO-Supported Iridium Metal Pair-Site Catalysts Are More Active and Resistant to CO Poisoning Than Analogous Single-Site Catalysts for Ethylene Hydrogenation and Hydrogen-Deuterium Exchange. *ACS Catal.* **2019**, *9*, 9545-9553. <http://dx.doi.org/10.1021/acscatal.9b03463>. (DA Dixon, S. Zhang, and M. Vasiliu supported by this proposal for all of the computational work and writing the manuscript.)
  91. Han, Q.; Rehman, M. U.; Wang, J.; Rykov, A.; Gutiérrez, O. Y.; Zhao, Y.; Wang, S.; Ma, X.; Lercher, J. A., The Synergistic Effect between Ni Sites and Ni-Fe Alloy Sites on Hydrodeoxygenation of Lignin-Derived Phenols. *Appl. Catal. B* **2019**, *253*, 348-358. <http://dx.doi.org/https://doi.org/10.1016/j.apcatb.2019.04.065>. (O.Y. Gutierrez, and J.A. Lercher were funded by this FWP. O.Y. Gutierrez was supported by this program for contributing to discussion of the results and writing of the manuscript; J.A. Lercher was supported by this program for discussion of the results, planning, and writing of the manuscript.)
  92. Hu, H.; Vasiliu, M.; Stein, T. H.; Qu, F.; Gerlach, D. L.; Dixon, D. A.; Shaughnessy, K. H., Synthesis, Structural Characterization, and Coordination Chemistry of (Trineopentylphosphine)Palladium(Aryl)Bromide Dimer Complexes ( $[(\text{Np}_3\text{P})\text{Pd}(\text{Ar})\text{Br}]_2$ ). *Inorg. Chem.* **2019**, *58*, 13299-13313. <http://dx.doi.org/10.1021/acs.inorgchem.9b02164>. (DA Dixon, TH Stein, and M. Vasiliu supported by the proposal for all of the computational work and writing the manuscript.)
  93. Jaegers, N. R.; Lai, J.-K.; He, Y.; Walter, E.; Dixon, D. A.; Vasiliu, M.; Chen, Y.; Wang, C.; Hu, M. Y.; Mueller, K. T.; Wachs, I. E.; Wang, Y.; Hu, J. Z., Mechanism by Which Tungsten Oxide Promotes the Activity of Supported  $\text{V}_2\text{O}_5/\text{TiO}_2$  Catalysts for  $\text{NO}_x$  Abatement: Structural Effects Revealed by  $^{51}\text{V}$  MAS NMR Spectroscopy. *Angew. Chem. Int. Ed.* **2019**, *58*, 12609-12616.

- <http://dx.doi.org/10.1002/anie.201904503>. (DA Dixon and M. Vasiliu supported by this proposal for all of the computational work and writing the manuscript.)
94. Kovarik, L.; Bowden, M.; Shi, D.; Szanyi, J.; Peden, C. H. F., Structural Intergrowth in  $\delta$ -Al<sub>2</sub>O<sub>3</sub>. *J. Phys. Chem. C* **2019**, *123*, 9454-9460. <http://dx.doi.org/10.1021/acs.jpcc.8b10135>. (L. Kovarik and J. Szanyi was funded by this program. L. Kovarik designed and carried out all the TEM experiments. J. Szanyi supervised the experimental work and contributed to writing the manuscript.)
  95. Li, S.; Dixon, D. A. *Chapter Eight - Mechanism of Oxide-Catalyzed Selective Oxidation: A Computational Perspective in Annual Reports in Computational Chemistry*; Dixon, D. A., Ed.; Elsevier, **2019**; Vol. 15; pp 287-333. (DA Dixon played an important role in writing the manuscript.)
  96. Palermo, A. P.; Schöttle, C.; Zhang, S.; Grosso-Giordano, N. A.; Okrut, A.; Dixon, D. A.; Frei, H.; Gates, B. C.; Katz, A., Spectroscopic Characterization of  $\mu$ - $\eta$ 1: $\eta$ 1-Peroxo Ligands Formed by Reaction of Dioxygen with Electron-Rich Iridium Clusters. *Inorg. Chem.* **2019**, *58*, 14338-14348. <http://dx.doi.org/10.1021/acs.inorgchem.9b01529>. (DA Dixon and S. Zhang supported by this proposal for all of the computational work and writing the manuscript.)
  97. Walsh, A. P.; Laureanti, J. A.; Katipamula, S.; Chambers, Geoffrey M.; Priyadarshani, N.; Lense, S.; Bays, J. T.; Linehan, J. C.; Shaw, W. J., Evaluating the Impacts of Amino Acids in the Second and Outer Coordination Spheres of Rh-bis(Diphosphine) Complexes for CO<sub>2</sub> Hydrogenation. *Faraday Discuss.* **2019**, *215*, 123-140. <http://dx.doi.org/10.1039/C8FD00164B>. (All authors were supported by this FWP, with the exception of Chambers, who provided a ligand and was supported by the EFRC.)
  98. Wei, R.; Fang, Z.; Vasiliu, M.; Dixon, D. A.; Andrews, L.; Gong, Y., Infrared Spectroscopic and Theoretical Studies of the 3d Transition Metal Oxyfluoride Molecules. *Inorg. Chem.* **2019**, *58*, 9796-9810. <http://dx.doi.org/10.1021/acs.inorgchem.9b00822>. (DA Dixon and M. Vasiliu supported by this proposal for all of the computational work and writing the manuscript.)
  99. Yu, Z.; Wang, A.; Liu, S.; Yao, Y.; Sun, Z.; Li, X.; Liu, Y.; Wang, Y.; Camaioni, D. M.; Lercher, J. A., Hydrodeoxygenation of Phenolic Compounds to Cycloalkanes over Supported Nickel Phosphides. *Catal. Today* **2019**, *319*, 48-56. <http://dx.doi.org/10.1016/j.cattod.2018.05.012>. (DM Camaioni and JA Lercher were funded by this FWP. DM Camaioni was supported by this program for writing the manuscript and scientific advisor. JA Lercher was supported by this program as science lead and for writing the manuscript.)
  100. Zhang, Y.; Zhao, R.; Sanchez-Sanchez, M.; Haller, G. L.; Hu, J.; Bermejo-Deval, R.; Liu, Y.; Lercher, J. A., Promotion of Protolytic Pentane Conversion on H-MFI Zeolite by Proximity of Extra-Framework Aluminum Oxide and Brønsted Acid Sites. *J. Catal.* **2019**, *370*, 424-433. <http://dx.doi.org/10.1016/j.jcat.2019.01.006>. (J. Hu, and J.A. Lercher were funded by this FWP. J. Hu was supported by this program for

contributing to NMR experiments; J.A. Lercher was supported by this program for discussion of the results and leading the work.)

## 2020

101. Barnett, K. L.; Vasiliu, M.; Stein, T. H.; Delahay, M. V.; Qu, F.; Gerlach, D. L.; Dixon, D. A.; Shaughnessy, K. H., Experimental and Computational Study of the Structure, Steric Properties, and Binding Equilibria of Neopentylphosphine Palladium Complexes. *Inorg. Chem.* **2020**, *59*, 5579-5592. <http://dx.doi.org/10.1021/acs.inorgchem.0c00266>. (DA Dixon, TH Stein, and M. Vasiliu supported by the proposal for all of the computational work and writing the manuscript.)
102. Bowden, M. E.; Ginovska, B.; Jones, M. O.; Karkamkar, A. J.; Ramirez-Cuesta, A. J.; Daemen, L. L.; Schenter, G. K.; Miller, S. A.; Repo, T.; Chernichenko, K.; Leick, N.; Martinez, M. B.; Autrey, T., Heterolytic Scission of Hydrogen within a Crystalline Frustrated Lewis Pair. *Inorg. Chem.* **2020**, *59*, 15295-15301. <http://dx.doi.org/10.1021/acs.inorgchem.0c02290>. (The authors (M.E.B., B.G., A.J.K., G.K.S., and T.A.) gratefully acknowledge support from this project.)
103. Bramley, G.; Nguyen, M.-T.; Glezakou, V.-A.; Rousseau, R.; Skylaris, C.-K., Reconciling Work Functions and Adsorption Enthalpies for Implicit Solvent Models: A Pt (111)/Water Interface Case Study. *J. Chem. Theory Comput.* **2020**, *16*, 2703-2715. <http://dx.doi.org/10.1021/acs.jctc.0c00034>. (Major contribution. G.B. (partial support), V.-A.G., M.-T.N., and R.R. were supported by this program.)
104. Confer, M. P.; Allayarov, S. R.; Kim, I. P.; Markin, I. V.; Jackson, V. E.; Dixon, D. A., Direct Fluorination of Tetrafluoroethylene at Low Temperatures. *J. Fluorine Chem.* **2020**, *232*, 109493. <http://dx.doi.org/10.1016/j.jfluchem.2020.109493>. (DA Dixon and M. P. Confer supported by this proposal for all of the computational work and writing the manuscript.)
105. Donaubauer, P. J.; Melzer, D. M.; Wanninger, K.; Mestl, G.; Sanchez-Sanchez, M.; Lercher, J. A.; Hinrichsen, O., Intrinsic Kinetic Model for Oxidative Dehydrogenation of Ethane over MoVTaNb Mixed Metal Oxides: A Mechanistic Approach. *Chem. Eng. J.* **2020**, *383*, 123195. <http://dx.doi.org/https://doi.org/10.1016/j.cej.2019.123195>. (J.A. Lercher was funded by this FWP for planing interpretation of data and writing of the manuscript.)
106. Ehrmaier, A.; Löbbert, L.; Sanchez-Sanchez, M.; Bermejo-Deval, R.; Lercher, J., Impact of Alkali and Alkali-Earth Cations on Ni-Catalyzed Dimerization of Butene. *ChemCatChem* **2020**, *12*, 3705-3711. <http://dx.doi.org/10.1002/cctc.202000349>. (J.A. Lercher was supported by this program for discussion of the results and leading the work.)
107. Jaegers, N. R.; Mueller, K. T.; Wang, Y.; Hu, J. Z., Variable Temperature and Pressure Operando MAS NMR for Catalysis Science and Related Materials. *Acc. Chem. Res.* **2020**, *53*, 611-619. <http://dx.doi.org/10.1021/acs.accounts.9b00557>. (Major support by BES program for the review of the catalyst applications.)
108. Laureanti, J. A.; Ginovska, B.; Buchko, G. W.; Schenter, G. K.; Hebert, M.; Zadvornyy, O. A.; Peters, J. W.; Shaw, W. J., A Positive Charge in the Outer

- Coordination Sphere of an Artificial Enzyme Increases CO<sub>2</sub> Hydrogenation. *Organometallics* **2020**, *39*, 1532-1544. <http://dx.doi.org/10.1021/acs.organomet.9b00843>. (Jointly funded lead contribution by this program. JWP partially supported by the USDA National Institute of Food and Agriculture.)
109. Lu, Y. B.; Zhang, Z. H.; Lin, F.; Wang, H. M.; Wang, Y., Single-Atom Automobile Exhaust Catalysts. *ChemNanoMat* **2020**, 1659-1682. <http://dx.doi.org/10.1002/cnma.202000407>. (H.W. acknowledges the support from this FWP.)
110. Marcinkowski, M. D.; Adamsen, K. C.; Doudin, N.; Sharp, M. A.; Smith, R. S.; Wang, Y.; Wendt, S.; Lauritsen, J. V.; Parkinson, G. S.; Kay, B. D.; Dohnálek, Z., Adsorption and Reaction of Methanol on Fe<sub>3</sub>O<sub>4</sub>(001). *J. Chem. Phys.* **2020**, *152*, 064703. <http://dx.doi.org/10.1063/1.5139418>. (MDM, ND, MAS, RSS, YW, BDK, and ZD were funded by this program. MDM, ND, MAS, YW acquired the data, carried out the analysis, and participated in the preparation of the manuscript. ZD, RSS, and BDK contributed to data analysis and manuscript preparation.)
111. Rousseau, R.; Glezakou, V.-A.; Selloni, A., Theoretical Insights into the Surface Physics and Chemistry of Redox-Active Oxides. *Nat. Rev. Mater.* **2020**, *5*, 460-475. <http://dx.doi.org/10.1038/s41578-020-0198-9>. (R.R and V.A.G. partially supported by program, R.R major contribution on the writing, A.S. funded by program at Princeton.)
112. Saal, T.; Blastik, Z. E.; Haiges, R.; Nirmalchandar, A.; Baxter, A. F.; Christe, K. O.; Vasiliu, M.; Dixon, D. A.; Beier, P.; Prakash, G. K. S., Protonation of CH<sub>3</sub>N<sub>3</sub> and CF<sub>3</sub>N<sub>3</sub> in Superacids: Isolation and Structural Characterization of Long-Lived Methyl- and Trifluoromethylamino Diazonium Ions. *Angew. Chem. Int. Ed.* **2020**, *59*. <http://dx.doi.org/10.1002/anie.202002750>. (DA Dixon and M. Vasiliu supported by this program for all of the computational work and writing the manuscript.)
113. Shreiber, S. T.; Kaplan, P. T.; Hughes, R. P.; Vasiliu, M.; Dixon, D. A.; Cramer, R. E.; Vicic, D. A., Syntheses, Solution Behavior, and Computational Bond Length Analyses of Trifluoromethyl and Perfluoroethyl Cuprate Salts. *J. Fluorine Chem.* **2020**, *234*, 109518. <http://dx.doi.org/10.1016/j.jfluchem.2020.109518>. (DA Dixon and M. Vasiliu supported by this proposal for all of the computational work and writing the manuscript.)
114. Singh, N.; Sanyal, U.; Ruehl, G.; Stoerzinger, K. A.; Gutiérrez, O. Y.; Camaioni, D. M.; Fulton, J. L.; Lercher, J. A.; Campbell, C. T., Aqueous Phase Catalytic and Electrocatalytic Hydrogenation of Phenol and Benzaldehyde over Platinum Group Metals. *J. Catal.* **2020**, *382*, 372-384. <http://dx.doi.org/10.1016/j.jcat.2019.12.034>. (D.M. Camaioni, J.L. Fulton, and J.A. Lercher were funded by this FWP. D. Camaioni and J.L. Fulton were supported by this program for supporting data analysis and interpretation of spectroscopic experiments. J.A. Lercher was supported by this program for planing and interpretation of data.)
115. Tran, B. L.; Neisen, B. D.; Speelman, A. L.; Gunasekara, T.; Wiedner, E. S.; Bullock, R. M., Mechanistic Studies on the Insertion of Carbonyl Substrates into Cu-H: Different Rate-Limiting Steps as a Function of Electrophilicity. *Angew. Chem. Int.*

- Ed.* **2020**, *59*, 8645-8653. <http://dx.doi.org/10.1002/anie.201916406>. (Lead contributions. B.L.T., B.D.N., A.L.S., E.S.W. support by DOE BES and R.M.B. T.G. was supported as part of the Center for Molecular Electrocatalysis, an Energy Frontier Research Center funded by the U.S. Department of Energy.)
116. Wang, Y.; Wen, B.; Dahal, A.; Kimmel, G. A.; Rousseau, R.; Selloni, A.; Petrik, N. G.; Dohnalek, Z., Binding of Formic Acid on Anatase TiO<sub>2</sub>(101). *J. Phys. Chem. C* **2020**, *124*, 20228-20239. <http://dx.doi.org/10.1021/acs.jpcc.0c06031>. (All experimental studies (YW, AD, GAK, NGP, and ZD) and theoretical contribution by RR were funded by this program.)
117. Zhang, S. G.; Li, H. X.; Appel, A. M.; Hall, M. B.; Bullock, R. M., Controlling P-C/C-H Bond Cleavage in Nickel Bis(Diphosphine) Complexes: Reactivity Scope, Mechanism, and Computations. *Organometallics* **2020**, *39*, 3306-3314. <http://dx.doi.org/10.1021/acs.organomet.0c00388>. (Leading, Zhang, Appel, and Bullock were supported by this project for experimental work, data analysis, and writing of the manuscript.)
118. Zheng, J.; Lee, I.; Khramenkova, E.; Wang, M.; Peng, B.; Gutierrez, O.; Fulton, J. L.; Camaioni, D.; Khare, R.; Jentys, A.; Haller, G.; Pidko, E.; Sanchez-Sanchez, M.; Lercher, J., Importance of Methane Chemical Potential for Its Conversion to Methanol on Cu-Exchanged Mordenite. *Chem. Eur. J.* **2020**, *26*, 7563-7567. <http://dx.doi.org/10.1002/chem.202000772>. (J. Zheng, M. Wang, B. Peng, O.Y. Gutierrez, J.L. Fulton, and D.M. Camaioni, were funded by this FWP. J. Zheng, M. Wang, and B. Peng were supported by this program for the experimental work and writing of the first drafts. O.Y. Gutierrez, J.L. Fulton, and D. Camaioni were supported by this program for supporting data analysis and writing of the manuscript.)
119. Zhu, Y.; Zheng, J.; Ye, J.; Cui, Y.; Koh, K.; Kovarik, L.; Camaioni, D. M.; Fulton, J. L.; Truhlar, D. G.; Neurock, M.; Cramer, C. J.; Gutiérrez, O. Y.; Lercher, J. A., Copper-Zirconia Interfaces in UiO-66 Enable Selective Catalytic Hydrogenation of CO<sub>2</sub> to Methanol. *Nat. Commun.* **2020**, *11*, 5849. <http://dx.doi.org/10.1038/s41467-020-19438-w>. (Jointly funded. Y.Z., L.K., D.M.C., J.F., and O. Y.G. acknowledge support from this project.)
120. Zhu, Y. F.; Zhang, X.; Koh, K.; Kovarik, L.; Fulton, J. L.; Rosso, K. M.; Gutierrez, O. Y., Inverse Iron Oxide/Metal Catalysts from Galvanic Replacement. *Nat. Commun.* **2020**, *11*, 3269. <http://dx.doi.org/10.1038/s41467-020-16830-4>. (Y. Zhu, L. Kovarik, J.L. Fulton, and O.Y. Gutierrez were supported by this program for leading the work and performing kinetic and characterization experiments.)

## 2021

121. Kwak, J. H.; Kim, Y.; Collinge, G.; Lee, M.-S.; Khivantsev, K.; Cho, S. J.; Glezakou, V.-A.; Rousseau, R.; Szanyi, J., Are All Single Atoms Created Equal? Surface Density Dependent Catalytic Activity of Single Pd Atoms Supported on Ceria. *Angew. Chem. Int. Ed.* **2021**. <http://dx.doi.org/https://doi.org/10.1002/anie.202105750>. (Major contribution from the BES Catalysis Program; Multiple PIs from both theory and experiment.)

122. Petrik, N. G.; Wang, Y.; Wen, B.; Wu, Y.; Ma, R.; Dahal, A.; Gao, F.; Rousseau, R.; Wang, Y.; Kimmel, G. A.; Selloni, A.; Dohnálek, Z., Conversion of Formic Acid on Single- and Nano-Crystalline Anatase TiO<sub>2</sub>(101). *J. Phys. Chem. C* **2021**, *125*, 7686-7700. <http://dx.doi.org/10.1021/acs.jpcc.1c00571>. (N.G.P., Ya.W, Yi.W., R.M., A.D., F.G., R.R., Yo.W., G.A.K., and Z.D. were supported by this project.)

*Publications jointly funded by this grant and other grants with relatively minor intellectual contribution from this grant*

## 2018

123. Bray, J.; Collinge, G.; Stampfl, C.; Wang, Y.; McEwen, J. S., Predicting the Electric Field Effect on the Lateral Interactions between Adsorbates: O/Fe(100) from First Principles. *Top. Catal.* **2018**, *61*, 763-775. <http://dx.doi.org/10.1007/s11244-018-0944-z>. (J.B and J.-S.M were supported by this program, G.C. funded by NSF supported through a Graduate research fellowship and the NSF EAPSI fellowship program, J.B. supported from the Achievement Rewards for College Scientists Foudnation. Y.W. Supported for conceiving the ideas and participating in interpreting results and writing the paper.)
124. Bray, J.; Hensley, A. J. R.; Collinge, G.; Che, F.; Wang, Y.; McEwen, J.-S., Modeling the Adsorbate Coverage Distribution over a Multi-Faceted Catalytic Grain in the Presence of an Electric Field: O/Fe from First Principles. *Catal. Today* **2018**, *312*, 92-104. <http://dx.doi.org/10.1016/j.cattod.2018.04.016>. (Y.W. Supported for conceiving the ideas and participating in interpreting results and writing the paper.)
125. Chen, J. G.; Crooks, R. M.; Seefeldt, L. C.; Bren, K. L.; Bullock, R. M.; Darensbourg, M. Y.; Holland, P. L.; Hoffman, B.; Janik, M. J.; Jones, A. K.; Kanatzidis, M. G.; King, P.; Lancaster, K. M.; Lymar, S. V.; Pfromm, P.; Schneider, W. F.; Schrock, R. R., Beyond Fossil Fuel-Driven Nitrogen Transformations. *Science* **2018**, *360*, eaar6611. <http://dx.doi.org/10.1126/science.aar6611>. (RM Bullock participated in the discussion at the DOE-BES workshop and helped write the paper, which contained intellectual contributions from all participants at the workshop.)
126. Du, L.; Shao, Y.; Sun, J.; Yin, G.; Du, C.; Wang, Y., Electrocatalytic Valorisation of Biomass Derived Chemicals. *Catal. Sci. Technol.* **2018**, *8*, 3216-3232. <http://dx.doi.org/10.1039/C8CY00533H>. (J.S and Y.W. supported for conceiving the ideas and participating in interpreting results and writing the paper.)
127. Hensley, A. J. R.; Wang, Y.; Mei, D.; McEwen, J.-S., Mechanistic Effects of Water on the Fe-Catalyzed Hydrodeoxygenation of Phenol. The Role of Brønsted Acid Sites. *ACS Catal.* **2018**, *8*, 2200-2208. <http://dx.doi.org/10.1021/acscatal.7b02576>. (D.Mei performed DFT calculations and Y.Wang participated in the interpretation of results and writing the manuscript.)
128. Hensley, A. J. R.; Wöckel, C.; Gleichweit, C.; Gotterbarm, K.; Papp, C.; Steinrück, H.-P.; Wang, Y.; Denecke, R.; McEwen, J.-S., Identifying the Thermal Decomposition Mechanism of Guaiacol on Pt(111): An Integrated X-ray Photoelectron Spectroscopy and Density Functional Theory Study. *J. Phys. Chem. C* **2018**, *122*, 4261-4273. <http://dx.doi.org/10.1021/acs.jpcc.7b10006>. (Y.W. Supported

for conceiving the ideas and participating in interpreting results and writing the paper.)

129. Jin, Q.; Chen, B.; Ren, Z.; Liang, X.; Liu, N.; Mei, D., A Theoretical Study on Reaction Mechanisms and Kinetics of Thiophene Hydrodesulfurization over MoS<sub>2</sub> Catalysts. *Catal. Today* **2018**, *312*, 158-167. <http://dx.doi.org/https://doi.org/10.1016/j.cattod.2018.02.013>. (DM was funded by this program to perform computational studies.)
130. Jin, Q.; Liu, N.; Chen, B.; Mei, D., Mechanisms of Semiconducting 2H to Metallic 1t Phase Transition in Two-Dimensional MoS<sub>2</sub> Nanosheets. *J. Phys. Chem. C* **2018**, *122*, 28215-28224. <http://dx.doi.org/10.1021/acs.jpcc.8b10256>. (DM was funded by this program to perform computational studies.)
131. Lee, M.-S.; McGrail, B. P.; Rousseau, R.; Glezakou, V.-A., Molecular Level Investigation of CH<sub>4</sub> and CO<sub>2</sub> Adsorption in Hydrated Calcium–Montmorillonite. *J. Phys. Chem. C* **2018**, *122*, 1125-1134. <http://dx.doi.org/10.1021/acs.jpcc.7b05364>. (This work was supported by the US Department of Energy, Office of Fossil Energy (M.-S.L., B.P.M. and V.-A.G.) and the Office of Basic Energy Science, Division of Chemical Sciences (R.R.)
132. Lo, B. T. W.; Ye, L.; Chang, G. G. Z.; Purchase, K.; Day, S.; Tang, C. C.; Mei, D.; Tsang, S. C. E., Dynamic Modification of Pore Opening of SAPO-34 by Adsorbed Surface Methoxy Species During Induction of Catalytic Methanol-to-olefins Reactions. *Appl. Catal. B* **2018**, *237*, 245-250. <http://dx.doi.org/https://doi.org/10.1016/j.apcatb.2018.05.090>. (DM was funded by this program to perform computational studies.)
133. Lo, B. T. W.; Ye, L.; Murray, C. A.; Tang, C. C.; Mei, D.; Tsang, S. C. E., Monitoring the Methanol Conversion Process in H-ZSM-5 Using Synchrotron X-ray Powder Diffraction-Mass Spectrometry. *J. Catal.* **2018**, *365*, 145-152. <http://dx.doi.org/https://doi.org/10.1016/j.jcat.2018.06.027>. (DM was funded by this program to perform computational studies.)
134. Nguyen, M.-T.; Wang, Z.; Rod, K. A.; Childers, M. I.; Fernandez, C.; Koech, P. K.; Bennett, W. D.; Rousseau, R.; Glezakou, V.-A., Atomic Origins of the Self-Healing Function in Cement–Polymer Composites. *ACS Appl. Mater. Interfaces* **2018**, *10*, 3011-3019. <http://dx.doi.org/10.1021/acsami.7b13309>. (R Rousseau and V-A Glezakou provided technical input on the analysis of the results of the polymer/surface interactions.)
135. Ren, Z.; Liu, N.; Chen, B.; Li, J.; Mei, D., Theoretical Investigation of the Structural Stabilities of Ceria Surfaces and Supported Metal Nanocluster in Vapor and Aqueous Phases. *J. Phys. Chem. C* **2018**, *122*, 4828-4840. <http://dx.doi.org/10.1021/acs.jpcc.7b10208>. (DM was funded by this program to perform computational studies.)
136. Ren, Z.; Liu, N.; Chen, B.; Li, J.; Mei, D., Nucleation of Cu<sub>n</sub> (n = 1–5) Clusters and Equilibrium Morphology of Cu Particles Supported on CeO<sub>2</sub> Surface: A Density Functional Theory Study. *J. Phys. Chem. C* **2018**, *122*, 27402-27411. <http://dx.doi.org/10.1021/acs.jpcc.8b07993>. (DM was funded by this program to perform computational studies.)

137. Zhou, J.; Zhao, Y.; Zhang, J.; Wang, Y.; Gutiérrez, O. Y.; Wang, S.; Li, Z.; Jin, P.; Wang, S.; Ma, X.; Lercher, J. A., A Nitrogen-Doped PtSn Nanocatalyst Supported on Hollow Silica Spheres for Acetic Acid Hydrogenation. *Chem. Commun.* **2018**, *54*, 8818-8821. <http://dx.doi.org/10.1039/C8CC03649G>. (O.Y.G, and J.A.L. acknowledge the support for their contribution by this project.)

## 2019

138. Cammarota, R. C.; Xie, J.; Burgess, S. A.; Vollmer, M. V.; Vogiatzis, K. D.; Ye, J.; Linehan, J. C.; Appel, A. M.; Hoffmann, C.; Wang, X.; Young, V. G.; Lu, C. C., Thermodynamic and Kinetic Studies of H<sub>2</sub> and N<sub>2</sub> Binding to Bimetallic Nickel-Group 13 Complexes and Neutron Structure of a Ni( $\eta^2$ -H<sub>2</sub>) Adduct. *Chem. Sci. J.* **2019**, *10*, 7029-7042. <http://dx.doi.org/10.1039/C9SC02018G>. (SAB, JCL, and AMA were supported by this program. MVV was supported by the NSF Graduate Research Fellowship. CCL acknowledges NSF. JX, JY and KDV were supported as part of the Inorganometallic Catalyst Design Center.)
139. Chen, L.; Zhang, S.; Persaud, R. R.; Smith, R. S.; Kay, B. D.; Dixon, D.; Dohnálek, Z., Understanding the Binding of Aromatic Hydrocarbons on Rutile TiO<sub>2</sub>(110). *J. Phys. Chem. C* **2019**, *123*, 16766-16777. <http://dx.doi.org/10.1021/acs.jpcc.9b03355>. (All theoretical contributions (DD, SZ, and RRP) were funded by this program.)
140. Clark, J. A.; Murray, A.; Lee, J.-m.; Autrey, T. S.; Collord, A. D.; Hillhouse, H. W., Complexation Chemistry in N,N-Dimethylformamide-Based Molecular Inks for Chalcogenide Semiconductors and Photovoltaic Devices. *J. Am. Chem. Soc.* **2019**, *141*, 298-308. <http://dx.doi.org/10.1021/jacs.8b09966>. (T Autrey was supported by this grant to direct the calorimetry experiments, assist with analysis of data and writing the manuscript.)
141. Ehrmaier, A.; Liu, Y.; Peitz, S.; Jentys, A.; Chin, Y.-H. C.; Sanchez-Sanchez, M.; Bermejo-Deval, R.; Lercher, J., Dimerization of Linear Butenes on Zeolite-Supported Ni<sup>2+</sup>. *ACS Catal.* **2019**, *9*, 315-324. <http://dx.doi.org/10.1021/acscatal.8b03095>. (JA Lercher was supported by this program for oversight of the work and editing the manuscript.)
142. Gentil, S.; Molloy, J. K.; Carrière, M.; Hobballah, A.; Dutta, A.; Cosnier, S.; Shaw, W. J.; Gellon, G.; Belle, C.; Artero, V.; Thomas, F.; Le Goff, A., A Nanotube-Supported Dicopper Complex Enhances Pt-free Molecular H<sub>2</sub>/Air Fuel Cells. *Joule* **2019**, *3*, 2020-2029. <http://dx.doi.org/10.1016/j.joule.2019.07.001>. (S.G., J.K.M., M.C., A.H., A.D., and G.G. conducted the experiments and analyzed the data. W.J.S., C.B., S.C., F.T., V.A., and A.L.G. analyzed and discussed the results. F.T., V.A., and A.L.G. designed the experiments and wrote the paper.)
143. Jaegers, N. R.; Khivantsev, K.; Kovarik, L.; Klas, D. W.; Hu, J. Z.; Wang, Y.; Szanyi, J., Catalytic Activation of Ethylene C-H Bonds on Uniform d<sup>8</sup> Ir(I) and Ni(II) Cations in Zeolites: Toward Molecular Level Understanding of Ethylene Polymerization on Heterogeneous Catalysts. *Catal. Sci. Technol.* **2019**, *9*, 6570-6576. <http://dx.doi.org/10.1039/C9CY01442J>. (Minor, J. Szanyi participated in experimental design, data interpretation and MS preparation.)

144. Khivantsev, K.; Jaegers, N.; Kovarik, L.; Gao, F.; Wang, Y.; Szanyi, J., Palladium/Zeolite Low Temperature Passive NO<sub>x</sub> Adsorbers (PNA): Structure-Adsorption Property Relationships for Hydrothermally Aged PNA Materials. *Emiss. Control. Sci. Technol.* **2019**, *6*, 126-138. <http://dx.doi.org/10.1007/s40825-019-00139-w>. (Partially supported, NMR part of work.)
145. Kollias, L.; Cantu, D. C.; Tubbs, M. A.; Rousseau, R.; Glezakou, V.-A.; Salvalaglio, M., Molecular Level Understanding of the Free Energy Landscape in Early Stages of Metal–Organic Framework Nucleation. *J. Am. Chem. Soc.* **2019**, *141*, 6073-6081. <http://dx.doi.org/10.1021/jacs.9b01829>. (V.-A.G. acknowledges partial support by this program.)
146. Lee, M.-S.; Glezakou, V.-A.; Rousseau, R.; McGrail, B. P., Molecular Simulation of the Catalytic Regeneration of nBuLi through a Hydrometalation Route. *Inorg. Chem.* **2019**, *58*, 3033-3040. <http://dx.doi.org/10.1021/acs.inorgchem.8b02910>. (R Rousseau and V-A Glezakou provided guidance on the planning, execution and analysis of the liquid phase catalysis simulations.)
147. Weber-Stockbauer, M.; Gutiérrez, O. Y.; Bermejo-Deval, R.; Lercher, J. A., Cesium Induced Changes in the Acid-Base Properties of Metal Oxides and the Consequences for Methanol Thiolation. *ACS Catal.* **2019**, *9*, 9245-9252. <http://dx.doi.org/10.1021/acscatal.9b02537>. (J.A.L. was supported by this program.)
148. Yang, G.; Akhade, S. A.; Chen, X.; Liu, Y.; Lee, M.-S.; Glezakou, V.-A.; Rousseau, R.; Lercher, J. A., The Nature of Hydrogen Adsorption on Platinum in the Aqueous Phase. *Angew. Chem. Int. Ed.* **2019**, *58*, 3527-3532. <http://dx.doi.org/10.1002/anie.201813958>. (JA Lercher was supported by this program as science lead and for writing the manuscript.)
149. Zhao, Y.; Wang, H.; Han, J.; Zhu, X.; Mei, D.; Ge, Q., Simultaneous Activation of CH<sub>4</sub> and CO<sub>2</sub> for Concerted C–C Coupling at Oxide–Oxide Interfaces. *ACS Catal.* **2019**, *9*, 3187-3197. <http://dx.doi.org/10.1021/acscatal.9b00291>. (DM was funded by this program to perform computational studies.)

## 2020

150. Braga, A. H.; Costa, N. J. S.; Philippot, K.; Gonçalves, R. V.; Szanyi, J.; Rossi, L. M., Structure and Activity of Supported Bimetallic NiPd Nanoparticles: Influence of Preparation Method on CO<sub>2</sub> Reduction. *Chem. Eur. J.* **2020**, *12*, 2967-2976. <http://dx.doi.org/10.1002/cctc.201902329>. (Minor, J. Szanyi mentored/supervised visiting student (AH Braga) with the DRIFTS measurements; helped data interpretation and MS preparation.)
151. Fang, Z.; Wang, L.-C.; Wang, Y.; Sikorski, E.; Tan, S.; Li-Oakey, K. D.; Li, L.; Yablonsky, G.; Dixon, D. A.; Fushimi, R., Pt-Assisted Carbon Remediation of Mo<sub>2</sub>C Materials for CO Disproportionation. *ACS Catal.* **2020**, *10*, 1894-1911. <http://dx.doi.org/10.1021/acscatal.9b05225>. (Minor, DA Dixon writing manuscript.)
152. Hensley, A. J. R.; deJoode, I.; Wang, Y.; McEwen, J.-S., Identifying Trends in the Field Ionization of Diatomic Molecules over Adsorbate Covered Pd(331) Surfaces. *Top. Catal.* **2020**, *63*, 1510-1521. <http://dx.doi.org/10.1007/s11244-020-01392-y>. (A.J.R.H., I.J., and J.-S.M. were primarily funded by this FWP.)

153. Koh, K.; Sanyal, U.; Lee, M.-S.; Cheng, G.; Song, M.; Glezakou, V.-A.; Liu, Y.; Li, D.; Rousseau, R.; Gutiérrez, O. Y.; Karkamkar, A.; Derewinski, M.; Lercher, J. A., Electrochemically Tunable Proton-Coupled Electron Transfer in Pd-Catalyzed Benzaldehyde Hydrogenation. *Angew. Chem. Int. Ed.* **2020**, *59*, 1501-1505. <http://dx.doi.org/10.1002/anie.201912241>. (O. Gutierrez and M. Derewinski were supported by this program for kinetic analysis, material synthesis and editing the manuscript.)
154. Laureanti, J.; Brandi, J.; Offor, E.; Engel, D.; Rallo, R.; Ginovska, B.; Martinez, X.; Baaden, M.; Baker, N. A., Visualizing Biomolecular Electrostatics in Virtual Reality with UnityMol-APBS. *Protein Sci.* **2020**, *29*, 237-246. <http://dx.doi.org/10.1002/pro.3773>. (Minor contribution, BG supported by this program. MB acknowledges support by the “Initiative d'Excellence” program from the French State.)
155. Lee, J.; Jang, E. J.; Oh, D. G.; Szanyi, J.; Kwak, J. H., Morphology and Size of Pt on Al<sub>2</sub>O<sub>3</sub>: The Role of Specific Metal-Support Interactions between Pt and Al<sub>2</sub>O<sub>3</sub>. *J. Catal.* **2020**, *385*, 204-212. <http://dx.doi.org/10.1016/j.jcat.2020.03.019>. (Minor contribution: J. Szanyi provided assistance for data analysis; helped in MS preparation.)
156. Lee, M.-S.; Saslow, S. A.; Um, W.; Kim, D.-S.; Kruger, A. A.; Rousseau, R.; Glezakou, V.-A., Impact of Cr and Co on <sup>99</sup>Tc Retention in Magnetite: A Combined Study of Ab Initio Molecular Dynamics and Experiments. *J. Hazard. Mater.* **2020**, *387*, 121721. <http://dx.doi.org/10.1016/j.jhazmat.2019.121721>. (R.R. and V.-A.G. were partially support by this program.)
157. Lopez-Ruiz, J. A.; Qiu, Y.; Andrews, E.; Gutierrez, O. Y.; Holladay, J. D., Electrocatalytic Valorization into H<sub>2</sub> and Hydrocarbons of an Aqueous Stream Derived from Hydrothermal Liquefaction. *J. Appl. Electrochem.* **2020**, 107-118. <http://dx.doi.org/10.1007/s10800-020-01452-x>. (M.D. was supported by this FWP.)
158. Materna, K. L.; Lalaoui, N.; Laureanti, J. A.; Walsh, A. P.; Rimgard, B. P.; Lomoth, R.; Thapper, A.; Ott, S.; Shaw, W. J.; Tian, H.; Hammarström, L., Using Surface Amide Couplings to Assemble Photocathodes for Solar Fuel Production Applications. *ACS Appl. Mater. Interfaces* **2020**, *12*, 4501-4509. <http://dx.doi.org/10.1021/acsami.9b19003>. (Minor. W.J.S., A.P.W., and J.A.L. were supported by the U.S. Department of Energy.)
159. Polino, D.; Grifoni, E.; Rousseau, R.; Parrinello, M.; Glezakou, V.-A., How Collective Phenomena Impact CO<sub>2</sub> Reactivity and Speciation in Different Media. *J. Phys. Chem. A* **2020**, *124*, 3963-3975. <http://dx.doi.org/10.1021/acs.jpca.9b11744>. (V.-A.G. scoped the research and together with R.R. performed some of the simulations. All authors contributed to the writing of the manuscript.)
160. Vollmer, M. V.; Ye, J.; Linehan, J. C.; Graziano, B. J.; Preston, A.; Wiedner, E. S.; Lu, C. C., Cobalt-Group 13 Complexes Catalyze CO<sub>2</sub> Hydrogenation Via a Co(-I)/Co(I) Redox Cycle. *ACS Catal.* **2020**, *10*, 2459-2470. <http://dx.doi.org/10.1021/acscatal.9b03534>. (Minor contribution. JC Linehan and A Preston were supported by this project to help collect and interpret high pressure

NMR spectroscopy data. ES Wiedner was supported by this project to help collect and interpret high pressure cyclic voltammetry data.)

161. Wang, S.; Li, S.; Dixon, D. A., Mechanism of Selective and Complete Oxidation in La<sub>2</sub>O<sub>3</sub>-Catalyzed Oxidative Coupling of Methane. *Catal. Sci. Technol.* **2020**, *10*, 2602-2614. <http://dx.doi.org/10.1039/D0CY00141D>. (Minor. DA Dixon was supported by this program and helped to interpret the computational results and write the paper.)
162. Wang, X.; Liu, N.; Zhang, Q.; Liang, X.; Chen, B.; Mei, D., Thermodynamic and Kinetic Roles of H<sub>2</sub> in Structure Evolution of Urchin-Like Co: A Density Functional Theory Study. *Particuology* **2020**, *48*, 2-12. <http://dx.doi.org/10.1016/j.partic.2018.08.007>. (DM was funded by this program to perform computational studies.)
163. Yao, Y.; Wu, X.; Gutiérrez, O. Y.; Ji, J.; Jin, P.; Wang, S.; Xu, Y.; Zhao, Y.; Wang, S.; Ma, X.; Lercher, J. A., Roles of Cu<sup>+</sup> and Cu<sup>0</sup> Sites in Liquid-Phase Hydrogenation of Esters on Core-Shell CuZn<sub>x</sub>@C Catalysts. *Appl. Catal. B* **2020**, *267*, 118698. <http://dx.doi.org/10.1016/j.apcatb.2020.118698>. (O.Y. Gutierrez, and J.A. Lercher were funded by this FWP. O.Y. Gutierrez and was supported by this program for contributing to discussion of the results and writing of the manuscript; J.A. Lercher was supported by this program for discussion of the results, planning, and writing of the manuscript.)
164. Zhang, J. H.; Sudduth, B.; Sun, J. M.; Wang, Y., Hydrodeoxygenation of Lignin-Derived Aromatic Oxygenates over Pd-Fe Bimetallic Catalyst: A Mechanistic Study of Direct C-O Bond Cleavage and Direct Ring Hydrogenation. *Catal. Lett.* **2020**. <http://dx.doi.org/10.1007/s10562-020-03352-3>. (Y.W. was partially supported by this program.)
165. Zhao, Y.; Zhu, X.; Wang, H.; Han, J.; Mei, D.; Ge, Q., Aqueous Phase Aldol Condensation of Formaldehyde and Acetone on Anatase TiO<sub>2</sub>(101) Surface: A Theoretical Investigation. *ChemCatChem* **2020**, *12*, 1220-1229. <http://dx.doi.org/10.1002/cctc.201901736>. (DM was funded by this program to perform computational studies.)

## 2021

166. Chu, Y.; Sanyal, U.; Li, X. S.; Qiu, Y.; Song, M.; Engelhard, M. H.; Davidson, S. D.; Koh, K.; Meyer, L. C.; Zheng, J.; Xie, X.; Li, D.; Liu, J.; Gutiérrez, O. Y.; Wang, Y.; Shao, Y., Tuning Proton Transfer and Catalytic Properties in Triple Junction Nanostructured Catalysts. *Nano Energy* **2021**, *86*, 106046. <http://dx.doi.org/https://doi.org/10.1016/j.nanoen.2021.106046>. (O.Y. Gutierrez and Y. Wang were funded by this FWP for coordination of experimental work, interpretation of data and writing of the manuscript.)
167. Pfriem, N.; Hintermeier, P. H.; Eckstein, S.; Kim, S.; Liu, Q.; Shi, H.; Milakovic, L.; Liu, Y.; Haller, G. L.; Baráth, E.; Liu, Y.; Lercher, J. A., Role of the Ionic Environment in Enhancing the Activity of Reacting Molecules in Zeolite Pores. *Science* **2021**, *372*, 952. <http://dx.doi.org/10.1126/science.abh3418>. (J.A.L. was funded by this Program.)

168. Sanyal, U.; Yuk, S. F.; Koh, K.; Lee, M. S.; Stoerzinger, K.; Zhang, D.; Meyer, L. C.; Lopez-Ruiz, J. A.; Karkamkar, A.; Holladay, J. D.; Camaioni, D. M.; Nguyen, M. T.; Glezakou, V. A.; Rousseau, R.; Gutiérrez, O. Y.; Lercher, J. A., Hydrogen Bonding Enhances the Electrochemical Hydrogenation of Benzaldehyde in the Aqueous Phase. *Angew. Chem. Int. Ed.* **2021**, *60*, 290-296. <http://dx.doi.org/10.1002/anie.202008178>. (DM Camaioni was supported by this program for writing the manuscript and scientific advisor. JA Lercher was supported by this program as science lead and for writing the manuscript.)
169. Shetty, M.; Wang, H.; Chen, F.; Jaegers, N.; Liu, Y.; Camaioni, D. M.; Gutiérrez, O. Y.; Lercher, J. A., Directing the Rate-Enhancement for Hydronium Ion Catalyzed Dehydration Via Organization of Alkanols in Nanoscopic Confinements. *Angew. Chem. Int. Ed.* **2021**, *60*, 2304-2311. <http://dx.doi.org/https://doi.org/10.1002/anie.202009835>. (D.M.C. and J.A.L. were supported by the FWP for contributing to the discussion of the results, planning, and writing of the manuscript.)

## Atomic-scale Design of Metal and Alloy Catalysts: A Combined Theoretical and Experimental Approach

Manos Mavrikakis,<sup>†</sup> James A. Dumesic,<sup>†</sup> Younan Xia<sup>‡</sup>

<sup>†</sup> Department of Chemical & Biological Engineering, University of Wisconsin–Madison

<sup>‡</sup> School of Chemistry & Biochemistry, Georgia Institute of Technology

### Presentation Abstract

The main objective of this combined theoretical and experimental project is to: *i) design* from first-principles, *ii) synthesize* using advanced *nanosynthesis* techniques, and *iii) experimentally evaluate new metal and alloy catalysts*, with unique *catalytic* properties for a number of important chemical reactions. Measurable impact can be found in a number of applications, including low-temperature fuel cells, hydrogen production and purification, and production of fuels and chemicals. The importance of the atomic-scale architecture of these new, theoretically designed catalysts, to their unique properties is driving the development of *new inorganic materials synthesis* approaches, which are capable of synthesizing the theoretically determined optimal, and in some cases, metastable, nanoscale catalytic architectures.

**Grant or FWP Number: DOE Grant No. DE-FG02-05ER15731** (Atomic-scale Design of Metal and Alloy Catalysts: A Combined Theoretical and Experimental Approach)

**Postdocs** (partially supported by this grant): Roberto Schimmenti (UW), Lang Xu (UW)  
**Students** (partially supported by this grant): Saurabh Bhandari (UW), Lisa Je (UW), Michael Rebarchik (UW), Trenton Wolter (UW), Minghao Xie (GIT)

### RECENT PROGRESS

#### *A Review of Computational Methods in Heterogeneous Catalysis*<sup>1</sup>

Computational methods have found an increasingly important role in heterogeneous catalysis. They have provided unprecedented atomic-scale insight into material properties and reaction mechanisms, enabling a fundamentals-based bottom-up approach for catalyst design. In this *Chem. Rev.* article, we critically analyzed recent advances in computational heterogeneous catalysis, with a focus on the applications of density functional theory (DFT) and microkinetic modeling methods for supported transition-metal catalysts.

We started with a survey of recent advancements in electronic structure methods and atomistic catalyst models toward a more accurate description for the catalytically active sites. We first discussed the development of higher-level theoretical methods with improved chemical accuracy over the conventional DFT under the generalized gradient approximation (GGA). Second, we reviewed progress in the development of efficient theoretical methods for large systems. Third, we surveyed typical types of atomistic models

used in computational studies. Lastly, we reviewed recently emerging methods for treating solvation effects in liquid-phase catalytic reactions.

Microkinetic models bridge the gap between nanoscale computational insights and macroscale experimental kinetics data. We reviewed the recent developments in two commonly used microkinetic modeling methods: mean-field microkinetic models (MF-MKMs) and kinetic Monte Carlo (KMC) simulations. For MF-MKM, we demonstrated that a *self-consistent* MF-MKM is required to accurately capture the nature of the active sites on a catalyst when the reaction is taking place, which involves a feedback loop among electronic structure calculations, MF-MKM, and parameter estimation based on experimentally measured reaction kinetics data. On-lattice KMC simulations explicitly track the positions of each adsorbate and are suitable for catalytic systems where the mean-field approximation breaks down. We showcased several recent KMC examples for catalysis by small metal-clusters. Specifically, we highlighted the unique functionality of KMC to treat catalyst reconstructions under *in situ* reactive environments.

The last topic covered in this review is research for accelerating *in silico* catalyst design and discovery. Approximations which capitalized on the similarity of binding sites across different metals (e.g., scaling relations between different thermodynamic quantities and Brønsted–Evans–Polanyi (BEP) relations between thermodynamic and kinetic quantities) have played a pivotal role in designing new catalysts in the past decade. However, the strongly correlated parameters can also be viewed as a limitation imposed on the catalyst performance. Therefore, we surveyed recent research efforts directed toward developing catalysts more active than those predicted by the scaling and BEP relations. We also reviewed the identification of fundamental-based reactivity descriptors for catalyst design purposes, with a focus on the classical *d*-band center model as well as more recent attempts to modify and improve the accuracy of the *d*-band center model.

In the near future, we foresee continued efforts in computational heterogeneous catalysis to probe surface phenomena and reaction mechanisms in the presence of complex, realistic reaction environments. These theoretical insights can be further translated into ideas for developing improved catalysts for important technological applications.

### ***Combining Computational Modeling with Reaction Kinetics Experiments for Elucidating the In-Situ Nature of the Active Site in Heterogeneous Catalysis***<sup>2,3</sup>

Due to the intrinsic errors in DFT and inadequate knowledge about catalytic site structures and reaction mechanisms, a MF-MKM constructed using DFT-derived energetics alone is often insufficient to conclusively infer the mechanistic details of a catalytic system. To address this, our group has developed an iterative approach for combining DFT-based MF-MKMs with reaction kinetics experiments (Figure 1). We start by hypothesizing an active site model, on which the thermodynamic and kinetic parameters for each elementary step are calculated with DFT and used to formulate an initial MF-MKM. We then perform parameter estimation, during which the DFT-derived parameters are adjusted until the

model-predicted reaction rates/orders match the data from reaction kinetics experiments, using a procedure developed relying on modern optimization algorithms. The model-experiment parity is examined based on three criteria: (1) Can the adjusted model accurately reproduce the experimental data? (2) Are the parameter adjustments within the typical error of DFT? (3) Are the model-predicted coverages of surface species consistent with those at which the DFT energetics were calculated? If all three criteria are satisfied, we conclude that the nature of the active sites is accurately described by our hypothesized site model. Otherwise, we use hints from the parameter estimation to adjust our hypothesized active site model and repeat this iterative procedure.

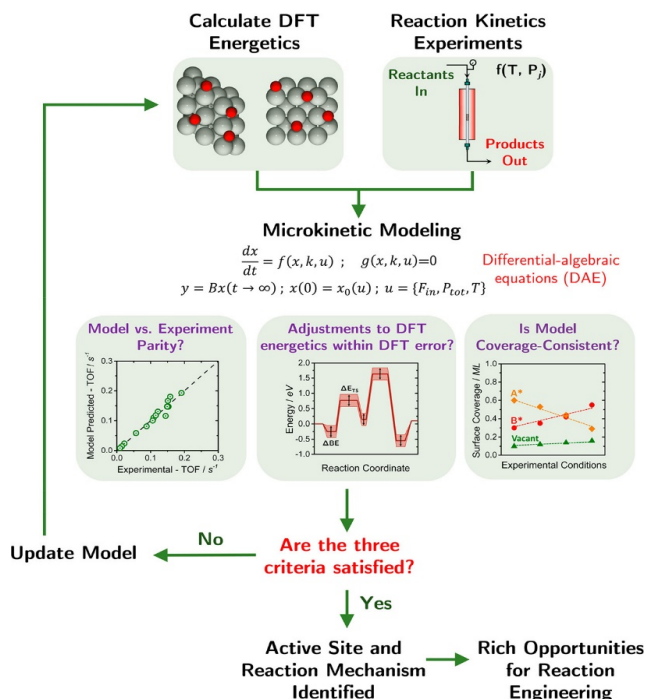


**Figure 1.** Iterative scheme for elucidating the nature of the catalytic active site and the reaction mechanism, using a combination of DFT, reaction kinetics experiments, and MF-MKM. From ref. 2.

The utility of this methodology was showcased in our recent study for formic acid (FA) decomposition on a carbon-supported Pt (Pt/C) catalyst.<sup>3</sup> We obtained the initial set of DFT parameters on clean Pt(111) and Pt(100) surfaces as the hypothesized active site models. Both the clean Pt(111) and Pt(100) MF-MKMs yielded CO coverages above 0.9 monolayer (ML) after parameter adjustments, contradicting the initial hypothesis of clean surfaces (used in the DFT work). Therefore, the active site models used in the new DFT calculations were adjusted by applying an intermediate CO coverage of 0.44 ML. The 0.44 ML CO-covered Pt(111) and Pt(100) models predicted CO coverages of 0.33 and 0.50 ML, respectively, after parameter adjustments, both in reasonable agreement with the initial assumption of 0.44 ML CO coverage. The 0.44 ML CO-covered Pt(111) model was able to capture our experimental measurements with parameter adjustments within the standard DFT error bar ( $\pm 0.2$  eV); on the other hand, the 0.44 ML CO-covered Pt(100) model required large adjustments beyond typical DFT errors to match the experimental data. Therefore, we concluded that, compared to possible models based on Pt(100), the 0.44 ML CO-covered Pt(111) is a more suitable model for the active sites on Pt/C catalysts during FA decomposition. This case study of FA decomposition on Pt/C catalysts demonstrated the powerfulness of our methodology for elucidating the nature of the catalytic active sites *under reaction conditions*, particularly when a surface species is present at a significant surface coverage.

***How Non-innocent Spectator Species Improve the Oxygen Reduction Reaction Activity of Single-atom Catalysts: Microkinetic Models informed by First-principles Calculations***<sup>4</sup>

Transition-metal single-atom catalysts (SACs) embedded in graphene-based 2D materials have emerged as a promising alternative to platinum catalysts for fuel cell applications. However, these catalysts are currently limited by their durability in harsh electrolyte environments and the lack of understanding of the nature of the active sites and the reaction mechanisms on these catalysts. In previous DFT studies, *onset potentials* have been typically estimated by a

purely thermodynamic analysis (i.e., the lowest potential required to make each electrochemical reduction step exergonic), which often deviate substantially from experimental values. Here, we modeled the oxygen reduction reaction (ORR) on 12 different SACs (Au, Co, Cr, Cu, Fe, Ir, Mn, Ni, Pd, Pt, Rh, and Ru) inside fourfold nitrogen-doped double vacancies in graphene. We hypothesized that ORR intermediates could exist on *both sides* of the metal center simultaneously and developed a reaction network comprised of all possible pair combinations of reaction intermediates adsorbed at either side of the metal center (Figure 2). Using DFT energetics, we performed a microkinetic analysis to predict the onset potential and dominant ORR mechanism for each SAC.

The onset potentials predicted from our microkinetic models deviated by up to 0.73 V compared to the values predicted by the purely thermodynamic model. This finding suggests that kinetic effects have a significant impact on electrocatalytic performance and should not be neglected. For weakly oxophilic SACs (Au, Cu, Ni, Pd, and Pt), the thermodynamic model was found to overestimate onset potentials when compared to values derived from our microkinetic analysis due to the kinetically relevant O<sub>2</sub> adsorption step. For more oxophilic metals (Cr, Fe, Mn, and Ru), our microkinetic analysis revealed a previously unknown reaction pathway near the onset potential, in which the adsorption of a second oxygen molecule at one side of the SAC facilitates the protonation of the hydroxyl intermediate adsorbed at the other side of the SAC. Accounting for this O<sub>2</sub>-assisted pathway also leads to broadening of the volcano peak when the calculated ORR onset potentials are plotted against the common ORR descriptor, namely the binding energy of atomic oxygen. This observation may explain why experimental onset potentials for single-atom electrocatalysts embedded in nitrogen-substituted graphene di-vacancies appear to be largely independent of the identity of the transition metal atom.

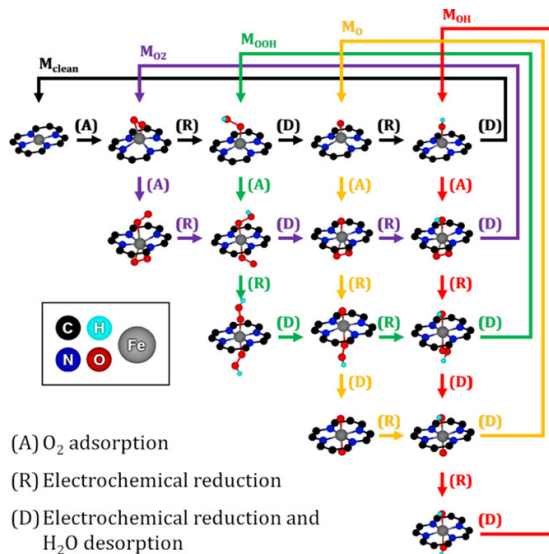


**Figure 2.** Full ORR mechanism considered in our combined DFT and microkinetic modeling study. From ref. 4.

## References

- (1) Chen, B. W. J.; Xu, L.; Mavrikakis, M. Computational Methods in Heterogeneous Catalysis. *Chem. Rev.* **2021**, *121*, 1007–1048.
- (2) Bhandari, S.; Rangarajan, S.; Mavrikakis, M. Combining Computational Modeling with Reaction Kinetics Experiments for Elucidating the In Situ Nature of the Active Site in Catalysis. *Acc. Chem. Res.* **2020**, *53*, 1893–1904.
- (3) Bhandari, S.; Rangarajan, S.; Maravelias, C. T.; Dumesic, J. A.; Mavrikakis, M. Reaction Mechanism of Vapor-Phase Formic Acid Decomposition over Platinum Catalysts: DFT, Reaction Kinetics Experiments, and Microkinetic Modeling. *ACS Catal.* **2020**, *10*, 4112–4126.
- (4) Rebarchik, M.; Bhandari, S.; Kropp, T.; Mavrikakis, M. How Noninnocent Spectator Species Improve the Oxygen Reduction Activity of Single-Atom Catalysts: Microkinetic Models from First-Principles Calculations. *ACS Catal.* **2020**, *10*, 9129–9135.

## Publications Acknowledging this Grant in 2018-2021

### Intellectually led by this grant

#### 2021

1. Gao, W.; Elnabawy, A. O.; Hood, Z. D.; Shi, Y.; Wang, X.; Roling, L. T.; Pan, X.; Mavrikakis, M.; Xia, Y.; Chi, M. Atomistic insights into the nucleation and growth of platinum on palladium nanocrystals, *Nat. Commun.* **2021**, *12*, 3215.
2. Peng, G.; Xu, L.; Glezakou, V.; Mavrikakis, M. Mechanism of Methanol Synthesis on Ni(110), *Catal. Sci. Technol.* **2021**, *11*, 3279–3294.
3. Elnabawy, A. O.; Herron, J. A.; Liang, Z.; Adzic, R. R.; Mavrikakis, M. Formic Acid Electrooxidation on Pt or Pd Monolayer on Transition-Metal Single Crystals: A First-Principles Structure Sensitivity Analysis, *ACS Catal.* **2021**, *11*, 5294–5309.
4. Li, S.; Rangarajan, S.; Scaranto, J.; Mavrikakis, M. On the structure sensitivity of and CO coverage effects on formic acid decomposition on Pd surfaces, *Surf. Sci.* **2021**, *709*, 121846.
5. Chen, B. W. J.; Bhandari, S.; Mavrikakis, M. Role of Hydrogen-bonded Bimolecular Formic Acid–Formate Complexes for Formic Acid Decomposition on Copper: A Combined First-Principles and Microkinetic Modeling Study, *ACS Catal.* **2021**, *11*, 4349–4361.
6. Zhu, J.; Xu, L.; Lyu, Z.; Xie, M.; Chen, R.; Jin, W.; Mavrikakis, M.; Xia, Y. Janus Nanocages of Platinum-Group Metals and Their Use as Effective Dual-Electrocatalysts, *Angew. Chem. Int. Ed.* **2021**, *60*, 10384–10392.
7. Chen, B. W. J.; Xu, L.; Mavrikakis, M.; Computational Methods in Heterogeneous Catalysis, *Chem. Rev.* **2021**, *121*, 1007–1048.
8. Tacey, S. A.; Chen, B. W. J.; Szilásvi, T.; Mavrikakis, M. An automated cluster surface scanning method for exploring reaction paths on metal-cluster surfaces, *Comput. Mater. Sci.* **2021**, *186*, 110010.

9. Schimmenti, R.; Mavrikakis, M. HCOOH Decomposition on Sub-Nanometer Pd<sub>6</sub> Cluster Catalysts: The Effect of Defective Boron Nitride Supports Through First Principles, *Appl. Catal. B Environ.* **2021**, *280*, 119392.

## 2020

10. Lopes, P. P.; Li, D.; Lv, H.; Wang, C.; Tripkovic, D.; Zhu, Y.; Schimmenti, R.; Daimon, H.; Kang, Y.; Snyder, J.; Becknell, N.; More, K. L.; Strmcnik, D.; Markovic, N. M.; Mavrikakis, M.; Stamenkovic, V. R. Eliminating dissolution of platinum-based electrocatalysts at the atomic scale, *Nat. Mater.* **2020**, *19*, 1207–1214 (2020).
11. Bhandari, S.; Rangarajan, S.; Mavrikakis, M. Combining Computational Modeling with Reaction Kinetics Experiments for Elucidating the *In Situ* Nature of the Active Site in Catalysis, *Acc. Chem. Res.* **2020**, *53*, 1893–1904.
12. Chen B. W. J.; Mavrikakis, M.; Formic Acid: A Hydrogen-Bonding Cocatalyst for Formate Decomposition, *ACS Catal.* **2020**, *10*, 10812–10825.
13. Salazar, N.; Rangarajan, S.; Rodríguez-Fernández, J.; Mavrikakis, M.; Lauritsen, J. V.; Site-dependent reactivity of MoS<sub>2</sub> nanoparticles in hydrodesulfurization of thiophene, *Nat. Commun.* **2020**, *11*, 4369.
14. Kropp, T.; Mavrikakis, M.; Effect of Strain on the Reactivity of Graphene Films, *J. Catal.* **2020**, *390*, 67–71.
15. Rebarchik, M.; Bhandari, S.; Kropp, T.; Mavrikakis, M. How Noninnocent Spectator Species Improve the Oxygen Reduction Activity of Single-atom Catalysts: Microkinetic Models from First-principles Calculations, *ACS Catal.* **2020**, *10*, 9129–9135.
16. Chen B. W. J.; Mavrikakis, M. How Coverage Influences Thermodynamic and Kinetic Isotope Effects for H<sub>2</sub>/D<sub>2</sub> Dissociative Adsorption on Transition Metals, *Catal. Sci. Technol.* **2020**, *10*, 671–689.
17. Liang, Z.; L. Song, L.; Elnabawy, A.O; Marinkovic, N; Mavrikakis, M.; Adzic, R. R. Platinum and Palladium Monolayer Electrocatalysts for Formic Acid Oxidation. *Top. Catal.* **2020**, *63*, 742–749.
18. Svenum, I.-H.; Herron, J. A.; Mavrikakis, M.; Venvik, H. J. Pd<sub>3</sub>Ag(111) as a Model System for Hydrogen Separation Membranes: Combined Effects of CO Adsorption and Surface Termination on the Activation of Molecular Hydrogen. *Top. Catal.* **2020**, *63*, 750–761.
19. Xu, L.; Bhandari, S.; Chen, J.; Glasgow, J.; Mavrikakis, M. Chloroform Hydrodechlorination on Palladium Surfaces: A Comparative DFT Study on Pd(111), Pd(100), and Pd(211). *Top. Catal.* **2020**, *63*, 762–776.
20. Göttl, F.; Murray, E.A.; Tacey, S.A.; Rangarajan, S.; Mavrikakis M. Comparing the performance of density functionals in describing the adsorption of atoms and small molecules on Ni(111). *Surf. Sci.* **2020**, *700*, 121675.
21. Göttl, F.; Murray, E. A.; Chen, B.W.J.; Jacobberger, R.M.; Arnold, M.S.; Mavrikakis, M. Exploring Driving Forces for Length Growth in Graphene Nanoribbons During Chemical Vapor Deposition of Hydrocarbons on Ge(001) via Kinetic Monte Carlo Simulations. *Appl. Surf. Sci.* **2020**, *527*, 146748.

22. Tacey, S.A.; Szilvási, T.; Schauer, J. J.; Mavrikakis M. Computational-chemistry-based evaluation of metal salts and metal oxides for application in mercury-capture technologies. *Ind. Eng. Chem. Res.* **2020**, *59*, 9015.
23. Bhandari, S.; Rangarajan, S.; Maravelias, C.T.; Dumesic, J. A.; Mavrikakis, M. Reaction Mechanism of Vapor-Phase Formic Acid Decomposition over Platinum Catalysts: DFT, Reaction Kinetics Experiments, and Microkinetic Modeling. *ACS Catal.* **2020**, *10*, 4112.

## 2019

24. Kropp, T.; Rebarchik, M.; Mavrikakis, M. On the Active Site for Electrocatalytic Water Splitting on Late Transition Metals Embedded in Graphene. *Catal. Sci. Technol.* **2019**, *9*, 6793–6799.
25. Cao, S.; Yang, M.; Elnabawy, A. O.; Trimpalis, A.; Li, S.; Wang, C.; Göttl, F.; Chen, Z.; Liu, J.; Shan, J.; Li, M.; Haas, T.; Chapman, K. W.; Lee, S.; Allard, L. F.; Mavrikakis, M.; Flytzani-Stephanopoulos, M. Single-Atom Gold Oxo-Clusters Prepared in Alkaline Solutions Catalyse the Heterogeneous Methanol Self-Coupling Reactions. *Nat. Chem.* **2019**, *11*, 1098–1105.
26. Szilvási, T.; Chen, B. W. J.; Mavrikakis, M. Identification of Stable Adsorption Sites and Diffusion Paths on Nanocluster Surfaces: An Automated Scanning Algorithm. *Npj Comput. Mater.* **2019**, *5*, 101.
27. Zhong, L.; Kropp, T.; Baaziz, W.; Ersen, O.; Teschner, D.; Schlögl, R.; Mavrikakis, M.; Zafeiratos, S. Correlation Between Reactivity and Oxidation State of Cobalt Oxide Catalysts for CO Preferential Oxidation. *ACS Catal.* **2019**, *9*, 8325–8336.
28. Cai, H.; Schimmenti, R.; Nie, H.; Mavrikakis, M.; Chin, Y.-H. C. Mechanistic Role of the Proton-Hydride Pair in Heteroarene Catalytic Hydrogenation. *ACS Catal.* **2019**, *9*, 9418–9437.
29. Chen, B. W. J.; Stamatakis, M.; Mavrikakis, M. Kinetic Isolation between Turnovers on Au<sub>18</sub> Nanoclusters: Formic Acid Decomposition One Molecule at a Time. *ACS Catal.* **2019**, *9*, 9446–9457.
30. Kropp, T.; Mavrikakis, M. Brønsted–Evans–Polanyi relation for CO oxidation on metal oxides following the Mars–van Krevelen mechanism. *J. Catal.* **2019**, *377*, 577–581.
31. Chen, B. W. J.; Mavrikakis, M. Effects of composition and morphology on the hydrogen storage properties of transition metal hydrides: Insights from PtPd nanoclusters. *Nano Energy* **2019**, *63*, 103858.
32. Kropp, T.; Mavrikakis, M. Transition Metal Atoms Embedded in Graphene: How Nitrogen Doping Increases CO Oxidation Activity. *ACS Catal.* **2019**, *9*, 6864–6868.
33. Li, S.; Singh, S.; Dumesic, J. A.; Mavrikakis, M. On the Nature of Active Sites for Formic Acid Decomposition on Gold Catalysts. *Catal. Sci. Technol.* **2019**, *9*, 2836–2848.
34. Zhu, J.; Chen, Z.; Xie, M.; Lyu, Z.; Chi, M.; Mavrikakis, M.; Jin, W.; Xia, Y. Iridium-Based Cubic Nanocages with 1.1-nm-Thick Walls: A Highly Efficient and Durable Electrocatalyst for Water Oxidation in an Acidic Medium. *Angew. Chem. Int. Ed.* **2019**, *58*, 7244–7248.
35. Chen, B. W. J.; Kirvassilis, D.; Bai, Y.; Mavrikakis, M. Atomic and Molecular Adsorption on Ag(111). *J. Phys. Chem. C* **2019**, *123*, 7551–7566.

36. Kropp, T.; Lu, Z.; Li, Z.; Chin, Y. H. C.; Mavrikakis, M. Anionic Single-Atom Catalysts for CO Oxidation: Support-Independent Activity at Low Temperatures. *ACS Catal.* **2019**, *9*, 1595–1604.
37. Lyu, Z.; Xie, M.; Aldama, E.; Zhao, M.; Qiu, J.; Zhou, S.; Xia, Y. Au@Cu Core-Shell Nanocubes with Controllable Sizes in the Range of 20–30 nm for Application in Catalysis and Plasmonics. *ACS Appl. Nano Mater.* **2019**, *2*, 1533–1540.
38. Bai, Y.; Kirvassilis, D.; Xu, L.; Mavrikakis, M. Atomic and Molecular Adsorption on Ni(111). *Surf. Sci.* **2019**, *679*, 240–253.

## 2018

39. Liu, Y.; Zhang, L.; Göttl, F.; Ball, M. R.; Hermans, I.; Kuech, T. F.; Mavrikakis, M.; Dumesic, J. A. Synthesis Gas Conversion over Rh-Mn-W<sub>x</sub>C/SiO<sub>2</sub> Catalysts Prepared by Atomic Layer Deposition. *ACS Catal.* **2018**, *8*, 10707–10720.
40. Elnabawy, A. O.; Herron, J. A.; Scaranto, J.; Mavrikakis, M. Structure Sensitivity of Formic Acid Electrooxidation on Transition Metal Surfaces: A First-Principles Study. *J. Electrochem. Soc.* **2018**, *165*, J3109–J3121.
41. Zhao, M.; Xu, L.; Vara, M.; Elnabawy, A. O.; Gilroy, K. D.; Hood, Z. D.; Zhou, S.; Figueroa-Cosme, L.; Chi, M.; Mavrikakis, M.; Xia, Y. Synthesis of Ru Icosahedral Nanocages with a Face-Centered-Cubic Structure and Evaluation of Their Catalytic Properties. *ACS Catal.* **2018**, *8*, 6948–6960.
42. Bai, Y.; Chen, B. W. J.; Peng, G.; Mavrikakis, M. Density Functional Theory Study of Thermodynamic and Kinetic Isotope Effects of H<sub>2</sub>/D<sub>2</sub> Dissociative Adsorption on Transition Metals. *Catal. Sci. Technol.* **2018**, *8*, 3321–3335.
43. Xu, L.; Lin, J.; Bai, Y.; Mavrikakis, M. Atomic and Molecular Adsorption on Cu(111). *Top. Catal.* **2018**, *61*, 736–750.
44. Tacey, S. A.; Szilvási, T.; Xu, L.; Schauer, J. J.; Mavrikakis, M. The Role of Iron-Oxide Aerosols and Sunlight in The Atmospheric Reduction of Hg(II) Species: A DFT+U Study. *Appl. Catal. B Environ.* **2018**, *234*, 347–356.
45. Bai, Y.; Mavrikakis, M. Mechanistic Study of Nitric Oxide Reduction by Hydrogen on Pt(100) (I): A DFT Analysis of the Reaction Network. *J. Phys. Chem. B* **2018**, *122*, 432–443.
46. Xu, L.; Kirvassilis, D.; Bai, Y.; Mavrikakis, M. Atomic and Molecular Adsorption on Fe(110). *Surf. Sci.* **2018**, *667*, 54–65.

**Jointly funded by this grant and other grants with intellectual leadership by other funding sources**

## 2021

47. Demir, B.; Kropp, T.; Gilcher, E. B.; Mavrikakis, M.; Dumesic, J. A. Effects of water on the kinetics of acetone hydrogenation over Pt and Ru catalysts, *J. Catal.* **2021**. <https://doi.org/10.1016/j.jcat.2021.03.013>
48. Xu, L.; Stangland, E. E.; Dumesic, J. A.; Mavrikakis, M. Hydrodechlorination of 1,2-Dichloroethane on Platinum Catalysts: Insights from Reaction Kinetics Experiments,

Density Functional Theory, and Microkinetic Modeling, *ACS Catal.* **2021**, *11*, 7890–7905.

## 2020

49. Demir, B.; Kropp, T.; Rivera-Dones, K. R.; Gilcher, E.B.; Huber, G.W.; Mavrikakis, M.; Dumesic, J. A. A Self-Adjusting Platinum Surface for Acetone Hydrogenation. *Proc. Natl. Acad. Sci. U.S.A* **2020**, *117*, 3446.

## 2019

50. Way, A. J.; Murray, E. A.; Göttl, F.; Saraswat, V.; Jacobberger, R. M.; Mavrikakis, M.; Arnold, M. S. Anisotropic Synthesis of Armchair Graphene Nanoribbon Arrays from Sub-5 nm Seeds at Variable Pitches on Germanium. *J. Phys. Chem. Lett.* **2019**, *10*, 4266–4272.
51. Jacobberger, R. M.; Murray, E. A.; Fortin-Deschênes, M.; Göttl, F.; Behn, W. A.; Krebs, Z. J.; Levesque, P. L.; Savage, D. E.; Smoot, C.; Lagally, M. G.; Desjardins, P.; Martel, R.; Brar, V.; Moutanabbir, O.; Mavrikakis, M.; Arnold, M. S. Alignment of Semiconducting Graphene Nanoribbons on Vicinal Ge(001). *Nanoscale* **2019**, *11*, 4864–4875.

## 2018

52. Özer, E.; Sinev, I.; Mingers, A.; Araujo, J.; Kropp, T.; Mavrikakis, M.; Mayrhofer, K.; Cuenya, B.; Strasser, P. Ir-Ni Bimetallic OER Catalysts Prepared by Controlled Ni Electrodeposition on Ir<sub>poly</sub> and Ir(111). *Surfaces* **2018**, *1*, 165–186.

### Awards or leadership activities during 2018-2020 calendar years

#### Awards:

1. **Robert Burwell Lectureship in Catalysis**, North American Catalysis Society (2021).
2. **Gabor A. Somorjai Award for Creative Research in Catalysis**, American Chemical Society (2019).
3. **Visiting Miller Research Professor**, Department of Chemistry, University of California – Berkeley (2018/19).
4. **Herman Pines Award**, Catalysis Club of Chicago (2019).
5. **WARF Named Professor** (2019 – present): University of Wisconsin – Madison.

#### Leadership:

1. **Vice-Chair, Gordon Research Conference on Chemical Reactions at Surfaces** (2019).
2. Meeting Co-Chair; **2019 DOE Catalysis Science PI Meeting**, 7/19.

3. **Department Chair**, Chemical & Biological Engineering, UW-Madison (2015-2018)
4. **Chair** of the College of Engineering (UW-Madison) **Promotions and Tenure Committee** (Fall 2020 - present).
5. **Editor-in-Chief**, *Surface Science* (2012 - 2020)
6. **Editorial Board** of *ACS Catalysis* (2012 - 2018)
7. **Editorial Board** of *ChemPhysChem* (2015 - present)
8. **Editorial Board** of *AICHE Journal* (2012- present)
9. **Editorial Board** of *Surface Science Reports* (2019 - present)
10. **Editorial Board** of *Surface Science* (2008 - present)
11. **Editorial Board** of *Catalysis Today* (2009 - present)

## Modulating Catalytic Properties of Metal Cationic Centers in Non-Stoichiometric Mixed Metal Oxides for Electrochemical Oxygen Reduction

Samji Samira, John Carl A. Camayang, Krishna Patel, Xiang-Kui Gu, and Eranda Nikolla  
Department of Chemical Engineering and Materials Sciences, Wayne State University,  
Detroit, Michigan-48202 (USA)

Efficient electrochemical transformations of molecular oxygen (oxygen reduction and evolution) for energy conversion/storage rely largely on the effective design of heterogenous electrocatalysts. Tuning the electrocatalytic properties of materials by controlling the electronic structure of active sites is a promising but challenging approach. Structural and compositional flexibilities of non-stoichiometric mixed metal oxides present unique opportunities toward this goal, as the reactivity of their metal cationic centers can be modified via ligand and charge transfer modes. Herein, theoretical calculations combined with experiments show that highly catalytically active  $4d/5d$  transition metal cations for oxygen reduction in alkaline media can be generated by tuning the distinct intrinsic oxophilicity of  $3d$  and  $4d/5d$  metal cations within the perovskite structure. Tailoring the perovskite composition is shown to switch catalytically poor Rh in supported catalysts to highly catalytic active Rh cationic centers within a perovskite framework ( $\text{LaNi}_{1-x}\text{Rh}_x\text{O}_3$ ,  $x \leq 0.01$ ). These findings open up opportunities for extrapolating the function of such catalytic systems to other targeted chemistries.

### DE-SC0020953: Tuning Catalytically Active Single Sites in Non-stoichiometric, Mixed Metal Oxides for Oxygen Electrocatalysis

**PI:** Eranda Nikolla

**Student(s):** Samji Samira, John Carl A. Camayang

**Institution:** Wayne State University, Detroit, MI

### RECENT PROGRESS

$\text{ABO}_3$  perovskites are utilized to demonstrate that the electrochemical activity of non-stoichiometric mixed metal oxides can be pushed beyond that of conventional  $3d$  transition metal-based oxides by introducing highly dispersed  $4d/5d$  transition metal cations in their B-site (*ACS Energy Lett.*, 6, 3, 1065–1072, 2021). The oxygen reduction reaction (ORR) is used as a probe reaction given its importance in governing the overall efficiency of electrochemical energy conversion and storage technologies. Density function theory (DFT) calculations were performed to study the energetics of ORR on highly dispersed  $4d/5d$  transition metal cations within the B-site of La-based perovskites ( $\text{LaB}_{0.94}\text{B}'_{0.06}\text{O}_3$ ; B=Mn, Co, Ni, Cu; B'=Pd, Pt, Rh, Ru, Ir, Os). In these studies, B/B' ratio was chosen such as to represent highly dispersed, spatially separated  $4d/5d$  metal cations in a pool of  $3d$  transition metal cations and  $\text{O}^{2-}$  anions. An associative direct four-electron mechanism in alkaline was used to study the ORR energetics (Figure 1a). ORR was assumed to occur on the B' cationic centers in all the considered perovskites. Theoretical ORR overpotentials for these B' containing oxides were calculated based on

the Gibbs free energy diagrams for ORR. A volcano relationship between the theoretical overpotential and OH\* adsorption energy was observed (Figure 1b), consistent with OH\* adsorption energy being effective at describing ORR activity. For perovskites on the left of this volcano, ORR was limited by OH\* removal, and thus B' cations characterized by weaker OH\* adsorption would lead to higher ORR activity. This results in a B-site dependent B' cationic activity trend with  $\text{LaCu}_{0.94}\text{B}'_{0.06}\text{O}_3$  and  $\text{LaMn}_{0.94}\text{B}'_{0.06}\text{O}_3$  (B'=Os, Ir, Ru) oxides exhibiting the lowest and highest theoretical overpotentials, respectively, at a given B' cationic composition. For perovskites on the right side of volcano, the ORR

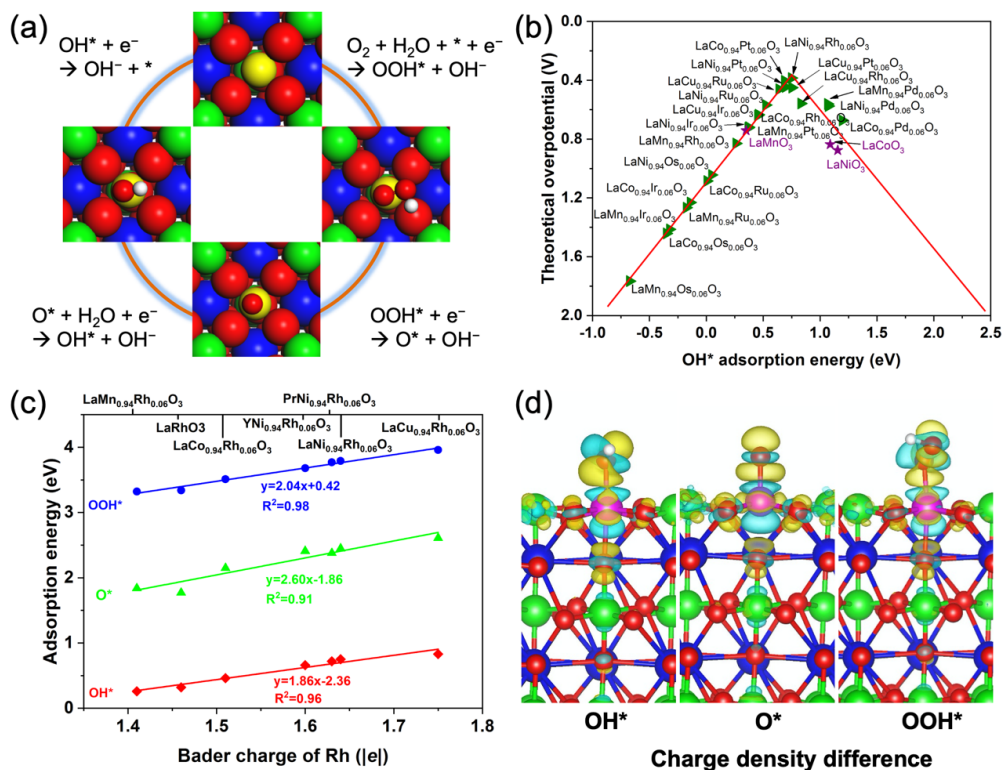


**Figure 1.** (a) Proposed mechanism for ORR in alkaline media. (b) Volcano relationship between the theoretical overpotential and the OH\* adsorption energy on  $\text{LaB}_{0.94}\text{B}'_{0.06}\text{O}_3$  (B=Mn, Co, Ni, Cu; B'=Pd, Pt, Rh, Ru, Ir, Os). (c) Linear correlations between the adsorption energies of ORR intermediates on Rh-based perovskites as a function of the calculated Bader charge of Rh cations. (d) Charge density difference for ORR intermediates adsorbed on  $\text{LaNi}_{0.94}\text{Rh}_{0.06}\text{O}_3$ . Cyan and yellow contours represent electron depletion and accumulation, respectively. Blue, green, magenta, red, and white spheres represent La, Ni, Rh, O, and H atoms, respectively. (*ACS Energy Lett.*, 6, 3, 1065–1072, 2021)

activity was limited by OOH\* formation, with stronger adsorption of OOH\* resulting in lower theoretical overpotential. To determine the underlying factors that governed the activity, the correlation between the adsorption energetics of intermediates and the electronic structure of B' cations was examined. Generally, B' cations in these oxides transferred electrons to the neighboring oxygen anions, based on their positive Bader charges. The extent of charge transfer became larger as the perovskite B-site cation varied from Mn, Co, Ni to Cu for a specific 4d/5d metal, leading to B' cations in  $\text{LaCu}_{0.94}\text{B}'_{0.06}\text{O}_3$  being the most oxidized with the weakest intermediate adsorption. This was a consequence of the variations in B–O bond strengths resulting in distinct ability of the oxygen anions to capture the electrons from the B' cation. The electronic structure change of the B' cation

as a function of the oxide composition (e.g.,  $\text{LaB}_{0.94}\text{B}'_{0.06}\text{O}_3$  ( $\text{B}'=\text{Pt, Rh, Ru, Ir}$ )) was directly correlated to the adsorption energetics and ORR theoretical overpotentials. This is because adsorption primarily involved charge transfer between the  $\text{B}'$  cation and the intermediates (Figure 1d). This suggests that activity enhancement of perovskites on the left of the volcano will require strategies to create an oxide environment that withdraws more electrons from  $\text{B}'$  cations (more reducible oxides characterized by weaker  $\text{B}-\text{O}$  bonds). This would make  $\text{B}'$  cations more oxidized than in the current perovskite environment, weakening  $\text{OH}^*$  adsorption and improving activity. On the right of the volcano, incorporating  $\text{B}'$  cations into less reducible oxides (characterized by stronger  $\text{B}-\text{O}$  bonds) should improve their activity due to the enhanced  $\text{OOH}^*$  adsorption as the  $\text{B}'-\text{O}$  bonds weaken. Effects from the A-site composition of  $\text{ANi}_{0.94}\text{B}'_{0.06}\text{O}_3$  ( $\text{A}=\text{Y, Pr, La}$ ) perovskites on the ORR energetics were less significant than those from variations in the B-site composition. Compositional changes of the A-site primarily altered the perovskite lattice parameters. Among the perovskites considered,  $\text{LaNi}_{0.99}\text{Rh}_{0.01}\text{O}_3$  provided the optimal compromise between predicted phase stability and ORR activity (Figure 1b), making it ideal for experimental testing.

$\text{LaNi}_{1-x}\text{Rh}_x\text{O}_3$  ( $0.005 \leq x \leq 0.02$ ) perovskites were synthesized with Rh content being fixed at 0.5-2 at% relative to Ni, to maximize the formation of highly dispersed and spatially separated Rh cations in  $-\text{Ni}-\text{O}-\text{Rh}-$  environments. Their performance was compared to  $\text{LaRhO}_3$  as a control, representing Rh cations in  $-\text{Rh}-\text{O}-\text{Rh}-$  environment. Rh oxide supported on  $\text{LaNiO}_3$  was also used as a control to represent Rh cations outside the  $\text{LaNiO}_3$  framework ( $w$  wt%  $\text{Rh}_2\text{O}_3/\text{LaNiO}_3$ ,  $0.15 \leq w \leq 0.58$ ). Phase-pure perovskite structures of  $\text{LaNi}_{1-x}\text{Rh}_x\text{O}_3$  and  $\text{LaRhO}_3$  were confirmed via X-ray diffraction (XRD), high angle annular dark field imaging using scanning transmission electron microscopy (HAADF-STEM), and energy dispersive X-ray spectroscopy (EDS) (Figure 2a-e). The near surface composition and electronic structure (extent of charge transfer) of Rh cations in  $\text{LaNi}_{1-x}\text{Rh}_x\text{O}_3$  were characterized using angle-resolved X-ray photoelectron spectroscopy (AR-XPS). An average oxidation state of  $+3.28 \pm 0.01$  was measured for cationic Rh in  $\text{LaNi}_{0.99}\text{Rh}_{0.01}\text{O}_3$  (Figure 2f), which was higher than Rh in the control catalysts (0.29 wt%  $\text{Rh}_2\text{O}_3/\text{LaNiO}_3$  (+3.16) and  $\text{LaRhO}_3$  (+3)). This is consistent with the lower oxophilicity of Ni in  $\text{LaNi}_{0.99}\text{Rh}_{0.01}\text{O}_3$  (characterized by  $-\text{Ni}-\text{O}-\text{Rh}-$  catalytic centers), leading to stronger  $\text{O}-\text{Rh}$  bonds and more oxidized Rh cations in the perovskite, consistent with the theoretical insights.

Electrochemical performance of the oxides was investigated using a thin-film approach in a three-electrode system containing  $\text{O}_2$ -saturated 0.1M KOH electrolyte solution. ORR activity of  $\text{LaNi}_{1-x}\text{Rh}_x\text{O}_3$  oxides was benchmarked using Pt/C, and state-of-the-art perovskite,  $\text{LaMnO}_3$ .  $\text{LaNi}_{1-x}\text{Rh}_x\text{O}_3$  oxides exhibited superior electrocatalytic performance, as shown in Figure 2g. For instance,  $\text{LaNi}_{0.99}\text{Rh}_{0.01}\text{O}_3$  exhibited a more positive potential (lower overpotential) at  $100 \mu\text{Acm}^{-2}_{\text{geo}}$  ( $0.916 \pm 0.004$  V) as compared to the control catalysts and  $\text{LaMnO}_3$  ( $0.887 \pm 0.003$  V). Mass activities of Rh-based oxides under similar conditions are shown in Figure 2h. The mass activity of  $\text{LaNi}_{0.995}\text{Rh}_{0.005}\text{O}_3$  was  $\sim 35$  times higher than that of 0.15 wt%  $\text{Rh}_2\text{O}_3/\text{LaNiO}_3$  at 0.80 V. The mass activity of  $\text{LaNi}_{0.995}\text{Rh}_{0.005}\text{O}_3$  was 80-fold higher as compared to commercial 5 wt% Rh/C at 0.80 V.

These results show that tailoring the electronic structure of the  $4d/5d$  metal cations via variations in the intrinsic oxophilicity within the perovskite framework can switch catalytically inert Rh and Rh oxide supported catalysts, to highly active Rh cationic centers in perovskites for ORR. These studies demonstrate the potential of exploring non-stoichiometric mixed metal oxides as frameworks for systematically tuning the electronic structure of  $4d/5d$  metal cations, consequently generating unique catalytic active centers for targeted electrocatalytic reactions of importance in energy conversion and storage technologies.

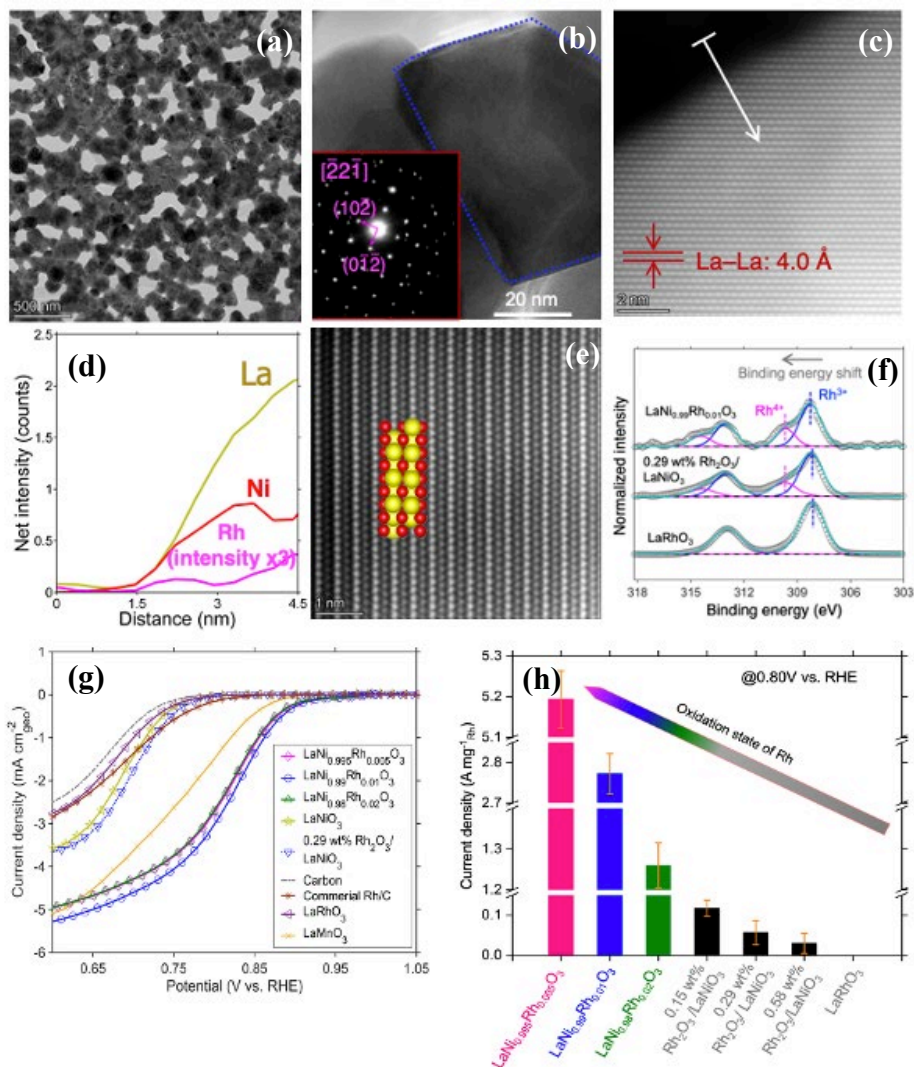


**Figure 2.** (a) TEM micrograph of  $\text{LaNi}_{0.99}\text{Rh}_{0.01}\text{O}_3$ . (b) HR-TEM micrograph of  $\text{LaNi}_{0.99}\text{Rh}_{0.01}\text{O}_3$  with the inset representing the SAED pattern along the  $[22\bar{1}]$  zone axis. (c) HAADF-STEM image of  $\text{LaNi}_{0.99}\text{Rh}_{0.01}\text{O}_3$ . (d) EDS line-scan for La, Ni, and Rh along the white arrow shown in (c). (e) Atomic resolution HAADF-STEM image of bulk  $\text{LaNi}_{0.99}\text{Rh}_{0.01}\text{O}_3$ . Yellow and red spheres represent A- and B-site cations, respectively. (f) HR-XPS of Rh  $3d$  core level region in  $\text{LaNi}_{0.99}\text{Rh}_{0.01}\text{O}_3$ , in comparison with 0.29 wt%  $\text{Rh}_2\text{O}_3/\text{LaNiO}_3$ , and  $\text{LaRhO}_3$ . (g) Background-subtracted  $\text{O}_2$ -saturated polarization curves in 0.1 M KOH at 1600 rpm for all the investigated perovskites. (h) Mass activities of Rh-based oxide electrocatalysts at an operating potential of 0.80 V vs. RHE. (*ACS Energy Lett.*, 6, 3, 1065–1072. 2021)

## **Publications Acknowledging this Grant in 2020-2021 (this grant started in 8/2020)**

(XXVII) *Exclusively funded by this grant;*

- Samira S., Camayang J. C. A., Patel K., Gu X-K, Nikolla E.\*, “Modulating Catalytic Properties of Targeted Metal Cationic Centers in Nonstoichiometric Mixed Metal Oxides for Electrochemical Oxygen Reduction”, *ACS Energy Lett.* 2021, 6, 1065–1072.
- Samira S.<sup>‡</sup>, Hong J.<sup>‡</sup>, Camayang J. C. A., Hoffman A. S., Bare S. R. \*, Nikolla E. \*, “Dynamic Surface Reconstruction Unifies the Electrocatalytic Oxygen Evolution Activity of Nonstoichiometric Mixed Metal Oxides”, **Submitted, August 2021.**

### **Awards during 2018-2020 calendar years**

- **WCC’s Rising Stars Award for 2019**, ACS Women Chemists Committee (WCC), 2019
- **2019 Young Innovator Award in NanoEnergy**, Nano Research, 2019
- **Career Development Chair Award**, Wayne State University, 2018
- **Department of Energy Early Career Research Award**, Office of Basic Energy Science, 2015-2020
- **Camille Dreyfus Teacher-Scholar Award**, 2016-2021

### **Scientific Leadership and Service to Catalysis Community (2018-2020 calendar years)**

- Associate Editor of Journal of Catalysis (3/2020- current)
- Director-at-Large of the North America Catalysis Society (2021-current)
- Past-Chair of the AIChE’s Catalysis and Reaction Engineering (CRE) Division (2020-current).
- Member of the Diversity and Inclusion Task Force for the AIChE’s Catalysis and Reaction Engineering (CRE) Division (2019-current).
- Chair of the AIChE’s Catalysis and Reaction Engineering (CRE) Division (2019-2020).
- Member of the budget committee for the U.S. bid for the 2020 International Congress on Catalysis.
- Member of the Website/Publicity Committee for the 2020 International Congress on Catalysis.
- Chair of the Student Travel Award Committee for the 2020 International Congress on Catalysis.
- Member of the Editorial Advisory Board for Journal of ACS Catalysis (2019-2020).
- Member of the Editorial Advisory Board for Journal of ACS Energy Letters (2021-current).
- Member of the Editorial Advisory Board for Industrial & Engineering Chemistry Research (2018-current).
- National Meetings Session Chair and co-Chair:
  - 2019 North American Catalysis Society Meeting
  - 2018 and 2019 AIChE Annual Meetings.

- Organized the “Power Hour” event at Gordon Research Conference on Catalysis 2018 to promote diversity and inclusion.
- Organized a “Design in Women” Workshop, The Midland Section of ACS and WCC to promote diversity and inclusion.

**Justin M. Notestein**

**Institute for Catalysis in Energy Processes (ICEP)**

Justin M. Notestein  
Chemical and Biological Engineering and Center for Catalysis and Surface Science,  
Northwestern University, Evanston IL 60208 USA

**Presentation Abstract**

The Institute for Catalysis in Energy Processes (ICEP) is a primary home for research in catalysis science at Northwestern University. 16 PIs are involved, mentoring approximately 20 postdoctoral fellows and graduate students and anchoring many more collaborations within Northwestern University and beyond. ICEP brings together researchers with expertise in computational modeling, materials synthesis, advanced characterization, and chemical kinetics to advance basic catalysis science. Leveraging our unique skillset, we focus on the development of more precise materials, with which we can achieve disruptive advances in our understanding and implementation of catalysis and new catalytic processes. In the current cycle we focus on oxidation catalysis across three mechanistically interlinked research thrusts and three crosscuts on tool development. This work was supported by the US Department of Energy, Office of Basic Energy Sciences, through a grant (DE-FG02-03ER15457) to the Institute for Catalysis for Energy Processes (ICEP) at Northwestern University.

**DE-FG02-03ER15457: Institute for Catalysis in Energy Processes (ICEP)**

**PI:** Justin M. Notestein<sup>1</sup> (lead)

**Additional PIs:** M. Bedzyk<sup>2</sup>, L. Broadbelt<sup>1</sup>, O. Farha<sup>3</sup>, J. Hupp<sup>3</sup>, H. Kim<sup>3</sup>, H. Kung<sup>1</sup>, M. Kung<sup>1</sup>, L. Marks<sup>2</sup>, T. Marks<sup>3</sup>, S. Nguyen<sup>3</sup>, K. Poepelmeier<sup>3</sup>, G. Schatz<sup>3</sup>, N. Schweitzer<sup>1</sup>, R. Snurr<sup>1</sup>, E. Weitz<sup>3</sup>

**Affiliations(s):** Northwestern University, Center for Catalysis and Surface Science and <sup>1</sup>Department of Chemical and Biological Engineering or <sup>2</sup>Department of Materials Science and Engineering or <sup>3</sup>Department of Chemistry

**RECENT PROGRESS**

***Introduction***

The overarching ICEP goal is targeted research to address the inhomogeneity challenge in heterogeneous catalysis: more precise materials are required to achieve disruptive advances in our understanding and implementation of catalysis and new catalytic processes. ICEP posits that catalyst inhomogeneity is a particularly serious problem in selective oxidation, where grand challenges remain outstanding due in part to a lack of control and understanding of catalyst active sites, which can activate O<sub>2</sub> and reactants down many different desired and undesired paths. We are in year 1 of the current cycle focusing on oxidation catalysis. The ICEP vision has been that we can create catalysts with unique

types of active sites in an atomistically controlled fashion so that we can move beyond indirect empiricism to definitive, predictive science. This directly attacks the two Grand Challenges identified in the 2007 DOE workshop report “Basic Research Needs: Catalysis for Energy” and is strongly aligned with four of five the Priority Research Directions (PRD) identified in the 2017 DOE workshop “Basic Research Needs for Catalysis Science”. The ICEP team is organized into complementary and interacting Thrusts and CrossCuts. Thrusts are mnemonically organized around steps in an idealized oxidation reaction cycle – substrate activation (Thrust 1), O<sub>2</sub> activation (Thrust 2), and non-redox shunts (Thrust 3). CrossCuts are organized around tool development in synthesis (CrossCut 1), characterization (CrossCut 2), and data-driven catalysis (CrossCut 3). Each of these are summarized below.

### *Thrust 1*

Thrust I develops expanded structure-function relationships for complex supported oxides and alloys that dynamically lose and gain O. CO oxidation, alkane oxidative dehydrogenation and alcohol oxidative dehydrogenation / coupling are foci of this Thrust. A major effort will be to synthesize and stabilize a wider range of atomically-precise oxidized sites than have been previously possible. Project 1 builds upon extensive experience to synthesize tunable nanoparticles stabilized by epitaxy with designed supports. Project 2 develops new routes into oxide clusters of precise size and composition. Both projects begin with homometallic catalysts and will move into bimetallics, intermetallics, and alloys. From this, we expect to develop powerful synthesis-structure-function relationships and to significantly advance the science underlying bond activation. In addition, these materials are designed to be amenable to computational screening and interrogation, something that has been previously challenging for many supported oxides and related structures. Both projects are multi-investigator and will use multimodal characterization to obtain the details of the metal/oxide interface structures, including XANES/EXAFS, EELS, aberration-corrected electron microscopy, XRD/XPS/XSW, and ab-initio DFT thermodynamics methods. In addition to steady state measurements, reactions will be followed with techniques such as SSITKA/FTIR.

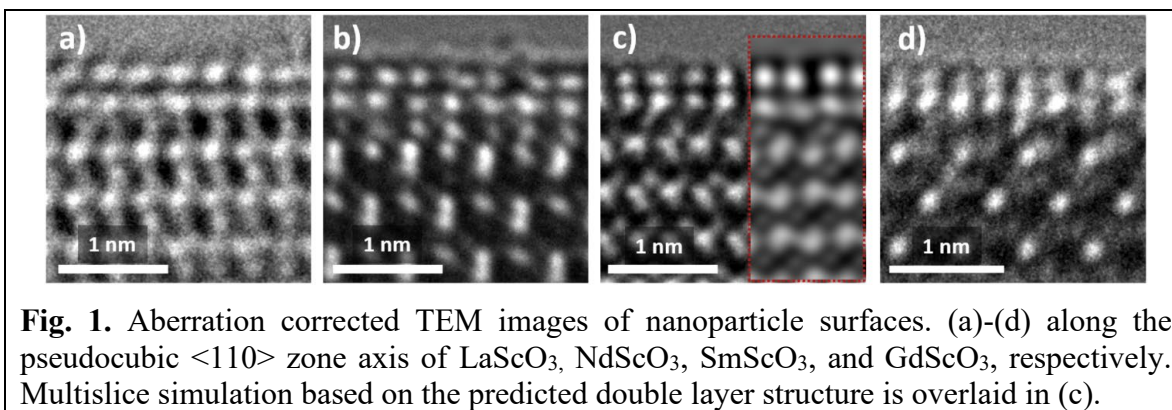
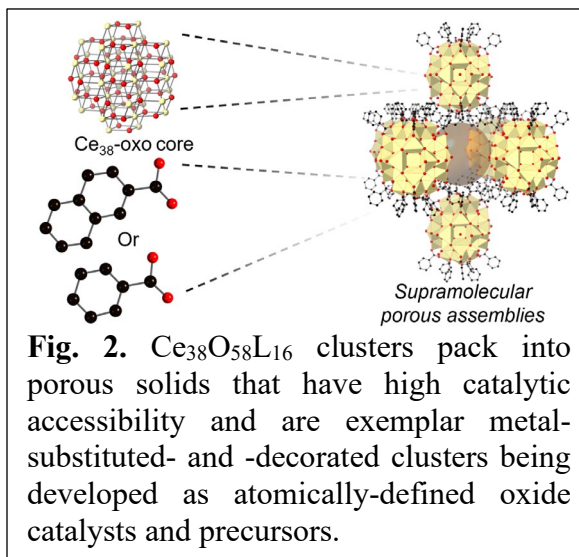


**Fig. 1.** Aberration corrected TEM images of nanoparticle surfaces. (a)-(d) along the pseudocubic  $\langle 110 \rangle$  zone axis of LaScO<sub>3</sub>, NdScO<sub>3</sub>, SmScO<sub>3</sub>, and GdScO<sub>3</sub>, respectively. Multislice simulation based on the predicted double layer structure is overlaid in (c).

**L. Marks and Poeppelmeier** made significant progress towards understanding nanoparticle LnScO<sub>3</sub> (Ln = La, Nd, Sm, Gd) supports. They identified and solved reconstructions on the (100) and (110) pseudocubic faces (**Fig. 1**) and they developed a novel synthesis method that controls water vapor pressure for greater shape and size control. A thermodynamic model was derived for supported, twinned particles, which are common

on these supports. (*J. Phys. Chem. C*, 2020) The tunable basicity of these supports determined catalytic performance in CO oxidation (*ACS Catal*, submitted) and reverse WGS for supported Au and Pt. (**Schweitzer** and **Notestein**). Computational investigations indicate an important role for *4f* electrons in the LnScO<sub>3</sub> supports. These materials are also growth substrates, so understanding their surfaces and electronic structure has broad applicability. In parallel, **Bedzyk** and **Schatz** determined the structure of Pt/SrTiO<sub>3</sub> (001) via X-ray standing wave measurements (see CrossCuts). Manuscripts are being developed.

**Farha** synthesized atom-precise oxide clusters Ce<sub>38</sub>O<sub>58</sub>L<sub>16</sub> (L=benzoic acid) (**Fig. 2**), Ce<sub>70</sub>/M Ce<sub>70</sub> (M = Cu, Ni, Zn, Co, Fe), and Ce<sub>12</sub>V<sub>6</sub>-L (L = sulfonate) and fully characterized their chemical and physical properties. Ce<sub>38</sub>O<sub>58</sub>L<sub>16</sub> is porous and catalytically active even in the solid state (*Chem. Mater*, 2020). CuCe<sub>70</sub> and FeCe<sub>70</sub> were more reactive in CO and alcohol oxidation, which was ascribed to favorable redox cycling of the dopant (e.g. Cu<sup>2+</sup>) with Ce<sup>3+</sup>/Ce<sup>4+</sup>. Ce<sub>12</sub>V<sub>6</sub>-L exhibited high reactivity and solubility and is being tested as a precursor for supported oxides catalysts for alkane oxidative dehydrogenation.



**Weitz, Bedzyk, and Schatz** are studying MoO<sub>x</sub> and VO<sub>x</sub> structures on θ-Al<sub>2</sub>O<sub>3</sub>, CeO<sub>2</sub>, and TiO<sub>2</sub>. XSW, IR and TPD are combined with DFT and *ab initio* molecular dynamics to refine the nature of adsorbed H, OH, O and H<sub>2</sub>O. The improved models will be used in further catalysis studies at variable water coverages and to further tailor ALD processes. This complements extensive work using *in situ* IR spectroscopy, TPR/O, and kinetics studies to address cyclohexane/cyclohexene oxidation over low coverage VO<sub>x</sub>/CeO<sub>2</sub> (*Appl. Catal. A*, submitted), VO<sub>x</sub>/TiO<sub>2</sub> (*J. Phys Chem C*, 2020), and VO<sub>x</sub>/CeO<sub>2</sub>/Al<sub>2</sub>O<sub>3</sub> (*J. Catal.*, 2020) also with **Notestein, Stair, and Snurr**.

### Thrust 2

Thrust 2 focuses on O<sub>2</sub> activation within complex cycles and at tailored interfaces. Hydroperoxides are effective at forming oxygenates and abstracting H atoms, so it is important to understand the mechanisms by which catalysts activate O<sub>2</sub> as peroxy/hydroperoxys, identify relationships between mechanism and catalyst properties, understand how selectivity is dictated by the structure of the activated O<sub>2</sub> and the nature of the reactant, and finally, to devise catalytic structures to influence selectivity. Our work focuses on inverse catalysts to interrogate the critical role of metal – oxide interfaces for supported catalysts (Project 1), and O<sub>2</sub> activation over framework vacancies as a part of Mars-van Krevelen cycles (Project 2). Materials and reaction mechanisms will be probed by SERS, SSTIKA experiments, and computational modeling. Alkane and alcohol dehydrogenation and olefin epoxidation will be emphasized.

**Kung** researched selective alcohol oxidation on Au, and measurements showed that aqueous 1,2-propanediol oxidation proceeded with stoichiometric H<sub>2</sub>O<sub>2</sub> production (*Appl. Catal. A*, 2020), proving a key hypothesis that hydroperoxyl mechanisms are involved in activating O<sub>2</sub> over these catalysts. Prior work implicated interfaces as alcohol oxidation active sites for Au decorated with TiO<sub>x</sub>. In support, **Snurr** modeled Au(111), anatase(001), and Au/anatase(001) interfaces using periodic DFT (VASP). CO, O, and O<sub>2</sub> adsorption were calculated, and isopropoxy adsorption is in progress. New postdocs have designed and benchmarked a system for coupled ODH and epoxidation / sulfoxidation with hydroperoxy species generated during O<sub>2</sub> activation.

In work also related to CrossCut 1, **Notestein**, **Stair**, and **L. Marks** used ALD techniques to overcoat supported Pt with a variety of additional oxides. It was demonstrated that sub-monolayer addition of Al<sub>2</sub>O<sub>3</sub> or TiO<sub>2</sub> on Pt/SiO<sub>2</sub> substantially altered the kinetics of CO<sub>2</sub> hydrogenation by controlling CO formation and desorption rates, shifting the mechanism from an Eley-Rideal type to a Langmuir-Hinshelwood type with the addition of the partial overcoat. (**Fig. 3**, *J. Phys. Chem. C*, 2021). Likewise, ALD techniques developed in ICEP were used to add thicker overcoats of In<sub>2</sub>O<sub>3</sub> on Pt/Al<sub>2</sub>O<sub>3</sub>. This enhanced In<sub>2</sub>O<sub>3</sub> reducibility, leading to low temperature reduction by H<sub>2</sub> or by H atoms spilled over from propane dehydrogenation on Pt. The abundance of interface sites on this catalyst gave world-leading performance in propane ODH (*Science*, 2021)

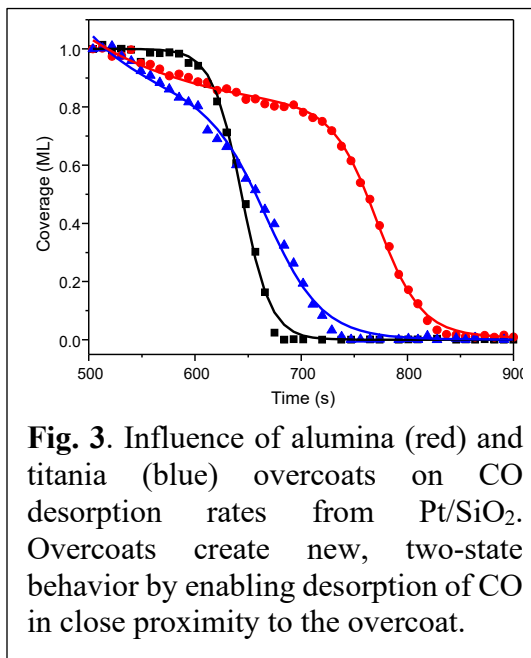


**Fig. 3.** Influence of alumina (red) and titania (blue) overcoats on CO desorption rates from Pt/SiO<sub>2</sub>. Overcoats create new, two-state behavior by enabling desorption of CO in close proximity to the overcoat.

### **Thrust 3**

Thrust 3 studies isolated metal oxo/dioxo sites that do not require redox to turn over. These are synthesized via atom-precise means and are amenable to spectroscopic and computational characterization. This thrust investigates acceptorless dehydrogenation and mechanistically related reactions including dehydration and hydrogenolysis (Project 1) and activation of H<sub>2</sub>O<sub>2</sub> to carry out epoxidation or sulfoxidation (Project 2). These reactions are important technologies on their own, but they also shed light on elementary steps and shunt reactions occurring during O<sub>2</sub>-driven selective oxidation catalysis. These materials will be studied through a combination of precision synthesis, reaction scoping, kinetics and mechanistic studies, DFT analysis of the supported catalyst structure and reaction pathways, and *ex situ* and *operando* structural, electronic, and vibrational characterization.

**T. Marks** expanded use of a carbon-supported, single-site Mo-dioxo catalyst. It is a dehydrogenation and dehydration catalyst, and it was recently demonstrated to depolymerize PET in H<sub>2</sub> to yield terephthalic acid and ethylene (*Angew. Chem. Int. Ed.* 2020). Reaction intermediates were isolated, characterized by EXAFS (**Bedzyk**), Raman (**Kim**), and compared to DFT models (**Schatz**), **Fig. 4**. Manuscripts are in preparation. Using the single-molecule atomic-resolution real-time electron microscope (SMART-EM) at U. Tokyo (with Prof. Eiichi Nakamura), isolated Mo-dioxo species and reaction intermediates were directly observed (*Bull. Chem. Soc. Japan*, 2021, cover). Together, these studies motivate future catalyst design and new reactions. On analogous materials, **Notestein** completed a study on isobutane non-oxidative dehydrogenation over MoOx/K-Al<sub>2</sub>O<sub>3</sub> (*J. Catal.* 2021). The active sites were assigned as Mo<sup>4+</sup> by a combination of XAS and TPR. Only the larger clusters formed deeply reduced sites responsible for coking.

Separately, **Notestein** compared Ti-SiO<sub>2</sub> and Nb-SiO<sub>2</sub> in vapor- and solution-phase olefin epoxidation with H<sub>2</sub>O<sub>2</sub> (*ACS Catal* 2020) using a uniquely designed reactor. After addressing heats

of adsorption, Nb-SiO<sub>2</sub> had the same transition state for activating H<sub>2</sub>O<sub>2</sub> in both phases, whereas Ti-SiO<sub>2</sub> required solvent stabilization. These studies connect back to Thrust 2.

In carryover work from a prior iteration of ICEP, **T. Marks** also completed studies on olefin polymerization by Cp\*ZrMe<sub>2</sub><sup>+</sup>X<sup>-</sup> in solution (X<sup>-</sup> = fluoroarylborate) and supported on sulfated alumina, with accompanying NMR (Pruski and Kobayashi at Ames Lab) and DFT (A. Motta, U. Rome). The homogeneous system produced atactic polypropylene, while the supported catalyst produced isotactic polypropylene via a “back-skip” enchainment mechanism, reflecting the environment imposed by the nearby surface. This phenomenon has never been observed for a structurally well-defined, supported molecular polymerization catalyst and has significant mechanistic implications for poorly understood heterogeneous Ziegler-Natta catalysts. (*ChemCatChem* 2021 and *ACS Catal* 2021)

### CrossCuts

Running perpendicular to the three thrusts are crosscuts addressing new synthesis tools using ALD, advanced characterization by X-ray standing wave (XSW) techniques at the Advanced Light Source and other synchrotrons, and data science approaches.

**Notestein** advanced the use of ALD and related approaches to synthesize catalysts. In addition to work discussed in Thrust 2, SiO<sub>2</sub> overcoating using techniques generated within ICEP generated new Brønsted acid sites at Nb<sub>2</sub>O<sub>5</sub>-SiO<sub>2</sub> interfaces, (*J. Catal.* 2021) and the

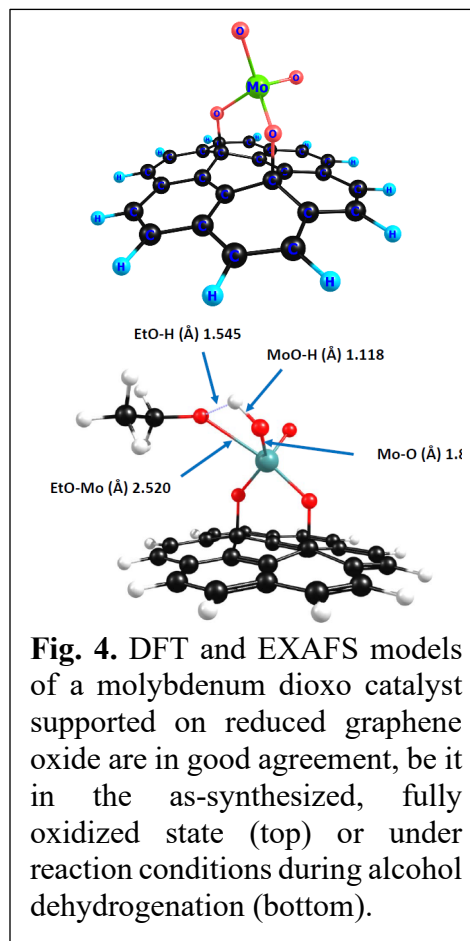


**Fig. 4.** DFT and EXAFS models of a molybdenum dioxo catalyst supported on reduced graphene oxide are in good agreement, be it in the as-synthesized, fully oxidized state (top) or under reaction conditions during alcohol dehydrogenation (bottom).

concept has been extended to other core oxides. The surface cavities generated by SiO<sub>2</sub> deposition on a templated Ti-SiO<sub>2</sub> catalyst were proven to introduce reactant stabilization during limonene epoxidation. (*ACS Catal.* 2020). Finally, work proceeds on developing direct spectroscopic evidence for size-selective cavities in templated ALD films. This is an extension of recent work by **Stair** on the mechanism of spontaneous pore formation in ALD-derived alumina overcoats (*ACS Appl. Mater. Inter.* 2020).

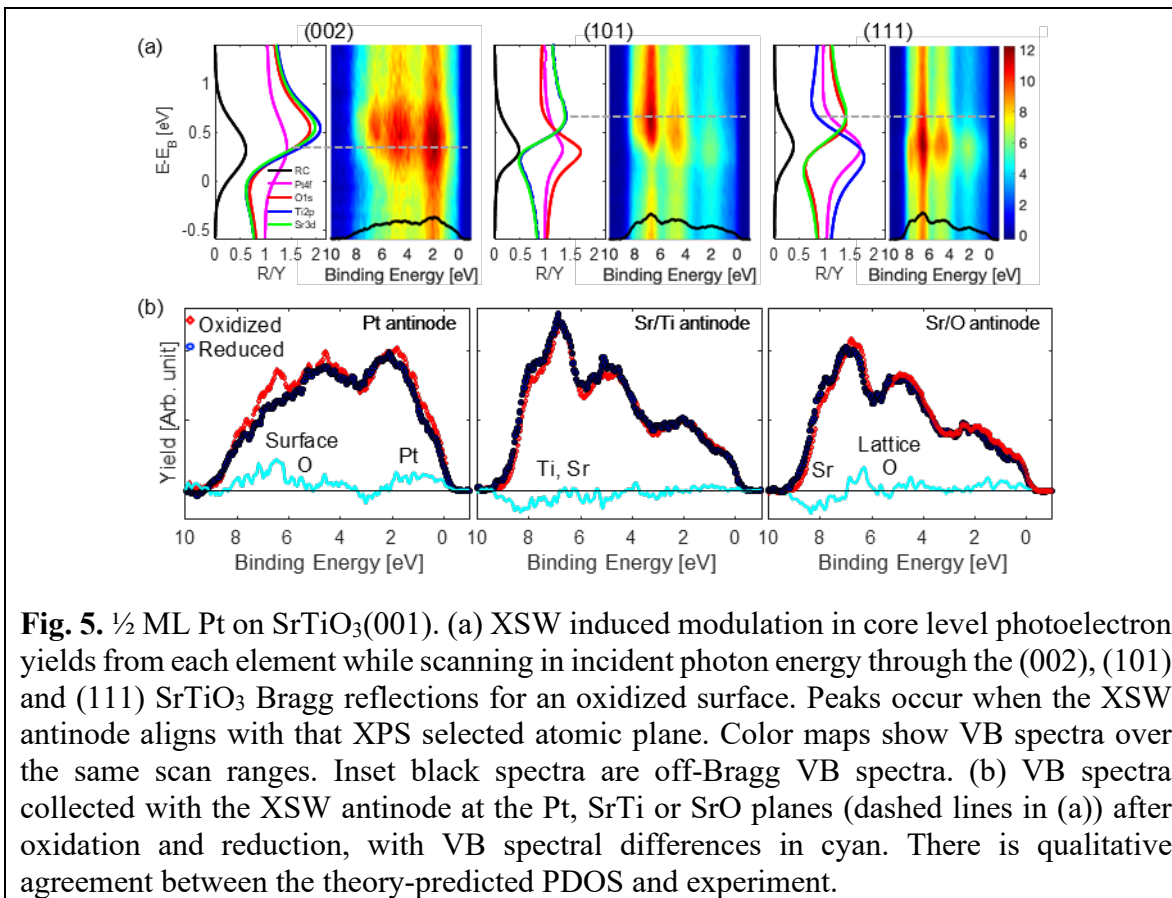
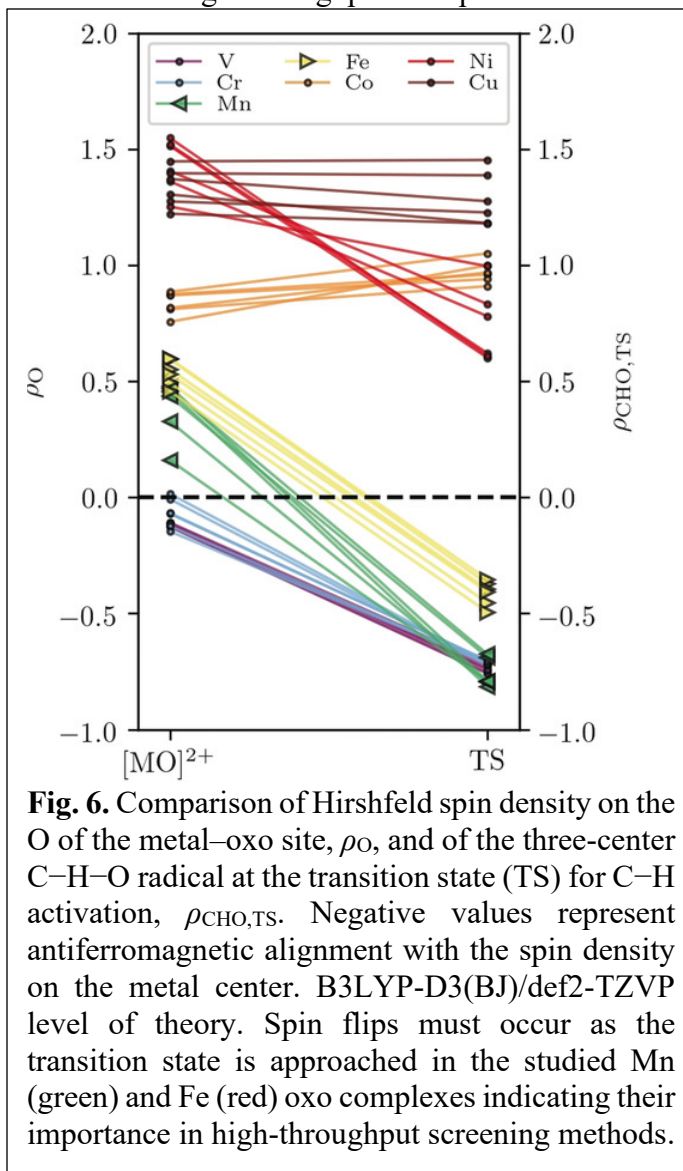


**Fig. 5.**  $\frac{1}{2}$  ML Pt on SrTiO<sub>3</sub>(001). (a) XSW induced modulation in core level photoelectron yields from each element while scanning in incident photon energy through the (002), (101) and (111) SrTiO<sub>3</sub> Bragg reflections for an oxidized surface. Peaks occur when the XSW antinode aligns with that XPS selected atomic plane. Color maps show VB spectra over the same scan ranges. Inset black spectra are off-Bragg VB spectra. (b) VB spectra collected with the XSW antinode at the Pt, SrTi or SrO planes (dashed lines in (a)) after oxidation and reduction, with VB spectral differences in cyan. There is qualitative agreement between the theory-predicted PDOS and experiment.

**Bedzyk** is carrying out XSW-XPS measurements of oxide-supported catalysts at Diamond Light Source I09 and Advanced Photon Source 5ID-C, as discussed in Thrust 1. Site-specific valence band (VB) spectroscopy for half-ML Pt on SrTiO<sub>3</sub>(001) is highlighted as the first measurement of site-specific VB contribution from surface atoms, (**Fig. 5**) and it agrees well with the DFT calculations from **Schatz**. Publications are in development.

**Snurr** used quantum-chemical calculations to investigate a family of metal–organic frameworks (MOFs) containing triazolate linkers for their ability to form terminal metal–oxo sites and activate methane (*Angew. Chem. Int. Ed.* 2020). Reactivity was widely tunable but complexly dependent on spin density, which has implications both for specific research discussed in Thrust 1 Project 2, as well as for accelerated discovery efforts (**Fig. 6**). In follow-up work (*J. Chem. Phys.*, 2021), **Snurr** directly addressed the need for accurate density functional approximations in high throughput computational studies, specifically for metal oxides. Commonly used generalized gradient approximation (GGA), GGA+*U*, and meta-GGA exchange-correlation functionals were compared for modeling redox-dependent binding of O<sub>2</sub> and N<sub>2</sub> at open metal sites. Although binding energies were strongly dependent on the given functional, the approaches often yielded the same qualitative trends and structure–property relationships.

The experimental corollary to this work was begun in the REACT core facility. **Schweitzer** has developed a library of ALD-derived oxide materials studied using methanol TPR, visible Raman, DRIFTS, and SSITKA-IR. Beyond specific findings, these materials validated experimental workflows that will be broadened out to cover more novel materials. A graduate student has been brought on specifically to address the interface between computation and experiment in this materials space.



## Publications Acknowledging this Grant in 2018-2021

### Leading Intellectual Contributions from ICEP

1. Ahn, S.; Nauert, S. L.; Hicks, K. E.; Ardagh, M. A.; Schweitzer, N. M.; Farha, O. K.; Notestein, J. M., Demonstrating the critical role of solvation in supported Ti and Nb epoxidation catalysts via vapor-phase kinetics. *ACS Catal.* **2020**, *10*, 2817-2825.
2. Ardagh, M. A.; Bregante, D. T.; Flaherty, D. W.; Notestein, J. M., Controlled deposition of silica on titania-silica to impart transport limitation-free confinement effects on epoxidation catalysts. *ACS Catal.* **2020**, *10*, 13008–13018.
3. Bae, J.; Samek, I. A.; Stair, P. C.; Snurr, R. Q., Investigation of the Hydrophobic Nature of Metal Oxide Surfaces Created by Atomic Layer Deposition. *Langmuir* **2019**, *35* (17), 5762-5769.
4. Bo, Z.; Sol, A.; Ardagh, M. A.; Schweitzer, N. M.; Canlas, C. P.; Farha, O. K.; Notestein, J. M., Synthesis and Stabilization of Small Pt Nanoparticles on TiO<sub>2</sub> Partially Masked by SiO<sub>2</sub>. *Applied Catalysis A* **2018**, *551*, 122-128.
5. Bo, Z.; Thornburg, N. E.; Peng, L.; Moreno, J. J. G.; Nolan, M.; Marks, L. D.; Notestein, J. M., Direct Visualization of Independent Ta Centers Supported on Two-Dimensional TiO<sub>2</sub> Nanosheets. *Nano Letters* **2019**, *19*, 8103-8108.
6. Bo, Z.; McCullough, L. R.; Dull, S.; Ardagh, M. A.; Wang, J.; Notestein, J. M., Strong Electrostatic Adsorption of Pt onto SiO<sub>2</sub> partially Overcoated Al<sub>2</sub>O<sub>3</sub> – Towards Single Atom Catalysts. *The Journal of Chemical Physics* **2019**, *151*.
7. Brydon, R. R. O.; Peng, A. Y.; Qian, L. P.; Kung, H. H.; Broadbelt, L. J., Microkinetic Modeling of Homogeneous and Gold Nanoparticle-Catalyzed Oxidation of Cyclooctene. *Industrial & Engineering Chemistry Research* **2018**, *57* (14), 4832-4840.
8. Chen, B.-R.; Crosby, L. A.; George, C.; Kennedy, R. M.; Schweitzer, N. M.; Wen, J.; Van Duyne, R. P.; Stair, P. C.; Poeppelmeier, K. R.; Marks, L. D.; Bedzyk, M. J., Morphology and CO Oxidation Activity of Pd Nanoparticles on SrTiO<sub>3</sub> Nanopolyhedra. *ACS Catalysis* **2018**, *8* (6), 4751-4760.
9. Cheng, E.; McCullough, L.; Noh, H.; Farha, O.; Hupp, J.; Notestein, J. M., Isobutane Dehydrogenation over Bulk and Supported Molybdenum Sulfide Catalysts. *Ind. Eng. Chem. Res.* **2020**, *59* (3), 1113–1122.
10. Cheng, E.; Notestein, J. M., Catalytic Dehydrogenation of Isobutane over Supported MoO<sub>x</sub>/K-Al<sub>2</sub>O<sub>3</sub>. *J. Catal.* **2021**, *397*, 212-222.
11. Cook, S.; Dylla, M. T.; Rosenberg, R. A.; Mansley, Z. R.; Snyder, G. J.; Marks, L. D.; Fong, D. D., The Vacancy-Induced Electronic Structure of the SrTiO<sub>3-δ</sub> Surface. *Advanced Electronic Materials* **2019**, *5* (1), 1800460.
12. Crosby, L. A.; Chen, B.-R.; Kennedy, R. M.; Wen, J.; Poeppelmeier, K. R.; Bedzyk, M. J.; Marks, L. D., All Roads Lead to TiO<sub>2</sub>: TiO<sub>2</sub>-Rich Surfaces of Barium and Strontium Titanate Prepared by Hydrothermal Synthesis *Chemistry of Materials* **2018**, *30* (3), 841-846.
13. Ding, J.; Huang, L.; Guojing, J.; Zeng, Y.; Chen, Z.; Eddings, E.G.; Fan, M.; Zhong, Q.; Kung, H.H., Modification of Catalytic Properties of Hollandite Manganese Oxide by Ag Intercalation for Oxidative Acetalization of Ethanol to Diethoxyethane. *ACS Catal.* **2021**, *11* (9), 5347-5357.
14. Engelhardt, C. M.; Kennedy, R. M.; Enterkin, J. A.; Poeppelmeier, K. R.; Ellis, D. E.; Marshall, C. L.; C., S. P., Structure Sensitivity of Acrolein Hydrogenation by Platinum Nanoparticles on Ba<sub>x</sub>Sr<sub>1-x</sub>TiO<sub>3</sub> Nanocuboids. *ChemCatChem* **2018**, *10* (3), 632-641.

15. George, C.; Littlewood, P.; Stair, P. C., Understanding Pore Formation in ALD Alumina Overcoats. *ACS Appl. Mater. Interfaces* **2020**, *12* (18), 20331-20343.
16. Hackler, R. A.; Kang, G.; Schatz, G. C.; Stair, P. C.; Van Duyne, R. P., Analysis of TiO<sub>2</sub> Atomic Layer Deposition Surface Chemistry and Evidence of Propene Oligomerization Using Surface-Enhanced Raman Spectroscopy. *Journal of the American Chemical Society* **2019**, *141* (1), 414-422.
17. Kennedy, R. M.; Crosby, L. A.; Ding, K.; Canlas, C. P.; Gulec, A.; Marks, L. D.; Elam, J. W.; Marshall, C. L.; Stair, P. C.; Poepelmeier, K. R., Replication of SMSI Via ALD: TiO<sub>2</sub> Overcoats Increase Pt-Catalyzed Acrolein Hydrogenation Selectivity. *Catalysis Letters* **2018**, *148* (8), 2223-2232.
18. Kratish, Y.; Li, J. Q.; Liu, S. F.; Gao, Y. S.; Marks, T. J., Polyethylene Terephthalate Deconstruction Catalyzed by a Carbon-Supported Single-Site Molybdenum-Dioxo Complex. *Angew. Chem.-Int. Edit.* **2020**, *59* (45), 19857-19861.
19. Kratish, Y.; Nakamuro, T.; Liu, Y. Q.; Li, J. Q.; Tomotsuka, I.; Harano, K.; Nakamura, E.; Marks, T. J., Synthesis and Characterization of a Well-Defined Carbon Nanohorn Supported Molybdenum Dioxo Catalyst by SMART-EM Imaging. Surface Structure at the Atomic Level. *Bull. Chem. Soc. Jpn.* **2021**, *94* (2), 427-432.
20. Li, J.; Liu, S.; Lohr, T. L.; Marks, T. J., Efficient Chemoselective Reduction of N-Oxides and Sulfoxides using a Carbon-Supported Molybdenum-Dioxo Catalyst and Alcohols. *ChemCatChem* **2019**, *11*, 4139-4146.
21. Limvorapitux, R.; Chen, H. Y.; Mendonca, M. L.; Liu, M. T.; Snurr, R. Q.; Nguyen, S. T., Elucidating the mechanism of the UiO-66-catalyzed sulfide oxidation: activity and selectivity enhancements through changes in the node coordination environment and solvent. *Catalysis Science & Technology* **2019**, *9* (2), 327-335.
22. Lin, W.; Wu, W.; Weitz, W.; Schatz, G. C., Molecular-level insight into the hydroxylated monomeric VO<sub>x</sub>/θ-Al<sub>2</sub>O<sub>3</sub>(010) and its adsorption of methanol. *Journal of Physical Chemistry C* **2019**, *123* (45), 27704-27711.
23. Liu, C.; Nauert, S. L.; Alsina, M. A.; Wang, D.; Grant, A.; He, K.; Weitz, E.; Nolan, M.; Gray, K. A.; Notestein, J. M., Role of surface reconstruction on Cu/TiO<sub>2</sub> nanotubes for CO<sub>2</sub> conversion. *Applied Catalysis B: Environmental* **2019**, *255*, 117754.
24. Liu, D. H.; Marks, T. J.; Li, Z., Catalytic One-Pot Conversion of Renewable Platform Chemicals to Hydrocarbon and Ether Biofuels through Tandem Hf(OTf)<sub>4</sub>+Pd/C Catalysis. *ChemSusChem* **2019**, *12*, 5217-5223.
25. Mansley, Z. R.; Marks, L. D., Modified Winterbottom Construction Including Boundaries. *J. Phys. Chem. C* **2020**, *124* (51), 28038-28043.
26. Marks, T.J.; Gao, Y.; Kratish, Y.; Li, J. METHODS FOR DEPOLYMERIZING POLYESTERS. US Patent PCT/US2021/026822. April 12, 2021.
27. Mouat, A. R.; Whitford, C. L.; Chen, B.-R.; Liu, S. S.; Perras, F. A.; Pruski, M.; Bedzyk, M. J.; Delferro, M.; Stair, P. C.; Marks, T. J., Synthesis of Supported Pd<sup>0</sup> Nanoparticles from a Single-Site Pd<sup>2+</sup> Surface Complex by Alkene Reduction. *Chemistry of Materials* **2018**, *30* (3), 1032-1044.
28. Nauert, S. L.; Savereide, L.; Notestein, J. M., Role of Support Lewis Acid Strength in Copper-Oxide-Catalyzed Oxidative Dehydrogenation of Cyclohexane. *ACS Catalysis* **2018**, *8* (8), 7598-7607.
29. Nauert, S. L.; Rosen, A. S.; Kim, H.; Snurr, R. Q.; Stair, P. C.; Notestein, J. M., Evidence for copper dimers in low-loaded CuO<sub>x</sub>/SiO<sub>2</sub> catalysts for cyclohexane

- oxidative dehydrogenation. *ACS Catalysis* **2018**, *8*, 9775-9789.
30. Otake, K.; Ahn, S.; Knapp, J.; Hupp, J. T.; Notestein, J. M.; Farha, O. K., Vapor-Phase Cyclohexene Epoxidation by Single-Ion Fe(III) Sites in Metal-Organic Frameworks. *Inorg. Chem.* **2021**, *60* (4), 2457-2463.
  31. Paull, R. J.; Mansley, Z. R.; Ly, T.; Marks, L. D.; Poeppelmeier, K. R., Synthesis of Gadolinium Scandate from a Hydroxide Hydrogel. *Inorganic Chemistry* **2018**, *57* (7), 4104-4108.
  32. Paull, R. J.; Ly, T.; Mansley, Z. R.; Poeppelmeier, K. R.; Marks, L. D., Controlled Two-Step Formation of Faceted Perovskite Rare-Earth Scandate Nanoparticles. *Crystals* **2019**, *9* (4).
  33. Peng, A.; Kung, M. C.; Brydon, R. R. O.; Ross, M. O.; Qian, L.; Broadbelt, L. J.; Kung, H. H., Noncontact Catalysis: Initiation of Selective Ethylbenzene Oxidation by Au Cluster-Facilitated Cyclooctene Epoxidation. *Sci. Adv.* **2020**, *6*, eaax6637.
  34. Peng, A.; Kung, M. C.; Ross, M. O.; Hoffman, B. M.; Kung, H. H., The Role of Co-ZSM-5 Catalysts in Aerobic Oxidation of Ethylbenzene. *Top. Catal.* **2020**, *63* (19-20), 1708-1716.
  35. Rosen, A. S.; Mian, M. R.; Islamoglu, T.; Chen, H. Y.; Farha, O. K.; Notestein, J. M.; Snurr, R. Q., Tuning the Redox Activity of Metal-Organic Frameworks for Enhanced, Selective O-2 Binding: Design Rules and Ambient Temperature O-2 Chemisorption in a Cobalt-Triazolate Framework. *J. Am. Chem. Soc.* **2020**, *142* (9), 4317-4328.
  36. Rosen, A. S.; Notestein, J. M.; Snurr, R. Q., Comparing GGA, GGA plus U, and meta-GGA functionals for redox-dependent binding at open metal sites in metal-organic frameworks. *J. Chem. Phys.* **2020**, *152* (22), 12.
  37. Rosen, A. S.; Notestein, J. M.; Snurr, R. Q., High-Valent Metal-Oxo Species at the Nodes of Metal-Triazolate Frameworks: The Effects of Ligand Exchange and Two-State Reactivity for C-H Bond Activation. *Angew. Chem.-Int. Edit.* **2020**, *59* (44), 19494-19502.
  38. Rosen, A. S.; Notestein, J. M.; Snurr, R. Q., Identifying promising metal-organic frameworks for heterogeneous catalysis via high-throughput periodic density functional theory. *Journal of Computational Chemistry* **2019**, *40* (12), 1305-1318.
  39. Rosen, A. S.; Notestein, J. M.; Snurr, R. Q., Structure-Activity Relationships That Identify Metal-Organic Framework Catalysts for Methane Activation. *ACS Catalysis* **2019**, *9* (4), 3576-3587.
  40. Samek, I. A.; Bobbitt, N. S.; Snurr, R. Q.; Stair, P. C., Interactions of VO<sub>x</sub> Species with Amorphous TiO<sub>2</sub> Domains on ALD-Derived Alumina-Supported Materials. *The Journal of Physical Chemistry C* **2019**, *123* (13), 7988-7999.
  41. Samek, I. A.; Bobbitt, N. S.; Snurr, R. Q.; Stair, P. C., Structure and Activity of Mixed VO<sub>x</sub>-CeO<sub>2</sub> Domains Supported on Alumina in Cyclohexane Oxidative Dehydrogenation. *J. Catal.* **2020**, *384*, 147-158.
  42. Tang, X.; Liu, C.; Long, E.; Lin, W.; Hackler, R.; Wang, X.; Marks, L.; Notestein, J.; Stair, P. Sub-monolayer is enough: Switching Reaction Channels on Pt/SiO<sub>2</sub> by Atomic Layer Deposition. *J. Phys. Chem. C* **2021**, accepted.
  43. Wasson, M. C.; Otake, K.; Gong, X. Y.; Strathman, A. R.; Islamoglu, T.; Gianneschi, N. C.; Farha, O. K., Modulation of crystal growth and structure within cerium-based metal-organic frameworks. *Crystengcomm* **2020**, *22* (47), 8182-8188.
  44. Wasson, M. C.; Zhang, X.; Otake, K. I.; Rosen, A. S.; Alayoglu, S.; Krzyaniak, M. D.;

- Chen, Z. J.; Redfern, L. R.; Robison, L.; Son, F. A.; Chen, Y. W.; Islamoglu, T.; Notestein, J. M.; Snurr, R. Q.; Wasielewski, M. R.; Farha, O. K., Supramolecular Porous Assemblies of Atomically Precise Catalytically Active Cerium-Based Clusters. *Chem. Mat.* **2020**, *32* (19), 8522-8529.
45. Wang, Z.; Hou, X.; Wu, Y. Y.; Shen, J.; Li, T.; Fang, C.; Kung, M. C.; Kung, H. H., Controlled Generation of TiO<sub>x</sub>-Au Interface Using Titanium Molecular Complex Bearing Pyridyl Anchors: Synthesis, Characterization and Catalysis. *Topics in Catalysis* **2018**, *61* (9), 800-809.
46. Wu, W. Q.; Kwon, S.; McCarthy, J. A.; Stair, P. C.; Weitz, E., Mechanistic Studies of the Oxidation of Cyclohexene to 2-Cyclohexen-1-one over ALD Prepared Titania Supported Vanadia. *J. Phys. Chem. C* **2020**, *124* (22), 11844-11862.
47. Wu, W.; Savereide, L. M.; Notestein, J. M.; Weitz, E., In-situ IR spectroscopy as a Probe of Oxidation/Reduction of Ce in Nanostructured CeO<sub>2</sub>. *Applied Surface Science* **2018**, *445*, 548-554.
48. Ye, J. Q.; Dombrowski, J. P.; Hu, X. B.; Whitney-Warner, J.; Guo, S. H.; Kung, M. C.; Kung, H. H., Production of H<sub>2</sub>O<sub>2</sub> during Au/C catalyzed aerobic oxidation of 1,2-propanediol. *Appl. Catal. A-Gen.* **2020**, *599*, 117616.
49. Zhang, J. L.; Motta, A.; Gao, Y. S.; Stalzer, M. M.; Delferro, M.; Liu, B. P.; Lohr, T. L.; Marks, T. J., Cationic Pyridylamido Adsorbate on Bronsted Acidic Sulfated Zirconia: A Molecular Supported Organohafnium Catalyst for Olefin Homo- and Co-Polymerization. *ACS Catalysis* **2018**, *8* (6), 4893-4901.
50. Zhang, X.; Yan, P.; Zhao, B.; Liu, K.; Kung, M. C.; Kung, H. H.; Chen, S.; Zhang, Z. C., Selective Hydrodeoxygenation of Guaiacol to Phenolics by Ni/Anatase TiO<sub>2</sub> Catalyst Formed by Cross-Surface Migration of Ni and TiO<sub>2</sub>. *ACS Catalysis* **2019**, *9* (4), 3551-3563.
51. Zhang, J. L.; Mason, A. H.; Wang, Y.; Motta, A.; Kobayashi, T.; Pruski, M.; Gao, Y. S.; Marks, T. J., Beyond the Active Site. Cp\*ZrMe<sub>3</sub>/Sulfated Alumina-Catalyzed Olefin Polymerization Tacticity via Catalyst...Surface Ion-Pairing. *ChemCatChem* **2021**, 2564–2569.
52. Zhang, J. L.; Mason, A. H.; Motta, A.; Cesar, L. G.; Kratish, Y.; Lohr, T. L.; Miller, J. T.; Gao, Y. S.; Marks, T. J., Surface vs Homogeneous Organo-Hafnium Catalyst Ion-Pairing and Ligand Effects on Ethylene Homo- and Copolymerizations. *ACS Catal.* **2021**, *11* (6), 3239-3250.
53. Zhang, F. R.; Hu, X. B.; Roth, E. W.; Kim, Y. W.; Nguyen, S. T., Template-Assisted, Seed-Mediated Synthesis of Hierarchically Mesoporous Core-Shell UiO-66: Enhancing Adsorption Capacity and Catalytic Activity through Iterative Growth. *Chem. Mat.* **2020**, *32* (10), 4292-4302.

### **Publications Acknowledging this Grant in 2018-2021**

#### **Secondary Support from ICEP**

1. Ahn, S.; Nauert, S. L.; Buru, C. T.; Rimoldi, M.; Choi, H.; Schweitzer, N. M.; Hupp, J. T.; Farha, O. K.; Notestein, J. M., Pushing the Limits on Metal-Organic Frameworks as a Catalyst Support: NU-1000 Supported Tungsten Catalysts for o-Xylene Isomerization and Disproportionation. *Journal of the American Chemical Society* **2018**, *140* (27), 8535-8543.

2. Amsterdam, S. H.; Stanev, T. K.; Zhou, Q.; Lou, A. J. T.; Bergeron, H.; Darancet, P.; Hersam, M. C.; Stern, N. P.; Marks, T. J., Electronic Coupling in Metallophthalocyanine–Transition Metal Dichalcogenide Mixed-Dimensional Heterojunctions. *ACS Nano* **2019**, *13* (4), 4183-4190.
3. Barger, C. J.; Motta, A.; Weidner, V. L.; Lohr, T. L.; Marks, T. J., La[N(SiMe<sub>3</sub>)<sub>2</sub>]<sub>3</sub>–Catalyzed Reduction of Esters with Pinacolborane –Scope and Mechanism of Ester Cleavage. *ACS Catalysis* **2019**, *9*, 9015-9024.
4. Chapovetsky, A.; Langeslay, R. R.; Celik, G.; Perras, F. A.; Pruski, M.; Ferrandon, M. S.; Wegener, E. C.; Kim, H.; Dogan, F.; Wen, J. G.; Khetrapal, N.; Sharma, P.; White, J.; Kropf, A. J.; Sattelberger, A. P.; Kaphan, D. M.; Delferro, M., Activation of Low-Valent, Multiply M-M Bonded Group VI Dimers toward Catalytic Olefin Metathesis via Surface Organometallic Chemistry. *Organometallics* **2020**, *39* (7), 1035-1045.
5. Celik, G.; Kennedy, R. M.; Hackler, R. A.; Ferrandon, M.; Tennakoon, A.; Patnaik, S.; LaPointe, A. M.; Ammal, S. C.; Heyden, A.; Perras, F. A.; Pruski, M.; Scott, S. L.; Poepelmeier, K. R.; Sadow, A. D.; Delferro, M., Upcycling Single-Use Polyethylene into High-Quality Liquid Products. *ACS Central Science* **2019**, *5* (11), 1795-1803.
6. Chen, Y.; Yang, L.; Wu, J.; Wang, G.; Huang, W.; Melkonyan, F. S.; Lu, Z.; Huang, Y.; Marks, T. J.; Facchetti, A., Performance, Morphology, and Charge Recombination Correlations in Ternary Squaraine Solar Cells. *Chemistry of Materials* **2018**, *30* (19), 6810-6820.
7. Chen, J. Z.; Motta, A.; Zhang, J. L.; Gao, Y. S.; Marks, T. J., Mechanism of Organoscandium-Catalyzed Ethylene Copolymerization with Amino-Olefins: A Quantum Chemical Analysis. *ACS Catalysis* **2019**, *9* (9), 8810-8818.
8. Chen, J.; Motta, A.; Wang, B.; Gao, Y.; Marks, T. J., Facilitating Polar Comonomer Enchainment in Zirconocene-Catalyzed, Masking Reagent-Free, Ethylene Copolymerization. *Angewandte Chemie International Edition* **2019**, *58*, 7030-7034.
9. Cho, S.; Park, W.; Kim, H.; Jokisaari, J. R.; Roth, E. W.; Lee, S.; Klie, R. F.; Lee, B.; Kim, D., Gallstone-Formation-Inspired Bimetallic Supra-nanostructures for Computed-Tomography-Image-Guided Radiation Therapy. *ACS Applied Nano Materials* **2018**, *1* (9), 4602-4611.
10. Cui, C.; Ji, X.; Wang, P.; Xu, G.; Chen, L.; Chen, J.; Kim, H.; Ren, Y.; Chen, F.; Yang, C.; Fan, X.; Luo, C.; Amine, K.; Wang, C., Integrating Multi-Redox Centers into one Framework for High Performance Organic Li-Ion Battery Cathode. *ACS Energy Lett.* **2020**, *5*, 224–231.
11. Dey, A. B.; Sanyal, M. K.; Keane, D. T.; Campbell, G. P.; Liu, B. H.; Farrer, I.; Ritchie, D. A.; Bedzyk, M. J., X-ray atomic mapping of quantum dots. *Phys. Rev. Mater.* **2020**, *4* (5), 056002.
12. Du, M.; Agrawal, A. M.; Chakraborty, S.; Garibay, S. J.; Limvorapitux, R.; Choi, B.; Madrahimov, S. T.; Nguyen, S. T., Matching the Activity of Homogeneous Sulfonic Acids: The Fructose-to-HMF Conversion Catalyzed by Hierarchically Porous Sulfonic-Acid-Functionalized Porous Organic Polymer (POP) Catalysts. *ACS Sustainable Chemistry & Engineering* **2019**, *7* (9), 8126-8135.
13. Gao, Y. S.; Chen, J. Z.; Wang, Y.; Pickens, D. B.; Motta, A.; Wang, Q. J.; Chung, Y. W.; Lohr, T. L.; Marks, T. J., Highly branched polyethylene oligomers via group IV-catalysed polymerization in very nonpolar media. *Nature Catalysis* **2019**, *2* (3), 236-242.

14. Gao, Y.; Christianson, M. D.; Wang, Y.; Chen, J.; Marshall, S.; Klosin, J.; Lohr, T. L.; Marks, T. J., Unusual Precatalyst  $\sigma$ -Ligand Effects on Phenoxyimine Zr-Catalyzed Ethylene/1-Octene Copolymerizations. *Journal of the American Chemical Society* **2019**, *141*, 7822–7830.
15. Goetjen, T. A.; Zhang, X.; Liu, J.; Hupp, J. T.; Farha, O. K., A Metal-Organic Framework Supported Single Site Chromium (III) Catalyst for Ethylene Oligomerization at Low Pressure and Temperature. *ACS Sustainable Chemistry & Engineering* **2019**, *7*, 2553-2557.
16. Hicks, K. E.; Rosen, A. S.; Syed, Z. H.; Snurr, R. Q.; Farha, O. K.; Notestein, J. M., Zr6O8 Node-Catalyzed Butene Hydrogenation and Isomerization in the Metal-Organic Framework NU-1000. *ACS Catal.* **2020**, *10* (24), 14959-14970.
17. Kang, D. E., J.W.; Libera, J.A.; Liang, Y.; Kim, H.; Mane, A. Method to remove undesired lithium carbonate and coating aluminum oxide on ceramic solid-state electrolytes. 2020.
18. Kwon, G.; Jang, H.; Lee, J.-S.; Mane, A.; Mandia, D. J.; Soltau, S. R.; Utschig, L. M.; Martinson, A. B. F.; Tiede, D. M.; Kim, H.; Kim, J., Resolution of Electronic and Structural Factors Underlying Oxygen-Evolving Performance in Amorphous Cobalt Oxide Catalysts. *Journal of the American Chemical Society* **2018**, *140* (34), 10710-10720.
19. Langeslay, R. R.; Sohn, H.; Hu, B.; Mohar, J. S.; Ferrandon, M.; Liu, C.; Kim, H.; Kropf, A. J.; Yang, C.; Niklas, J.; Potuektov, O. G.; Alp, E. E.; Ignacio-de Leon, P.; Sattelberger, A. P.; Hock, A. S.; Delferro, M., Nuclearity effects in supported, single-site Fe(II) hydrogenation pre-catalysts. *Dalton Transactions* **2018**, *47* (32), 10842-10846.
20. Lin, W.; Schatz, G. C., Mechanisms of Formaldehyde and C<sub>2</sub> Formation from Methylene Reacting with CO<sub>2</sub> Adsorbed on Ni(110). *The Journal of Physical Chemistry C* **2018**, *122* (25), 13827-13833.
21. Lyu, J.; Gong, X.; Lee, S.; Gnanasekaran, K.; Zhang, Z.; Wasson, M. C.; Wang, X.; Bai, P.; Guo, X.; Gianneschi, N. C.; Farha, O. K., In Situ Monitoring of Phase Transition in Metal–Organic Frameworks through Variable Temperature Liquid-Cell Transmission Electron Microscopy and X-Ray Diffraction. *J. Am. Chem. Soc.* **2020**, *142*, 4609–4615.
22. Liu, C.; Notestein, J. M.; Weitz, E.; Gray, K. A., Photo-Initiated Reduction of CO<sub>2</sub> by H<sub>2</sub> on Silica Surface. *ChemSusChem* **2018**, *11* (7), 1163-1168.
23. McCullough, L. R.; Cheng, E. S.; Gosavi, A. A.; Kilos, B. A.; Barton, D. G.; Weitz, E.; Kung, H. H.; Notestein, J. M., Gas phase acceptorless dehydrogenative coupling of ethanol over bulk MoS<sub>2</sub> and spectroscopic measurement of structural disorder. *Journal of Catalysis* **2018**, *366*, 159-166.
24. Moribe, S.; Chen, Z.; Alayoglu, S.; Syed, Z. H.; Islamoglu, I.; Farha, O. K., Ammonia Capture within Isoreticular Metal–Organic Frameworks with Rod Secondary Building Units. *ACS Materials Letters* **2019**, *1*, 476-480.
25. Moody, M. J.; Henning, A.; Jurca, T.; Shang, J. Y.; Bergeron, H.; Balla, I.; Olding, J. N.; Weiss, E. A.; Hersam, M. C.; Lohr, T. L.; Marks, T. J.; Lauhon, L. J., Atomic Layer Deposition of Molybdenum Oxides with Tunable Stoichiometry Enables Controllable Doping of MoS<sub>2</sub>. *Chemistry of Materials* **2018**, *30* (11), 3628-3632.
26. Moreau, L. M.; Jones, M. R.; Roth, E. W.; Wu, J.; Kewalramani, S.; O'Brien, M. N.;

- Chen, B.-R.; Mirkin, C. A.; Bedzyk, M. J., The Role of Trace Ag in the Synthesis of Au Nanorods *Nanoscale* **2019**, *11*, 11744-11754.
27. Savereide, L.; Nauert, S. L.; Roberts, C. A.; Notestein, J. M., The effect of support morphology on CoO<sub>x</sub>/CeO<sub>2</sub> catalysts for the reduction of NO by CO. *Journal of Catalysis* **2018**, *366*, 150-158.
  28. Savereide, L.; Gosavi, A.; Hicks, K. E.; Notestein, J. M., Identifying properties of low-loaded CoO<sub>x</sub>/CeO<sub>2</sub> via X-ray Absorption Spectroscopy for NO reduction by CO. *Journal of Catalysis* **2020**, *381*, 355-362.
  29. Teich, J.; Dvir, R.; Henning, A.; Hemo, E.; Moody, M. J.; Jurca, T.; Cohen, H.; Marks, T. J.; Rosen, B.; Lahuon, L.; Ismach, A., Light and Complex 3D MoS<sub>2</sub>/graphene Heterostructures as an Efficient Catalyst for HER. **2019** (submitted).
  30. Wang, F.; Chen, Z.; Chen, H.; Goetjen, T. A.; Li, P.; Wang, X.; Alayoglu, S.; Ma, K.; Chen, Y.; Wang, T.; Islamoglu, T.; Fang, Y.; Snurr, R. Q.; Farha, O. K., Interplay of Lewis and Brønsted Acid Sites in Zr-Based Metal–Organic Frameworks for Efficient Esterification of Biomass-Derived Levulinic Acid. *ACS Applied Materials & Interfaces* **2019**, *11* (35), 32090-32096.
  31. Wang, T. T.; Gong, W. B.; He, X.; Kou, Z. H.; Tan, G.; Zhou, S. J.; Yu, H. T.; Fan, M. H.; Kung, H. H., Synthesis of Highly Nanoporous beta-Silicon Carbide from Corn Stover and Sandstone. *ACS Sustain. Chem. Eng.* **2020**, *8* (39), 14896-14904.
  32. Wolek, A. T. Y.; Ardagh, M. A.; Pham, H.N.; Alayoglu, S.; Abhaya, D.K.; Notestein, J. M., Creating Brønsted Acidity at the SiO<sub>2</sub>-Nb<sub>2</sub>O<sub>5</sub> Interface. *J. Catal.* **2021**, *394*, 387-396.
  33. Yan, H.; He, K.; Samek, I.A.; Jing, D.; Nanda, M.G.; Stair, P.C.; Notestein, J.M. Tandem In<sub>2</sub>O<sub>3</sub>-Pt/Al<sub>2</sub>O<sub>3</sub> catalyst for coupling propane dehydrogenation to selective H<sub>2</sub> combustion at the nanoscale. *Science* **2021**, *371*, 1257-1260.
  34. Yang, Y.; Zhang, X.; Kanchanakungwankul, S.; Lu, Z. Y.; Noh, H.; Syed, Z. H.; Farha, O. K.; Truhlar, D. G.; Hupp, J. T., Unexpected "Spontaneous" Evolution of Catalytic, MOF-Supported Single Cu(II) Cations to Catalytic, MOF-Supported Cu(0) Nanoparticles. *Journal of the American Chemical Society* **2020**, *142* (50), 21169-21177.
  35. Yuan, W.; Ma, Q.; Liang, Y.; Sun, C.; Narayanachari, K. V. L. V.; Bedzyk, M. J.; Takeuchi, I.; Haile, S. M., Unusual trends in the enhanced Ce<sup>3+</sup> surface concentration in ceria-zirconia catalyst materials. *J. Mater. Chem. A.* **2020**, *8*, 9850-9858.
  36. Zee, D. Z.; Harris, T. D., Enhancing catalytic alkane hydroxylation by tuning the outer coordination sphere in a heme-containing metal-organic framework. *Chem. Sci.* **2020**, *11* (21), 5447-5452.

### **Publications Acknowledging this Grant in 2018-2021**

#### **Reviews and Perspectives**

1. Chen, Z. J.; Wasson, M. C.; Drout, R. J.; Robison, L.; Idrees, K. B.; Knapp, J. G.; Son, F. A.; Zhang, X.; Hierse, W.; Kuhn, C.; Marx, S.; Hernandez, B.; Farha, O. K., The state of the field: from inception to commercialization of metal-organic frameworks. *Faraday Discuss.* **2021**, *225* (0), 9-69.
2. Hargreaves, J. S. J.; Chung, Y. M.; Ahn, W. S.; Hisatomi, T.; Domen, K.; Kung, M. C.; Kung, H. H., Minimizing energy demand and environmental impact for sustainable NH<sub>3</sub> and H<sub>2</sub>O<sub>2</sub> production-A perspective on contributions from thermal, electro-, and photo-catalysis. *Appl. Catal. A-Gen.* **2020**, *594*, 117419.

- Jones, L. O.; Mosquera, M. A.; Schatz, G. C.; Ratner, M. A., Embedding Methods for Quantum Chemistry: Applications from Materials to Life Sciences. *J. Am. Chem. Soc.* **2020**, *142* (7), 3281-3295.
- Ma, K. K.; Idrees, K. B.; Son, F. A.; Maldonado, R.; Wasson, M. C.; Zhang, X.; Wang, X. J.; Shehayeb, E.; Merhi, A.; Kaafarani, B. R.; Islamoglu, T.; Xin, J. H.; Farha, O. K., Fiber Composites of Metal-Organic Frameworks. *Chem. Mat.* **2020**, *32* (17), 7120-7140.
- Mosquera, M. A.; Jones, L. O.; Ratner, M. A.; Schatz, G. C., Quantum embedding for material chemistry based on domain separation and open subsystems. *Int. J. Quantum Chem.* **2020**, *120* (21), 13.
- Wasson, M. C.; Buru, C. T.; Chen, Z. J.; Islamoglu, T.; Farha, O. K., Metal-organic frameworks: A tunable platform to access single-site heterogeneous catalysts. *Applied Catalysis A* **2019**, *586*, 20.
- Zhang, X.; Chen, Z. J.; Liu, X. Y.; Hanna, S. L.; Wang, X. J.; Taheri-Ledari, R.; Maleki, A.; Li, P.; Farha, O. K., A historical overview of the activation and porosity of metal-organic frameworks. *Chem. Soc. Rev.* **2020**, *49* (20), 7406-7427.
- Zhang, X.; Wasson, M. C.; Shayan, M.; Berdichevsky, E. K.; Ricardo-Noordberg, J.; Singh, Z.; Papazyan, E. K.; Castro, A. J.; Marino, P.; Ajoyan, Z.; Chen, Z. J.; Islamoglu, T.; Howarth, A. J.; Liu, Y. Y.; Majewski, M. B.; Katz, M. J.; Mondloch, J. E.; Farha, O. K., A historical perspective on porphyrin-based metal-organic frameworks and their applications. *Coord. Chem. Rev.* **2021**, *429*, 22.

### Select Leadership Activities by ICEP PIs

National Academy of Science (T. Marks, Schatz)  
National Academy of Engineering (Broadbelt, T. Marks)

Editorial Board Chair, *Energy & Environmental Science* (Hupp)  
Editor-in-Chief, *Applied Catalysis A* (Kung)  
Editor-in-Chief (2005-2019), *Journal of Physical Chemistry* (Schatz),

#### Editing and Editorial Boards:

- *ACS Applied Materials & Interfaces* (Farha)
- *Acta Crystallographia A* (L. Marks)
- *Adsorption* (Snurr)
- *Adsorption Science & Technology* (Snurr)
- *Applied Catalysis A* (Notestein)
- *Current Opinion in Chemical Engineering* (Snurr)
- *Industrial Engineering & Chemistry Research* (Broadbelt, Kung)
- *Journal of Physical Chemistry* (Weitz)
- *Molecular Systems Design & Engineering* (Snurr)
- *Solid State Chemistry* (Poepelmeier)

Scientific Advisory Council, Materials Science Division, Argonne Nat. Lab (Bedzyk)  
Deputy Director, DOE EFRC for Inorganometallic Catalyst Design (Hupp)  
Scientific Advisory Board, Joint Center for Artificial Photosynthesis (Hupp)

Meeting Chair, 26<sup>th</sup> Meeting of the North American Catalysis Society, (Notestein)  
Board Member, Max Planck Institute for Chemical Physics of Solids (Poepelmeier)  
Catalysis Club of Chicago President 2019-2020 (Schweitzer)

**Select Awards by ICEP Members in 2020-2021**

Ernest W. Thiele Award (Chicago Section of AIChE):

Linda Broadbelt

McBride Award (Northwestern University's Highest Staff Service Award):

Yosi Kratish (Postdoc, T. Marks Lab)

Presidential Fellow (Northwestern University's Highest Graduate Student Award):

Andrew Rosen (Notestein and Snurr Labs)

**Fundamental studies of the multifunctional electrocatalysis on heteroatom-doped carbon (CN<sub>x</sub>) catalysts**

Umit S. Ozkan, Dishari Basu, Vance Gustin, Deeksha Jain, Qiang Zhang, Jonathan Hightower, Seval Gunduz, Aravind Asthagiri, Yehia Khalifa<sup>1</sup>, Anne Co<sup>1</sup>  
The Ohio State University, Department of Chemical and Biomolecular Engineering  
<sup>1</sup>The Ohio State University, Department of Chemistry and Biochemistry

**Presentation Abstract**

Nitrogen-doped carbon nanostructures (CN<sub>x</sub>) are widely studied for electrocatalytic technologies such as PEM fuel cells owing to their economic feasibility and versatile applicability. Previously, we demonstrated the dual functionalities of CN<sub>x</sub> for both electrocatalytic oxygen reduction and oxygen evolution reactions (ORR & OER respectively). While continuing the quest to understand the nature of active sites on CN<sub>x</sub> for ORR, in this reporting period, we have ventured into the exploration of its versatility as an electrocatalyst for the bromine evolution reaction (BER) as well. Thus, our current efforts have focused on: (i) investigating the potential of CN<sub>x</sub> as an electrocatalyst for BER compared to other nitrogen devoid carbon supports (e.g., Vulcan carbon) using a combination of experimental and computational (density functional theory, DFT) methods (ii) investigating the potential of CN<sub>x</sub> as a support for platinum (Pt) catalyzed BER compared to commercial carbon supported Pt (iii) using post reaction characterization and DFT as aids for gaining insights into the role of nitrogen functionalities at different stages during ORR (iv) using in-situ surface characterization, DFT calculations and bicarbonate ion as molecular probe for investigating the nature of ORR active centers in CN<sub>x</sub>. Thus, our efforts are targeted towards exploring the applicability of CN<sub>x</sub> as an electrocatalyst or as a support, as well as gaining fundamental insights into its structural properties responsible for electrocatalytic ORR and BER, using ex-situ and in-situ characterization techniques, molecular probes and DFT calculations.

**Grant Number:** DE-FG02-07ER15896

**Grant Title:** Fundamental studies of the multifunctional electrocatalysis on heteroatom-doped carbon (CN<sub>x</sub>) catalysts

**P.I.:** Umit S. Ozkan, **Co-PIs:** Aravind Asthagiri, Anne Co

**Students:** Dishari Basu, Vance Gustin, Deeksha Jain, Qiang Zhang, Jonathan Hightower

**Undergraduate students:** Judy Garzanich, Koleen Avery, Corey Sceranka, Benjamin Rudzinski, Callista Krebs, Benjamin Naragon

**Collaborators:** Seval Gunduz, Yehia Khalifa

## RECENT PROGRESS

### CNx as Electrocatalysts for Bromine Evolution Reaction

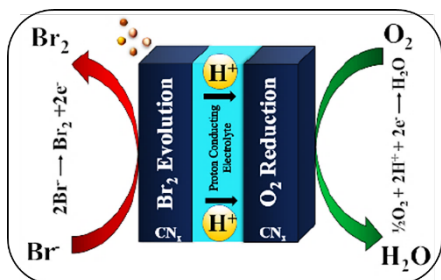


Figure 1: CN<sub>x</sub> proposed to be used as an oxygen depolarized cathode and anodic bromine evolution electrocatalyst for bromine generation

Direct oxidation of bromide ions to generate bromine has been applied in the context of purifying water to prevent the formation of carcinogenic by-products and for bromine generation from electrolysis of brine. Owing to its previously demonstrated halide poisoning resistance during ORR, CN<sub>x</sub> has the potential to be applied as an oxygen depolarized cathode catalyst (Figure 1). We further explored its potential as the anodic electrocatalyst during bromine evolution reaction (BER).

Figure 2(a) shows the negligible current evolution associated with the concurrent oxygen evolution

reaction (OER) and increasing BER current density with increasing dissolved bromide (Br<sup>-</sup>) concentration which begins at a Br<sup>-</sup> concentration as low as 5mM. The current density at 1.2 V, which is higher than the thermodynamic BER potential of 1.07 V, can be used a measure of the BER activity. As shown in Figure 2(b), the current density associated with BER at 1.2V increases with increasing bromide (Br<sup>-</sup>) concentration. Figure 2(c) compares the BER activity in terms of current density at 1.2V and 1.3V on the three

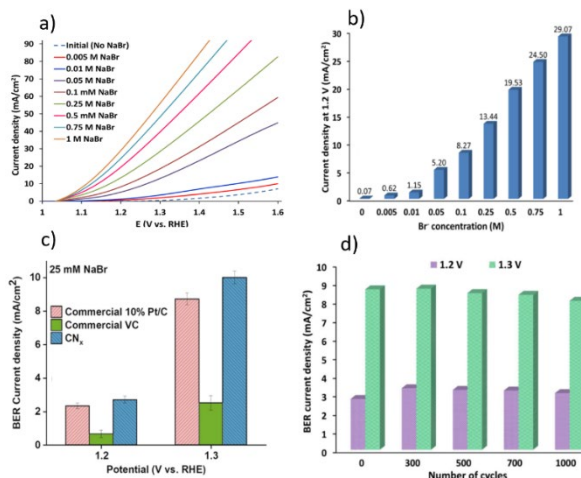


Figure 2: a) LSVs of CN<sub>x</sub> in presence of increasing concentrations of dissolved Br<sup>-</sup> ions and b) BER current density at 1.2 V with varying concentration of dissolved Br<sup>-</sup> ions c) Comparison of BER activity of CN<sub>x</sub>, 10% Pt/C and VC in presence of 25mM Br<sup>-</sup>. Potential hold experiments are reported at 1.2 and 1.3 V. d) Results of accelerated durability testing on CN<sub>x</sub> with 25mM Br<sup>-</sup>

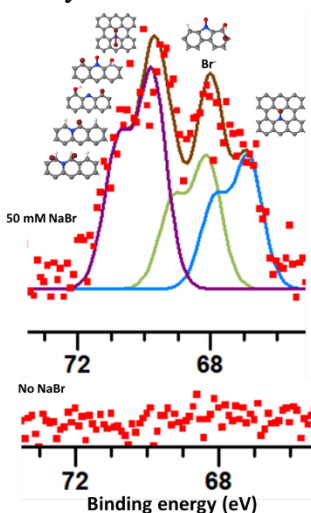


Figure 3: Br-3d XPS spectra collected on electrode tips before (bottom) and after (top) exposure to BER conditions

model catalysts – CN<sub>x</sub>, 10% Pt/C (commercial) and Vulcan

Carbon (VC, commercial). At 25 mM Br<sup>-</sup> concentration, the BER activity of CN<sub>x</sub> is better than 10% Pt/C which is especially significant while considering the much higher cost of the latter. Figure 2(d) demonstrates the stability of CN<sub>x</sub> after cycling under highly oxidizing potentials even up to 1000 cycles in presence of 25mM dissolved Br<sup>-</sup> ion.

Post reaction XPS characterization on the electrode tips (shown in Figure 3) in conjunction with DFT studies were used to propose a plausible BER mechanism over CN<sub>x</sub> sites. This study outlines guidelines for the design of electrocatalysts and the explores the nature of active sites on CN<sub>x</sub> materials for electrochemical bromine production.

## CNx supported Platinum for electrocatalytic Bromine Evolution

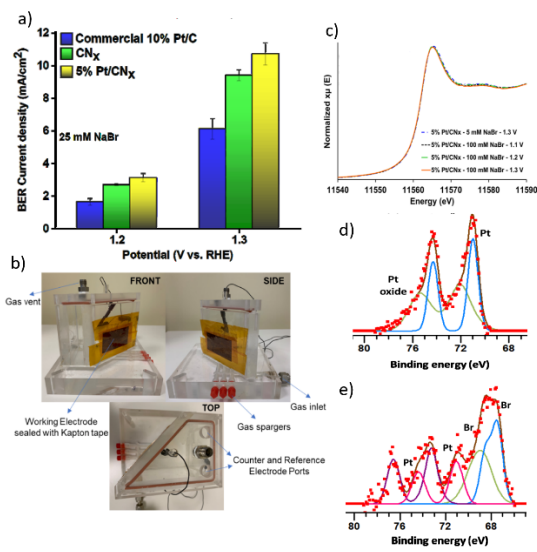


Figure 4: a) BER activity of 5% Pt/CNx compared to 10% Pt/VC and CNx with 25mM NaBr dissolved b) Operando XAS cell c) Operando XANES spectra of 5% Pt/CNx collected during BER with 5 mM and 100 mM NaBr at 1.1V-1.3V d) Post reaction XPS spectra collected in the Pt 4f region on the bare 5% Pt/CNx ink e) Post reaction XPS spectra collected in the Pt 4f region on 5% Pt/CNx held at 1.2 V with 50 mM dissolved NaBr

Figure 4(a) shows the synergistic effect of supporting Pt on CNx during BER. As compared to commercial Vulcan carbon supported Pt catalysts with 10% Pt loading (10% Pt/C), the BER activity of 5% Pt/CNx is found to be better. CNx, when used as a catalyst support, can allow lower loading of Pt with higher BER activity as compared to both CNx as well as commercial 10% Pt/C, indicating a synergistic effect between the Pt and CNx catalyst support. An in-situ XAS cell was designed to study the oxidation state of Pt during BER and OER as shown in Figure 4(b). The results in Figure 4(c) indicate that the bulk structure of Pt remains stable under BER conditions in the range of potentials between 1.1 and 1.3 V whereas post reaction XPS (Figure 4(d) and 4(e)) confirms that BER on Pt/CNx occurs on the surface, showing Br<sup>-</sup> adsorption on Pt sites in the Pt 4f XPS region.

## Changes in Active Sites on CNx Under ORR: A Combined Post-Reaction Characterization and DFT Study

Post-reaction XPS and DFT calculations can be useful in identifying changes that occur in

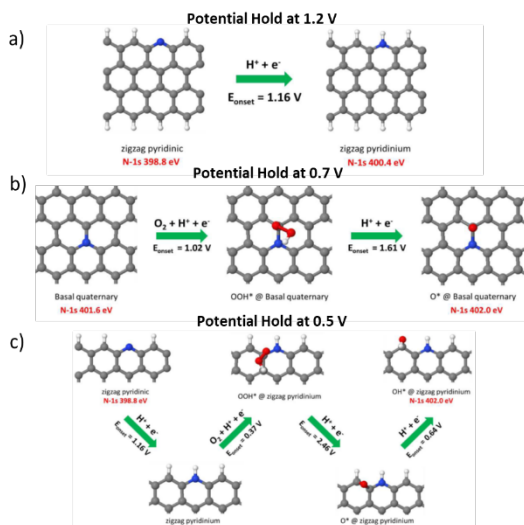


Figure 5: a) Protonation of zigzag pyridinic N sites to zigzag pyridinium on application of 1.2 V b) Formation of ORR intermediates on basal quaternary sites during potential hold at 0.7 V. c) ORR proceeding via the associative mechanism at 0.5 V on carbon next to zigzag pyridinium sites

nitrogen functionalities in CNx type catalysts under ORR conditions. Phenomena such as protonation and formation of ORR intermediates that take place on the electrode surface at various applied overpotentials in acidic electrolytes can result in significant changes in the nitrogen distribution in CNx that can be quantified and explained using post-reaction XPS measurements and DFT calculations as shown in Figure 5(a)- 5(c). Even before reaching the onset potential, ORR intermediates are formed on the carbon sites adjacent to nitrogen in CNx, however, strongly adsorbed intermediates prevent the reaction from turning over completely.

### Bicarbonate Poisoning of CN<sub>x</sub> Catalysts for ORR

In this phase of the study, we used the bicarbonate ion as a molecular probe, in conjunction with DFT models and NAP-XPS experiments to investigate the activity of CN<sub>x</sub> catalysts. Electrochemical measurements showed a decrease in the ORR activity of CN<sub>x</sub> after exposure to bicarbonate ions through CO<sub>2</sub> saturation of the electrolyte as shown in Figure 6(a). The poisoning effect of the bicarbonate ions was confirmed through sodium bicarbonate additions experiments, shown in Figure 6 (b).

DFT predictions indicated that partial poisoning of the active sites in CN<sub>x</sub> could occur as a result of strong HCO<sub>3</sub><sup>-</sup> adsorption confirming the experimental results. By combining NAP-XPS

experiments of CN<sub>x</sub> samples in the presence of oxygen and carbon dioxide with DFT calculations, the impact of bicarbonate poisoning was evaluated (Figure 7). High resolution N1s spectra

showed a decrease in the pyridinic nitrogen content for pristine CN<sub>x</sub> between the UHV and 2 mbar O<sub>2</sub> spectrum indicating adsorption on those sites. The bicarbonate poisoned CN<sub>x</sub>-HCO<sub>3</sub><sup>-</sup> sample showed minimal change in pyridinic nitrogen content, supporting the

hypothesis that the bicarbonate adsorption poisons the ORR active sites. Examination of the N1s difference spectra showed two peaks in the pyridinic nitrogen region for pristine CN<sub>x</sub> (398 eV and 399 eV) and only one peak (398 eV) for poisoned CN<sub>x</sub>. These results suggest that the higher binding energy peaks may be more susceptible to HCO<sub>3</sub><sup>-</sup> poisoning. The N1s difference spectra of pristine CN<sub>x</sub> in the presence of CO<sub>2</sub> showed weak adsorption behavior on zigzag pyridinic nitrogen (398 eV), and armchair/basal quaternary nitrogen (401.4 eV and 402.4 eV) confirming DFT predictions.

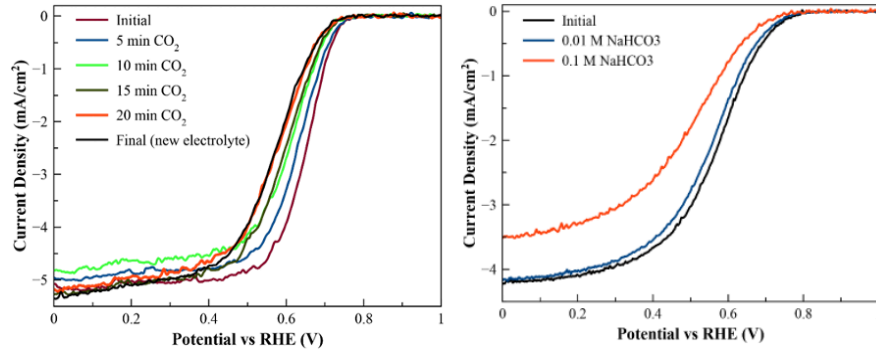


Figure 6: Polarization curves of CN<sub>x</sub> in 0.1 M HClO<sub>4</sub> electrolyte with (a) incremental exposure to carbon dioxide (b) with various concentrations of NaHCO<sub>3</sub>

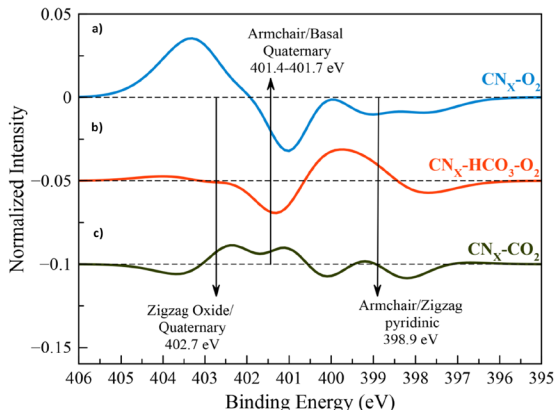


Figure 7: NAP-XPS N1s difference spectra of UHV spectra subtracted from i) for pristine CN<sub>x</sub> under 2 mbar O<sub>2</sub>, ii) ex-situ poisoned CN<sub>x</sub>-HCO<sub>3</sub><sup>-</sup> under 2 mbar O<sub>2</sub> and iii) pristine CN<sub>x</sub> under 2 mbar CO<sub>2</sub>

## Publications Acknowledging this Grant in 2018-2021

Please classify your publications into two categories according to the source of support for the work published:

(XXVIII) *Intellectually led by this grant*

1. Jain, D.; Gustin, V.; Basu, D.; Gunduz, S.; Deka, D. J.; Co, A. C.; Ozkan, U. S., Phosphate tolerance of nitrogen-coordinated-iron-carbon (FeNC) catalysts for oxygen reduction reaction: A size-related hindrance effect. *Journal of Catalysis* **2020**, *390*, 150-160.
2. Jain, D.; Zhang, Q.; Gustin, V.; Hightower, J.; Gunduz, S.; Co, A. C.; Miller, J. T.; Asthagiri, A.; Ozkan, U. S., Experimental and DFT Investigation into Chloride Poisoning Effects on Nitrogen-Coordinated Iron–Carbon (FeNC) Catalysts for Oxygen Reduction Reaction. *The Journal of Physical Chemistry C* **2020**, *124* (19), 10324-10335.
3. Jain, D.; Ozkan, U. S., Electrocatalytic applications of heteroatom-doped carbon nanostructures: thinking beyond PEM fuel cells. *The Royal Society of Chemistry* **2020**; Vol. 32.
4. Jain, D.; Zhang, Q.; Hightower, J.; Gustin, V.; Asthagiri, A.; Ozkan, U. S., Changes in Active Sites on Nitrogen-Doped Carbon Catalysts Under Oxygen Reduction Reaction: A Combined Post-Reaction Characterization and DFT Study. *ChemCatChem* **2019**, *11* (24), 5945-5950.
5. Zhang, Q.; Asthagiri, A., Solvation effects on DFT predictions of ORR activity on metal surfaces. *Catalysis Today* **2019**, *323*, 35-43.
6. Mamtani, K.; Ozkan, U. S., Nitrogen-Doped Carbon Nanostructures as Oxygen Reduction Reaction (ORR) and Oxygen Evolution Reaction (OER) Electrocatalysts in Acidic Media. *Handbook of Graphene, Volume 5: Energy, Healthcare, and Environmental Applications* **2019**, 373.
7. Jain, D.; Mamtani, K.; Gustin, V.; Gunduz, S.; Celik, G.; Waluyo, I.; Hunt, A.; Co, A. C.; Ozkan, U. S., Enhancement in Oxygen Reduction Reaction Activity of Nitrogen-Doped Carbon Nanostructures in Acidic Media through Chloride-Ion Exposure. *ChemElectroChem* **2018**, *5*, 1966–1975.
8. Mamtani, K.; Singh, D.; Dogu, D.; Jain, D.; Millet, J.-M. M.; Ozkan, U. S., Effect of acid-washing on the nature of bulk characteristics of nitrogen-doped carbon nanostructures as oxygen reduction reaction electrocatalysts in acidic media. *Energy & Fuels* **2018**, *32* (10), 11038-11045.
9. Mamtani, K.; Jain, D.; Dogu, D.; Gustin, V.; Gunduz, S.; Co, A. C.; Ozkan, U. S., Insights into oxygen reduction reaction (ORR) and oxygen evolution reaction (OER) active sites for nitrogen-doped carbon nanostructures (CNx) in acidic media. *Applied Catalysis B: Environmental* **2018**, *220*, 88-97.

(XXIX) *Jointly funded by this grant and other grants with intellectual leadership by other funding sources*

1. Deka, D. J.; Kim, J.; Gunduz, S.; Jain, D.; Shi, Y.; Miller, J. T.; Co, A. C.; Ozkan, U. S., Coke formation during high-temperature CO<sub>2</sub> electrolysis over AFeO<sub>3</sub> (A= La/Sr) cathode: Effect of A-site metal segregation. *Applied Catalysis B: Environmental* **2021**, *283*, 119642.

2. Gunduz, S.; Deka, D. J.; Kim, J.; Wilson, M.; Warren, M.; Ozkan, U. S., Incident-angle dependent operando XAS cell design: investigation of the electrochemical cells under operating conditions at various incidence angles. *RSC Advances* **2021**, *11* (12), 6456-6463.
3. Deka, D. J.; Kim, J.; Gunduz, S.; Aouine, M.; Millet, J.-M. M.; Co, A. C.; Ozkan, U. S., Investigation of hetero-phases grown via in-situ exsolution on a Ni-doped (La, Sr) FeO<sub>3</sub> cathode and the resultant activity enhancement in CO<sub>2</sub> reduction. *Applied Catalysis B: Environmental* **2021**, *286*, 119917.
4. Deka, D. J.; Kim, J.; Gunduz, S.; Ferree, M.; Co, A. C.; Ozkan, U. S., Temperature-induced changes in the synthesis gas composition in a high-temperature H<sub>2</sub>O and CO<sub>2</sub> co-electrolysis system. *Applied Catalysis A: General* **2020**, *602*, 117697.
5. Deka, D. J.; Gunduz, S.; Kim, J.; Fitzgerald, T.; Shi, Y.; Co, A. C.; Ozkan, U. S., Hydrogen production from water in a solid oxide electrolysis cell: effect of Ni doping on lanthanum strontium ferrite perovskite cathodes. *Industrial & Engineering Chemistry Research* **2019**, *58* (50), 22497-22505.
6. Deka, D. J.; Gunduz, S.; Fitzgerald, T.; Miller, J. T.; Co, A. C.; Ozkan, U. S., Production of syngas with controllable H<sub>2</sub>/CO ratio by high temperature co-electrolysis of CO<sub>2</sub> and H<sub>2</sub>O over Ni and Co-doped lanthanum strontium ferrite perovskite cathodes. *Applied Catalysis B: Environmental* **2019**, *248*, 487-503.
7. Dogu, D.; Gunduz, S.; Meyer, K. E.; Deka, D. J.; Ozkan, U. S., CO<sub>2</sub> and H<sub>2</sub>O Electrolysis Using Solid Oxide Electrolyzer Cell (SOEC) with La and Cl-doped Strontium Titanate Cathode. *Catalysis Letters* **2019**, *149* (7), 1743-1752.

#### **Awards or leadership activities during 2018-2020 calendar years**

- 2018 The Ohio State University, College of Engineering, Lumley Interdisciplinary Research Award
- 2019 Honored by an Endowed Professorship created in her name (Ozkan Professorship)
- 2019 Honored by a special issue of *Catalysis Today* (Volume 323, 270 pages, 2019).
- Served as the Vice-Chair of the 17th International Congress in Catalysis (ICC-2020).
- Serves on the Board of Directors of the North American Catalysis Society (2000-present)
- Serves on the Executive Committee of the ACS Energy and Fuels Division
- Serves on Editorial Boards of
  - *Catalysis Today*
  - *Journal of Molecular Catalysis*
  - *Catalysis Letters*
  - *Topics in Catalysis*
  - *The Royal Society of Chemistry, Catalysis Book Series*
  - *Catalysis Reviews, Science and Engineering*
  - *Applied Catalysis B*

- *Catalysis Review*
- *ACS Applied Energy Materials*
- *Nature Sustainability*
- *Journal of Catalysis*
- *ACS Catalysis*.

## Crystalline Matrix Isolation of Catalysts and Catalyst Intermediates

David C. Powers  
Texas A&M University, Department of Chemistry

### Presentation Abstract

Direct characterization of the reactive intermediates responsible for bond-breaking and -making during catalysis is inherently challenging due to the fleeting lifetimes of these species. Classical matrix isolation strategies rely on cryogenic synthesis and unreactive matrices to enable spectroscopic observation of transient species. Here, we will present our progress towards developing complementary crystalline matrix isolation chemistry that enables structural elucidation by *in situ* diffraction-based experiments. Application to the characterization of reactive metal–ligand (M–L) multiply bonded species, including Rh<sub>2</sub> nitrenes and Co iminyl radicals, will be highlighted. Further, progress toward the development of new molecular photoprecursors, based on *N*-haloamide ligands, has broadened the scope of reactive M–N fragments that can be accessed photochemically. To utilize the characterized reactive fragments in catalytic bond-forming reactions, we have developed new synthetic strategies to achieve atomistic control over the chemical structure and materials properties of porous catalyst materials. Progress based on metallopolymerization chemistry will be described as a strategy to achieve catalyst-controlled selectivity in hydrocarbon functionalization chemistry and to overcome mass-transport limitations in porous materials catalysis.

### DE-SC0018977: Lattice-Templated Catalysts for Selective Hydrocarbon Upgrading

**Postdoc(s):** Debabrata Sengupta

**Student(s):** Anuvab Das, Gerard P. Van Trieste III, Chen-Hao Wang

### RECENT PROGRESS

***Experimentally Establishing the Structures of Reactive Intermediates Involved in C–H Functionalization Reactions.*** X-ray crystallography is an invaluable tool in design and development of organometallic catalysis, but application typically requires species to display sufficiently high solution concentrations and lifetimes for single crystalline samples to be obtained. *In crystallo* organometallic chemistry relies on chemical reactions that proceed within the single-crystal environment to access crystalline samples of reactive organometallic fragments that are unavailable by alternate means. Previously, we have demonstrated *in situ* photocrystallography as a technique for the structural characterization of reactive M–L multiple bonded complexes. In 2019, we demonstrated the characterization of a Rh<sub>2</sub> adamantyl nitrene complex generated by photolysis of a Rh<sub>2</sub>

adamantylazide adduct within a single crystal matrix. While the characterized  $Rh_2$  adamantylnitrene provided insight regarding the electronic structure of the transient nitrene intermediates, facile nitrenoid rearrangement prevented observation of C–H functionalization chemistry. During this funding cycle, we demonstrated *in crystallo* synthesis and characterization of  $Rh_2$  nitrenoids that participate in catalytic C–H amination (Figure 1). This discovery was enabled by the use of *ortho*-biphenylazide as a nitrene photoprecursor; in this case intramolecular C–H amination is facile from the incipient nitrene intermediate. Further, we observe the impact of coordinating substrate, which is present in excess during catalysis, on the structure of transient  $Rh_2$  nitrenoids. By providing structural characterization of authentic C–H functionalization intermediates, and not kinetically stabilized model complexes, these experiments provide the opportunity to define critical structure-activity relationships.

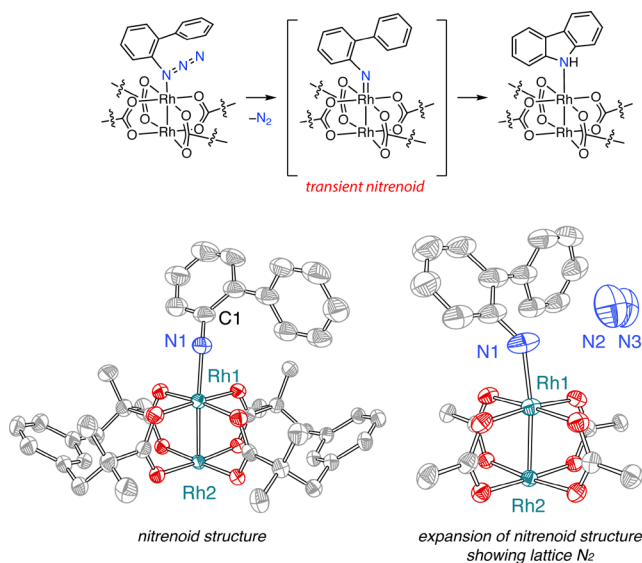


**Figure 1.** *In crystallo* C–H amination via a transient nitrenoid intermediate. Confinement within the extended crystalline lattice enables structural characterization of fleeting reactive intermediates.

We have extended the *in crystallo* synthesis and characterization of transient M–N fragments to the characterization of Co iminyl radicals that mediate catalytic C–H amination chemistry. In collaboration with Prof. Ted Betley, we studied the *in crystallo* chemistry of four-coordinate Co(II) organoazide complex ( $^A L$ )CoBr(N<sub>3</sub>(C<sub>6</sub>H<sub>4</sub>-*p*-*t*Bu)) ( $^A L$  = 5-mesityl-1,9-(2,4,6-Ph<sub>3</sub>C<sub>6</sub>H<sub>2</sub>)dipyrrin). This complex participates in a number of transformations that can be interpreted in light of the intermediacy of a Co(III) iminyl ( $^A L$ )CoBr(N(C<sub>6</sub>H<sub>4</sub>-*p*-*t*Bu)) or Co(IV) imido ( $^A L$ )CoBr(N(C<sub>6</sub>H<sub>4</sub>-*p*-*t*Bu)) complex. *In crystallo* N<sub>2</sub> extrusion enabled characterization of the putative intermediate by single-crystal X-ray diffraction and supported the formulation of this reactive intermediate as a Co iminyl radical adduct (Figure 2).

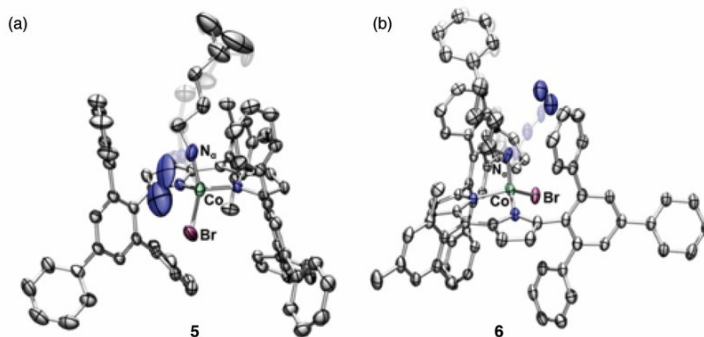


**Figure 2.** Solid-state structures of Co(III) iminyl radical intermediates generated by solid-state N<sub>2</sub> extrusion from Co(II) organoazide precursors.

**Development of Novel Molecular Photoprecursors.** Manganese complexes supported by macrocyclic tetrapyrrole ligands represent an important platform for nitrene transfer catalysis and have been applied to both C–H amination and olefin aziridination catalysis. The reactivity of the transient high-valent Mn nitrenoids that mediate these processes renders characterization of these species challenging. Here we report the synthesis and nitrene transfer photochemistry of a family of Mn(III) *N*-haloamide complexes (Figure 3). The  $S = 2$  *N*-haloamide complexes are characterized by  $^1\text{H}$  NMR, UV-vis, IR, high-frequency and -field EPR (HF-EPR) spectroscopies, and single-crystal X-ray diffraction. Photolysis of these complexes

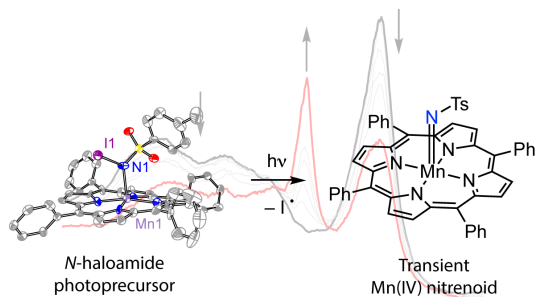


**Figure 3.** Photosynthesis of transient Mn(IV) nitrenoids is enabled by the development of specific intraligand-fragmentation photoreactions of *N*-haloamide ligands.

results in the formal transfer of a nitrene equivalent to both C–H bonds, such as the  $\alpha$ -C–H bonds of tetrahydrofuran, and olefinic substrates, such as styrene, to afford aminated and aziridinated products, respectively. Low-temperature spectroscopy and analysis of kinetic isotope effects for C–H amination indicate halogen-dependent photoreactivity: Photolysis of *N*-chloroamides proceeds via initial cleavage of the Mn–N bond to generate Mn(II) and amidyl radical intermediates; in contrast, photolysis of *N*-iodoamides proceeds via N–I cleavage to generate a Mn(IV) nitrenoid (*i.e.*,  $\{\text{MnNR}\}^7$  species). These results establish *N*-haloamide ligands as viable precursors in the photosynthesis of metal nitrenes and highlight the power of ligand design to provide access to reactive intermediates in group-transfer catalysis.

**Achieving Rational Synthetic Control over Lattice-Isolated Catalyst Sites.** Metal-organic frameworks (MOFs) have attracted significant attention as porous catalyst platforms due to the synthetic modularity of these materials and the diversity of lattice-confined catalytic sites that are readily embedded within periodic crystalline frameworks. MOFs offer platforms to heterogenize molecular catalysts, stabilize novel coordination motifs, and leverage confinement effects in catalysis. Crystallinity allows diffraction-based methods to be employed in the characterization of these catalysts. Access to crystalline MOFs typically requires reversible construction of the metal–ligand (M–L) bonds that connect the secondary building units (SBUs), which provides a mechanism to anneal defects during crystallization. While the required M–L bond reversibility is often promoted by synthesis at elevated temperature, access to crystalline materials based on either transition metals with characteristic slow exchange kinetics or highly basic donor ligands remains a synthetic challenge. We have developed metallopolymerization strategies to enable the incorporation of kinetically inert catalyst sites into porous media and the enable atomistic control over the primary coordination sphere of these ions to enable catalyst-controlled selectivity to be achieved with porous catalyst materials.

Polymerization of kinetically inert Ru<sub>2</sub> metallomonomers via labile Ag–N bonds provides access to a family of atomically precise single-crystalline Ru<sub>2</sub>-based coordination polymers with varied network topology and primary coordination sphere (e.g., polymerization of **1** with Ag(I) ions to afford [Ag(**1**)], Figure 1). These materials are not available from classical solvothermal methods. By modulating the geometry and connectivity of the metallomonomers, the resultant structures can be varied from 1-D chains to 2-D sheets and 3-D networks (Figure 4). The modularity of the metallopolymerization strategy enables the primary coordination sphere of lattice-bound Ru<sub>2</sub> nodes to be systematically varied within single-crystalline, atomically precise materials.

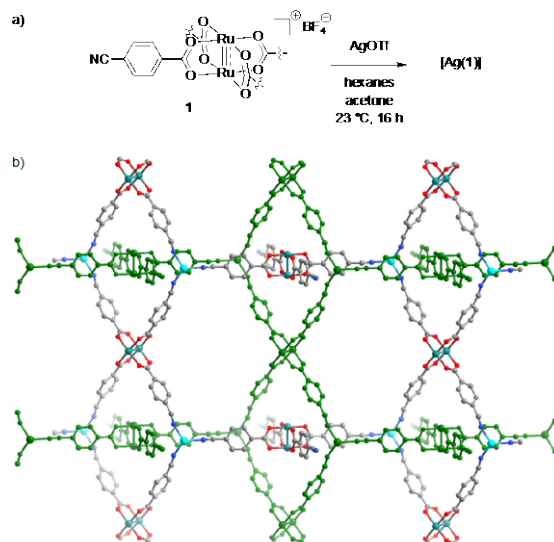


**Figure 4.** (a) Diffusion of hexanes into an acetone solution of Ru<sub>2</sub>(4-CN-OBz)<sub>4</sub>BF<sub>4</sub> (**1**) and AgOTf affords orange-colored block-shaped crystals of [Ag(**1**)]. (b) A 2D extended coordination polymer was revealed by single-crystal X-ray Diffraction (SCXRD). The second interpenetrated layer is marked green.

## Publications Acknowledging this Grant in 2018-2021

(XXX) Intellectually led by this grant

- Hyun, S.-M.; Reid, K. A.; Vali, S. W.; Lindahl, P. A.; Powers, D. C. *Cis-Divacant Octahedral Fe(II) in a Dimensionally Reduced Family of 2-(Pyridin-2-yl)pyrrolide Complexes*. *ChemRxiv*, **2021**, DOI: 10.33774/chemrxiv-2021-t8vdn).
- Van Trieste, G. P., III; Hicks, M. H.; Das, A.; Bhuvanesh, N.; Ozarowski, A.; Telser, J.; Powers, D. C. Nitrene Photochemistry of Manganese *N*-Haloamides. *ChemRxiv*, **2021**, DOI: 10.33774/chemrxiv-2021-plww9).
- Reid, K. R.; Powers, D. C. *In Crystallo* Organometallic Chemistry. *Chem. Commun.* **2021**, 57, 4993–5003. DOI: 10.1039/D1CC01684A.
- Ezazi, A. A.; Gao, W.-Y. Powers, D. C. Leveraging Exchange Kinetics for the Synthesis of Atomically Precise Porous Catalysts. *ChemCatChem* **2021**, 13, 2117–2131. DOI: 10.1002/cctc.202002034.
- Das, A.; Wang, C.-H.; Van Trieste, G. P., III; Sun, C.-J.; Chen, Y.-S.; Reibenspies, J. H.; Powers, D. C. *In Crystallo* Snapshots of Rh<sub>2</sub>-Catalyzed C–H Amination. *J. Am. Chem. Soc.* **2020**, 142, 19862–19867. DOI: 10.1021/jacs.0c09842. (Pre-

print: *ChemRxiv*, **2020**, DOI: 10.26434/chemrxiv.12934784.v1). (Highlighted in: *Nat. Rev. Chem* **2021**, 5, 2.)

- Gao, W.-Y.; Van Trieste, G. P., III; Powers, D. C. Synthesis of Atomically Precise Single-Crystalline Ru<sub>2</sub>-Based Coordination Polymers. *Dalton Trans.* **2020**, 49, 16077–16081. DOI: 10.1039/D0DT02233K. (Pre-print: *ChemRxiv*, **2020**, DOI: 10.26434/chemrxiv.12556160.v1).
- Hyun, S.-M.; Upadhyay, A.; Das, A.; Burns, C. P.; Sung, S.; Beaty, J. D.; Bhuvanesh, N.; Nippe, M.; Powers, D. C. Kinetic versus Thermodynamic Metalation Enables Synthesis of Isostructural Homo- and Heterometallic Trinuclear Clusters. *Chem. Commun.* **2020**, 56, 5893–5896. (Pre-print: *ChemRxiv*, **2020**, DOI: 10.26434/chemrxiv.12056028.v1).
- Gao, W.-Y.; Sur, A.; Wang, C.-H.; Lorz, G. R.; Antonio, A. M.; Ezazi, A. A.; Bhuvanesh, N.; Bloch, E. D.; Powers, D. C. Atomically Precise Crystalline Materials Based on Kinetically Inert Metal Ions via Reticular Mechanopolymerization. *Angew. Chem. Int. Ed.* **2020**, 59, 10878–10883. (Pre-print: *ChemRxiv*, **2020**, DOI: 10.26434/chemrxiv.11879304.v1).
- Das, A.; Van Trieste, G. P., III; Powers, D. C. Crystallography of Reactive Intermediates. *Comm. Inorg. Chem.* **2020**, 40, 116–158. DOI: 10.1080/02603594.2020.1747054.
- Wang, C.-H.; Gao, W.-Y.; Powers, D. C. Measuring and Modulating Substrate Confinement during Nitrogen-Atom Transfer in a Ru<sub>2</sub>-Based Metal-Organic Framework. *J. Am. Chem. Soc.* **2019**, 141, 19203–19207. DOI: 10.1021/jacs.9b09620. (Pre-print: *ChemRxiv*, **2019**, DOI: 10.26434/chemrxiv.9784514.v1).
- Das, A.; Chen, Y.-S.; Reibenspies, J. H.; Powers, D. C. Characterization of a Reactive Rh<sub>2</sub> Nitrenoid by Crystalline Matrix Isolation. *J. Am. Chem. Soc.* **2019**, 141, 16232–16236. DOI: 10.1021/jacs.9b09064. (Pre-print: *ChemRxiv*, **2019**, DOI: 10.26434/chemrxiv.9273395.v1).
- Gao, W.-Y.; Ezazi, A. A.; Wang, C.-H.; Moon, J.; Abney, C.; Wright, J.; Powers, D. C. Metallopolymers as a Strategy to Translate Ligand-Modulated Chemoselectivity to Porous Catalysts. *Organometallics*, **2019**, 38, 3436–3443. DOI: 10.1021/acs.organomet.9b00162. (Pre-print: *ChemRxiv*, **2019**, DOI: 10.26434/chemrxiv.7538747.v1).
- Gao, W.-Y.; Cardenal, A. D.; Wang, C.-H.; Powers, D. C. In Operando Analysis of Diffusion in Porous Metal-Organic Framework Catalysts. *Chem. Eur. J.* **2019**, 25, 3465–3476. DOI: 10.1002/chem.201804490. (Invited Mini-Review).
- Wang, C.-H.; Gao, W.-Y.; Ma, Q.; Powers, D. C. Templating Metastable Pd<sub>2</sub> Carboxylate Aggregates. *Chem. Sci.* **2019**, 10, 1823–1830. DOI: 10.1039/C8SC04940H.

(XXXI) Jointly funded by this grant and other grants with intellectual leadership by other funding sources

- Baek, Y.; Das, A.; Zheng, S.-L.; Powers, D. C.; Betley, T. A. C–H Amination Mediated by Organoazide-bound Dipyrinato Cobalt Complexes and the

- Corresponding Cobalt Nitrene Intermediates. *J. Am. Chem. Soc.* **2020**, *142*, 11232–11243. DOI: 10.1021/jacs.0c04252.
2. Cardenal, A. D.; Maity, A.; Gao, W.-Y.; Ashirov, R.; Hyun, S.-M.; Powers, D. C. Iodosylbenzene Coordination Chemistry Relevant to Metal-Organic Framework Catalysis. *Inorg. Chem.* **2019**, *58*, 10543–10553. DOI: 10.1021/acs.inorgchem.9b01191.

#### **Awards or leadership activities during 2018-2020 calendar years**

Association of Former Students College Level Teaching Award	2021
NIH Outstanding Investigator Award (MIRA – Maximizing Investigators' Research Award)	2020
Alfred P. Sloan Fellowship	2020
Montague-Center for Teaching Excellence Scholar	2019
ACS Organic Division Academic Young Investigator	2019
NSF CAREER Award	2019
Thieme Chemistry Journal Award	2019
DOE Early Career Award	2018

**Catalysis for Advanced Fuel Synthesis:  
Conversion of C-O and C-H bonds**

José A. Rodriguez, Ping Liu, Sanjaya D. Senanayake, Jinguang Chen  
and Michael G. White

Brookhaven National Laboratory, Chemistry Department

**Presentation Abstract**

This research program pursues an understanding the behavior and performance of catalysts that use C1 chemistry for the synthesis of fuels and high-value chemical by elucidating catalytically important properties of well-defined surfaces, surface films, powders and nanostructures. It addresses the conversion and manipulation of C-O and C-H bonds in small molecules. The main focus these days is on the activation and conversion of CO<sub>2</sub> and CH<sub>4</sub> to oxygenates, olefins or syngas. The program conducts a systematic study of the catalytic properties of metal-oxide, metal-carbide and metal-sulfide interfaces with the aim of controlling catalytic activity and selectivity. Emphasis is placed on understanding basic principles of surface reactivity, full characterization of active phases, and on mechanistic studies as a function of surface structure and composition. A major cross cutting thrust is the development of characterization techniques and theoretical methods for the study of catalytic processes in real time reaction conditions. Different types of interfaces, generated by combining non-expensive metals (Cu, Ni and Co) with oxides (CeO<sub>2</sub>, TiO<sub>2</sub>, ZrO<sub>2</sub>, In<sub>2</sub>O<sub>3</sub>), nitrides (Mo<sub>2</sub>N) or carbides (Mo<sub>2</sub>C, MoC, TiC), are being manipulated to produce unique binding sites which will be able to adsorb and transform molecules that have a low reactivity (CO<sub>2</sub>, CH<sub>4</sub>, CO, etc) and are of interest in C1 chemistry. At the NSLS-II, facilities are being developed for the integration of IR spectroscopy with XRD and XAFS, for performing high-pressure studies (up to 20atm), and for enabling NEXAFS as a tool for in-situ studies of surface chemistry. In the area of theory, new methodologies are being explored and tested for the modeling of reaction networks in catalytic processes such as machine learning and sophisticated approaches for kinetic Monte Carlo simulations.

**FWP-BNL-CO040: Catalysis for Advanced Fuel Synthesis and Energy, Conversion of C-O and C-H bonds**

**Co-PIs:** Ping Liu, Sanjaya Senanayake, Jinguang Chen, and Michael G. White

**Postdoc(s):** Ning Rui, Mausumi Mahapatra, Luis Betancourt, Vikram Mehar, Xuelong Wang, Juan Jimenez, Zongyuan Liu, Dimitriy Vovchok

**Student(s):** Erwei Huang, Ivan Orozco, Rina Rosales, Rui Shi, Yi Tian, Jindong Kang, Kaixi Deng, Wenjie Liao, Yilin Ma, Luolin Shi, Jason Wang, Feng Zhang

**Affiliations(s):** All the students are from SUNY Stony Brook, most of them from the Department of Chemistry

## RECENT PROGRESS

C1 chemistry involves the conversion of molecules that contain one carbon atom into valuable products. C1 chemistry is expected to become a major area of interest for the transportation fuel and chemical industries in the relatively near future. In general, the feedstocks for C1 chemistry include natural gas (mostly methane), carbon monoxide, carbon dioxide, methanol and synthesis gas (a mixture of carbon monoxide and hydrogen). Thus, a fundamental understanding of the conversion of C-O and C-H bonds is essential for controlling C1 chemistry. The Catalysis Group at BNL has been quite active in this area. The systems under investigation involved pure metal catalysts or catalysts that contained compounds of metals with light elements (C, N, O, S). We have developed and applied synchrotron-based techniques for *in-situ* characterization (AP-XPS, XRD, PDF, XAS) to understand catalyst function in operating environments. Theoretical methods for catalytic science have also been advanced (optimized KMC, reaction network analysis). In the last three and a half years (2018-2021 period), this program has led research published in 79 articles and collaborated on 12 additional articles led by external collaborators.<sup>1-91</sup> In the last three years, major research achievements are:

- Characterization and identification of inverse oxide/metal systems (ZnO/Cu, ZrO<sub>2</sub>/Cu, SnO<sub>x</sub>/Cu) as active catalysts for CO<sub>2</sub> and CH<sub>4</sub> conversion.<sup>1,11,46,47,63,74</sup>
- Discovery of the essential role that complex metal-oxide, metal-carbide and metal-nitride interfaces play in the catalysis associated with C1 chemistry.<sup>6,7,10,28,30,31,70</sup>
- Combining CO<sub>2</sub> reduction with propane oxidative dehydrogenation over bimetallic catalysts.<sup>52,69,70</sup>
- Using CO<sub>2</sub> and ethane in the production of C3 oxygenates.<sup>43,69,70</sup>
- Study of the role of alkali metal atoms as vital centers and promoters of the activity of catalysts used for CO oxidation, the water-gas shift and CO<sub>2</sub> hydrogenation.<sup>3,23,51,73</sup>
- Synthesis, characterization and study of atomically precise metal and metal oxide clusters as model catalysts.<sup>47,75</sup>
- Detailed proof through *operando* studies that metal/oxide catalysts are dynamic entities that change as a function of reaction conditions during the water-gas shift, CO<sub>2</sub> hydrogenation and alkane dry reforming reactions.<sup>7,13,15,18,28,36,70,71</sup>
- Breaking simple scaling relations through metal-support interactions: Understanding room temperature activation of methane on M-CeO<sub>2</sub> (M= Co, Ni, Fe, Pt, Ru) and Ni-TiC surfaces.<sup>30,48,76</sup>
- Discovering of the essential role of site confinement in improving activity/selectivity in DRM on single site Ni/MgO catalysts.<sup>8,21</sup>
- Participation in the design and implementation of instrumentation to carry out *in-situ* quick XAFS/IR and XRD/IR studies at the NSLS-II and APS. Active participants in the Synchrotron Catalysis Consortium and the design of the end stations for three beam lines (IOS, XPD, QAS) at the NSLS-II.<sup>10,13,43,83</sup>
- Development of theoretical tools for the study of catalysis science using machine learning, reaction network analysis, and advanced Kinetic Monte Carlo. Identification of fundamental descriptors for C1 catalysis.<sup>8,49,53,73</sup>

These are examples of the research done during the 2018-2021 years:

### A. Inverse oxide/metal systems (ZnO/Cu, ZrO<sub>2</sub>/Cu, SnO<sub>x</sub>/Cu) as active catalysts for CO<sub>2</sub> and CH<sub>4</sub> conversion

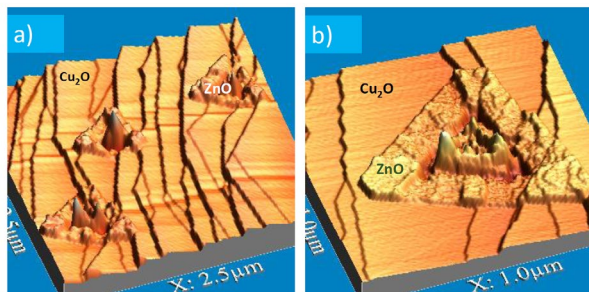


**Figure 1:** Three Dimensional (3D) view of ZnO islands deposited on a Cu<sub>x</sub>O/Cu(111) substrate

create a catalytically active metal-oxide interface. We have performed a systematic study using scanning tunneling microscopy (STM) to investigate the growth modes of ZnO on Cu(111) under different preparation conditions.<sup>11,19</sup> Zn was deposited on Cu(111) or CuO<sub>x</sub>/Cu(111) surfaces under various conditions. When Zn was deposited at 300 K with subsequent exposure to O<sub>2</sub> at higher temperatures (400-550 K), small particles of ZnO (< 20 nm in size) were produced on the surface. For Zn deposition onto CuO<sub>x</sub>/Cu(111) at elevated temperatures (450-600 K) in an oxygen ambient, large ZnO islands (300-650 nm in size) were produced which were very rough and spread over several terraces of Cu(111), See Figure 1. XPS/Auger spectra showed that all the preparation conditions led to the formation of ZnO/CuO<sub>x</sub>/Cu(111) surfaces where the oxidation state of zinc was uniform.<sup>11,19</sup>

We studied the catalytic activity of the ZnO/CuO<sub>x</sub>/Cu(111) systems and found they were active for the oxidation of CO, the water-gas shift and the hydrogenation of CO<sub>2</sub>, see Figure 2. However, the small ZnO structures prepared by the first approach had a limited stability at temperatures above 500 K.<sup>1,11,19</sup>

In our studies, we did not see graphite-like structures as seen for the powder catalyst under reaction conditions by Lunkenbein et al.<sup>11,19</sup> However, in catalytic tests, we found that our ZnO/CuO<sub>x</sub>/Cu(111) systems were much more active for CO<sub>2</sub> hydrogenation than Cu(111). Figure

Mixtures of CuO-ZnO are frequently used as catalysts for the WGS and the synthesis of methanol.<sup>1</sup> A recent transmission electron microscopy (TEM) study by Lunkenbein, et al. has revealed that strong metal-support interactions between Cu and ZnO lead to the formation of a ZnO overlayer on top of the Cu particles in an industrial Cu/ZnO/Al<sub>2</sub>O<sub>3</sub> catalyst under reaction conditions.<sup>1</sup> Such formation of an oxide overlayer on Cu could

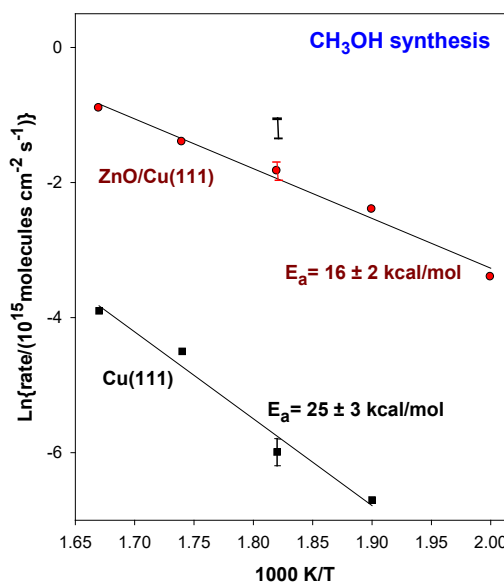


**Figure 2:** Methanol synthesis on clean Cu(111) and on a copper surface pre-covered with 0.3 ML of ZnO.

2 compares the catalytic activity of Cu(111) to a system where  $\sim 30\%$  of the copper substrate was covered with ZnO. The ZnO overlayer was prepared at 600 K to induce the formation of big ZnO islands. The addition of ZnO to the copper substrate enhanced the catalytic activity by two to three orders of magnitude. For this sample, the measured line shape for the Zn LMM Auger spectra suggested the presence of ZnO on the copper surface during reaction. These experimental results are consistent with the predictions of DFT and KMC calculations and show the importance of an oxide-metal interface in CO<sub>2</sub> hydrogenation.<sup>1,11,19</sup>

In another set of experiments, mass selected cluster methods were used to prepare well-defined nanostructures of ZrO<sub>2</sub> on an oxidized CuO<sub>x</sub>/Cu(111) substrate.<sup>47</sup>

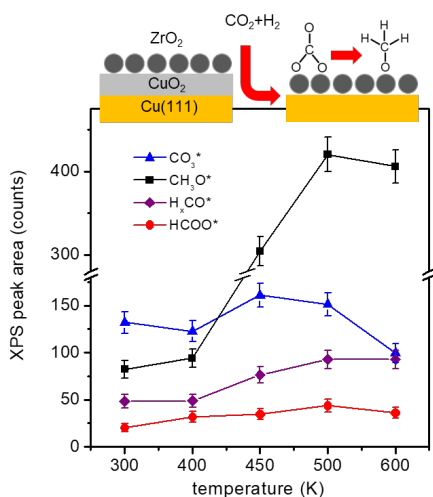


**Figure 3:** Temperature dependent C1s peak intensities representing the relative surface concentrations of reaction intermediates on a 0.3 ML ZrO<sub>2</sub>/Cu(111) surface under CO<sub>2</sub> hydrogenation conditions (CO<sub>2</sub> + 3H<sub>2</sub>, 0.7mbar). The peak intensities were taken from least squares fits of the C1s spectra obtained using near ambient pressure XPS.

The ZrO<sub>2</sub>/CuO<sub>x</sub>/Cu(111) surfaces were very active towards mixtures of CO<sub>2</sub>/H<sub>2</sub> typically used for the synthesis of methanol.<sup>47</sup> Experiments with AP-XPS and IRAS were useful to follow the formation and conversion of key reaction intermediates, see Figure 3. At a ZrO<sub>2</sub> coverage of 0.3 ML, the temperature profiles of the intermediates suggest a modified “formate” pathway in which CO<sub>2</sub> is bound on the oxide as carbonate species, which then undergo a series of hydrogenation and C-O bond breaking steps to form methoxy, which is the final surface species leading to methanol. At higher oxide coverage, it was observed the formation of alkyl intermediates which may signal a competing reaction pathway to methanation.<sup>47</sup>

## B. Alkali-promoted selective CO<sub>2</sub> conversion to methanol and ethanol.

Experimental and theoretical studies indicate that cesium promotes the rates of methanol and ethanol formation on Cu/ZnO(000 $\bar{1}$ ) catalysts.<sup>73</sup> A combination of XPS and calculations based on density functional theory and Kinetic Monte Carlo was used to study this phenomenon, see Figure 4. The results pinpointed the effects of doped alkali on the binding of reaction intermediates and transition states, and the operating reaction pathways, being able to promote the CO<sub>2</sub>

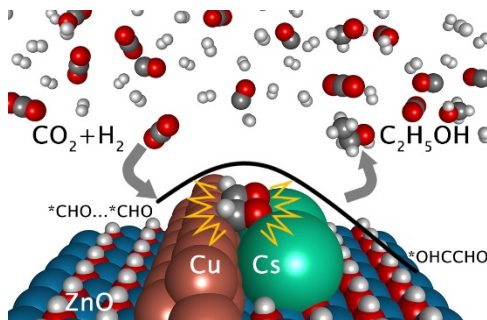


**Figure 4** The path for the formation of ethanol through Cs-mediated CHO to CHO coupling on Cu/ZnO(000 $\bar{1}$ ).

conversion and more importantly the selectivity to methanol and ethanol. Descriptors were identified, which well described the catalytic behaviors and therefore were useful for the rational design of better Cu-based catalysts for CO<sub>2</sub> hydrogenation.<sup>73</sup> The work provided a better understanding of C-C bond formation and developed a descriptor-based method for rational screening of complex catalysts at a theoretical level.<sup>73</sup>

### C. Novel metal/nitride and metal/carbide catalysts for C1 chemistry

Strong bonding interaction between a transition metal and a supporting substrate is an effective strategy to immobilize sub-nm scale clusters or atoms in heterogeneous catalysis. While such interactions are well-studied for oxide substrates, we recently showed that similar effects occur on a Mo<sub>2</sub>N surface.<sup>31</sup> Combined experimental and theoretical studies have confirmed that strong metal-support interactions between face-centered cubic (fcc) structured  $\gamma$ -Mo<sub>2</sub>N and cobalt is an effective approach to anchor sub-nm Co clusters and prevent their aggregation. We studied the reactivity and stability of such Co/Mo<sub>2</sub>N systems for the hydrogenation of CO<sub>2</sub>.<sup>31</sup>

The hydrogenation of CO<sub>2</sub>, the water-gas shift reaction, and the activation of methane were also investigated on novel catalysts generated by the deposition of metals on carbide surfaces.<sup>2,4,25,27,30,32</sup> For small Cu and Au clusters supported on TiC or MoC, strong admetal  $\leftrightarrow$  C<sub>surface</sub> interactions induce charge polarization over the surface. As a result, there is a significant enhancement in the catalytic activity when going from metal bulk surfaces to carbide-supported small clusters, and systems such as Au/MoC and Au/TiC display a high catalytic activity for the low-temperature water-gas shift reaction.

Methane is an extremely stable molecule which interacts poorly with surfaces of late transition metals such as Ni(111) or Pt(111). At room temperature, the sticking coefficient of methane on these surfaces is negligible ( $< 10^{-8}$ ). Combining experiments with X-ray photoemission and accurate DFT based calculations, we have shown that small Ni clusters dispersed on TiC(001) are able to capture and dissociate methane at room temperature.<sup>30</sup> In DFT calculations, a small energy barrier of  $< 0.5$  eV is predicted for CH<sub>4</sub> dissociation into adsorbed methyl and atomic hydrogen species (Figure 5).<sup>30</sup> In addition, the calculated reaction free energy profile at 300 K and 1 atm of CH<sub>4</sub> shows no effective energy barriers in the system. We found a similar trend for the deposition of small Pt clusters on the carbide surface. A comparison to other reported systems that activate methane at room temperature, including oxide and zeolite-based materials, indicates that the metal/carbide systems activate distinct chemistry. The discovery of a carbide-based surface able to activate methane at low temperatures is promising for the design of new types of catalysts for efficient conversion of methane into value-added chemicals.<sup>30,33,45,58</sup>

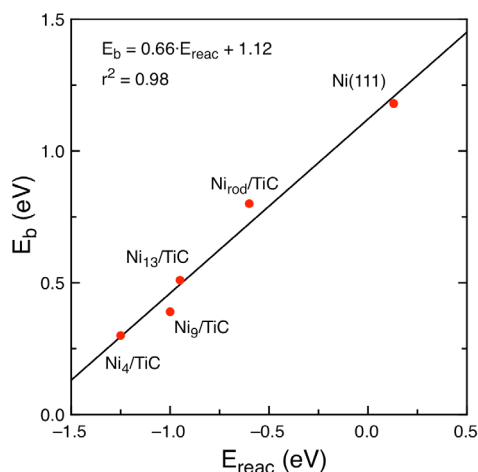


**Figure 5:** Energy barrier ( $E_b$ ) for CH<sub>4</sub> to CH<sub>3</sub>+H dissociation on the Ni/TiC systems and on Ni(111) versus the reaction energy ( $E_{\text{reac}}$ ).

### C. Novel bimetallic and metal-oxide interfaces for the conversion of methane and light alkanes with CO<sub>2</sub>.

During this funding cycle, we have found that ceria is a versatile oxide with chemical properties that can be tuned to perform the activation and dry conversion of methane and light alkanes using CO<sub>2</sub>.<sup>6,10,69,70,76</sup> Studies were performed for the deposition of

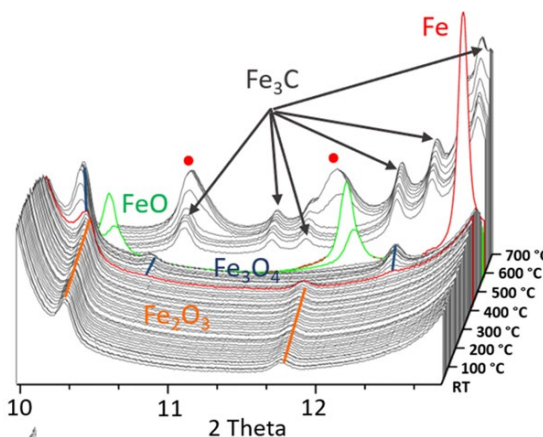


**Figure 6.** In-situ XRD profile of FeO<sub>x</sub>/CeO<sub>2</sub> sample during reaction with methane as a function of temperature.

non-expensive metals on ceria powders which had the shape of nanospheres, nanorods or nanocubes.<sup>7</sup> The strength of the metal-support interactions and the surface chemistry for the activation of CH<sub>4</sub> and CO<sub>2</sub> depended on the orientation for the ceria support and the nature of the admetal.<sup>7</sup> Good activity has been seen after depositing metals such as Ni, Co or Fe.<sup>10</sup> As a consequence of strong metal-support interactions, the M/CeO<sub>2</sub> systems (M= Ni, Co, Fe) dissociate methane at room temperature and massive reaction, with the formation of metal carbides in some cases, was

observed at elevated temperatures with XPS, XANES and XRD (Figure 6).<sup>10</sup>

Technically, the dry reforming of methane (DRM) is an effective way for utilizing two major greenhouse gases, CO<sub>2</sub> and CH<sub>4</sub>. to produce syngas, which can be used as the feedstock for catalytic processes, such as Fischer-Tropsch and methanol synthesis. However, conventional Ni catalysts for the DRM deactivate quickly due to sintering of the active metal phase and carbon deposition via the Boudouard reaction ( $2\text{CO} \rightarrow \text{C} + \text{CO}_2$ ) and/or CH<sub>4</sub> decomposition ( $\text{CH}_4 \rightarrow \text{C} + 4\text{H}$ ). It has been shown that this deactivation process can be avoided by depositing small clusters of Ni on MgO and CeO<sub>2</sub>. This phenomenon was studied in detail using DFT and KMC calculations on the Ni/MgO system. At large coverages of Ni, the size of the Ni particles is not confined and deactivation by massive carbon deposition can occur. In contrast, at lower coverage the KMC simulations predict that the site confinement of a single site catalyst such as Ni<sub>4</sub>/MgO helps to balance the activations of CO<sub>2</sub> and CH<sub>4</sub>, which is essential to achieve high yield and a useful H<sub>2</sub>/CO ratio of 1, while preventing the poisoning of active sites during the DRM reaction.<sup>8</sup>

Bimetallic-derived catalysts have been used for simultaneously upgrading CO<sub>2</sub> and underutilized ethane into value-added chemicals, such as synthesis gas and olefins.<sup>69,70</sup> For example, the dry reforming of ethane with CO<sub>2</sub> was achieved over a PtNi/CeO<sub>2</sub> bimetallic catalyst.<sup>69,70</sup> The PtNi bimetallic catalyst showed an improvement in both activity and stability in comparison to the corresponding monometallic catalysts.<sup>69,70</sup> The formation of a PtNi alloy and the partial reduction of Ce<sup>4+</sup> to Ce<sup>3+</sup> under reaction conditions were demonstrated by in situ AP-XPS, XRD and XAFS measurements. In another project, a tandem of two reactors was used to combine CO<sub>2</sub> and ethane in the production of C<sub>3</sub> oxygenates.<sup>43,70</sup> In the first reactor, a Fe<sub>3</sub>Ni<sub>1</sub>/CeO<sub>2</sub> catalyst facilitated CO<sub>2</sub>-assisted dehydrogenation and reforming of ethane to produce ethylene, CO, and H<sub>2</sub>. While in the second reactor, a RhCo<sub>x</sub>/MCM-41 catalyst enable CO insertion for the production of C<sub>3</sub> oxygenates (propanal and 1-propanol) via heterogeneous hydroformylation.<sup>43,70</sup>

## Publications for this grant (2018-2021)

In the last two and a half years, 79 articles have been published with this grant as the main driver or the main provider of ideas, plus 12 articles in collaboration with external collaborators.

*\*\* Mainly generated by this grant*

### **2018:**

1. Palomino, R.M.; Ramirez, P.J.; Liu, Z.; Waluyo, I.; Orozco, I.; Senanayake, S.D.; Rodriguez, J.A. Hydrogenation of CO<sub>2</sub> on ZnO/Cu(100) and ZnO/Cu(111) Catalysts: Role of Copper Structure and Metal-Oxide Interface in Methanol Synthesis, *J. Phys. Chem. B*, **2018**, *122*, 794-798.
2. Jimenez-Orozco, C.; Florez, E.; Moreno, A.; Liu P.; Rodriguez, J.A. Acetylene and Ethylene Adsorption on a  $\beta$ -Mo<sub>2</sub>C(100) Surface: A Periodic DFT Study on the Role of C- and Mo-terminations for Bonding and Hydrogenation Reactions, *J. Phys. Chem. C*, **2017**, *121*, 19786-19791.
3. Rodriguez, J.A.; Grinter, D.C.; Ramírez, P.J.; Stacchiola, D.J.; Senanayake, S.D. High Activity of Au/K/TiO<sub>2</sub>(110) for CO Oxidation: Alkali Enhanced Dispersion of Au and Bonding of CO, *J. Phys. Chem. C*, **2018**, *122*, 4324-4328.
4. Kunkel, C.; Viñes, F.; Ramírez, P.J.; Rodriguez, J.A.; Illas, F. Combining Theory and Experiment for Multitechnique Characterization of Activated CO<sub>2</sub> on Transition Metal Carbide (001) Surfaces, *J. Phys. Chem. C*, **2018**, *123*, 7567-7576.
5. Vovchok, D.; Guild, C. J.; Dissanayake, S.; Llorca, J.; Stavitski, E.; Liu, Z.; Palomino, R. M.; Waluyo, I.; Li, Y.; Frenkel, A. I.; Rodriguez, J. A.; Suib, S. L.; Senanayake, S. D. Characterization of Mesoporous Co/CeO<sub>2</sub> Catalysts for the High Temperature Water-Gas Shift, *J. Phys. Chem. C*, **2018**, *122*, 8998-9008.
6. Zhang, F.; Liu, Z.; Zhang, S.; Akter, N.; Palomino, R.M.; Vovchok, D.; Orozco, I.; Salazar, D.; Rodriguez, J.A.; Llorca, J.; Lee, J.; Kim, D.; Xu, W.; Frenkel, A.; Li, Y.; Kim, T.; Senanayake, S.D. *In-situ* Elucidation of the Active State of Co-CeO<sub>2</sub> Catalysts in the Dry Reforming of Methane: The Important Role of the Reducible Oxide Support and Interactions with Cobalt, *ACS Catal.* **2018**, *8*, 3550-3560.
7. Lin, L.; Yao, S.; Liu, Z.; Zhang, F.; Li, N.; Vovchok, D.; Martínez-Arias, A.; Castañeda, R.; Lin, J.; Senanayake, S. D.; Su, D.; Ma, D.; Rodriguez, J. A. *In-situ* Characterization of Cu/CeO<sub>2</sub> Nanocatalysts for CO<sub>2</sub> Hydrogenation: Morphological Effects of Nanostructured Ceria on the Catalytic Activity, *J. Phys. Chem. C*, **2018**, *122*, 12934-12943.

8. Zuo, Z.; Liu, S.; Wang, Z.; Liu, C.; Huang, W.; Huang, J.; Liu, P. “Dry reforming of Methane on single site Ni/MgO catalysts: importance of site confinement”, *ACS Catal.*, **2019**, *8*, 9821–9835.
9. Voychok, D.; Guild, C. J.; Llorca, J.; Palomino, R. M.; Waluyo, I.; Rodriguez, J. A.; Suib, S. L.; Senanayake, S. D. Structural and Chemical State of Doped and Impregnated Mesoporous Ni/CeO<sub>2</sub> Catalysts for the Water-Gas Shift. *Appl. Catal. A Gen.* **2018**, *567*, 1–11.
10. Zhang, F.; Yao, S.; Liu, Z.; Gutiérrez, R. A.; Vovchok, D.; Cen, J.; Xu, W.; Ramírez, P. J.; Kim, T.; Senanayake, S. D.; et al. Reaction of Methane with MO<sub>x</sub>/CeO<sub>2</sub> (M = Fe, Ni, and Cu) Catalysts: In Situ Studies with Time-Resolved X-Ray Diffraction. *J. Phys. Chem. C* **2018**, *122*, 28739–28747.
11. Mahapatra, M.; Kang, J.; Ramírez, P. J.; Hamlyn, R.; Rui, N.; Liu, Z.; Orozco, I.; Senanayake, S. D.; Rodriguez, J. A. Growth, Structure, and Catalytic Properties of ZnO<sub>x</sub> Grown on CuO<sub>x</sub>/Cu(111) Surfaces. *J. Phys. Chem. C* **2018**, *122*, 26554–26562.
12. Piñero, J.J.; Ramírez, P.J.; Bromley, S.T.; Illas, F.; Viñes, F.; Rodriguez, J.A. Diversity of Adsorbed Hydrogen on TiC (001) Surface at High Coverages, *J. Phys. Chem. C*, **2018**, *122*, 26554-26562.
13. Voychok, D.; Guild, C. J.; Llorca, J.; Palomino, R. M.; Waluyo, I.; Rodriguez, J. A.; Suib, S. L.; Senanayake, S. D. Structural and Chemical State of Doped and Impregnated Mesoporous Ni/CeO<sub>2</sub> Catalysts for the Water-Gas Shift. *Appl. Catal. A Gen.* **2018**, *567*, 1–11.
14. Liu, Z.; Yao, S.; Johnston-Peck, A.; Xu, W.; Rodriguez, J. A.; Senanayake, S. D. Methanol Steam Reforming over Ni-CeO<sub>2</sub> model and Powder Catalysts: Pathways to High Stability and Selectivity for H<sub>2</sub>/CO<sub>2</sub> production. *Catal. Today* **2018**, *311* 74-80.
15. Hamlyn, R.; Mahapatra, M.; Grinter, D.; Xu, F.; Luo, S.; Palomino, R.; Kattel, S.; Waluyo, I.; Liu, P.; Stacchiola, D.; Senanayake, S.; Rodriguez, J. A. “Imaging the Ordering of a Weakly Adsorbed Two-dimensional condensate: ambient-pressure microscopy and spectroscopy of CO<sub>2</sub> molecules on rutile TiO<sub>2</sub>(110)”, *Phys. Chem. Chem. Phys.* **2018**, *20*, 13122-13126.
16. Liu, S.; White, M.G.; Liu, P. Oxygen Reduction Reaction on Ag(111) in Alkaline Solution: A Combined Density Functional Theory and Kinetic Monte Carlo Study, *ChemCatChem* **2018**, *10*, 540-549. **(Cover art)**
17. Liu, S.; Liu, P. Optimized Pt-based Catalysts for Oxygen Reduction Reaction in Alkaline Solution: A First Principle Study, *J. Electrochem. Soc.* **2018**, *165*, J3090-J3094 **(Invited)**.

18. Carrillo, P.; Shi, R.; Teeluck, K.; Senanayake, S. D.; White, M. G. In-Situ Formation of FeRh Nanoalloys for Oxygenate Synthesis. *ACS Catal.* **2018**, *8* (8), 7279-7286.

19. Mahapatra, M.; Gutiérrez, R. A.; Kang, J.; Rui, N.; Hamlyn, R.; Liu, Z.; Orozco, I.; Ramírez, P. J.; Senanayake, S. D.; Rodriguez, J. A. The Behavior of Inverse Oxide/Metal Catalysts: CO Oxidation and Water-Gas Shift Reactions over ZnO/Cu(111) Surfaces. *Surf. Sci.* **2018**, *681*, 116–121.

**2019:**

20. Liu, Z.; Senanayake, S. D.; Rodriguez, J. A. Chapter 5 - Catalysts for the Steam Reforming of Ethanol and Other Alcohols. In *Ethanol*; Basile, A., Iulianelli, A., Dalena, F., Veziroğlu, T. N., Eds.; Elsevier, 2019; pp 133–158 (invited).

21. Rodriguez, J. A.; Zhang, F.; Liu, Z.; Senanayake, S. D. Methane Activation and Conversion on Well-Defined Metal-Oxide Surfaces: In Situ Studies with Synchrotron-Based Techniques. In *Catalysis: Volume 31*; The Royal Society of Chemistry, 2019; Vol. 31, pp 198–215 (invited).

22. Senanayake, S. D.; Liu, P.; Rodriguez, J. A. Preface: Virtual Special Issue in Honor of Dr. Jan Hrbek. *Surf. Sci.* 2019, *680*, A1.

23. Waluyo, I.; Mudiyansele, K.; Xu, F.; An, W.; Liu, P.; Boscoboinik, J. A.; Rodriguez, J. A.; Stacchiola, D. J. Potassium-Promoted Reduction of Cu<sub>2</sub>O/Cu(111) by CO, *J. Phys. Chem. C* **2019**, *123*, 8057-8066.

24. Flege, J. I.; Hocker, J.; Sadowski, J. T.; Senanayake, S. D.; Falta, J. Nucleation, Morphology, and Structure of Sub-Nm Thin Ceria Islands on Rh(111). *Surf. Interface Anal.* **2019**, *51*, 110–114.

25. Prats, H.; Posada-Perez, S.; Rodriguez, J.A.; Sayos, R.; Illas, F. Kinetic Monte Carlo Simulations Unveil Synergic Effects at Work on Bifunctional Catalysts, *ACS Catal.* 2019, *9*, 9117-9126.

26. Simonovis, J. P.; Hunt, A.; Senanayake, S. D.; Waluyo, I. Subtle and Reversible Interactions of Ambient Pressure H<sub>2</sub> with Pt/Cu(111) Single-Atom Alloy Surfaces. *Surf. Sci.* **2019**, *679*, 207–213.

27. Koverga, A.A.; Florez, E.; Dorkis, L.; Rodriguez, J.A. CO, CO<sub>2</sub>, and H<sub>2</sub> Interactions with (0001) and (001) Tungsten Carbide Surfaces: Importance of Carbon and Metal Sites, *J. Phys. Chem. C*, **2019**, *123*, 8871-8876.

28. Liu, Z. ; Zhang, F.; Rui, N.; Rodriguez, J.A.; Senanayake, S.D. Highly Active Ceria-Supported Ru Catalyst for the Dry Reforming of Methane: In Situ Identification of Ru<sup>δ+</sup>-Ce<sup>3+</sup> Interactions for Enhanced Conversion, *ACS Catal.* 2019, *9*, 3349-3359.

29. Lin, L.; Yao, S.; Rui, N.; Han, L.; Zhang, F.; Gerlak, C. A.; Liu, Z.; Cen, J.; Song, L.; Senanayake, S. D.; Rodriguez, J.A. Conversion of CO<sub>2</sub> on a Highly Active and Stable

Cu/FeOx/CeO<sub>2</sub> Catalyst: Tuning Catalytic Performance by Oxide-Oxide Interactions. *Catal. Sci. Technol.* **2019**, *9*, 3735-3742.

**30.** Prats, H.; Gutierrez, R.A.; Piñero, J.J.; Viñes, F.; Bromley, S.T.; Ramirez, P.J.; Rodriguez, J.A.; Illas, F. R. Room Temperature Methane Capture and Activation by Ni Clusters Supported on TiC(001): Effects of Metal–Carbide Interactions on the Cleavage of the C–H Bond. *J. Am. Chem. Soc.* **2019**, *141*, 5303-5313.

**31.** Yao, S.; Lin, L.; Liao, W.; Li, N.; Rui, N.; Liu, Z.; Cen, J.; Zhang, F.; Su, D.; Senanayake, S.; Liu, P.; Ma, D.; Chen, J.G.; Rodriguez, J. A. Exploring Metal–Support Interactions to Immobilize Subnanometer Co Clusters on  $\gamma$ -Mo<sub>2</sub>N: A Highly Selective and Stable Catalyst for CO<sub>2</sub> Activation, *ACS Catal.* **2019**, *9*, 9087-9097.

**32.** Jimenez-Orozco, C.; Florez, E.; Moreno, A.; Rodriguez, J.A. Metal Carbide Surfaces as Catalysts for Olefin and Alkyne Conversion: Binding and Hydrogenation of Ethylidene, *J. Phys.: Conf. Ser.* **2019**, *1247*, 012003.

**33.** Jimenez-Orozco, C.; Florez, E.; Montoya, A.; Rodriguez, J.A. Binding and Activation of Ethylene on Tungsten Carbide and Platinum Surfaces, *Phys. Chem. Chem. Phys.* **2019**, *21*, 17332-17336.

**34.** Orozco, I.; Huang, E.; Gutiérrez, R.A.; Liu, Z.; Zhang, F.; Mahapatra, M.; Kang, J.; Kersell, H.; Nemsak, S.; Ramírez, P.J.; Senanayake, S.D.; Liu, P.; Rodriguez, J.A. Hydroxylation of ZnO/Cu(1 1 1) Inverse Catalysts under Ambient Water Vapor and the Water–gas Shift Reaction, *J. Phys. D: Appl. Phys.*, **2019**, *52*, 454001.

**35.** Rodriguez, J. A.; Remesal, E. R.; Ramírez, P. J.; Orozco, I.; Liu, Z.; Graciani, J.; Senanayake, S. D.; Sanz, J. F. Water-Gas Shift Reaction on K/Cu(111) and Cu/K/TiO<sub>2</sub>(110) Surfaces: Alkali Promotion of Water Dissociation and Production of H<sub>2</sub>. *ACS Catal.* **2019**, *9* (12), 10751.

**36.** Vovchok, D.; Tata, J.; Orozco, I.; Zhang, F.; Palomino, R. M.; Xu, W. Q.; Harper, L.; Khatib, S. J.; Rodriguez, J. A.; Senanayake, S. D. Location and Chemical Speciation of Cu in ZSM-5 during the Water-Gas Shift Reaction. *Catal. Today* **2019**, *323*, 216–224.

**37.** Zhang, H. T.; Liu, C.; Liu, P.; Hu, Y. H. Mo<sub>6</sub>S<sub>8</sub>-Based Single-Metal-Atom Catalysts for Direct Methane to Methanol Conversion, *J. Chem. Phys.* **2019**, *151*, 024304. (invited).

## **2020:**

**38.** López Cámara, A.; Cortés Corberán, V.; Martínez-Arias A.; Barrio, L.; Si, R.; Hanson, J.C.; Rodriguez, J.A. Novel Manganese-promoted Inverse CeO<sub>2</sub>/CuO Catalyst: *In situ* Characterization and Activity for the Water-gas Shift Reaction, *Catal. Today*, **2020**, *24*.

39. Zhang, F.; Liu, Z.; Chen, X.; Rui, N.; E. Betancourt, L.; Lin, L.; Xu, W.; Sun, C.; M. Milinda Abeykoon, A.; A. Rodriguez, J.; et al. Effects of Zr Doping into Ceria for the Dry Reforming of Methane over Ni/CeZrO<sub>2</sub> Catalysts: In Situ Studies with XRD, XAFS, and AP-XPS. *ACS Catal.* **2020**, *10*, 3274.
40. Rui, N.; Zhang, F.; Sun, K.; Liu, Z.; Xu, W.; Stavitski, E.; Senanayake, S.D.; Rodriguez, J.A.; Liu, C.-J. Hydrogenation of CO<sub>2</sub> to Methanol on a Au<sup>+</sup>-In<sub>2</sub>O<sub>3-x</sub> Catalyst, *ACS Catal.* **2020**, *10*, 11307.
41. Winter, L.R.; Ashford, B.; Hong, J.; Murphy, A.B.; Chen, J.G. Identifying Surface Reaction Intermediates in Plasma Catalytic Ammonia Synthesis, *ACS Catal.* **2020**, *10*, 14763.
42. Kang, J.; Mahapatra, M.; Rui, N.; Orozco, I.; Shi, R.; Senanayake, S.D. Rodriguez, J.A. Growth and structural studies of In/Au(111) alloys and InO<sub>x</sub>/Au(111) inverse oxide/metal model catalysts, *J. Chem. Phys.* **2020**, *152*, 054702 (invited)
43. Xie, Z.; Xu, Y.; Xie, M.; Chen, X.; Lee, J.H.; Stavitski, E.; Kattel, S.; Chen, J.G. Reactions of CO<sub>2</sub> and Ethane Enable CO Bond Insertion for Production of C<sub>3</sub> Oxygenates, *Nature Communications*, **2020**, *11*, 1887
44. Hamlyn, R. C. E.; Mahapatra, M.; Orozco, I.; Waluyo, I.; Hunt, A.; Rodriguez, J. A.; White, M. G.; Senanayake, S. D. Structure and Chemical State of Cesium on Well-Defined Cu(111) and Cu<sub>2</sub>O/Cu(111) Surfaces. *J. Phys. Chem. C*, **2020**, *124*, 3107.
45. Figueras, M.; Gutierrez, R.A.; Prats, H.; Viñes, F.; Ramirez, P.J.; Illas, F.; Rodriguez, J.A. Boosting the Activity of Transition Metal Carbides towards Methane Activation by Nanostructuring, *Phys. Chem. Chem. Phys.* **2020**, *22*, 7110.
46. Shi, R.; Mahapatra, M.; Kang, J.; Orozco, I.; Senanayake, S.D.; Rodriguez, J.A. Preparation and Structural Characterization of ZrO<sub>2</sub>/CuOx/Cu(111) Inverse Model Catalysts, *J. Phys. Chem. C*, **2020**, *124*, 10502.
47. Ma, Y.; Wang, K.; Goodman, K.R.; Head, A.R.; Stacchiola, D.J. Reactivity of a Zirconia-Copper Inverse catalyst for CO<sub>2</sub> Hydrogenation, *J. Phys. Chem. C* **2020**, *124*, 22158.
48. Senanayake, S.D.; Rodriguez, J.A.; Weaver, J. Low Temperature Activation of Methane on Metal-Oxide and Complex Interfaces: Insights from Surface Science, *Accounts of Chem. Res.* **2020**, *53*, 1488 (invited).
49. Liu, Z.; Huang, E.; Orozco, I.; Liao, W.; Palomino, R. M.; Rui, N.; Duchoň, T.; Nemšák, S.; Grinter, D. C.; Mahapatra, M.; Liu, P.; Rodriguez, J. A.; Senanayake, S. D., Water-promoted interfacial pathways in methane oxidation to methanol on a CeO<sub>2</sub>/Cu<sub>2</sub>O catalyst. *Science* **2020**, *368*, 513.

- 50.** Jiang, X.; Nie, X.; Guo, X.; Song, C.; Chen, J.G. Recent Advances in Carbon Dioxide Hydrogenation to Methanol via Heterogeneous Catalysis, *Chemical Reviews*, **2020**, *120*, 7984.
- 51.** Hamlyn, R.C.E.; Mahapatra, M.; Orozco, I.; Hunt, A.; Waluyo, I.; White, M.G.; Senanayake, S.D.; Rodriguez, J.A. Morphology and Chemical Behavior of Model  $\text{CsO}_x/\text{Cu}_2\text{O}/\text{Cu}(111)$  Nanocatalysts for Methanol Synthesis: Reaction with  $\text{CO}_2$  and  $\text{H}_2$ , *J. Chem. Phys.*, **2020**, *152*, 044701.
- 52.** Niu, X.; Nie, X.; Yang C.; Chen, J.G.  $\text{CO}_2$ -assisted propane aromatization over phosphorous-modified Ga/ZSM-5 catalysts, *Catal. Sci. & Tech.*, **2020**, *10*, 1881.
- 53.** Liao, W.; Liu, P., Methanol Synthesis from  $\text{CO}_2$  Hydrogenation over a Potassium-Promoted  $\text{Cu}_x\text{O}/\text{Cu}(111)$  ( $x \leq 2$ ) Model Surface: Rationalizing the Potential of Potassium in Catalysis. *ACS Catal.* **2020**, *10*, 5723.
- 54.** Wang, J.; Ma, Y.; Tong, X.; Stacchiola, D.J.; White, M.G. Morphology and Reactivity of Size-selected Titanium Oxide Nanoclusters on Au(111), *J. Chem. Phys.*, **2020**, *152*, 054714 (cover art)
- 55.** Nie, X.; Ren, X.; Tu, C.; Song, C.; Guo, X; Chen, J.G. Computational and Experimental Identification of Strong Synergy of Fe/ZnO Catalyst in Promoting Acetic Acid Synthesis from  $\text{CH}_4$  and  $\text{CO}_2$ , *Chemical Communications*, **2020**, *56*, 3983
- 56.** Xie, Z.; Tian, D.; Xie, M.; Yang, S.; Xu, Y.; Rui, N.; Lee, J.H.; Senanayake, S.D.; Li, K.; Wang, H.; Kattel, S.; Chen, J.G. Interfacial Active Sites for  $\text{CO}_2$ -Assisted Selective Cleavage of C-C/C-H Bonds in Ethane, *Chem*, **2020**, *6*, 2703.
- 57.** Vovchok, D.; Zhang, C.; Hwang, S.; Jiao, L.Y.; Zhang, F.; Liu, Z.Y.; Senanayake, S.D.; Rodriguez, J.A. Deciphering Dynamic Structural and Mechanistic Complexity in Cu/CeO<sub>2</sub>/ZSM-5 Catalysts for the Reverse Water-Gas Shift Reaction, *ACS Catal.* **2020**, *10*, 10216.
- 58.** Figueras, M.; Gutierrez, R.A.; Prats, H.; Viñes, F.; Ramirez, P.J.; Rodriguez, J.A. Illas, F. Supported Molybdenum Carbide Nanoparticles as Hot Hydrogen Reservoirs for Catalytic Applications, *J. Phys. Chem. Lett.* **2020**, *11*, 8437.
- 59.** Deng, K.; Lin, L.; Rui, N.; Vovchok, D.; Zhang, F.; S. Zhang, S.; Senanayake, S.D.; Kim, T.; Rodriguez, J.A. Studies of  $\text{CO}_2$  Hydrogenation over Cobalt/Ceria Catalysts with *In-situ* Characterization: The Effect of Cobalt Loading and Metal-Support Interactions on the Catalytic Activity, *Catal. Sci. & Technol.* **2020**, *10*, 6468.
- 60.** Mahapatra, M.; Betancourt, L.E.; Liu, Z.; Vovchok, D.; Simonovis, J.P.; Rodriguez, J.A.; S.D. Senanayake, S.D. In Situ Characterization of Metal/Oxide Catalysts for  $\text{CO}_2$  Conversion: From Fundamental Aspects to Real Catalyst Design, In: Heterogeneous

Catalysis for Energy Applications (Edited by Tomas R. Reina and Jose A. Odriozola), chapter 13, pages 431-458, Royal Society of Chemistry, **2020 (invited)**.

**61.** Rodriguez, J.A. Activation of Gold on Metal Carbides: Novel Catalysts for C1 Chemistry, *Frontiers in Chemistry*, **2020**, 7, 1 (**invited**).

**62.** Carrillo, P.; Shi, R.; Senanayake, S. D.; White, M. G. In Situ Structural Study of Manganese and Iron Oxide Promoted Rhodium Catalysts for Oxygenate Synthesis, *Appl. Catal. A Gen.* **608** **2020** 117845.

**63.** Wu, C.; Lin, L.; Liu, J.; Zhang, J.; Zhang, F.; Zhou, T.; Rui, N.; Yao, S.; Deng, Y.; Yang, F.; Xu, W.; Luo, J.; Zhao, Y.; Yan, B.; Wen, X-D.; Rodriguez, J.A.; Ma, D. Inverse ZrO<sub>2</sub>/Cu as a Highly Efficient Methanol Synthesis Catalyst from CO<sub>2</sub> Hydrogenation, *Nature Commun.* **2020**, 11, 5767.

## **2021**

**64.** Orozco, I.; Huang, E.; Mahapatra, M.; Shi, R.; Kang, J.; Nemšák, S.; Senanayake, S. D.; Liu, P.; Rodriguez, J. A., In Situ Studies of Methanol Decomposition Over Cu(111) and Cu<sub>2</sub>O/Cu(111): Effects of Reactant Pressure, Surface Morphology, and Hot Spots of Active Sites. *J. Phys. Chem. C* **2021**, 125, 558.

**65.** Tu, C.; Nie, X.; Chen, J.G. Insight into Acetic Acid Synthesis from the Reaction of CH<sub>4</sub> and CO<sub>2</sub>, *ACS Catal.*, **2021**, 11, 3384.

**66.** Wang, Y.; Winter, L.R.; Chen J.G.; Yan, B. CO<sub>2</sub> Hydrogenation over Heterogeneous Catalysts at Atmospheric Pressure: From Electronic Properties to Product Selectivity, *Green Chemistry*, **2021**, 23, 249.

**67.** Zhang, H.; Wang, X.; Frenkel, A. I.; Liu, P., Rationalization of promoted reverse water gas shift reaction by Pt<sub>3</sub>Ni alloy: Essential contribution from ensemble effect. *J. Chem. Phys.*, **2021**, 154, 014702.

**68.** Orozco, I.; Huang, E.; Mahapatra, M.; Kang, J.; Shi, R.; Nemšák, S.; Tong, X.; Senanayake, S. D.; Liu, P.; Rodríguez, J. A., Understanding Methanol Synthesis on Inverse ZnO/CuO<sub>x</sub>/Cu Catalysts: Stability of CH<sub>3</sub>O Species and Dynamic Nature of the Surface. *J. Phys. Chem. C*, **2021**, 125, 6673.

**69.** Xie, Z.; Winter, L.R.; Chen, J.G. “Bimetallic-Derived Catalysts and Their Application in Simultaneous Upgrading of CO<sub>2</sub> and Ethane”, *Matter*, **2021**, 3, 408.

**70.** Xie, Z.; Gomez, E.; Chen, J.G. Simultaneously Upgrading CO<sub>2</sub> and Light Alkanes into Value-added Products, *AIChE Journal*, **2021**, 67, e17249 (**Cover Perspective Article**)

71. Rui, N.; Zhang, X.; Zhang, F.; Liu, Z.; Cao, X.; Xie, Z.; Zou, R.; Senanayake, S.D.; Yang, Y.; Rodriguez, J. A.; Liu, C.-J. Highly Active Ni/CeO<sub>2</sub> Catalyst for CO<sub>2</sub> Methanation: Preparation and Characterization, *Appl. Catal. B Environ.* **2021**, *282*, 119581.
72. Winter, L.R.; Chen, J.G. N<sub>2</sub> Fixation by Plasma-Activated Processes, *Joule*, **2021**, *5*, 300.
73. Wang, X.; Ramírez, P. J.; Liao, W.; Rodriguez, J. A.; Liu, P., Cesium-Induced Active Sites for C–C Coupling and Ethanol Synthesis from CO<sub>2</sub> Hydrogenation on Cu/ZnO(000 $\bar{1}$ ) Surfaces. *J. Am. Chem. Soc.* **2021**, <https://doi.org/10.1021/jacs.1c03940>.
74. Kang, J.; Rui, N.; Huang, E.; Tian, Y.; Mahapatra, M.; Rosales, R.; Orozco, I.; Shi, R.; Senanayake, S. D.; Liu, P.; Rodriguez, J. A., Surface characterization and methane activation on SnO<sub>x</sub>/Cu<sub>2</sub>O/Cu(111) inverse oxide/metal catalysts. *Phys. Chem. Chem. Phys.* **2021**, <http://dx.doi.org/10.1039/D1CP02829D>.
75. Wang, J.; Ma, Y.; Mahapatra, M.; Kang, J.; Senanayake, S.D.; Tong, X.; Stacchiola, D.J.; White, M.G. Surface Structure of Mass-selected Niobium Oxide Nanoclusters on Au(111), *Nanotechnology*, accepted. DOI:
76. Zhang, F.; Gutiérrez, R.A.; Lustemberg, P.G.; Liu, Z.; Rui, N.; Wu, T.; Ramírez, P.J.; Xu, W.; Idriss, H.; Ganduglia-Pirovano, M.V.; Senanayake, S.D.; Rodriguez, J.A. Metal-support Interactions and C1 Chemistry: Transforming Pt-CeO<sub>2</sub> into a Highly Active and Stable Catalyst for the Conversion of Carbon Dioxide and Methane, *ACS Catal.* **2021**, *11*, 1613.
77. Danielis, M.; Betancourt, L.E.; Orozco, I.; Divins, N.J.; Llorca, J.; Rodríguez, J.A.; Senanayake, S.D.; Colussi, S.; Trovarelli, A. A Methane Oxidation Activity and Nanoscale Characterization of Pd/CeO<sub>2</sub> Catalysts Prepared by Dry Milling Pd Acetate and Ceria, *Appl. Catal. B Environ.* **2021**, *282*, 119567
78. Li, Y.; Kottwitz, M.; Vincent, J. L.; Enright, M. J.; Liu, Z.; Zhang, L.; Huang, J.; Senanayake, S. D.; Yang, W.-C. D.; Crozier, P. A.; et al. Dynamic Structure of Active Sites in Ceria-Supported Pt Catalysts for the Water Gas Shift Reaction. *Nat. Commun.*, **2021**, *12*, 1–9.
79. Zhou, J.; Du, L.; Braedt, D. L.; Miao, J.; Senanayake, S. D. Growth, Sintering, and Chemical States of Co Supported on Reducible CeO<sub>2</sub>(111) Thin Films: The Effects of the Metal Coverage and the Nature of the Support *J. Chem. Phys.* **2021**, *154*, 4.

*\*\* Jointly funded by this grant with leading contributions from another grant*

## **2018**

**80.** Ma, Z.; Zhang, Y.; Liu, S.; Xu, W.; Wu, L.; Hsieh, Y.-C.; Liu, P.; Zhu, Y.; Sasaki, K.; Renner, J. N.; Ayers, K. E.; Adzic, R. R.; Wang, J. X. Reaction Mechanism for Oxygen Evolution on RuO<sub>2</sub>, IrO<sub>2</sub>, and RuO<sub>2</sub>@IrO<sub>2</sub> Core-shell Nanocatalysts, *J. Electroanal. Chem.* **2018**, *819*, 296-305.

**81.** K. A. Kuttiyiel, S. Kattel, S. Cheng, J. H. Lee, L. Wu, Y. Zhu, G. Park, P. Liu, K. Sasaki, J. G. Chen, R. R. Adzic, “Au-doped stable L10 structured platinum cobalt ordered intermetallic nanoparticle catalysts for enhanced electrocatalysis”, *ACS Appl. Energy Mater.* **2018**, *1*, 3771–3777.

## **2019**

**82.** Zhou, Z.; Liu, P.; Yang, F.; Bao, X. Interface-Confined Triangular FeOx Nanoclusters on Pt(111), *J. Chem. Phys.* **2019**, *151*, 214704. (Invited).

## **2020**

**83.** Frenkel, A.; Rodriguez, J.A.; Chen, J.G. Synchrotron Consortia for Catalysis and Electrocatalysis Research, *Synchrotron Radiation News*, **2020**, *33*, 2

**84.** Lozano-Reis, P.; Sayos, R.; Rodriguez, J.A.; Illas, F. Structural, Electronic and Magnetic Properties of Ni Nanoparticles Supported on the TiC(001) Surface, *Phys. Chem. Chem. Phys.* **2020**, *22*, 26145.

**85.** Ke, W.; Liu, Y.; Wang, X.; Qin, X.; Chen, L.; Palomino, R. M.; Simonovis, J. P.; Lee, I.; Waluyo, I.; Rodriguez, J. A.; Frenkel, A. I.; Liu, P.; Zaera, F., Nucleation and Initial Stages of Growth during the Atomic Layer Deposition of Titanium Oxide on Mesoporous Silica. *Nano Letters* **2020**, *20*, 6884.

**86.** Koverga, A.A.; Florez, E.; Dorkis, L.; Rodriguez, J.A. Promoting Effect of Tungsten Carbide on Catalytic Activity of Cu for CO<sub>2</sub> Reduction *Phys. Chem. Chem. Phys.* **2020**, *22*, 13666.

**87.** Marcos, F.C.F.; Linb, L.; Betancourt, L.E.; Senanayake, S.D.; Rodriguez, J.A.; Assaf, J.M.; R. Giudici, R.; Assaf, E.M. Insights into the Methanol Synthesis Mechanism via CO<sub>2</sub> Hydrogenation over Cu-ZnO-ZrO<sub>2</sub> Catalysts: Effects of Surfactant/Cu-Zn-Zr Molar Ratio, *Journal of CO<sub>2</sub> Utilization*, **2020**, *41*, 101215.

**88.** Salvatore, K.L.; Deng, K.; Yue, S.; McGuire, S.; Rodriguez, J.A.; Wong, S.W. Optimized Microwave-based Synthesis of Thermally-Stable Inverse Catalytic Core-Shell Motifs for CO<sub>2</sub> Hydrogenation, *ACS Applied Materials and Interfaces*, **2020**, *12*, 32591.

**89.** Jimenez-Orozco, C.; Florez, E.; Viñes, F.; Rodriguez, J.A.; Illas, F. Critical Hydrogen Coverage Effect on the Hydrogenation of Ethylene Catalyzed by  $\delta$ -MoC (001): An *Ab Initio* Thermodynamic and Kinetic Study Jimenez-Orozco, *ACS Catal.* **2020**, *10*, 6213.

## **2021**

**90.** Bell, C. N.; Lee, D. C.; Drexler, M. N.; Rouleau, C. M.; Sasaki, K.; Senanayake, S. D.; Williams, M. D.; Alamgir, F. M.. Substoichiometric Tuning of the Electronic Properties of Titania, *Thin Solid Films* **2021**, *717*, 138437.

**91.** Koverga, A.A.; Flórez, E.; Jimenez-Orozco, C.; Rodriguez, J.A. Not All Platinum Surfaces are the Same: Effect of the Support on Fundamental Properties of Platinum Adlayer and its Implications for the Activity toward the Hydrogen Evolution Reaction, *Electrochimica Acta*, **2021**, *368*, 137598

**Catalysis Beyond the Active Site: Identification and quantification of distinct active sites in Hf-Beta zeolites for transfer hydrogenation catalysis**

Yuriy Román-Leshkov, John R. Di Iorio, and Blake A. Johnson  
Department of Chemical Engineering, Massachusetts Institute of Technology

**Presentation Abstract**

Lewis acidic zeolites are microporous crystalline materials that offer promise as catalysts for the activation and conversion of biomass-derived precursors in the liquid-phase due to their unique water-tolerance and synthetic versatility. Despite the significant progress made in characterizing different framework heteroatom coordination environments that exist in Lewis acidic zeolites with probe molecule adsorption and spectroscopy, methods to reliably quantify site counts remain indefinite and are primarily limited to Sn and Ti Lewis acid sites. Here, methods to quantify framework Lewis acidic Hf<sup>4+</sup> sites in zeolite Beta (Hf-Beta) with two Lewis base titrants (pyridine, deuterated acetonitrile) were developed using infrared (IR) spectroscopy. IMECs measured for IR peaks reflecting pyridine bound to Lewis acidic Hf sites ( $\epsilon(\text{Hf}; 1448 \text{ cm}^{-1})$ :  $1.54 \pm 0.21$ ) and CD<sub>3</sub>CN bound to open ( $\epsilon(\text{Hf}; 2313 \text{ cm}^{-1})$ :  $2.40 \pm 0.22$ ) and closed ( $\epsilon(\text{Hf}; 2307 \text{ cm}^{-1})$ :  $3.55 \pm 0.41$ ) Hf sites, gave similar counts for the total number of Lewis acidic sites across six Hf-Beta zeolites (Si/Hf = 100-413). Consistent with previous reports with Sn-Beta catalysts where open Sn sites are responsible for catalytic turnover, apparent first and zero-order MPVO rate constants (0.01-1 M cyclohexanone in 2-butanol; per total Hf, 373 K) correlated with the total number of open Hf sites, per total Hf, but not with the total number of closed Hf sites or total Lewis acid site counts. Precise mechanistic interpretation of liquid-phase zeolite catalysis necessitates the development of synthetic, spectroscopic, and kinetic methods that can decouple such complex active site structures and probe the interactions that occur between confined active sites, solvent and reactant molecules, and adsorbed intermediates and transition states. The characterization methods reported herein enable normalization of initial MPVO turnover rates on Hf-Beta zeolites by their number of open Hf sites, as required prior to interpreting the consequences of varying active site identity, solvation, and pore topology in liquid-phase catalysis.

**Grant or FWP Number: DE-SC0016214**

**RECENT PROGRESS**

*Solvent Effects in Lewis Acid Zeolites*

The disruption of ordered water molecules confined within hydrophobic reaction pockets alters the energetics of adsorption and catalysis, but a mechanistic understanding of how nonaqueous solvents influence catalysis in microporous voids remains unclear. Here, we use kinetic analyses coupled with IR spectroscopy to study how alkanol hydrogen-bonding networks confined within hydrophobic and hydrophilic zeolite catalysts modify reaction free energy landscapes. Hydrophobic Beta zeolites containing framework Sn atoms

catalyze the transfer hydrogenation reaction of cyclohexanone in a 2-butanol solvent  $10\times$  faster than their hydrophilic analogues. This rate enhancement stems from the ability of hydrophobic Sn-Beta to inhibit the formation of extended liquid-like 2-butanol oligomers and promote dimeric H-bonded 2-butanol networks. These different intraporous 2-butanol solvent structures manifest as differences in the activation and adsorption enthalpies and entropies that comprise the free energy landscape of transfer hydrogenation catalysis. The ordered H-bonding solvent network present in hydrophobic Sn-Beta stabilizes the transfer hydrogenation transition state to a greater extent than the liquid-like 2-butanol solvent present in hydrophilic Sn-Beta, giving rise to higher turnover rates on hydrophobic Sn-Beta. Additionally, reactant adsorption within hydrophobic Sn-Beta is driven by the breakup of intraporous solvent–solvent interactions, resulting in positive enthalpies of adsorption that are partially compensated by an increase in the solvent reorganization entropy. Collectively, these results emphasize the ability of the zeolite pore to regulate the structure of confined nonaqueous H-bonding solvent networks, which offers an additional dimension to modulate adsorption and reactivity.

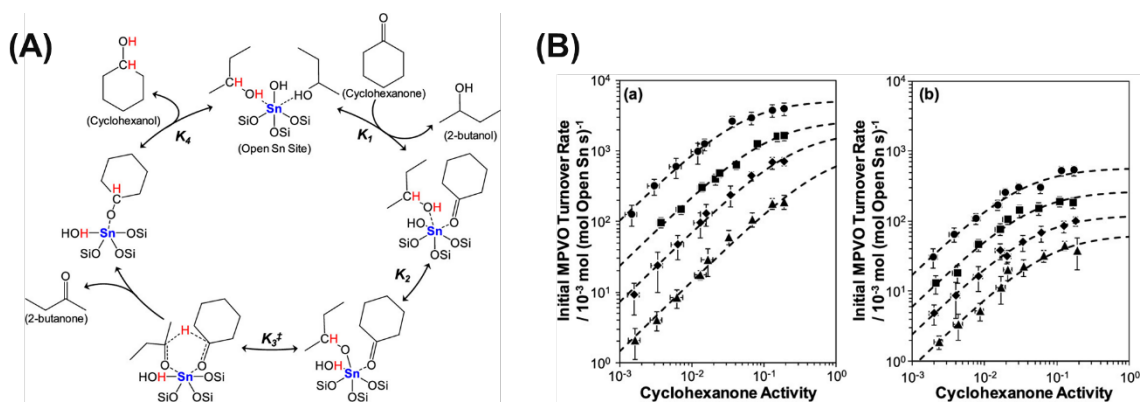


**Figure 1.** (A) Proposed MPVO Reaction mechanism between 2-butanol and cyclohexanone over an open Sn site in a 2-butanol solvent. (B) Cyclohexanol formation rates (per open Sn site) measured on (a) Sn-Beta-F and (b) Sn-Beta-OH as a function of cyclohexanone activity (0.01–1 M cyclohexanone) in 2-butanol at 333 K (▲), 353 K (◆), 373 K (■), and 393 K (●).

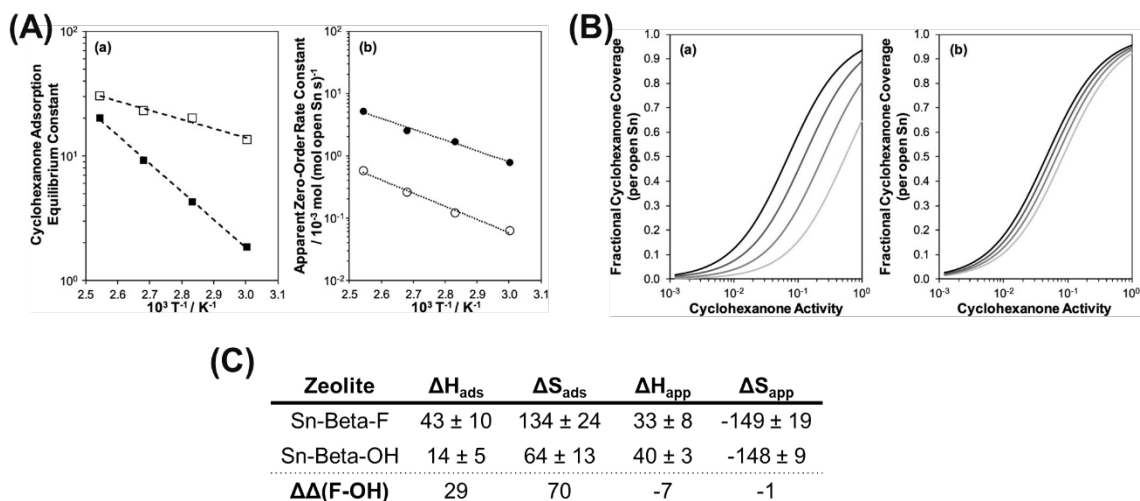


**Figure 2.** (A) Cyclohexanone adsorption equilibrium constants (a) and apparent zero-order rate constants (b) per open Sn site determined by regression to initial MPVO turnover rates (per open Sn site) measured on Sn-Beta-F (filled) and Sn-Beta-OH (open) in a 2-butanol solvent as a function of temperature (333–393 K). Dashed lines are exponential fits to the data. (B) Fractional cyclohexanone coverage (per open Sn site) as a function of temperature (333–393 K light to dark) and cyclohexanone activity (0.01–1 M cyclohexanone) in a 2-butanol solvent on (a) Sn-Beta-F and (b) Sn-Beta-OH. (C) Values of  $\Delta H_{\text{ads}}$ ,  $\Delta S_{\text{ads}}$ ,  $\Delta H_{\text{app}}$ , and  $\Delta S_{\text{app}}$  determined from experimental kinetics measured on Sn-Beta-F and Sn-Beta-OH in a 2-butanol solvent. Units of  $\Delta H$  are  $\text{kJ mol}^{-1}$  and units of  $\Delta S$  are  $\text{J mol}^{-1} \text{K}^{-1}$ .

### *Controlled Formation of Lewis Acidic Active Sites*

The selective incorporation of isolated framework Lewis acid sites at specific crystallographic positions in high-silica zeolites was achieved by applying a rationalized post-synthetic grafting methodology. The removal of framework Ge atoms from a Ge-BEC zeolite with low concentrations of Ge in the framework ( $\text{Si/Ge} \sim 150$ ) followed by grafting allows the synthesis of Sn-BEC zeolites with Sn atoms positionally biased into the double-4-ring (D4R) crystallographic positions of the BEC framework. Spectroscopic characterization using solid-state nuclear magnetic resonance (NMR) coupled with theoretical calculations revealed that Sn atoms preferentially form open Sn sites in the D4R of Sn-BEC. This observation was supported by IR spectra of adsorbed deuterated acetonitrile ( $\text{CD}_3\text{CN}$ ), a known titrant of Sn sites in zeolites. The catalytic implications of selective incorporation of open Sn sites in Sn-BEC were probed using the Meerwein–Ponndorf–Verley–Oppenauer (MPVO) reaction. Although the MPVO turnover rates normalized by the total number of open Sn sites were comparable on Sn-BEC and a conventional Sn-Beta catalyst synthesized in fluoride media (Sn-Beta(F)), Sn-BEC demonstrated higher per gram reaction rates because of its larger fraction of open sites compared to Sn-Beta(F). These results highlight the advantage of placing active sites in targeted locations within a zeolite structure.

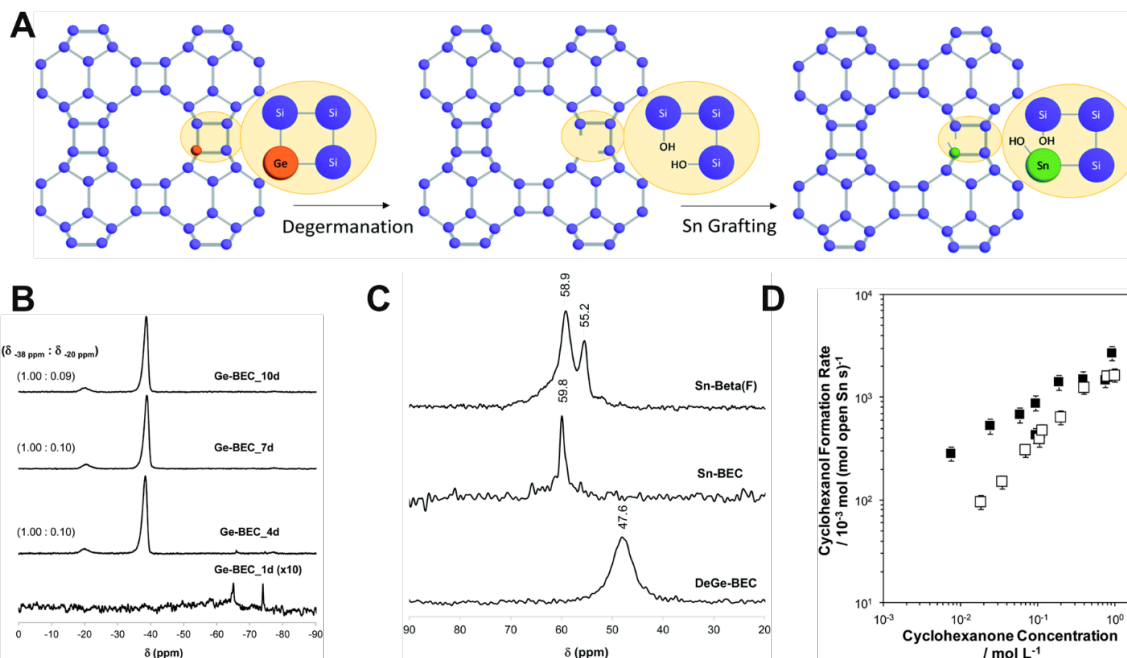


**Figure 3.** (A) Schematic representation of the multi-step synthesis procedure to selectively place Sn in d4rs of high-silica BEC zeolites. (B)  $^{19}\text{F}$  MAS NMR spectra of the as-prepared Ge-containing BEC materials after different crystallization times. The measured signal ratios are included for all Ge-BEC samples. (C)  $^{31}\text{P}$  MAS NMR spectra of TMPO dosed on DeGe-BEC, Sn-BEC and Sn-Beta-F at P/Sn = 0.5 loading. (D) Cyclohexanol formation rates (373 K, per open Sn site) measured on Sn-BEC (solid squares) and Sn-Beta(F) (open squares) zeolites. Error bars represent propagated experimental uncertainty.

### Quantification of Active Sites in Hf-Beta Zeolites

Mechanistic interpretation of kinetic data measured on different metallosilicate zeolites requires that turnover rates be rigorously normalized by the total number of active sites that catalyze such reactions. This is critical for the comparison of transfer hydrogenation rates across different catalysts and reaction solvents because open sites, not closed sites, have been reported to be the active site for this class of reactions in Lewis acidic zeolites containing different heteroatoms (e.g., Sn, Hf, Zr). Efforts to quantify these different site types, however, has primarily focused on characterizing Sn-containing zeolites using various titrants (e.g., CD<sub>3</sub>CN, pyridine, trimethylphosphine oxide) and spectroscopic methods (e.g., IR and NMR) despite reports that Hf-containing zeolites routinely demonstrate exceptional performance, compared to Sn, for a range of catalytic transformations of oxygenates in the liquid phase. Here, we demonstrate methods to quantify different Lewis acid sites in Hf-Beta zeolites using infrared spectroscopic measurements of adsorbed pyridine and CD<sub>3</sub>CN titrants. Additionally, turnover rates on

transfer hydrogenation catalysis appear to correlate with the total number of  $2310\text{ cm}^{-1}$  sites, and not the sites at  $2305\text{ cm}^{-1}$ , suggesting that the  $2310\text{ cm}^{-1}$  belongs to open Hf sites (i.e.,  $\text{Hf}(\text{OSi})_3\text{OH}$ ).

.....

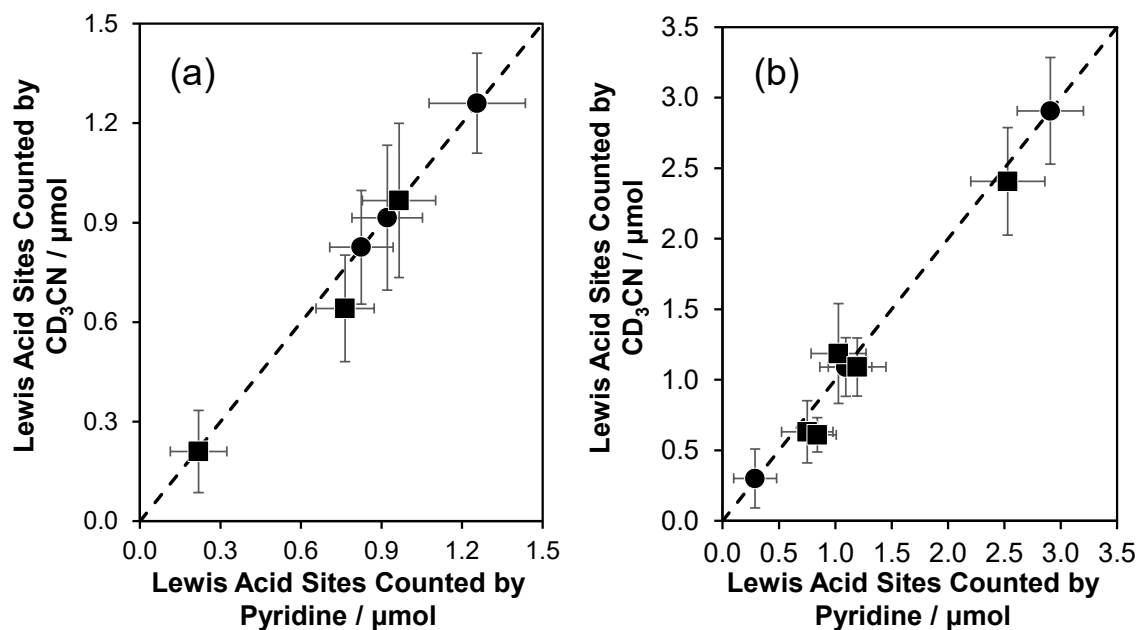


**Figure 4.** Number of Lewis acidic Hf sites counted by pyridine and  $\text{CD}_3\text{CN}$  on (a) six different Sn-Beta zeolites with  $\text{Si}/\text{Sn} = 81-337$  and (b) 8 different Hf-Beta zeolites with  $\text{Si}/\text{Hf} = 100-413$ . Circles represent samples used for the fitting of  $\text{CD}_3\text{CN}$  IMECs and squares are additional M-Beta samples not used in IMEC fitting. Dashed line is a parity line. Error bars reflect propagated experimental uncertainties.

.....

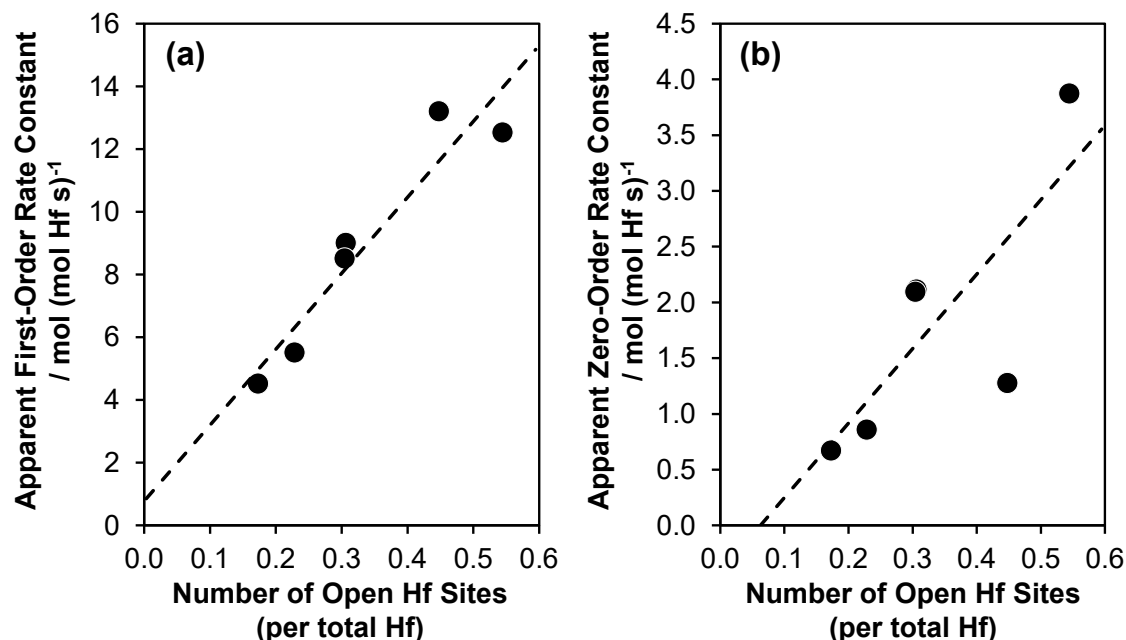


**Figure 5.** Apparent first-order (a) and zero-order (b) MPVO rate constants (per total Hf, 373 K) as a function of the total number of open Hf sites ( $2313 \text{ cm}^{-1}$ , per total Hf). Dashed lines represent linear regressions to the data sets.

---

#### Publications Acknowledging this Grant in 2018-2021

1. Di Iorio, J.R.; Johnson, B.A.; Román-Leshkov, Y. Ordered Hydrogen-Bonded Alcohol Networks Confined in Lewis Acid Zeolites Accelerate Transfer Hydrogenation Turnover Rates. *J. Am. Chem. Soc.* **2020**, *142*, 19379-19392.
2. Rodríguez-Fernández, A. †; Di Iorio, J.R. †; Paris, C.; Boronat, M.; Corma, A.; Román-Leshkov, Y.; Moliner, M. Catalytic implications of selective active site placement in Lewis acid zeolites. *Chem. Sci.*, **2020**, *11*, 10225-10235.
3. Bagi, S.; Wright, A.M.; Oppenheim, J.; Dinca, M.; Román-Leshkov, Y. Accelerated Synthesis of a  $\text{Ni}_2\text{Cl}_2(\text{BTDD})$  Metal–Organic Framework in a Continuous Flow Reactor for Atmospheric Water Capture. *ACS Sus. Chem. Eng.*, **2020**, *9*, 3996-4003.
4. Johnson, B.A.; Di Iorio, J.R.; Román-Leshkov, Y. Tailoring Distinct Reactive Environments in Lewis Acid Zeolites for Liquid Phase Catalysis. *Acc. Mater. Res.*, Accepted.
5. Johnson, B.A. †; Di Iorio, J.R. †; Román-Leshkov, Y. Identification and quantification of distinct active sites in Hf-Beta zeolites for transfer hydrogenation catalysis. *J. Catal.*, Submitted.

*All work intellectually led by this grant*

**Awards or leadership activities during 2018-2020 calendar years**

Robert T. Haslam (1911) Chair Professorship	<b>2021</b>
Duncan & Suzanne Mellichamp Emerging Leader Lectureship, UCSB	<b>2019</b>
ACS Early Career in Catalysis Award (Inaugural)	<b>2019</b>
Bose Fellow	<b>2019</b>
Rutherford Aris Award, NASCRE	<b>2019</b>
AICHE Catalysis and Reaction Engineering Division Young Investigator Award (Inaugural)	<b>2018</b>
Robert Augustine Award granted by the ORCS	<b>2018</b>

Aaron D. Sadow

**Uniform catalytic environments at the interface: characterization of sites and distributions, catalytic activity, and reaction mechanisms**

Aaron D. Sadow, Takeshi Kobayashi, Marek Pruski, Frédéric A. Perras, Long Qi, Igor I. Slowing  
Ames Laboratory, U.S. DOE, Iowa State University, Ames, IA 50011-3111

**Presentation Abstract**

The mission of the Ames Lab collaborative Program in Catalysis Science is to enable efficient and selective transformations by developing new catalytic principles for uniting the best features of homogeneous and heterogeneous catalysis in 3D environments. The overarching goal of this fundamental research is to synthesize and study highly uniform solid catalysts that mediate the difficult carbon-oxygen and carbon-hydrogen bond cleavage reactions, which are needed to utilize bioderived feedstocks and abundant hydrocarbons for chemical synthesis. To this end our research team combines expertise in mesoporous and nanostructured catalyst synthesis, organometallic chemistry, kinetics and mechanisms of catalytic reactions, and solid-state (SS)NMR, including the ultrasensitive dynamic nuclear polarization (DNP) technique. Uniform materials are essential because their spectroscopic features characterize the most important and most pertinent species and functionality for affecting the overall catalytic properties, thus facilitating the rational improvement of catalysts. Unfortunately, catalytic species operating at the solid-liquid interface rarely approach the ideal homogeneity (sometimes) epitomized by chemistry in a single phase. To address this gap, our team combines advanced materials synthesis and surface organometallic chemistry with cutting-edge NMR spectroscopic methods to construct uniform organometallic catalytic sites, distributed evenly in the uniform environments created by pores of hierarchical functionalized mesoporous materials. These species represent several classes of catalysts commonly applied in hydrogenations and hydrodeoxygenations of oxygenates or in C-H bond activations, which are nonetheless currently limited. Using the uniform materials and operando spectroscopy, we elucidate molecular-level mechanisms, including those involved in complex reaction networks, and then ameliorate the features that constrain catalytic performance.

**AL-03-380-011: Homogeneous and Interfacial Catalysis in 3D Controlled Environments**

**Postdoc(s):** Junlei Cui, Pranaw Kunal, Guillaume Laurent, Yuting Li, Alexander Paterson, Guocang Wang

**Student(s):** Kevin Basemann, Puranjan Chatterjee, Yang-Yun Chu, Pranjali Naik

## RECENT PROGRESS

**Zinc-silane and zinc-alcohol intermediates in dehydrocoupling.** We sought new catalytic methods for silylation of silica surfaces to create uniform materials for organometallic sites. Zinc alkyl compounds supported by the *N,N*-bidentate phenyl-bis(4,4-dimethyl-oxazolinato) ligand ( $\text{PhBOX}^{\text{Me}_2}\text{ZnR}$ ; R = Me, Et) catalyze the dehydrocoupling of primary or secondary silanes and alcohols to give silyl ethers and hydrogen. The three-coordinate organozinc pre-catalysts are synthesized by reaction of  $\text{ZnR}_2$  (R = Me, Et) and 1,1-bis-(4,4-dimethyl-2-oxazoliny)phenylmethane ( $\text{Ph}_2\text{BOX}^{\text{Me}_2}$ ).  $\text{PhBOX}^{\text{Me}_2}\text{ZnMe}$  and  $\text{R}'\text{OH}$  (R' = Me, *i*Pr, 3,5- $\text{C}_6\text{Me}_2\text{H}_3$ ) react to form monomeric  $\text{PhBOX}^{\text{Me}_2}\text{ZnOR}'$  (R' = Me, *i*Pr, 3,5- $\text{C}_6\text{Me}_2\text{H}_3$ ) as likely catalytic intermediates. In  $\text{PhBOX}^{\text{Me}_2}\text{ZnR}$ -catalyzed dehydrocoupling reactions, primary and secondary silanes react with small, medium, and large alcohols to give varying degrees of substitutions, from mono-alkoxylation to tri-alkoxylation, while tri-substituted silanes do not react with MeOH under these conditions.<sup>25</sup> The

$\text{PhBOX}^{\text{Me}_2}\text{ZnMe}$ -catalyzed reaction of  $\text{PhSiH}_3$  and methanol affords high turnover numbers, up to  $10^7$ , under solvent-free conditions. Remarkably, several rate laws characterize the  $\text{PhBOX}^{\text{Me}_2}\text{ZnMe}$ -catalyzed reaction of 3,5-dimethylphenol (ArylOH) and  $\text{PhMeSiH}_2$ . The catalytic rate laws vary considerably, depending on the concentrations of the aryl

alcohol and silane reactants (Figure 1). A ternary rate law ( $\text{rate} \propto [\text{Zn}]^1[\text{PhMeSiH}_2]^1[\text{ArylOH}]^1$ ) was measured under conditions with excess ArylOH (25-1.5 equiv. compared to  $\text{PhMeSiH}_2$ ); furthermore, kinetic data indicate saturation and then inhibition occurs at high  $[\text{ArylOH}]$ . Alternatively, second-order and first-order rate laws ( $\text{rate} \propto [\text{Zn}]^1[\text{PhMeSiH}_2]^1[\text{ArylOH}]^0$  and  $\text{rate} \propto [\text{Zn}]^1[\text{PhMeSiH}_2]^0[\text{ArylOH}]^0$ ) were determined for lower concentrations of ArylOH (1-1.4 and 0.037-0.80 equiv compared to  $\text{PhMeSiH}_2$ ). The latter two rate laws were shown to be mechanistically related, through saturation in  $\text{PhMeSiH}_2$ . Two catalytic mechanisms are proposed to account for the changes in rate law with reactant concentrations, which also affect the apparent reaction rates and have important implications for comparisons of catalytic performance and design of selective zinc catalysts. A proposed sequence which accounts for saturation behavior and zero-order silane dependence invokes reversible coordination of hydrosilane to the unsaturated, three-coordinate zinc center prior to  $\sigma$ -bond metathesis.

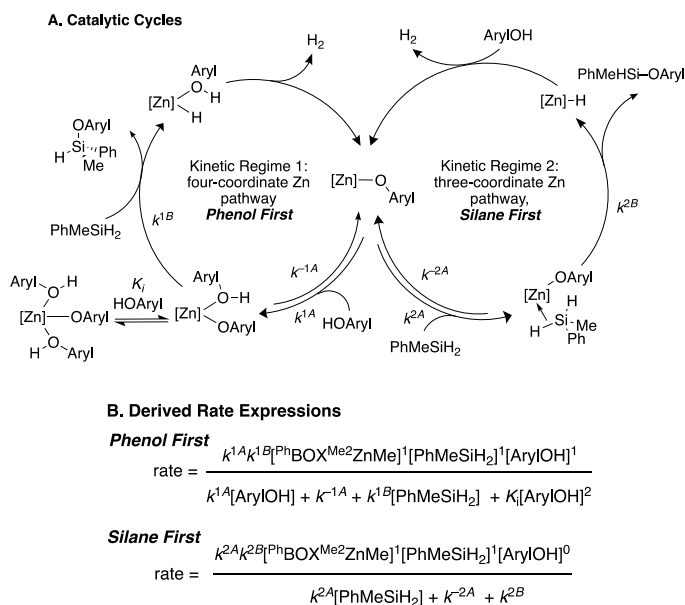


**Figure 1.** Proposed mechanisms for dehydrocoupling of silanes and alcohols derived from observed rate laws.

**Facile and precise control of size in ligand-free catalytic nanoparticles.** Studying structure-sensitive reactions requires the synthesis of catalytic nanoparticles with precisely controlled sizes. Conventional nanoparticle synthesis utilizes capping agents to adjust their size and prevent aggregation. However, capping agents typically block access to the surface of the catalytic particles. Removal of capping agents can lead to undesired nanoparticle sintering and surface disruption. Here, we demonstrate the facile production of size-controlled Pd nanoparticles by directly forming them inside the pores of ordered mesoporous silica nanoparticles (MSN).<sup>26</sup> MSN have narrow pore width distributions that can be adjusted during their synthesis.

Deposition precipitation of Pd(NH<sub>3</sub>)<sub>4</sub>Cl<sub>2</sub> at controlled pH followed by mild hydrogenation yielded Pd nanoparticles inside MSN pores.

The Pd particle size distributions matched closely the pore width distributions of the MSN supports (Figure 2) indicating that confinement in the pores is an effective way to restrict nanoparticle growth. CO pulsed chemisorption of the materials confirmed the Pd surface was accessible and provided an additional estimation

of particle size that corresponded well with the one observed by HAADF STEM analysis.

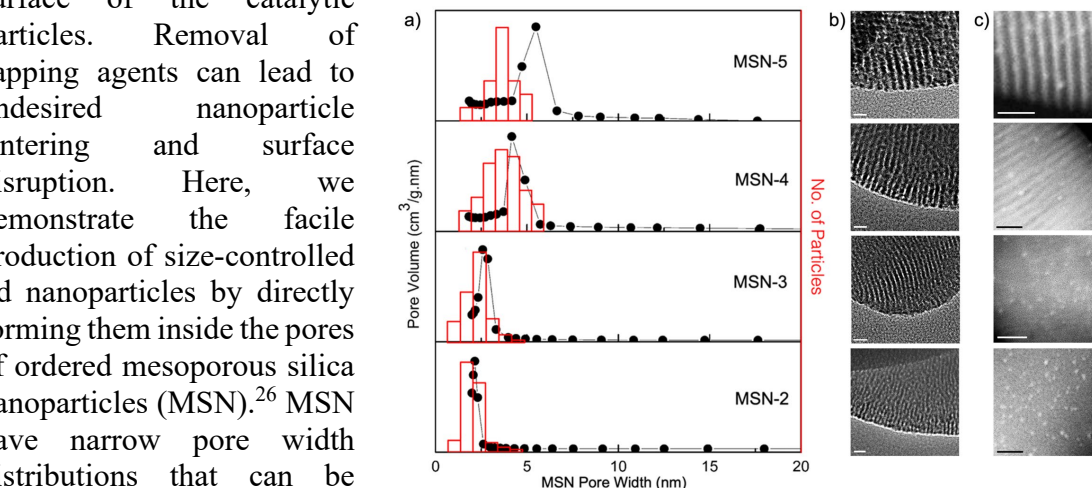


**Figure 2.** a) Overlaid pore width distributions of MSN supports (black scatter plot) with size distributions (red histograms) of Pd nanoparticles produced inside of them. b) TEM images of the original MSN and c) HAADF-STEM images of the nanoparticles in each material. All scale bars are 10 nm.

of particle size that corresponded well with the one observed by HAADF STEM analysis.

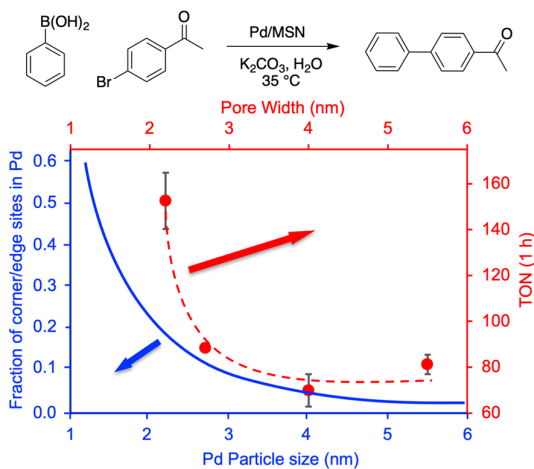


**Figure 3.** a) Catalytic activity of Pd/MSN as a function of pore width (red scatter plot, trace, and axes), and statistical estimation of the fraction of edges and corners in fcc Pd truncated cuboctahedra as a function of their size (blue trace and axes).

The Pd/MSN materials with different Pd particle sizes were then used as catalysts for Suzuki-Miyaura cross coupling and phenol hydrogenation reactions. Structure sensitivity was observed for both reactions. A dramatic increase in catalytic activity (normalized to accessible Pd surface) was observed for both types of reaction when particle size decreased below 2.5 nm, demonstrating structure sensitivity of the processes. Comparison of the change in reactivity with the estimated fraction of corners and edges in truncated cuboctahedra suggested a correlation between abundance of low coordinated metallic sites and catalytic activity (Figure

3). Furthermore, CO chemisorption DRIFTS revealed a blue shift in the  $\nu_{\text{C=O}}$  for the smallest particles with respect to those larger than 2.5 nm suggesting a higher backbonding capacity that may also be responsible for their enhanced reactivity.

**Substrate binding on  $\text{CeO}_2$  support defects enhances reactivity in Pd catalyzed hydrodehalogenation reactions.** The catalytic activity of Pd/ $\text{CeO}_2$  for the hydrodehalogenation (HDH) of halophenols benefits from the interaction of hydroxyl groups in the substrate with the support. The Hammett plot of the reaction shows that increasing the electron density on halo-aromatic substrates enhances the rates of HDH (Figure 4a). The high halophenol HDH activity of the catalyst can be attributed to electron-rich phenoxide species generated upon dissociative adsorption of the substrate onto the support. Formation of these phenoxide species is evidenced by NMR, DRIFT, XP and Raman spectroscopies. The catalytic cycle of halophenol HDH on Pd/ $\text{CeO}_2$  seems to follow a sequence of dissociative adsorption, oxidative addition, and reductive elimination, with the last step being turnover limiting (Figure 4b). The catalytic activity depends strongly on the nature of the halogen. Arranging the rates of Pd/ $\text{CeO}_2$ -catalyzed HDH as a function of halogen size gives a volcano plot. This reactivity order is likely due to a balance between the relative barriers for C-X bond cleavage and H-X desorption during the oxidative addition and reductive elimination steps of the reaction, respectively. The HDH reactivity order, however, favors conversion of larger halides when the reaction is performed on mixed substrates (*i.e.* halophenols containing different halogens, or mixtures of different halophenols). The likely reason for this difference is that larger halides have lower BDE and therefore undergo oxidative addition faster than the smaller halides. However, once the larger halide is chemisorbed on the catalyst it blocks active sites for reaction with the smaller halides. The strong adsorption of iodine on Pd results in poor HDH activity. However, addition of pyridine to the reaction mixture facilitates reductive elimination in the form of pyridinium iodide, which ultimately restores catalyst turnover.

**Divergent reaction pathways for C-O cleavage by size-controlled Pd catalysts.** Precious metals are ideal catalysts for cleaving strong covalent bonds such as carbon-oxygen linkages in biomass. However, the high costs and low natural abundance of these critical elements demand us to design effective and robust catalysts with high atom economy. Therefore, we synthesized several Pd-based catalysts with different dispersion based on distinctive metal-support interaction and studied their catalytic performance for C-O hydrogenolysis. The speciation of Pd was achieved with a series of characterization

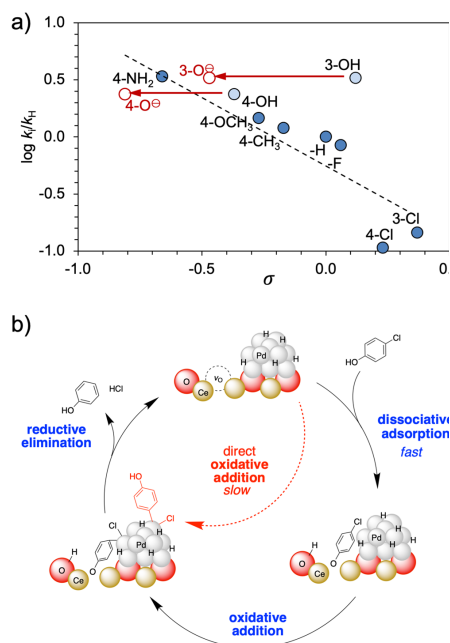


**Figure 4.** a) Hammett plot for the Pd/ $\text{CeO}_2$  catalyzed HDH of substituted halophenols, replacing the  $\sigma$  of -OH substituents with that of -O<sup>-</sup> leads to improved alignment with the correlation trend; b) proposed cycle of the Pd/ $\text{CeO}_2$  catalyzed HDH.

including X-ray absorption spectroscopy and electron microscopy. High surface area ceria<sup>64</sup> leads to the formation of single-atom Pd while other supports (silica, gamma-alumina, and titania) render Pd nanoparticles of different sizes. Catalytic studies were carried out with PPE as a lignin beta-O-4 model compound (Figure 5) containing both an alpha-OH group and beta-ether linkage. Results shows the Pd dispersion has significant impact on both activity and selectivities. Single-atom Pd on ceria catalyze the cleavage of the ether linkage to produce 1-phenylethanol but all other catalysts with Pd nanoparticles primarily activate the alpha-OH group to produce PEB. In the presence of larger Pd nanoparticles, PPE also undergoes arene hydrogenation as undesired side products. Further kinetics indicate that the conversion of PPE by Pd/Ceria catalyst is of zero-order rate law on hydrogen pressure, indicating the reaction can operate with low pressure and agreeing with our recent observation.<sup>18, 46</sup> Overall, the mechanistic and kinetic studies indicate that atomic-precise synthesis of catalysts can bring new opportunities in strong-bond activation and enable effective chemical and energy transformation by making every atom count.

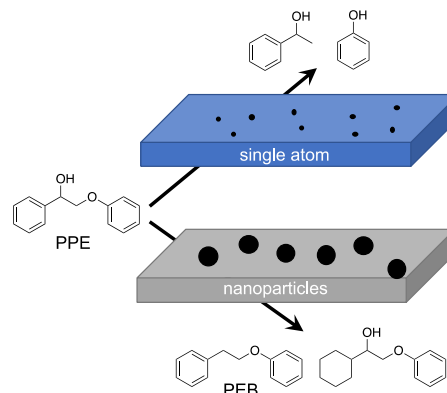


**Figure 5.** Divergent bond activation mechanism induced by Pd single atom and nanoparticles.

**Detailed Structures of Catalytic Active Sites through Sensitivity-Enhanced NMR.** Structural homogeneity at the active site is a necessity for obtaining highly selective catalysts. While much effort has been placed toward the synthesis of active sites with predetermined structures to achieve high activity, selectivity, and stability, to a large degree the structures of active sites in heterogeneous catalysts remain imprecise. This lack of high-resolution structural information has led to difficulties in rationalizing reaction outcomes, and the design of bespoke catalytic active sites.

At present, nuclear magnetic resonance (NMR) spectroscopy is the only tool capable of providing unambiguous and quantitative structural metrics (internuclear distances) with the range and scale required to elucidate full, three-dimensional, structures of sites situated on amorphous surfaces. Sensitivity, however, prevented the realization of this potential. We have demonstrated that, with sensitivity enhancement provided through dynamic nuclear polarization (DNP), it is possible to measure a large number of information-rich distances from surface sites.<sup>29</sup> In particular, by developing large multispin simulations of rotational-echo double-resonance (REDOR) data, we were able to measure accurate vertical distances between natural abundance <sup>13</sup>C sites in a organoiridium(III) pincer complex and the <sup>27</sup>Al sites in the Al<sub>2</sub>O<sub>3</sub> support. Each such distance reveals nontrivial information relating to the orientation, and in turn configuration, of the catalytic active site. The data together fully determines the positions, and orientation of the ligands relative to the support and enables, in combination with density functional theory and X-ray absorption spectroscopy, for the complete determination of the three-dimensional structure of the active site. In particular, we found that the bulky pincer ligand formed an angle of ~35° relative to the surface, and had a single, THF-capped, open coordination site in a very accessible location (Figure 6). The intimate knowledge of the three-dimensional catalytic

pocket in this and other catalysts will enable for unprecedented active site design in heterogeneous catalysis.

In another study<sup>61</sup> we applied  $^1\text{H}$  detection under fast-MAS to enable the measurement of homo- and heteronuclear proximities in a sulfated alumina-supported  $\text{Cp}^*\text{Zr}(\text{CH}_3)_3$  olefin polymerization catalyst. These correlation experiments, together with quantitative  $^{13}\text{C}$  NMR, helped determine the chemical composition and the physical conformation of the catalyst. Crucially, it was found that the complex grafted through methide transfer rather than protonolysis, leading to an electrostatically-bound complex:

$[\text{AlO}_x(\text{CH}_3)]^- [\text{ZrCp}^*(\text{CH}_3)_2]^+$ , as observed through a 2:1 ratio of Zr-CH<sub>3</sub> and Al-CH<sub>3</sub>  $^{13}\text{C}$  NMR signals.  $^1\text{H}$  homonuclear correlation experiments were able to confirm this through the detection of proximities between the Cp\* and Al-CH<sub>3</sub>  $^1\text{H}$  sites. Moving forward, the development of methodology to detect intermolecular proximities on surfaces, and in particular between surface functionalities and organometallic complexes, will enable us to improve catalytic activity and selectivity through the generation of localized microenvironments.

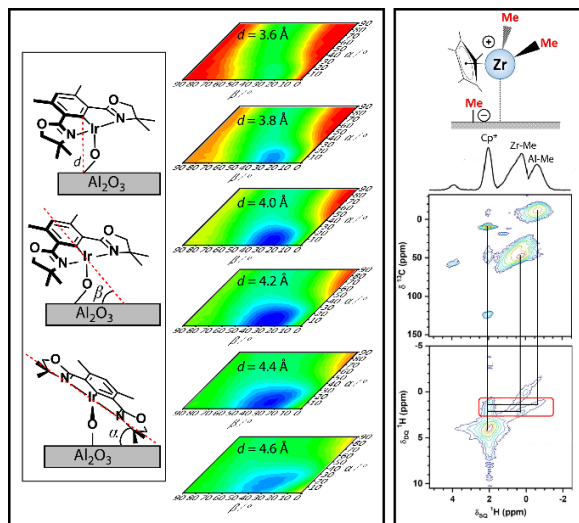


**Figure 6.** (left) Agreement between experimental and simulated REDOR data are plotted as an RMSD as a function of the orientation of the complex, defined in a polar coordinate system. (right)  $^1\text{H}$  detected  $^1\text{H}$ - $^{13}\text{C}$  and  $^1\text{H}$ - $^1\text{H}$  correlation experiments showing the formation of an electrostatically-bound Zr complex, in close proximity to a surface Al methyl.

## Publications Acknowledging this Grant in 2018-2021

### Source of support for the work published:

(I) *Intellectually led by this grant*<sup>1-31</sup>

(II) *Jointly funded by this grant and other grants with intellectual leadership by other funding sources*<sup>32-63</sup>

1. Wang, Z.; Opembe, N.; Kobayashi, T.; Nelson, N. C.; Slowing, I. I.; Pruski, M., Quantitative Atomic-scale Structure Characterization of Ordered Mesoporous Carbon Materials by Solid State NMR. *Carbon* **2018**, *131*, 102-110. doi:10.1016/j.carbon.2018.01.087
2. Reinig, R. R.; Fought, E. L.; Ellern, A.; Windus, T. L.; Sadow, A. D., Cobalt(II) Acyl Intermediates in Carbon-Carbon Bond Formation and Oxygenation. *Dalton Trans.* **2018**, *47*, 12147-12161. doi:10.1039/C8DT02661K
3. Perras, F. A.; Wang, J. S.; Manzano, J. S.; Chaudhary, U.; Opembe, N.; Johnson, D. D.; Slowing, I. I.; Pruski, M., Optimal Sample Formulations for DNP SENS: The

- Importance of Radical-Surface Interactions. *Curr. Opin. Colloid Interface Sci.* **2018**, *33*, 9-18.
- Perras, F. A.; Kobayashi, T.; Pruski, M., Growing Signals from the Noise: Challenging Nuclei in Materials DNP. *Emagres* **2018**, *7*, 35-50. doi:10.1002/9780470034590.emrstm1556
  - Perras, F. A.; Boteju, K. C.; Slowing, I. I.; Sadow, A. D.; Pruski, M., Direct  $^{17}\text{O}$  Dynamic Nuclear Polarization of Single-site Heterogeneous Catalysts. *Chem. Commun.* **2018**, *54*, 3472-3475. doi:10.1039/C8CC00293B
  - Manzano, S. J.; Singappuli-Arachchige, D.; Parikh, B. L.; Slowing, I. I., Fine-tuning the Release of Molecular Guests from Mesoporous Silicas by Controlling the Orientation and Mobility of Surface Phenyl Substituents. *Chem. Eng. J.* **2018**, *340*, 73-80. doi:10.1016/j.cej.2017.12.015
  - Maluta, J. R.; Machado, S. A. S.; Chaudhary, U.; Manzano, J. S.; Kubota, L. T.; Slowing, I. I., Development of a Semigraphitic Sulfur-doped Ordered Mesoporous Carbon Material for Electroanalytical Applications. *Sens. Actuators, B* **2018**, *257*, 347-353. doi:10.1016/j.snb.2017.10.164
  - Kobayashi, T.; Singappuli-Arachchige, D.; Slowing, I. I.; Pruski, M., Spatial Distribution of Organic Functional Groups Supported on Mesoporous Silica Nanoparticles (2): A Study by  $^1\text{H}$  Triple-Quantum Fast-MAS Solid-State NMR. *Phys. Chem. Chem. Phys.* **2018**, *20*, 22203-22209. doi:10.1039/C8CP04425B
  - Kobayashi, T.; Nishiyama, Y.; Pruski, M., Heteronuclear Correlation Solid-state NMR Spectroscopy with Indirect Detection under Fast Magic-angle Spinning. In *Modern Methods in Solid-state NMR: A Practitioner's Guide*, The Royal Society of Chemistry: 2018; pp 1-38.
  - Boteju, K. C.; Wan, S.; Venkatesh, A.; Ellern, A.; Rossini, A. J.; Sadow, A. D., Rare Earth Arylsilazido Compounds with Inequivalent Secondary Interactions. *Chem. Commun.* **2018**, *54*, 7318-7321. doi:10.1039/C8CC03186J
  - Singappuli-Arachchige, D.; Kobayashi, T.; Wang, Z.; Burkhow, S. J.; Smith, E. A.; Pruski, M.; Slowing, I. I., Interfacial Control of Catalytic Activity in the Aldol Condensation: Combining the Effects of Hydrophobic Environments and Water. *ACS Catal.* **2019**, *9*, 5574-5582. doi:10.1021/acscatal.9b00195
  - Reinig, R. R.; Ellern, A.; Sadow, A. D., Heteroleptic Four-Coordinate Tris(oxazoliny)borato Iron(II) Compounds. *Inorg. Chem.* **2019**, *58*, 6044-6051. doi:10.1021/acs.inorgchem.9b00359
  - Perras, F. A.; Wang, Z.; Kobayashi, T.; Baiker, A.; Huang, J.; Pruski, M., Shedding light on the atomic-scale structure of amorphous silica–alumina and its Brønsted acid sites. *Phys. Chem. Chem. Phys.* **2019**, *21*, 19529-19537. doi:10.1039/C9CP04099D
  - Patnaik, S.; Sadow, A. D., Interconverting Lanthanum Hydride and Borohydride Catalysts for C=O Reduction and C–O Bond Cleavage. *Angew. Chem. Int. Ed.* **2019**, *58*, 2505-2509. doi:10.1002/anie.201813305
  - Kobayashi, T.; Wang, Z.; Pruski, M., Homonuclear Dipolar Recoupling of Arbitrary Pairs in Multi-spin Systems Under Magic Angle Spinning: A Double-Frequency-selective ZQ-SEASHORE Experiment. *Solid State Nucl. Magn. Reson.* **2019**. doi:10.1016/j.ssnmr.2019.05.006

16. Kobayashi, T.; Pruski, M., Spatial Distribution of Silica-Bound Catalytic Organic Functional Groups Can Now Be Revealed by Conventional and DNP-Enhanced Solid-State NMR Methods. *ACS Catal.* **2019**, *9*, 7238-7249. doi:10.1021/acscatal.9b02017
17. Biswas, A.; Ellern, A.; Sadow, A. D., CO Displacement in an Oxidative Addition of Primary Silanes to Rhodium(I). *Inorg. Chem.* **2019**, *58*, 3815-3824. doi:10.1021/acs.inorgchem.8b03425
18. Zhou, H.; Wang, H.; Sadow, A. D.; Slowing, I. I., Toward hydrogen economy: Selective guaiacol hydrogenolysis under ambient hydrogen pressure. *Appl. Catal. B* **2020**, *270*, 118890-118899. doi:10.1016/j.apcatb.2020.118890
19. Wang, Z.; Patnaik, S.; Eedugurala, N.; Manzano, J. S.; Slowing, I. I.; Kobayashi, T.; Sadow, A. D.; Pruski, M., Silica-Supported Organolanthanum Catalysts for C–O Bond Cleavage in Epoxides. *J. Am. Chem. Soc.* **2020**, *142*, 2935-2947. doi:10.1021/jacs.9b11606
20. Singappuli-Arachchige, D.; Slowing, I. I., Control of interfacial pH in mesoporous silica nanoparticles via surface functionalization. *J. Chem. Phys.* **2020**, *152*, 034703. doi:10.1063/1.5138912
21. Qi, L.; Chen, J.; Zhang, B.; Nie, R.; Qi, Z.; Kobayashi, T.; Bao, Z.; Yang, Q.; Ren, Q.; Sun, Q.; Zhang, Z.; Huang, W., Deciphering a Reaction Network for the Switchable Production of Tetrahydroquinoline or Quinoline with MOF-Supported Pd Tandem Catalysts. *ACS Catal.* **2020**, *10*, 5707-5714. doi:10.1021/acscatal.0c00899
22. Manzano, J. S.; Wang, H.; Kobayashi, T.; Naik, P.; Lai, K. C.; Evans, J. W.; Slowing, I. I., Kinetics of the functionalization of mesoporous silica nanoparticles: Implications on surface group distributions, adsorption and catalysis. *Microporous Mesoporous Mater.* **2020**, *305*, 110276. doi:10.1016/j.micromeso.2020.110276
23. Luo, Z.; Nie, R.; Nguyen, V. T.; Biswas, A.; Behera, R. K.; Wu, X.; Kobayashi, T.; Sadow, A.; Wang, B.; Huang, W.; Qi, L., Transition metal-like carbocatalyst. *Nat. Commun.* **2020**, *11*, 4091. doi:10.1038/s41467-020-17909-8
24. Hafezisefat, P.; Lindstrom, J. K.; Brown, R. C.; Qi, L., Non-catalytic oxidative depolymerization of lignin in perfluorodecalin to produce phenolic monomers. *Green Chem.* **2020**, *22*, 6567-6578. doi:10.1039/D0GC02505D
25. Patnaik, S.; Kanbur, U.; Ellern, A.; Sadow, A. D., Hydrosilane  $\sigma$ -Adduct Intermediates in an Adaptive Zinc-Catalyzed Cross-dehydrocoupling of Si–H and O–H Bonds. *Chem. Eur. J.* **2021**, *27*, 10428-10436. doi:10.1002/chem.202101146
26. Naik, P. J.; Chatterjee, P.; Chen, S.; Huang, W.; Slowing, I. I., Regulating the Catalytic Activity of Pd Nanoparticles by Confinement in Ordered Mesoporous Supports. *ChemCatChem* **2021**, *13*, 539-542. doi:10.1002/cctc.202001594
27. Eedugurala, N.; Wang, Z.; Kanbur, U.; Ellern, A.; Pruski, M.; Sadow, A. D., Synthesis and Characterization of Tris(oxazolonyl)borato Copper(II) and Copper(I) Complexes. *Helv. Chim. Acta* **2021**, *104*, e2000209. doi:10.1002/hlca.202000209
28. Boteju, K. C.; Venkatesh, A.; Chu, Y.-Y.; Wan, S.; Ellern, A.; Rossini, A. J.; Sadow, A. D., Ancillary Steric Effects on the Activation of SiH Bonds in Arylsilazido Rare-Earth Compounds. *Organometallics* **2021**, *40*, 1654-1669. doi:10.1021/acs.organomet.1c00162
29. Perras, F. A.; Paterson, A. L.; Syed, Z. H.; Kropf, A. J.; Kaphan, D. M.; Delferro, M.; Pruski, M., Revealing the Configuration and Conformation of Surface

- Organometallic Catalysts with DNP-Enhanced NMR. *J. Phys. Chem. C* **2021**, *125*, 13433-13442. doi:10.1021/acs.jpcc.1c03176
30. Chen, J.; Qi, L.; Zhang, B.; Chen, M.; Kobayashi, T.; Bao, Z.; Yang, Q.; Ren, Q.; Huang, W.; Zhang, Z., Tandem synthesis of tetrahydroquinolines and identification of the reaction network by operando NMR. *Catal. Sci. Technol.* **2021**, *11*, 4332-4341. doi:10.1039/D1CY00418B
  31. Naik, P. J.; An, Y.; Sedinkin, S. L.; Masching, H.; Freppon, D.; Smith, E. A.; Venditti, V.; Slowing, I. I., Non-Innocent Role of the Ceria Support in Pd-Catalyzed Halophenol Hydrodehalogenation. *ACS Catal.* **2021**, 10553-10564. doi:10.1021/acscatal.1c02716
  32. Mouat, A. R.; Whitford, C. L.; Chen, B. R.; Liu, S. S.; Perras, F. A.; Pruski, M.; Bedzyk, M. J.; Delferro, M.; Stair, P. C.; Marks, T. J., Synthesis of Supported Pd-0 Nanoparticles from a Single-Site Pd<sup>2+</sup> Surface Complex by Alkene Reduction. *Chem. Mater.* **2018**, *30*, 1032-1044. doi:10.1021/acs.chemmater.7b04909
  33. Klet, R. C.; Kaphan, D. M.; Liu, C.; Yang, C.; Kropf, A. J.; Perras, F. A.; Pruski, M.; Hock, A. S.; Delferro, M., Evidence for Redox Mechanisms in Organometallic Chemisorption and Reactivity on Sulfated Metal Oxides. *J. Am. Chem. Soc.* **2018**, *140*, 6308-6316. doi:10.1021/jacs.8b00995
  34. Khazdozian, H. A.; Manzano, J. S.; Gandha, K.; Slowing, I. I.; Nlebedim, I. C., Recycled Sm-Co Bonded Magnet Filaments for 3D Printing of Magnets. *AIP Advances* **2018**, *8*, 056722. doi:10.1063/1.5007669
  35. Kaphan, D. M.; Klet, R. C.; Perras, F. A.; Pruski, M.; Yang, C.; Kropf, A. J.; Delferro, M., Surface Organometallic Chemistry of Supported Iridium(III) as a Probe for Organotransition Metal-Support Interactions in C-H Activation. *ACS Catal.* **2018**, *8*, 5363-5373. doi:10.1021/acscatal.8b00855
  36. García, A.; Slowing, I. I.; Evans, J. W., Pore Diameter Dependence of Catalytic Activity: p-Nitrobenzaldehyde Conversion to an Aldol Product in Amine-Functionalized Mesoporous Silica. *J. Chem. Phys.* **2018**, *149*, 024101. doi:10.1063/1.5037618
  37. Camacho-Bunquin, J.; Ferrandon, M.; Sohn, H.; Yang, D. L.; Liu, C.; Ignacio-de Leon, P. A.; Perras, F. A.; Pruski, M.; Stair, P. C.; Delferro, M., Chemoselective Hydrogenation with Supported Organoplatinum(IV) Catalyst on Zn(II)-Modified Silica. *J. Am. Chem. Soc.* **2018**, *140*, 3940-3951. doi:10.1021/jacs.7b11981
  38. Syed, Z. H.; Kaphan, D. M.; Perras, F. A.; Pruski, M.; Ferrandon, M. S.; Wegener, E. C.; Celik, G.; Wen, J.; Liu, C.; Dogan, F.; Goldberg, K. I.; Delferro, M., Electrophilic Organoiridium(III) Pincer Complexes on Sulfated Zirconia for Hydrocarbon Activation and Functionalization. *J. Am. Chem. Soc.* **2019**, *141*, 6325-6337. doi:10.1021/jacs.9b00896
  39. Qi, L.; Chamas, A.; Jones, Z. R.; Walter, E. D.; Hoyt, D. W.; Washton, N. M.; Scott, S. L., Unraveling the Dynamic Network in the Reactions of an Alkyl Aryl Ether Catalyzed by Ni/ $\gamma$ -Al<sub>2</sub>O<sub>3</sub> in 2-Propanol. *J. Am. Chem. Soc.* **2019**, *141*, 17370-17381. doi:10.1021/jacs.9b09071
  40. Pei, Y.; Zhang, B.; Maligal-Ganesh, R. V.; Naik, P. J.; Goh, T. W.; MacMurdo, H. L.; Qi, Z.; Chen, M.; Behera, R. K.; Slowing, I. I.; Huang, W., Catalytic properties of intermetallic platinum-tin nanoparticles with non-stoichiometric compositions. *J. Catal.* **2019**, *374*, 136-142. doi:10.1016/j.jcat.2019.04.013

41. Manzano, J. S.; Wang, H.; Slowing, I. I., High Throughput Screening of 3D Printable Resins: Adjusting the Surface and Catalytic Properties of Multifunctional Architectures. *ACS Appl. Polym. Mater.* **2019**, *1*, 2890-2896. doi:10.1021/acsapm.9b00598
42. Huang, X.-M.; Perras, F. A.; Manzano, J. S.; Slowing, I. I.; McNabb, A.; Pruski, M., The Anomalous Solidification of Concrete Grindings from Acid Treatment. *Cem. Concr. Res.* **2019**, *116*, 65-69. doi:10.1016/j.cemconres.2018.11.010
43. Carnahan, S. L.; Lampkin, B. J.; Naik, P.; Hanrahan, M. P.; Slowing, I. I.; VanVeller, B.; Wu, G.; Rossini, A. J., Probing O–H Bonding through Proton Detected 1H–17O Double Resonance Solid-State NMR Spectroscopy. *J. Am. Chem. Soc.* **2019**, *141*, 441-450. doi:10.1021/jacs.8b10878
44. Johnson, R. L.; Perras, F. A.; Hanrahan, M. P.; Mellmer, M.; Garrison, T. F.; Kobayashi, T.; Dumesic, J. A.; Pruski, M.; Rossini, A. J.; Shanks, B. H., Condensed Phase Deactivation of Solid Brønsted Acids in the Dehydration of Fructose to Hydroxymethylfurfural. *ACS Catal.* **2019**, *9*, 11568-11578. doi:10.1021/acscatal.9b03455
45. Chamas, A.; Qi, L.; Mehta, H. S.; Sears, J. A.; Scott, S. L.; Walter, E. D.; Hoyt, D. W., High Temperature/Pressure MAS-NMR for the Study of Dynamic Processes in Mixed Phase Systems. *Magn. Reson. Imaging* **2019**, *56*, 37-44. doi:10.1016/j.mri.2018.09.026
46. Zhou, H.; Wang, H.; Perras, F. A.; Naik, P.; Pruski, M.; Sadow, A. D.; Slowing, I. I., Two-step conversion of Kraft lignin to nylon precursors under mild conditions. *Green Chem.* **2020**, *22*, 4676-4682. doi:10.1039/D0GC01220C
47. Zhang, W.; Xu, C.; Kobayashi, T.; Zhong, Y.; Guo, Z.; Zhan, H.; Pruski, M.; Huang, W., Hydrazone-Linked Heptazine Polymeric Carbon Nitrides for Synergistic Visible-Light-Driven Catalysis. *Chem. Eur. J.* **2020**, *26*, 7358-7364. doi:10.1002/chem.202000934
48. Sedinkin, S. L.; An, Y.; Naik, P.; Slowing, I. I.; Venditti, V., An organogel library for solution NMR analysis of nanoparticle suspensions in non-aqueous samples. *J. Magn. Reson.* **2020**, *321*, 106874. doi:10.1016/j.jmr.2020.106874
49. Schroer, G.; Deischer, J.; Zensen, T.; Kraus, J.; Pöppler, A.-C.; Qi, L.; Scott, S.; Delidovich, I., Structure-performance correlations of cross-linked boronic acid polymers as adsorbents for recovery of fructose from glucose–fructose mixtures. *Green Chem.* **2020**, *22*, 550-562. doi:10.1039/C9GC03151K
50. Manzano, J. S.; Wang, H.; Qi, L.; Slowing, I. I., Macroscale Control of Reactivity using 3D Printed Materials with Intrinsic Catalytic Properties. *Appl. Catal., A* **2020**, *605*, 117794. doi:10.1016/j.apcata.2020.117794
51. Han, Y.; Slowing, I. I.; Evans, J. W., Surface structure of linear nanopores in amorphous silica: Comparison of properties for different pore generation algorithms. *J. Chem. Phys.* **2020**, *153*, 124708. doi:10.1063/5.0021317
52. Egner, T. K.; Naik, P.; An, Y.; Venkatesh, A.; Rossini, A. J.; Slowing, I. I.; Venditti, V., ‘Surface Contrast’ NMR Reveals Non-innocent Role of Support in Pd/CeO<sub>2</sub> Catalyzed Phenol Hydrogenation. *ChemCatChem* **2020**, *12*, 4160-4166. doi:10.1002/cctc.202000608
53. Dong, B.; Mansour, N.; Pei, Y.; Wang, Z.; Huang, T.; Filbrun, S. L.; Chen, M.; Cheng, X.; Pruski, M.; Huang, W.; Fang, N., Single Molecule Investigation of

- Nanoconfinement Hydrophobicity in Heterogeneous Catalysis. *J. Am. Chem. Soc.* **2020**. doi:10.1021/jacs.0c05905
54. Chen, J.; Zhang, B.; Qi, L.; Pei, Y.; Nie, R.; Heintz, P.; Luan, X.; Bao, Z.; Yang, Q.; Ren, Q.; Zhang, Z.; Huang, W., Facile Fabrication of Hierarchical MOF–Metal Nanoparticle Tandem Catalysts for the Synthesis of Bioactive Molecules. *ACS Appl. Mater. Interfaces* **2020**, *12*, 23002-23009. doi:10.1021/acsami.0c05344
  55. Chapovetsky, A.; Langeslay, R. R.; Celik, G.; Perras, F. A.; Pruski, M.; Ferrandon, M. S.; Wegener, E. C.; Kim, H.; Dogan, F.; Wen, J.; Khetrapal, N.; Sharma, P.; White, J.; Kropf, A. J.; Sattelberger, A. P.; Kaphan, D. M.; Delferro, M., Activation of Low-Valent, Multiply M–M Bonded Group VI Dimers toward Catalytic Olefin Metathesis via Surface Organometallic Chemistry. *Organometallics* **2020**, *39*, 1035-1045. doi:10.1021/acs.organomet.9b00787
  56. An, Y.; Naik, P.; Slowing, I. I.; Venditti, V., Substrate–Support Interactions Mediate Hydrogenation of Phenolic Compounds by Pd/CeO<sub>2</sub> Nanorods. *ACS Appl. Nano Mater.* **2020**, *3*, 11282-11288. doi:10.1021/acsanm.0c02381
  57. Perras, F. A.; Paterson, A. L., High Field Solid-State NMR of Challenging Nuclei in Inorganic Systems. In *Reference Module in Chemistry, Molecular Sciences and Chemical Engineering*, Elsevier: 2021.
  58. Matsuki, Y.; Kobayashi, T.; Fukazawa, J.; Perras, F. A.; Pruski, M.; Fujiwara, T., Efficiency analysis of helium-cooled MAS DNP: case studies of surface-modified nanoparticles and homogeneous small-molecule solutions. *Phys. Chem. Chem. Phys.* **2021**, *23*, 4919-4926. doi:10.1039/D0CP05658H
  59. Sluiter, J. B.; Michel, K. P.; Addison, B.; Zeng, Y.; Michener, W.; Paterson, A. L.; Perras, F. A.; Wolfrum, E. J., Direct determination of cellulosic glucan content in starch-containing samples. *Cellulose* **2021**, *28*, 1989-2002. doi:10.1007/s10570-020-03652-2
  60. Paterson, A. L.; Liu, D.-J.; Kanbur, U.; Sadow, A. D.; Perras, F. A., Observing the three-dimensional dynamics of supported metal complexes. *Inorg. Chem. Front.* **2021**, *8*, 1416-1431. doi:10.1039/D0QI01241F
  61. Zhang, J.; Mason, A. H.; Wang, Y.; Motta, A.; Kobayashi, T.; Pruski, M.; Gao, Y.; Marks, T. J., Beyond the Active Site. Cp\*ZrMe<sub>3</sub>/Sulfated Alumina-Catalyzed Olefin Polymerization Tacticity via Catalyst–Surface Ion-Pairing. *ChemCatChem* **2021**, *13*, 2564-2569. doi:10.1002/cctc.202100406
  62. Chen, M.; Yan, Y.; Gebre, M.; Ordonez, C.; Liu, F.; Qi, L.; Lamkins, A.; Jing, D.; Dolge, K.; Zhang, B.; Heintz, P.; Shoemaker, D. P.; Wang, B.; Huang, W., Thermal Unequilibrium of PdSn Intermetallic Nanocatalysts: From In Situ Tailored Synthesis to Unexpected Hydrogenation Selectivity. *Angew. Chem. Int. Ed.* **2021**, *60*, 18309-18317. doi:10.1002/anie.202106515
  63. Li, G.; Wang, B.; Kobayashi, T.; Pruski, M.; Resasco, D. E., Optimizing the Surface Distribution of Acid Sites for Cooperative Catalysis in Condensation Reactions Promoted by Water. *Chem Catal.* **2021**, *in press*.
  64. Nelson, N. C.; Manzano, J. S.; Sadow, A. D.; Overbury, S. H.; Slowing, I. I., Selective Hydrogenation of Phenol Catalyzed by Palladium on High-Surface-Area Ceria at Room Temperature and Ambient Pressure. *ACS Catal.* **2015**, *5*, 2051-2061. doi:10.1021/cs502000j

### **Awards or leadership activities during 2018-2020 calendar years**

- Frédéric Perras: DOE Early Career Award (2020)  
Frédéric Perras: Banting postdoctoral fellowship (2016-2018)  
Igor Slowing: Society of Hispanic Professional Engineers, Noche de Ciencias Conference (2021)  
Igor Slowing: Advisory Board in Program of Exascale Software for Interfacial Catalysis, Computational Chemical Sciences, US DOE (2019 – present)  
Igor Slowing: International Thesis Committee, University of Ghent, Belgium (2019)  
Igor Slowing: Highly Cited Researcher (Top 1 % in world) Clarivate Analytics, ISI Web of Science (2018)  
Igor Slowing: ACS Midwest Regional Meeting organizing committee (2018)  
Igor Slowing: ACS Ames Local Section Chair (2018)  
Igor Slowing: Visiting Professor, Department of Chemistry, Huazhong University, China (2017-2020)  
Aaron Sadow: Director of Institute for Cooperative Upcycling of Plastics (iCOUP) DOE-EFRC (2020)  
Aaron Sadow: Fulbright Fellowship (2020)  
Aaron Sadow: Helvetica Chimica Acta Editorial Advisory Board (2018-2020)

**Plasma-Catalyst Modeling for Materials Selection**

William F. Schneider and Hanyu Ma

Department of Chemical and Biomolecular Engineering, 250 Nieuwland Science Hall,  
University of Notre Dame, Indiana, 46556

**Presentation Abstract**

Reliable kinetic models are essential to rationalize observations and to guide the selection of appropriate plasma-catalyst combinations. Kinetic models coupling plasma- and heterogeneous-catalytic-chemistries, however, are primitive. Here, we combine reduced plasma chemistries and DFT-parameterized surface reactions to model NO formation from N<sub>2</sub> oxidation, an alternative nitrogen fixation process. We first show plasma excited species can enhance turnover frequencies of both Pt and Au. The enhancing potential is a function of plasma species and their densities. We then compare NO production between plasma/Pt and plasma/Au with an integral reactor model and explore the dependence of NO production as a function of plasma conditions, reactor configurations and chemical compositions. Plasma/Pt generates more NO than plasma/Au under most thermal and plasma parametric conditions. Plasma/Au outperforms plasma/Pt under high plasma excitations at low temperatures. These results highlight that selection of plasma-catalyst combinations should consider the properties of plasmas, materials and the coupling of the two.

**DE - SC0021107: Coordinated Interrogation and Modeling in Ammonia Oxidation Catalysis**

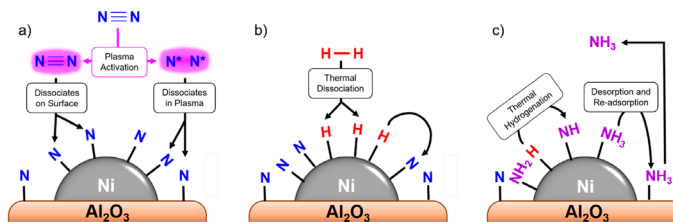
**Postdoc(s):** Dr. Hanyu Ma

**Student(s):** Anshuman Goswami, Craig Waitt, Patrick Barboun, Hope Odor

**RECENT PROGRESS**

**Ammonia Synthesis**

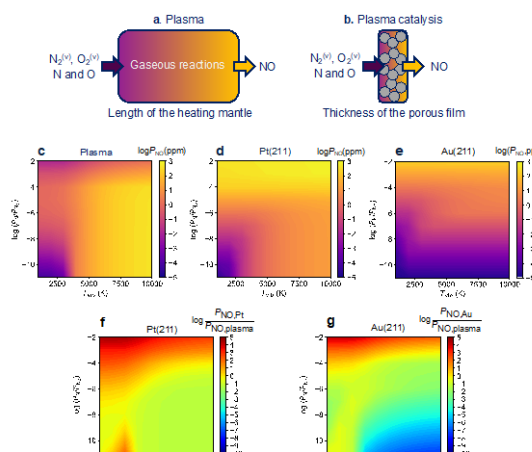
Ample literature evidence from our group and others indicates that ammonia can be formed at or near ambient conditions in a dielectric barrier discharge (non-thermal) plasma integrated with a catalytic surface. Our prior work (*Nature Catal.* **2018**, <https://doi.org/10.1038/s41929-018-0045-1>) reveals that at least one mode of action of the plasma is to decrease the demands on the catalytic surface to dissociate nitrogen. To provide more clarity into the influence of the optimal catalytic material, we performed experiments at the Spallation Neutron Source at Oak Ridge National Laboratory and density functional perturbation theory to probe the relationship between exposure of a catalytic Ni surface to N<sub>2</sub> and/or H<sub>2</sub> plasma and the formed surface species. Both experiments and



models highlight the appearance of chemisorbed hydrogen and of partially to fully hydrogenated nitrogen in the  $N_2/H_2$  plasma, in contrast to a plasma-free control. Further, we find that a sequential exposure to  $N_2$  plasma and to  $H_2$  without plasma leads to the same surface intermediates, highlighting the role of  $N_2$  excitations specifically on ammonia synthesis. This work recently appeared in *ACS Energy Letters*.

### Nitrogen oxidation

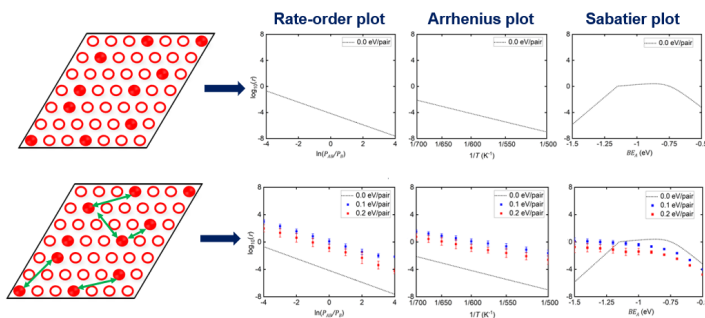
Nitrogen oxidation to NO is an alternative route to nitrogen fixation that, owing to the fact that it is endothermic, is particularly well suited to plasma promotion. Nitrogen oxidation in thermal plasmas has a long history, and recent evidence indicates that the same is possible in non-thermal plasmas. We have developed a modeling framework to assess the potential for plasma-catalyst combinations to promote nitrogen oxidation over a Pt catalyst, based on a reduced model for plasma-phase chemistry and DFT-predicted results for surface catalytic chemistry. The models highlight the sensitivity of NO productivity to plasma conditions (radical density, vibrational temperature, and mixing ratio) and reveal plasma regimes well suited to catalytic promotion of NO production.



Experiments performed by collaborators at the Dutch Institute for Fundamental Energy Research (DIFFER) agree well with model predictions. The work is particularly significant in that it demonstrates quantitatively a plasma-catalytic coupling at conditions at which intrinsic plasma and catalytic contributions alone are negligible and which produces NO at concentrations that exceed thermal equilibrium. This work is under consideration for publication at *Nature Communications* and in press at the *Journal of Physics:D*.

### Microkinetic modeling methods

One of the key observations in the work above is the important role of adsorbate coverage in controlling rates and selectivities. Both DFT calculations and experiments reveal that adsorption and activation energies are sensitive to the coverage of adsorbates, reflecting adsorbate-adsorbate interactions. Those interactions can be evaluated using DFT and captured explicitly in spatially resolved models that incorporate lateral interactions, for instance using a cluster expansion or similar representation of adsorbate distributions. These models are typically solved stochastically using kinetic Monte Carlo. While robust, the kMC are more expensive to solve, difficult to differentiate to recover apparent orders



and activation energies, and less amenable to screening than are more conventional mean-field microkinetic models. In support of the modeling efforts above, we are exploring the consequences of lateral interactions on predicted kinetic behavior, using a combination of kMC-based lattice models and mean field models. Work reveals the influence of interactions on apparent kinetics and suggests strategies for appropriately and efficiently incorporating these interactions into coverage-aware mean-field models. This work is in preparation for *Journal of Catalysis*.

A second dimension of this general problem is the development of models to describe the translational entropy of adsorbates, as this too relates to adsorbate coverage. We are exploring approaches that circumvent the conventional strategies of assuming functional forms for translation, including the harmonic oscillator or hindered translator. This work is in revision for *The Journal of Physical Chemistry*.

### **Publications Acknowledging this Grant in 2018-2021**

#### *(III) Intellectually led by this grant*

1. H. Ma and W. F. Schneider, "Plasma-Catalyst Modeling for Materials Selection: Challenges and Opportunities in Nitrogen Oxidation," *J. Phys. D: Appl. Phys.* **2021**, in press. (invited article)

#### *(IV) Jointly funded by this grant and other grants with intellectual leadership by other funding sources*

1. P. Barboun, L. Daemen, C. Waitt, Z. Wu, W. F. Schneider, and J. C. Hicks, "Inelastic Neutron Scattering Observation of Plasma-Promoted Nitrogen Reduction Intermediates on Ni/V-Al<sub>2</sub>O<sub>3</sub>," *ACS Energy Lett.* **2021**, 6, 2048–2053. <https://doi.org/10.1021/acsenergylett.1c00643>
2. Bogaerts, A.; Tu, X.; Whitehead, J. C.; Centi, G.; Lefferts, L.; Guaitella, O.; Azzolina-Jury, F.; Kim, H.-H.; Murphy, A. B.; Schneider, W. F.; Nozaki, T.; Hicks, J. C.; Rousseau, A.; Thevenet, F.; Khacef, A.; Carreon, M. The 2020 Plasma Catalysis Roadmap. *J. Phys. D: Appl. Phys.* **2020**, 53, 443001. <https://doi.org/10.1088/1361-6463/ab9048>

### **Awards or leadership activities during 2018-2020 calendar years**

1. Chair, Department of Chemical and Biomolecular Engineering,
2. Chair-elect, Division of Catalysis Science and Technology (CATL), American Chemical Society, 2019-2020
3. Executive Editor, *The Journal of Physical Chemistry C*, 2020-present
4. Organizer, "Recent Advances in Plasma-Enhanced Catalysis," American Chemical Society National Meeting, Spring 2019, Spring 2020
5. 2018 Giuseppe Parravano Award, Michigan Catalysis Society
6. Co-author, "The 2020 Plasma Catalysis Roadmap - Plasma Catalysis Modeling" (*J. Physics D: Applied Physics*)
7. Notre Dame site lead, CISTAR NSF ERC

**Oxidation of O-H and N-H Bonds with Non-Precious-Metal-Catalysts**

Shannon S. Stahl  
Department of Chemistry, University of Wisconsin-Madison

**Presentation Abstract**

We have been exploring two fundamental reaction classes relevant to non-precious-metal-catalyzed aerobic oxidation of organic molecules: (1) Cu-catalyzed oxidation of N–H bonds, including methods for aerobic oxidative coupling of N–N bonds, and (2) Fe-catalyzed oxidation of O–H bonds. The studies of N–H oxidation and oxidative N–N bond formation is motivated by the prevalence of N–N bonds in industrial chemicals (e.g., azo dyes, hydrazine), together with the growing interest in the use of ammonia as liquid hydrogen carrier for energy-conversion applications. Our studies of aerobic and electrochemical oxidative N–N coupling reactions provide unique insights into the kinetic and thermodynamic principles underlying these reactions and set the stage for new routes to leverage ammonia as a hydrogen carrier. The Fe-catalyzed efforts build upon our previous work on Cu/nitroxyl-catalyzed aerobic alcohol reactions in which the nitroxyl cocatalyst is generated via oxidation of a hydroxylamine O–H bond under the aerobic reaction conditions. In this work we have been exploring homogeneous and heterogeneous Fe-based catalysts in an effort to elucidate the principles of redox cooperativity in these catalyst systems.

**DE-FG02-05ER15690:**

**Oxidation of O-H and N-H Bonds with Non-Precious-Metal-Catalysts**

**Postdoc(s):** Jack Twilton, Fei Wang, Michael C. Ryan, James B. Gerken

**Student(s):** Jordan E. Nutting, Melissa N. Hopkins

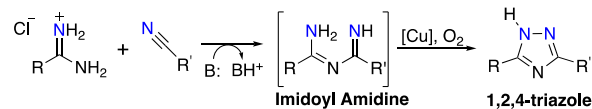
**RECENT PROGRESS**

***Copper-Catalyzed Aerobic N–H Bond Oxidation and Oxidative Coupling of N–N Bonds.***

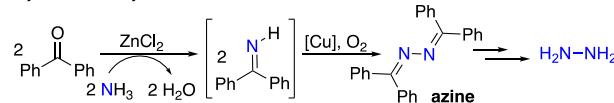
Several of our research efforts have focused on Cu-catalyzed N–H oxidation and oxidative N–N coupling. Organometallic chemists and other catalysis researchers are well versed in carbon-hydrogen and carbon-heteroatom bond formation. But, aside from the extensive study of water oxidation to molecular oxygen, comparatively little attention has been given to catalytic methods for heteroatom-heteroatom bond formation. The mechanistic principles underlying Cu-catalyzed N–N bond-forming reactions are similarly poorly developed and understood. This topic has particular relevance to the use of ammonia as a hydrogen-carrier, including the development of fuel cells capable of using hydrazine or ammonia as the fuel.

We have been characterizing the mechanism of N–N coupling reactions. Such reactions have applications in the energy sector, such as oxidation of ammonia into hydrazine or dinitrogen. In a study completed in 2020 (ref 5), we investigated the mechanism of two related copper-catalyzed oxidative aerobic N–N coupling reactions, one involving the synthesis of a relevant triazole and the other relevant to the oxidative conversion of ammonia to hydrazine. Analysis of catalytic and stoichiometric N–N coupling reactions support an "oxidase"-type catalytic mechanism with two redox half-reactions: (1) aerobic oxidation of a Cu<sup>I</sup> catalyst and (2) Cu<sup>II</sup>-promoted N–N coupling (Fig 1). Both reactions feature turnover-limiting oxidation of Cu<sup>I</sup> by O<sub>2</sub>, and this step is inhibited by the N–H substrate(s) (Fig 2). The results highlight the unexpected facility of the N–N coupling step and establish a foundation for development of improved catalysts for these transformations.

**A. Aerobic N–N Coupling of sp<sup>2</sup>-hybridized Nitrogen (Hayashi, Nagasawa)**  
*Nagasawa Triazole Synthesis*



*Hayashi Azine Synthesis*



**B. "Oxidase"-Type Catalytic Mechanism of N–N Coupling Reaction**

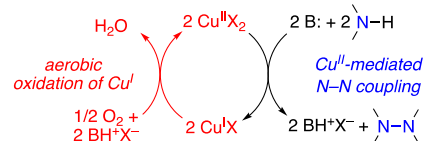


**Fig 1.** Copper-catalyzed aerobic N–N coupling.

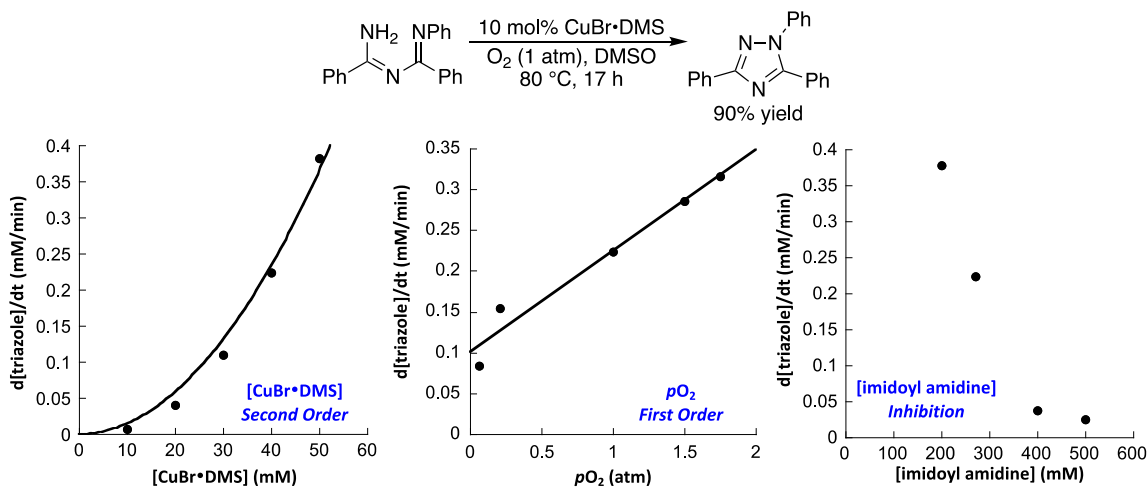


**Fig 2.** Kinetic data for Cu-catalyzed 1,2,4-triazole synthesis.

Hydrazine is an important industrial chemical and fuel that has attracted considerable attention for use in liquid fuel cells. Ideally, hydrazine could be prepared via direct oxidative coupling of ammonia, but thermodynamic and kinetic factors limit the viability of this approach. We performed a study that evaluated three different electrochemical strategies for the oxidative homocoupling of benzophenone imine, a readily accessible ammonia surrogate (ref 6, Fig 3). Hydrolysis of the resulting benzophenone azine affords hydrazine and benzophenone, with the latter amenable to recycling. The three different electrochemical N–N coupling methods include (1) a proton-coupled electron-transfer process promoted by a phosphate base, (2) an iodine-mediated reaction involving intermediate N–I bond formation, and (3) a copper-catalyzed N–N coupling process.

Analysis of the thermodynamic efficiencies for these electrochemical imine-to-azine oxidation reactions reveals low overpotentials ( $\eta$ ) for the copper and iodine mediated processes (390 and 470 mV, respectively), but a much higher value for the proton-coupled pathway ( $\eta \sim 1.6$  V). A similar approach is used to assess molecular electrocatalytic methods for electrochemical oxidation of ammonia to dinitrogen (Fig 4). The results of these studies lay the foundation for future targeted electrocatalytic efforts toward N-N bond coupling.

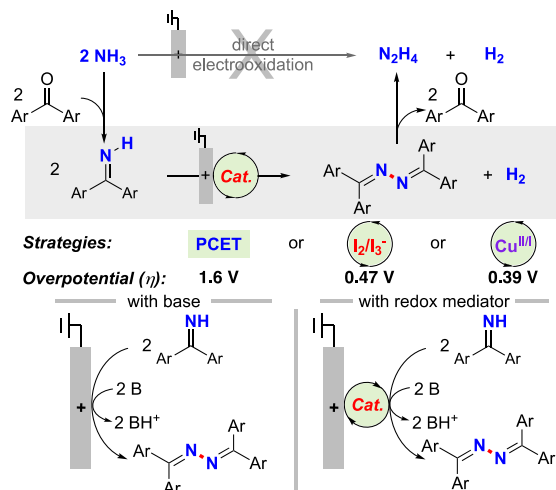


**Fig 3.** Strategies for electrocatalytic hydrazine synthesis.

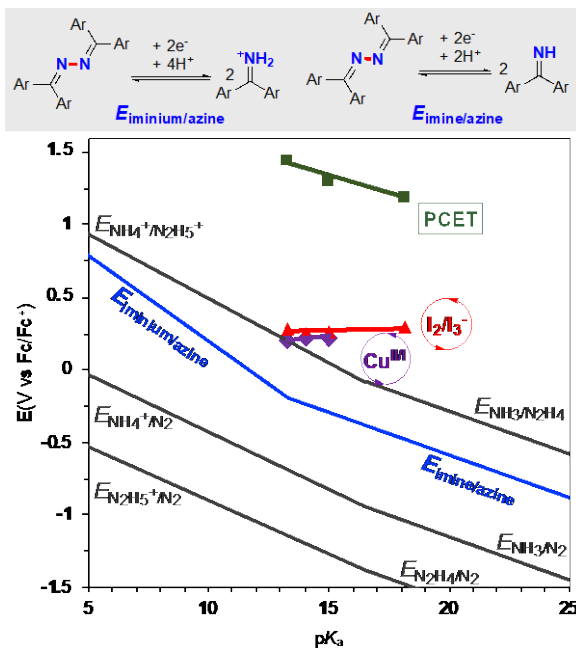


**Fig 4.** Pourbaix-type diagram for azine/benzophenone imine,  $N_2/NH_3/N_2H_4$  species, and redox potentials for the three electrochemical processes.

Complementary to our work on oxidative/dehydrogenative N-N coupling, we initiated a study of catalytic aerobic dehydrogenation of hydrazones (ref 8). This double N-H dehydrogenation reaction affords diazo compounds, which are an important lynchpin for site selective Rh-catalyzed insertion into C-H bonds. The reaction proceeds under mild conditions (air, 0 to 20 °C) with a catalyst composed of  $Cu(OAc)_2$  and a pyridine additive. Kinetic analysis of the reaction mixture and a series of linear free-energy relationships (Fig 5A) established a mechanistic framework involving a turnover limiting deprotonation of a Cu-hydrazone adduct by the pyridine additive (Fig 5B). With these insights in hand, improved catalyst systems leveraging more basic pyridine additives were identified, and an electronically and structurally diverse array of substrates furnish the corresponding diazo compounds in excellent yields, often within minutes at room temperature.

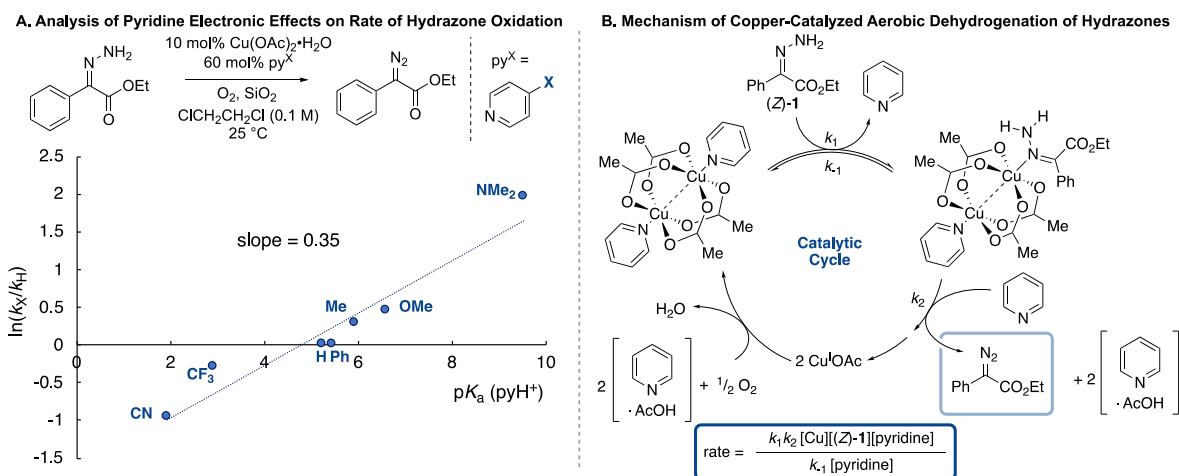


**Fig 5.** Mechanistic studies and proposed mechanism of copper-catalyzed aerobic dehydrogenation of hydrazones.

### **Mechanistic Studies of Iron(III) Nitrate/Aminoxyl-Catalyzed Aerobic Alcohol Oxidation.**

We have investigated the mechanism of iron(III) nitrate/TEMPO co-catalyzed aerobic oxidation of alcohols to identify the nature of the co-catalyst cooperativity and chemoselectivity in aerobic polyol oxidations (ref 9, Fig 6). Using an electrochemical technique called cyclic step chronoamperometry (CSCA) that

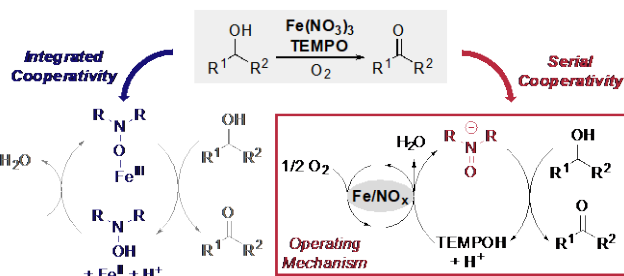


**Fig 6.** Integrated vs. serial cooperativity mechanisms of Fe(NO<sub>3</sub>)<sub>3</sub>/TEMPO-catalyzed aerobic alcohol oxidation.

employs a rotating disk electrode we have identified that in the presence of iron(III) nitrate, TEMPO first undergoes disproportionation followed by oxidation to the oxoammonium. This reactivity is not observed with other metal nitrate salts, highlighting the unique reactivity of iron(III) nitrate with aminoxyls. We then examined the chemoselectivity of the TEMPO-iron(III) nitrate system for aerobic oxidation of polyols and compared this reactivity with our group's previously reported Cu/TEMPO and NO<sub>x</sub>/TEMPO catalyst systems. The iron(III) nitrate and NO<sub>x</sub> systems demonstrate similar chemoselectivity: oxidation of 2° benzylic alcohols was preferred over oxidation of 1° benzylic alcohols; 2° benzylic > 1° aliphatic; and 2° aliphatic > 1° aliphatic (Fig 7). The opposite selectivity was observed for the Cu/TEMPO system. All together, these results support the hypothesis that the TEMPO-iron(III) nitrate system for aerobic alcohol oxidation proceeds through generation of a reactive oxoammonium intermediate rather than the Fe<sup>III</sup>/TEMPO adduct that has been proposed previously (analogous to the Cu/TEMPO mechanism). This study shows how chemoselectivity changes for different modes of catalyst cooperativity in aerobic alcohol oxidation.

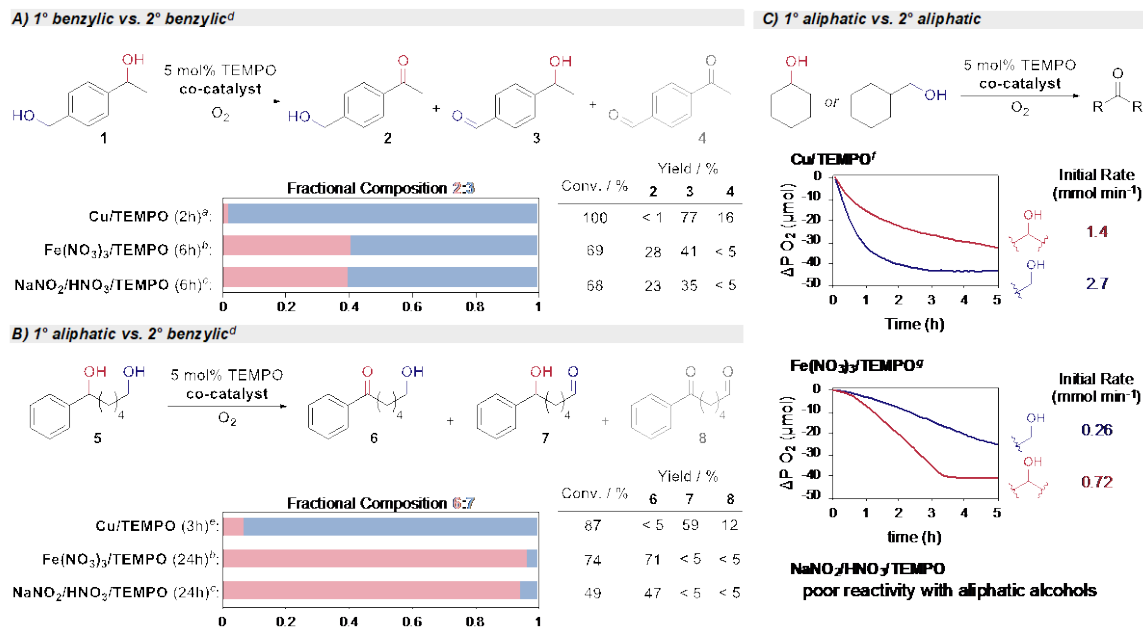


**Fig 7.** Comparison of chemoselectivity and functional group compatibility with different aminoxyl cocatalyst systems for aerobic alcohol oxidation.

## Publications Acknowledging this Grant in 2018-2021

*Intellectually led by this grant*

1. Lennox, A. J. J.; Nutting, J. E.; Stahl, S. S. Selective Electrochemical Generation of Benzylic Radicals Enabled by Ferrocene-Based Electron-Transfer Mediators. *Chem. Sci.* **2018**, *9*, 356-361.
2. Ryan, M. C.; Martinelli, J. R.; Stahl, S. S. Cu-Catalyzed Aerobic Oxidative N–N Coupling of Carbazoles and Diarylamines Including Selective Cross-Coupling. *J. Am. Chem. Soc.* **2018**, *140*, 9074-9077.
3. Das, A.; Nutting, J. E.; Stahl, S. S. Electrochemical C–H Oxygenation and Alcohol Dehydrogenation Involving Fe-oxo Species Using Water as the Oxygen Source. *Chem. Sci.* **2019**, *10*, 7542-7548.
4. Ryan, M. C.; Whitmire, L. D.; McCann, S. D.; Stahl, S. S. Copper/TEMPO Redox Redux: Analysis of PCET Oxidation of TEMPOH by Copper(II) and the Reaction of TEMPO with Copper(I). *Inorg. Chem.* **2019**, *58*, 10194-10200.
5. Ryan, M. C.; Kim, Y.-J.; Gerken, J. B.; Wang, F.; Aristov, M. M.; Martinelli, J. R.; Stahl, S. S. Mechanistic Insights into Copper-Catalyzed Aerobic Oxidative Coupling of N–N Bonds. *Chem. Sci.* **2020**, *11*, 1170-1175.
6. Wang, F.; Gerken, J. B.; Bates, D. M.; Kim, Y. J.; Stahl, S. S. Electrochemical Strategy for Hydrazine Synthesis: Development and Overpotential Analysis of Methods for Oxidative N–N Coupling of an Ammonia Surrogate. *J. Am. Chem. Soc.* **2020**, *142*, 12349-12356.
7. Wang, F.; Stahl, S. S. Electrochemical Oxidation of Organic Molecules at Lower Overpotential: Accessing Broader Functional Group Compatibility with Electron-Proton Transfer Mediators. *Acc. Chem. Res.* **2020**, *53*, 561-574.

8. Liu, W.; Twilton, J.; Wei, B.; Lee, M.; Hopkins, M. N.; Bacsa, J.; Stahl, S. S.; Davies, H. M. L. Copper-Catalyzed Oxidation of Hydrazones to Diazo Compounds Using Oxygen as the Terminal Oxidant. *ACS Catal.* **2021**, *11*, 2676-2683.
9. Nutting, J. E.; Mao, K.; Stahl, S. S. Iron(III) Nitrate/TEMPO-Catalyzed Aerobic Alcohol Oxidation: Distinguishing between Serial versus Integrated Redox Cooperativity. *J. Am. Chem. Soc.* **2021**, *143*, 10565-10570.

*Jointly funded by this grant and other grants with intellectual leadership by other funding sources*

1. Anson, C. W.; Stahl, S. S. Mediated Fuel Cells: Soluble Redox Mediators and Their Applications to Electrochemical Reduction of O<sub>2</sub> and Oxidation of H<sub>2</sub>, Alcohols, Biomass, and Complex Fuels. *Chem. Rev.* **2020**, *120*, 3749-3786.
2. Salazar, C. A.; Thompson, B. J.; Knapp, S. M. M.; Myers, S. R.; Stahl, S. S. Multichannel Gas-Uptake/Evolution Reactor for Monitoring Liquid-Phase Chemical Reactions. *Rev. Sci. Instrum.* **2021**, *92*, 044103.

## **Awards**

- ACS Catalysis Lectureship Award for the Advancement of Catalytic Science 2020
- Wisconsin Alumni Research Foundation (WARF) Technology Innovation Award, Finalist 2019
  - six finalists selected from >400 invention disclosures submitted to WARF; for "One-Step Process to Generate Lignin-Derived Aromatics from Raw Biomass"
- Steenbock Professorship of Chemical Sciences 2018

**Catalytic Selective Oxidations with Porous Transition Metal Oxides**

Steven L. Suib  
University of Connecticut

**Presentation Abstract**

The detection and potential correlation of reactive oxygen species (ROS) in selective oxidations is a significant recent area of research. Generally, a description of the elementary steps of a catalytic process should include the study of the kinetics and equilibria of chemisorption, identification of the real adsorbed species present at the catalyst surface, and the behavior of such species in catalytic reactions. For catalytic oxidations, the role of oxygen is of particular interest. No one method can reliably monitor the multitude of reactive oxygen species that are produced. A combination of characterization of materials; reactants and intermediates; and analyses of reactive oxygen species is key to a better understanding of these selective heterogeneous catalytic oxidations. Reactive Oxygen Species (ROS) define highly reactive oxygen-bearing molecules typically formed due to the incomplete reduction of molecular oxygen. Four major ROS are observed, comprising superoxide radical anion ( $O_2^{\cdot-}$ ), hydrogen peroxide ( $H_2O_2$ ), (singlet oxygen ( $^1O_2$ ), and hydroxyl radical ( $\cdot OH$ ). Other ROS include ozone ( $O_3$ ), ozonide ( $O_3^-$ ), and oxide ( $O^{2-}$ ), although they do not often appear in common selective catalytic oxidation reactions. These different ROS are typically difficult to track, especially in heterogeneous systems, and the methods used to study them are generally complicated, expensive, and time consuming. This is the subject of our research.

**Grant or FWP Number: DE-FG02-86ER13622: CATALYTIC SELECTIVE OXIDATIONS WITH POROUS TRANSITION METAL OXIDES**

**Postdoc(s):** None

**Student(s):** Laura Achola, Jared Fee, Inosh Perera, Shubahashish Subhashish

**RECENT PROGRESS**

Methods to determine reactive oxygen species (ROS) were used to study the heterogeneous aerobic oxidative coupling of amines to imines where reactive oxygen species play an integral role in the mechanism. Three different catalysts were studied; cobalt doped mesoporous manganese oxide, mesoporous copper aluminum mixed metal oxide, and mesoporous copper sulfide material. The first catalyst ( $Cu_{meth}Al_{butox}$ ) was used for the heterogeneous aerobic oxidative coupling of amines to imines. Here, the generation of  $\cdot OH$ ,  $H_2O_2$ ,  $O_2^{\cdot-}$  and  $^1O_2$  was confirmed by various methods. These observations led to a mechanism (See **Figure 1**) that included all four of the observed ROS. Interestingly, a radical cation was also trapped using BHT (butylated hydroxytoluene) and the adduct presence confirmed using GC-MS.



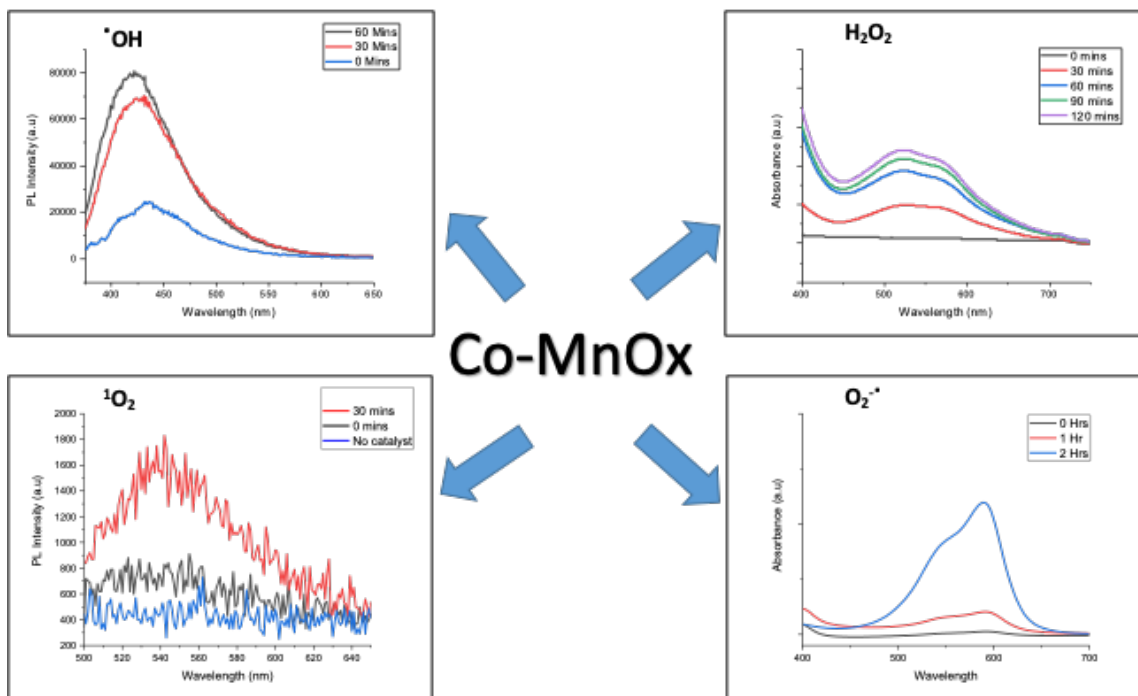


**Figure 2.** Hydroxyl Radical test, Peroxide test, Singlet Oxygen, and Superoxide Anion test for the 1%Co-MnO<sub>x</sub> Catalyst System.

The detection of the three ROS, suggested further study to find out the terminal ROS. Therefore, ROS quenchers curcumin and butylated hydroxytoluene were introduced to scavenge the superoxide anion radical and hydroxyl radical, respectively. The quenching of hydroxyl radicals inhibited the formation of imines. Whereas, a considerable amount (~15 %) of imine was obtained, despite quenching superoxide anions. This confirmed the hydroxyl radical to be the terminal ROS.

The third catalyst was a hydrothermally synthesized mesoporous copper sulfide. This catalyst was used for the visible-light-driven catalytic process for amine to imine transformations. In this system, the presence of superoxide radical anion (O<sub>2</sub><sup>•-</sup>), hydrogen peroxide (H<sub>2</sub>O<sub>2</sub>), singlet oxygen (<sup>1</sup>O<sub>2</sub>) and hydroxyl radical (\*OH) were detected and therefore reactive oxygen species were investigated using different detection methods. Multiple reactive oxygen species were detected in the reaction mixture using UV-vis and fluorescence spectroscopy in the presence of different indicators. Among these, superoxide radical anions and singlet oxygen (produced by the reaction between superoxide anion (O<sub>2</sub><sup>•-</sup>) electron holes (h<sup>+</sup>) on the surface) are prone to abstract electrons, which is required to drive the reaction forward. Hence, to identify the ROS responsible for this process, specific quenchers were used. In the presence of p-benzoquinone (pBQ), the superoxide radical anion quencher, no significant drop in conversion (93%) was observed as compared to the unquenched system (97%). However, the conversion decreased significantly to 37% in the presence of sodium azide (NaN<sub>3</sub>), a singlet oxygen quencher. This indicated the major role played by singlet oxygen in catalyzing the meso-CuS driven photocatalytic transformation of amines to imines. This led us to propose a reaction mechanism using singlet oxygen, which initiated the reaction by abstracting electrons from the substrate and produced superoxide radical anions.

Additionally, copper oxide supported on mesoporous manganese oxide (meso Cu/MnOx) was synthesized by an inverse micelle templated evaporation induced self-assembly procedure. The catalyst had exceptional catalytic activity in the aerobic oxidative coupling of terminal alkynes with a conversion and selectivity of >99% in both homocoupling and cross-coupling of alkynes using optimized reaction conditions. The labile lattice oxygen of the mesoporous Cu/MnOx was implicated in the deprotonation of the alkyne proton, as supported by TPD and TGA studies. Therefore, further studies were conducted to investigate the reactive oxygen species in this system. The afore-mentioned methods were used to detect  $\cdot\text{OH}$ ,  $\text{H}_2\text{O}_2$ ,  $\text{O}_2^{\cdot-}$  and  $^1\text{O}_2$ . Only  $\cdot\text{OH}$  and  $\text{H}_2\text{O}_2$  species were found to be present in this system. Some of these data are shown in **Figure 3**.

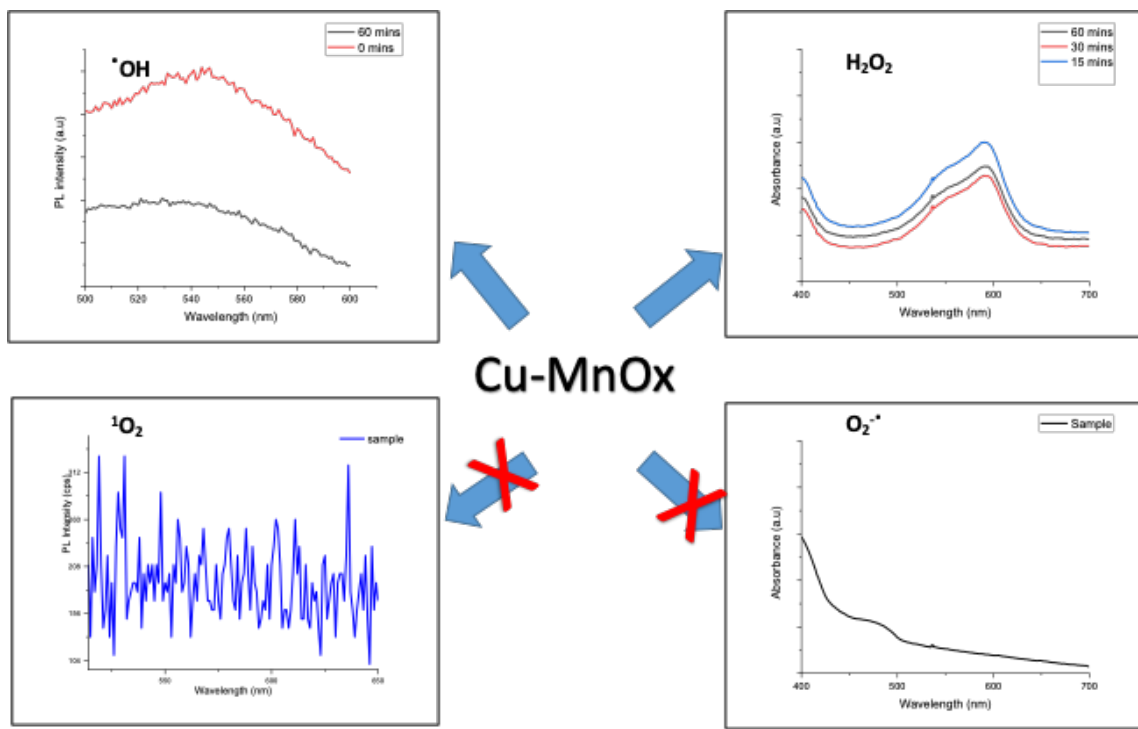


**Figure 3.** Hydroxyl radical test, Peroxide test, Singlet oxygen, and superoxide anion test for the 1%Cu-MnO<sub>x</sub> catalyst system.

The above studies are just a few examples of the role of ROS in selective oxidations. Some key findings of this research are the following:

1. ROS must be analyzed under *in situ/in operando* conditions.
2. The same catalyst can produce different ROS for different reactions.
3. Quenchers have been developed to selectively kill specific ROS leaving one or more species that are active in such reactions.

## Publications Acknowledging this Grant in 2018-2021

(V) *Intellectually led by this grant*

Sahoo, S.; Suib, S. L.; Alpay, S. P., Graphene Supported Single Atom Transition Metal Catalysts for Methane Activation, *ChemCatChem*, 2018, **10**, 3229-3235. Top downloaded paper.

Zhong, W.; Jiang, T.; Dang, Y.; He, J.; Chen, S. Y.; Kuo, C. H.; Kriz, D.; Meng, Y.; Meguerdichian, A.; Suib, S. L., Mechanism studies on methyl orange dye degradation by perovskite-type  $\text{LaNiO}_3$  under dark ambient conditions, *Appl. Catal. A*, 2018, **554**, 54-63.

Zhong, W.; Jiang, T.; Dang, Y.; He, J.; Chen, S. Y.; Kuo, C. K.; Kriz, D.; Meng, Y.; Meguerdichian, A. G.; Suib, S. L., Mechanism studies on Methyl Orange dye degradation by perovskite-type  $\text{LaNiO}_{3-\delta}$  under dark ambient conditions, *Appl. Catal., A: Gen.*, 2018, **549**, 302-309.

Liu, B.; Jin, L.; Zhong, W.; Lopes, A.; Suib, S. L.; He, J., Ultrafine and Ligand-Free Precious Metal (Ru, Ag, Au, Rh and Pd) Nanoclusters Supported on Phosphorus-Doped Carbon, *Chem. Eur. J.*, 2018, **24**, 2565-2569.

Moharreri, E.; Hines, W.; Biswas, S.; Perry, D.; He, J.; Murray-Simmons, D.; Suib, S. L., Comprehensive Magnetic Study of Nanostructured Mesoporous Manganese Oxide Materials and Implications for Catalytic Behavior, *Chem. Mat.*, 2018, **30**, 1164-1177.

Meguerdichian, A.; Jafari, T.; Shakil, M. M.; Miao, R.; Achola, L.; Macharia, J.; Shirazi, A. A.; Suib, S., Synthesis and Electrocatalytic Activity of Ammonium Nickel Phosphate,  $\text{NH}_4\text{NiPO}_4 \cdot 6\text{H}_2\text{O}$  and  $\beta$ -Nickel Pyrophosphate,  $\beta\text{-Ni}_2\text{P}_2\text{O}_7$  Catalysts for Electrocatalytic Decomposition of Urea, *Inorg. Chem.*, 2018, **57**, 1815-1823.

Hincapie, B.; Llano, S. M.; Garces, H. F.; Espinal, D.; Suib, S. L.; Garces, L. J., Epoxidation of Cyclopentene by a Low Cost and Environmentally Friendly Bicarbonate/Peroxide/Manganese System, *Ads. Sci. & Tech.*, 2018, **36**, 9-22.

Yin, S.; Zhong, W.; Guild, C. J.; Shi, J.; Suib, S. L.; Cotica, L. F.; Jain, M., Effect of Gd Substitution on the structural, magnetic, and magnetocaloric Properties of  $\text{HoCoO}_3$ , *J. Appl. Phys.*, 2018, **123**, 053904/1-053904/6.

Nie, Y. C.; Yu, F.; Wang, L. C.; Xing, Q. J.; Liu, X.; Pei, Y.; Zou, J. P.; Dai, W. L.; Li, Y.; Suib, S. L., Photocatalytic Degradation of Organic Pollutants Coupled with Simultaneous Photocatalytic  $\text{H}_2$  Evolution over Graphene Quantum  $\text{TiO}_2$ -g- $\text{C}_3\text{N}_4$  Composite Catalysts: Performance and mechanism, *Appl. Catal., B: Env.*, 2018, **227**, 312-321.

Liu, C.; Luo, W.; Liu, J.; Sun, L.; Yang, Y.; Liu, G.; Wang, F.; Zhong, W.; Guild, C.; Suib, S. L., Pt/Ferric Hydroxyphosphate: An Effective Catalyst for the Selective Hydrogenation of  $\alpha,\beta$ -Unsaturated Aldehydes (Ketones) into  $\alpha,\beta$ -Unsaturated Alcohols, *Catal. Lett.*, 2018, **148**, 555-563.

Ouyang, J.; Zheng, C.; Gu, W.; Zhang, Y.; Yang, H.; Suib, S. L. Textural properties determined CO<sub>2</sub> capture of tetraethylenepentamine loaded SiO<sub>2</sub> nanowires from  $\alpha$ -sepiolite *Chem. Eng. J.*, 2018, **337**, 342-350.

Dey, S.; Zhou, Y.; Sun, Y.; Jenkins, J. A.; Kriz, D.; Suib, S. L.; Chen, O.; Zou, S.; Zhao, J., Excitation wavelength dependent photon anti-bunching/bunching from single quantum dots near gold nanostructures, *Nanoscale*, 2018, **10**, 1038-1046.

King'onde, C. K.; Garces, H. F.; Suib, S. L., Nano-Structures & Nano-Objects, End to End and Side by Side Alignment of Short Octahedral Molecular Sieve (OMS-2) Nanorods into Long Microyarn Superarchitectures and Highly Flexible Membranes, *Nano-Str. Nano-Obj.*, 2018, **14**, 49-56.

Vovchok, D.; Guild, C. J.; Dissanayake, S.; Llorca, J.; Stavitski, E.; Liu, Z.; Palomino, R.; Waluyo, I.; Li, Y.; Frenkel, A. I.; Rodriguez, J. A.; Suib, S. L.; Senanayake, S. D.; In Situ Characterization of Mesoporous Co/CeO<sub>2</sub> Catalysts for the High-Temperature Water-Gas Shift, *J. Phys. Chem. C*, 2018, **122**, 8998-9008.

Dixit, C. K.; Bhakta, S.; Macharia, J.; Furtado, J.; Suib, S. L.; Rusling, J. F., Novel Epoxy-Silica Nanoparticles to Develop Non-Enzymatic Colorimetric Probe for Analytical Immuno/Bioassays, *Anal. Chim. Acta*, 2018, **1028**, 77-85.

Weerakoddy, C.; Guild, C.; Achola, L.; Palo, J.; Suib, S. L., Effects of microwave and ultrasound exposure to microsphere particles made out of different classes of inorganic and organic materials, *J. Ind. Eng. Chem.*, 2018, **65**, 26-30.

Meguerdichian, A.; Shirazi A., Al.; Moharreri, E.; Achola, L.; Murphy, S.; Macharia, J.; Zhong, W.; Jafari, T.; Suib, S., Synthesis of Large Mesoporous-Macroporous and High Pore Volume, Mixed Crystallographic Phase Manganese Oxide, Mn<sub>2</sub>O<sub>3</sub>/Mn<sub>3</sub>O<sub>4</sub> Sponge, *Inorg. Chem.*, 2018, **57**, 6946-6956.

Luo, Y.; Tan, W.; Suib, S. L.; Qiu, G.; Liu, F., Dissolution and phase transformation processes of hausmannite in acidic aqueous systems under anoxic conditions, *Chem Geol.*, 2018, **487**, 54-62.

Liu, L.; Jia, Z.; Tan, W.; Suib, S. L.; Ge, L.; Qiu, G.; Hua, R., Abiotic photomineralization and transformation of iron oxide nanominerals in aqueous systems, *Env. Sci.: Nano*, 2018, **5**, 1169-1178.

Dutta, B.; March, S.; Achola, L.; Sahoo, S.; He, J.; Amin, A.; Wu, Y.; Poges, S.; Pamir A., S.; Suib, S. L., Mesoporous Cobalt/Manganese Oxide: A Highly Selective Bifunctional Catalyst for Amine–Imine Transformations, *Green Chem.*, 2018, **20**, 3180 - 3185.

Zhang, T.; Liu, L.; Tan, W.; Suib, S. L.; Qiu, G.; Liu, F., Photochemical formation and Transformation of Birnessite: effects of cations on micromorphology and crystal structure, *Env. Sci. Technol.*, 2018, **52**, 6864-6871.

Ouyang, J.; Mu, D.; Zhang, Y.; Yang, H.; Suib, S., Selective Fabrication of Barium Carbonate Nanoparticles in Halloysite Lumen, *Minerals*, 2018, **8**, 296/1-296/13.

Shakil, M. M.; El-Sawy, A.; Tasnim, H.; Meguerdichian, A.; Jin, J.; Dubrosky, J.; Suib, S., Single and Multi-Doped Transition Metal (Mn, Fe, Co, and Ni) ZnO and Their Electrocatalytic Activities for Oxygen Reduction Reaction, *Inorg. Chem.*, 2018, **57**, 9977-9987.

Lv, H.; Chen, X.; Xu, D.; Hu, Y.; Zheng, H.; Suib, S. L.; Liu, B., Ultrathin PdPt Bimetallic Nanowires with Enhanced Electrocatalytic Performance for Hydrogen Evolution Reaction, *Appl. Catal. B: Env.*, **238**, 525-532.

Gupta, A.; Mittal, M.; Singh, M. K.; Suib, S. L.; Pandey, O. P., Visible light induced photocatalytic degradation characteristics of NbC/C nano-composite synthesized at low temperature, *Sci. Rep.*, 2018, **8**, 1-7.

Weerakkody, C.; Rathnayake, D.; He J.; Dutta, B.; Kerns, P.; Achola, L.; Suib, S. L., Enhanced Catalytic Properties of Molybdenum Promoted Mesoporous Cobalt Oxide: Structure-Surface-Dependent Activity for Selective Synthesis of 2-Substituted Benzimidazoles, *ChemCatChem*, 2019, **11**, 528-537.

Biswas, S.; Khanna, H. S.; Nizami, Q. A.; Caldwell, D. R.; Cavanaugh, K. T.; Howell, A. R.; Raman, S.; Suib, S. L.; Nandi, P., Heterogeneous Catalytic Oxidation of Amides to Imides by Manganese Oxides, *Sci. Rep.*, 2018, **8**, 1-8.

Vovchok, D.; Guild, C. J.; Llorca, J.; Palomino, R. M.; Waluyo, I.; Rodriguez, J. A.; Suib, S. L., Senanayake, S. D. Structural and Chemical State of Doped and Impregnated Mesoporous Ni/CeO<sub>2</sub> Catalysts for the Water-gas Shift, *Appl. Catal. A*, 2018, **567**, 1-11.

Zou, X.; Chen, T.; Zhang, P.; Chen, D.; He, J.; Dang, Y.; Ma, Z.; Chen, Y.; Toloueinia, P.; Zhu, C.; Xie, J.; Liu, H., Suib, S. L., High catalytic performance of Fe-Ni/Palygorskite in the steam reforming of toluene for hydrogen production, *Appl. Energy*, 2018, **226**, 827-837.

Liu, L.; Tan, W. F.; Suib, S.; Qiu, G.; Zheng, L.; Huang, Q.; Liu, C., Effective Zinc Adsorption Driven by Electrochemical Redox Reactions of Birnessite Nanosheets Generated by Solar Photochemistry, *ACS Sust. Chem. & Eng.*, 2018, **6**, 13907-13914.

Sun, L.; Liu, J.; Luo, W.; Yang, Y.; Wang, F.; Weerakkody, C.; Suib, S. L., Preparation of Amorphous Copper-chromium Oxide Catalysts for selective Oxidation of Cyclohexane, *Mol. Cat.*, 2018, **460**, 16-26.

Yin, S.; Seehra, M. S.; Guild, C. J.; Suib, S. L.; Poudel, N.; Lorenz, B.; Jain, M., Magnetic and Magnetocaloric Properties of HoCoO<sub>3</sub> Tuned by Selective Rare-earth Doping, *Phys. Rev. B*, 2017, **95**, 184421/1-184421/12.

Genuino, H. C.; Valenciac, D.; Suib, S. L., Insights into the Structure-Property-Activity Relationship in Molybdenum-Doped Octahedral Molecular Sieve Manganese Oxides for Catalytic Oxidation, *Cat. Sci. Tech.*, 2018, **8**, 6493 - 6502.

Ouyang, J.; Zhao, Z.; Yang, H.; He, J.; Suib, S. L., Surface Redox Characters and Synergetic Catalytic Properties of Macroporous Ceria-Zirconia Solid Solutions, *J. Haz. Mat.*, 2019, **366**, 54-64.

Lawson, M.; Horn, J.; Wong-Ng, W.; Espinal, L.; Nguyen, H. G.; Kaduk, J.; Lapidus, S. H.; Meng, Y.; Suib, S.; Li, L., Carbon Capture and Storage Properties of Porous Octahedral Molecular Sieve, *Powder Diff.*, 2019, **34**, 13-20.

Dutta, B.; Wu, Y.; Chen, J.; Wang, J.; He, J.; Sharafeldin, M. Kerns, P.; Jin, L.; Dongare, A.; Rusling, J.; Suib, S., Partial Surface Selenization of Cobalt Sulfide Microspheres for Enhancing the Hydrogen Evolution Reaction, *ACS Catalysis*, 2018, **9**, 456-465.

Weerakkody, C.; Rathnayake, D.; He J.; Dutta, B.; Kerns, P.; Achola, L.; Suib. S. L., Enhanced Catalytic Properties of Molybdenum Promoted Mesoporous Cobalt Oxide: Structure-Surface-Dependent Activity for Selective Synthesis of 2-Substituted Benzimidazoles, *ChemCatChem*, 2019, **11**, 528-537.

Chen, S. Y.; Tang, W.; He, J.; Miao, R.; Lin, H. J.; Song, W.; Wang, S.; Gao, P.; Suib, S. L., Copper Manganese Oxide Enhanced Nanoarray-Based Monolithic Catalysts for Hydrocarbon Oxidation, *J. Mat. Chem. A*, 2018, **6**, 19047-19057.

Premaratne, G.; Niroula, J.; Patel, M.; Zhong, W.; Suib, S.; Kalkan, A. K.; Krishnan, S., Electrochemical and Surface Plasmon Correlation of Serum Autoantibody Immunoassay with Binding Insights: Graphenyl vs. Mercapto-Monolayer Surface, *Anal. Chem.*, 2018, **90**, 12456-12463.

Ouyang, J.; Zhao, Z.; Suib, S. L.; Yang, H., Degradation of Congo Red Dye by a  $\text{Fe}_2\text{O}_3@ \text{CeO}_2\text{-ZrO}_2/\text{Palygorskite}$  Composite Catalyst: Synergetic Effects of  $\text{Fe}_2\text{O}_3$ , *J. Coll. Int. Sci.*, 2018, **539**, 135-145.

Wang, Y.; Wu, Y.; Shirazi Amin, A.; Kerns, P.; Fee, J.; He, J.; Jin, L.; Maric, R.; Suib, S., Direct Construction of Mesoporous Metal Sulfides via Reactive Spray Deposition Technology, *ACS Appl. Energy Mat.*, 2019, **2**, 2370-2374.

Yang, Y.; Su, X.; Zhang, L.; Kerns, P.; Achola, L.; Hayes, V.; Quardokus, R.; Suib, S. L.; He, J., Intercalating  $\text{MnO}_2$  Nanosheets with Transition Metal Cations to Enhance Oxygen Evolution, *ChemCatChem*, 2019, **11**, 1689-1700.

Dissanayake, D.; Achola, L.; Kerns, P.; Rathnayake, D.; He, J.; Macharia, J.; Suib, S. L., Aerobic Oxidative Coupling of Amines to Imines by Mesoporous Copper Aluminum Mixed Metal Oxides via Generation of Reactive Oxygen Species (ROS), *Appl. Catal. B: Env.*, 2019, **249**, 32-41.

Muya, R. K.; Achola, L.; Njagi, E. C.; Ombaka, O.; Suib, S. L., Synthesis Characterization and Applications of Transition Metal Doped Manganese oxide Catalysts, *Res. J. Life Sci. BioInf. Pharm. Chem. Sci.*, 2019, **5**, 16-30.

Lv, H.; Sun, L.; Xu, D.; Suib, S. L., Liu, B., One-Pot Aqueous Synthesis of Ultrathin Trimetallic PdPtCu Nanosheets for the Electrooxidation of Alcohols, *Green Chem.*, 2019, **21**, 2367-2374.

Wang, C.; Zou, X.; Liu, H.; Chen, T.; Suib, S. L.; Chen, D.; Xie, J.; Li, M.; Sun, F., Highly Efficient catalyst of palygorskite-Supported manganese Oxide for Formaldehyde Oxidation at Ambient and Low Temperature: Performance, Mechanism and Reaction Kinetics, *Appl. Surf. Sci.*, 2019, **486**, 420-430.

Shakil, M. M.; Meguerdichian, A.; Tasnim, H.; Shirazi A., Alireza; S. M.; Suib, S. L., Syntheses of ZnO with Different Morphologies: Catalytic Activity Towards Coumarin Synthesis via the Knoevenagel Condensation Reaction, *Inorg. Chem.*, 2019, **58**, 5703-5714.

Dutta, B.; Clarke, R.; Raman, S.; Shaffer, T. D.; Achola, L.; Nandi, P.; Suib, Steven L., Lithium Promoted mesoporous manganese oxide catalyzed oxidation of allyl ethers, *Nature Comm.*, 2019 **10**, 1-6.

He, J.; Chen, S. Y.; Tang, W.; Dang, Y.; Kerns, P.; Miao, R.; Dutta, B.; Gao, P. X.; Suib, S., Microwave-Assisted Integration of Transition Metal Oxide Nanocoatings on Manganese Oxide Nanoarray Monoliths for Low Temperature CO Oxidation, *Appl. Catal. B: Env.*, 2019, **255**, 117766.

Deljoo, B.; Jafari, T.; Miao, R.; Nieh, M. P.; Suib, S. L.; Aindow, M., Surfactant selection as a strategy for tailoring the structure and properties of UCT manganese oxides, *Mat. Des.*, 2019, **180**, 107902.

Moharreri, E.; Biswas, S.; Deljoo, B.; Kriz, D.; Lim, S.; Elliott, S.; Dissanayake, S.; Dabaghian, M.; Aindow, M.; Suib, S. L., Aerobic Self-Esterification of Alcohols Assisted by Mesoporous Manganese and Cobalt Oxide, *ChemCatChem*, 2019, **11**, 3413-3422.

Suib, S. L.; Prech, J.; Cejka, J.; Kuwahara, Y.; Mori, K.; Yamashita, H., Some Novel Porous Materials for Selective Catalytic Oxidations, *Materials Today*, 2020, **32**, 244-259.

Dutta, B.; Achola, L.; Clarke, R.; Sharma, V.; He, J.; Kerns, P.; Suib, S. L., Photocatalytic Transformation of Amines to Imines by Meso-porous Copper Sulfides, *ChemCatChem*, 2019, **11**, 4262-4265.

Liu, L.; Tan, W.; Suib, S. L.; Qiu, G.; Zheng, L.; Su, S., Enhanced adsorption removal of arsenic from mining wastewater using birnessite under electrochemical redox reactions, *Chem. Eng. J.*, 2019, **375**, 122051.

Dutta, B.; Achola, L. A.; Clarke, R.; Sharma, V.; He, J.; Kerns, P.; Suib, S. L., Photocatalytic Transformation of Amines to Imines by Meso-porous Copper Sulfides, *ChemCatChem*, 2019, **11**, 4262-4265.

Dang, Y.; He, J.; Wu, T.; Yu, L.; Kerns, P.; Wen, L.; Ouyang, J.; Suib, S., Constructing Bifunctional 3D Holey and Ultrathin CoP Nanosheets for Efficient Overall Water Splitting, *ACS Appl. Mat. Int.*, 2019, **11**, 29879-29887.

He, J.; Wu, T.; Chen S. Y.; Miao, R.; Dang, Y.; Zhong, W.; Wang, M.; Jiang, T.; Suib, S., Structure-Property Relationship of Graphene Coupled Metal (Ni, Co, Fe) (Oxy)Hydroxides for Efficient Electrochemical Evolution of Oxygen, *J. Catal.*, 2019, **377**, 619-628

Moharreri, E.; Pardakhti, M.; Srivastava, R.; Suib, S., Energy-Geometry Dependency of Molecular Structures: A Multistep Machine Learning Approach, *ACS Comb. Sci.*, 2019, **21**, 614-621.

Pardakhti, M.; Jafari, T.; Tobin, Z.; Dutta, B.; Moharreri, E.; Saveh S. N.; Suib, S.; Srivastava, Ranjan, Trends in Solid Adsorbent Materials Development for CO<sub>2</sub> Capture, *ACS Appl. Mat. Int.*, 2019, **11**, 34533-34559.

Wang, C.; Chen, T.; Liu, H.; Xie, J.; Li, M.; Han, Z.; Zhao, Y.; Dong, S.; He, H.; Zou, X.; Suib, S. L., Promotional catalytic oxidation of airborne formaldehyde over mineral-supported MnO<sub>2</sub> at ambient temperature, *Appl. Clay Sci.*, 2019, **182**, 105289.

Lv, H.; Xu, D.; Sun, L.; Henzie, J.; Suib, S.; Yamauchi, Y.; Liu, Be. Ternary Palladium-Boron-Phosphorus Alloy Mesoporous Nanospheres for Highly Efficient Electrocatalysis, *ACS Nano*, 2019, **13**, 12052-12061.

Megeurdichian, A.; Tabassum, L.; Dubrosky, J. P.; Shakil, M. R.; Macharia, J.; Toloueinia, P.; Tasnim, H.; Kapuge, T. K.; Willis, W. S.; Suib, S. L., Facile Preparation of Porous Manganese Oxide Foams, Sponges, and Merged Spherical Networks, Using Polydopamine/Dextran for Catalytic Oxidation of SelectCyclohexane, *Micropor. Mesopor. Mat.*, 2020, **295**, 109740 -109751.

Nabavinia, M.; Kanjilal, B.; Hesketh, A.; Wall, P.; Amin, A. A.; Kerns, P.; Stanzione, J. F.; Suib, S. L.; Liu, F.; Noshadi, I., One-Pot Aqueous and Template-Free Synthesis of Mesoporous Polymeric Resins, *Catalysts*, 2019, **9**, 782 - 797.

Meguerdichian, A. G.; Tabassum, L.; Tasnim, H.; Kapuge, T.; Shirazi-Amin, A.; Shakil, M. R.; Toloueinia, P.; Achola, L. A.; Willis, W. S.; Suib · S. L., Modified Solution Combustion Synthesis (SCS) of Nickel Oxide, NiO Sphere Clusters Using Glucans and Sodium Salts: Application for Electrocatalytic Decomposition of Urea, *Micropor. Mesopor. Mat.*, 2020, **295**, 109750 - 109763.

Thalgaspitiya, W.; Kapuge, T.; Rathnayake, D.; He, J.; Willis, W. S.; Suib, S. L., A Novel Generalized Metal Dissolution Approach for the Synthesis of Mixed Valent Mesoporous Metal Oxides, *Mat. Today*, 2020, **35**, 50-68.

Achola, L. A.; Ghebrehiwet, A.; Macharia, J.; Kerns, P.; He, J.; Fee, J.; Tinson, C.; Shi, J.; March, S.; Jain, M.; Suib, S. L., Enhanced Visible-Light-Assisted Peroxymonosulfate Activation on Cobalt-Doped Mesoporous Iron Oxide for Orange II Degradation, *Appl. Catal. B: Env.*, 2020, **263**, 118332 - 18342.

Meng, Y.; Zhang, X.; Hung, W. H.; He, J.; Sheng, T. Y.; Kuang, Y.; Kenney, M.; Shyue, J. J.; Liu, Y.; Stone, K. H.; Suib, S. L.; Lin, M.; Liang, Y.; Dai, H., Highly Active Oxygen Evolution Integrated with Efficient CO<sub>2</sub> to CO Electroreduction, *Proc. Nat. Acad. Sci.*, 2019, **116**, 23915-23922.

Li, G.; Dissanayake, S.; Suib, S. L.; Resasco, D. E.; Activity and Stability of Mesoporous CeO<sub>2</sub> and ZrO<sub>2</sub> Catalysts for the Self-Condensation of Cyclopentanone, *Appl. Catal. B Env*, 2020, **267**, 118373.

Kapuge, T. K.; Thalgaspitiya, W. R. K.; Rathnayake, D.; He, H.; Kerns, P.; Suib, S. L., Photo-generated reactive oxygen species assisted tandem amine homocoupling and amine-alcohol cross-coupling reaction on mesoporous spinel cobalt oxide, *Appl. Catal. B*, 2020, **268**, 118386 - 18404.

Shu, Z.; Liu, L.; Tan, W.; Suib, S. L.; Qiu, G.; Yang, X.; Zheng, L.; Liu, F., Solar Irradiation Induced Transformation of Feerrihydrate in the Presence od Aqueous Fe<sup>2+</sup>, *Env. Sci. Tech.*, 2019, **53**, 8854–8861.

Dissanayake, S. L.; Wasalathanthri, N. D.; Amin, A. S.; He, J.; Poges, S.; Rathnayake, D.; Suib, S. L., Mesoporous Co<sub>3</sub>O<sub>4</sub> Catalysts for VOC Elimination: Oxidation of 2-propanol, *Appl. Catal. A*, 2020, **590**, 117366 - 117374.

Wang, X.; Seelen, E. A.; Mazrui, N. M.; Kerns, P.; Suib, S. L.; Zhao, J.; Mason, R. P., The Interaction of Mercury and Methylmercury with Chalcogenide Nanoparticles, *Env. Poll.*, 2019, **255**, 113346 - 113355.

Hu, M.; Jin, L.; Su, X.; Bamonte, S.; Lu, X.; Gao, P.; Suib, S. L.; Liu, B.; He, J., Polymer-assisted co-assembly towards synthesis of mesoporous titania encapsulated monodisperse PdAu for highly selective hydrogenation of phenylacetylene, *ChemCatChem*, 2020, **12**, 1476-1482.

Thalgaspitiya, W. R. K.; Kapuge T. K.; He, J.; Kerns, P.; Meguerdichian, A.; Suib, S. L., A Novel, Mesoporous Molybdenum Doped Titanium Dioxide/ Reduced Graphene Oxide Composite as a Green, Highly Efficient Solid Acid Catalyst for Acetalization, *Dalton Trans.*, 2020, **49**, 3786 - 3795.

Wang, J.; Dang, Y.; Meguerdichian, A.; Dissanayake, S.; Kankanam-Kapuge, T.; Bamonte, S.; Tobin, Z.; Achola, L.; Suib, S., Water Harvesting from the Atmosphere in Arid Areas with Manganese Dioxide, *Env. Sci. & Tech. Lett.*, 2020, **7**, 48-53.

Thalgaspitiya, W.; Kapuge, T.; He, J.; Rathnayake, D.; Kerns, P.; Suib, S., Mesoporous Molybdenum-Tungsten Mixed Metal Oxide: A Solid Acid Catalyst for Green, Highly Efficient sp<sup>3</sup>-sp<sup>2</sup> C-C coupling reactions, *ACS Appl. Mat. Int.*, 2020, **12**, 5990-5998.

Thalgaspitiya, W. R. K.; Kapuge, T. K.; Rathnayake, D.; He, J.; Willis, W. S.; Suib, S. L., Generalized Synthesis of High Surface Area Mesoporous Metal Titanates as Efficient Heterogeneous Catalysts, *Appl. Mat. Today*, 2020, **19**, 100570-100574.

He, Y.; Yang, K. R.; Yu, Z.; Fishman, Z. S.; Achola, L. A.; Tobin, Z. M.; Heinlein, J. A.; Hu, S.; Suib, S. L.; Batista, V. S.; et al, Catalytic manganese Oxide nanostructures for the reverse Water gas Shift Reaction, *Nanoscale*, 2019, **11**, 16677-16688.

Moharrerri, E.; Pardakhti, M.; Srivastava, R.; Suib, S. L., Energy-Geometry Dependency of Molecular Structures: A Multistep Machine Learning Approach, *ACS Comb. Sci.*, 2019, **21**, 614-621.

Xing, Y.; Jia, G.; Liu, Z.; Fang, S.; Zhao, C.; Guo, X.; Suib, S. L., Development of Highly Selective Support for CO Hydrogenation to light olefins with Partially Passivated Iron Catalysts, *ChemCatChem*, 2019, **11**, 3187-99.

Yu, L.; Zhang, J.; Dang, Y.; He, J.; Tobin, Z.; Kerns, P.; Dou, Y.; Jiang, Y.; He, Y.;

Suib, S. L., In Situ Growth of Ni<sub>2</sub>P-Cu<sub>3</sub>P Bimetallic Phosphide with Bicontinuous Structure on Self Supported NiCuC Substrate as an Efficient Hydrogen evolution Reaction Electrocatalyst, *ACS Catal.*, 2019, **9**, 6919-6928.

Chen, Y.; Chen, T.; Liu, H.; Zhang, P.; Wang, C.; Dong, S.; Chen, D.; Xie, J.; Zou, X.; Suib, S. L.; Li, C.. High catalytic performance of the Al-promoted Ni/Palygorskite catalysts for dry reforming of methane, *Appl. Clay Sci.*, 2020, **188**, 105498 - 105508.

Jin, L.; Su, X.; Shi, J.; Shih, K. C.; Cintron, D.; Cai, T.; Nieh, M. P.; Chen, O.; Suib, S. L.; Jain, M.; He, J., Crystalline Mesoporous Complex Oxides: Porosity-Controlled Electromagnetic Response, *Adv. Funct. Mat.*, 2020, **30**, 1909491 -1909500.

Wu, Y.; Fee, J.; Tobin, Z.; Shirazi, A.; Kerns, P.; Dissanayake, S.; Mirich, A.; Suib, S., Amorphous Manganese Oxides: A New Approach for Reversible Aqueous Zinc-Ion Batteries, *ACS Appl. Energy Mat.*, 2020, **3**, 1627-1633.

Hu, M. Yang, W.; Tan, H.; Jin, L.; Zhang, L.; Kerns, P.; Dang, Y.; Dissanayake, S.; Zhu, Y.; Liu, B.; Suib, S. L.; He, J., Template-free synthesis of mesoporous and crystalline transition metal oxide nanoplates with abundant surface defects, *Matter*, 2020, **264**, 118553 – 118559.

Deljoo, B.; Tan, H.; Suib, S. L.; Aindow, M., Thermally activated structural transformations in manganese oxide nanoparticles under air and argon atmospheres, *J. Mat. Sci.*, 2020, **55**, 7247-7258.

Thalgaspitiya, W. R. K.; Kapuge, T. K.; He, J.; Rathnayake, D.; Suib, S. L., High Surface Area Mesoporous Tungsten Oxide for Fast, Green Oxidation of Organosulfur Compounds in Crude Oil, *Appl. Mat. Today*, 2020, **19**, 100616 -100621.

Sarvi, B.; Hosseini, S. M.; Akbari, M. S. A.; Deljoo, B.; El-Sawy, A.; Amin, A. S.; Aindow, M.; Suib, S. L.; Najafpour, M. M., New findings and current controversies in the reaction of ruthenium red and ammonium cerium(IV) nitrate: Focus on the precipitated compound, *Cat. Sci. Tech.*, 2020, **10**, 2491-2502.

Yu, L.; Zhang, J.; Zeng, J.; He, J.; Kerns, P.; Murphy, S.; Suib, S.; Dang, Y.; Dou, Y., Self-Grown NiCuOx Hybrids on a Porous NiCuC Substrate as an HER Cathode in Alkaline Solution, *Appl. Surf. Sci.*, 2020, **515**, 146117–146125.

Yu, L.; Rowe, D.; Perera, I.; Zhang, J.; Suib, S.; Xin, X.; Wei, M., Intrafibrillar Mineralized Collagen-Hydroxyapatite-Based Scaffolds for Bone Regeneration, *ACS Appl. Mat. Int.*, 2020, **12**, 18235-18249.

Toloueinia, P.; Khassaf, H.; Shirazi, A. A.; Tobin, Z.; Alpay, S. P.; Suib, S., Moisture-Induced Structural Degradation in Methylammonium Lead Iodide Perovskite Thin Films, *ACS Appl. Energy Mat.*, 2020, **3**, 8240-8248.

Liu, B.; Hu, M J.; Dang, Y.; Suib, S. L.; He, J., Supported Pt Nanoparticles on Mesoporous Titania for Selective Hydrogenation of Phenylacetylene, *Frontiers Chem.*, 2020, **8**, 581512–581520.

Zhou, X.; Wu, D.; Jin, Z.; Song, X.; Wang, X.; Suib, S. L., Significantly increased Raman Enhancement of Defect Rich O-Incorporated 1T-MoS<sub>2</sub> Nanosheets, *J. Mat. Sci.*, 2020, **55**, 16374-16384.

Zhang, T.; Liu, L.; Tan, W.; Suib, S. L.; Qiu, G., Formation and Transformation of Manganese (III) Intermediates in the Photochemical Generation of Manganese (IV) Oxide Minerals, *Chemosphere*, 2021, **262**, 128082 - 128090.

Thalgaspitiya, W. R. K.; Kankanam Kapuge, T.; He, J.; Deljoo, B.; Meguerdichian, A. G.; Aindow, M.; Suib, S. L., Multifunctional Transition Metal Doped Titanium Dioxide Reduced Graphene oxide Composites as highly Efficient Adsorbents and Photocatalysts, *Micropor. Mesopor. Mat.*, 2020, **307**, 110521 - 110528.

Kibona, T. E.; Achola, L.; Kerns, P.; Macharia, J.; King'ondy, C. K.; Suib, S. L., Highly Microporous Parinari Curatellifolia Carbon Nanomaterials for Supercapacitors, *Nano-Structures & Nano-Objects*, 2020, **22**, 100445-100454.

Shi, J.; Sauyet, T.; Dang, Y.; Suib, S.; Seehra, M.; Jain, M. Structure-property correlations and scaling in the magnetic and magnetocaloric properties of GdCrO<sub>3</sub> particles, *J. Phys. Cond. Matt.*, 2021, **33**, 205801-205812.

Luo, Y.; Tan, W.; Suib, S. L.; Qiu, G.; Liu, F., Epitaxial Growth mechanisms of Heterogeneous Catalytic Oxidation of Mn(II) on Manganite Under Oxidic Conditions, *Chem. Geol.*, 2020, **547**, 119670 - 119677.

He, Y.; Guo, F.; Yang, K.; Heinlein, J.; Bamonte, S.; Fee, J.; Hu, S.; Suib, S. L.; Haller, G.; Batista, V.; Pfefferle, L., In situ Identification of Reaction Intermediates and Mechanistic Understandings of Methane Oxidation over Hematite: A Combined Experimental and Theoretical Study, *J. Am. Chem. Soc.*, 2020, **142**, 17119-17130.

Fan, Y.; Huang, Y.; Linthicum, W.; Liu, F.; Berings, A.; Dang, Y.; Xu, Z.; Chang, S. Y.; Ling, J.; Huey, B.; D.; Suib, S.; Ma, A.; Gao, P.; Lu, X.; Lei, Y.; Shaw, M.; Li, B., Towards Long-term Accurate and Continuous Monitoring of Nitrate in Wastewater Using PTFE (polytetrafluoroethylene)- Solid-state Ion-selective electrodes (S-ISEs), *ACS Sensor*, 2020, **5**, 3182-3193.

Dissanayake, S.; Vora, N.; Achola, L.; Dang, Y.; He, J.; Tobin, Z.; Lu, X.; Mirich, A.; Gao, P. X.; Suib, S. L., Synergistic Catalysis by Mn Promoted Ceria for Molecular Oxygen Assisted Epoxidation, *Appl. Cat. B*, 2020, **282**, 119573 - 119583.

Rathnayake, D.; Perera, I.; Shirazi Amin, A.; Kerns, P.; Dissanayake, S.; Suib, S. L., Mesoporous Crystalline Niobium Oxide with High Surface Area: A Solid Acid Catalyst for Alkyne Hydration, *ACS Appl. Mat. Int.*, 2020, **12**, 47389-47396.

Wang, W.; He, Y.; He, J.; Dang, Y.; Kankanmkapuge, T.; Gao, W.; Cong, R.; Suib, S. L.; Yang, T., Identification of Key Oxidative Intermediates and the Function of Chromium Dopants in PKU-8: Catalytic Dehydrogenation of Sec-Alcohols with tert-Butylhydroperoxide, *Cat. Sci. Tech.*, 2021, **11**, 1365 - 1374.

Khanna, H.; Eddy, N.; Dang, Y.; Bhosale, T.; Shubhashish, S.; Suib, S.; Nandi, P., Nanoporous Co/Mn Mixed Metal Oxides Templated via Polysulfones for Amine Oxidation, *ACS Applied Nano Materials*, 2020, **3**, 11923-11932.

Amin, A. S.; Toloueinia, P.; Wu, Y.; Meguerdichian, A. G.; Kerns, P.; Suib, S. L., Effect of lithium incorporation on tweaking the electrocatalytic behavior of tantalum-based oxides, *J. Mat. Chem. A*, 2020, **8**, 23413 – 23426.

Tabassum, L.; Tasnim, H.; Meguerdichian, A.; Willis, W.; Macharia, J.; Price, C.; Dang, Y.; Suib, S., L., Enhanced Catalytic Activity of Vanadium-Doped Mesoporous Octahedral Molecular Sieve-2 (K-OMS-2) Towards Hydrogen Evolution Reaction (HER), *ACS Appl. Energy Mat.*, 2020, **3**, 12185-12193.

Saeidi, S.; Najari, S.; Concepcion, P.; Hessel, V.; Suib, S. L., Recent advances in CO<sub>2</sub> hydrogenation to value-added products — Current challenges, development and future directions, *Prog. Energy Combust. Sci.*, 2021, **85**, 100905 - 100968.

Shubhashish, S.; Khanna, H.; Achola, L.; Shirazi A., A.; Willis, W.; Suib, S., Selective Oxidative Coupling of Amines Using Mesoporous MoO<sub>x</sub> Catalysts, *ACS Appl. Nano*, 2021, **4**, 2086-2097.

Hu, M.; Jin, L.; Dang, Y.; Suib, S. L.; He, J.; Liu, B. Supportd Pt Nanoparticles on Mesoporous Titania for Selectrive Hydrogeneation of Phenylacetylene, *Frontiers Chem.*, 2020, **8**, 581512-581520.

Feng, X.; Jiao, Q.; Chen, W.; Dang, Y.; Dai, Z.; Suib, S. L.; Zhang, J.; Zhao, Y.; Li, H.; Feng, C., Cactus like NiCo<sub>2</sub>S<sub>4</sub>@NiFe LDH Hollow Spheres as an Effective Oxygen Bifunctional Electrocatalyst, *Appl. Cat., B: Env.*, 2021, **286**, 119869 - 119880.

Wang, X.; Yan, P.; Kerns, P.; Suib, S. L.; Loew, L. M.; Zhao, J., Voltage Dependent Photoluminescence of Carbon Dots, *J. Electrochem. Soc.*, 2020, **167**, 147515 - 147520.

Shirazi-Amin, A.; Toloueinia, P.; Wu, Y.; Meguerdichian, A. G.; Kerns, P.; Suib, S. L., Effect of Lithium Inorporation on Tweaking the Electrocatalytic Behavior of Tantalum-Based Oxides, *J. Mat Chem. A: Mat. Energy Sust.*, 2020, **8**, 23413-23426.

Meng, Y.; Liu, Y.; He, J.; Sun, V.; Palmieri, A.; Gu, Y.; Zheng, X.; Dang, Y.; Huang, X.;

Mustain, W.; Suib, S.; Large Scale Synthesis of Manganese Oxide/Reduced Graphene Oxide Composites as Anode Materials for Long Cycle Lithium Ion Batteries, *ACS Appl. Energy Mat.*, 2021 in press.

Suib, S. L.; Jain, M., Comparison of the Dielectric and Magnetocaloric Properties of Bulk and Thin Films of  $\text{GdFe}_{0.5}\text{Cr}_{0.5}\text{O}_3$ , *J. Appl. Phys.*, 2021, in press.

(VI) *Jointly funded by this grant and other grants with intellectual leadership by other funding sources*

Luo, Z.; Kriz, D. A.; Miao, R.; Kuo, C. H.; Zhong, W.; Guild, C.; He, J.; Willis, W.; Dang, Y.; Suib, S. L.; Nandi, P.,  $\text{TiO}_2$  Supported Gold-Palladium Catalyst for Effective Syngas Production from Methane Partial Oxidation, *Appl. Catal. A.*, 2018, **554**, 54-63.

Kriz, D. A.; Nizami, Q. A.; He, J.; Jafari, T.; Dang, Y.; Kerns, P.; Meguerdichian, A. G.; Suib, S. L.; Nandi, P., Partial Oxidation of Methane to Synthesis Gas Using Supported Ga-containing Bimetallic Catalysts and a Ti-Promoter, *ChemCatChem*, 2018, **10**, 4300-4308.

Wasalathanthri, N. D.; Guild, C.; Nizami, Q. A.; Dissanayake, S. L.; He, J.; Kerns, P.; Fee, J.; Achola, L.; Rathnayake, D.; Weerakkody, C.; Suib, S. L.; Nandi, P., Niobium-substituted Octahedral Molecular Sieve (OMS-2) Materials in Selective Oxidation of Methanol to Dimethoxymethane, *RSC Advances*, 2019, **9**, 32665 – 32673.

Ernst, A. T.; Kerns, P.; Nardi, A.; Brody, H. D.; Dongare, A. M.; Lee, S. W.; Champagne, V. K.; Suib, S. L.; Aindow, M., Surface States of Gas-Atomized Al 6061 Powders – Effect of Heat treatment, *Appl. Surf. Sci.*, 2020, **534**, 147643 - 147654.

Ma, X.; Zhong, W.; Zhao, J.; Suib, S. L.; Lei, Y., Self Heating Enabled One Pot Synthesis of Fluorescent Carbon Dots, *Eng. Sci.*, 2020, **9**, 44-49.

### **Awards 2018 – 2021**

National Academy of Inventors, Fellow, 2018

ACS Excellence in Review Award, 2019

OCSD Wall of Honor, 2020

I&EC Research 2020 Excellence in Review Award

AAAS Fellow, 2020

### **Major Journal Leadership**

Associate Editor – The Chemist, Recent Patents on Materials Science

Associate Editor - Recent Patents on Catalysis

Associate Editor – The International Journal of Chemical Research

Editor in Chief, Materials

Specialty Chief Editor, Frontiers in Green and Environmental Chemistry

Review Editor, Frontiers in Materials

Field Chief Editor, Frontiers in Chemistry

Nathaniel K. Szymczak and Corey R. J. Stephenson

## Tandem Upgrading and Alkylations Using Ethanol as a Building Block

Nathaniel K. Szymczak, Corey R. J. Stephenson,  
Zhongyuan Li, Alex Davies  
University of Michigan

### Presentation Abstract

This presentation will outline our efforts to develop new routes to access diversified chemicals from ethanol (EtOH). Using a Ru-pincer-based catalyst, we established the viability of a single pot cascade reaction sequence to use the products of a Guerbet reaction (ethanol to 1-butanol) with carbon pronucleophiles to form new carbon-carbon bonds. Representative substrate classes containing acidic C-H bonds were assessed and evaluated a one-pot tandem reaction sequence to directly upgrade ethanol to butylated and hexylated products. We will show how the physical reaction parameters were optimized, including the effects of stoichiometry, temperature, time, base-, counter ion-, and catalyst identity. Reactions using representative carbon pronucleophiles provided butylated products in yields ranging from 50-90%. Ligand redesign will be described as a strategy to modify the properties of a Ru-pincer-based catalyst for these multi-step reactions. Ongoing efforts include developing conditions and catalyst variants that improve the reaction activity and/or selectivity in addition to promoting photochemically-driven alcohol upgrading.

### DE - SC0020191: Catalytic Upgrading of Renewable Feedstock

**PI:** Lead PI(s) Name(s) (*include only if different from above*)

**Postdoc(s):** Zhongyuan Li, Alex Davies

**Student(s):** Emily Nolen

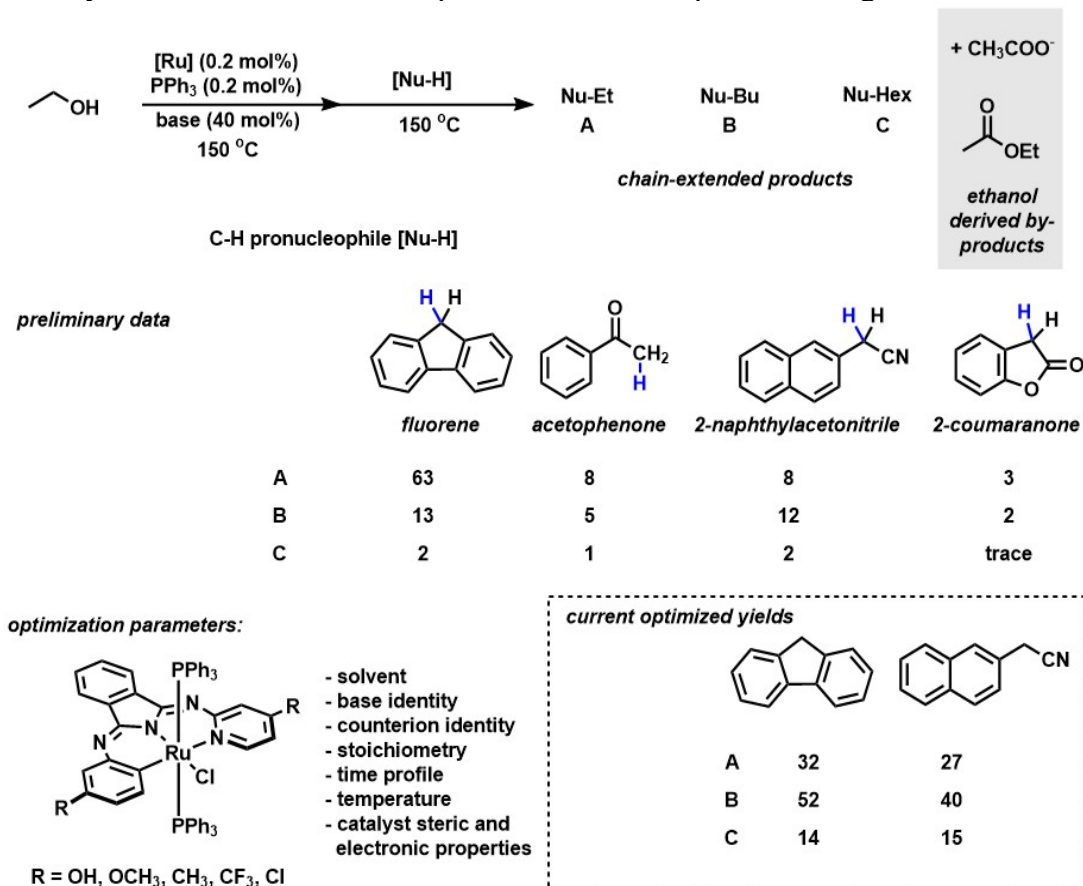
**Affiliations(s):** (*include only if different from above*)

### RECENT PROGRESS

#### ***Carbon-carbon bond forming reactions using alcohol feedstocks/reagents.***

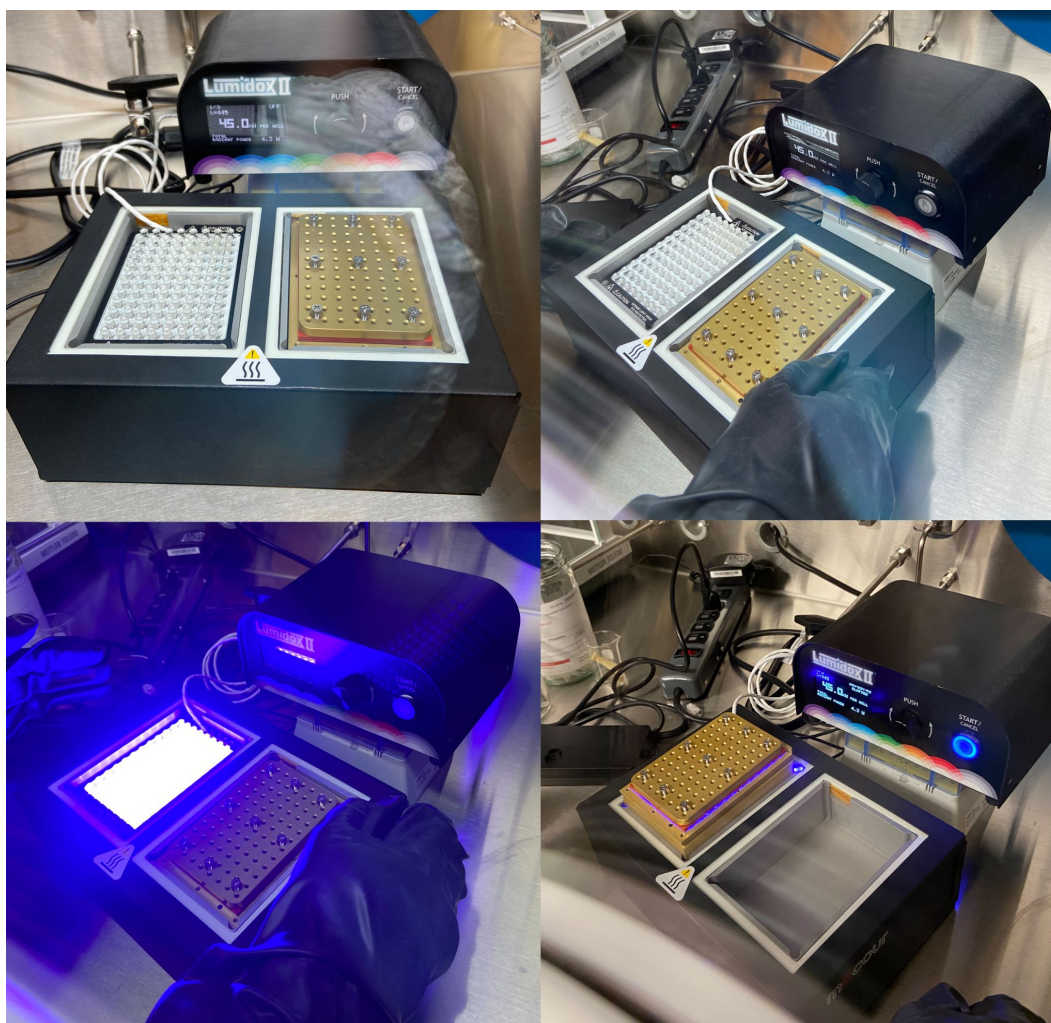
A major focus of this project is to provide new routes to platform chemicals from EtOH. To accomplish this task, we targeted a single pot cascade reaction sequence to intercept the products of the initial Guerbet reaction (ethanol to 1-butanol). To increase the value of ethanol-derived products, we evaluated carbon-carbon bond forming reactions using carbon pronucleophiles. We identified four representative substrates containing acidic C-H bonds amenable to a tandem Guerbet/alkylation reaction: fluorene, 2-naphthylacetonitrile, acetophenone, and 2-coumaranone. The critical challenge to overcome for these reactions is to minimize the amount of ethanol present prior to the addition of the carbon pronucleophile. Our previous results for ethanol upgrading were performed in neat ethanol, and an extensive solvent screen revealed that using co-solvents has a large impact on the ratio of ethanol to 1-butanol, ranging from 180 : 1 (DMF) to 1 : 2 (mesitylene). Using mixtures that mimic the reaction components after the ethanol

upgrading reaction, we evaluated the second (alkylation) step of the reaction sequence with each carbon pronucleophile using 1-butanol as the substrate. Reactions using fluorene, 2-naphthylacetonitrile, acetophenone, and 2-coumaranone provided butylated products in 51, 91, 20, and 55 % yields, respectively. We combined the results of both sets of optimization data and evaluated a one-pot tandem reaction sequence to directly upgrade ethanol to butylated and hexylated products using fluorene as a representative substrate. The reaction yields and selectivity profiles were initially highly variable and sensitive to solvent volume and stir rate; these properties necessitated extensive controls and replicate data to ensure batch to batch reproducibility. After optimizing the physical reaction parameters, we evaluated the effects of stoichiometry, temperature, time, base-, counter ion-, and catalyst identity. Interestingly, we found that the yields and selectivity are not favorably influenced by electronic modifications (para-substitution using -OH, -OCH<sub>3</sub>, -CH<sub>3</sub>, -CF<sub>3</sub>, -Cl), or steric modifications (para-substitution using -mesitylene) to the catalyst structure. This outcome implicates a selectivity-determining step that does not involve a metal-coordinated substrate. Given this information, we probed other hypothesized selectivity-determining steps and uncovered an important result that the base counter cation plays a large role to influence both the Guerbet reaction (ratio of ethanol to 1-butanol: 40 mol% LiOtBu = 5.5:1; 40 mol% NaOtBu = 1.8:1; 40 mol% KOtBu = 0.45:1.) and the tandem reaction selectivity (yield of ethylated, butylated and hexylated products for 40 mol% NaOtBu = 64, 13 and 2%; 40 mol% KOtBu = 32, 52 and 14%). We are continuing to optimize these reactions to maximize the yields of butylated and hexylated products and ultimately assess the mechanistic implications of our empirical findings.



***Assemble experimental apparatus needed for high throughput reaction development as well as reaction monitoring during illumination.***

A major focus of Aims 2 & 3 of the project is to target photochemically-driven reactions as well as reactor design principles to provide new routes to platform chemicals from EtOH. The Stephenson laboratory in collaboration with MéCour Temperature Control have recently developed and produced a double-position thermal unit which allows efficient high-throughput experimentation of both photochemical and thermal reactions. The unit is designed to house both a 96-well Lumidox II LED array (390 nm or 456 nm) with a 96-well plate, or 96/384/1536-well plates for thermal reactivity profiling. The unit supports precise temperature regulation between  $-40$  to  $150$  °C allowing for robust temperature control and in depth analysis of the effect of temperature on a given reaction. Furthermore, the Lumidox II LED arrays are equipped with a control unit which allows for light intensity adjustments. Despite significant delays in the acquisition and installation of the thermal unit due to the pandemic, the Stephenson laboratory is now equipped with a state-of-the-art photochemical batch reactor which supports up to 192 simultaneous reactions on micromole scale.



**Ligand and Surface Cooperativity in the Stabilization of Metal-Ligand Single-site Catalysts at Surfaces**

Steven L. Tait  
Department of Chemistry, Indiana University

**Presentation Abstract**

Metal-ligand complexation offers the opportunity to both stabilize and chemically tune single transition metal atoms on a support surface. This offers a solution to grand challenges in heterogeneous catalysis to achieve high levels of selectivity by controlling the chemical uniformity of metal catalyst sites at surfaces. Here, we examine the significant roles of the coordinating ligands and of the oxide support on catalyst structure, activity, and stability. Defect sites on the support have a strong influence on the state of the metal centers and show a significant impact on reaction activity, even for comparable loading levels. We also see strong influences due to changing functional group substituents in the ligands or by changing the ligand to metal loading ratio on the catalyst. By loading the metal and ligand directly on the oxide support, it is possible to maintain a close contact of the metal to the oxide, which can facilitate heterolytic activation and spillover during the reaction. These systems are shown to be active for the catalysis of hydrosilylation reactions in solution and for hydrogenation in flow reactor experiments.

**DE-SC0021390: Rational Design of Metal-ligand Single Atom Heterogeneous Catalysts**

**PIs:** Steven L. Tait, Kenneth G. Caulton

**Postdoc:** Nicholas Maciulis

**Students:** Ayanna Culmer-Gilbert, Brendan Godsel, Fereshteh Rezvani, Eman Wasim

**RECENT PROGRESS**

***Overview***

In this project, we are conducting experiments to advance study of single-atom heterogeneous catalysts on support surfaces that are defined and stabilized by a metal-ligand coordination strategy. The combination of metal-ligand and metal-support interactions provides well-defined coordination centers on high-surface area oxide supports that achieve scalable, high reaction selectivity in gas flow reactions and in solution-phase batch reactions. We characterize these systems before, during, and after reactions. The central goal of our work is to advance understanding of single-atom catalysts on solid supports through a metal-ligand complexation strategy to enable high activity, high selectivity, and robust stability.

## Ligand-coordinated Ir Single-atom Catalysts Stabilized on Oxide Supports for Ethylene Hydrogenation and Their Evolution under a Reductive Atmosphere

We have studied a novel series of oxide-supported Ir-ligand single-atom catalysts (SACs) for ethylene hydrogenation. Ir SACs were synthesized using a one-step impregnation method developed by our group, using one of two ligands, either 1,10-Phenanthroline-5,6-dione (PDO) or 3,6-Di-2-pyridyl-1,2,4,5-tetrazine (DPTZ, Fig. 1), on powder supports of either CeO<sub>2</sub> or MgO. Characterization by XAS, XPS, and CO adsorption proved that Ir exist principally as highly uniform, cationic single-atoms. Ir SACs show significantly higher durability and metal utilization efficiency than Ir nanoparticle (NP) catalysts during ethylene hydrogenation at 100 °C, as well as excellent stability, as no Ir aggregates were detected after > 10 h reaction.

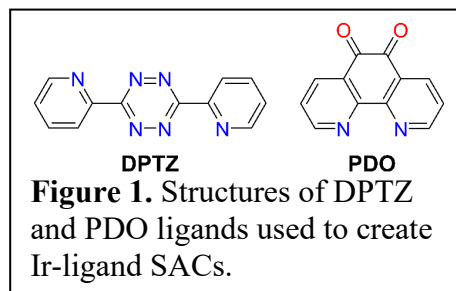


**Figure 1.** Structures of DPTZ and PDO ligands used to create Ir-ligand SACs.

The activity of the ligand stabilized supported catalysts (LCSCs) of Ir can be tuned by ligand and support effects: PDO and CeO<sub>2</sub> are superior to DPTZ and MgO, respectively. This tunability is attributed to differences in H<sub>2</sub> activation capability, which results from differences in support reducibility, electron density on Ir, and, potentially, the local coordination environment of Ir.

As for the ligand effect, we think Ir-PDO/CeO<sub>2</sub> activate H<sub>2</sub> better than Ir-DPTZ/CeO<sub>2</sub>, likely because Ir on the former is more electron deficient, as a result of electron tuning by the ligand. Ligand geometry can also affect the coordination between Ir and reactants sterically. It may also influence the interaction between ligand molecular orbitals and Ir valence orbitals, impacting catalysis indirectly through electronic effects. The ligand effect highlights the extra tunability Ir-ligand SACs have over typical SACs without ligands. As is observed in homogeneous catalysis, the ligand can exert both electronic and geometric effects on the metal center. Inspired by the ligand and support effects, we are exploring broader ligand space and support engineering strategies to enhance the performance of metal-ligand SACs.

We also discovered that Ir single atoms evolve dynamically during H<sub>2</sub>-D<sub>2</sub> exchange experiments. The changes in H<sub>2</sub>-D<sub>2</sub> exchange activity indicate that the structure of Ir single atoms is dynamic under H<sub>2</sub>. *In situ* XAS was conducted on Ir-PDO/MgO SAC during H<sub>2</sub>-He-H<sub>2</sub> treatment. The sample was heated to 100 °C under 20% H<sub>2</sub> in 0.75 h, and further treated with H<sub>2</sub> at 100 °C for 6 h. Then the gas was switched to He at 100 °C for ~ 5.5 h, after which H<sub>2</sub> was re-introduced for 6.5 h. During the entire experiment, Ir L3-edge X-ray absorption spectra were collected continuously, with results summarized in **Fig. 2**.

During the initial H<sub>2</sub> treatment stage, white line intensity,  $N(\text{Ir-O/N})$ , and  $N(\text{Ir-Cl})$  decrease continuously, suggesting a loss of Ir-O/N and Ir-Cl coordination (**Figs. 2a** and **2d**). **Fig. 2a** also shows a slight absorption edge shift to higher energy and the appearance of a secondary feature centered at ~6 eV beyond the white line (highlighted in  $\Delta\text{XANES}$ ). This feature, with its well-defined position, has been recognized by multiple studies as a highly unique feature from the metal-H  $\sigma^*$  antibonding orbitals,<sup>84-87</sup> and no alternative explanation exists in literature, *i.e.*, it indicates metal hydride formation. The formation of Ir-H is consistent with decreased white line intensity, which is an indicator of Ir reduction. Overall, these results strongly indicate that under H<sub>2</sub>, Ir-O/N and Ir-Cl coordination is

gradually replaced by Ir–H. The replacement is associated with the initial activation and the following irreversible deactivation in H<sub>2</sub>-D<sub>2</sub> exchange.

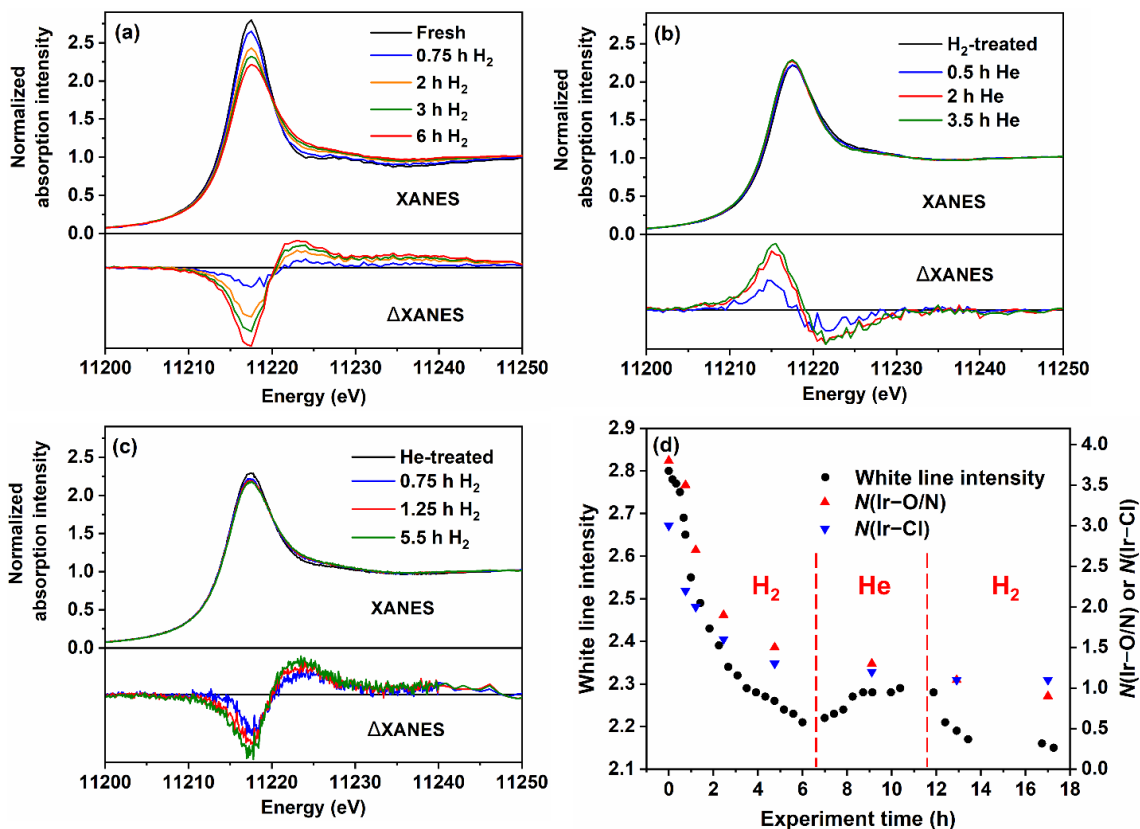


**Figure 2.** *In situ* Ir L3-edge XAS on Ir-PDO/MgO SAC during H<sub>2</sub>-He-H<sub>2</sub> treatment. XANES region after normalization during (a) the initial H<sub>2</sub> stage (including heating to 100 °C from room temperature), (b) He stage, and (c) the second H<sub>2</sub> stage. (d) XANES white line intensity (black dots),  $N(\text{Ir-O/N})$  (red triangles), and  $N(\text{Ir-Cl})$  (blue triangles) from EXAFS fitting during the entire experiment.

This work presents a new type of Ir hydrogenation SACs that are more durable, efficient, and tunable than supported Ir NPs, while more stable than homogeneous Ir complexes. It also offers fundamental understanding regarding the ligand and support effect, as well as the evolution of Ir single-atoms under H<sub>2</sub>, instructing future design of stable, effective hydrogenation SACs.

### ***Tuning Ligand-coordinated Single Metal Atoms on TiO<sub>2</sub> and their Dynamic Response during Hydrogenation Catalysis***

We investigate the effect of the choice of organic ligand on the activity and stability of TiO<sub>2</sub>-supported single-atom Pt-ligand catalysts for ethylene hydrogenation. The activity of these catalysts shows a significant dependence on the choice of ligand and also correlates with coordination number for Pt-ligand and Pt-Cl. Of the three ligands examined in our study, the one with the lowest Pt coordination number, 1,10-phenanthroline-5,6-dione (PDO), shows the lowest reaction temperature and highest reaction rate, likely due to those metal sites being more accessible to reactant adsorption.

*In situ* XAS experiments show that the activity also correlates with good heterolytic dissociation of hydrogen, which is supported by OH/OD exchange experiments and is the rate-determining step of the hydrogenation reaction.

Our measurements of reaction order on the Pt-ligand LCSCs indicate first-order dependence on H<sub>2</sub> pressure. According to the Horviti–Polanyi mechanism, first-order kinetics in H<sub>2</sub> indicate that the H<sub>2</sub> dissociation is the rate-determining step for the hydrogenation reaction. For the Pt-ligand LCSCs studied here, the single-site character of the catalyst does not allow for two neighboring Pt to facilitate H–H activation, so a heterolytic hydrogen dissociation pathway, involving hydrogen spillover to the oxide support, occurs on the surface. We compare this hydrogen dissociation to DRIFTS measurement of OH/OD exchange under D<sub>2</sub> flow. The Pt-PDO/TiO<sub>2</sub> catalyst, which shows the highest hydrogenation activity, also shows the highest OD intensity at 30 °C, indicating that the high hydrogenation activity of the catalyst at 30 °C may be related to the efficient heterolytic hydrogen dissociation process and efficient H atom spillover. Pt-BPDCA (at similar Pt loading) shows a significantly lower OD intensity compared to Pt-PDO, which suggests lower hydrogen dissociation ability of the less-active Pt-BPDCA at 30 °C. Pt-DPTZ/TiO<sub>2</sub> (measured with 3-fold lower Pt loading) also exhibits less OH/OD exchange than Pt-PDO at 30 °C. Unlike the Pt LCSCs, OH/OD exchange on Pt NPs/TiO<sub>2</sub> may also be facilitated by a homolytic hydrogen dissociation process on the particles.

In these *in situ* XAS experiments up to 190 °C, the supported Pt-ligand catalyst shows excellent stability against structural and chemical change. Instead of Pt, the PDO ligand can be coordinated with Ir on TiO<sub>2</sub> to form Ir LCSCs that show slow activation by loss of Ir-Cl bonds, then excellent stability in the hydrogenation of ethylene. These results provide the chance to engineer ligand-coordinated supported catalysts at the single-atom catalyst (SAC) level by the choice of ligand and enable new applications at relatively high temperature.

### ***Ongoing work***

We have developed synthesis protocols for a new series of ligands that allow us to add functional groups to enhance interaction with the support surface, thereby increasing stability. Symmetric substitution of two COOH or methyl groups raised concerns about steric restriction of substrate access to the catalyst active site, so we also developed protocols for asymmetric substitution. Our results on this so far have demonstrated that we can show a significant improvement in the recyclability of Pt-ligand catalysts over eight reaction batch cycles for alkene hydrosilylation reactions.

We have conducted experiments to better understand our observation of high selectivity in acetylene hydrogenation with an increase in diketone phenanthroline (PDO) ligand during synthesis in collaboration with researchers at the University of Central Florida conducting DFT calculations. We have discovered a direct role of PDO ligands in shuttling H atoms for highly selective hydrogenation of acetylene. Our new results show the role that metal-ligand complexes in heterogeneous catalysts can play for achieving high performing reactions.

## Publications Acknowledging this Grant in 2018-2021

### *(VII) Intellectually led by this grant*

1. Chen, L.; Ali, I. S.; Sterbinsky, G. E.; Zhou, X.; Wasim, E.; Tait, S. L. Ligand-coordinated Ir Single-atom Catalysts Stabilized on Oxide Supports for Ethylene Hydrogenation and Their Evolution under a Reductive Atmosphere. *Catal. Sci. & Tech.* **2021**, *11*, 2081-2093. DOI: [10.1039/D0CY01132K](https://doi.org/10.1039/D0CY01132K)
2. Zhou, X.; Sterbinsky, G. E.; Wasim, E.; Chen, L.; Tait, S. L. Tuning Ligand-coordinated Single Metal Atoms on TiO<sub>2</sub> and their Dynamic Response during Hydrogenation Catalysis. *ChemSusChem* **2021**, *in press*. DOI: [10.1002/cssc.202100208](https://doi.org/10.1002/cssc.202100208)
3. Ali, I. S.; Chen, L.; Rezvani, F.; Zhou, X.; Tait, S. L. Tuning Coordinated Supported Catalysts: Carboxylic Acid-Based Ligands to Improve Ceria-Supported Pt Catalysts for Hydrosilylation. **2021**, *submitted*.
4. Zhou, X.; Rezvani, F.; Sterbinsky, G. E.; Tait, S. L. Titania Supported Rh-Ligand Coordinated Catalyst: Identification of Active Complex for CO Oxidation. **2021**, *manuscript in preparation*.

### *(VIII) Jointly funded by this grant and other grants with intellectual leadership by other funding sources*

5. Morris, T. W.; Din, N. U.; Wisman, D. L.; Duncan, D. A.; Le, D.; Wasim, E.; Rahman, T. S.; Tait, S. L. Impact of Oxygen Binding on Surface Trans Effect in Metal-Ligand Complexes at Surfaces by X-Ray Standing Wave Spectroscopy. **2021**, *manuscript in preparation*.

## Awards or leadership activities during 2018-2020 calendar years

2019 Visiting Fellow at the University of Science and Technology of China, Chinese Academy of Sciences, President's International Fellowship Initiative

2018 Visiting Professor of Chemistry and International Visiting Fellow of the Institute of Advanced Study, University of Warwick

Diversity Affairs Committee, 2016 – present, IU Chemistry

IU Catalysis Club, faculty advisor, 2016 – present

Chair, Graduate Admissions Committee, 2016-2019, IU Chemistry

Associate Director, IU Electron Microscopy Center, 2020 – present

Research Affairs Committee, Bloomington Faculty Council, 2020 – present

Review Panel, Institute for Advanced Studies, 2018 – present

Editor, Surface Science Reports, 2019 – present

Editorial Advisory Board, Surface Science, 2018 – present

ACS COLL Division Programming Chair, 2021 – present

American Chemical Soc., Society Committee on Publications, Associate, 2020 – present

American Vacuum Soc., Surface Science Div., Executive Board Member, 2017 – 2019

AVS Prairie Section, Executive Board Member, 2018 – present

ACS Alternate Councilor, ACS Colloids and Surface Chemistry Division, 2015 – 2020

ACS COLL Division Programming Committee, 2015 – present

American Chemical Society (ACS) Committee on Ethics, Committee Member 2017-2019, Associate Committee Member, 2015-2016

Organizer of eight recurring symposia on “Surface Chemistry,” ACS National Meetings: Atlanta (hybrid), August 2021; San Antonio (online), April 2021; San Francisco (online), August 2020; Philadelphia (online), March 2020; San Diego, August 2019; Orlando, April 2019; Boston, August 2018; New Orleans, April 2018.

Organizer of Symposium on “Adsorption and Reaction at Surfaces: Symposium in Honor of Charles T. Campbell,” with Jose Rodriguez and David Starr, ACS National Meeting, San Diego, August 2019.

Organizer of Symposium on “Supramolecular Assemblies at Surfaces: Non-covalent, Covalent, and Coordination Bonding,” ACS National Meeting, Orlando, April 2019, with Federico Rosei.

Organizer of Symposium on “Charge Transfer in Metal-Organic Systems at Surfaces,” Institute of Advanced Study, Univ. of Warwick, November 2018, with Giovanni Costantini and Nian Lin.

Fonds Wetenschappelijk Onderzoek (FWO, Belgian Research Foundation) Review College, 2021-2023

External Reviewer: Indian Institute of Science Education and Research, Pune; National University of Singapore (2020).

## M-edge XANES Spectroscopy of Transition Metal Catalysts

Josh Vura-Weis  
University of Illinois at Urbana-Champaign, Department of Chemistry

### Presentation Abstract

Optimizing reaction mechanisms at transition metal catalysts requires a detailed understanding of each step in the catalytic cycle, but transition states and many reactive intermediates are too complex and short-lived to characterize with existing spectroscopic tools. We use transient M-edge XANES spectroscopy in the extreme ultraviolet (XUV) spectral region to resolve these intermediates using femtosecond time resolution. This tabletop, in-lab technique probes the metal center directly, and the spectra share the element-, oxidation state-, spin state-, and ligand field-specificity of traditional hard X-ray absorption spectroscopy. We used this technique, in combination with optical transient absorption spectroscopy, to show that the low photochemical quantum yield of  $\mu$ -oxo bridged Fe(III) porphyrins is due to rare formation of the active Fe<sup>IV</sup>=O state. We continued our investigation of Co<sub>4</sub>O<sub>4</sub> cubane catalysts, and showed that the strong spin-orbit coupling in these systems enables single-step  $\Delta S=2$  intersystem crossing in high yield, opening up new options for multistate reactivity.

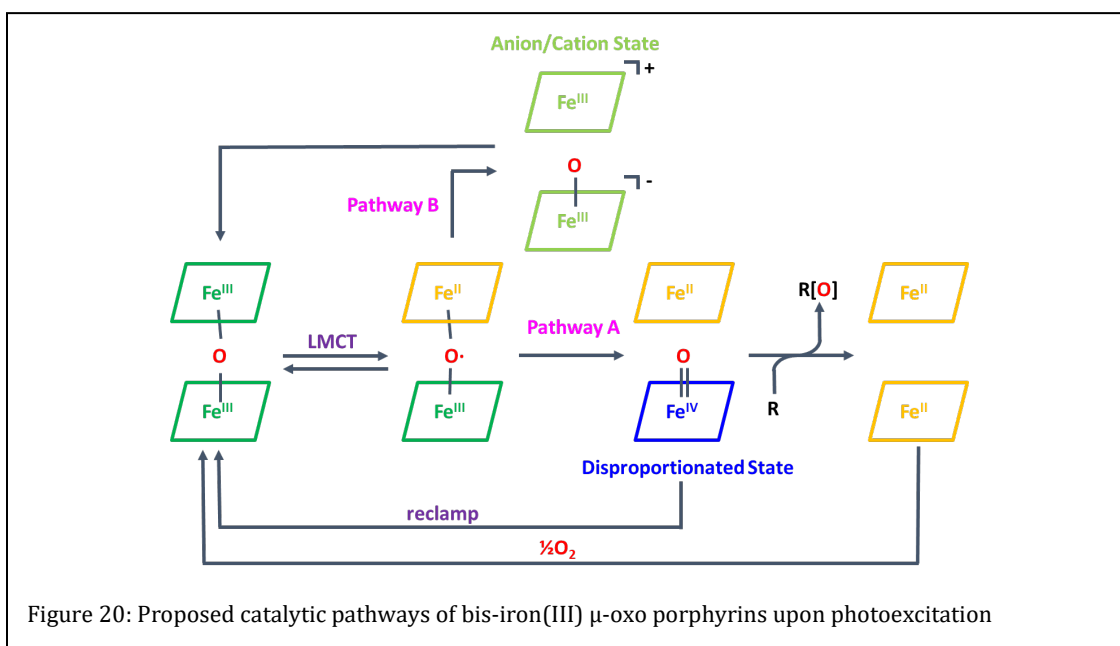
### **DE-SC0018904: Catalytic Reaction Intermediates Revealed with Femtosecond M-edge XANES**

**Students:** Clare Leahy, Yusef Shari'ati, Kori Sye

### RECENT PROGRESS

#### *Identification of catalytic intermediates in "Pacman" porphyrins using transient UV/Vis and M-edge XANES*

Much of our work in the past year has been uncovering the reason for low quantum yield in porphyrin photocatalysts. Previous work in other groups on bis-iron(III)  $\mu$ -oxo porphyrins has shown that the quantum yield of product formation (molecules oxidized vs photons absorbed) is less 0.01%. We sought to determine the why the yield is so low (what happens to molecules that are photoexcited but do not catalyze a reaction?). Two primary pathways have been proposed for the behavior of these molecules after photoexcitation, as shown in Figure 1.



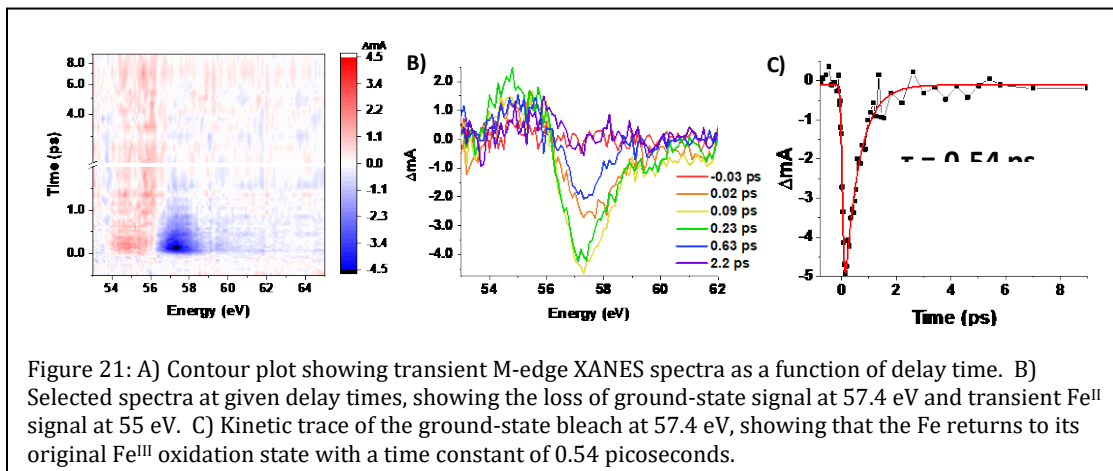
In the desired pathway (Pathway A), illumination at 350-400 nm excites a mixed ligand-to-metal charge transfer (LMCT) /  $\pi$ - $\pi^*$  state, creating a species with one  $\text{Fe}^{\text{III}}$  and one  $\text{Fe}^{\text{II}}$  center and bridging  $\text{O}^\cdot$  radical. In the desired pathway (Pathway A), disproportionation follows to form the catalytically active  $[\text{Fe}^{\text{II}} \text{Fe}^{\text{IV}}=\text{O}]$  species, which can then oxidize hydrocarbons. In the second pathway (labeled Pathway B), the stacked porphyrin splits into  $\text{Fe}^{\text{III}}\text{TPP}^+$ , where the cation is localized on the porphyrin ring, and  $\text{Fe}^{\text{III}}\text{TPPO}^-$ , where the anion is localized on the porphyrin ring. This state will be referred to as the Anion/Cation state. Notably, the oxidation state of the metal centers in this state is unchanged from the parent molecule.

The ability to differentiate between these two pathways is important from a fundamental perspective, given the low photon-to-product quantum yield. There are several possible “failure modes” for this catalyst:

- 1) The system relaxes from the LMCT state to the ground state before either Pathway A or B
- 2) The system proceeds primarily along Pathway A, but catalysis from the  $\text{Fe}^{\text{IV}}=\text{O}$  species is slow, so reclamping occurs before hydrocarbon oxidation
- 3) The system proceeds primarily along Pathway B, so the active  $\text{Fe}^{\text{IV}}=\text{O}$  state is rarely formed.

Previous optical transient absorption studies gave conflicting answers to this question, because it is difficult to ascertain the metal oxidation state from the change in the porphyrin UV/Visible spectrum (which is dominated by  $\pi$ - $\pi^*$  transitions). We performed transient M-edge XANES spectroscopy with 50-fs time resolution to identify the true pathway. This core-level technique (which probes  $3p \rightarrow 3d$  transition) is element-, oxidation state-, and spin-selective. As shown in Figure 2, photoexcitation at 400 nm creates an immediate ground-state bleach of the  $\text{Fe}^{\text{III}}$  signal at 57.4 eV and creation of a

new positive feature at 55 eV. As we showed in earlier transient absorption studies of Fe<sup>III</sup> tetraphenylporphyrin chloride (Fe<sup>III</sup>TPPCl), this is a signature of the Fe<sup>II</sup> center in the LMCT state. Surprisingly, this Fe<sup>II</sup> signal disappears with a time constant of only 0.54 ps, as does the Fe<sup>III</sup> ground-state bleach. This result indicates that little if any Fe<sup>IV</sup> is formed, ruling out the desired Pathway A as a major product.



Despite this observation that the metal has returned to its original Fe<sup>III</sup> oxidation state in less than a picosecond, optical transient absorption spectroscopy reveals porphyrin signals that last for approximately 700 ps. By comparing these transients to model complexes, we assign them to the porphyrin-centered anion and cation states shown in Pathway B of Figure 1.

In summary, through a combination of transient M-edge XANES (which primarily reports on the metal) and optical transient absorption (which primarily reports on the porphyrin ligand), we have shown that the reason that  $\mu$ -oxo bridged Fe(III) porphyrins have low photochemical quantum yield for catalysis is that the active Fe<sup>IV</sup>=O species is only a minor product of the initial photoexcitation. We are currently exploring whether the addition of electron withdrawing/donating groups on the two porphyrins can better promote the desired disproportionation reaction.

### *Multistate reactivity and excited-state dynamics in Co<sub>4</sub>O<sub>4</sub> cubanes*

We have also continued our study of catalytic intermediates in Co<sub>4</sub>O<sub>4</sub> cubanes that are catalysts for water oxidation. In these systems, we seek to understand whether the second oxidation of the cluster leads to a single Co<sup>V</sup>=O that reacts with a nearby Co<sup>III</sup>-OH in an acid-base mechanism to form the O-O bond, or whether two Co<sup>IV</sup>-O\* centers are formed and form the O-O bond through radical coupling. As part of this work, we append perylenediimide (PDI) chromophores to the Co<sub>4</sub>O<sub>4</sub> cluster so that we can trigger the cluster oxidation with a photon and time-tag the intermediates. As shown in Figure 4, we used optical transient absorption spectroscopy to show that the chromophore does inject a hole into the Co<sub>4</sub>O<sub>4</sub> on the picosecond timescale, with recombination in ~100 ps. However, we noted that the quantum yield for this charge separation was only ~25%, so much of the initial singlet excited state on the PDI was being quenched through an unknown mechanism.

This observation led us to study the inherent photophysics of the cubane itself. This and other cubanes have been incorporated into both homogeneous and heterogeneous photocatalytic assemblies, but little attention has been paid to the potential deactivation pathways caused by the manifold of excited (d,d) states present in the catalyst.

Using our tabletop transient M-edge XANES spectrometer, we excited the cubane into its  $^1(d,d)$  states at 550 nm and tracked an intricate

cascade of intersystem crossing (ISC) events. As shown in Figure 3, the  $t_{2g} \rightarrow e_g$  excitation into the  $^1T_1$  excited state populates antibonding orbitals and causes elongation of the Co-ligand bonds. In only 38 femtoseconds, the cobalt center undergoes two spin flips with 100% quantum yield, forming a  $^5T_2$  state. This result, while the fastest  $\Delta S=2$  intersystem crossing in a 3d transition metal yet observed, is not especially surprising. Previous work on  $Fe^{II}$  complexes such as  $Fe(bpy)_3^{2+}$  has shown that spin-vibronic coupling is sufficiently strong to enable two  $\Delta S=1$  intersystem crossing events in rapid succession. However, the next step is to our knowledge unprecedented. Only 94 femtoseconds after the forward-ISC from  $^1T_1$  to  $^3T_2$  to  $^5T_2$ , a second curve-crossing is reached, between the  $^5T_2$  state and the  $^1A_1$  ground state. While 70% of the excited-state molecules relax to the bottom of the  $^5T_2$  surface and then to the lower-energy  $^3T_1$  state, 30% undergo a single-step  $\Delta S=2$  back-ISC.

The yield of this two-quantum spin flip on a single crossing of the surfaces is much higher than expected, possibly due to an “external heavy-atom effect” from the neighboring Co atoms. Many transition metal catalysts are known to exhibit multi-state reactivity, in which the catalyst changes spin states during the catalytic cycle. The high yield of this  $\Delta S=2$  process suggests that a larger range of spin states should be considered in these reactions.

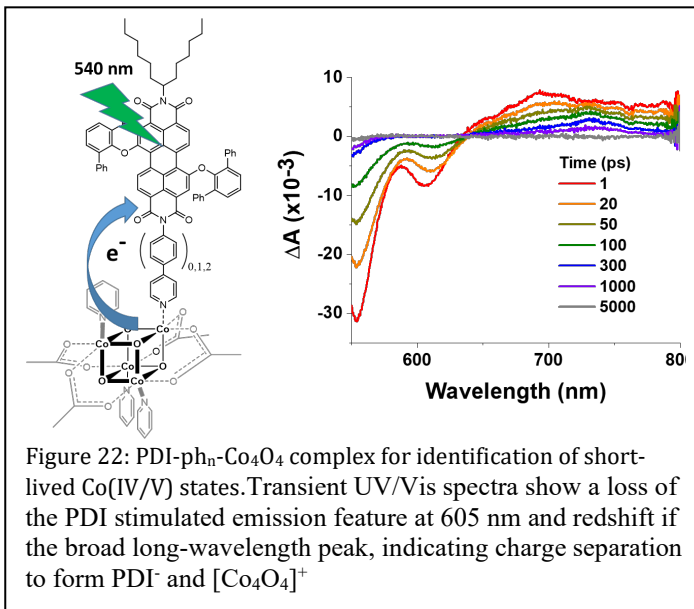


Figure 22: PDI-ph<sub>n</sub>-Co<sub>4</sub>O<sub>4</sub> complex for identification of short-lived Co(IV/V) states. Transient UV/Vis spectra show a loss of the PDI stimulated emission feature at 605 nm and redshift if the broad long-wavelength peak, indicating charge separation to form PDI<sup>-</sup> and [Co<sub>4</sub>O<sub>4</sub>]<sup>+</sup>

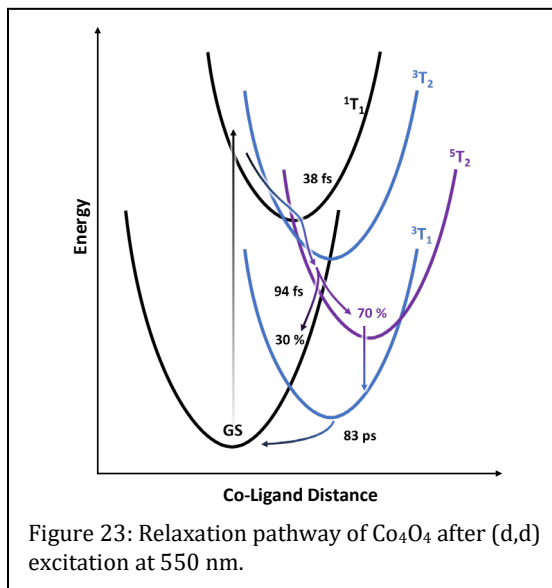


Figure 23: Relaxation pathway of Co<sub>4</sub>O<sub>4</sub> after (d,d) excitation at 550 nm.

### **Publications Acknowledging this Grant in 2017-2021:**

Leahy, C.A.; Drummond, M.J.; Vura-Weis, J.; Fout, A.R.; “Synthesis of a series of M(II) (M = Mn, Fe, Co) chloride complexes with both inter- and intra-ligand hydrogen bonding interactions“, *Dalton Transactions, In Press*

Shari’ati, Y.; Vura-Weis, J.; “Polymer Thin Films as Universal Substrates for Extreme Ultraviolet Absorption Spectroscopy of Molecular Transition Metal Complexes”; *Submitted to J Synch Rad*

### **2018-2020 Awards and Leadership Activities**

- Organized a symposium on ultrafast XUV/X-ray spectroscopy in chemistry for the American Chemical Society national meeting in Fall 2018
- Organized a symposium on High-Harmonic Generation and XUV Spectroscopy at the 2019 International Symposium on Molecular Spectroscopy
- Chair of the International Symposium on Molecular Spectroscopy, 2021-2025
- Editorial Board Member, Journal of Molecular Spectroscopy (2020-)
- LCLS Review Panel, Chemical Science Division, 2019, 2020, 2021

Timothy H. Warren

## Uncovering Redox Non-Innocent Hydrogen-Bonding in Cu(I)-Diazene Complexes

Evan J. Gardner,<sup>†</sup> Sean C. Marguet,<sup>‡</sup> Caitlyn R. Cobb,<sup>†</sup> Dominic M. Pham,<sup>†</sup> Josalyne A. M. Beringer,<sup>†</sup> Jeffery A. Bertke,<sup>†</sup> Hannah S. Shafaat,<sup>\*,‡</sup> and Timothy H. Warren<sup>\*,†,§</sup>

<sup>†</sup>Department of Chemistry, Georgetown University, Box 51277-1227, Washington, D.C. 20057, United States

<sup>‡</sup>The Ohio State University, 100 West 18th Avenue, Columbus, Ohio 43210, United States

<sup>§</sup>Department of Chemistry, Michigan State University, East Lansing, MI 48824, United States

### Presentation Abstract

The life-sustaining reduction of N<sub>2</sub> to NH<sub>3</sub> is thermoneutral yet kinetically challenged by high energy intermediates such as N<sub>2</sub>H<sub>2</sub>. Exploring intramolecular H-bonding as a potential strategy to stabilize diazene intermediates, we employ a series of [<sup>x</sup>HetTpCu]<sub>2</sub>(μ-N<sub>2</sub>H<sub>2</sub>) complexes that exhibit H-bonding between pendant aromatic N-heterocycles (<sup>x</sup>Het) such as pyridine and a bridging *trans*-N<sub>2</sub>H<sub>2</sub> ligand at copper(I) centers. X-ray crystallography and IR spectroscopy clearly reveal H-bonding in [<sup>pyMe</sup>TpCu]<sub>2</sub>(μ-N<sub>2</sub>H<sub>2</sub>) while low temperature <sup>1</sup>H NMR studies coupled with DFT analysis reveals a dynamic equilibrium between two closely related, symmetric H-bonded structural motifs. Importantly, the <sup>x</sup>Het pendant negligibly influences the electronic structure of <sup>x</sup>HetTpCu<sup>I</sup> centers in <sup>x</sup>HetTpCu(CNAr<sup>2,6-Me2</sup>) complexes that lack H-bonding as judged by nearly indistinguishable ν(CN) frequencies (2113 - 2117 cm<sup>-1</sup>). Nonetheless, H-bonding in the corresponding [<sup>x</sup>HetTpCu]<sub>2</sub>(μ-N<sub>2</sub>H<sub>2</sub>) complexes results in marked changes in ν(NN) (1398 - 1419 cm<sup>-1</sup>) revealed through rRaman studies. Due to the closely matched N-H BDE's of N<sub>2</sub>H<sub>2</sub> and the neutral pyH<sup>0</sup> cation radical, the aromatic N-heterocyclic pendants may encourage partial H-atom transfer (HAT) from N<sub>2</sub>H<sub>2</sub> to <sup>x</sup>Het through redox non-innocent H-bonding in [<sup>x</sup>HetTpCu]<sub>2</sub>(μ-N<sub>2</sub>H<sub>2</sub>). DFT studies reveal modest thermodynamic barriers for concerted transfer of both H-atoms of coordinated N<sub>2</sub>H<sub>2</sub> to the <sup>x</sup>Het pendants to generate tautomeric [<sup>x</sup>HetH<sup>+</sup>TpCu]<sub>2</sub>(μ-N<sub>2</sub>) complexes, identifying metal-assisted concerted dual HAT as a thermodynamically favorable pathway for N<sub>2</sub> / N<sub>2</sub>H<sub>2</sub> interconversion.

**Grant or FWP Number: Grant or FWP Number:** DE-SC001779

Catalytic Interconversion of Ammonia and Dinitrogen at Base Metals

**Student(s):** Mahdi Raghbi Borougeni, Evan J. Gardner, Christine Greene, David Lucas Kane, Josalyne A. M. Beringer

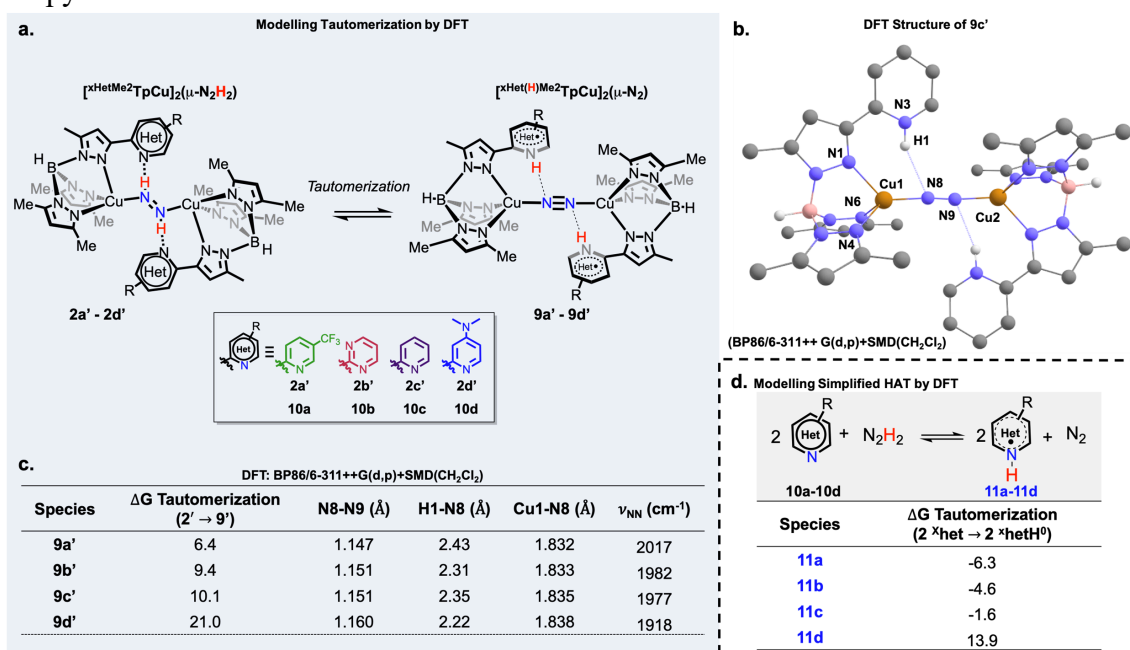
**Postdoc(s):** Dr. Estak Ahmed

## RECENT PROGRESS

### *Diazeno - dinitrogen interconversion via redox non-innocent H-bonding*

We have performed a detailed synthetic, spectroscopic, and computational study on the first set of metal-diazeno complexes  $[\text{xHet}^{\text{Me}_2}\text{TpCu}]_2(\mu\text{-N}_2\text{H}_2)$  with tunable H-bonding via pendant aromatic N-heterocycles such as pyridine. These studies reveal that the pyridine arms are redox non-innocent, leading to unusual shifts in  $\nu(\text{NN})$  towards high energy for the most electron-poor N-heterocycles. We attribute this to a contribution of the redox tautomer in which H-atom from diazeno are transferred to the aromatic N-heterocycle to give pyridinium-type radicals resulting in a metal-dinitrogen complex  $[\text{xHet}^{\text{H}}\text{TpCu}]_2(\mu\text{-N}_2)$ .

This study reveals that pyridinium radicals  $\text{pyH}^0$  and  $\text{N}_2$  are well matched for H-atom transfer to give  $\text{py}$  and  $\text{N}_2\text{H}_2$ , especially considering concerted, dual H-atom transfer from the pyridinium radicals.

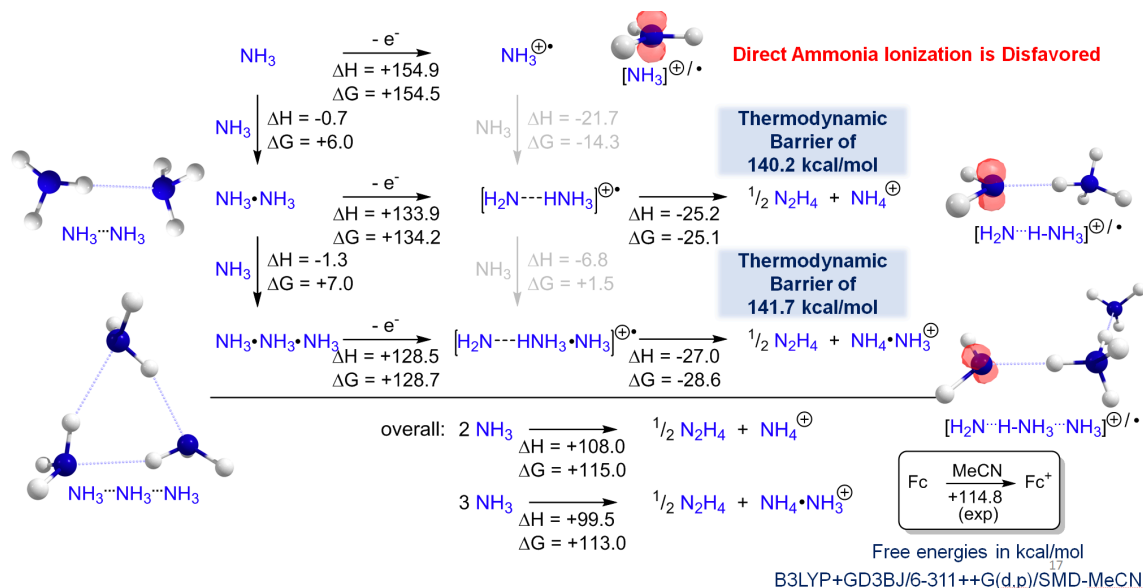


### *Ammonia oxidation via ferrocene derivatives*

Ferrocenium ( $\text{Fc}^+$ ) stoichiometrically and catalytically oxidizes  $\text{NH}_3$  to  $\text{N}_2$ . While first order in  $[\text{Fc}^+]$ , kinetic studies reveal a mixed 2<sup>nd</sup> / 3<sup>rd</sup> order in  $[\text{NH}_3]$ :  $\text{rate} = (k_2[\text{NH}_3]^2 + k_3[\text{NH}_3]^3)[\text{Fc}^+]$ . Additionally, there is evidence for ion pairing with the  $\text{PF}_6^-$  anion as the observed rate exhibits an inverse first-order dependence on  $[\text{PF}_6^-]$ . Employing simple ferrocene derivatives that include 1,1'-dimethylferrocene (1,1'- $\text{Me}_2\text{Fc}$ ) and the sulfonated species 1,1'- $\text{Me}_2\text{FcSO}_3\text{K}$ , this electrocatalytic system that generates  $\text{N}_2$  exhibits modest overpotentials (0.81 - 0.94 V) for catalytic ammonia oxidation compared to other reported molecular electrocatalysts (1.0 - 1.7 V). Perhaps more importantly, some of these robust catalysts operate in energy-dense, liquid ammonia in which many coordination compounds would be converted to Werner complexes  $[\text{M}(\text{NH}_3)_6]^{n+}$  inactive towards ammonia oxidation.

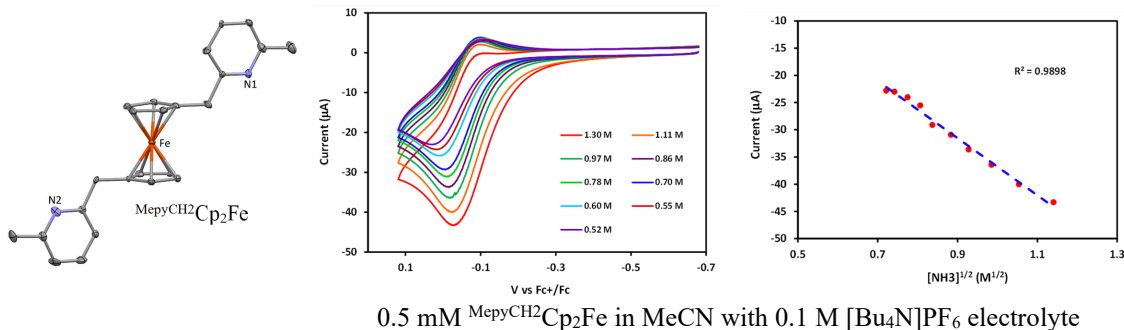
We interpret the 2<sup>nd</sup> and 3<sup>rd</sup> order dependence of  $[\text{NH}_3]$  in stoichiometric ammonia oxidation to reflect the need to pre-assemble ammonia dimers  $[\text{NH}_3 \cdot \text{NH}_3]$  and trimers

$[\text{NH}_3 \cdot \text{NH}_3 \cdot \text{NH}_3]$  around ferrocenium prior to 1-electron oxidation. While the B3LYP level of theory predicts that the formation of these aggregates are endergonic at +6 and +13 kcal/mol, respectively, they are *much* easier to ionize than free  $\text{NH}_3$  giving overall thermodynamic barriers of 25.0 and 26.7 kcal/mol vs. the  $\text{Fc}^+/\text{Fc}$  couple in MeCN.



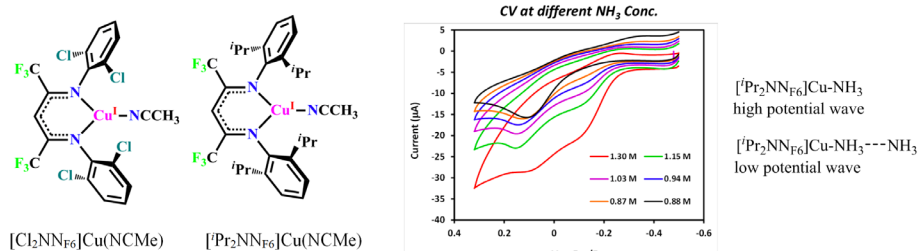
### Ammonia oxidation via ferrocenes with pendant amine arms

We have begun to explore strategies to encourage  $\text{NH}_3$  to engage in related H-bonding interactions near the ferrocenium catalyst that could accelerate ammonia oxidation by thermodynamically lowering the oxidation potential of  $\text{NH}_3$  while accelerating outer-sphere electron transfer. Preparation of  $^{\text{MepyCH}_2}\text{Cp}_2\text{Fe}$  that possesses oxidation resistant 2,6-lutidine pendant arms results in a much more active ammonia oxidation catalyst than ferrocene alone. While unsubstituted  $\text{Cp}_2\text{Fe}$  requires high concentrations of ammonia (> 3 M) to observe electrocatalytic ammonia oxidation, ammonia oxidation readily occurs in 0.55 - 1.3 M ammonia solutions containing 0.5 mM  $^{\text{MepyCH}_2}\text{Cp}_2\text{Fe}$ . Moreover, the onset potential for ammonia oxidation is lower at ca. -0.2 V vs.  $\text{Fc}^+/\text{Fc}$  corresponding to a lower overpotential for ammonia oxidation. Analysis by cyclic voltammetry suggests that the reaction is now first order in  $\text{NH}_3$  with  $\text{TOF}_{\text{max}} = 0.22 \text{ s}^{-1}$  ( $[\text{NH}_3] = 1.3 \text{ M}$ ). Thus, the pendant pyridyl groups play crucial roles in ammonia oxidation, perhaps via H-bonded  $[\text{NH}_3 \cdot \text{py}]$  or  $[\text{py} \cdot \text{NH}_3 \cdot \text{py}]$  intermediates that facilitate 1-electron ammonia oxidation to  $[\text{NH}_2 \cdot \text{py}]^{+/\bullet}$  species that couple to form  $\text{N}_2\text{H}_4$ . Once formed,  $\text{N}_2\text{H}_4$  undergoes rapid oxidation by Fc-based electrocatalysts.

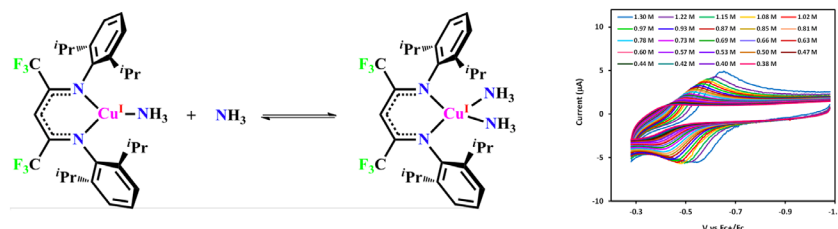


### Electrocatalytic ammonia oxidation by copper $\beta$ -diketiminates

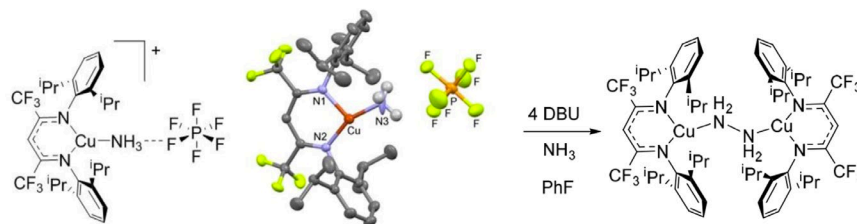
Two copper  $\beta$ -diketiminato catalysts  $[\text{Cl}_2\text{NNF}_6]\text{Cu}$  and  $[\text{}^i\text{Pr}_2\text{NNF}_6]\text{Cu}$  serve as electrocatalysts for ammonia oxidation in MeCN with  $[\text{NH}_3] = 1.3 \text{ M}$ . The more electron-poor  $[\text{Cl}_2\text{NNF}_6]\text{Cu}$  exhibits an onset potential of 0.14 V vs.  $\text{Fc}^+/\text{Fc}$  with  $\text{TOF}_{\text{max}} = 0.14 \text{ s}^{-1}$  while the more electron-rich  $[\text{}^i\text{Pr}_2\text{NNF}_6]\text{Cu}$  shows two distinct electrocatalytic waves with onset potentials of -0.25 V and -0.1 V with  $\text{TOF}_{\text{max}}$  of 0.06 and  $0.11 \text{ s}^{-1}$ , respectively. Each leads to long-lived electrocatalysis under CPE conditions with current densities of ca. 0.8 and  $0.5 \text{ mA/cm}^2$  at 1 mM [catalyst] and 1.3 M  $[\text{NH}_3]$  in MeCN using a graphite rod working electrode.



Mechanistic investigation by a combination of cyclic voltammetry and DFT studies reveal two ways that two  $\text{NH}_3$  may coordinate to the copper(I)  $\beta$ -diketiminato monoammine complexes  $[\text{Cu}^{\text{I}}]-\text{NH}_3$ . Each exhibits a fully reversible, low potential wave that cathodically shifts from ca. -0.35 to -0.55 V (vs.  $\text{Fc}^+/\text{Fc}$ ) as the ammonia concentration is increased from 0.4 to 1.3 M. We attribute this to the equilibrium formation of  $[\text{Cu}^{\text{I}}](\text{NH}_3)_2$  complexes that possess a reversible  $\text{Cu}^{\text{II}}/\text{Cu}^{\text{I}}$  couple indicating that  $\{[\text{Cu}^{\text{II}}](\text{NH}_3)_2\}^+$  are stable towards ammonia oxidation. On the other hand, we attribute the two electrocatalytic waves observed with  $[\text{}^i\text{Pr}_2\text{NNF}_6]\text{Cu}$  to originate from  $[\text{Cu}^{\text{I}}]-\text{NH}_3$  and  $[\text{Cu}^{\text{I}}]-\text{NH}_3\cdot\text{NH}_3$  species. Adding electron-density via H-bonding in the  $[\text{Cu}^{\text{I}}]-\text{NH}_3\cdot\text{NH}_3$  species would cathodically shift the oxidation wave.



We have isolated a key intermediate in ammonia oxidation by copper(II). Addition of  $\text{NH}_3$  to  $\{[\text{}^i\text{Pr}_2\text{NNF}_6]\text{Cu}\}\text{PF}_6$  (obtained by oxidation of  $[\text{}^i\text{Pr}_2\text{NNF}_6]\text{Cu}$  with  $\text{AgPF}_6$  in fluorobenzene) leads to  $\{[\text{}^i\text{Pr}_2\text{NNF}_6]\text{Cu}-\text{NH}_3\}\text{PF}_6$  confirmed by X-ray crystallography. Importantly, addition of  $\text{NH}_3$  / DBU to  $\{[\text{}^i\text{Pr}_2\text{NNF}_6]\text{Cu}-\text{NH}_3\}\text{PF}_6$  leads to  $\{[\text{}^i\text{Pr}_2\text{NNF}_6]\text{Cu}\}(\mu\text{-N}_2\text{H}_4)$ , demonstrating that deprotonation leads to hydrazine formation. This presumably occurs via the highly reactive  $[\text{Cu}^{\text{II}}]-\text{NH}_2$  intermediate.



## Publications Acknowledging this Grant in 2018-2021

(I) *Intellectually led by this grant*

Gardner, E. J.; Cobb, C. R.; Bertke, J. A.; Warren, T. H.\* “Tris(pyrazolyl)borate Copper Hydroxide Complexes Featuring Tunable Intramolecular H-bonding” *Inorg. Chem.* **2019**, *58*, 11248-11255.

Gardner, E. J.; Marguet, S. C.; Cobb, C. R.; Pham, D. M.; Beringer, J. A. M.; Bertke, J. A.; Shafaat, H. S.\*; Warren, T. H.\* Uncovering Redox Non-Innocent H-Bonding in Cu(I)-Diazene Complexes *J. Am. Chem. Soc.* **2021**, *143*, ASAP. doi: 10.1021/jacs.1c04108

Boroujeni, M. R.; Greene, C.; Bertke, J. A.; Cundari, T. R.; Warren, T. H.\* Chemical and Electrocatalytic Ammonia Oxidation by Ferrocenium (under revision): *preprint: ChemRxiv* **2019**, <https://doi.org/10.26434/chemrxiv.9729635.v1>.

## Awards or leadership activities during 2018-2020 calendar years

Chair, Inorganic Reaction Mechanisms Gordon Research Conference, Galveston, TX (2019)

*Comprehensive Organometallic Chemistry IV* section editor (groups 8-10; 30 contributions)

*Chemical Society Reviews* Editorial Advisory Board (since 2019)

*Inorganic Syntheses* Editorial Board (since 2014)

*Inorganic Chemistry* Editorial Advisory Board (2016-2019)

Awards Co-chair of ACS Division of Inorganic Chemistry Executive Committee (2013 - 2018)

Chairperson, Michigan State University Department of Chemistry (present)

Chairperson, Georgetown University Department of Chemistry (2017-2021)

Chair, Georgetown Environment Initiative (2015-2019)

Jason F. Weaver

**Steady state oxidation of CH<sub>4</sub> on an IrO<sub>2</sub>(110) film investigated using near-ambient pressure x-ray photoelectron spectroscopy**

Rachel Martin<sup>1)</sup>, Minkyu Kim<sup>2)</sup>, Christopher J. Lee<sup>1)</sup>, Vikram Mehar<sup>1)</sup>, Aravind Asthagiri<sup>2)</sup>, Jason F. Weaver<sup>1)</sup>

<sup>1)</sup>Department of Chemical Engineering, University of Florida, Gainesville, FL 32611

<sup>2)</sup>Department of Chemical and Biomolecular Engineering, The Ohio State University, Columbus, OH 43210

**Presentation Abstract**

The IrO<sub>2</sub>(110) surface promotes the C-H bond activation of light alkanes (C<sub>1</sub>-C<sub>3</sub>) at temperatures as low as 100 K, producing adsorbed alkyl fragments that remain stable to nearly 400 K. These characteristics may provide opportunities for developing IrO<sub>2</sub>-based catalysts that can selectively and efficiently convert light alkanes to value-added products. In this presentation, I will discuss recent work in which we used near-ambient pressure X-ray photoelectron spectroscopy (NAP-XPS) to investigate the steady state oxidation of CH<sub>4</sub> on IrO<sub>2</sub>(110) films at total pressures up to about 2 Torr as a function of the CH<sub>4</sub>-O<sub>2</sub> mixture composition and surface temperature. Our results show that IrO<sub>2</sub>(110) thin films (~10 layers) remain stable at temperatures up to 650 K during exposure to CH<sub>4</sub>-O<sub>2</sub> mixtures with at least 90% CH<sub>4</sub>, enabling the oxide surface to promote CH<sub>4</sub> oxidation under steady state conditions. Evaluation of O 1s spectra reveals that CO<sub>x</sub> species as well as bridging and on-top OH groups form in high coverages during CH<sub>4</sub> oxidation. Both quantitative analysis of species coverages and the C 1s binding energies indicate that the dominant adsorbed intermediates have a 2:1 O:C molar ratio, as represented by the stoichiometric formula CH<sub>y</sub>O<sub>2</sub>, and that the types and relative proportions of these intermediates are largely insensitive to the temperature and mixture composition. These findings provide important information for guiding the development of first-principles models of CH<sub>4</sub> oxidation kinetics on IrO<sub>2</sub>(110) surfaces and identifying conditions needed to modify reaction selectivity.

**DE-FG02-03ER15478: Alkane Oxidation on Late Transition-Metal Oxide Surfaces**

**Postdoc(s):** M. Kim

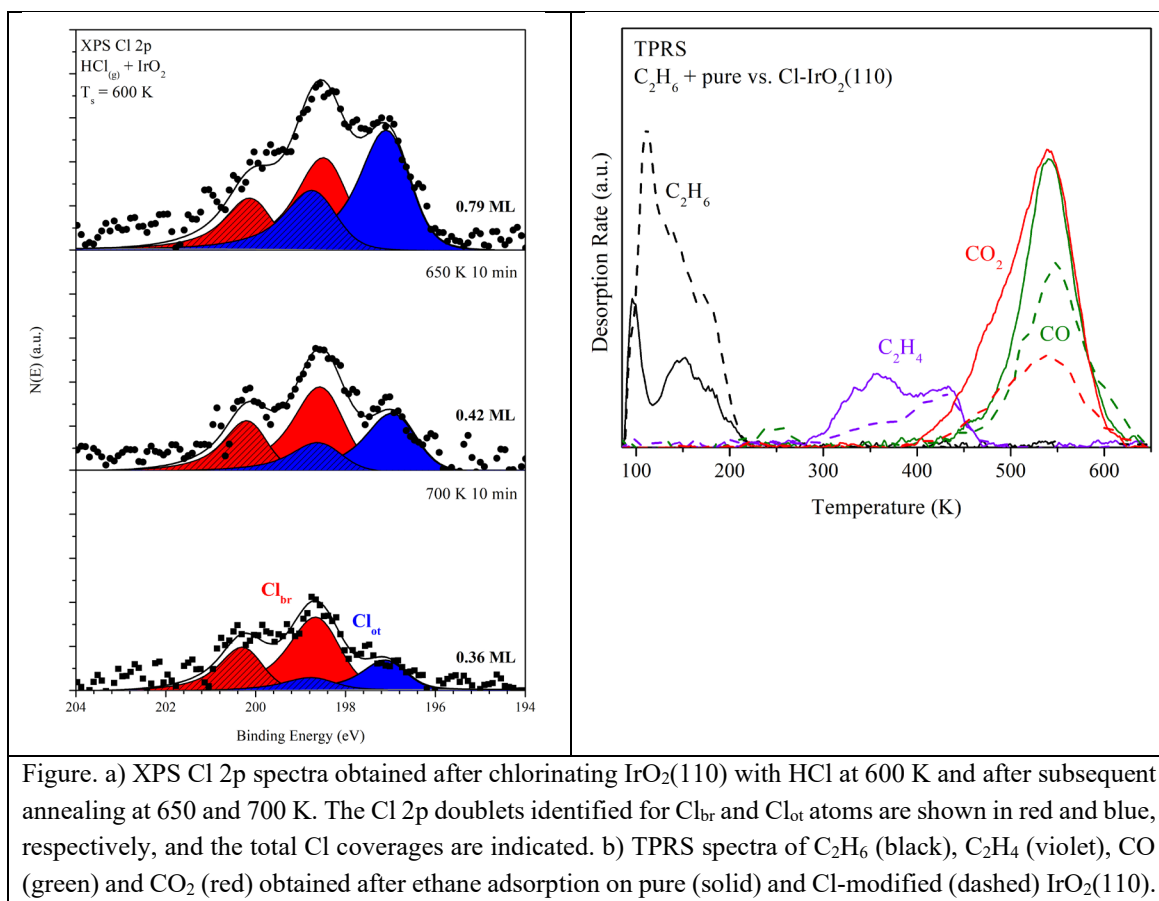
**Student(s):** R. Martin, A. Franklin, T. Li, V. Mehar, C. Lee, Y. Bian, F. Feng, J. Jamir

## RECENT PROGRESS

### Chlorination of IrO<sub>2</sub>(110) surfaces

We have been investigating the chlorination of IrO<sub>2</sub>(110) and its influence on the surface reactivity toward light alkanes. Our experiments demonstrate that HCl dissociates on the IrO<sub>2</sub>(110) surface and can cause up to ~0.8 ML of Cl to incorporate into the surface layer. We have been studying how preparation conditions influence the distribution of Cl atoms among surface sites, including adsorption on top of Ir<sub>cus</sub> atoms vs. replacement of bridging-O atoms (O<sub>br</sub>) to generate Cl<sub>ot</sub> vs. Cl<sub>br</sub> atoms, respectively. We find that the coverages of Cl<sub>ot</sub> and Cl<sub>br</sub> species can be accurately quantified from XPS Cl 2p spectra. Our results show that both Cl<sub>br</sub> and Cl<sub>ot</sub> atoms are generated in approximately equal quantities on IrO<sub>2</sub>(110) during exposure to gaseous HCl at 600 K. However, subsequent annealing in UHV to 650-700 K selectively eliminates the Cl<sub>ot</sub> atoms and enables the preparation of Cl-modified IrO<sub>2</sub>(110) surfaces with high coverages of both Cl<sub>br</sub> atoms and vacant Ir<sub>cus</sub> sites needed for alkane adsorption and activation. We find that partial surface chlorination suppresses the reactivity of IrO<sub>2</sub>(110) toward ethane and improves the selectivity toward ethylene formation. We are continuing to investigate the mechanisms of IrO<sub>2</sub>(110) surface chlorination and alkane dehydrogenation to identify optimal conditions that promote selective conversion to alkenes.

We have also conducted extensive DFT calculations and microkinetic modeling to study IrO<sub>2</sub>(110) chlorination and ethane dehydrogenation. The calculations predict that partial replacement of O<sub>br</sub> atoms by Cl<sub>br</sub> atoms can significantly enhance the selectivity of C<sub>2</sub>H<sub>6</sub> dehydrogenation to C<sub>2</sub>H<sub>4</sub> because the Cl atoms are inactive toward the hydrocarbon fragments and replace O-atoms that would otherwise oxidize the desired C<sub>2</sub>H<sub>4</sub> product. Our predictions suggest that the ethylene selectivity could be increased to as much as 80% by IrO<sub>2</sub>(110) chlorination. Validation of these predictions would represent a significant and intriguing advance because it would demonstrate that a controlled modification of the IrO<sub>2</sub>(110) surface enables selective and efficient ethane dehydrogenation to ethylene.



## Publications Acknowledging this Grant in 2018-2021

### (IX) Intellectually led by this grant

1. R. Martin, M. Kim, C.J. Lee, V. Mehar, S. Albertin, U. Hejral, L.R. Merte, A. Asthagiri and J.F. Weaver, "Isothermal reduction of IrO<sub>2</sub>(110) films by methane investigated using *in situ* x-ray photoelectron spectroscopy". *ACS Catal.* **2021**, *11*, 5004-5016.
2. R. Martin, M. Kim, A. Asthagiri and J.F. Weaver, "Alkane activation and oxidation on late transition-metal oxides: Challenges and opportunities". *ACS Catal.* **2021**, *11*, 4682-4703.
3. R. Martin, M. Kim, C.J. Lee, V. Mehar, S. Albertin, U. Hejral, L.R. Merte, E. Lundgren, A. Asthagiri and J.F. Weaver, "High resolution x-ray photoelectron spectroscopy of an IrO<sub>2</sub>(110) film on Ir(100)". *J. Phys. Chem. Lett.* **2020**, *11*, 7184-7189.
4. S.D. Senanayake, J.A. Rodriguez and J.F. Weaver, "Low temperature activation of methane on metal-oxides and complex interfaces: Insights from surface science". *Acc. Chem. Res.* **2020**, *53*, 1488-1497.
5. M. Kim, A. Franklin, R. Martin, Y. Bian, J.F. Weaver and A. Asthagiri, "Methane oxidation kinetics on IrO<sub>2</sub>(110): Effects of local surface hydroxide species". *J. Catal.*

2020, 383, 181-192.

6. R. Martin, M. Kim, C.J. Lee, M. Shariff, F. Feng, R.J. Meyer, A. Asthagiri and J.F. Weaver, "Molecular chemisorption of N<sub>2</sub> on IrO<sub>2</sub>(110)". *J. Chem. Phys.* **2020**, *152*, 074712.
7. M. Kim, A. Franklin, R. Martin, F. Feng, T. Li, Z. Liang, A. Asthagiri and J.F. Weaver, "Adsorption and oxidation of CH<sub>4</sub> on oxygen-rich IrO<sub>2</sub>(110)". *J. Phys. Chem. C* **2019**, *123*, 27603-27614.
8. Y. Bian; T. Li and J.F. Weaver, "Structure and reactivity of iridium oxide layers grown on Ir(100) at sub-ambient O<sub>2</sub> pressures". *J. Phys. D: Appl. Phys.* **2019**, *52* 434002.
9. Mehar, V.; Kim, M.; Shipilin, M.; Van den Bossche, M.; Gustafson, J.; Merte, L. R.; Hejral, U.; Gronbeck, H.; Lundgren, E.; Asthagiri, A.; Weaver, J. F., "Understanding the intrinsic surface reactivity of single-layer and multilayer PdO(101) on Pd(100)". *ACS Catal* **2018**, *8*, 8553-8567.
10. Martin, R.; Kim, M.; Franklin, A.; Bian, Y.; Asthagiri, A.; Weaver, J. F., "Adsorption and oxidation of propane and cyclopropane on IrO<sub>2</sub>(110)". *Phys. Chem. Chem. Phys.* **2018**, *20*, 29264 - 29273.
11. Li, T.; Kim, M.; Liang, Z.; Asthagiri, A.; Weaver, J. F., "Dissociative chemisorption and oxidation of H<sub>2</sub> on the stoichiometric IrO<sub>2</sub>(110) surface". *Top. Catal.* **2018**, *61*, 397-411.
12. Li, T.; Kim, M.; Liang, Z.; Asthagiri, A.; Weaver, J., "Hydrogen oxidation on oxygen-rich IrO<sub>2</sub>(110)". *Catalysis, Structure and Reactivity* **2018**, *4*, 1-13.
13. Kim, M.; Pan, L.; Weaver, J. F.; Asthagiri, A., "Initial reduction of the PdO(101) surface: Role of oxygen vacancy formation kinetics". *J. Phys. Chem. C* **2018**, *122*, 26007-26017.
14. Bian, Y. X.; Kim, M.; Li, T.; Asthagiri, A.; Weaver, J. F., "Facile dehydrogenation of ethane on the IrO<sub>2</sub>(110) surface". *J. Am. Chem. Soc.* **2018**, *140*, 2665-2672.

(X) *Jointly funded by this grant and other grants with intellectual leadership by other funding sources;*

1. Busch, M.; Mehar, V.; Merte, L. R.; Shipilin, M.; Lundgren, E.; Weaver, J. F.; Gronbeck, H., "Adsorption of NO on Fe<sub>3</sub>O<sub>4</sub>(111)". *Chem. Phys. Lett.* **2018**, *693*, 84-87.

## **J. Weaver**

### *Awards (2018-20)*

- 2019 Recipient of the Doctoral Dissertation Adviser/Mentoring Award, Wertheim College of Engineering, University of Florida.
- 2018 Awarded the ExxonMobil Gator Alumni Endowed Professorship in Chemical Engineering, University of Florida for the three-year period from 2018-2021.

### *Leadership activities (2018-20)*

Member of the Working Group for the Catalysis theme of the Lund Institute for Neutron and X-ray Science, Lund, Sweden. (<https://www.linxs.se>) (2020-present)

Organizer of a Symposium for the Spring ACS meeting, Catalysis Science Division titled, “Multi-functional surfaces for cooperativity in catalysis”, Philadelphia, PA March 22-23, 2020. (Meeting was cancelled)

Organizer, International Workshop titled “Functional Materials at Work”, (April 3-6, 2018) Fort Myers Beach, FL.

Member, Heterogeneous Catalysis Focus Topic Program Committee, American Vacuum Society (2017 – present).

Member of the Editorial Board of *Surface Science* (2016 – present).

## **A. Asthagiri**

### *Leadership activities (2018-20)*

Organizer of a Symposium for the Spring ACS meeting, Catalysis Science Division titled, “Bridging Surface Science to Catalysis”, San Antonio, TX March 21-25, 2021.

Organizer of a Symposium for the Spring ACS meeting, Catalysis Science Division titled, “Bridging Surface Science to Catalysis”, Philadelphia, PA March 22-23, 2020. (Meeting was cancelled)

Associate Chair of Department of Chemical & Biomolecular Engineering, The Ohio State University (2019 – present)

**Atomically Precise Metal and Metal Oxide Clusters as Model Catalysts**

Michael G. White,<sup>1,2</sup> Yilin Ma,<sup>1</sup> Jason Wang<sup>1</sup>, Luolin Shi<sup>1</sup> and Matthew Bonney<sup>1</sup>

<sup>1</sup>Department of Chemistry, Stony Brook University, Stony Brook, NY 11794

<sup>2</sup>Chemistry Division, Brookhaven National Laboratory, Upton, NY 11973

**Presentation Abstract**

This project is guided by the premise that tuning the interface between metals and metal oxides at the nanoscale can lead to multifunctional catalysts with higher performance. The metal-oxide interface modifies the atomic and electronic structure of the components and creates unique sites for binding, spillover and reaction of intermediates. We use mass-selected cluster methods to prepare well-defined metal-oxide interfaces between atomically precise metal or metal oxide clusters that are deposited onto a single crystal or thin film supports. Cluster deposition is uniquely suited to exploring the size dependence of reactivity of sub-nm clusters, down to single atoms, and can be applied to a wide range of metal-oxide combinations and interfaces. Recent studies have focused on understanding the reactivity and surface structure of small oxide clusters deposited on metal surfaces that are used as model inverse catalysts for parallel reactivity studies. STM imaging of small Ti and Nb oxide clusters deposited on Au(111) surface exhibit surprisingly different binding sites and morphologies that strongly depend on cluster stoichiometry. These observations suggest that the surface morphology is largely controlled by the metal-oxygen coordination which in turn determines the isolated cluster structures and cluster-surface interaction energies. Similar experiments are currently being performed on Cu(111) where oxide cluster binding is anticipated to be stronger. Ambient pressure XPS and IRRAS studies were also carried out on ZrO<sub>2</sub>/Cu<sub>2</sub>O/Cu(111) and Cu<sub>2</sub>/ZrO<sub>2</sub>/ZnO(0001) surfaces as model catalysts for CO<sub>2</sub> hydrogenation to methanol. The Cu-ZrO<sub>2</sub> interface is thought to be key for improving the catalytic performance over the commercial Cu/ZnO/Al<sub>2</sub>O<sub>3</sub> catalyst. Zirconia was deposited as small amorphous nanoparticles and both surfaces were found to be active for CO<sub>2</sub> binding and conversion to reaction intermediates as identified by XPS and IRRAS measurements under reaction conditions. The temperature profiles of the intermediates suggest a modified “formate” pathway in which CO<sub>2</sub> is bound on the oxide as carbonate species, which then undergo a series of hydrogenation and C-O bond breaking steps to form methoxy, which is the final surface species leading methanol. At higher Cu coverage on the Cu<sub>2</sub>/ZrO<sub>2</sub>/ZnO surface, we also observed the formation of alkyl intermediates which may signal a competing pathway to methanation.

**FWP-BNL-CO040: Catalysis for Advanced Fuel Synthesis**

**FWP ERKCC96: Fundamentals of Catalysis and Chemical Transformations**

**PIs:** Miaofang Chi, Sheng Dai, Stephan Irle, De-en Jiang (UC-Riverside), Felipe Polo-Garzon, Aditya (Ashi) Savara, Zili Wu (lead PI), Zhenzhen Yang

**Postdoc(s):** Yang He, Zhennan Huang, Yifan Sun, Xinbin Yu

**Student(s):** Francis Okejiri (UTK), Kristen Wang (UC-Riverside)

**Affiliation (s):** Oak Ridge National Laboratory

**RECENT PROGRESS**

The overarching goal of this program *is to control catalytic activity and selectivity through tuning the local environment around the active sites on the surface and at the oxide-metal interface of complex oxides*. The vision of our research is that by fundamentally understanding the composition, geometric and electronic structure and interaction among catalytic sites and the reaction pathways, we will be able to precisely assemble the desired local environment of a catalyst to control selectivity and activity. Specifically, we focus on understanding and controlling catalytic reactions involving C-H bond cleavage and formation and C=O bond activation that are known to be dependent on the local environment of the catalytic sites including local surface structure (first coordination shell) as well as geometric and electronic structures (beyond first coordination shell) at the metal-support interfaces. We summarize here our recent progress. **In the first part**, we aim to mechanistically understand how to control the local structure of active sites on surfaces to tune reaction pathways and selectivity by harnessing the chemical tunability of complex oxides. To understand the catalytic consequence of composition and structure of oxides on C-H and C=O activation, we chose complex oxides including perovskites and high entropy oxides (HEOs) because of the wide tunability of the cations and anions that can result in tunable surface local environment and catalytic chemistry. **In the second part**, we aim to understand how local geometric and electronic structure can be tailored at the metal-oxide face and interface to control reaction pathways and catalytic selectivity. These include stabilization of single atoms with oxide supports, utilizing low-temperature induced strong metal support interaction (SMSI) to stabilize and tune the catalytic properties of metal nanoparticles, core-shell structures to enhance metal-support interactions and catalysis, and visualizing the formation of SMSI layer with electron microscopy coupled with machine learning method.

**Part 1 – Surface local composition and structure effect in complex oxide catalysis**

The goal of this part of work is to achieve a fundamental understanding of how the local environment arising from composition and structure variation on complex oxide surfaces controls the reaction pathways and catalytic selectivity involved in the activation of C-H and C-O bonds. We address this goal by studying the adsorption and reaction of oxygenates and hydrocarbons over ternary oxides including perovskites and mixed oxides where both surface and bulk structure and composition at the cation and anion sites were tuned. A key focus over the last year was to understand the impact of *surface reconstruction* of complex oxides on both acid-base and redox reactions whose mechanism were studied via reaction kinetic measurements, DRIFTS/Raman, ambient pressure X-ray photoelectron spectroscopy (AP-XPS), advanced electron microscopy, and microcalorimetry. Density

functional theory (DFT) has enhanced our understanding of the reaction mechanism, the surface structure and composition of perovskites and provided predictive catalytic descriptors.

**Surface composition effect on C-H activation in methane over complex oxides.**

The goal of this study is to unveil reactivity descriptors for CH<sub>4</sub> activation over perovskites, using CH<sub>4</sub> combustion as a model reaction. In previous work, we showed that both surface segregation of Sr and creation of step-surfaces of SrTiO<sub>3</sub> (STO) can significantly impact the rate

of methane conversion in both combustion (Polo-Garzon *et al.*)<sup>49,72</sup> and oxidative coupling (OCM) (Bai *et al.*)<sup>65</sup> (Fig 1). It was also found that surface reconstruction is tied to changes on surface basic and acidic sites. Our accomplishments studying the surface reconstruction and acid-base properties of perovskites, with focus on STO, puts our team in an ideal position to unveil the connections between various surface properties, linked to surface reconstruction, and catalytic performance for CH<sub>4</sub> combustion. Accounting for surface reconstruction on the study of CH<sub>4</sub> catalysis over perovskites is currently understudied, and we hypothesize it can help elucidate reactivity descriptors over an ample set of perovskites with different elemental composition. Recently, we expanded our study to find reactivity descriptors for CH<sub>4</sub> combustion over perovskite catalysts with different elemental compositions (A=La, Sr; B=Ti, Zr, Mn, Co) that provide variation in basicity and redox properties. An array of top surface characterization techniques, kinetic experiments (including isotope labelling experiments) and DFT calculations are currently being carried out to find the density and intrinsic reactivity of active sites.

**Bridging pressure and materials gaps over complex oxide surfaces** One of the challenges in catalysis research is the so-called pressure and material gaps between surface science and reactor studies. The goal of our past experiments was to understand how the pressure and material gaps affect the reactivity and selectivity over complex oxides using alcohol conversion as the probe reaction. Perovskites are used in our research and these perovskites are chosen for their ability in cationic substitution and reducibility, which enables tuning the local environments in a way that builds upon our existing knowledge. We have performed experiments with controlled gas fluxes on the surface under high vacuum conditions, as this enables extraction of intrinsic chemical kinetics in the absence of mass transfer limitations. However, when compared to experiments performed at >1 mTorr, there can often be differences in the intrinsic kinetics, due to changes in the surface or adsorbate states, and this can lead to so-called 'pressure gaps'. Thus, we also compare the information that we extract to experiments under higher pressures on either powders, single crystal samples, or both.

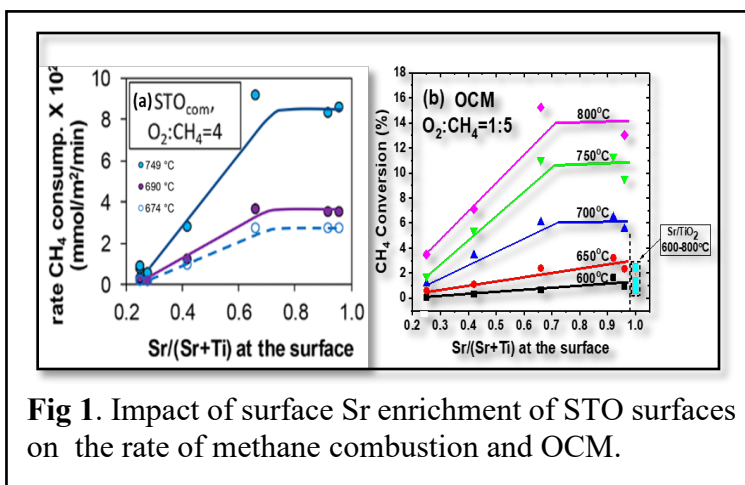
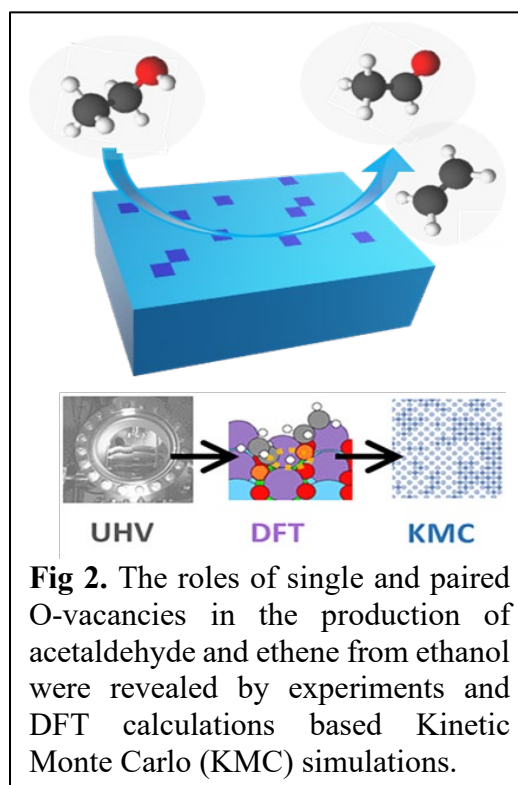


**Fig 1.** Impact of surface Sr enrichment of STO surfaces on the rate of methane combustion and OCM.

In one of our recent studies, we sought to understand the effects of oxygen vacancies in ethanol conversion over  $\text{La}_{0.7}\text{Sr}_{0.3}\text{MnO}_{3-x}(100)$  (Chen et al.)<sup>38</sup>. We ascertained that both ethene and acetaldehyde were formed by catalysis with the primary site for holding the intermediate being oxygen vacancies. Yet an increase in oxygen vacancies resulted in changing the selectivity to more greatly favor acetaldehyde. Using DFT calculations and kinetic Monte Carlo simulations, we found that adjacent (neighboring) surface oxygen vacancies on a  $\text{La}_{0.7}\text{Sr}_{0.3}\text{MnO}_3$  metal oxide catalyst switched catalytic conversion of ethanol from ethene to acetaldehyde (**Fig 2**). The experiments and simulations showed that on this catalytic surface, adjacent oxygen vacancies produced aldehyde while oxygen vacancies without neighboring oxygen vacancies produced ethene. This trend has since been confirmed in our experiments over powders. Understanding that adjacent oxygen vacancies can affect the reaction selectivity may help to design new or more selective catalytic process.

In a second study, we investigated how surface intermediates on adjacent sites could be used for C-C coupling to create acetone and crotonaldehyde from ethanol over  $\text{La}_{0.7}\text{Sr}_{0.3}\text{MnO}_3$ . It was found that acetone could be produced with a high selectivity (~40%) when an excess of water was cofed. Based on isotopic labeling and density functional theory studies, it was concluded that the most likely pathway was an aldol addition pathway involving an aldehyde outside an oxygen vacancy and an enolate in an oxygen vacancy. How could this pathway be consistent with the above conclusion that oxygen vacancies led to ethene and aldehyde? It was found that at low pressures, acetaldehyde and ethene were the main products. However, as the pressure reached the Torr range with an excess of water present, acetone became the primary carbon containing product over *both* the  $\text{La}_{0.7}\text{Sr}_{0.3}\text{MnO}_3(100)$  single crystal sample and the  $\text{La}_{0.7}\text{Sr}_{0.3}\text{MnO}_3$  powder. This change in selectivity with pressure reflects the need for the two reactants in the aldol addition step to find each other, and that a pressure gap is the reason that no substantial acetone production had been observed in previous high vacuum experiments of ethanol conversion over  $\text{La}_{0.7}\text{Sr}_{0.3}\text{MnO}_3(100)$ .

**Understanding local environment impact on hydrogenation reactions over oxides**  
Hydrogenation of aromatic rings promoted by earth-abundant metal composites under mild conditions is an attractive and challenging subject. In our recent work (Chen et al.)<sup>36</sup>, a simple active site creation and stabilization strategy was employed to obtain a  $\text{Cu}^+$ -containing ternary mixed oxide catalyst –  $\text{CuCeCoO}_x$  for the hydrogenation of benzene under mild conditions (373 K with 5 bar  $\text{H}_2$ ). The ternary oxide showed much higher activity than that of the corresponding binary counterparts and even exceeded the



performance of commercial noble metal catalysts (e.g., Pd/C). The local environment around  $\text{Cu}^+$  sites plays a crucial role in the catalytic hydrogenation of benzene: at the  $\text{CuOx-CeO}_2$  interface,  $\text{CeO}_2$  functions as a hydrogen dissociation and transfer medium while  $\text{Cu}^+$  hydrogenates the benzene ring; at the  $\text{CuOx-CoOx}$  interface,  $\text{CoOx}$  stabilizes the unstable  $\text{Cu}^+$  species and thus the hydrogenation reaction. This work unlocks a new opportunity to design highly efficient earth-abundant heterogeneous catalysts via tuning interface interactions.

Different from the tuning of cations in oxides, the ability of substituting the oxygen anion sites in complex oxides with an anion of different electronegativity such as hydride ( $\text{H}^-$ ) can also greatly impact the surface property and catalysis. Considering the reactivity of hydride species in metals such as Pd, we hypothesize that the hydride in perovskite oxyhydrides (POHs) could, in an analog to the MvK mechanism of lattice oxygen, spearhead a new mechanism of hydrogenation reaction. Our preliminary study using bare  $\text{BaTiO}_{3-x}\text{H}_x$  for the hydrogenation of acetylene showed quite promising performance: when the hydride content is at a certain value ( $x=0.03$  in this case), the POH exhibits almost 10-times higher conversion at similarly high selectivity to ethylene than the pure oxide form of perovskite, and the benchmark oxide-based hydrogenation catalyst – ceria. Currently we are carrying out neutron scattering studies of the reactivity and dynamics of the lattice hydride in POH during the hydrogenation reaction. On the computational side, an initial work focus (Wang *et al.*)<sup>18</sup> is to identify the stable surface termination of the POH under catalytically relevant temperatures and pressure using first-principle thermodynamics based on DFT. Using  $\text{BaTiO}_{2.5}\text{H}_{0.5}$  as a model, five low index facets, including (100), (010), (210), (011), and (211), and their various terminations for a total of 47 different surfaces have been examined for relative stability at different temperatures (700, 500, 300 K) and gas environments ( $10-15 \leq P_{\text{O}_2} \leq 1$  atm,  $10-15 \leq P_{\text{H}_2} \leq 100$  atm). The most stable ones are found to be (010)- $\text{Ba}_2\text{O}_2$ , (210)- $\text{Ti}_2\text{O}_2$ , and (211)- $\text{Ba}_2\text{O}_4\text{H}$  surface terminations. These polar surfaces are stabilized by charge compensation. This work provides important insights into the stable surfaces of perovskite oxyhydrides for future studies of the mechanism of hydrogenation reactions, which is currently on going.

## **Part 2 - Tuning metal-support interface for enhanced stability and catalysis**

The goal of second part of our work is to understand how local environment can be tailored at the metal-support interface to control catalytic activity, selectivity and stability. Our hypothesis is that tuning the local environment arising from the chemical and electronic interactions between metal nanoparticles and oxides can provide enhanced stability and an amplification of catalytic activity and selectivity of the supported metal centers. In the past year, we have explored various ways to tailor the interfacial structure and electronic property to achieve highly stable metal single atoms and nanoparticles (NPs) with enhanced catalytic stability, reactivity and selectivity. The stabilization was achieved via either maximization of configurational entropy of complex oxides or novel approaches to the strong metal-support interactions (SMSI).

***Stabilization of single metal sites by complex oxides for methane activation:*** The local environment of an oxide support including the surface composition and structure plays a key role in interacting with a metal. The goal of this study was to create highly stable and reactive single atom catalysts (SACs) by tuning the interfacial interaction with complex oxides carrying rich surface compositional and structural environments. We previously

showed that both small Au NPs and Au SAC supported on LaFeO<sub>3</sub>-MCF (mesoporous cellular foam silica) (Tian et al.)<sup>21</sup> displayed high sintering-resistance, catalytic activity and stability for CO oxidation, thanks to the strong interfacial interaction from the heterostructured perovskite. We recently extended the support from perovskites to high entropy oxides (HEOs) and showed that Pd SAs can be well stabilized on the high-entropy fluorite oxides (CeZrHfTiLa)O<sub>x</sub> (HEFO) up to 900 °C. Pd1@HEFO exhibits not only low-temperature CO oxidation activity but also outstanding resistance to thermal and hydrothermal degradation, which was attributed to the maximum configurational entropy of the support host (Xu et al.)<sup>16</sup>.

In exploring geometric environmental effect of oxide support on the stability of SACs, we recently explored computationally the thickness effect of the oxide support, with a goal to create 2D transition-metal oxides (TMOs) for interacting with metal sites. Excitingly, free-standing monolayer perovskites have been created recently, opening up an unexplored territory for catalysis. As a starting point, by DFT calculation using rutile TiO<sub>2</sub> as a typical TMO, we show that the band gap, which varies with the thickness of the 2D rutile TiO<sub>2</sub>(110) in an odd-even pattern, is a very useful descriptor to correlate with the reactivity of 2D TiO<sub>2</sub> and that of the single atom catalyst supported on them (Xu *et al.*)<sup>2</sup>. The smallest band gap appears for 3L-TiO<sub>2</sub>(110) which has the weakest Ti-O bonding; in other words, the local M-O bonding is influenced by the thickness of the 2D TMO, which in turn impacts

the interaction with the supported metal. **Fig 3** shows the structure of Pt<sub>1</sub> on three-layer (3L) 2D TiO<sub>2</sub>(110). Interestingly, methane can chemisorb on Pt<sub>1</sub> in this case (**Fig 3b**), followed by a facile heterolytic C-H cleavage. We further demonstrate that the band gap can be used to control

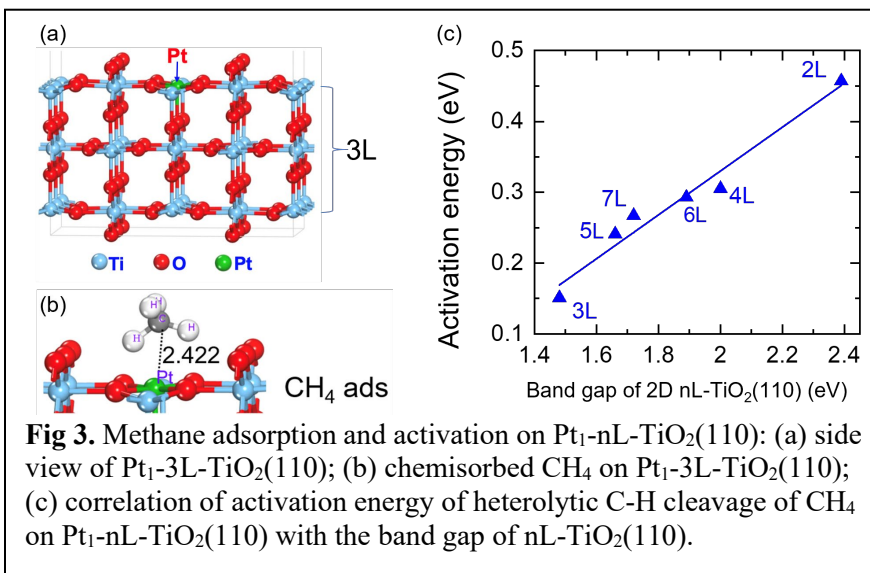


**Fig 3.** Methane adsorption and activation on Pt<sub>1</sub>-nL-TiO<sub>2</sub>(110): (a) side view of Pt<sub>1</sub>-3L-TiO<sub>2</sub>(110); (b) chemisorbed CH<sub>4</sub> on Pt<sub>1</sub>-3L-TiO<sub>2</sub>(110); (c) correlation of activation energy of heterolytic C-H cleavage of CH<sub>4</sub> on Pt<sub>1</sub>-nL-TiO<sub>2</sub>(110) with the band gap of nL-TiO<sub>2</sub>(110).

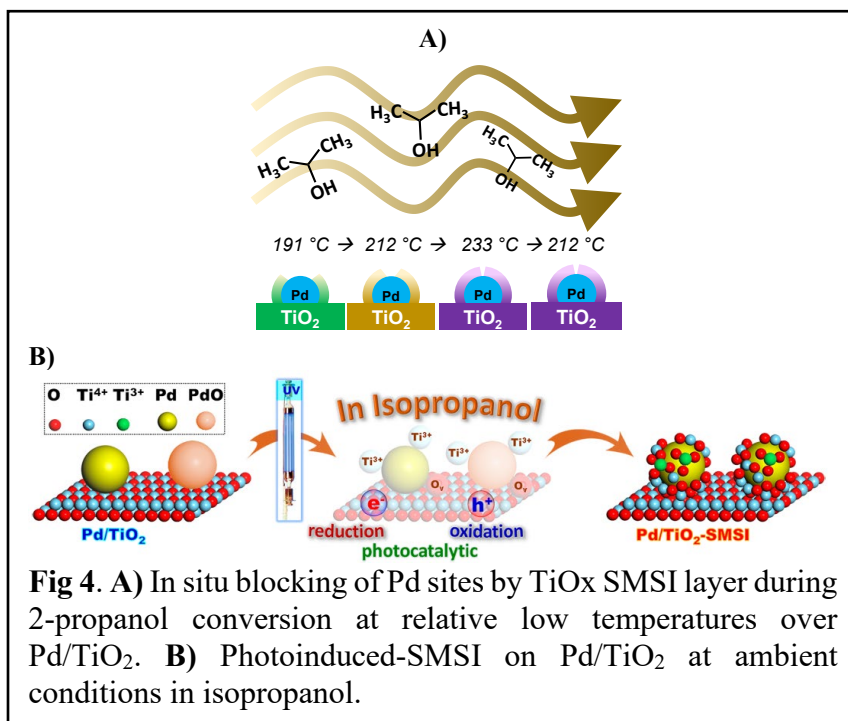
methane adsorption and its first C-H cleavage to achieve facile methane activation, because the correlation of methane adsorption and activation energy (**Fig 3c**) with the band gap of the 2D TiO<sub>2</sub>(110). Hence, our work provides a very useful guiding principle to prepare 2D TMOs of desired thickness and band gap for supporting metal single atoms and nanoparticles for catalysis. We plan to further expand this approach to the activation and conversion of methane over SACs stabilized over 2D perovskites and high-entropy oxides. **New pathways to tune Strong metal-support interaction (SMSI) for enhanced catalysis.** A significant portion of our efforts focuses on achieving a deep understanding of SMSI and utilizing it for enhanced catalysis. In the past year, we have uncovered a novel method to induce SMSI at much lower temperatures down to room temperature, thus preventing

sintering of metal nanoparticles that can occur during traditional SMSI formation conditions ( $\text{H}_2$  treatment at  $>300\text{ }^\circ\text{C}$ ). In addition, we developed a ML method to characterize SMSI when weak signals prevent identification via electron microscopy inspection. These studies are described below.

Classical SMSI is commonly associated with  $\text{H}_2$ -treatment at high temperature ( $>300\text{ }^\circ\text{C}$ ). Alcohols can reduce metal oxides, and thus we hypothesized that catalytic conversion of alcohols can promote SMSI *in situ*. We showed, via IR spectroscopy of CO adsorption and electron energy loss spectroscopy (EELS), that during 2-propanol conversion over Pd/TiO<sub>2</sub>, coverage of Pd sites occurs due to SMSI at low reaction temperatures, as low as  $\sim 190\text{ }^\circ\text{C}$  (**Fig 4A**) (Polo-Garzon *et al.*)<sup>6</sup>. Emergence of SMSI during reaction (*in situ*) explains apparent catalyst deactivation when the reaction temperature is varied. Steady-state isotopic transient kinetic analysis (SSITKA) shows that the intrinsic reactivity of the catalytic sites does not change with temperature when SMSI is promoted *in situ*, rather the number of available active sites changes (when a TiO<sub>x</sub> layer migrates over Pd NPs). SMSI generated during reaction fully reverses upon exposure to O<sub>2</sub> at room temperature for  $\sim 15$  h, which may have made its identification elusive up to now. This work questions the existence of SMSI under reaction conditions upon exposure of the catalyst to reactants capable of reducing the surface.

Motivated by the achievement of SMSI at low temperature ( $\sim 190\text{ }^\circ\text{C}$ ) upon 2-propanol treatment, our team sought and found a strategy to promote SMSI under ambient conditions: a photochemistry-driven methodology (**Fig 4B**) (Chen *et al.*)<sup>11</sup>. Encapsulation of Pd nanoparticles in Pd/TiO<sub>2</sub> with a TiO<sub>x</sub> overlayer, the presence of Ti<sup>3+</sup> species, and suppression of CO adsorption were achieved upon UV irradiation. The key lied in the

generation of separated photoinduced reductive electrons ( $\text{e}^-$ ) and oxidative holes ( $\text{h}^+$ ), which subsequently triggered the formation of Ti<sup>3+</sup> species/oxygen vacancies ( $\text{O}_v$ ) and then interfacial Pd– $\text{O}_v$ –Ti<sup>3+</sup> sites, affording SMSI in Pd/TiO<sub>2</sub>. UV-induced SMSI promoted full hydrogenation of the alkyne group in phenyl-acetylene, whereas the base



Pd/TiO<sub>2</sub> led to semi and full hydrogenation. This indicates that the UV-induced SMSI enhanced the hydrogenation capabilities of the catalyst. The SMSI layer was reversible,

and the photo-driven procedure could be extended to Pd/ZnO and Pt/TiO<sub>2</sub>.

In addition to the novel alcohol-induced low temperature formation of SMSI, we also recently devised an approach to synthesize artificial SMSI layer with non-reducible and non-oxide support – boron nitride (Chen et al.)<sup>34</sup>. Highly crystalline and nanoporous hexagonal boron nitride (h-BN) 2D layers over metal particles were demonstrated via in situ encapsulation and reduction using NaBH<sub>4</sub>, NaNH<sub>2</sub>, and noble metal (Pd) salts as precursors. The as-prepared nanocatalysts exhibited robust thermal stability and sintering resistance to withstand thermal treatment at up to 950 °C, rendering them with high catalytic efficiency and durability in CO oxidation even in the presence of H<sub>2</sub>O and hydrocarbon simulated to realistic exhaust systems. This work extends the support materials in traditional SMSI systems from reducible oxides to non-oxides and provides potential for stabilizing diverse metal nanoparticles with various support compositions and architectures.

Precisely detecting the formation of SMSI layer especially at its early stage and determining its chemistry, however, is a challenging task. Scanning transmission electron microscopy (STEM) is the most commonly used technique for such an analysis but often suffers from a low signal strength due to the thickness and the electron beam sensitivity of the surface encapsulation layer. This can lead to the potential misinterpretation or overlooking of the encapsulation signal. Recently, using Pd/TiO<sub>2</sub> as a prototype system, we develop and demonstrate an unsupervised machine learning method that allows us to reveal the presence and chemical information of the SMSI encapsulation layer that is otherwise hidden in STEM-electron energy loss spectroscopy (EELS) datasets (Blum et al.<sup>13</sup>, **Fig 5**). This method not only provides a robust tool for the analysis of trace SMSI in catalysts, but is generally applicable to any materials and spectroscopy datasets of any material systems where revealing a trace signal is critical.

**Predictive understanding of metal – support interactions** Overcoming the limitation of DFT in handling catalytic systems of sub-nanometer size, newly developed density-functional tight-binding (DFTB) parameters were employed in steered molecular dynamics (SMD) simulations of the Pt/TiO<sub>2</sub> system to evaluate the free energy profile for the nucleation of a Pt<sub>6</sub> cluster due to Pt atom attachment to an existing Pt<sub>5</sub> cluster. The simulations were carried out on the rutile (110) surface at temperatures of 400, 600, and 800 K, and we approximate the Gibbs free energy profile was computed as the potential of mean force (PMF) associated with the reaction coordinate. To obtain a statistical sampling, the PMFs were computed from the pulling work of over 100 SMD trajectories using Jarzynski's equality. While the effects of temperature on the amplitude of the first barrier is similar to the case of single Pt atom diffusion on the rutile (110) surface, the second barrier changed more noticeably with the temperature. It was reduced from 11 kcal/mol at

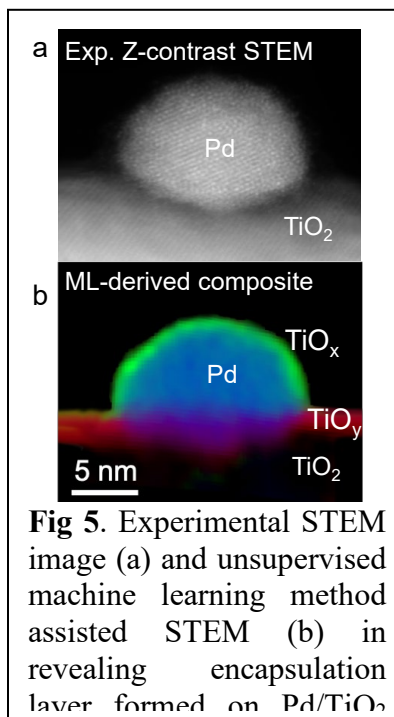


**Fig 5.** Experimental STEM image (a) and unsupervised machine learning method assisted STEM (b) in revealing encapsulation layer formed on Pd/TiO<sub>2</sub>

400 K to ~6 kcal/mol at 800 K. By analyzing the SMD trajectories, we found that the energy decrease of the second barrier is due to the dynamics of the Pt<sub>5</sub> cluster, as it distorts toward the Pt single atom at the position of the second energy barrier. This distortion induces the early formation of the Pt<sub>5</sub>+Pt<sub>1</sub> complex, stabilizing the transition state. To enable such sintering simulations in the presence of reactants/products during catalysis, we are now working on the parameterization of Pt with H, C, O, N, as well as Sr. This is the first step toward DFTB-based studies of surface dynamic evolution processes including the formation of SMSI occurring at Pt-clusters on TiO<sub>2</sub> and SrTiO<sub>3</sub> support interfaces, paving the way for the design of new metal catalysts on active supports.

## **Publications Acknowledging this Grant (ERKCC96) in 2018 –2021 (total – 132)**

### **(I) Intellectually led by this grant (total – 91)**

1. Zhang, Z.; Yao, S.; Hu, X.; Okejiri, F.; He, K.; Liu, P.; Tian, Z.; Dravid, V. P.; Fu, J.; Zhu, X.; Dai, S., Sacrificial Synthesis of Supported Ru Single Atoms and Clusters on N-doped Carbon Derived from Covalent Triazine Frameworks: A Charge Modulation Approach. *Advanced Science* **2021**, *8* (3), 2001493.
2. Xu, X.; Wang, X.; Jiang, D.-e., Band Gap as a Novel Descriptor for the Reactivity of 2D Titanium Dioxide and its Supported Pt Single Atom for Methane Activation. *J. Phys. Chem. Lett.* **2021**, *12* (10), 2484-2488.
3. Wang, Z.; Rong, J.; Lv, J.; Chong, R.; Zhang, L.; Wang, L.; Chang, Z.; Wang, X., Chelation-mediated in-situ formation of ultrathin cobalt (oxy)hydroxides on hematite photoanode towards enhanced photoelectrochemical water oxidation. *J. Energy Chem.* **2021**, *56*, 152-161.
4. Wang, S.; Wu, Z.; Dai, S.; Jiang, D.-e., Deep Learning Accelerated Determination of Hydride Locations in Metal Nanoclusters. *Angew. Chem. Int. Ed.* **2021**, *60* (22), 12289-12292.
5. Sun, Y.; Dai, S., High-entropy materials for catalysis: A new frontier. *Science Advances* **2021**, *7* (20), eabg1600.
6. Polo-Garzon, F.; Blum, T. F.; Bao, Z.; Wang, K.; Fung, V.; Huang, Z.; Bickel, E. E.; Jiang, D.-e.; Chi, M.; Wu, Z., In Situ Strong Metal–Support Interaction (SMSI) Affects Catalytic Alcohol Conversion. *ACS Catal.* **2021**, *11* (4), 1938-1945.
7. Liu, T.; Jiang, D.-e., Understanding the interaction between carboxylates and coinage metals from first principles. *The Journal of Chemical Physics* **2021**, *155* (3), 034301.
8. Leng, Y.; Zhang, Z.; Chen, H.; Du, S.; Liu, J.; Nie, S.; Dong, Y.; Zhang, P.; Dai, S., Overcoming the phase separation within high-entropy metal carbide by poly(ionic liquid)s. *Chem. Commun.* **2021**, *57* (30), 3676-3679.
9. He, X.; Walter, M.; Jiang, D.-e., Understanding Superatomic Ag Nanohydrides. *Small* **2021**, 2004808.
10. Gao, W.; Elnabawy, A. O.; Hood, Z. D.; Shi, Y.; Wang, X.; Roling, L. T.; Pan, X.; Mavrikakis, M.; Xia, Y.; Chi, M., Atomistic insights into the nucleation and growth of platinum on palladium nanocrystals. *Nat. Commun.* **2021**, *12* (1), 3215.
11. Chen, H.; Yang, Z.; Wang, X.; Polo-Garzon, F.; Halstenberg, P. W.; Wang, T.; Suo, X.; Yang, S.-Z.; Meyer, H. M.; Wu, Z.; Dai, S., Photoinduced Strong Metal–Support Interaction for Enhanced Catalysis. *J. Amer. Chem. Soc.* **2021**, *143* (23), 8521-8526.

12. Chen, H.; Wang, W.; Yang, Z.; Suo, X.; Lu, Z.; Xiao, W.; Dai, S., Alkaline salt-promoted construction of hydrophilic and nitrogen deficient graphitic carbon nitride with highly improved photocatalytic efficiency. *J. Mater. Chem. A* **2021**, *9* (8), 4700-4706.
13. Blum, T.; Graves, J.; Zachman, M. J.; Polo-Garzon, F.; Wu, Z.; Kannan, R.; Pan, X.; Chi, M., Machine Learning Method Reveals Hidden Strong Metal-Support Interaction in Microscopy Datasets. *Small Methods* **2021**, *n/a* (n/a), 2100035.
14. Zhang, Y.; Mullins, D. R.; Savara, A., Surface Reactions and Catalytic Activities for Small Alcohols over LaMnO<sub>3</sub>(100) and La<sub>0.7</sub>Sr<sub>0.3</sub>MnO<sub>3</sub>(100): Dehydrogenation, Dehydration, and Oxidation. *J. Phys. Chem. C* **2020**, *124* (6), 3650-3663.
15. Zhang, X.; Savara, A.; Getman, R. B., A Method for Obtaining Liquid-Solid Adsorption Rates from Molecular Dynamics Simulations: Applied to Methanol on Pt(111) in H<sub>2</sub>O. *J. Chem. Theory Comput.* **2020**, *16* (4), 2680-2691.
16. Xu, H.; Zhang, Z.; Liu, J.; Do-Thanh, C.-L.; Chen, H.; Xu, S.; Lin, Q.; Jiao, Y.; Wang, J.; Wang, Y.; Chen, Y.; Dai, S., Entropy-stabilized single-atom Pd catalysts via high-entropy fluorite oxide supports. *Nat. Commun.* **2020**, *11* (1), 3908.
17. Wu, P.; Tan, S.; Moon, J.; Yan, Z.; Fung, V.; Li, N.; Yang, S.-Z.; Cheng, Y.; Abney, C. W.; Wu, Z.; Savara, A.; Momen, A. M.; Jiang, D.-e.; Su, D.; Li, H.; Zhu, W.; Dai, S.; Zhu, H., Harnessing strong metal-support interactions via a reverse route. *Nat. Commun.* **2020**, *11* (1), 3042.
18. Wang, K.; Fung, V.; Wu, Z.; Jiang, D.-e., Stable Surface Terminations of a Perovskite Oxyhydride from First Principles. *J. Phys. Chem. C* **2020**, *124* (34), 18557-18563.
19. Wang, F.; Wu, Z., Preface to Special Issue on Advances in Ceria Catalysis. *Chin. J. Catal.* **2020**, *41* (6), 899-900.
20. Wan, Q.; Fung, V.; Lin, S.; Wu, Z.; Jiang, D.-e., Perovskite-supported Pt single atoms for methane activation. *J. Mater. Chem. A* **2020**, *8* (8), 4362-4368.
21. Tian, C.; Zhang, H.; Zhu, X.; Lin, B.; Liu, X.; Chen, H.; Zhang, Y.; Mullins, D. R.; Abney, C. W.; Shakouri, M.; Chernikov, R.; Hu, Y.; Polo-Garzon, F.; Wu, Z.; Fung, V.; Jiang, D.-e.; Liu, X.; Chi, M.; Liu Jimmy, J.; Dai, S., A new trick for an old support: Stabilizing gold single atoms on LaFeO<sub>3</sub> perovskite. *Appl. Catal. B: Environ.* **2020**, *261*, 118178.
22. Savara, A.; Walker, E. A., CheKiPEUQ Intro 1: Bayesian Parameter Estimation Considering Uncertainty or Error from both Experiments and Theory. *ChemCatChem* **2020**, *12* (21), 5385-5400.
23. Savara, A., Microkinetic simulation and fitting of the temperature programmed reaction of methanol on CeO<sub>2</sub>(111): H<sub>2</sub> and H<sub>2</sub>O + V production. *React. Kinet. Mech. Catal.* **2020**, *129* (1), 181-203.
24. Polo-Garzon, F.; Blum, T. F.; Fung, V.; Bao, Z.; Chen, H.; Huang, Z.; Mahurin, S. M.; Dai, S.; Chi, M.; Wu, Z., Alcohol-Induced Low-Temperature Blockage of Supported-Metal Catalysts for Enhanced Catalysis. *ACS Catal.* **2020**, *10*, 8515-8523.
25. Moon, J.; Cheng, Y.; Daemen, L. L.; Li, M.; Polo-Garzon, F.; Ramirez-Cuesta, A. J.; Wu, Z., Discriminating the Role of Surface Hydride and Hydroxyl for Acetylene Semi-Hydrogenation over Ceria Through in situ Neutron and Infrared Spectroscopy. *ACS Catal.* **2020**, *10* (9), 5278-5287.
26. Liu, J.; Wang, L.; Okejiri, F.; Luo, J.; Zhao, J.; Zhang, P.; Liu, M.; Yang, S.; Zhang, Z.; Song, W.; Zhu, W.; Liu, J.; Zhao, Z.; Feng, G.; Xu, C.; Dai, S., Deep

Understanding of Strong Metal Interface Confinement: A Journey of Pd/FeOx catalysts. *ACS Catal.* **2020**, *10*, 8950-8959.

27. Kammert, J.; Moon, J.; Wu, Z., A review of the interactions between ceria and H<sub>2</sub> and the applications to selective hydrogenation of alkynes. *Chin. J. Catal.* **2020**, *41* (6), 901-914.
28. Huang, R.; Fung, V.; Wu, Z.; Jiang, D.-e., Understanding the conversion of ethanol to propene on In<sub>2</sub>O<sub>3</sub> from first principles. *Catal. Today* **2020**, *350*, 19-24.
29. Fung, V.; Hu, G.; Wu, Z.; Jiang, D.-e., Hydrogen in Nanocatalysis. *J. Phys. Chem. Lett.* **2020**, *11* (17), 7049-7057.
30. Fung, V.; Hu, G.; Wu, Z.; Jiang, D.-e., Descriptors for Hydrogen Evolution on Single Atom Catalysts in Nitrogen-Doped Graphene. *J. Phys. Chem. C* **2020**, *124* (36), 19571-19578.
31. Doyle, P. J.; Savara, A.; Raiman, S. S., Extracting meaningful standard enthalpies and entropies of activation for surface reactions from kinetic rates. *React. Kinet. Mech. Catal.* **2020**, *129* (2), 551-581.
32. Ding, Y.; Zhang, P.; Xiong, H.; Sun, X.; Klyushin, A.; Zhang, B.; Liu, Z.; Zhang, J.; Zhu, H.; Qiao, Z.-A.; Heumann, S.; Dai, S., Tuning regioselective oxidation toward phenol via atomically dispersed iron sites on carbon. *Green Chem.* **2020**, *22* (18), 6025-6032.
33. Dai, S., Across the Board: Sheng Dai on Catalyst Design by Entropic Factors. *ChemSusChem* **2020**, *13* (7), 1915-1917.
34. Chen, H.; Yang, S.-Z.; Yang, Z.; Lin, W.; Xu, H.; Wan, Q.; Suo, X.; Wang, T.; Jiang, D.-e.; Fu, J.; Dai, S., Sinter-Resistant Nanoparticle Catalysts Achieved by 2D Boron Nitride-Based Strong Metal-Support Interactions: A New Twist on an Old Story. *ACS Cent. Sci.* **2020**, *6* (9), 1617-1627.
35. Chen, H.; Sun, Y.; Yang, S.; Wang, H.; Dmowski, W.; Egami, T.; Dai, S., Self-regenerative noble metal catalysts supported on high-entropy oxides. *Chem. Commun.* **2020**, *56* (95), 15056-15059.
36. Chen, H.; Lin, W.; Zhang, Z.; Yang, Z.; Jie, K.; Fu, J.; Yang, S.-z.; Dai, S., Facile benzene reduction promoted by a synergistically coupled Cu-Co-Ce ternary mixed oxide. *Chem. Sci.* **2020**, *11* (22), 5766-5771.
37. Chen, H.; Jie, K.; Jafta, C. J.; Yang, Z.; Yao, S.; Liu, M.; Zhang, Z.; Liu, J.; Chi, M.; Fu, J.; Dai, S., An ultrastable heterostructured oxide catalyst based on high-entropy materials: A new strategy toward catalyst stabilization via synergistic interfacial interaction. *Appl. Catal. B: Environ.* **2020**, *276*, 119155.
38. Chen, B.; Xiong, C.; Jiang, D.-e.; Savara, A., Ethanol Conversion over La<sub>0.7</sub>Sr<sub>0.3</sub>MnO<sub>3-x</sub>(100): Autocatalysis, Adjacent O-Vacancies, Disproportionation, and Dehydrogenation. *ACS Catal.* **2020**, *10* (21), 12920-12931.
39. Bao, Z.; Fung, V.; Polo-Garzon, F.; Hood, Z. D.; Cao, S.; Chi, M.; Bai, L.; Jiang, D.-e.; Wu, Z., The interplay between surface facet and reconstruction on isopropanol conversion over SrTiO<sub>3</sub> nanocrystals. *J. Catal.* **2020**, *384*, 49-60.
40. Zhao, C.; Watt, C.; Kent, P. R.; Overbury, S. H.; Mullins, D. R.; Calaza, F. C.; Savara, A.; Xu, Y., Coupling of Acetaldehyde to Crotonaldehyde on CeO<sub>2-x</sub>(111): Bifunctional Mechanism and Role of Oxygen Vacancies. *J. Phys. Chem. C* **2019**, *123* (13), 8273-8286.

41. Zhang, Z.; Yang, S.; Hu, X.; Xu, H.; Peng, H.; Liu, M.; Thapaliya, B. P.; Jie, K.; Zhao, J.; Liu, J.; Chen, H.; Leng, Y.; Lu, X.; Fu, J.; Zhang, P.; Dai, S., Mechanochemical Nonhydrolytic Sol–Gel–Strategy for the Production of Mesoporous Multimetallic Oxides. *Chem. Mater.* **2019**, *31* (15), 5529-5536.
42. Zhang, Y.; Mullins, D. R.; Savara, A., Effect of Sr Substitution in LaMnO<sub>3</sub>(100) on Catalytic Conversion of Acetic Acid to Ketene and Combustion-Like Products. *J. Phys. Chem. C* **2019**, *123* (7), 4148-4157.
43. Yang, X.; Li, Q.; Lu, E.; Wang, Z.; Gong, X.; Yu, Z.; Guo, Y.; Wang, L.; Guo, Y.; Zhan, W.; Zhang, J.; Dai, S., Taming the stability of Pd active phases through a compartmentalizing strategy toward nanostructured catalyst supports. *Nat. Commun.* **2019**, *10* (1), 1611.
44. Yan, Y.; Zhang, Z.; Bak, S.-M.; Yao, S.; Hu, X.; Shadike, Z.; Do-Thanh, C.-L.; Zhang, F.; Chen, H.; Lyu, X.; Chen, K.; Zhu, Y.; Lu, X.; Ouyang, P.; Fu, J.; Dai, S., Confinement of Ultrasmall Cobalt Oxide Clusters within Silicalite-1 Crystals for Efficient Conversion of Fructose into Methyl Lactate. *ACS Catal.* **2019**, *9* (3), 1923-1930.
45. Xu, H.; Liu, J.; Zhang, Z.; Liu, S.; Lin, Q.; Wang, Y.; Dai, S.; Chen, Y., Design and Synthesis of Highly-Dispersed WO<sub>3</sub> Catalyst with Highly Effective NH<sub>3</sub>–SCR Activity for NO<sub>x</sub> Abatement. *ACS Catal.* **2019**, *9* (12), 11557-11562.
46. Wu, P.; Wu, Z.; Mullins, D. R.; Yang, S.-Z.; Han, X.; Zhang, Y.; Foo, G. S.; Li, H.; Zhu, W.; Dai, S.; Zhu, H., Promoting Pt catalysis for CO oxidation via the Mott–Schottky effect. *Nanoscale* **2019**, *11* (40), 18568-18574.
47. Polo-Garzon, F.; Luo, S.; Cheng, Y.; Page, K. L.; Ramirez-Cuesta, A. J.; Britt, P. F.; Wu, Z., Neutron Scattering Investigations of Hydride Species in Heterogeneous Catalysis. *ChemSusChem* **2019**, *12* (1), 93-103.
48. Polo-Garzon, F.; Fung, V.; Nguyen, L.; Tang, Y.; Tao, F.; Cheng, Y.; Daemen, L. L.; Ramirez-Cuesta, A. J.; Foo, G. S.; Zhu, M.; Wachs, I. E.; Jiang, D.-e.; Wu, Z., Elucidation of the Reaction Mechanism for High-Temperature Water Gas Shift over an Industrial-Type Copper–Chromium–Iron Oxide Catalyst. *J. Amer. Chem. Soc.* **2019**, *141* (19), 7990-7999.
49. Polo-Garzon, F.; Bao, Z.; Zhang, X.; Huang, W.; Wu, Z., Surface Reconstructions of Metal Oxides and the Consequences on Catalytic Chemistry. *ACS Catal.* **2019**, *9* (6), 5692-5707.
50. Peng, H. G.; Zhang, X. H.; Han, X.; You, X. J.; Lin, S. X.; Chen, H.; Liu, W. M.; Wang, X.; Zhang, N.; Wang, Z.; Wu, P.; Zhu, H. Y.; Dai, S., Catalysts in Coronas: A Surface Spatial Confinement Strategy for High-Performance Catalysts in Methane Dry Reforming. *ACS Catal.* **2019**, *9* (10), 9072-9080.
51. Peng, H.; Dong, T.; Zhang, L.; Wang, C.; Liu, W.; Bao, J.; Wang, X.; Zhang, N.; Wang, Z.; Wu, P.; Zhang, P.; Dai, S., Active and stable Pt-Ceria nanowires@silica shell catalyst: Design, formation mechanism and total oxidation of CO and toluene. *Appl. Catal. B: Environ.* **2019**, *256* (5), 117807.
52. Okejiri, F.; Zhang, Z.; Liu, J.; Liu, M.; Yang, S.; Dai, S., Room-Temperature Synthesis of High-Entropy Perovskite Oxide Nanoparticle Catalysts through Ultrasonication-Based Method. *ChemSusChem* **2019**, *13* (1), 111-115.
53. Matera, S.; Schneider, W. F.; Heyden, A.; Savara, A., Progress in Accurate Chemical Kinetic Modeling, Simulations, and Parameter Estimation for Heterogeneous Catalysis. *ACS Catal.* **2019**, *9* (8), 6624-6647.

54. Liu, X.; Hood, Z. D.; Zheng, Q.; Jin, T.; Foo, G. S.; Wu, Z.; Tian, C.; Guo, Y.; Dai, S.; Zhan, W.; Zhu, H.; Chi, M., Optimizing the structural configuration of FePt-FeOx nanoparticles at the atomic scale by tuning the post-synthetic conditions. *Nano Energy* **2019**, *55*, 441-446.
55. Liu, M.; Zhang, Z.; Okejiri, F.; Yang, S.; Zhou, S.; Dai, S., Entropy-Maximized Synthesis of Multimetallic Nanoparticle Catalysts via a Ultrasonication-Assisted Wet Chemistry Method under Ambient Conditions. *Adv. Mater. Interfaces* **2019**, *6* (0), 1900015.
56. Leng, Y.; Liu, J. X.; Zhang, Z. H.; Chen, H.; Zhang, P. F.; Dai, S., Polyoxometalates as bifunctional templates: engineering metal oxides with mesopores and reactive surfaces for catalysis. *J. Mater. Chem. A* **2019**, *7* (48), 27297-27303.
57. Leng, Y.; Jiang, Y.; Peng, H.; Zhang, Z.; Liu, M.; Jie, K.; Zhang, P.; Dai, S., Heterogeneity of polyoxometalates by confining within ordered mesopores: toward efficient oxidation of benzene to phenol. *Catal. Sci. Technol.* **2019**, *9* (9), 2173-2179.
58. Lee, K. H.; Vuong, V. Q.; Fung, V.; Jiang, D. E.; Irle, S., Density-Functional Tight-Binding for Platinum Clusters and Bulk: Electronic vs Repulsive Parameters. *MRS Adv.* **2019**, *4* (33-34), 1821-1832.
59. Kong, L.; Zhao, J.; Han, S.; Zhang, T.; He, L.; Zhang, P.; Dai, S., Facile Synthesis of Copper Containing Ordered Mesoporous Polymers via Aqueous Coordination Self-Assembly for Aerobic Oxidation of Alcohols. *Ind. Eng. Chem. Res.* **2019**, *58* (16), 6438-6445.
60. Hou, S.; Chen, N.; Zhang, P.; Dai, S., Heterogeneous viologen catalysts for metal-free and selective oxidations. *Green Chem.* **2019**, *21* (6), 1455-1460.
61. Gao, Y.; Huang, R.; Wang, J.; Wu, Z.; Jiang, D.-e., Effect of Hydrogen-Induced Metallization on Chemisorption. *J. Phys. Chem. C* **2019**, *123* (24), 15171-15175.
62. Fung, V.; Hu, G.; Tao, F.; Jiang, D.-e., Methane Chemisorption on Oxide-Supported Pt Single Atom. *ChemPhysChem* **2019**, *20* (17), 2217-2220.
63. Chen, H.; Yang, Z.; Zhang, Z.; Chen, Z.; Chi, M.; Wang, S.; Fu, J.; Dai, S., Construction of a Nanoporous Highly Crystalline Hexagonal Boron Nitride from an Amorphous Precursor for Catalytic Dehydrogenation. *Angew. Chem. Int. Ed.* **2019**, *131* (31), 10736-10740.
64. Chen, H.; Lin, W.; Zhang, Z.; Jie, K.; Mullins, D. R.; Sang, X.; Yang, S.-Z.; Jafta, C. J.; Bridges, C. A.; Hu, X.; Unocic, R. R.; Fu, J.; Zhang, P.; Dai, S., Mechanochemical Synthesis of High Entropy Oxide Materials under Ambient Conditions: Dispersion of Catalysts via Entropy Maximization. *ACS Mater. Lett.* **2019**, *1*, 83-88.
65. Bai, L.; Polo-Garzon, F.; Bao, Z.; Luo, S.; Moskowitz, B. M.; Tian, H.; Wu, Z., Impact of Surface Composition of SrTiO<sub>3</sub> Catalysts for Oxidative Coupling of Methane. *ChemCatChem* **2019**, *11* (8), 2107-2117.
66. Zhang, P.; Chen, N.; Chen, D.; Yang, S.; Liu, X.; Wang, L.; Wu, P.; Phillip, N.; Yang, G.; Dai, S., Ultra-Stable and High-Cobalt-Loaded Cobalt@Ordered Mesoporous Carbon Catalysts: All-in-One Deoxygenation of Ketone into Alkylbenzene. *ChemCatChem* **2018**, *10* (15), 3299-3304.
67. Xiao, W.; Yang, S.; Zhang, P.; Li, P.; Wu, P.; Li, M.; Chen, N.; Jie, K.; Huang, C.; Zhang, N.; Dai, S., Facile Synthesis of Highly Porous Metal Oxides by Mechanochemical Nanocasting. *Chem. Mater.* **2018**, *30* (9), 2924-2929.

68. Wu, Z.; Mullins, D. R.; Allard, L. F.; Zhang, Q.; Wang, L., CO oxidation over ceria supported Au<sub>22</sub> nanoclusters: Shape effect of the support. *Chin. Chem. Lett.* **2018**, *29* (6), 795-799.
69. Tang, Q.; Hu, G.; Fung, V.; Jiang, D.-e., Insights into Interfaces, Stability, Electronic Properties, and Catalytic Activities of Atomically Precise Metal Nanoclusters from First Principles. *Acc. Chem. Res.* **2018**, *51* (11), 2793-2802.
70. Prati, L.; Villa, A.; Jouve, A.; Beck, A.; Evangelisti, C.; Savara, A., Gold as modifier of metal nanoparticles: effect on structure and catalysis. *Faraday Discuss.* **2018**, *208*, 395-407.
71. Polo-Garzon, F.; Wu, Z., Acid-base catalysis over perovskites: a review. *J. Mater. Chem. A* **2018**, *6* (7), 2877-2894.
72. Polo-Garzon, F.; Fung, V.; Liu, X.; Hood, Z. D.; Bickel, E. E.; Bai, L.; Tian, H.; Foo, G. S.; Chi, M.; Jiang, D.-e.; Wu, Z., Understanding the Impact of Surface Reconstruction of Perovskite Catalysts on CH<sub>4</sub> Activation and Combustion. *ACS Catal.* **2018**, *9*, 10306-10315.
73. Peng, H.; Rao, C.; Zhang, N.; Wang, X.; Liu, W.; Mao, W.; Han, L.; Zhang, P.; Dai, S., Confined Ultrathin Pd-Ce Nanowires with Outstanding Moisture and SO<sub>2</sub> Tolerance in Methane Combustion. *Angew. Chem. Int. Ed.* **2018**, *57* (29), 8953-8957.
74. Mullins, D. R., Variations in the surface chemistry of methanol with CeO<sub>2</sub>(100) at low and elevated pressures. *Surf. Interface Anal.* **2018**, *50* (10), 913-920.
75. Lukosi, M.; Tian, C.; Li, X.; Mahurin, S. M.; Meyer, H. M.; Foo, G. S.; Dai, S., Tuning the Core-Shell Structure of Au<sub>144</sub>@Fe<sub>2</sub>O<sub>3</sub> for Optimal Catalytic Activity for CO Oxidation. *Catal. Lett.* **2018**, *148* (8), 2315-2324.
76. Liu, Y.; Zhang, P.; Liu, J.; Wang, T.; Huo, Q.; Yang, L.; Sun, L.; Qiao, Z.-A.; Dai, S., Gold Cluster-CeO<sub>2</sub> Nanostructured Hybrid Architectures as Catalysts for Selective Oxidation of Inert Hydrocarbons. *Chem. Mater.* **2018**, *30* (23), 8579-8586.
77. Liu, F.; Huang, K.; Zheng, A.; Xiao, F.-S.; Dai, S., Hydrophobic Solid Acids and Their Catalytic Applications in Green and Sustainable Chemistry. *ACS Catal.* **2018**, *8* (1), 372-391.
78. Leng, Y.; Zhang, C.; Liu, B.; Liu, M.; Jiang, P.; Dai, S., Synergistic Activation of Palladium Nanoparticles by Polyoxometalate-Attached Melem for Boosting Formic Acid Dehydrogenation Efficiency. *ChemSusChem* **2018**, *11* (19), 3396-3401.
79. Huang, W.; Wu, Z.; Tang, J.; Wei, W. D.; Guo, X., Surface chemistry connecting heterogeneous catalysis, photocatalysis and plasmonic catalysis. *Chin. Chem. Lett.* **2018**, *29* (6), 725-726.
80. Huang, R.; Fung, V.; Zhang, Y.; Mullins, D. R.; Wu, Z.; Jiang, D.-e., Understanding Methanol Coupling on SrTiO<sub>3</sub> from First Principles. *J. Phys. Chem. C* **2018**, *122* (13), 7210-7216.
81. Hu, G.; Wu, Z.; Jiang, D.-e., Stronger-than-Pt hydrogen adsorption in a Au<sub>22</sub> nanocluster for the hydrogen evolution reaction. *J. Mater. Chem. A* **2018**, *6*, 7532-7537.
82. Hu, G.; Wu, Z.; Jiang, D.-e., First Principles Insight into H<sub>2</sub> Activation and Hydride Species on TiO<sub>2</sub> Surfaces. *J. Phys. Chem. C* **2018**, *122* (35), 20323-20328.
83. Hu, G.; Wu, Z.; Dai, S.; Jiang, D.-e., Interface Engineering of Earth-Abundant Transition Metals by Boron Nitride for Selective Electroreduction of CO<sub>2</sub>. *ACS Appl. Mater. Inter.* **2018**, *10* (7), 6694-6700.

84. Fung, V.; Wu, Z.; Jiang, D.-e., New Bonding Model of Radical Adsorbate on Lattice Oxygen of Perovskites. *J. Phys. Chem. Lett.* **2018**, *9* (21), 6321-6325.
85. Fung, V.; Polo-Garzon, F.; Wu, Z.; Jiang, D.-e., Exploring perovskites for methane activation from first principles. *Catal. Sci. Technol.* **2018**, *8* (3), 702-709.
86. Foo, G. S.; Hood, Z. D.; Wu, Z., Shape Effect Undermined by Surface Reconstruction: Ethanol Dehydrogenation over Shape-Controlled SrTiO<sub>3</sub> Nanocrystals. *ACS Catal.* **2018**, *8* (1), 555-565.
87. Dong, H.; Li, Y.; Jiang, D.-e., First-Principles Insight into Electrocatalytic Reduction of CO<sub>2</sub> to CH<sub>4</sub> on a Copper Nanoparticle. *J. Phys. Chem. C* **2018**, *122* (21), 11392-11398.
88. Ding, S.; Tian, C.; Zhu, X.; Wang, H.; Wang, H.; Abney, C. W.; Zhang, N.; Dai, S., Engineering nanoporous organic frameworks to stabilize naked Au clusters: a charge modulation approach. *Chem. Commun.* **2018**, *54* (40), 5058-5061.
89. Chen, H.; Shi, X.; Liu, J.; Jie, K.; Zhang, Z.; Hu, X.; Zhu, Y.; Lu, X.; Fu, J.; Huang, H.; Dai, S., Controlled synthesis of hierarchical ZSM-5 for catalytic fast pyrolysis of cellulose to aromatics. *J. Mater. Chem. A* **2018**, *6* (42), 21178-21185.
90. Chen, H.; Fu, J.; Zhang, P.; Peng, H.; Abney, C. W.; Jie, K.; Liu, X.; Chi, M.; Dai, S., Entropy-stabilized metal oxide solid solutions as CO oxidation catalysts with high-temperature stability. *J. Mater. Chem. A* **2018**, *6*, 11129-11133
91. Chan-Thaw, C.; Savara, A.; Villa, A., Selective Benzyl Alcohol Oxidation over Pd Catalysts. *Catalysts* **2018**, *8* (10), 431.

***(II) Jointly funded by this grant and other grants with intellectual leadership by other funding sources (total - 41)***

92. Zhu, X.; Gao, Y.; Wang, X.; Haribal, V.; Liu, J.; Neal, L. M.; Bao, Z.; Wu, Z.; Wang, H.; Li, F., A tailored multi-functional catalyst for ultra-efficient styrene production under a cyclic redox scheme. *Nat. Commun.* **2021**, *12* (1), 1329.
93. Zhu, M.; Tian, P.; Cao, X.; Chen, J.; Pu, T.; Shi, B.; Xu, J.; Moon, J.; Wu, Z.; Han, Y.-F., Vacancy engineering of the nickel-based catalysts for enhanced CO<sub>2</sub> methanation. *Appl. Catal. B: Environ.* **2021**, *282*, 119561.
94. Moon, J.; Cheng, Y.; Daemen, L.; Novak, E.; Ramirez-Cuesta, A. J.; Wu, Z., On the Structural Transformation of Ni/BaH<sub>2</sub> During a N<sub>2</sub>-H<sub>2</sub> Chemical Looping Process for Ammonia Synthesis: A Joint In Situ Inelastic Neutron Scattering and First-Principles Simulation Study. *Topic Catal.* **2021**, *64*, 685-692.
95. Liu, X.; Li, B.; Han, G.; Liu, X.; Cao, Z.; Jiang, D.-e.; Sun, Y., Electrocatalytic synthesis of heterocycles from biomass-derived furfuryl alcohols. *Nat. Commun.* **2021**, *12* (1), 1868.
96. Lawson, S.; Farsad, A.; Adebayo, B.; Newport, K.; Schueddig, K.; Lowrey, E.; Polo-Garzon, F.; Rezaei, F.; Rownaghi, A. A., A Novel Method of 3D Printing High-Loaded Oxide/H-ZSM-5 Catalyst Monoliths for Carbon Dioxide Reduction in Tandem with Propane Dehydrogenation. *Advanced Sustainable Systems* **2021**, *5* (3), 2000257.
97. Hutama, A. S.; Marlina, L. A.; Chou, C.-P.; Irle, S.; Hofer, T. S., Development of Density-Functional Tight-Binding Parameters for the Molecular Dynamics Simulation of Zirconia, Ytria, and Ytria-Stabilized Zirconia. *ACS Omega* **2021**, *6* (31), 20530-20548.

98. Cao, Y.; Liu, T.; Chen, T.; Zhang, B.; Jiang, D.-e.; Xie, J., Revealing the etching process of water-soluble Au<sub>25</sub> nanoclusters at the molecular level. *Nat. Commun.* **2021**, *12* (1), 3212.
99. Bhasker-Ranganath, S.; Rahman, M. S.; Zhao, C.; Calaza, F.; Wu, Z.; Xu, Y., Elucidating the Mechanism of Ambient-Temperature Aldol Condensation of Acetaldehyde on Ceria. *ACS Catal.* **2021**, 8621-8634.
100. Barboun, P. M.; Daemen, L. L.; Waitt, C.; Wu, Z.; Schneider, W. F.; Hicks, J. C., Inelastic Neutron Scattering Observation of Plasma-Promoted Nitrogen Reduction Intermediates on Ni/ $\gamma$ -Al<sub>2</sub>O<sub>3</sub>. *ACS Energy Letters* **2021**, *6* (6), 2048-2053.
101. Zhang, L.; Zhang, X.; Qian, K.; Li, Z.; Cheng, Y.; Daemen, L. L.; Wu, Z.; Huang, W., Activation and surface reactions of CO and H<sub>2</sub> on ZnO powders and nanoplates under CO hydrogenation reaction conditions. *J. Energy Chem.* **2020**, *50*, 351-357.
102. Yuk, S. F.; Lee, M.-S.; Collinge, G.; Zhang, J.; Padmaperuma, A. B.; Li, Z.; Polo-Garzon, F.; Wu, Z.; Glezakou, V.-A.; Rousseau, R., Mechanistic Understanding of Catalytic Conversion of Ethanol to 1-Butene over 2D-Pillared MFI Zeolite. *J. Phys. Chem. C* **2020**, *124* (52), 28437-28447.
103. Yang, J.; Xiao, W.; Chi, X.; Lu, X.; Hu, S.; Wu, Z.; Tang, W.; Ren, Z.; Wang, S.; Yu, X.; Zhang, L.; Rusydi, A.; Ding, J.; Guo, Y.; Gao, P.-X., Solar-driven efficient methane catalytic oxidation over epitaxial ZnO/La<sub>0.8</sub>Sr<sub>0.2</sub>CoO<sub>3</sub> heterojunctions. *Appl. Catal. B: Environ.* **2020**, *265*, 118469.
104. Yang, H.; Chen, X.; Hu, G.; Chen, W.-T.; Bradley, S. J.; Zhang, W.; Verma, G.; Nann, T.; Jiang, D.-e.; Kruger, P. E.; Wang, X.; Tian, H.; Waterhouse, G. I. N.; Telfer, S. G.; Ma, S., Highly efficient electrocatalytic hydrogen evolution promoted by O–Mo–C interfaces of ultrafine  $\beta$ -Mo<sub>2</sub>C nanostructures. *Chem. Sci.* **2020**, *11* (13), 3523-3530.
105. Wang, X.; Wang, Z.; García de Arquer, F. P.; Dinh, C.-T.; Ozden, A.; Li, Y. C.; Nam, D.-H.; Li, J.; Liu, Y.-S.; Wicks, J.; Chen, Z.; Chi, M.; Chen, B.; Wang, Y.; Tam, J.; Howe, J. Y.; Proppe, A.; Todorović, P.; Li, F.; Zhuang, T.-T.; Gabardo, C. M.; Kirmani, A. R.; McCallum, C.; Hung, S.-F.; Lum, Y.; Luo, M.; Min, Y.; Xu, A.; O'Brien, C. P.; Stephen, B.; Sun, B.; Ip, A. H.; Richter, L. J.; Kelley, S. O.; Sinton, D.; Sargent, E. H., Efficient electrically powered CO<sub>2</sub>-to-ethanol via suppression of deoxygenation. *Nat. Energy* **2020**, *5*, 478-486.
106. Walker, E. A.; Ravisankar, K.; Savara, A., CheKiPEUQ Intro 2: Harnessing Uncertainties from Data Sets, Bayesian Design of Experiments in Chemical Kinetics. *ChemCatChem* **2020**, *12* (21), 5401-5410.
107. Shu, Y.; Chen, H.; Chen, N.; Duan, X.; Zhang, P.; Yang, S.; Bao, Z.; Wu, Z.; Dai, S., A Principle for Highly Active Metal Oxide Catalysts via NaCl-Based Solid Solution. *Chem* **2020**, *6* (7), 1723-1741.
108. Liu, K.-G.; Gao, X.-M.; Liu, T.; Hu, M.-L.; Jiang, D.-e., All-Carboxylate-Protected Superatomic Silver Nanocluster with an Unprecedented Rhombohedral Ag<sub>8</sub> Core. *J. Amer. Chem. Soc.* **2020**, *142* (40), 16905-16909.
109. Feng, D.; Dong, Y.; Zhang, L.; Ge, X.; Zhang, W.; Dai, S.; Qiao, Z.-A., Holey Lamellar High Entropy Oxide as Ultra-Highly Active Heterogeneous Catalyst for Solvent-free Aerobic Oxidation of Benzyl Alcohol. *Angew. Chem. Int. Ed.* **2020**, *59* (44), 19503-19509.

110. Chevrier, D. M.; Conn, B. E.; Li, B.; Jiang, D.-e.; Bigioni, T. P.; Chatt, A.; Zhang, P., Interactions between Ultrastable Na<sub>4</sub>Ag<sub>44</sub>(SR)<sub>30</sub> Nanoclusters and Coordinating Solvents: Uncovering the Atomic-Scale Mechanism. *ACS Nano* **2020**.
111. Cao, Y.; Fung, V.; Yao, Q.; Chen, T.; Zang, S.; Jiang, D.-e.; Xie, J., Control of single-ligand chemistry on thiolated Au<sub>25</sub> nanoclusters. *Nat. Commun.* **2020**, *11* (1), 5498.
112. Zhou, M.; Higaki, T.; Hu, G.; Sfeir, M. Y.; Chen, Y.; Jiang, D.-e.; Jin, R., Three-orders-of-magnitude variation of carrier lifetimes with crystal phase of gold nanoclusters. *Science* **2019**, *364* (6437), 279-282.
113. Zheng, K.; Fung, V.; Yuan, X.; Jiang, D.-e.; Xie, J., Real Time Monitoring of the Dynamic Intracluster Diffusion of Single Gold Atoms into Silver Nanoclusters. *J. Amer. Chem. Soc.* **2019**, *141* (48), 18977-18983.
114. Yusuf, S.; Neal, L.; Bao, Z.; Wu, Z.; Li, F., Effects of Sodium and Tungsten Promoters on Mg<sub>6</sub>MnO<sub>8</sub>-Based Core-Shell Redox Catalysts for Chemical Looping—Oxidative Dehydrogenation of Ethane. *ACS Catal.* **2019**, *9* (4), 3174-3186.
115. Ye, J.; Bai, L.; Liu, B.; Tian, H.; Hu, J.; Polo-Garzon, F.; Mayes, R. T.; Wu, Z.; Fang, Y.-X., Fabrication of Pillared ZSM-5 Framework for Shape Selectivity of Ethane Dehydroaromatization. *Ind. Eng. Chem. Res.* **2019**, *58* (17), 7094-7106.
116. Wu, H.; Zeng, M.; Li, Z.; Zhu, X.; Tian, C.; Xia, C.; He, L.; Dai, S., Coupling FeNi alloys and hollow nitrogen-enriched carbon frameworks leads to high-performance oxygen electrocatalysts for rechargeable zinc-air batteries. *Sustain. Energ. Fuels* **2019**, *3* (1), 136-141.
117. Tan, S.; Sayed, F.; Yang, S.; Li, Z.; Wu, J.; Ajayan, P. M., Strong Effect of B-Site Substitution on the Reactivity of Layered Perovskite Oxides Probed via Isopropanol Conversion. *ACS Mater. Lett.* **2019**, *1* (2), 230-236.
118. Hülsey, M. J.; Zhang, B.; Ma, Z.; Asakura, H.; Do, D. A.; Chen, W.; Tanaka, T.; Zhang, P.; Wu, Z.; Yan, N., In situ spectroscopy-guided engineering of rhodium single-atom catalysts for CO oxidation. *Nat. Commun.* **2019**, *10* (1), 1330.
119. Dong, H.; Liu, C.; Li, Y.; Jiang, D.-e., Computational screening of M/Cu core/shell nanoparticles and their applications for the electro-chemical reduction of CO<sub>2</sub> and CO. *Nanoscale* **2019**, *11* (23), 11351-11359.
120. You, B.; Zhang, Y.; Yin, P.; Jiang, D.-e.; Sun, Y., Universal molecular-confined synthesis of interconnected porous metal oxides-N-C frameworks for electrocatalytic water splitting. *Nano Energy* **2018**, *48*, 600-606.
121. Yao, Q.; Fung, V.; Sun, C.; Huang, S.; Chen, T.; Jiang, D.-e.; Lee, J. Y.; Xie, J., Revealing isoelectronic size conversion dynamics of metal nanoclusters by a noncrystallization approach. *Nat. Commun.* **2018**, *9* (1), 1979.
122. Nair, L. V.; Hossain, S.; Takagi, S.; Imai, Y.; Hu, G.; Wakayama, S.; Kumar, B.; Kurashige, W.; Jiang, D.-e.; Negishi, Y., Hetero-bicosahedral [Au<sub>24</sub>Pd(PPh<sub>3</sub>)<sub>10</sub>(SC<sub>2</sub>H<sub>4</sub>Ph)<sub>5</sub>Cl<sub>2</sub>]<sup>+</sup> nanocluster: selective synthesis and optical and electrochemical properties. *Nanoscale* **2018**, *10* (40), 18969-18979.
123. Lu, M.; Lepore, A. W.; Choi, J.-S.; Li, Z.; Wu, Z.; Polo-Garzon, F.; Hu, M. Z., Acetic Acid/Propionic Acid Conversion on Metal Doped Molybdenum Carbide Catalyst Beads for Catalytic Hot Gas Filtration. *Catalysts* **2018**, *8* (12), 643.
124. Liu, C.; Camacho-Bunquin, J.; Ferrandon, M.; Savara, A.; Sohn, H.; Yang, D.; Kaphan, D. M.; Langeslay, R. R.; Ignacio-de Leon, P. A.; Liu, S.; Das, U.; Yang, B.; Hock, A. S.; Stair, P. C.; Curtiss, L. A.; Delferro, M., Development of activity-descriptor

relationships for supported metal ion hydrogenation catalysts on silica. *Polyhedron* **2018**, *152*, 73-83.

125. Li, W.; He, D.; Hu, G.; Li, X.; Banerjee, G.; Li, J.; Lee, S. H.; Dong, Q.; Gao, T.; Brudvig, G. W.; Waagele, M. M.; Jiang, D.-e.; Wang, D., Selective CO Production by Photoelectrochemical Methane Oxidation on TiO<sub>2</sub>. *ACS Centr. Sci.* **2018**, *4* (5), 631-637.

126. Kim, M.; Tang, Q.; Narendra Kumar, A. V.; Kwak, K.; Choi, W.; Jiang, D.-e.; Lee, D., Dopant-Dependent Electronic Structures Observed for M<sub>2</sub>Au<sub>36</sub>(SC<sub>6</sub>H<sub>13</sub>)<sub>24</sub> Clusters (M = Pt, Pd). *J. Phys. Chem. Lett.* **2018**, *9* (5), 982-989.

127. Hossain, S.; Ono, T.; Yoshioka, M.; Hu, G.; Hosoi, M.; Chen, Z.; Nair, L. V.; Niihori, Y.; Kurashige, W.; Jiang, D.-e.; Negishi, Y., Thiolate-Protected Trimetallic Au~20Ag~4Pd and Au~20Ag~4Pt Alloy Clusters with Controlled Chemical Composition and Metal Positions. *J. Phys. Chem. Lett.* **2018**, *9* (10), 2590-2594.

128. Duchesne, P. N.; Li, Z. Y.; Deming, C. P.; Fung, V.; Zhao, X.; Yuan, J.; Regier, T.; Aldabahi, A.; Almarhoon, Z.; Chen, S.; Jiang, D.-e.; Zheng, N.; Zhang, P., Golden single-atomic-site platinum electrocatalysts. *Nat. Mater.* **2018**, *17*, 1033-1039.

129. Choi, W.; Hu, G.; Kwak, K.; Kim, M.; Jiang, D.-e.; Choi, J.-P.; Lee, D., Effects of Metal-Doping on Hydrogen Evolution Reaction Catalyzed by MAu<sub>24</sub> and M<sub>2</sub>Au<sub>36</sub> Nanoclusters (M = Pt, Pd). *ACS Appl. Mater. Inter.* **2018**, *10* (51), 44645-44653.

130. Chen, T.; Fung, V.; Yao, Q.; Luo, Z.; Jiang, D.-e.; Xie, J., Synthesis of Water-Soluble [Au<sub>25</sub>(SR)<sub>18</sub>]- Using a Stoichiometric Amount of NaBH<sub>4</sub>. *J. Amer. Chem. Soc.* **2018**, *140* (36), 11370-11377.

131. Bugnet, M.; Overbury, S. H.; Wu, Z.; Aires, F. J. C. S.; Meunier, F.; Epicier, T., Visualizing and Quantifying the Cationic Mobility at {100} Surfaces of Ceria: Application to CO<sub>2</sub> Adsorption/Desorption Phenomena in the Environmental Transmission Electron Microscope. *Microsc. Microanal.* **2018**, *24* (S1), 1940-1941.

132. Artyushkova, K.; Mullins, D. R.; Gregoratti, L.; Yu, X. Y., Foreword to special section on “Near Ambient and Synchrotron Surface Analysis (NAXPS)”. *Surf. Interface Anal.* **2018**, *50* (10), 911-912.

## **Awards and leadership activities during 2018 – 2020 of ORNL BES Catalysis team (FWP ERKCC96)**

### **Zili Wu**

#### **Award:**

- 2019 - Excellence in Catalysis Award from the Catalysis Society of Metropolitan New York

#### **Leadership activities**

- Advisory Committees: External Advisory Board of Institute of Catalysis for Energy Processes (ICEP), Northwestern University, 2017 – present.
- International Scientific Committee of 3<sup>rd</sup> Fundamentals and Applications of Cerium Oxide in Catalysis, 2018 and 2020.
- Editorial Board: *Chin J. Catal.* 2014 – present; *Chin. Chem. Lett.* 2016 – present
- Symposium organizer

- “Advances in Catalysis with Ceria & Other Reducible Oxides” symposium, 258th ACS National Meeting & Exposition, August 25-29, 2019, San Diego, CA; Co-organizer.
- “Catalytic Chemistry over Metal Oxides” symposium, 257th ACS National Meeting & Exposition, Orlando, FL, March 31 - April 4, 2019; lead organizer.
- “In Situ & Operando Spectroscopy Microscopy Studies of Catalysis” symposium, 257th ACS National Meeting & Exposition, Orlando, FL, March 31 - April 4, 2019; co-organizer.
- “Catalytic Insights from In-Situ/Operando X-ray & Neutron Techniques” symposium, 256th ACS National Meeting & Exposition, Boston, MA, Aug. 19 - 23, 2018; lead organizer.

## **Sheng Dai**

### **Award**

- Winner of the 2020 Max Bredig Award for Ionic Liquids and Molten Salts from Electrochemical Society
- 2019 American Chemical Society's Award in Separations Science & Technology
- MRS Fellow, 2019
- 2019 Thompson-Reuters List of the World’s Most Influential Chemists
- 2018 IMMA Award from the International Mesoporous Materials Society
- American Association for the Advancement of Science (AAAS) Fellow, 2018
- 2018 Thompson-Reuters List of the World’s Most Influential Chemists and Materials Scientists

### **Leadership activities**

- Editorial or advisory boards of *ChemSusChem* (Wiley), *Batteries & Supercaps* (Wiley), *ChemistrySELECT* (Wiley), and *Green Energy & Environment* (KeAi & Elsevier).
- Treasurer, International Mesoporous Materials Society, 2013-2018.
- Council member, International Mesoporous Materials Society, 2013-2018.
- Serve on the review panel, Material Synthesis near Room Temperature, Deutsche Forschungsgemeinschaft (German Research Foundation), Max Planck Institute for Chemical Physics of Solids, 2013-2020.
- Symposium organizer
  - International Advisory Committee, The 8th International Congress on Ionic Liquids (COIL 8), Beijing, China on May 13-17, 2019
  - International Advisory Committee, The 6th Asian-Pacific Congress on Ionic Liquid & Green Processes (APCIL-6), Yonago, Japan, Oct. 31-Nov. 3, 2018.
  - Co-organizer for Symposium: The 10th International Mesoporous Materials Symposium (IMMS10), September 10-13th, 2018 at the UCLA Campus in Los Angeles, California
  - Co-organizer for Symposium: “Porous Materials and Nanocomposites for Catalysis Nanotechnology (Symposium NM04) ” in the MRS 2018 Spring Meeting, April 2-6, 2018, Phoenix, Arizona

## **De-en Jiang**

### **Leadership activities**

Symposium/workshop organizer

- Co-Chair, Gordon Research Conference on Atomically Precise Nanochemistry, Galveston, TX, February 9 - 14, 2020.
- "Computational Materials Chemistry" Telluride Workshop, focus on electrochemical interfaces, July 16-20, 2019, Telluride, CO; lead organizer.
- "Catalytic Chemistry over Metal Oxides" symposium, 257th ACS National Meeting & Exposition, Orlando, FL, March 31 - April 4, 2019; co-organizer.
- "Nanometal: Synthesis, Properties, and Applications" Symposium, 2018 Materials Research Society Fall Meeting, Boston, MA, Nov. 25-30, 2018; lead organizer.
- "Fundamental Understandings of Interfaces in Catalysis", 256th ACS National Meeting & Exposition, Boston, MA, Aug. 19 - 23, 2018; sole organizer.
- "Interplay between theory and experimental in nanocatalysis", Mesilla Workshop, Feb. 3-7, 2018, Mesilla, NM; lead organizer.

## **Ashi Savara**

### **Leadership activities**

- 2017- 2019 ACS Catalysis Science and Technology Division Representative on ACS National Meetings Multidisciplinary Program Planning Group
- 2018, 2019 ACS Catalysis Science and Technology Division Councilor
- 2017- 2019 ACS Catalysis Science and Technology Division Spring Program Chair
- 2017- 2019 ACS Environmental Chemistry Division Membership Chair
- Symposium lead organizer:
  - "Catalysis for Environmental and Energy Applications" Division: ENVR & CATL. 258th ACS National Meeting, San Diego, CA. August 25-29, 2019.
  - "Advances in Methods for Comparing Molecular & Supramolecular Simulations to Experiments" Division: CATL & PHYS & COMP & CINF. 257th ACS National Meeting, Orlando, FL. March 31- April 04, 2019.
  - "Elucidation of Mechanisms & Kinetics on Surfaces" Division: CATL & PHYS & INOR & ENFL & ENVR. 257th ACS National Meeting, Orlando, FL. March 31- April 04, 2019.
  - "ACS Award in Surface Chemistry: Symposium in Honor of Hajo Freund" Division: COLL & CATL & PHYS. 257th ACS National Meeting, Orlando, FL. March 31- April 04, 2019.
  - "Catalysis for Environmental and Energy Applications" Division: ENVR & CATL. 256th ACS National Meeting, Boston, MA. August 19-23, 2018.
  - "Towards Comprehension of Scale-Up & Multiscale Modeling of Catalysts" Division: CATL & ENFL & COMP. 255th ACS National Meeting, New Orleans, LA. March 18-22, 2018.

- “Elucidation of Mechanisms & Kinetics on Surfaces” Division: CATL & ENVR. 255th ACS National Meeting, New Orleans, LA. March 18-22, 2018.

### **Miaofang Chi**

#### **Awards**

- 2019, the K.F.J. Heinrich Award, Microanalysis Society (MAS).
- 2019, DOE-BES Early Career Research Award.
- 2018, Global highly cited researchers, Clarivate Analytics.

#### **Leadership activities**

- Committee Chair, Award Committee for Microscopy Society of America (MSA), 2019- present;
- 2019, International Advisory Board member of the International Conference on Electroceramics (International Electrochemical Society).
- Editorial Board, Materials Today, 2019 – present.
- Conference organizer, The 17th Frontiers of Electron Microscopy in Materials Science International Conference (FEMMS), Asheville, NC 2019.

### **Stephan Irle**

#### **Leadership activities**

- American Association for the Advancement of Science (AAAS) Fellow, 2018
- Author Profile, *Angew. Chem. Int. Ed.* **57**, 6732 (2018). [DOI: 10.1002/anie.201712472](https://doi.org/10.1002/anie.201712472)

## LIST OF PARTICIPANTS

First Name	Last Name	Email
Frank	Abild-Pedersen	abild@slac.stanford.edu
Anastassia	Alexandrova	ana@chem.ucla.edu
Aaron	Appel	aaron.appel@pnnl.gov
Yotam	Ardon	yardon@sas.upenn.edu
Tom	Autrey	tom.autrey@pnnl.gov
Simon	Bare	srbare@slac.stanford.edu
Bart	Bartlett	bartmb@umich.edu
Dishari	Basu	basu.75@osu.edu
Michael	Bedzyk	bedzyk@northwestern.edu
Alexis	Bell	alexbell@berkeley.edu
Wesley	Bernskoetter	bernskoetterwh@missouri.edu
Guy	Bertrand	gbertrand@ucsd.edu
Aditya	Bhan	abhan@umn.edu
Dipti	Bhave	dbhave@umass.edu
Elizabeth	Biddinger	ebiddinger@ccny.cuny.edu
Jennifer	Bigelow	jennifer.bigelow@pnnl.gov
Suzanne	Blum	blums@uci.edu
Monika	Blum	mblum@lbl.gov
Michael	Boreen	mboreen@berkeley.edu
Jeffery	Bricker	jeffery.bricker@uop.com
Morris	Bullock	morris.bullock@pnnl.gov
Jeffery	Byers	jeffery.byers@bc.edu
Karen Vannessa	Caballero	k.caballeroperez@wsu.edu
Donald	Camaioni	donald.camaioni@pnnl.gov
Charles	Campbell	charliec@uw.edu
Matteo	Cargnello	mcargnello@stanford.edu
Puranjan	Chatterjee	puranjan@iastate.edu

---

Yanna	Chen	yanna.chen@northwestern.edu
Peng	Chen	pc252@cornell.edu
Jingguang	Chen	jgchen@columbia.edu
Yaxin	Chen	yaxin.chen@northwestern.edu
Linxiao	Chen	linxiao.chen@pnnl.gov
Jingyi	Chen	chenj@uark.edu
Miaofang	Chi	chim@ornl.gov
Paul	Chirik	pchirik@princeton.edu
Andrei	Chirila	andrei.chirila@pnnl.gov
Phillip	Christopher	pchristopher@ucsb.edu
Geoff	Coates	gc39@cornell.edu
Richard	Crooks	crooks@cm.utexas.edu
Ayanna	Culmer-Gilbert	aculmer@iu.edu
Thomas	Cundari	t@unt.edu
Sheng	Dai	dais@ornl.gov
Anusheela	Das	anusheeladas2021@u.northwestern.edu
Abhaya	Datye	datye@unm.edu
Paul	Dauenhauer	hauer@umn.edu
Alex	Davies	amdavies@umich.edu
Robert	Davis	rjd4f@virginia.edu
Max	Delferro	delferro@anl.gov
David	Dixon	dadixon@ua.edu
Zdenek	Dohnalek	zdenek@pnnl.gov
Dawn	Duan	dawnduan@u.northwestern.edu
Daniel	Ess	dhe@chem.byu.edu
Chris	Fecko	christopher.fecko@science.doe.gov
David	Flaherty	dwflhrt@illinois.edu
Alison	Fout	Fout@illinois.edu
Mike	Gagne	mgagne@unc.edu

---

---

Aigerim	Galyamova	Aigerimg@utexas.edu
Yafei	Gao	gaoyafe@iu.edu
Lijun	Gao	lijungao@ucsb.edu
Feng	Gao	feng.gao@pnnl.gov
Carlos	Garcia	carlos.garciavargas@wsu.edu
Bruce	Gates	bcgates@ucdavis.edu
Bojana	Ginovska	bojana.ginovska@pnnl.gov
Vanda	Glezakou	Vanda.Glezakou@pnnl.gov
Karen	Goldberg	kig@sas.upenn.edu
Alan	Goldman	alanguardman@gmail.com
Raymond	Gorte	gorte@seas.upenn.edu
Rajamani	Gounder	rgounder@purdue.edu
Lars	Grabow	grabow@uh.edu
Lauren	Greenlee	greenlee@psu.edu
T Brent	Gunnoe Gutierrez	tbg7h@virginia.edu
Oliver	Tinoco	oliver.gutierrez@pnnl.gov
Lillian	Hale	Lily.hale@pnnl.gov
John	Hartwig	jhartwig@berkeley.edu
Nilay	Hazari	nilay.hazari@yale.edu
Tony	Heinz	tony.heinz@stanford.edu
Graeme	Henkelman	henkelman@utexas.edu
Alyssa	Hensley	alyssa.rose@wsu.edu
Ive	Hermans	hermans@chem.wisc.edu
Clemens	Heske	heske@unlv.nevada.edu
Andreas	Heyden	heyden@cec.sc.edu
Adam	Hoffman	ashoff@slac.stanford.edu
Patrick	Holland	patrick.holland@yale.edu
Jian	Hu	Jianzhi.Hu@pnnl.gov
Wenda	Hu	wenda.hu@wsu.edu

---

---

Zhennan	Huang	huangz@ornl.gov
Weixin	Huang	weixin.huang@wsu.edu
Joseph	Hupp	j-hupp@northwestern.edu
Stephan	Irle	irles@ornl.gov
Anant	Jain	anantj16@sas.upenn.edu
Seung Soon	Jang	seungsoon.jang@mse.gatech.edu
Michael	Janik	mjanik@psu.edu
Thomas	Jaramillo	jaramillo@stanford.edu
Friederike	Jentoft	fcjentoft@umass.edu
De-en	Jiang	djiang@ucr.edu
Dong	Jiang	dong.jiang@wsu.edu
William	Jones	jones@chem.rochester.edu
Christopher	Jones	christopher.jones@chbe.gatech.edu
David	Kaphan	kaphand@anl.gov
Abhi	Karkamkar	abhi.karkamkar@pnnl.gov
Alexander	Katz	askatz@berkeley.edu
Bruce	Kay	bruce.kay@pnnl.gov
Sheima	Khatib	sheima.khatib@ttu.edu
Konstantin	Khivantsev	Konstantin.Khivantsev@pnnl.gov
Sungmin	Kim	sungmin.kim@pnnl.gov
Mansu	Kim	mansu.kim@northwestern.edu
Greg	Kimmel	gregory.kimmel@pnnl.gov
Takeshi	Kobayashi	takeshi@iastate.edu
Shane	Kosir	shane.kosir@wsu.edu
Yosi	Kratish	yosi.kratish@northwestern.edu
Jeremy	Kropf	kropf@anl.gov
Pranaw	Kunal	pranaw@ameslab.gov
Harold	Kung	hkung@northwestern.edu
Rob	Lavroff	lavroff@g.ucla.edu

---

---

Thuy	Le	thuy.le@pnnl.gov
Christopher	Lee	christopher.lee@pnnl.gov
Johannes	Lercher	johanneslercher@hotmail.com
Wenjie	Li	wl697@cornell.edu
Junrui	Li	junrui.li@wsu.edu
Jiaqi	Li	jiaqili2015@u.northwestern.edu
Yixiao	Li	yixiao.li@wsu.edu
Suljo	Linic	linic@umich.edu
Cong	Liu	congliu@anl.gov
Liang	Liu	liang.liu@pnnl.gov
Jian	Liu	jian.liu@northwestern.edu
Yiqi	Liu	yiqliu2023@u.northwestern.edu
Ping	Liu	pingliu3@bnl.gov
Charles	Machan	machan@virginia.edu
Mausumi	Mahapatra	mausumi@pnnl.gov
Konstantin	Mamedov	km6uq@virginia.edu
Zachary	Mansley	zacharymansley2021@u.northwestern.edu
Smaranda	Marinescu	smarines@usc.edu
Tobin	Marks	t-marks@northwestern.edu
Abraham	Martinez	abraham.martinez@berkeley.edu
Manos	Mavrikakis	emavrikakis@wisc.edu
Andrew	May	amay000@citymail.cuny.edu
Charles	McCrorry	cmccrory@umich.edu
Jean-Sabin	McEwen	js.mcewen@wsu.edu
Eric	McFarland	mcfar@ucsb.edu
Will	Medlin	medlin@colorado.edu
Raul	Miranda	raul.miranda@science.doe.gov
Liviu	Mirica	mirica@illinois.edu
Karl	Mueller	karl.mueller@pnnl.gov

---

---

Jennifer	Napoles	napolj2@unlv.nevada.edu
Matthew	Neurock	mneurock@umn.edu
Eranda	Nikolla	erandan@wayne.edu
Justin	Notestein	j-notestein@northwestern.edu
Christopher	O'Connor	christopher.oconnor@pnnl.gov
Tadashi	Ogitsu	ogitsu1@llnl.gov
Umit	Ozkan	ozkan.1@osu.edu
Chris	Paolucci	cp9wx@virginia.edu
Gerard	Parkin	parkin@columbia.edu
Anyang	Peng	lly9y3@u.northwestern.edu
Frederic	Perras	fperras@ameslab.gov
Craig	Plaisance	plaisance@lsu.edu
Felipe	Polo-Garzon	pologarzonf@ornl.gov
Patricia	Poths	patriciapoths@chem.ucla.edu
David	Potts	dspotts2@illinois.edu
David	Powers	powers@chem.tamu.edu
Long	Qi	lqi@ameslab.gov
Kenneth	Raymond	knr4uc@gmail.com
Austin	Reese	ajr349@cornell.edu
Daniel	Resasco	resasco@ou.edu
Fereshteh	Rezvani	frezvani@iu.edu
Jeffrey	Rimer	jrimer@central.uh.edu
Robert	Rioux	rnr189@psu.edu
Jose	Rodriguez	rodriguez@bnl.gov
Jennifer	Roizen	jennifer.roizen@science.doe.gov
Beatriz	Roldan Cuenya	roldan@fhi-berlin.mpg.de
Yuriy	Roman	yroman@mit.edu
Roger	Rousseau	roger.rousseau@pnnl.gov
Aaron	Sadow	sadow@iastate.edu

---

---

Miquel	Salmeron	mbsalmeron@lbl.gov
Aditya	Savara	savaraa@ornl.gov
Anthony	Savoy	anthony.savoy@wsu.edu
Gregory	Schenter	greg.schenter@pnnl.gov
Julian	Schmid	julian.schmid@pnnl.gov
William	Schneider	wschneider@nd.edu
Neil	Schweitzer	neil.schweitzer@northwestern.edu
Susannah	Scott	sscott@ucsb.edu
Sanjaya	Senanayake	ssenanay@bnl.gov
Linda	Severs	Linda.severs@ornl.gov
Christo	Sevov	sevov.1@osu.edu
Marcus	Sharp	marcus.sharp@pnnl.gov
Wendy	Shaw	Wendy.Shaw@pnnl.gov
Carsten	Sievers	carsten.sievers@chbe.gatech.edu
Wade	Sisk	wade.sisk@science.doe.gov
Igor	Slowing	Igor.Slowing@science.doe.gov
Jeremy	Smith	smith962@indiana.edu
Randall	Snurr	snurr@northwestern.edu
Shannon	Stahl	stahl@chem.wisc.edu
Corey	Stephenson	crjsteph@umich.edu
Albert	Stiegman	stiegman@chem.fsu.edu
Juliette	Strasser	jstrasser@utexas.edu
JINGYI	SUI	B9t8a7@u.northwestern.edu
Steven	Suib	steven.suib@uconn.edu
Yifan	Sun	suny@ornl.gov
Junming	Sun	Junming.sun@wsu.edu
Jin	Suntivich	jsuntivich@cornell.edu
Charles	Sykes	charles.sykes@tufts.edu
Janos	Szanyi	janos.szanyi@pnnl.gov

---

---

Nathaniel	Szymczak	nszym@umich.edu
Steven	Tait	tait@indiana.edu
Sara	Thoi	sarathoi@jhu.edu
Don	Tilley	tdtilley@berkeley.edu
Ian	Tonks	itonks@umn.edu
Chris	Torres	chris3@illinois.edu
Ba	Tran	ba.tran@pnnl.gov
Franck	Ulm	franck_ulm@berkeley.edu
David	Vicic	vicic@lehigh.edu
Fernando	Vila	fdv@uw.edu
Johannes	Voss	vossj@slac.stanford.edu
Josh	Vura-Weis	vuraweis@illinois.edu
Israel	Wachs	iew0@lehigh.edu
Aone	Wang	aone.wang@oneatinc.com
Xingjie	Wang	xingjie.wang@northwestern.edu
Huamin	Wang	huamin.wang@pnnl.gov
Bin	Wang	wang_cbme@ou.edu
Yong	Wang	wang42@wsu.edu
Timothy	Warren	thw@georgetown.edu
Eman	Wasim	emwasim@iu.edu
Megan	Wasson	meganwasson2022@u.northwestern.edu
Steven	Watt	swatt@gradcenter.cuny.edu
Jason	Weaver	weaver@che.ufl.edu
Marcus	Weck	mw125@nyu.edu
Eric	Weitz	weitz@northwestern.edu
Michael	White	mgwhite@bnl.gov
ross	widenhoefer	rwidenho@chem.duke.edu
Eric	Wiedner	eric.wiedner@pnnl.gov
Kirsten	Winther	winther@stanford.edu

---

---

Zili	Wu	wuz1@ornl.gov
Zhenzhen	Yang	zyang17@utk.edu
Peidong	Yang	p_yang@berkeley.edu
Rocky	Ye	ry279@cornell.edu
Shuhao	Zhang	shuhao.zhang@northwestern.edu
Bin	Zhang	biz517@lehigh.edu
Zihao	Zhang	zihao.zhang@pnnl.gov

---

Cover images courtesy of: Jinguang Chen (Columbia University), David W. Flaherty (University of Illinois, Urbana-Champaign), Suzanne A. Blum (University of California, Irvine), Patrick L. Holland (Yale University), Jeffrey D. Rimer (University of Houston) and Frank Abild-Pedersen (SLAC).



U.S. DEPARTMENT OF  
**ENERGY**

Office of  
Science